

*Argonne National Laboratory*

**CHEMICAL ENGINEERING**

**DIVISION**

**SEMIANNUAL REPORT**

**July-December 1964**

## LEGAL NOTICE

This report was prepared as an account of Government sponsored work. Neither the United States, nor the Commission, nor any person acting on behalf of the Commission:

A. Makes any warranty or representation, expressed or implied, with respect to the accuracy, completeness, or usefulness of the information contained in this report, or that the use of any information, apparatus, method, or process disclosed in this report may not infringe privately owned rights; or

B. Assumes any liabilities with respect to the use of, or for damages resulting from the use of any information, apparatus, method, or process disclosed in this report.

As used in the above, "person acting on behalf of the Commission" includes any employee or contractor of the Commission, or employee of such contractor, to the extent that such employee or contractor of the Commission, or employee of such contractor prepares, disseminates, or provides access to, any information pursuant to his employment or contract with the Commission, or his employment with such contractor.

ANL-6925

Chemical Separations Processes  
for Plutonium and Uranium  
(TID-4500, 44th Ed.)  
AEC Research and  
Development Report

Argonne National Laboratory

9700 South Cass Avenue  
Argonne, Illinois 60440

# CHEMICAL ENGINEERING DIVISION SEMIANNUAL REPORT

July-December, 1964

R. C. Vogel, Division Director  
Milton Levenson, Associate Division Director  
F. R. Masten, Assistant Division Director

May, 1965

Preceding Semiannual Reports:

ANL-6800	July-December, 1963
ANL-6900	January-June, 1964

Operated by The University of Chicago  
under  
Contract W-31-109-eng-38  
with the  
U.S. Atomic Energy Commission



# Table of Contents

<b>SUMMARY</b> .....	1
<b>I. COMPACT PYROCHEMICAL PROCESSES</b> .....	21
A. Pyrochemical Process Development .....	21
1. Melt Refining .....	21
2. Processes Employing Liquid Metal Solvents .....	25
B. Fuel Processing Facilities for EBR-II .....	53
1. Technical Assistance and Service Equipment Development .....	53
2. Process Equipment Development .....	55
C. Fuel Cycle Facility Operations .....	68
1. Operations and Investigations with Equipment for Recovery of Irradiated Fuel .....	68
2. Operations with Equipment for Fuel Fabrication .....	76
3. Fuel Surveillance Program .....	86
4. Performance of Process Auxiliaries .....	86
D. Chemistry of Liquid Metals .....	90
1. Liquid Sodium Chemistry .....	90
2. Thermodynamics Studies .....	94
E. Preparation of Fuels for Fast Reactors .....	97
1. Preparation of Uranium Monocarbide by a Liquid-Metal Process .....	97
2. Preparation of Uranium Monocarbide by a Fluid-Bed Process .....	99
3. Homogeneous Precipitation of UC and (U-Pu)C from Fused Salts .....	101
4. Studies of Mobile Blanket Fuels for Fast Reactors .....	103
<b>II. FUEL CYCLE APPLICATIONS OF VOLATILITY AND FLUIDIZATION TECHNIQUES</b> .....	107
A. Laboratory Investigations .....	110
1. Fluid-Bed Fluorination of $U_3O_8$ - $PuO_2$ Mixtures .....	110
2. Fluorination of $UO_2$ - $PuO_2$ Pellets in a 2-inch Diameter Fluidized-Bed Reactor .....	116
3. Phase Studies .....	120
4. Reactions of $PuF_6$ .....	122
5. Alpha Radiation Decomposition Rate of Plutonium Hexafluoride .....	123
6. Corrosion of Materials .....	126
7. Fluorination of Waste Samples from Rocky Flats Plant .....	128
8. Neptunium Chemistry .....	130
9. Fission Product Chemistry: Behavior of $MoO_3$ , $MoO_2$ , and $SnF_4$ Under Fluorination Conditions .....	132
B. Engineering-Scale Investigations of Fluid-Bed Fluoride Volatility Processes .....	132
1. Development of Fluid-Bed Fluoride Volatility Processes for the Recovery of Uranium and Plutonium from Uranium Dioxide Fuels .....	132
2. Process Studies on the Recovery of Uranium from Highly Enriched Uranium Alloy Fuels .....	147
3. The Corrosion of Nickel-200 in Fluoride Volatility Process Environments .....	158
4. Basic Studies of Fluidized-Bed Behavior Related to Process Operations .....	163
<b>III. HIGH TEMPERATURE REACTOR MATERIALS DEVELOPMENT</b> .....	165
A. Current Status of High Temperature Phase Relations and Thermodynamic Properties in the Uranium-Urania System .....	165
B. Experimentation in the Uranium-Urania System .....	170
1. Effusion Vapor Pressure Studies .....	170
2. Mass Spectrometric Effusion Studies .....	171
3. Transpiration Studies of Vaporization .....	171
4. Uranium-Urania Phase Diagram Studies .....	171
C. Uranium-Uranium Monosulfide Phase Diagram Studies .....	173
<b>IV. CALORIMETRY</b> .....	175
A. Combustion of Phosphorus in Fluorine .....	175
B. Combustion of Sulfur in Fluorine .....	177
C. Combustion of Silicon Carbide and Graphite in Fluorine .....	177
D. Combustions of Magnesium, Aluminum, Yttrium, Lanthanum, Gadolinium, and Holmium in Fluorine .....	179

E.	Combustion of Tantalum Diboride in Fluorine.....	181
F.	Fluorine Flow Calorimeter; Combustion of Uranium Monosulfide in Fluorine....	182
G.	High Temperature Enthalpy Calorimetry.....	183
	1. 1500°C Drop Calorimeter.....	183
	2. 2500°C Drop Calorimeter.....	185
<b>V.</b>	<b>REACTOR SAFETY</b> .....	187
A.	Metal-Water Reactions.....	187
	1. Studies of Metal-Water Reactions by the High Pressure Furnace Method....	187
	2. Reaction of Refractory Metals with Steam.....	190
	3. Studies of Metal-Water Reactions by the Laser Heating Method.....	198
	4. Studies in TREAT of Uranium Dioxide Fuel.....	204
	5. Scale-Up Experiments in TREAT.....	209
	6. Water Hammer Evaluation.....	213
	7. Calculation of the Extent of Metal-Water Reaction During a Loss-of-Coolant Accident.....	215
B.	Fast Reactor Safety Studies.....	226
	1. Fuel- and Cladding-Coolant Interaction Studies.....	226
C.	Metal Oxidation and Ignition Kinetics.....	227
	1. Ignition of Irradiated Uranium.....	227
<b>VI.</b>	<b>ENERGY CONVERSION</b> .....	235
A.	Lithium Hydride Cell Studies.....	236
B.	Electrode Kinetics.....	237
C.	Intermetallic Systems.....	238
	1. Sodium-Bismuth Solubility Studies.....	238
	2. Intermetallic Compounds in Molten Salt Solutions.....	240
D.	Liquid-Vapor Relationships in the Regeneration of the Na-Bi Cell.....	241
E.	Regenerative Emf Cells—Engineering Studies.....	242
	1. Engineering Thermodynamic Studies.....	243
	2. Experimental Sodium-Bismuth Cell.....	245
	3. Frozen Electrolyte-Silicon Rubber Insulation-Seal.....	246
	4. Engineering Material Study.....	246
<b>VII.</b>	<b>NUCLEAR CONSTANTS</b> .....	249
A.	Neutron Inelastic Scattering.....	249
B.	Fast Neutron Capture.....	249
C.	Capture-to-Fission Ratios in EBR-II.....	251
<b>VIII.</b>	<b>ANALYTICAL RESEARCH AND DEVELOPMENT</b> .....	253
A.	Uranium-235 Fast Fission Yields of Molybdenum-95, -97, -98, and -100.....	253
B.	Uranium-235 Fast Fission Yields of Ruthenium-101, -102, and -104.....	253
C.	Irradiations in EBR-II.....	254
<b>IX.</b>	<b>STUDIES AND EVALUATIONS</b> .....	255
A.	General Objectives.....	255
B.	Cost Evaluation of Metal-Fueled Fast Reactors.....	255
C.	Divisional Study of Reprocessing of Fast Reactor Plutonium Fuels.....	259

## SUMMARY

### Chemical Engineering Division Semiannual Report

#### I. Compact Pyrochemical Processes (pages 21 to 106)

The first core loading of the EBR-II reactor will be processed for recycle to the reactor by melt refining. Development work on the melt refining process has been completed, and processing of irradiated fuel by this method has been started recently in the EBR-II Fuel Cycle Facility.

Further investigations have been conducted on halide slagging, a melt refining-type process in which rare earth fission products in discharged uranium or uranium-plutonium fuel alloys are preferentially oxidized by an oxidizing agent such as  $MgCl_2$  and extracted from the molten fuel alloy into an overlying chloride flux. Potential advantages of halide slagging are lower operating temperatures ( $\sim 1150^\circ C$ ) than those required for melt refining ( $\sim 1400^\circ C$ ), short liquation times (one hour or less), and high product yields ( $\sim 99\%$ ). To determine the behavior of fission product zirconium during halide slagging, a uranium-5 w/o fission alloy containing 0.68 w/o zirconium and 0.45 w/o cerium was contacted under static conditions with  $CaCl_2$  to which 160% of the quantity of  $MgCl_2$  required to oxidize the cerium and zirconium had been added. The system was liquated for one hour at  $1200^\circ C$ . No zirconium was removed from the alloy. The cerium removal (97%) was in agreement with earlier results.

The large-scale application of the halide slagging process requires the availability of large beryllia crucibles. The technology of fabricating large beryllia crucibles by pressing and sintering has not been developed. Therefore, the concept of a beryllia-coated crucible (beryllia plasma-sprayed on the inside surfaces) was explored. In a single test in a beryllia-coated Alundum crucible, molten flux seeped into the walls of the crucible. This approach, therefore, does not appear promising.

Various materials, principally high melting point carbides, borides, and nitrides, are being investigated for containing uranium and its alloys at temperatures from their melting points to several hundred degrees above their melting points. Of the materials tested,

only HfC and NbN, which were not attacked in 24-hour tests by uranium at  $1400^\circ C$ , appear promising, as does the previously tested  $ZrB_2$ ,  $TiB_2$ ,  $CrB_2$ , TiC, NbC, and TaC were severely attacked.

Work was continued on the purification of argon from nitrogen by getting the nitrogen on hot titanium sponge. This purification procedure may be used in the future for removing nitrogen from the argon atmosphere of the EBR-II Fuel Cycle Facility and could also be used for the purification of glovebox atmospheres. The kinetics of the nitrogen-titanium sponge reaction at  $900^\circ C$  have been measured at nitrogen concentrations in argon of 300, 1000, and 5000 ppm. At these concentrations, the reaction apparently follows a modified exponential rate law. Operation of a 10-cfm pilot plant was also continued to provide information on the durability of components for large volume purification systems. After 1000 hours of trouble-free operation, the pilot plant was shut down in order to charge fresh titanium. After 650 additional hours of operation, operations were again stopped when an oil leak developed in the gas blower. Seals in the gas blower were found to have failed because of inadequate lubrication. Modifications have been made in the blower to insure adequate lubrication of the seals and operation of the pilot plant was resumed in late November.

Work was continued on an EBR-II fuel recovery process which supplements melt refining. Known as the skull reclamation process, it effects recovery and purification of melt refining crucible residues. These residues are first converted by controlled oxidation to oxide powders which are poured from the crucible. Reduction of the oxide and purification of the uranium is then accomplished in a series of six process steps conducted in molten metal (zinc-magnesium systems) and molten halide salt media. These latter steps are being conducted on a pilot plant scale of about 2 kg of skull oxide per process batch, which compares to a plant batch size of 7 kg of skull oxide. The pilot plant equipment has been operated since startup in an open glovebox, but this glovebox has now been closed up and

operations are continuing in a dry-air (150 ppm H<sub>2</sub>O) atmosphere.

The operation of the pilot plant equipment has been improved steadily through the course of the runs. Reliable operation of agitators and heated molten salt and molten metal transfer lines has been achieved. However, a problem in several runs has been foaming of the flux. This has occurred in the step in which magnesium and zinc are added to reduce uranium oxides suspended in the molten flux. Foaming has been attributed to the hydrogen formed upon removal of residual water of hydration by reaction of water with the magnesium. It has been prevented in a recent run by pretreatment of the flux with magnesium at 700°C.

The major remaining operational problems are (1) reduction of the amounts of uranium precipitates which are entrained in metal waste streams, (2) control of salt fumes, and (3) fabrication of reliable tungsten crucibles. It is believed that the entrainment of uranium precipitates can be reduced to satisfactory levels by simply eliminating gas sparging of the molten metal supernatants which results when the transfer lines are back-flushed prior to transfer of the supernatant solution. Fume traps containing calcium metal turnings are effective in removing salt fumes, but have been inadequately tested. When properly used, pressed-and-sintered tungsten crucibles have performed satisfactorily, but their bulkiness and heavy weight are disadvantages. Therefore, relatively light weight welded tungsten and spun tungsten crucibles are being examined. A welded crucible failed by cracking in and near a weld after the equivalent of three pilot plant runs. Although a small (4-in. dia. by 6-in. high) spun tungsten crucible stood up well under test conditions, the larger spun crucible (10½ in. OD by 18½ in. high) has not yet been tested.

A number of uranium product solutions (about 10 w/o uranium and 12 w/o magnesium in zinc), the product of the pilot plant runs, have been retorted in beryllia crucibles to produce uranium ingots. With the possible exception of zirconium whose removal is on the low side, fission product concentrations are satisfactorily low and the product should be satisfactory for returning to the main EBR-II fuel stream via the melt refining operation.

Development work has continued on liquid metal processes for the recovery of plutonium and uranium from fast breeder reactor fuel alloys. The basic separations in the current process concepts are accomplished through differences in the partition behavior of the fuel constituents between liquid metal and molten salt solvents.

Because mechanical decladding of highly irradiated metallic reactor fuels may not be feasible, chemical

decladding procedures are under study. With a molten chloride solvent of the proper composition to provide the correct amount of complexing potential, it has been found possible to separate vanadium-20 w/o titanium cladding from uranium fuel alloy by treatment with chlorine. The chlorination reaction causes titanium and vanadium chlorides to be removed by volatilization, whereas the uranium remains in the salt as complexed UCl<sub>4</sub>. During the course of these studies, regions of liquid immiscibility were found in the systems KCl-CaCl<sub>2</sub>-BaCl<sub>2</sub>-UCl<sub>4</sub> and NaCl-KCl-CaCl<sub>2</sub>-UCl<sub>4</sub>. Initial studies indicate than an alternative decladding procedure, in which the clad fuel is hydrided, causing the cladding to split open, and subsequent dehydriding and dissolution of the fuel in liquid metal, may be feasible.

Further determinations of the distribution coefficients of plutonium, praseodymium, and lanthanum between 30 m/o NaCl-20 m/o KCl-50 m/o MgCl<sub>2</sub> and various liquid alloys of magnesium have been made. Drastic variations in the distribution coefficients of plutonium and rare earths are possible through changes in the composition of the metal phase. Aluminum-magnesium alloys, because they result in very low distribution coefficients for rare earths, appear to be useful for the removal of rare earth fission products from recycled salt streams. Copper-magnesium alloys provide a plutonium-praseodymium separation factor of at least 240, which may permit a single-stage extraction for this separation in a liquid metal process.

In another distribution study, distribution coefficients of yttrium and californium between LiCl-MgCl<sub>2</sub> salt mixtures and Zn-6 w/o Mg alloy were measured. The separation factor was small, about 8. This result suggests the possibility of rare earth fission product separations from transplutonium elements by multistage liquid metal-molten salt extractions.

X-ray data have shown that delta-phase U<sub>2</sub>Zn<sub>17</sub> precipitated from U-Cd-Mg-Zn solutions undergoes substitution of cadmium and magnesium for the zinc, with a corresponding expansion of the unit cell.

Work was continued on a program to develop the engineering technology required for the separation of plutonium and uranium from fission products by multistage extractions between molten metal and molten salt phases. Preliminary batch extractions indicate rapid transfer of uranium across metal-salt interfaces. A conceptual design has been developed for a prototype extraction facility, construction of which may be started in the next year. A loop facility has already been constructed for the purpose of testing components, e.g., valves, pumps, and flowmeters, required for the extraction facility.

Several steels (types 304 and 405 stainless steels,

Croloy 2¼, and 1019 and 1020 carbon steel) have been examined as potential materials of construction for the prototype extraction facility. Type 405 stainless steel was selected on the basis of: (1) superior corrosion resistance to the metal and salt systems, (2) good resistance to external air oxidation, and (3) good stability of plutonium in Cd-Mg-Zn solutions contained in crucibles fabricated of 405 stainless steel.

Improved performance of an eddy-current induction probe for measuring the depth of liquid metals has been achieved by winding the primary and secondary coils of nichrome wire on a grooved alumina tube. The probe is operated in a well similar to a thermocouple well. One such probe has given reproducible readings (equivalent to  $\pm 1/8$  in. of cadmium) over a 3-month period; during this time it was at temperatures above 350°C for more than 300 hr and was cycled at least thirty times between room temperature and 700°C. Calibration data have been obtained for the output signal strength as a function of cadmium liquid level and temperature. The instrument should be easily adaptable to remotely operated high-temperature equipment since there are no moving parts.

The ternary system, LiCl-KCl-MgCl<sub>2</sub>, is of interest as a potential flux to be used for the extraction of rare earth fission products from liquid metal solutions of uranium and plutonium. Liquidus temperatures of the ternary system have been determined over the entire composition range. To obtain satisfactory distribution coefficients for process separations, the salt should contain at least 50 m/o MgCl<sub>2</sub> and as much LiCl as possible. A liquid region was found to exist below 500°C in a wide composition band extending from 29 to 60 m/o MgCl<sub>2</sub> on the KCl-MgCl<sub>2</sub> edge of a ternary diagram to 23 to 55 m/o KCl on the LiCl-KCl edge. A minimum liquidus temperature, 336°C, lies at about 40 m/o LiCl, 50 m/o KCl and 10 m/o MgCl<sub>2</sub>. These results indicate that suitable compositions which are liquid at reasonable process temperatures are available in the LiCl-KCl-MgCl<sub>2</sub> system.

The binary system Pu-Mg is being considered for use in certain liquid metal processes for plutonium fuel alloys. Although some information is available on the solid phases in this system, a liquid immiscibility curve has not been determined, nor have the liquidus temperatures outside the miscibility region been firmly established. Preliminary determinations of the miscibility gap by a two-phase sampling procedure show liquid immiscibility from about 8.5 to 84 a/o magnesium at 625°C, and a consolute temperature in the vicinity of 975°C.

Scouting studies have indicated that it may be possible to remove certain cations from molten halide solvents by ion exchange techniques. Barium ion was

extracted from a KBr-AlBr<sub>3</sub> melt (mole ratio 1:1) by solid potassium hexatitanate with a distribution coefficient of 10<sup>3</sup> ( $K_d = w/o$  in solid /  $w/o$  in salt).

Work is in progress on the determination of the critical constants of alkali metals. The densities of liquid and vapor phases are to be obtained from room temperature to the critical temperature by measuring the gamma radiation emanating from the vapor and liquid regions of the alkali metal, which is held within a small capsule. Preliminary runs made with irradiated cesium indicate that it has a critical temperature near 1660°C.

In studies of the boiling of mercury, the surface temperature of the mercury was measured using the mercury itself as one leg of a thermocouple. This thermocouple system involved the use of a single chromel wire which penetrated the vaporizing surface from above and formed a thermocouple with the mercury. The effect of a step temperature difference at various positions along the immersed portion of the wire has been analyzed to indicate the magnitude of the error in the surface temperature measurement caused by a temperature gradient beneath the mercury surface. It was determined that an error of +1°C in surface temperature would result from a temperature gradient of 165°C/in. across a 0.2-in. thick surface layer. The gradient was the maximum found in the mercury boiling studies.

A torsion-wire oscillating-cup viscometer has been built for measurement of the viscosities of liquid metals.

The construction of the EBR-II Fuel Cycle Facility in Idaho has been completed and the facility is in operation. The Chemical Engineering Division at Argonne, Illinois, continues to give technical assistance in the repair and modification of equipment in the EBR-II Fuel Cycle Facility. One of the current modifications has been the installation of a Chemical Engineering Division designed slip clutch on the hoist drive of Air Cell and Argon Cell operating manipulators. This slip clutch is needed to protect the hoist mechanism and cables from damage resulting from overloads. Four of the eight hoist drives have been modified. Installation of the slip clutch and service tests of the complete drive unit were carried out at Argonne, Illinois, after which the drive unit was returned to Idaho. By modifying two spare hoist units first, it was possible to perform the required modifications without interrupting the use of in-cell manipulators.

A slip clutch has been developed by the Chemical Engineering Division which transmits a torque while it is slipping that is nearly equal to the torque at which it first starts to slip. The clutch consists of a

driven steel clutch disc that is enclosed in a tight-fitting cylindrical housing. The housing is filled with molybdenum disulfide powder and is attached to an output shaft. This clutch is very compact in design, is economical to fabricate, and is expected to be highly resistant to radiation.

As part of an argon atmosphere environmental system for the testing of equipment and processes, a large, purified argon enclosure, 24 ft long by 2 ft wide by 14 ft high, has been designed by and is being installed in the Chemical Engineering Division (Building 310). In this enclosure, plant-sized equipment for the skull reclamation process will be tested and evaluated in an atmosphere equivalent to that of the EBR-II Argon Cell.

Construction of the large enclosure is nearing completion. After installation of ancillary equipment is completed, the enclosure will be leak-tested. Installation of prototype skull reclamation equipment will then follow the leak tests. The argon purification and circulation equipment and two smaller inert atmosphere glove box enclosures have already been installed. The argon purification system and one glove box enclosure are in operation.

Development of plant-scale equipment for the skull reclamation process continues. A prototype M-2 skull reclamation furnace is under construction. It will be heated by resistance heaters which are mounted as hinged half-cylinders surrounding the furnace shell. The hinged construction permits the heaters to be opened at appropriate times in the process to promote cooling of the furnace. The crucible is of pressed and sintered tungsten construction. Crucible contents will be stirred by an agitator assembly mounted on the furnace top. Since it is required that the furnace operate as a sealed unit, it was necessary to develop a satisfactory seal and bearing assembly for the agitator shaft that would be capable of withstanding the operating temperatures of the furnace (800°C), the dry argon atmosphere, and corrosive metal or salt flux fumes. An experimental seal and bearing assembly has been developed and is under test.

A heated transfer line is used for the transfer of molten metal and molten flux from the M-2 skull reclamation furnace to a transfer receiver. A prototype plant-size transfer line, fabricated of Mo-30 w/o W, is undergoing operational tests. A transfer receiver of an earlier design is being used for these tests until fabrication of the prototype transfer receiver is completed. The design of the prototype plant transfer receiver provides means for purging the transfer line, collecting the process fumes which accompany the transferred material, and weighing the material trans-

ferred at each process step to maintain precise control of raw material charges for succeeding process steps.

Fifteen retorting and uranium consolidation operations have been conducted in a modified melt refining furnace which is located in an inert atmosphere glove box. The retorting and consolidation operations constitute the final step in the present flowsheet for the skull reclamation process. In this step, zinc and magnesium are distilled from an alloy having a nominal composition of Zn-12 w/o Mg-10 w/o U. After the Zn-Mg has been distilled, the uranium remaining in the retorting crucible is consolidated by melting to form a metallic button. Two-liter beryllia crucibles have been used in these runs; plant-scale operations will require crucibles having a capacity of about 11 liters. Although beryllia crucibles have the advantage of providing easy removal of the metallic button from the crucible, they are subject to cracking and are difficult to fabricate in the size required for plant use. Therefore, a few exploratory experiments have been made to determine whether a tungsten crucible could be used successfully for the distillation operation. Since the uranium product remaining in the crucible after the distillation adheres to a tungsten crucible and makes removal of the uranium difficult, hydriding of the uranium product to convert it to a free-flowing, easily removable powder is being tested. The hydrided powder could then be transferred to a small, durable, readily available beryllia crucible for vacuum melting to produce uranium metal; the need for an 11-liter beryllia crucible would thereby be eliminated. Preliminary hydriding experiments have been successful, but further tests are needed before a decision can be made regarding the application of the hydriding step to the skull reclamation process.

The installation, preliminary testing, and modification to facilitate operation of equipment provided for the EBR-II Fuel Cycle Facility in Idaho was substantially completed and initial operations with irradiated fuel were carried out. This facility provides for the fully remote recovery and refabrication of fuel discharged from the EBR-II reactor after a decay cooling period as short as two weeks.

Modifications were made to the interbuilding fuel transfer coffin. These included motorizing the sliding top shield plug, and providing a mercury dump tank for emergency cooling. A fuel element removal machine was installed on the assembly dismantler and its operability was demonstrated. Tool bits of a new material (steel containing cobalt) were provided for the fuel element decanner. The speed of the decanner was reduced, after motion picture studies revealed an interaction between the decanner and the fuel chopper.

A series of  $^{131}\text{I}$  tracer experiments carried out on the melt refining process (and related process steps) showed that most of the iodine liberated on heating was retained by the furnace (including the fume trap) or the in-cell filter and that only a very small fraction escaped to the off-gas system. The off-gas delay tank was also found to be very effective in retaining iodine. The skull oxidation furnace was installed and found to perform satisfactorily. In tests with it, little or no iodine was found to volatilize during oxidation. Similarly, little iodine was lost from the uranium charge during injection casting.

An irradiated core subassembly which had attained a maximum burnup of about 0.1 a/o in the EBR-II reactor was placed in the interbuilding fuel transfer coffin. While in the coffin, sodium adhering to the subassembly was removed. The subassembly was then transferred to the Air Cell where it was dismantled without difficulty. In the Argon Cell, eighty fuel elements were deanned and melt refined along with about one-half their weight of unirradiated alloy. The ingot obtained had a weight equal to 92.7% of the charge. Fission product decontamination (except for higher than expected removal of zirconium) corresponded closely with results of small-scale tests. The skull remaining was oxidized satisfactorily, and the skull oxide was dumped from the crucible into a zinc can.

In the area of fuel fabrication, the equipment for injection casting, pin processing, welding, leak testing, bonding, and final assembly was placed into operation with some modifications. The use of an immersion thermocouple and a disposable mold pallet was effected for injection casting. Because of difficulties in feeding the pin processing machine automatically, the demolder module was separated from the pin processing machine and a master-slave manipulator was provided for feeding. Modifications were made to the welding operation to permit use of an argon shroud gas. The bonding machine was modified by substituting pneumatic actuation for electrical actuation. A new assembly straightness checking machine was provided.

By the use of the fuel fabrication equipment, 75 kg of unirradiated enriched fuel was cast to yield 418 acceptable castings. Assembly and recycle of this material has not been completed, but over 250 acceptable canned fuel elements have been obtained. Rebonding and retesting were carried out on 2500 fuel elements which were obtained from the disassembly, in Argonne, Illinois, of unirradiated subassemblies intended for EBR-II dry and wet critical tests. Some 1800 additional elements were found suitable for reassembly (the scrap will also be reclaimed). Twenty-

two subassemblies were fabricated from unirradiated alloy. The single ingot of irradiated alloy was carried through the injection casting and pin processing operations to yield 36 acceptable castings.

The Argon Cell atmosphere pressure control and purification systems continued in satisfactory operation. Although it has been possible to reduce the oxygen and water levels in the cell atmosphere to 8 and 5 ppm, respectively, the water and oxygen concentrations are each being purposely maintained at  $40 \pm 20$  ppm. The Argon Cell is being operated at the higher oxygen and water concentrations because of high wear rates of carbon bearings and motor brushes that were attributed to operation at the lower concentrations. The air in-leakage rate to the cell has been maintained at about 0.003 scfm at a negative cell pressure of 3 in. of  $\text{H}_2\text{O}$ .

Correction of minor difficulties with in-cell cranes and manipulators has continued. A special tool was devised for replacing crane bridge-drive units.

An area has been provided for on-site burial of high-level-activity wastes, and 30 of the 2500 holes (12 ft deep, steel-lined) planned for the area have been dug. A bottom-dumping shielded cask and a special trailer for transport of the cask have been provided. A 6-ft long steel can of waste will be dropped in each hole and covered with gravel, after which a cap will be welded on the liner.

Experiments on the analysis of sodium for oxygen by the fast neutron activation method are continuing. Promising results for reducing the correction necessitated by the oxygen content of the sample encapsulation material were obtained by the use of 2S aluminum.

Two reactions have been compared for liberating carbon dioxide from the  $\text{Na}_2\text{O}-\text{Na}_2\text{CO}_3$  mixture produced by the dry oxidation method for analysis of carbon in sodium. Liberation of carbon dioxide by either the high temperature reaction with silica or the room temperature reaction with aqueous sulfuric acid have been shown to be equivalent.

The carbon content of liquid sodium which was in contact with graphite and sampled through  $5\mu$ -porosity stainless steel filters was found to vary erratically. This variation suggests that the carbon was present as particulate matter capable of passing through the  $5\mu$ -porosity filters.

The reaction of liquid sodium with trace quantities of gaseous contaminants in helium is being studied to appraise their significance with respect to the operation of nuclear reactors. Helium containing oxygen, nitrogen, carbon dioxide, carbon monoxide, hydrogen and methane was circulated through liquid sodium at temperatures in the range 190 to 455°C. Oxygen and

carbon dioxide were rapidly and completely consumed. Carbon monoxide probably reacted completely, whereas nitrogen was probably unaffected. Hydrogen reacted partially and methane reacted only at the highest temperature.

Thermodynamic properties of the intermetallic compound  $\text{NdCd}_{11}$  have been studied by the emf method. The standard free energy of formation at  $400^\circ\text{C}$  is  $-37.6$  kcal/mole.

Thermodynamic properties of binary liquid sodium-potassium alloys have been determined using an absorption spectrophotometric method. The results indicate positive departures from Raoult's Law. The system also deviates from regular solution behavior ( $\Delta S^{28} \neq 0$ ).

The eutectic temperatures in the  $\text{LnCd-Ln}$  fields of lanthanon-cadmium systems have been measured for  $\text{Ln} = \text{La, Ce, Pr, Nd, Sm, Eu, Gd}$  and  $\text{Yb}$ . The observed eutectic temperatures were used with the ideal freezing point lowering equation to derive an average mole fraction of  $\text{Ln} = 0.650 \pm 0.033$  at the eutectic in the pseudobinary system  $\text{LnCd-Ln}$ . Conversely, this value was used to estimate each of the eutectic temperatures for  $\text{LnCd-Ln}$  fields where  $\text{Ln} = \text{Tb, Dy, Ho, Er, Tm, Lu}$  and  $\text{Y}$ .

Refractory compounds of the actinide elements show promise as reactor fuels capable of withstanding high temperatures and large burnups. Methods are being investigated for the preparation of refractory fuels. The more promising methods are being used to prepare sufficient quantities of these refractory fuels for use in fuel element fabrication and irradiation tests.

The liquid-metal precipitation process for the preparation of uranium monocarbide (UC) has produced a product with good pressing and sintering properties. This process involves the addition of carbon to uranium dissolved in a zinc-magnesium solution, reacting the mixture for 8 to 19 hr at  $800^\circ\text{C}$ , removal of most of the supernatant zinc-magnesium solution through a transfer tube, and retorting of the precipitated UC to remove residual zinc and magnesium. Since the last report period, two runs on a 500-g scale have been completed using fully enriched uranium metal. The oxygen content of the UC product has been reduced to about 0.2 w/o during the series of runs, and the total carbon content of the UC products has been consistently near or below the maximum of 5.2 w/o desired by the Metallurgy Division for fuel element fabrication and irradiation studies. A significant increase in product yield (61.6% to 83.5%) in recent runs has been obtained by increasing the reaction and settling times and by changing the configuration of the transfer tube so that less UC product has been entrained in

the zinc-magnesium supernatant during its removal from the UC product through the transfer tube.

A fluid-bed method for the preparation of UC from powdered uranium metal and a hydrocarbon gas is being studied. In this method uranium metal particles are fluidized with propane and hydrogen at 500 to  $700^\circ\text{C}$  to form the monocarbide. Several successful preparations of UC have been made. The total carbon content of the UC product varies with the hydrogen and propane concentrations of the fluidizing gas. In runs at  $600^\circ\text{C}$ , with a run time of 5 to 6 hr and at a fluidizing velocity of 0.25 ft/sec, the total carbon content gradually decreased from 6.5 w/o to 5.3 w/o when the hydrogen concentration was increased from 10 v/o to 70 v/o. Above 70 v/o  $\text{H}_2$ , the total carbon content decreased sharply; at 80 v/o  $\text{H}_2$  with a run time of 5 hr at  $600^\circ\text{C}$ , the total carbon content of the UC was 3.2 w/o. At  $700^\circ\text{C}$  the reaction rate was somewhat higher than at  $600^\circ\text{C}$ . At  $700^\circ\text{C}$  and at a hydrogen concentration of 80 v/o, the total carbon content was 5.4 w/o after 3 hr, whereas at  $600^\circ\text{C}$ , it was 3.2 w/o after 5 hr at the same hydrogen concentration. Current effort is being focused on defining the conditions to produce stoichiometric UC and decrease the oxygen contamination of the product.

Work on the precipitation of uranium monocarbide-plutonium monocarbide solid solutions from fused salts containing  $\text{UCl}_3$ ,  $\text{PuCl}_3$  and  $\text{Mg}_2\text{C}_3$  has been suspended. X-ray diffraction analysis indicated the presence of sesquicarbide phases when the plutonium content of the carbide precipitate approached 10 w/o plutonium. The precipitated carbide product was therefore heterogeneous instead of the desired homogeneous solid solution of uranium and plutonium monocarbides. The presence in the carbide product of free carbon, probably produced by the precipitation reaction, and the difficulty of preparing pure  $\text{Mg}_2\text{C}_3$  also discouraged further interest in this procedure.

A preliminary evaluation of potential mobile blanket fuels for fast breeder reactors indicates that a paste of UN in sodium is an attractive choice. Accordingly, experimentation in preparation and testing of UN-sodium pastes has begun. Uranium mononitride of high bulk density, 8.0 g/cc, was prepared by reaction of uranium with nitrogen at 200 to 400 mm Hg pressure at a temperature which was varied from  $1050^\circ\text{C}$  at the beginning of nitriding to  $1300^\circ\text{C}$  at the conclusion. Analysis of the product for nitrogen by combustion to  $\text{U}_3\text{O}_8$  and correction for the 0.095% oxygen content of the sample yielded a nitrogen content of 5.60% as compared to the nitrogen content of stoichiometric UN of 5.557%. Sessile drop studies of the wetting of UN, US, UP, and UC by molten sodium at about  $250^\circ\text{C}$  indicated contact angles of about the same

magnitude as reported in the literature for  $\text{UO}_2$ . For the above ceramics, quite large angles were observed ( $130^\circ$  to  $157^\circ$ ).

## II. Fuel Cycle Applications of Volatility and Fluidization Techniques (pages 107 to 164)

Laboratory-scale fluid-bed fluorinations of mixtures of uranium, plutonium, and fission product element oxides are being performed in support of the fluid-bed fluoride volatility process. This laboratory work is being performed to determine the optimum reaction conditions under which the retention of plutonium in the inert fluid bed material (alumina) is minimized, and to obtain general information applicable to the operation of the pilot plant.

Experiments were performed to determine the feasibility of reusing an alumina bed for several addition-fluorinations of a  $\text{U}_3\text{O}_8$ - $\text{PuO}_2$ -fission product mixture. In these experiments about 300 g of the solid reaction mixture was fed into an alumina bed at  $450^\circ\text{C}$  and fluorinated using 20 v/o fluorine in nitrogen. This step was followed by recycle-fluorination periods of 5 hr at  $450^\circ\text{C}$ , 5 hr at  $500^\circ\text{C}$ , and 10 hr at  $550^\circ\text{C}$ , using 100% fluorine. In one series of experiments in which the fission product mixture did not contain  $\text{MoO}_3$ , the plutonium level in the alumina bed after the second addition-fluorination cycle (0.0036 w/o) corresponded to volatilization of 99% of the plutonium. After the seventh addition-fluorination cycle, the plutonium level was 0.0088 w/o, corresponding to volatilization of 99.4% of the plutonium. An eighth addition-fluorination cycle was performed by adding as much plutonium as in the previous seven cycles; the plutonium concentration of the alumina at the end of the cycle was 0.025 w/o, corresponding to cumulative volatilization of 99.2% of the plutonium. For a comparable series in which  $\text{MoO}_3$  was present in the fission product mixture, it was found that about seven cycles would be necessary before 99% of the plutonium would be volatilized.

The fluoride content and surface area of the alumina bed were measured after each addition-fluorination cycle for one of the series of reuse experiments. It was observed that the fluoride content of the alumina was 1.4 w/o after one addition-fluorination cycle, and increased by increments of 0.5 w/o for each additional cycle. The surface area of the alumina bed increased by about  $0.06 \text{ m}^2/\text{g}$  (the initial surface area of the 120 mesh alumina was  $0.011 \text{ m}^2/\text{g}$ ) per addition-fluorination cycle for the first three cycles and then remained relatively constant at about  $0.19 \text{ m}^2/\text{g}$  for the final two

cycles. These data indicate that fluorination and attrition of the alumina would not be significant on reuse of the bed material.

The use of a nonfluidized, static bed fluorination procedure was explored. In these experiments only  $\text{PuO}_2$  and fission products were fluorinated, using three recycle-fluorination periods. The alumina beds for two experiments contained an average of 0.075 w/o plutonium after fluorination, indicating that the use of a static bed under these conditions would not result in adequate removal of plutonium.

An investigation was made of the effect of gas flow rate during the recycle-fluorination periods on plutonium retention in the alumina bed. For these experiments only  $\text{PuO}_2$  and fission product oxides were fluorinated in a  $1\frac{1}{2}$ -in. dia. reactor, using 100% fluorine and three recycle-fluorination periods. Gas flow rates of 4, 6, 7, and 8 liters/min were used. The results showed that a gas flow rate of less than 6 liters/min is not sufficient to insure a satisfactorily low plutonium concentration in the alumina bed of 0.004 w/o or less.

The decladding scheme being considered at the present time will involve the HF-promoted oxidation of stainless steel. This chemical decladding operation will leave a mixture of uranium and plutonium fluorides and oxyfluorides, fission product fluorides, and iron oxides in the alumina bed for the subsequent fluorination step. An investigation was therefore started to determine the effect of the presence of iron oxides in the reaction mixture upon plutonium retention in the alumina bed. In these studies, the mixture of uranium, plutonium and decladding products was in the alumina bed at the start of the fluorination reaction. This procedure differed from previous studies wherein the uranium and plutonium were admitted to the fluorination reactor over a period of several hours. Experiments were performed using a solid reaction mixture containing  $\text{UO}_2\text{F}_2$ ,  $\text{PuF}_4$ , fission product fluorides, iron oxides prepared by the reaction of an  $\text{HF-O}_2$  mixture with 304 stainless steel, and sintered (Aleo type T-61) alumina. The experiments were performed using three fluorination periods at a gas flow rate of 8 liters/min. In the first fluorination period at  $450^\circ\text{C}$ , the initial fluorine concentration in the gas phase was increased from 5 to 20 v/o in nitrogen over a period of about one hour as the major part of the uranium was fluorinated. This was followed by recycle-fluorination periods of 4 hr at  $450^\circ\text{C}$ , 5 hr at  $500^\circ\text{C}$  and 10 hr at  $550^\circ\text{C}$  using 100% fluorine. In two of the experiments single batches of feed were fluorinated, while in the third experiment, reuse of the alumina bed material was evaluated.

The results of these experiments showed that the plutonium concentration in the alumina bed was not significantly increased either by the presence of iron

oxides in the reaction mixture, or by the presence of the entire solid reaction mixture in the reactor at the start of the fluorination. For the two experiments which involved the fluorination of single batches of the feed mixture, the plutonium concentrations in the alumina were 0.0087 and 0.010 w/o, respectively. In an experiment to demonstrate the reuse of alumina bed material, the final alumina bed from the second test was used as the starting bed for the fluorination of an additional batch of the same feed material. The final plutonium concentration in the bed after fluorination of this additional batch of feed was 0.014 w/o. If this plutonium level is maintained for seven addition-fluorination cycles, a recovery of 99% of the plutonium fed to the reaction system as  $\text{PuF}_6$  can be achieved from feed material containing stainless steel decladding products.

The retention of plutonium by Alcoa Type T-61 alumina was determined. One experiment was performed using a solid reaction charge containing  $\text{PuO}_2$ , fission product oxides, and T-61 alumina. The reaction procedure employed the usual three recycle-fluorination periods and a gas phase of 100% fluorine. The alumina bed after this fluorination contained 0.0026 w/o plutonium. This result is similar to results obtained, under the same reaction conditions, in experiments using the high purity Type RR alumina.

A 2-in. dia. fluidized bed reactor has been constructed to investigate the fluoride-promoted oxidative-decladding of clad  $\text{UO}_2\text{-PuO}_2$  pellets with mixtures of hydrogen fluoride in oxygen and the fluorination of these pellets with elemental fluorine. Experimental work with this unit will be carried out in support of the fluid-bed fluoride volatility pilot plant. Two preliminary runs with unclad  $\text{UO}_2$  pellets have been carried out in order to check out all equipment items. The equipment was found to perform satisfactorily.

Experimental studies of solid-liquid equilibria in the system  $\text{UF}_6\text{-PuF}_6$  are to be carried out. The results will be useful in the choice of conditions for the separation of  $\text{UF}_6$  and  $\text{PuF}_6$  in the fluid-bed fluoride volatility process. Construction of all of the apparatus necessary for these experimental studies is complete; the apparatus has been installed in a glovebox and is presently being tested with pure  $\text{UF}_6$ . A study of the vapor-liquid equilibria in the system  $\text{PuF}_6\text{-UF}_6$  has been started to provide information useful in the choice of process conditions for the separation of  $\text{UF}_6$  and  $\text{PuF}_6$ , as well as data of more fundamental interest. Construction of the apparatus has been completed and the testing of the equipment with mixtures of ethanol-water has been performed.  $\text{UF}_6$  has been introduced into the system, and the experimental procedures planned for  $\text{PuF}_6\text{-UF}_6$  mixtures are being checked out.

Studies of the chemical behavior of  $\text{PuF}_6$  are con-

tinuing with an investigation of the  $\text{PuF}_6$  sorption capacity of calcium fluoride ( $\text{CaF}_2$ ), lithium fluoride ( $\text{LiF}$ ), and sodium fluoride ( $\text{NaF}$ ). The  $\text{PuF}_6$  retention by  $\text{NaF}$ ,  $\text{LiF}$ , and  $\text{CaF}_2$  at  $100^\circ\text{C}$  is low. The  $\text{PuF}_6/\text{NaF}$  mole ratios were 0.0057 and 0.014 at 25 and  $100^\circ\text{C}$ , respectively. A  $\text{PuF}_6/\text{LiF}$  mole ratio of 0.024 was found for a 96-hr exposure of  $\text{LiF}$  at  $25^\circ\text{C}$  to 125 mm of  $\text{PuF}_6$ , followed by a 1-hr exposure at  $100^\circ\text{C}$ . Calcium fluoride (0.109 mole) at  $100^\circ\text{C}$  was exposed to 4.4 g of  $\text{PuF}_6$  for 0.75 hr in a flow system. A  $\text{PuF}_6/\text{CaF}_2$  mole ratio of  $2.1 \times 10^{-5}$  was found in the product. Further work on these systems is planned, but with emphasis on preparing the  $\text{PuF}_6$ -metal fluoride complexes.

Studies of the decomposition of gaseous  $\text{PuF}_6$  to fluorine and  $\text{PuF}_4$  by alpha radiation were continued with a series of short-duration  $\text{PuF}_6$  decomposition experiments. The experiments were carried out in 127-cc prefluorinated nickel vessels. At the end of each experiment, the fluorine and undecomposed  $\text{PuF}_6$  were removed, by pumping, from the  $\text{PuF}_4$ . To prepare the  $\text{PuF}_4$  for determination of plutonium by alpha counting, the spheres, after removal of the valves, were dissolved in nitric acid-aluminum nitrate solutions. The valves were separately washed with an acid solution which was added to the solution used for dissolution of the spheres. Separate analysis of a valve wash solution indicated that plutonium equivalent to 1.98 mg  $\text{PuF}_6$  had been deposited on the exposed valve components during emptying and filling of the vessels. The deposition of  $\text{PuF}_4$  within the valve has been attributed to corrosion of the phosphor-bronze bellows by  $\text{PuF}_6$ . On the basis of this finding, a correction of 1.98 mg  $\text{PuF}_6$  was made to the amount of  $\text{PuF}_6$  initially put into the vessels and to the total plutonium found in the nitrate solution. The rate of  $\text{PuF}_6$  decomposition was then calculated.

The rate of  $\text{PuF}_6$  decomposition was found to be high for short durations but decreased rapidly with increasing storage times. For 100 mm of  $\text{PuF}_6$  stored at  $26 \pm 2^\circ\text{C}$ , the average decomposition rates and their standard deviations were (in % per day)  $2.20 \pm 0.50$  (0.5 day),  $1.12 \pm 0.28$  (1.0 day),  $0.92 \pm 0.24$  (2.0 days),  $0.50 \pm 0.12$  (5.0 days),  $0.35 \pm 0.06$  (8.0 days),  $0.29 \pm 0.03$  (12 days) and  $0.27 \pm 0.10$  (16.0 days). The fact that  $\text{PuF}_6$  decomposition rate decreases rapidly with time and earlier reported observation that the decomposition rate is affected by the extent of exposed surface suggest the  $\text{PuF}_6$  interacts with the prefluorinated surfaces of the nickel vessel. Either the chemical reaction is essentially complete after eight days or it proceeds thereafter at a rate which changes with time too slowly to be detected by use of the present techniques. However, the available data

are not sufficient to determine the relative contribution of this chemical reaction and of the back reaction ( $\text{PuF}_4 + \text{F}_2 \rightarrow \text{PuF}_6$ ) which has a small influence on results in short-term experiments.

Studies of gas-phase alpha-induced decomposition of  $\text{PuF}_6$  have been hampered by the inability to isolate alpha-induced decomposition from other modes of decomposition, such as chemical reaction with the vessels and thermal decomposition. These studies have shown, however, that reuse of the vessel would result in less  $\text{PuF}_6$  decomposition and that part of the plutonium remains deposited in the equipment used to handle  $\text{PuF}_6$  until the plutonium is removed by fluorination. No further experiments on the alpha decomposition of  $\text{PuF}_6$  are planned at the present time.

A corrosion program in support of the fluid-bed fluoride volatility process has been initiated. Two types of experiments are planned at temperatures up to 550°C to determine the rate of corrosion of nickel-200: (a) small-scale static runs conducted in a tube furnace wherein nickel coupons will be exposed to volatile fission product fluorides, and (b) exposure of nickel coupons to the gaseous atmospheres of the 2-in. dia. fluid-bed reactor under actual operating conditions. A survey of the unclassified literature concerning the corrosion of nickel and Monel by  $\text{UF}_6$ ,  $\text{PuF}_6$ , and fluorine is included.

At the request of the Rocky Flats Division of the Dow Chemical Company, an examination of a direct fluorination technique for the recovery of plutonium from waste stream materials has been completed. Interest on the part of Rocky Flats stemmed from the potential savings which may be attained by using a simple, direct method of plutonium removal from a variety of waste materials. Elemental fluorine, at a flow rate of 200 ml/min for either 5 or 10 hr, was used to produce  $\text{PuF}_6$  from three types of waste samples in boat reaction vessels at 500 or 550°C. The materials used, together with the corresponding plutonium analyses (by Rocky Flats) are (1) skull oxide, 87.13 w/o Pu; (2) incinerator ash, 11.6 w/o Pu; (3) sweepings, 58.8 w/o Pu. The plutonium removal was 99% or better in all tests except those which involved processing of incinerator ash. In these tests, plutonium removals of 82.2% and 98.4% were obtained. Reaction rates were obtained at two temperatures (500 and 550°C) for one type of waste material, an impure  $\text{PuO}_2$  (the skull oxide). Plutonium removal from skull oxide was observed to proceed at a low rate during the initial fluorination period, which is attributed to the conversion of  $\text{PuO}_2$  to  $\text{PuF}_4$ . Impurity content of the collected  $\text{PuF}_6$  was not measured.

Fluorination of these waste samples containing plutonium resulted in removal of essentially all of the

contained plutonium by conversion of plutonium to the hexafluoride and subsequent volatilization. Both temperatures and rates of reaction appear relatively favorable for process application.

A study of the chemistry of  $\text{NpF}_6$  has been initiated, which involves the preparation of neptunium hexafluoride and characterization of the solid residues. This will be followed by spectral studies of the hexafluoride and the solid-vapor equilibrium in the system  $\text{NpF}_6\text{-NpF}_4\text{-F}_2$ . The apparatus has been constructed. Information in the literature on neptunium fluorides has been reviewed.

The results of tests in which  $\text{MoO}_3$  was reacted with mixtures of fluorine and nitrogen (and/or oxygen) revealed that under the conditions of the experiments (450°C, tube reactor), only a small fraction (3 to 5%) of the molybdenum was converted to  $\text{MoF}_6$ . The remainder of the molybdenum was probably in the form of  $\text{MoOF}_4$  or possibly  $\text{MoF}_5$ . In another test, it was found that  $\text{MoF}_6$  does not react with oxygen at 450°C. Treatment of  $\text{MoO}_3$  with a mixture of  $\text{HF}$ , oxygen, and nitrogen at 550°C resulted in formation of a slightly volatile compound of molybdenum, probably  $\text{MoO}_2\text{F}_2$ . Treatment of  $\text{MoO}_2$  with mixtures of fluorine, nitrogen and oxygen at 450°C resulted in formation of a slightly volatile compound, probably  $\text{MoO}_2\text{F}_2$ . In all these reactions, little or no  $\text{MoF}_6$  was formed.

Engineering-scale development work is in progress on the fluid-bed fluoride volatility process for the recovery of uranium and plutonium from spent uranium dioxide fuels. The main steps in this process will be studied with unirradiated sintered  $\text{UO}_2\text{-PuO}_2$  pellets in an engineering-scale alpha facility that is now in the final stages of installation. A fluorination pilot plant for processing batches of fuel to a mixed  $\text{UF}_6\text{-PuF}_6$  product and a converter system for converting the hexafluoride mixture to dense mixed particles have been installed in the facility. The converter unit will also be used in the study of the thermal decomposition of  $\text{PuF}_6$  to  $\text{PuF}_4$  as a means of separating plutonium from uranium. It is also planned to install a distillation unit in the facility which will provide design information on mixed uranium-plutonium hexafluoride systems.

Shakedown work with  $\text{UO}_2$  pellets was started in the fluorinator using the two-zone oxidation-fluorination procedure. A charge of 2.2 kg of  $\text{UO}_2$  pellets (3-in. bed depth) was processed in a 24-in. deep bed of alumina. Final bed analyses showed that more than 99.9 w/o of the uranium had been removed from the alumina bed. A material balance determined by weight of material collected in the main product condenser and in the sodium fluoride backup trap accounted for 99.97% of the charge. The quantity of  $\text{UF}_6$  transferred from

the product condenser to the final product receiver corresponded to 97.4% of the charge. Overall results and performance of all the main equipment components were satisfactory.

Installation of the converter system is essentially complete. The 2-in. dia. reactor and auxiliary equipment are described.

Performance tests of the main alpha facility systems, such as scrubbers and ventilation controls, and development of special operating procedures, such as the procedure for vertically bagging large equipment in and out of the boxes, were nearly completed. Safety procedures are being given a final evaluation. Installation of windows has started. Upon completion of this work, a short period of shakedown testing with  $UF_6$  will follow and then work with plutonium will begin.

Development work on the decladding and fluorination of  $UO_2$  fuels was continued. Initial studies were carried out on the processing of stainless steel-clad  $UO_2$  with  $HF-O_2$  mixtures in fluidized beds of alumina. An investigation conducted in a bench-scale reactor (1½-in. dia.) showed that the destructive oxidation of stainless steel occurred readily at 550°C using a 40 v/o  $HF$ -oxygen mixture (up to 20 v/o nitrogen diluent). Respective penetration rates for types 304 and 347 stainless steels were 30 and 13 mils/hr. The penetration rates ranged from 2 to 33 mils/hr over the temperature range 500 to 600°C.

The complete processing of a simulated fuel bundle was demonstrated in a pilot-scale facility (3-in. dia. reactor). The fuel bundle, six 3-ft long type 304 stainless steel tubes (0.43-in. ID, 0.020-in. wall thickness) containing a total of 4.5 kg of cylindrical  $UO_2$  pellets, was completely reacted in a 3-hr period at 550°C with a 40 v/o  $HF$ -60 v/o oxygen mixture. The bed consisted mainly of alumina,  $\alpha-Fe_2O_3$ , and  $UO_2F_2$  in the proportions of 2.1 to 1 to 2.1. The  $UO_2F_2$  was mainly in the form of fines (<325 mesh). To facilitate the processing of a bed containing a large proportion of reactive fines, the fluorination was conducted in two parts. The bulk (~82%) of the uranium was recovered in a 6.5-hr period at 400°C with dilute fluorine introduced at approximately the middle of the bed. The main fluidizing gas stream (nitrogen) was fed at the bottom. This was followed by an 11-hr period at 450°C, with the fluorine being fed at the bottom of the column along with the diluent gas. The fluorine concentration was increased gradually to a final value of about 90%. A final concentration of uranium in the alumina bed of 0.05 w/o indicated a recovery of about 99.9% of the uranium in the charge. The iron oxide was converted to  $FeF_3$  during the fluorination step. Overall fluorine efficiency was 67%, and was maintained at a high level through the use of fluorine recycle.

An exploratory run in the bench-scale reactor established the feasibility of processing  $UO_2$ -stainless steel cermet fuel by the  $HF$ -oxygen, fluorine route. A miniature fuel assembly of four plates, weighing 90 g, was processed. The plates were made of 18 w/o  $UO_2$ -stainless steel (type 304) cermet. The destructive oxidation was conducted at 550°C for 4 hr with 40 v/o  $HF$ , 40 v/o oxygen and 20 v/o nitrogen. The fluorination of the oxidation products was initiated at 250°C with about 2 v/o fluorine (in nitrogen) as the feed gas and completed at 550°C with 95 v/o fluorine. The total time for fluorination was 11 hr. High recovery (greater than 99%) of the uranium in the charge was indicated by the low level of uranium found in the alumina bed at the end of the fluorination. The final concentration of uranium in the bed was 0.005 w/o, which corresponds to 0.2% of the uranium in the charge.

The investigation of the method of decladding stainless steel by reaction with aqueous hydrochloric acid in an air-fluidized bed of inert solids was concluded during this period. Final tests were conducted in a 3-in. dia. column. A ½-in. dia. rod, 12 in. in length, of type 304 stainless steel was used in these tests. The rate of attack on the stainless steel was low, but increased with an increase in the acid content in the bed. For liquid contents of 0.16, 2.7, and 15.0 w/o  $HCl$  in  $H_2O$  the corrosion penetration rates were 0.01, 0.06, and 0.12 mils/hr, respectively. This work has been terminated in favor of the more promising all-gas method involving  $HF$ -oxygen mixtures.

Studies of the cleanup of cell exhaust air contaminated with  $PuF_6$  were continued. New equipment for studying the hydrolysis and filtration of air-borne  $PuF_6$  was constructed. The first experiment with a dilute  $PuF_6$  gas stream indicated that the hydrolysis rates of  $PuF_6$  and  $UF_6$  were similar. The rate of hydrolysis of  $PuF_6$  was no more than twice that of  $UF_6$ , nor less than that of  $UF_6$ .

Development studies of a fluid-bed fluoride volatility process for the recovery of uranium from highly enriched uranium-alloy fuels were continued. The process cycle includes hydrochlorination and fluorination steps in which the fuel charge is reacted while immersed in a fluid bed of alumina, which serves as a heat transfer medium. Mathematical analyses were made of the data accumulated in the bench-scale studies on unirradiated uranium-Zircaloy and uranium-aluminum alloy fuels. The analyses show the effect of process conditions on uranium loss during hydrochlorination and on uranium loss by retention by alumina after fluorination. Operating conditions that tended to decrease the partial pressure of the  $UF_6$  in the gas phase during fluorination resulted in lower uranium retention. Evaluation of the effect of particle

size on HCl utilization efficiency showed that HCl utilization increased with a decrease in the ratio of plate spacing to particle size. The HCl utilization efficiency increased with an increase in the particle size distribution of the bed material; that is, a mixture of a broad range of particle sizes resulted in higher efficiencies than beds of narrow size fractions. Since the overall objectives of this bench-scale work have been met, namely, the establishment of a satisfactory operating sequence and the evaluation of packed beds of alumina as high-temperature filters, experimental studies on this phase of the program have been terminated. A topical report (ANL-6829) on the work with zirconium alloys has been issued.

Full-scale operations are continuing in the pilot-plant facility installed to demonstrate the fluid-bed volatility process for the recovery of uranium from enriched uranium alloy fuels. The current work was concentrated on the processing of aluminum-uranium fuels which are typical of those used in the MTR and ETR. Each fuel element weighed about 6.0 kg and contained about 280 g of uranium.

Five experiments were completed; four included the hydrochlorination, hydrofluorination, and fluorination steps, and one involved only the hydrochlorination step. The processing conditions used in the HCl and HF steps were based on previous experience with the pilot-plant facility whereas the conditions used in the fluorination step were previously established in bench-scale studies.

An increase in reaction rate and HCl utilization of about 25% was demonstrated using a multicharge technique wherein additional fuel elements are charged after about 60 to 80% of the previous fuel element has been hydrochlorinated. Using this technique the hydrochlorination time for a single aluminum-uranium fuel element is 4 to 5 hr. The HCl utilization, using once-through flow, was over 50%. The uranium losses by transport through the packed-bed filter were as low as 0.14% using a 12-in. deep bed of 14 to 48 mesh alumina. The fluid-bed pyrohydrolysis reactor for converting the waste metal chlorides to oxides operated satisfactorily in all experiments.

More than 99% of the uranium was removed from the reactor and filter beds, based on the overall uranium balance, even though temperature excursions occurred and caused caking at the top surface of the packed-bed filter during the fluorination step of each of the current runs. These temperature excursions have only been encountered while processing aluminum fuels and probably can best be eliminated by fluidizing the packed-bed filter during the fluorination step to facilitate the removal of heat and thereby prevent caking.

A corrosion program in support of the fluid-bed

volatility program has been completed. The results of both laboratory tube furnace and in-plant tests are summarized. These results show that: (1) for conditions of static or near-static reagent flow, the corrosion rate of nickel by fluorine alternated with HCl and fluorine alternated with oxygen is about 1 to 4 mils/yr, and is close to the rate exhibited by nickel when exposed to fluorine alone, (2) the corrosion rate found for coupons exposed to fluoride volatility environments consisting of hydrogen chloride, hydrogen fluoride, and fluorine (in-plant tests) was in the range 12 to 40 mils/yr with the higher values obtained for specimens in contact with the fluidized bed, (3) the corrosion rate of nickel welds made with nickel-200 filler was found to be much lower than the corrosion rate of nickel welds made with nickel-61 filler metal (1 to 4 mils/yr as compared with 67 to 1315 mils/yr), and (4) thermal-cycling and exposing coupons to air between simulated process cycles had little or no effect upon the corrosion rate of nickel.

Exploratory studies on the measurement of particle residence times at solid surfaces in contact with a gas-fluidized bed have been initiated. Knowledge of particle residence times would be helpful in estimating the heat transfer properties of fluidized beds. Beds composed of particles of contrasting color (mainly white particles with a small fraction of black particles) were employed. Direct photographic observation of individual black particles in a test area yields the desired information but interpretation of the data was found to be prohibitively tedious and time-consuming. Attempts are being made to develop an autocorrelation technique for use in determining residence times as functions of the physical and flow properties of the systems under investigation.

A program of fluid-bed volatility studies with irradiated fuel materials on a bench-scale level has commenced. During the current period, the equipment was assembled and tested in a series of experiments using nonirradiated fuel materials. The equipment was then installed in the Senior Cave Facility of the Chemical Engineering Division and the first run with irradiated fuel (5-yr-cooled uranium-Zircaloy alloy fuel) was completed. Operationally the run with irradiated material was highly successful; however, analytical results for the run are not yet available.

The charge materials for the runs with nonirradiated material included Zircaloy-uranium alloy and aluminum-uranium alloy. The experimental conditions were similar to those developed in the bench-scale and pilot-plant work on highly enriched fuels but included also a system of sodium fluoride traps for  $UF_6$  collection and purification. A small charge of  $UO_2$  pellets was also processed to  $UF_6$  using the HF-oxygen

step for pulverizing the fuel and fluorine for recovery of the uranium.

Considerable effort was expended in making the main operating units leak-tight. Sealing of the equipment was achieved by the use of annealed, nickel-plated copper wire gaskets. Redesign of the fixed-bed filter was required to reduce the uranium loss to the off-gas condenser to a satisfactory level, and in the final runs high recoveries and essentially complete accountability of the uranium were achieved.

---

### III. High Temperature Reactor Materials Development (pages 165 to 174)

A program directed toward the development of certain high temperature reactor materials is under way, the objective being to build up a reservoir of basic data which may be used for screening and evaluation. The study will be concerned with the chemical stability of potential high temperature fuels, i.e., uranium oxides, phosphides, sulfides, arsenides, nitrides, and their solid solutions; and with the reactions of these fuels with hydrogen, its contaminants, and refractory structural materials such as tungsten, rhenium, molybdenum, tantalum, and certain alloys. These studies will be done quantitatively to yield thermodynamic and phase-diagram information. Selected systems are to be investigated in an integrated way using several methods which are mutually supporting. Progress in the application of these methods is itemized below.

*Phase Diagram Studies.* Studies of the uranium-uranium system have shown that a wide two-liquid immiscibility gap exists at elevated temperatures. The monotectic composition occurs at an oxygen-to-uranium ratio of 1.30 and at a temperature of  $\sim 2500^\circ\text{C}$ . The hypostoichiometric phase boundary of uranium has been determined in the range 1600 to  $2500^\circ\text{C}$ . Verification of these measurements is in progress.

A study of the uranium-uranium monosulfide phase diagram has been initiated.

*Effusion Vapor Pressure Studies.* The total vapor pressure of uranium-bearing species over the two-phase system uranium (liquid, saturated with uranium) plus uranium (solid, saturated with uranium) has been measured. Some additional measurements to verify these results will be made using a smaller effusion orifice. The vapor pressures over this system vary from a factor of 10 to 4 higher than those over stoichiometric

uranium dioxide in the range 1300 to  $2000^\circ\text{C}$ , respectively.

*Mass Spectrometric Effusion Studies.* Measurements of the relative concentrations of vaporizing species have been carried out for the same two-phase system noted in the preceding paragraph and also for stoichiometric uranium. The results are not reported at this time because of instrumentation uncertainties which need to be resolved. However, the nature of the tentative results has stimulated a thermodynamic analysis which leads clearly to the conclusion that the partial pressure of the  $\text{UO}_2(\text{g})$  species passes through a maximum at the stoichiometric composition  $\text{UO}_2$ .

*Transpiration Studies of Vaporization.* The extension of the vapor pressure measurements in the uranium-uranium system to higher temperatures than those possible in the effusion measurements is to be carried out by use of the transpiration method. Preliminary testing of the apparatus shows it to be functioning very well.

---

### IV. Calorimetry (pages 175 to 185)

A series of calorimetric combustions of phosphorus in fluorine has been carried out to obtain the enthalpy of formation of phosphorus pentafluoride. Calorimetric combustions of sulfur in fluorine using the same techniques and apparatus have been started.

Analysis of the results of the combustions of  $\alpha$ - and  $\beta$ -silicon carbide in fluorine has revealed the following. A reliable value for the enthalpy of combustion in fluorine of  $\beta$ -silicon carbide was obtained. Two samples of  $\alpha$ -silicon carbide yielded discordant results which appear to be associated with incomplete combustions and/or excessive amounts of side-products. The use of a more finely divided  $\alpha$ -silicon carbide may resolve the problem, and such a sample has been obtained. The results of the  $\beta$ -silicon carbide study yield a value for its enthalpy of formation whose principal source of uncertainty is the uncertainty of the enthalpy of formation of carbon tetrafluoride. A redetermination of the enthalpy of formation of carbon tetrafluoride will be undertaken.

The technique developed for combustion in fluorine of metals that form nonvolatile fluorides has been used for combustions of magnesium, aluminum, yttrium, lanthanum, gadolinium, and holmium. The studies with magnesium and aluminum were redeterminations in attempts to eliminate some uncertainties in previous results. An attempt has been made to correlate the combustion behavior of these metals with

their physical properties and the properties of their product fluorides.

A series of combustions of tantalum diboride in fluorine has been completed using the combustion technique previously employed for the diborides of zirconium, hafnium, and niobium. The first seven combustions of the series had been performed but the results had not been calculated at the time of writing the preceding semiannual report, ANL-6900. The last five combustions were performed recently under somewhat different conditions, which were chosen to decrease a suspected blank correction for fluorine expansion. Agreement between the two series indicates that the corrections are being properly applied.

For some of the work planned in the calorimetry program, particularly for the combustion of uranium compounds in fluorine, a fluorine flow calorimeter is desirable. Since a flow system has certain advantages over a static system, particularly control of the rate and extent of reaction, a preliminary flow reaction system was constructed for tests with uranium monosulfide. The results of these tests were very encouraging since nearly complete combustions of US were obtained.

The 1500°C high temperature enthalpy calorimeter has been assembled, tested, modified, and reassembled for further tests. A complete discussion of the various tests that have been performed and an analysis of the current capabilities of the apparatus are given. At present it appears that measurement of enthalpy increments with 0.1% accuracy is a realistic estimate.

---

## V. Reactor Safety (pages 187 to 233)

The experimental program to determine rates of reaction of molten reactor fuels and cladding metals with water is continuing. In general, it has been necessary to study the reaction of each metal of interest by several methods. One of these techniques utilizes a high pressure furnace which was designed especially for isothermal studies of steam with stainless steel and aluminum. The initial series of experiments in the furnace was designed to simulate the environment of a loss-of-coolant accident. In these experiments simulated fuel rods consisting of a series of UO<sub>2</sub> pellets sealed in an 8-in. length of either 304 stainless steel or Zircaloy-2 tubing were exposed to steam at a temperature which increased to a maximum during a period of about 8 min. The maximum temperature reached at the top end of the fuel rods was about 1500°C. The fuel rods were maintained at this tem-

perature for about 3 hr in an atmosphere of steam at 15 psig. The upper two-thirds of the cladding on both fuel rods had reacted completely, as was evidenced by their appearance and by the quantity of hydrogen collected. The stainless steel cladding formed a foamed oxide which flowed downward, baring several of the oxide pellets; the Zircaloy formed an intact tube of white oxide.

A study of the kinetics of reaction of refractory metals with steam was undertaken (1) to determine the suitability of these metals for materials of construction in high temperature metal-water studies, and (2) to extend knowledge of high temperature metal-water reactions in general. The following metals were investigated through the technique of induction heating in flowing steam at 1 atm pressure: molybdenum (1100 to 1700°C), rhenium (850 to 1700°C), tungsten (1050 to 1700°C), niobium (1050 to 1500°C), and tantalum (950 to 1300°C). Eudiometer measurements of the hydrogen evolved showed that molybdenum, rhenium, and tungsten followed linear rate laws in their reactions with steam. Niobium also obeyed linear kinetics after a brief induction period, and tantalum followed a para-linear rate law, that is, an initial parabolic rate of reaction, followed by transition to a linear rate. It was concluded that the high reaction rates observed for all five metals precluded their use as materials of construction for high temperature metal-water studies. A discussion is presented of the probable mechanism of each reaction.

One of the experimental techniques used to study metal-water reactions was designed to permit observation of the reactions of small particles under nonisothermal conditions. This method uses energy from a pulsed ruby laser to heat single particles of metal submerged in water. The experiment is designed to study not only the chemical reaction of particles with water but also to study the transient energy exchange and hydrodynamic effects. In recent work aluminum-water reactions under various conditions were studied. The samples are squares of one mil thick foil which form spheres when fully melted by the laser pulse. The extent of reaction is determined by hydrogen analysis of the reaction cell contents. By using foil squares 0.5, 1.0, and 2.0 mm on a side, spheres of 230, 360, and 575 $\mu$  dia. were formed. Average extents of reaction in water at 25°C were 17, 8, and 10%, respectively. Average deviations for these values are about 25%. In water at 25°C the extent of reaction was independent of laser output energy over a wide range (10 to 50 joules). These extents of reaction indicate reaction of a layer of aluminum approximately 7 $\mu$  thick for each particle. With water at 100°C and laser energies between 16 and 40 joules, no reaction was observed for particles 360 $\mu$  in dia.; with

laser energies above 45 joules, virtually complete reaction occurred. The reaction threshold at about 40 joules seems to be related to heating the particle above the melting point of  $Al_2O_3$  (2300°K). The residues from the completely reacted particles were hollow spherical shells of aluminum oxide; the incompletely oxidized particles had thin oxide skins. There was no evidence for appreciable oxide smoke formation. High speed motion pictures showed that a time of about 170 msec was required for complete reactions. For the cases of 0 to 18% reaction, 5 to 15 msec was required for the reaction. These data indicate that the rates of combustion are not greatly different in the two cases: combustion simply proceeds for a longer time. Plans for the immediate future include measurements with water at 25°C and 1 atm argon overpressure, and experiments at pressures up to 10 atm.

The third general method of studying metal-water reactions involves nuclear heating of typical reactor fuel materials in TREAT. In these studies, small fuel specimens are submerged in water in high-pressure autoclaves which are then placed at the center of TREAT and subjected to severe nuclear transients. Experiments were performed with unclad  $UO_2$  specimens with the objectives of determining the extent of reaction of  $UO_2$  with water and the degree of fragmentation of  $UO_2$  in the absence of metal cladding. A transient which caused partial melting of  $UO_2$  (2700°C) produced about 6 ml  $H_2$ (STP)/g  $UO_2$ , corresponding to an average composition of  $UO_{2.07}$ . More energetic transients which brought  $UO_2$  into the vaporization region (3300°C) produced about 17 ml  $H_2$  (STP)/g  $UO_2$  (average composition,  $UO_{2.19}$ ). X-ray diffraction analyses indicating final compositions of  $UO_{2.12}$  to  $UO_{2.17}$  gave support to the hypothesis that  $UO_2$  was reacting with water. It now appears likely that some of the hydrogen released in previous experiments with stainless steel-clad and Zircaloy-clad  $UO_2$  fuel pins resulted from the  $UO_2$ -water reaction.

Two experiments in TREAT were completed using a 9-element bundle of uranium rods which contained 100 times the quantity of metal contained in single pin transient meltdowns performed previously. One significant feature of the more energetic of the two scale-up transients was that there was clear evidence in the reactor power-time record for the change in geometry of the test subassembly. Evidently the meltdown perturbed the reactivity of the TREAT reactor itself. In the first experiment, CEN-196S, the 91 Mw-sec transient on a 157-msec period gave complete meltdown of the subassembly with 10.7% uranium-water reaction. In the second experiment, CEN-197S, a transient of 222 Mw-sec on a 140-msec period gave an estimated 56% uranium-water reaction.

A simple mathematical model was developed for the analysis of water hammers caused by reactor excursions. The model was based on Newton's second law and on the acoustic equation for particle velocity of an ideal shock wave. It was shown that only a gross estimate of the rate of steam generation during the excursion is required in order to predict the velocity of the water column and the impact pressure. A comparison was made of the predictions of the model with published observations of the SL-1 accident. The values for the impact velocity and the impact pressure calculated from the model are 126 ft/sec and 8500 psi compared with the reported values for SL-1 of 159 ft/sec and 10,000 psi. In modeling the SL-1 accident it was assumed that there was a linear rate of steam generation for 0.1 sec with a total energy transfer to the water of 50 Mw-sec.

A calculational study was initiated to demonstrate the application of metal-water reaction data to the analysis of a reactor loss-of-coolant accident. The initial effort makes use of the proposed LOFT (Loss of Flow Test) reactor as a model with the exception that the calculations were made for a 25-mil Zircaloy-clad core rather than the 15-mil stainless steel-clad core proposed in the LOFT design. The core was divided into ten power sections using the reported power distribution in the LOFT reactor.

The rate of the zirconium-water reaction was calculated using the parabolic rate law for the case of unlimited steam. A constant rate equal to the supply of steam was used to calculate the reaction when limited amounts of steam were assumed to be available. An energy balance equating the internal energy of each section to the chemical energy and decay energy developed in each section was used to calculate the temperature-time history of the ten sections. A flat temperature profile through the fuel pins was assumed and heat losses were ignored. The presence of the support structures was also ignored. The extent of reaction of the entire core was then calculated by summing the contributions from each core section.

The extent of reaction at the time the core reached average temperatures equal to the melting point of the zirconium cladding (1850°C), and the melting point of the uranium core (2800°C) were calculated as follows:

1. With unlimited steam: 40% and 62%, respectively.
2. With a 1000 lb/hr steam flow through the core: 21% and 41%, respectively.
3. With a 100 lb/hr steam flow through the core: 6% and 13%, respectively.

The strong interdependence of the core temperature history and the extent of reaction was demonstrated. The course of the accident subsequent to core col-

lapse would depend upon how much water was present in the reactor vessel following blowdown. The possibility of a steam explosion or a violent metal-water reaction following collapse is discussed. Two additional chemical reactions that could affect the course of the accident, the hydriding of zirconium and the reaction of steam with  $\text{UO}_2$ , are discussed.

A program of studies of potential problems in the field of fast reactor safety has been initiated. Work has begun in three general areas of investigation. These are:

1. Studies of the chemical and physical interactions of fuel and cladding materials with molten sodium at high temperature.
2. Studies of fuel migration and segregation in mixed uranium-plutonium fuels.
3. Studies of the transient boiling characteristics of molten sodium.

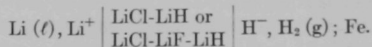
At present, most of the effort is directed toward literature studies and construction of apparatus.

The effect of prior irradiation of uranium on ignition in oxygen and air was investigated to assess the magnitude of additional ignition hazard of irradiated uranium over unirradiated metal. Four types of 20% enriched specimens were studied using the burning curve ignition test. One group of samples was irradiated in MTR to 0.79% burnup of the  $^{235}\text{U}$ . A second group was irradiated to 1.71% burnup. A third group was not irradiated; however, these samples were loaded into irradiation capsules, exposed to NaK coolant, and thermocycled in a manner approximating the thermal history of irradiated specimens. The fourth group of specimens consisted of untreated control samples. During irradiation samples were tightly constrained in tantalum-lined steel jackets to prevent dimensional changes. In spite of the constraint some surface roughening occurred. Nominal ignition temperatures in oxygen were as follows: unirradiated (control and thermocycled), 600°C; irradiated to 0.79% burnup, 400°C; irradiated to 1.71% burnup, 360°C. In air, the irradiated samples showed greater self-heating and spontaneous thermocycling than unirradiated samples; however, no clear-cut evidence of ignition was observed.

## VI. Energy Conversion (pages 235 to 247)

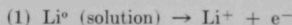
Investigations on the regenerative emf cells for the conversion of heat into electrical energy were continued. Two types of cells are being studied, bimetallic concentration cells and a lithium hydride cell.

The lithium hydride cell studies have been extended. Voltage measurements were made on a number of unsaturated lithium hydride cells of the type:



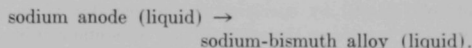
Using these data and the previously determined standard emf of a saturated lithium hydride cell, calculations have been made for the activities, activity coefficients, and emf-temperature coefficients of lithium hydride at various concentrations in the electrolyte. The activities showed strong positive deviations from ideality, an effect which leads to lower cell voltages than would be the case if the systems were ideal. Activity coefficients ranged from 2.5 to 3.5. The  $(\partial E/\partial T)_P$  varied from about  $-6 \times 10^{-4}$  volts/deg for the high mole fractions of lithium hydride to  $8 \times 10^{-4}$  volts/deg for the very dilute solutions of lithium hydride in lithium chloride. The cell for which the emf-temperature coefficient is zero has a concentration of lithium hydride in lithium chloride below one mole percent.

The electrode kinetic studies, which are necessary to characterize the operation of a galvanic lithium hydride cell, have begun to yield useful experimental results with a tungsten wire microelectrode. At all potentials positive with respect to a liquid lithium metal electrode as reference zero, an anodic process occurs at the tungsten microelectrode. Presumably, this is the oxidation of dissolved lithium metal in the fused salt solution. When the hydrogen gas-hydride ion equilibrium is established and the microelectrode polarized, the current-voltage curve can be interpreted as the resultant of the anodic oxidation of lithium and the cathodic reduction of hydrogen.



A limiting current plateau is observed for both processes.

The sodium-bismuth cell has been selected for the initial engineering studies. The overall cell reaction is



The solubilities in the fused salt electrolyte of both the alkali metal anode and the intermetallic compound formed at the cathode result in an irreversible transfer of material between the electrodes. The solubility of  $\text{Na}_3\text{Bi}$  in the ternary eutectic mixture 53.2 m/o NaI, 31.6 m/o NaCl, 15.2 m/o NaF ranged from 1.8 m/o  $\text{Na}_3\text{Bi}$  at 560°C to 8.5 m/o  $\text{Na}_3\text{Bi}$  at 840°C. The solubility of sodium in this electrolyte ranged from 0.3

m/o at 546°C to 0.9 m/o at 697°C. By proper selection of cell operating variables and cell components, the rates of transfer of both cathode and anode material can be minimized.

Solutions of the alkali metal tellurides and bismuthides have been studied by means of absorption spectra in order to better understand the phenomena involved in the solubility of intermetallic compounds in molten salts. The solutions are highly colored and the spectra exhibit intense charge transfer bands. The spectrum of each alkali telluride is characterized by an absorption peak in addition to a charge transfer band. Molar extinction coefficient values of from 600 to 800 have been calculated for several alkali metal telluride absorption peaks. These values indicate low oscillator strengths and forbidden transitions. Tentative spectra have been obtained for  $K_3Bi$  in  $LiCl-KCl$  eutectic and in  $CsCl$ .

The relative possible extents of regeneration of the sodium-bismuth bimetallic cell alloy were determined by examining the metal separation obtained under various thermal gradients. The intermetallic compound  $Na_3Bi$  was placed in sealed and evacuated tubes. In four experiments, the tubes were all 900°C at the hot end and 525, 616, 651, and 712°C at the cool end. The final residue compositions in the hot end of the tube (as compared with 75 a/o sodium for the  $Na_3Bi$  starting material) were 15, 48, 54, and 62 a/o sodium, respectively, with increasing condensate temperature. In all the experiments, less than one part per thousand bismuth was found in the sodium condensate. Transpiration experiments were also run; they showed that the vapor in equilibrium with a 50 a/o Na-Bi liquid alloy at 900°C contains about 3.5 a/o bismuth. This indicates that fractionation must have occurred in the sealed-tube experiments to obtain the high sodium purity in the condensate; such fractionation would lead to an inefficiency in cyclic operation of a regenerative system. The deposition of a solid, identified as  $Na_3Bi$ , at intermediate sites in the temperature gradient of the sealed tubes, indicates the importance of determining the solid and liquid-vapor equilibrium. It may be possible to avoid the formation of solid  $Na_3Bi$  by operating the regenerator at increased pressure, or the problem may be eliminated by a slight refluxing of fused salt electrolyte.

Engineering thermodynamic studies on the regeneration of sodium-bismuth, sodium-tin, lithium-tin, and lithium hydride cell systems have been made.

Experimental studies are being conducted on the non-faradaic or irreversible transfer (i.e., transfer without corresponding production of cell current) of sodium from the anode to the cathode in sodium-bismuth bimetallic cells. Cell current or faradaic

efficiencies of about 80% have been experimentally obtained while operating at 75% of the open circuit voltage.

Experimental work has begun to study a frozen electrolyte-silicone rubber insulator-seal for closed cells which can be operated in an air atmosphere. An experimental stainless steel sodium-bismuth cell without regenerator with such an insulator-seal has been constructed and is in operation at temperatures from 550 to 600°C.

Corrosion studies of bismuth and tin on materials of construction are being conducted. Tin is a more attractive cathode metal than bismuth because both its vapor pressure and melting point are lower. Static corrosion studies of tin on tantalum, tungsten, and molybdenum-30 w/o tungsten up to 1000°C indicate that these show promise as materials of construction. Dynamic corrosion tests of tin on these materials will be conducted. Static and dynamic corrosion tests of bismuth on mild steel and stainless steel indicate that both may be suitable for the low temperature section of a sodium-bismuth system, i.e., the cell, which would operate at temperatures up to 600°C. However, refractory metals will be required for the high temperature section, i.e., the regenerator, which would operate at about 1000°C or higher.

---

## VII. Nuclear Constants (pages 249 to 251)

The cross section for the production of the 0.741 MeV level of niobium-93 by neutron inelastic scattering has been measured at several neutron energies up to 1.2 MeV.

Radiative capture cross sections are reported for gadolinium-158 and erbium-170 as a function of neutron energies between 4 keV and 2 MeV.

Samples of uranium and plutonium isotopes have been prepared and are being placed in EBR-II for irradiations. Measurements will be made of the ratios of capture cross sections to fission cross sections as a function of position in the reactor.

---

## VIII. Analytical Research and Development (pages 253 to 254)

A program for the development of analytical methods for the determination of burnup of fast reactor fuels and for the measurement of fast fission yields

is being carried out. Determinations of the uranium-235 fast fission yields of molybdenum-95, -97, -98, and -100 and ruthenium-101, -102, and -104 are being carried out and will be completed shortly. Plans are being made to irradiate 100-mg amounts of plutonium-239, uranium-235, and uranium-233 in EBR-II until 25% of the fissile atoms have been consumed. These irradiated materials will be used to obtain fission yield data of increased accuracy.

---

#### **IX. Studies and Evaluations** (pages 255 to 263)

Studies and evaluations have been initiated of the feasibility and costs of projected applications of Chemical Engineering Division research and development projects. The major activities thus far have been concerned with two projects: (1) a Divisional economic study of fuels and reprocessing methods for fast reactors and (2) a contribution to an interdivisional conceptual design study and a feasibility and economic analysis of a large metal-fuel fast breeder power reactor and its integrated fuel cycle system.



ARGONNE NATIONAL LABORATORY

Chemical Engineering Division  
Semiannual Report



July - December, 1964

SEMIA<sup>N</sup>N<sup>U</sup>AL R<sup>E</sup>P<sup>O</sup>R<sup>T</sup>



# I

## Compact Pyrochemical Processes\* \*\*

Compact pyrochemical processes for the recovery of fissionable and fertile materials from discharged reactor fuels offer promise of achieving a reduction in fuel cycle costs associated with nuclear power. Savings are expected to result from rapid recycle of the fuel and a corresponding decrease in fuel inventory, a minimum of chemical conversion steps, small volumes and resultant compact equipment, direct production of solid wastes, decreased criticality problems because of the absence of aqueous solutions, and possible retention of valuable alloying agents in metallic fuels. Since the major objectives of these processes are repair of irradiation damage and restoration of fuel reactivity, high decontamination from fission products is not essential.

For high-burnup plutonium fuels, the buildup of activity from the higher plutonium isotopes precludes direct handling of the processed fuel, even if it is fully decontaminated from fission products.

The pyrochemical processes currently under development or in use are melt refining (a simple melting procedure for metallic fuels) and various processes for core and blanket materials which employ liquid metals and molten salts as processing media.

The melt refining process is in the most advanced state of development and it is currently being used to process the first core loading of the second Experimental Breeder Reactor (EBR-II),\*\*\* located in Idaho.

### A. PYROCHEMICAL PROCESS DEVELOPMENT

#### 1. Melt Refining (L. BURRIS, R. K. STEUNENBERG, R. D. PIERCE)

The fuel in the first core loading of EBR-II consists of approximately 50% enriched uranium alloyed with about 5 w/o noble metal fission product elements (fissium). The fuel rods are deacid, chopped into about 2-in. long segments and melt refined in a zirconia crucible. Operation of this process with irradiated fuel has been started in the EBR-II Fuel Cycle Facility (see Section II C 1 f). Although no laboratory development work has been done on the present melt refining process during the last reporting period, a modification of melt refining that involves the use of a flux (halide slugging) is being investigated. The halide slugging procedure shows promise for the processing of uranium-plutonium alloy fuels.

\* A summary of this section is given on pages 1 to 7.

\*\* These processes have hitherto been called pyrometallurgical processes, but in order to convey better their applicability to ceramic fuels, such as oxides and carbides, and to emphasize the compact nature of these processes, they are now referred to as "compact pyrochemical" processes.

#### a. BEHAVIOR OF ZIRCONIUM AND CERIUM DURING HALIDE SLAGGING (N. R. CHELLEW, J. T. FEENEY, W. A. PEHL†)

Previous investigations of a halide slugging process in which uranium-plutonium-fissium alloy was melted in contact with chloride fluxes containing  $MgCl_2$  as an oxidant showed that selective removal of rare earth fission products from the alloy can be accomplished by controlling the amount of  $MgCl_2$  in the flux (see ANL-6900, p. 46). The data reported here were obtained in a recent experiment primarily to determine the behavior of zirconium during the halide slugging of uranium-fissium alloy.

The synthetic fuel alloy used in the experiment was uranium-5 w/o fissium containing 0.68 w/o zirconium

\*\*\* The melt refining operations are conducted in the Fuel Cycle Facility, which is adjacent to the EBR-II reactor building.

† High Temperature Semi-Works Group.

TABLE I-1. DISTRIBUTION OF ZIRCONIUM IN HALIDE SLAGGING EXPERIMENT CONDUCTED WITH CHLORIDE FLUX

Charge Alloy (w/o):	94 U, 2.46 Mo, 1.96 Ru, 0.28 Rh, 0.19 Pd, 0.68 Zr, 0.01 Nb, 0.45 Ce
Charge Salt:	83.0 m/o (85.0 w/o) CaCl <sub>2</sub> , 17.0 m/o (15.0 w/o) MgCl <sub>2</sub>
Crucible:	High-purity BeO
Melt Conditions:	Charge heated one hour under argon atmosphere
Oxidant:	MgCl <sub>2</sub>

Fraction	Weight	
	Total (g)	Zirconium (g)
Charge Alloy	15.765	0.108
Salt	3.194	0
Product Alloy	15.684	0.110
Salt	2.672	$5 \times 10^{-5}$

and 0.45 w/o cerium. The cerium was employed as a stand-in for rare earth fission product elements. The flux consisted of CaCl<sub>2</sub> mixed with a 60% excess of MgCl<sub>2</sub> over the stoichiometric amount required for complete oxidation of the metallic cerium and zirconium to CeCl<sub>3</sub> and ZrCl<sub>4</sub>. Both salts were purified by standard techniques prior to use. Chemical analyses showed the purified CaCl<sub>2</sub> and MgCl<sub>2</sub> to contain 0.08 and 0.02 w/o oxygen, respectively.

In the halide slagging experiment, the alloy and salt were charged to a high-purity beryllia crucible, heated under an atmosphere of argon to 1200°C, held at this temperature for one hour, and cooled. The salt was removed from the metal ingot by washing with distilled water. The metal was subsequently dissolved in acid. The two solutions were then analyzed for the pertinent elements.

The distribution of zirconium in the charge and product fractions is shown in Table I-1. Essentially complete retention of the zirconium by the metal phase occurred during the halide slagging, when MgCl<sub>2</sub> was used as the oxidant. The small amount of zirconium in the salt (0.05% of that in the original charge) probably can be attributed to contamination of the salt phase during preparation of the analytical samples. Analyses of the charge and product alloys for cerium indicated that 97% of the cerium had been extracted from the metal. The percentage of cerium removal is in good agreement with the results obtained earlier by Bennett under similar conditions, but on a larger scale (see ANL-6900, p. 46).

The weight loss of the alloy during the experiment (0.08 g) corresponded within 0.01 g to the amount of

cerium removed. However, the flux underwent a weight loss of 0.52 g. Since the amount of MgCl<sub>2</sub> present initially in the flux (0.48 g) was close to the observed weight loss, it was suspected that vaporization of MgCl<sub>2</sub> had occurred. The vapor pressure of pure MgCl<sub>2</sub> is about 170 mm Hg at 1200°C. Analysis of the flux after the experiment, however, indicated that 88% of the excess MgCl<sub>2</sub> was still present. When the crucible and its contents were exposed to laboratory air after the experiment, the exterior surface of the beryllia became wet. This observation suggests that some of the hygroscopic flux had permeated the crucible during the slagging operation.

In general, the experiment showed that zirconium is not removed from uranium-fission alloy by chloride slagging when MgCl<sub>2</sub> is used as the oxidizing agent. The nearly complete removal of cerium under these conditions is in agreement with earlier results. Work is currently in progress to determine the behavior of plutonium, and to investigate further the apparent penetration of the beryllia crucible by the flux.

## b. CONTAINER MATERIALS FOR HALIDE SLAGGING (G. A. BENNETT, I. O. WINSCH, W. H. SPICER)

Laboratory-scale experiments which established the feasibility of purifying a uranium-plutonium-fission alloy by melting under a chloride flux were described in the previous semiannual report (ANL-6900, p. 46). Since previous runs have shown beryllia to be the only crucible which will hold up in the presence of both uranium and salts (ANL-6800, p. 35), the large-scale application of this procedure requires the availability of a reliable beryllia crucible for handling plant-scale charges (10 to 50 kg). An isopressed beryllia crucible was used in the laboratory-scale experiments (~700 g charge), but it is doubtful whether large isopressed beryllia crucibles would be satisfactory because of increased permeability to molten salts or even if acceptable from this standpoint, whether they could be fabricated at a reasonable cost for the 50-kg batches of fuel (somewhat less than half the critical mass of plutonium-containing fuel alloys). Alternatives may be thixotropically cast beryllia crucibles and crucibles of materials other than beryllia which are coated on the inside with beryllia. Beryllia deposited by plasma-spraying has appeared to adhere well to such inexpensive substrate materials as silicon carbide (ANL-6900, p. 63) and alundum (ANL-6725, p. 75) when such beryllia-coated samples were repeatedly thermal cycled to 900°C in an argon atmosphere.

The concept of a coated crucible was explored in a run in which a uranium-plutonium-fission alloy (420 g) was melted together with a 75 m/o BaCl<sub>2</sub>-25 m/o CaCl<sub>2</sub>

flux (120 g) in a 4¼-in. OD by 4¼-in. high alundum crucible having beryllia plasma-sprayed on the inside surface. The melt was held at 1150°C for 1 hr and then the crucible contents were poured into a mold. At the conclusion of the run, it was apparent that the molten salt had soaked into the crucible walls. Consequently, this approach does not appear promising.

### c. MATERIALS FOR CONTAINMENT OF MOLTEN URANIUM AND ITS ALLOYS (G. A. BENNETT, I. O. WINSCH, N. QUATTROPANI)

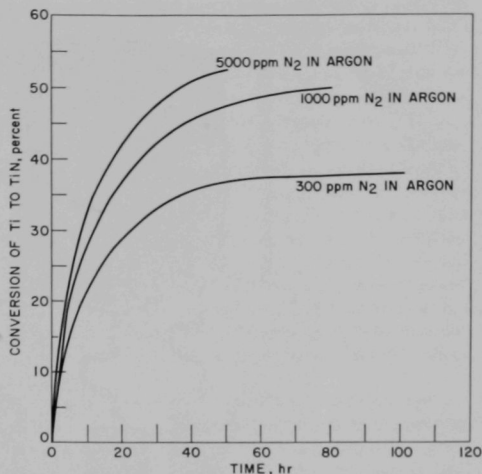
Materials are being investigated for containing uranium and uranium alloys at temperatures from near the melting points to several hundred degrees above the melting points. The work reported previously (ANL-6900, p. 48) has been extended to four additional materials: hafnium carbide, niobium nitride, niobium carbide and tantalum carbide. For these tests the experimental materials in the form of rods 1-in. dia. by 1-in. long were partially submerged in a bath of molten uranium in an argon atmosphere. After being exposed to molten uranium at 1400°C for 24 hr, the rods were withdrawn from the melt and examined for attack.

Hafnium carbide and niobium nitride were not attacked under the test conditions; moreover, niobium nitride was wetted only slightly, if at all. Niobium carbide was wetted and attacked. Tantalum carbide was wetted and suffered severe intergranular corrosion.

Hafnium carbide, niobium nitride, and zirconium diboride (previously tested) are the most promising of the materials which have been investigated. These materials will be tested further and other similar materials, now on order, will also be tested.

### d. REMOVAL OF NITROGEN FROM ARGON WITH TITANIUM SPONGE (M. KYLE, J. ARNTZEN)

A method is under development for removing nitrogen contamination from argon by getting the nitrogen on hot titanium sponge. Although this method will have general utility for purifying argon from nitrogen, the major incentive for its development is a possible future need to remove nitrogen from the argon atmosphere in the Argon Cell of the EBR-II Fuel Cycle Facility. Two sets of experimental equipment have been constructed: (1) equipment for a study of the kinetics of nitrogen removal from argon on hot titanium sponge, and (2) a pilot plant for obtaining overall process performance data and information on component reliability. Studies are being conducted with argon containing initial nitrogen concentrations between 100 and 50,000 ppm.



108-8713

FIG. I-1. Kinetics of Reaction of Titanium Sponge with Nitrogen Impurity in Argon at 900°C. (Based on the reaction  $Ti + \frac{1}{2} N_2 \rightarrow TiN$ .)

#### (1) Kinetics of Nitrogen Removal from Argon with Titanium Sponge

The equipment and experimental procedure for this study were described in ANL-6800, p. 54. In essence, a series of small titanium sponge beds are contacted at 900°C with a flowing stream of argon gas containing the desired concentration of nitrogen. The gas flow rate is maintained high enough so that the nitrogen concentration in the gas stream is not significantly reduced in passing through the beds. One bed at a time is removed and analyzed to provide data on the amount of reaction obtained by any given time. Data on the kinetics of the nitrogen-titanium sponge reaction have now been obtained at a temperature of 900°C and concentrations of 5000, 1000, and 300 ppm nitrogen in argon. Typical reaction rate curves for these nitrogen concentrations are shown in Figure I-1. Data are also being obtained at 50,000 and 100 ppm nitrogen. The data shown in Figure I-1 indicate that the reaction probably follows a parabolic or modified exponential rate law and is dependent upon the concentration of nitrogen in the gas phase. An attempt will be made to correlate all data obtained into a single equation which would be useful in the design of engineering-scale equipment.

#### (2) Pilot Plant for Nitrogen Removal from Argon

A pilot plant-scale unit designed to demonstrate the removal of nitrogen impurity from argon gas on a

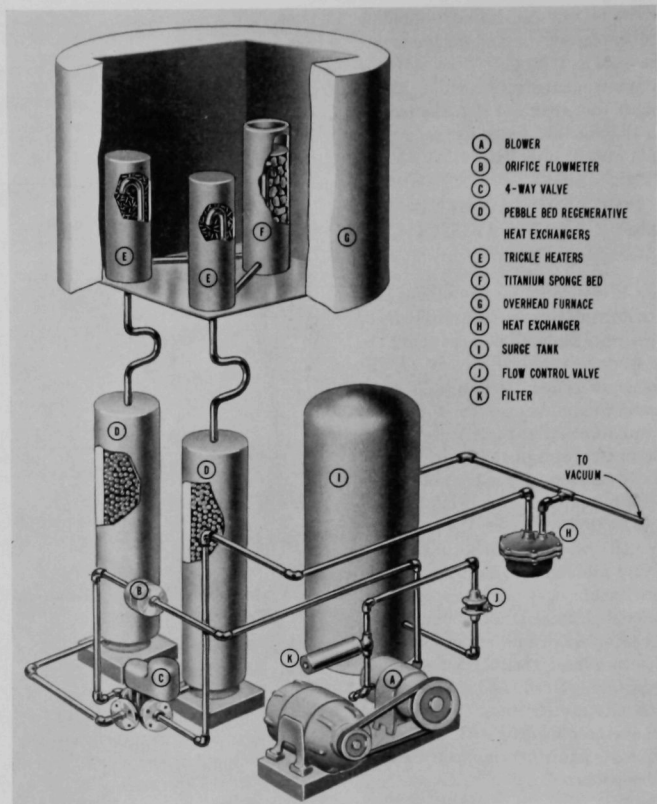


FIG. I-2. Pilot Plant for Study of Nitrogen Removal from Argon.

108-7356

large scale has been in operation. For the convenience of the reader, a schematic diagram of this unit is again shown in Figure I-2. Operating at a gas circulation rate of about 10 cfm, this unit will provide information on component design and reliability for large-volume purification systems. Nitrogen concentrations of between 100 and 5,000 ppm in argon will be used. Detailed information on the design, flow pattern, temperature distribution, and previous operating experience of this system was presented in previous reports (ANL-6800, p. 58 and ANL-6900, p. 50). When 1000 hr of operation were completed in April 1964, the loop was shut down for inspection of all components. The titanium metal sponge was also replaced at that time.

Inspection of the loop disclosed no evidence of deterioration of any process vessel. All instrumentation

and control systems were operating as designed. A small leak was discovered on the outboard oil seal on the shaft of the blower used to circulate the gas stream. The leak was sufficiently small that dismantling of the blower to rework the seal did not seem necessary. The electrical connections had failed on the leads to the booster heating coils on the trickle heaters. These heaters are located in the large furnace ahead of the titanium bed and the connections were made in the hot zone of the furnace. These heaters have an extended heat transfer surface and serve to insure proper preheat of the gas entering the titanium bed. Because it has been found that the trickle heaters receive enough heat from the furnace to perform satisfactorily without the booster coils, it has not been necessary to repair the high temperature connections.

**TABLE I-2. CONVERSION OF TITANIUM TO TITANIUM MONONITRIDE IN THE PILOT PLANT LOOP**

Temperature: 900°C  
 Weight of Titanium Sponge: 25 lb  
 Circulation Rate: 10 cfm  
 Exposure Time: 850 hr to Ar  
 150 hr to 650 ppm N<sub>2</sub> in Ar

Bed Position <sup>a</sup>	Conversion to TiN <sup>b</sup> (%)
Top	44.0
3-in. depth	46.9
6-in. depth	35.4
9-in. depth	35.0
12-in. depth	45.1
Bottom	46.5

<sup>a</sup> Bed approximately 14 in. high.

<sup>b</sup> Computed assuming the following reaction:  $Ti + \frac{1}{2}N_2 \rightarrow TiN$ .

The titanium metal sponge which was removed from the loop gettering bed after 1000 hr of operation (including about 150 hr exposure to 650 ppm nitrogen in argon), was submitted for a modified micro-Kjeldahl determination of the amount of absorbed nitrogen. Results are presented in Table I-2.

In order to obtain the highest possible average conversion of the sponge during the run and also alternately to recover and store heat on two regenerative heat exchangers, the direction of flow through the titanium bed was periodically reversed. This flow reversal through the titanium bed produced the expected conversion profile with the lowest conversion near the center of the bed. The average conversion was about 42%. If 50% conversion of titanium to the nitride could

be obtained in plant operation, the cost of gettering material for a titanium system would be about \$130 per lb mole of nitrogen removed. This cost is about 60% of that for a similar calcium system and 7% of that for a uranium system, based on similar conversions. Thus the results of this run are very encouraging.

The loop was restarted on June 5, 1964, at a gas concentration of 100 ppm nitrogen in argon. Shutdown of the loop, after 650 hr of continuous operation, was required because of oil leakage into the circulating gas stream. An inspection of the blower used to circulate the reacting gas revealed the failure of both the inboard and outboard shaft seals located on the upper blower lobe. The lower lobe seals had not deteriorated significantly. The seal failures permitted oil to leak into the interior of the blower and subsequently into the circulating gas.

The seal failures appear to have been a result of inadequate seal lubrication and insufficient spring tension on the seal faces. The blower has been repaired by replacing the face seals with seals of higher spring tension. The blower will now be operated on its side so that both the upper and lower seals will receive better lubrication.

The oil contamination of the gas stream resulted in poisoning of the titanium sponge, causing the titanium bed to lose its reactivity with nitrogen. Prior to this poisoning of titanium, for a period of about 600 hr, the nitrogen concentration of the circulating gas decreased from 100 ppm to less than 20 ppm nitrogen on passing through the bed at 900°C at a flow rate of 10 cfm. The conversion of the bed at that time was equivalent to about 30% titanium mononitride. After the titanium metal sponge had been replaced, the loop was placed in operation again during November 1964.

## 2. Processes Employing Liquid Metal Solvents

(L. BURRIS, R. K. STEUNENBERG, R. D. PIERCE)

Several processes are being developed which employ liquid metals and salts as processing media. The skull reclamation process is under development for recovery of the fissionable material remaining in the crucible residue (skull) after a melt refining operation. Skull reclamation runs are now being conducted in a pilot plant which has a capacity of about one-third that proposed for the EBR-II plant equipment. Laboratory and engineering work is also underway in the development of processes for recovery of advanced fast reactor fuels which contain plutonium. Fundamental chemical and engineering studies are in progress in support of process development work.

### a. DEVELOPMENT OF THE SKULL RECLAMATION PROCESS (L. BURRIS, R. D. PIERCE)

The skull reclamation process is being developed as an auxiliary process to melt refining for processing the first fuel loading of the EBR-II reactor. The process has two purposes: (1) recovery of uranium from the skull remaining in the crucible after melt refining, and (2) separation of fission products from the uranium. The skull material is expected to contain between 5 and 10% of the uranium charged to melt refining. The recovered and purified uranium will be returned to the main EBR-II fuel cycle via the melt refining step. The skull reclamation

mation process provides for removal of all nonvolatile fission products in the EBR-II fuel cycle.

### (1) Pilot Plant Studies of the Skull Reclamation

**Process** (I. O. WINSCH, T. F. CANNON, P. MACK, K. L. NISHIO, K. R. TOBIAS, N. QUATTROPANI, G. TEATS, L. KIRKEL\*)

Operation of a pilot plant for study and demonstration of the skull reclamation process on an engineering scale was continued during the past period. About 2 kg of skull oxide (containing about 75% uranium) is processed in each run. (In full-scale operations in the EBR-II Fuel Cycle Facility, 7 kg of skull oxide will be processed in each run.) Seven skull reclamation process demonstration runs were started during the past period (5 completed), making a total of 18 demonstration runs that have been completed to date in the pilot plant.

#### (a) Flowsheet

The skull reclamation process flowsheet has not been significantly changed in some time and has been described in detail in an ANL report (ANL-6818). The flowsheet is depicted in Figure I-3. This figure presents a slight process modification which involves delaying the waste flux transfer until after the uranium precipitation step (identified in Fig. I-3 as the intermetallic compound decomposition step) rather than after the reduction step. This change permits keeping the transfer line (an inverted U-tube) in a fixed position throughout the process.

#### (b) Equipment Performance

All process steps up to the retorting (solvent evaporation) step are performed in a 9½-in. ID tungsten crucible. The crucible is inductively heated in a bell jar furnace which is part of the pilot plant described in ANL-6687, p. 37. The bell jar allows performance of the steps in an inert atmosphere and permits pressurization of the system for transfer of molten metals or salts through a transfer line to an external container.

The equipment has been operated in an open glovebox through Run SKR-18. The box has now been enclosed and Runs SKR-19 and SKR-20 were made with a dry-air atmosphere (about 150 ppm H<sub>2</sub>O) in the box. This modification virtually eliminates moisture pickup by the flux when the furnace is open between runs.

**Flux Foaming.** A flux foaming problem attributable to water of hydration in the flux developed during the reduction step of several process demonstration runs. Several methods of flux pretreatment, such as vacuum melting and contacting the molten flux with magnesium to remove the water, have been tried as alternates to the

proven technique of bubbling hydrogen chloride through molten flux. The magnesium pretreatment, a simple foundry-type operation at 700°C, in which magnesium and any water in the flux react to form hydrogen, was used in preparing flux for Run SKR-20. There was no foaming during this run. Therefore, this procedure will be used for preparing flux for future runs.

Some of the plastic films which have been used to package flux have been found to be quite permeable to water vapor. Saran, which is relatively impermeable to water vapor, is now being used. As an additional precaution, fluxes are stored in sealed cans or dry-atmosphere gloveboxes.

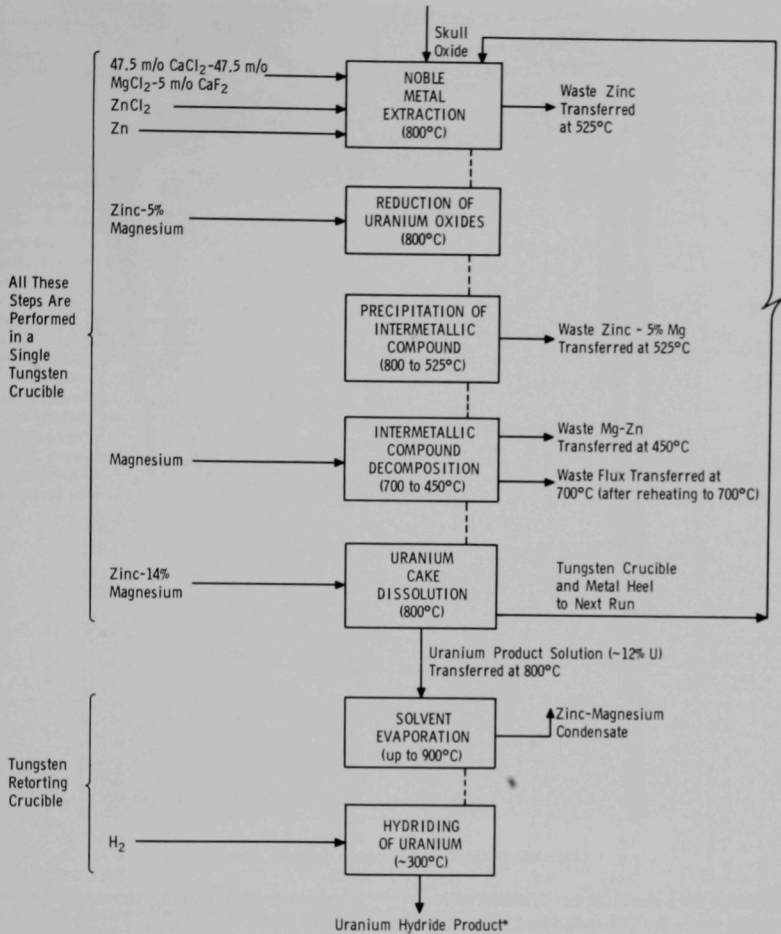
**Phase Transfer.** Waste and product streams are removed from the process crucible through molybdenum-30 w/o tungsten (Mo-W) transfer lines. These lines, which were discussed in ANL-6900, p. 59, have operated well. A photograph of the latest transfer line prior to insulation and canning is presented in Figure I-4. In this design, a stainless steel sheath previously used to cover the Mo-W tube has been eliminated. The electrical heaters are wound directly around the Mo-W transfer tube, covered with insulation, and then canned with a leak-tight stainless steel enclosure. The annular space is evacuated initially and then filled with argon to prevent oxidation of the Mo-W tube. This transfer tube (¾-in. OD by ⅜-in. ID) is 72 in. long. The larger inside diameter as compared to the former ⅝-in. ID will reduce the likelihood of plugs forming in the tubes. The extension of the tube beyond the heater at the outlet end was cut off prior to placing the tube in service.

The efficiency of fission product removal is limited by the transfer efficiency of the waste phases; therefore, transfers of about 90 percent are designed. The phase transfer efficiencies experienced in nine of the latest skull reclamation process demonstration runs are presented in Table I-3. These efficiencies are more consistent and considerably better than those observed in earlier runs (ANL-6800, pp. 70-73). The relatively low transfer efficiencies experienced with the uranium product solutions are due to the small total volumes of product solutions, as compared to the larger volumes of the waste supernatants. The portion of the product which is not transferred would be recycled through the next run (see Fig. I-3).

In several of the process steps, a liquid metal phase is pressure transferred from beneath a frozen flux. In order to provide a path through the flux for the pressurizing gas, the agitator is operated during the time the flux is freezing. A hexagonal agitator shaft has proved highly satisfactory for insuring an adequate opening through the frozen flux.

**Fuming.** Some vaporization of flux and metal phases or "fuming" occurs in the skull reclamation process

\* CEN Machine Shop.



\*The uranium hydride product may be decomposed and consolidated into a metal button in a beryllia crucible for return to melt refining, or it may be returned directly to melt refining.

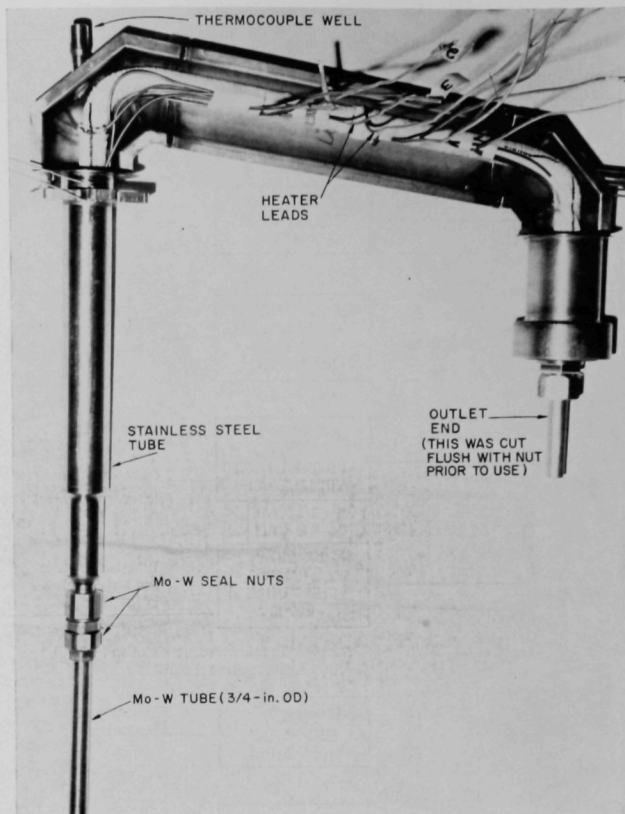
FIG. I-3. Flowsheet for Skull Reclamation Process.

108-8567

runs and a light deposit of flux is found on the inside of the bell jar wall at the conclusion of each run. In Runs SKR-18 and SKR-19, an attempt was made to eliminate the fuming problem. A perforated metal basket containing calcium metal turnings to react with vaporized flux was located in the top section of the tungsten crucible. At the completion of these runs, the interior of the bell jar furnace assembly was relatively

free of vaporized metal and flux. The trap proved to be effective even though flux foaming had occurred during these runs and had resulted in wetting of the calcium with gross amounts of flux. The calcium fume traps will be used in future runs.

*Process Time.* Modifications have been made in the process to reduce the overall time required for a run. Initial runs required about 32 hr for completion; later



108-8734

FIG. I-4. Molybdenum-Tungsten Transfer Line.

runs have required only about 18 hr. Without adverse effect, processing times for the individual steps of the process have been reduced as follows:

- 1) noble metal extraction: 8 hr to 1 hr
- 2) reduction of uranium oxides: 4 hr to 1 hr
- 3) intermetallic compound decomposition: 4 hr to 1 hr
- 4) product dissolution: 2 hr to 1 hr

Still further reductions in some of these processing times are thought possible.

Forced circulation of argon gas through the bell jar is employed to hasten cooling of the melt in the crucible during the noble metal extraction and the uranium precipitation steps. The forced cooling system has worked well. Plugging of the gas-circulation lines, which had been a problem earlier, has been prevented

by periodically cleaning the areas which are known trouble spots.

*Reaction Temperatures.* In several runs, the reaction temperature employed in the noble metal extraction, reduction, and intermetallic decomposition steps was reduced from 800°C to 700°C. The reduction of uranium oxides could be successfully completed at the lower temperature. Moreover, operation at the lower temperature reduced fuming of the flux and metal. However, operation at the lower temperature was found to be questionable because (1) the rates of reduction of uranium and zirconium oxides are lowered and (2) the reduction of uranium into a saturated zinc solution at 700°C may produce finer crystals, which settle less readily than those produced by cooling an initially unsaturated solution from 800°C. Further work is required to establish the optimum operating temperature.

TABLE I-3. PHASE TRANSFER EFFICIENCIES IN SKULL RECLAMATION PROCESS RUNS

Process Step <sup>a</sup> and Phase Transferred	Percent of Total Phase Transferred								
	SKR-9	SKR-10	SKR-11	SKR-12	SKR-13	SKR-14	SKR-15	SKR-16	SKR-17
Noble Metal Leach Waste Zinc	96.3	92.0	95.5	94	97.8	90.3	91	96.5	95.1
Intermetallic Precipitation 5 w/o Mg-Zn Supernatant	82.1	91.3	91.6	96	89.3	86.4	84	89.3	88.9
Intermetallic Decomposition 50 w/o Mg-Zn Supernatant	95.6	—	88.1	87.5	92.0	88.0	89	90.4	89.9
Product Dissolution 12 w/o Mg-Zn Product Solution	90.5 <sup>b</sup>	—	87	85.5	80.5	80.2	83 <sup>c</sup>	87.5 <sup>d</sup>	85.8
Flux Waste Flux	81.5 <sup>e</sup>	—	1.8	1.8	6.1	88.5 <sup>e</sup>	89 <sup>e</sup>	80.2 <sup>e</sup>	6.1

<sup>a</sup> See Figure I-3.

<sup>b</sup> 1.2% of the original flux transferred with the metal product.

<sup>c</sup> 5.7% of the original flux transferred with the metal product.

<sup>d</sup> 0.6% of the original flux transferred with the metal product.

<sup>e</sup> Flux transferred prior to dissolution of precipitated uranium.

<sup>f</sup> In these runs, between 30 and 78% of the flux foamed out of the crucible during the reduction step. Therefore, the efficiency of flux transfer could not be determined.

<sup>g</sup> Flux transferred with uranium product solution.

TABLE I-4. URANIUM MATERIAL BALANCE IN SKULL RECLAMATION PROCESS RUNS

(See Table I-3 for phase transfer efficiencies)

Run No.	Wt. of U Charged (g)	% of U in Product Solution	% of U in Samples and on Crucible Wall Above Melt	% of U in Waste Streams				U Accounted For (%)
				Noble Metal Extract	Waste Flux	Supernatant of Intermet. Ppt.	Supernatant of U Ppt.	
SKR-9	1550	100	—	0.044	0.5	2.35	2.1	105
SKR-10	1550	—	—	0.58	—	3.5	—	—
SKR-11	1540	93	0.14	0.15	7 <sup>a</sup>	1.7	2.0	105
SKR-12	1606	88	0.16	0.19	1.0 <sup>a</sup>	18.0	0.5	108
SKR-13	1540	97	0.23	0.79	1.1 <sup>a</sup>	1.3	0.9	101
SKR-14	1520	100	0.15	0.17	1.1	9.0	1.1	112
SKR-15	1540	108	0.22	0.35	0.7	8.0	4.0	121
SKR-16	1510	100	0.12	0.11	2.0	2.0	1.6 <sup>b</sup>	106
SKR-17	1545	87	0.06	0.17	1.1 <sup>a</sup>	12.5	4.0 <sup>b</sup>	105

<sup>a</sup> Based on residual flux transferred—foaming occurred during reduction step.

<sup>b</sup> Transfer at 500°C instead of 450°C.

One hour has proved adequate for the dissolution of the product at 800°C. The temperature of this step has been set at 800°C in order to dissolve all the uranium in as little as possible of the 14 w/o Mg-Zn solution without excessive zinc vaporization.

### (c) Process Results

The analytical results which show the behavior of uranium in the pilot plant runs through Run SKR-8 have been presented previously (ANL-6900, p. 55). The results for Runs SKR-9 through SKR-17 are now available and are reported below.

**Uranium Recovery.** The uranium material balances for nine runs are summarized in Table I-4. The overall uranium balance was high in all but one run. This imbalance is probably a result of (1) analytical uncertainties in the charge and product solution samples and (2) the uncertainty in the quantity of product solution left in the crucible as a heel. However, values for uranium losses in the waste streams are accurate. It is hoped to keep the uranium losses to less than 5% in the skull reclamation process to permit an overall process recovery of about 99.5% for the EBR-II fuel cycle.

Losses of uranium in the noble metal extraction step are slightly greater than the expected value (<0.1%)

TABLE I-5. FISSION PRODUCT MATERIAL BALANCES IN SKULL RECLAMATION PROCESS RUNS

Run No.	% of Fission Product Charged											Total % of Fission Product Accounted for			
	Noble Metal Extract		Supernatant, Intermetallic Ppt.		Supernatant, Intermetallic De-comp.	Waste Flux		Product Solution							
	Mo	Ru	Ce	Zr	Ce	Ce	Zr	Mo	Ru	Ce	Zr	Mo	Ru	Ce	Zr
SKR-9	25	79	3	42	39	30	—	55	17	8	41	75	96	80	83
SKR-10	58	92	0.6	60	—	—	—	—	—	—	—	—	—	—	—
SKR-11	42	73	4	62	38	6	11	15	20	25	28	57	93	73	101
SKR-12	71	97	12	70	21	5	2	23	12	37	28	94	109	75	100
SKR-13	60	89	4	53	38	35	5	39	21	5	36	99	110	82	94
SKR-14	45	75	—	45	23	45	—	41	16	6	34	86	91	74	79
SKR-15	57	82	—	42	32	37	—	44	14	13	50	101	96	82	92
SKR-16	61	74	—	47	36	31	—	28	17	5	30	89	91	72	77
SKR-17	60	84	—	54	39	29	6	17	9	5	19	77	89	87	69

but continue to be less than 1% and therefore present no real problem. Increasing the oxidation potential of the flux by adding zinc chloride, as will be done in Run SKR-22 and subsequent runs in which a recycled heel will be present from the previous run, should lower this loss to the expected level.

A uranium loss of 0.5 to 1% in the waste flux appears to be inherent in the process, apparently as a result of a chemical equilibrium in the reduction step. The high loss experienced in Run SKR-11 (7%) was a result of too low an agitation rate during the reduction step. The 2% loss in Run SKR-16 was the result of using insufficient time (1 hr) to complete the reduction at a relatively low temperature (700°C).

The uranium losses in the intermetallic precipitation step present a more serious challenge. The minimum uranium loss, that which is due to the solubility of uranium in the waste stream, is only about 0.5%, but the losses have been increased to 1.3 to 18% as a result of considerable entrainment of uranium. Smaller losses (1 to 2%) had been demonstrated in smaller scale runs (ANL-6900, p. 64). The two factors which are believed to have promoted the high losses are backflushing of argon through the transfer line and agitation during the cooling period of the intermetallic precipitation step. The backflushing is maintained to avoid crystallization in the transfer line. As discussed earlier, mechanical agitation is employed to maintain a vent through the freezing flux. These operating procedures are being modified to decrease the uranium entrainment. Agitation will be stopped as soon as the flux has become frozen, and an adequate time will be allowed for settling of the uranium-zinc crystals. Backflushing will also be stopped when the agitation is stopped. It is

felt that the uranium loss in this step can be reduced to about 1% by these changes in procedure.

The solubility of uranium in the waste stream from the intermetallic decomposition step will cause a minimum uranium loss of 0.8% at 450°C or 1.1% at 500°C. Higher losses, experienced in some of these runs, can be prevented if the settling period is increased and if backflushing is discontinued sooner or even eliminated. Based on earlier experience in both small-scale runs and blanket processing studies, uranium losses in this step should be reducible to a very low level.

*Fission Product Removal.* Fission product removals are shown in Table I-5. Except in Runs SKR-11 and SKR-12, cerium removals have been good, ranging between 87 and 95%. In Runs SKR-11 and SKR-12, the flux was transferred with the product solution, which resulted in back extraction of cerium into the product solutions. The overall cerium material balances have been low for an as yet unexplained reason.

Zirconium removals have ranged between 50 and 81%. Incomplete reduction of zirconium oxide in the reduction step has limited the removal of this fission product. The reduction steps in recent runs have been performed with more rapid agitation (~700 rpm) for the purpose of increasing the zirconium reduction and thereby making the zirconium available for removal in the waste zinc-5 w/o magnesium solution. A zirconium removal of at least 85% is desired in order to compensate adequately for zirconium introduced as zirconia powder spalled from the melt refining crucible (see ANL-6900, p. 53).

Ruthenium and molybdenum are insoluble in the zirconium metal extract at the phase transfer temperature of 525°C. An agitation rate of about 400 rpm keeps the

TABLE I-6. RETORTING TO FORM URANIUM PRODUCT INGOTS. RUNS SKR-13 THROUGH SKR-17

Run No.	Charge (from U Diss. Step)		Distillate Mg-Zn (kg)	Product													
				Total (kg)	Uranium		Fission Product Concentration (%)				% of Fission Product Charged				Mg (ppm)	Be (ppm)	Zn (%)
	kg	% of Charge <sup>a</sup> to Retorting			Ce	Zr	Mo	Ru	Ce	Zr	Mo	Ru					
SKR-13	11.29	1.18	9.95	1.1	1.05	89.2	0.13	1.24	0.75	0.36	2	27	26	18	—	20	—
SKR-14	11.92	1.16	9.48	0.92	0.84	72.2 <sup>b</sup>	0.25	0.94	0.87	0.22	3	17	22	9	25	5	<0.4
SKR-15	12.92	1.39	11.30	1.37	1.25	90.0	0.16	1.4	0.88	0.23	3	38	38	14	400	25	<1
SKR-16	13.14	1.26	11.50	1.24	1.17	93.0	0.22	0.96	0.65	0.24	4	24	26	14	8	100	—
SKR-17	13.17	1.14	11.20	1.10	1.02	90.0	0.32	0.54	0.42	0.15	5	12	14	8	2700	31	1-10

<sup>a</sup> Based on U product solution analyses.

<sup>b</sup> Beryllia crucible developed a crack. Analysis of the material recovered in the secondary accounts for about 17% of the uranium charged.

ruthenium and molybdenum in suspension in the zinc during the transfer. This has resulted in excellent removals of ruthenium (79 to 91%) and good removals of molybdenum (45 to 85%). An approximately 60% removal is satisfactory for molybdenum. The reason for the consistently lower decontamination of uranium from molybdenum than from ruthenium is not understood but is being explored.

**Retorted Uranium Products.** A number of zinc-14 w/o magnesium-10 w/o uranium product solutions have been retorted in a beryllia crucible to remove the magnesium-zinc and produce uranium ingots. Analyses of the retorted products from Runs SKR-13 through SKR-17 are shown in Table I-6. Overall removals of fission products, as indicated by the analytical results for the retorted products, were generally lower than the removals indicated by analyses of the product solutions. In the five runs summarized, the results indicate uranium discrepancies of about 7% in the final uranium products. Analyses of the distillates from several of these runs have shown uranium entrainment to be negligible (<0.01%). Therefore, the discrepancies are believed to be the result of inaccuracies in sampling or analysis of the uranium product solutions. This is being investigated. The 28% loss of uranium in SKR-14 was largely a result of a crack which developed in the beryllia crucible and allowed a portion of the product solution to leak into the secondary graphite crucible.

Magnesium and zinc contamination of the product has been low (Table I-6). Beryllium and carbon contamination of the product resulting from the use of beryllia crucibles and graphite condensers has not been significant. Carbon analyses are not reported in Table I-6, but results obtained for two runs have indicated

about 0.01% carbon, which is well below the maximum specified for reactor grade uranium. A small amount of flux which was carried over into the beryllia retorting crucible with the product solution was mechanically removed prior to retorting. The product from Run SKR-20, in which the residual flux was charged to the retort, is expected to contain somewhat more magnesium than did the products from Runs SKR-13 to SKR-17.

With the possible exception of zirconium whose removal is on the low side, fission product concentrations are satisfactorily low and the product should be satisfactory for returning to the main EBR-II fuel stream via the melt refining operation.

## (2) Small Scale Support Studies (I. O. WINSCH, K. R. TOBIAS)

**Zirconium Behavior.** In both the large and small scale skull reclamation process demonstration runs, as little as 75% of the expected amount of zirconium has appeared in the supernatant solution which was removed after precipitation and settling of a uranium-zinc intermetallic compound (~U<sub>2</sub>Zn<sub>23</sub>). Possible explanations for this are: (1) coprecipitation of the zirconium with the uranium-zinc intermetallic compound, a phenomenon which could be enhanced by the presence of other fission product elements in solution, (2) reduction of the zirconium solubility caused by the presence of other fission product elements, and (3) adsorption of zirconium on equipment surfaces.

Observations made in small-scale demonstration tests suggested a possible correlation between the amount of ruthenium present and the zirconium removal efficiencies. Therefore, several runs were made

in which the concentration of ruthenium was varied between wide limits. About 23% of the zirconium precipitated or coprecipitated when an abnormally large amount of ruthenium was present (0.06% in solution, which corresponds to only a 30% removal of ruthenium in the noble metal extraction step of the Skull Reclamation Process). Only 9 to 12% zirconium precipitated when the concentration of ruthenium was very low, i.e., less than 0.01%. Therefore, it appears that a significant coprecipitation of zirconium occurs and that it is increased by the presence of ruthenium. However, the effect of ruthenium should be small if the ruthenium is properly removed in the noble metal extraction step.

The precipitation or coprecipitation of zirconium was not perceptibly increased by the presence of cerium at a full process level concentration of 0.3%. Cerium, and other rare earth elements, are the major fission product constituents of intermetallic precipitation melts.

In order to investigate possible adsorption of zirconium on equipment surfaces, coupons of tantalum, tungsten, and molybdenum-30 w/o tungsten were suspended in a 5 w/o Mg-Zn solution containing  $^{90}\text{Zr}$  tracer and its  $^{90}\text{Nb}$  daughter. Analysis of coupons immersed for short periods (less than 2 hr) indicated that only 15 to 20% of the activity on the coupon surfaces was zirconium (the remainder was niobium). The total amount of zirconium adsorbed on the surfaces of the coupons represented a very small per-

centage (<0.1%) of the total zirconium present. Analysis of coupons immersed for longer periods (24 hr) showed that essentially all of the zirconium activity on the coupon surfaces had been replaced by niobium activity. These results show that significant zirconium losses cannot be accounted for by interaction with the reaction crucible, agitator, or transfer line surfaces.

It is concluded that zirconium removal in the supernatant solution of the intermetallic precipitation step has been somewhat less than expected because of slight and somewhat variable precipitation of the zirconium with the uranium-zinc intermetallic compound, depending on the amount of ruthenium present.

### (3) Procurement and Testing of Crucibles for the Skull Reclamation Process (G. A. BENNETT,

I. O. WINSCH, N. P. QUATTROPANI, W. H. SPICER)

Two crucibles are required in the skull reclamation process: (1) a tungsten or tungsten-coated crucible in which the reaction and precipitation steps are performed and (2) a smaller beryllia, beryllia-coated, tungsten, or tungsten-coated crucible in which the retorting step is performed.

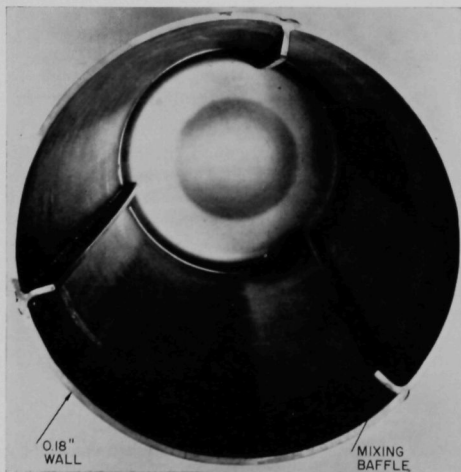
#### (a) Tungsten Crucibles

Four fabrication procedures have been investigated for producing the tungsten crucibles which have been employed: (1) pressing and sintering, (2) welding, (3) spinning, and (4) plasma spraying.

*Pressed and Sintered Crucibles.* Four small (4¼-in. ID) pressed and sintered tungsten crucibles have been in service for about 2½ yr for miscellaneous process studies related to skull reclamation process development. All four crucibles still appear to be in excellent condition. Two larger (10-in. ID) crucibles containing integral mixing baffles on the walls were employed in the skull reclamation pilot plant.

One of these larger pressed and sintered tungsten crucibles failed after many months of service in the skull reclamation process by cracking under the expansion stresses imposed during remelting of a full metal and flux charge. The second crucible, which was a manufacturer's reject because of the high porosity of the walls and the presence of several cracks in the walls, was repaired by plasma spraying the outside of the crucible with tungsten. The tungsten coating sealed the cracks and initially eliminated seepage of molten metals through the walls. However, over months of service, metal seepage gradually increased to the point that it was necessary to discontinue use of the crucible. A new pressed-and-sintered crucible has been obtained but has not been used.

*Helicarc Welded Tungsten Crucible.* An engineering-scale (10⅝-in. OD) welded tungsten crucible with in-



108-7647A

FIG. I-5. Welded Tungsten Crucible. (10⅝-in. OD by 21-in. high).

tegral mixing baffles was obtained for testing in the skull reclamation process pilot plant. A photograph of this crucible prior to its use is presented in Fig. 1-5. It was used in three pilot plant runs and for the melting of six metal waste streams for sampling. It was not visibly affected by these operations, but in the next skull reclamation run, an irregular, circumferential crack extending around about one-third the circumference of the crucible appeared in and above the lower circumferential weld. It has been postulated that a combination of incomplete stress relief after welding of the crucible and too rapid heating of the crucible in the brittle temperature region (up to 400°C) may have induced failure by thermal shock. Because of the relatively light weight of the welded crucible (~80 lb) as compared to a pressed-and-sintered tungsten crucible (~500 lb), a welded crucible has several advantages over the bulky pressed-and-sintered crucible, e.g., ease of handling and a lower heat capacity which permits faster heating and cooling cycles. Therefore, methods of improving the integrity of a welded crucible will be sought.

*Spun Tungsten Crucible.* Because of the excellent performance of a small (4-in. OD by 6-in. high) spun tungsten crucible (ANL-6900, p. 62), attempts were made to procure an engineering-scale spun crucible. Only one fabricator, Metallwerk Plansee (The Austrian affiliate of the National Research Corporation), agreed to fabricate such a crucible. This crucible will measure 18½ in. high by 10½ in. OD by 0.18 in. thick. Separate mixing baffles are also being fabricated for insertion in the crucible.

*Tungsten Crucible Formed by Plasma Spraying.* Crucibles of nearly any shape or size can be produced by spraying tungsten on a mandrel. Crucibles formed in this manner and subsequently fired under hydrogen to only 1000°C have been porous to zinc and flux melts. In an attempt to overcome the porosity problem, a plasma sprayed crucible is to be fired at 2500°C in hydrogen.

#### (b) Beryllia Crucibles

In the current EBR-II Skull Reclamation Process, beryllia is one of the crucible materials being considered for the final uranium retorting step. Beryllia crucibles have desirable characteristics for use in this step of the skull reclamation process. They do not react significantly with the solvent metals, magnesium and zinc, or with molten uranium, the product of the retorting operation. In work to date, beryllia has not been wetted by uranium, which indicates that the product might be removed from the crucible as a solid ingot. The required size of the beryllia retorting crucible for the EBR-II plant is about 8 in. OD by 15 in. high.

Isopressed beryllia crucibles used in early experiments cracked during retorting. However, a new BeO mix developed by the Brush Beryllium Company is considered superior to that used for the earlier crucibles. Crucibles prepared from this mix will be tested. Considerable attention has also been given to thixotropically cast beryllia crucibles which are reputed to be less subject to thermal shock and easier to fabricate in large sizes than isopressed crucibles. Thixotropically cast crucibles supplied by Brush Beryllium Company and by Coors Porcelain Company have been used in retorting studies reported in the section, *Recovery of Uranium Product*. In these studies, the magnesium and zinc have been evaporated from alloys containing about 12 w/o Mg-10 w/o U-78 w/o Zn on a scale of about 5 to 6 kg. The crucibles (5¼-in. dia. by 9-in. high) have been used for a number of times, but the gradual development and growth of cracks has resulted in crucible failures after a maximum of nine uses.

A larger, 12-in. OD by 20-in. high, thixotropically cast crucible was exposed successively to 5 w/o Mg-4 w/o U-Zn, 50 w/o Mg-Zn plus precipitated U, and 12 w/o Mg-10 w/o U-Zn at temperatures of 500 to 800°C. The crucible cracked circumferentially and in the base. To date, the integrity of large thixotropically cast beryllia crucibles has been poor, certainly insufficient for process use.

Because beryllia crucibles have not given an acceptable performance in retorting operations, increasing attention is being given to the use of tungsten crucibles for retorting. The uranium cannot be consolidated by melting in tungsten because the uranium wets the tungsten and sticks to it. However, the uranium product, which exists as a sponge after retorting, need not be melted but, to permit easy removal from the crucible, can be converted to a powder by hydriding at about 300°C and dehydriding at about 400°C under vacuum. Preliminary experiments have shown tungsten to be completely satisfactory when product removal is effected by the hydriding-dehydriding steps. Additional information on the performance of tungsten crucibles will be forthcoming in the next semiannual report.

#### (c) Coated Crucibles

Coated crucibles are being fabricated by plasma spraying a layer of tungsten or beryllia on an inexpensive substrate material which is readily available in large sizes. The most promising substrate materials are silicon carbide and alundum. Should such crucibles prove satisfactory, the cost of crucibles for the skull reclamation process could be greatly reduced. Small (4¼-in. OD by 4¼-in. high) silicon carbide crucibles have been prepared both with beryllia and with tung-

TABLE I-7. EFFECT OF SALT COMPOSITION ON URANIUM VOLATILIZATION AND VANADIUM AND TITANIUM RETENTION DURING CHLORINATION OF URANIUM AND VANADIUM-20 w/o TITANIUM ALLOY IN MOLTEN SALTS

Salt Composition (m/o)					Grams salt per gram U	Temperature (°C)	Time (hr)	Liters Cl <sub>2</sub> per gram U (S.T.P.)	% Uranium Volatilized	% Vanadium plus Titanium Retained
CaCl <sub>2</sub>	BaCl <sub>2</sub>	LiCl	NaCl	KCl						
65	35	—	—	—	1.5	650	1.7	1.2	24	—
32	18	50	—	—	1.7	650	1.5	1.5	10	—
32	18	—	50	—	1.75*	650	1.5	1.5	5	—
					3.5	650	1.2	2.5	2.7	0.1
32	18	—	—	50	1.8	650	1.5	1.5	0.9	0.2
30	—	—	40	30	1.0	600	0.7	0.8	0.5	0.2
27	—	—	33	40	1.2	600	0.8	0.8	~0	0.2
—	—	—	50	50	1.0	700	0.7	0.5	~0.1	5.5

\* Two experiments performed with this solvent to show the effect of the quantity of salt used.

sten coatings, and similar alundum crucibles have been coated with beryllia. All of these crucibles were thermal cycled without adverse effect. Testing of the crucibles with zinc and salt solutions has just begun. The first tungsten-coated crucible satisfactorily contained a zinc solution but allowed a small amount of flux to weep through the tungsten coating and into the silicon carbide.

(d) *Silicon Carbide Crucibles* (M. L. KYLE, W. F. PEHL)

Two runs were conducted to test the corrosion resistance of a substrate material by itself to Zn-Mg-U/halide flux systems. In these tests, conducted at 900°C and 800°C, a silicon oxynitride-bonded silicon carbide crucible\* (apparent porosity 15%) was subjected to a Zn-5 w/o Mg-2 w/o U/halide flux (CaCl<sub>2</sub>, MgCl<sub>2</sub>, CaF<sub>2</sub>) system. After 48 hr of exposure, it was found that the flux had leaked through the crucible wall and collected in the secondary (graphite) containment vessel. No evidence of corrosion or penetration by the metal phase was evident. It is concluded that silicon oxynitride-bonded silicon carbide is not sufficiently dense for containment of halide fluxes.

**b. PROCESSES FOR FAST BREEDER REACTOR FUELS** (L. BURRIS, R. K. STEUNENBERG, R. D. PIERCE)

Processes employing liquid metal and molten salt solvents are being developed for fast breeder reactor fuels that contain uranium and plutonium. Although the major effort is concerned with processes for metallic fuels, oxide and carbide fuels can also be accommodated by slight modifications of the process flowsheets.

\* Crystalon 63, a product of The Norton Company, Worcester, Mass.

(1) **Chemical Decladding** (D. A. WENZ)

Vanadium-titanium alloys continue to be considered seriously as a cladding material for fast breeder reactor fuels (ANL-6936, p. 24). Two approaches to the chemical removal of vanadium-20 w/o titanium cladding have been under study. One approach is a chlorination procedure; the other involves hydriding of the fuel followed by dissolution in liquid cadmium.

(a) *Chlorination Studies*

Exposure of uranium clad with vanadium-20 w/o titanium to chlorine in a molten chloride mixture has been found to result in dissolution of the uranium to form UCl<sub>4</sub> and volatilization of the titanium and vanadium as the chlorides. A series of experiments has been performed to determine a salt composition, ratio of salt to fuel, temperature, and amount of chlorine to be added in order to obtain a maximum separation of uranium from vanadium and titanium. The experimental results are summarized in Table I-7. It is evident from these data that with an increased concentration of alkali metal chlorides in the salt, there was less uranium lost by volatilization, presumably through the formation of complexes with UCl<sub>4</sub>. Of the alkali metal chlorides used, the tendency toward complex formation decreased in the order KCl > NaCl > LiCl. The tendency of the salt toward complex formation must be limited by appropriate control of the composition so that the vanadium and titanium chlorides are not retained by the salt solution. According to the results shown in Table I-7, this balance can be achieved by using the proper concentrations of alkali metal chlorides in mixtures with alkaline earth chlorides. When uranium-5 w/o fissionable clad with vanadium-20 w/o titanium alloy was chlorinated in 40 m/o NaCl-30 m/o KCl-30 m/o CaCl<sub>2</sub> at 600°C, the reaction rate was considerably lower than

when uranium was chlorinated, apparently because the fission elements inhibited the reaction. Most of the zirconium and molybdenum that did react were volatilized, while the other noble metals remained in the melt.

During the course of the chlorination studies, immiscible liquid phases were observed at certain compositions in the  $\text{KCl-CaCl}_2\text{-BaCl}_2\text{-UCl}_4$  and  $\text{NaCl-KCl-CaCl}_2\text{-UCl}_4$  quaternary systems. The two liquid phases were each sampled at  $600^\circ\text{C}$  at one composition in the  $\text{KCl-CaCl}_2\text{-BaCl}_2\text{-UCl}_4$  system. Analytical data on the samples (Table I-8) show that the lower phase contained primarily  $\text{KCl}$  and  $\text{UCl}_4$ , whereas the upper phase was mostly  $\text{CaCl}_2$  and  $\text{BaCl}_2$ .

Although the results of these studies indicate that a separation of uranium from vanadium-titanium cladding can be effected by chlorination in a salt mixture, the procedure is somewhat unattractive for process use because of the corrosiveness of the system and the low chlorination rate of uranium-fission alloy.

#### (b) Selective Dissolution of Uranium

Since uranium is known to be appreciably soluble in liquid cadmium (ANL-6900, Fig. I-6, p. 68) and since vanadium-20 w/o titanium alloy had proved to be essentially unaffected by long periods of exposure to this solvent, several attempts were made to dissolve uranium selectively from a uranium rod clad with vanadium-20 w/o titanium alloy tubing which was open at the ends. A Soxhlet-type extraction apparatus made of type 304 stainless steel was used to assure a continuous supply of fresh cadmium to the rod at temperatures of  $500$  to  $550^\circ\text{C}$ . The results indicated that the dissolution rate of uranium was much too low for a practical process.

Modification of this procedure by including a hydriding step before the uranium dissolution step was therefore investigated. A uranium-5 w/o fission rod (0.144-in. dia. by 0.5-in. long) was placed inside a piece of vanadium-20 w/o titanium tubing having an OD of 0.19 in. and a wall thickness of 0.015 in.; the ends of the vanadium-20 w/o titanium tubing were sealed. This simulated fuel pin was then exposed to 2 atm of hydrogen pressure for a period of 3 hr at  $250^\circ\text{C}$ . The uranium-fission alloy was hydrided, apparently by diffusion of the hydrogen through the vanadium-20 w/o titanium cladding. The cladding split open, probably as a result of the volume increase that occurs during the hydriding of uranium.

Although uranium-fission alloy forms a coarser powder than does uranium during hydriding, it is possible that a mechanical separation of the cladding fragments from the uranium-fission powder might

TABLE I-8. COMPOSITIONS OF IMMISCIBLE LIQUID PHASES IN THE SYSTEM  $\text{KCl-CaCl}_2\text{-BaCl}_2\text{-UCl}_4$   
Temperature:  $600^\circ\text{C}$

Phase	Composition (m/o)			
	KCl	CaCl <sub>2</sub>	BaCl <sub>2</sub>	UCl <sub>4</sub>
Upper	17.6	50.5	26.8	6.1
Lower	53.0	6.8	9.4	30.8

be developed. It appears, however, that a more satisfactory procedure might be first to dehydride the powder and dissolve the resulting metallic powder in liquid cadmium and then to separate the cladding by filtration. Further studies of the dehydriding procedure are in progress.

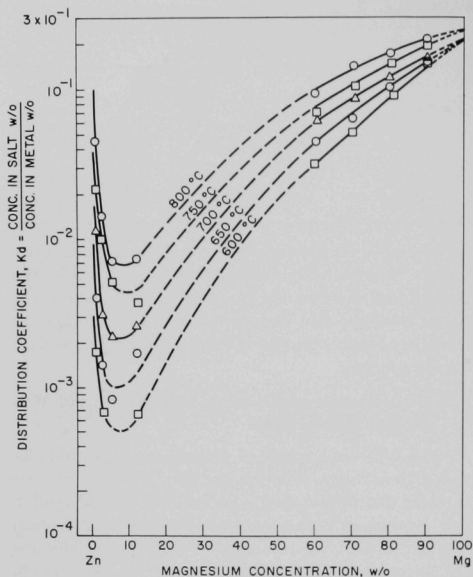
#### (2) Distribution of Elements between Liquid Metals and Molten Salts

Since some separations of fissionable and fertile elements from fission products are effected by differences in their distribution behavior in liquid metal-molten salt systems, it is necessary to determine distribution coefficients that are pertinent to the process. This information is useful not only for process application, but also in deriving fundamental data on the activity coefficients for the components of liquid metal solutions.

##### (a) Distribution of Plutonium between 30 m/o NaCl-20 m/o KCl-50 m/o MgCl<sub>2</sub> and Zn-Mg Alloys (I. JOHNSON, J. B. KNIGHTON, J. W. WALSH, J. D. SCHILB)

The distribution of plutonium between 30 m/o NaCl-20 m/o KCl-50 m/o MgCl<sub>2</sub> and Zn-Mg alloys has been determined at various magnesium concentrations over the temperature range of  $600$  to  $800^\circ\text{C}$ . The liquid salt and metal phases containing the plutonium were mixed in a tantalum crucible under an argon atmosphere; then, filtered samples of the two phases were withdrawn and analyzed. The results are shown in Figure I-6.

The purpose of these measurements was to supply data for the computation of the activity coefficient of plutonium in magnesium as a function of temperature. At an average plutonium concentration of 0.08 a/o, the activity coefficient of plutonium in magnesium remained at an essentially constant value of  $9.2 \pm 0.9$  over the range of  $600$  to  $800^\circ\text{C}$ . Further thermodynamic information on this system at higher temperatures should be forthcoming when a determination of the liquid immiscibility gap in the system plutonium-magnesium is completed (see Sect. I-A-2-c-(2)).



108-8712

Fig. I-6. Distribution of Plutonium between 30 m/o NaCl-20 m/o KCl-50 m/o MgCl<sub>2</sub> Salt and Zn-Mg Alloy at 600°C, 650°C, 700°C, 750°C, and 800°C.

Mixing Rate: 300 rpm  
Crucible: tantalum  
Atmosphere: argon

(b) *Distribution of Praseodymium between 30 m/o NaCl-20 m/o KCl-50 m/o MgCl<sub>2</sub> and Various Magnesium Alloys* (J. B. KNIGHTON, R. MANCINI\*, J. W. WALSH)

The distribution coefficients of various elements between liquid metal alloys and molten salts can be varied drastically by changing the composition of the liquid metal phase. In order to examine the possibility of exploiting this effect for process separations, the distribution behavior of praseodymium between 30 m/o NaCl-20 m/o KCl-50 m/o MgCl<sub>2</sub> and various binary alloys of magnesium was investigated. Praseodymium was chosen because it is representative of the rare earth fission product elements and because <sup>142</sup>Pr with a 19.2-hr half-life is a convenient tracer for radiochemical analysis. The salt and metal phases containing praseodymium were mixed in a tantalum crucible under an argon atmosphere at 600°C; then, filtered samples of the two phases were taken.

The results are presented in Figure I-7, where the praseodymium distribution coefficients are shown as a function of magnesium concentration in the binary alloys Cu-Mg, Ni-Mg, Cd-Mg, Pb-Mg, Zn-Mg, Sb-Mg, and Al-Mg. The composition regions selected for this study were those with melting points below 600°C as reported by Hansen and Anderko.<sup>1</sup> The data obtained show a very pronounced effect of alloy composition upon the distribution behavior of praseodymium. The praseodymium distribution favors the salt phase when Cu-Mg or Ni-Mg alloys are used, but it shifts strongly to the metal with Sb-Mg and Al-Mg alloys. These differences are the greatest at low magnesium concentrations. The distribution coefficient curves should all converge at 100% magnesium, as indicated by the dashed portions of the curves in Figure I-7. The common point at 100% magnesium is an extrapolated value, however, since the melting point of pure magnesium is about 50°C higher than the temperature of 600°C that was used in the experimental determinations.

These data show that Sb-Mg or Al-Mg alloys can be used to purify molten salts that have been used to extract rare earth fission products from solutions containing uranium and plutonium in Zn-Mg or Cd-Mg. The very low praseodymium distribution coefficients of 10<sup>-3</sup> to 10<sup>-4</sup> indicate that a single contact with a small volume of Sb-Mg or Al-Mg alloy should provide adequate rare earth removal for recycle of the salt. The rare earth fission products would thereby be consolidated in a compact metallic ingot for convenient disposal. Since Al-Mg alloy appeared more promising for this use, it was selected for further study.

(c) *Distribution of Lanthanum Between 30 m/o NaCl-20 m/o KCl-50 m/o MgCl<sub>2</sub> and Al-Mg Alloys* (J. B. KNIGHTON, AND R. MANCINI)

An experiment was performed to determine the distribution coefficient and solubility of lanthanum, a major rare earth fission product, between 30 m/o NaCl-20 m/o KCl-50 m/o MgCl<sub>2</sub> and Al-Mg alloys. Magnesium concentrations of 13, 20, and 30 w/o were chosen, since the minimum in the praseodymium distribution coefficient had occurred in this composition region of the Al-Mg system. The measurements were made over the temperature range 550 to 900°C. The results shown in Figure I-8 indicate appreciable solubility of lanthanum (2.23 w/o at 550°C) in the Al-20 w/o Mg alloy. The lanthanum solubility increased with rising aluminum concentration and with increasing temperature up to about 700°C. Above this tem-

<sup>1</sup> M. Hansen and K. Anderko, "Constitution of Binary Alloys," Second Edition, McGraw-Hill Book Co., Inc., New York, 1958.

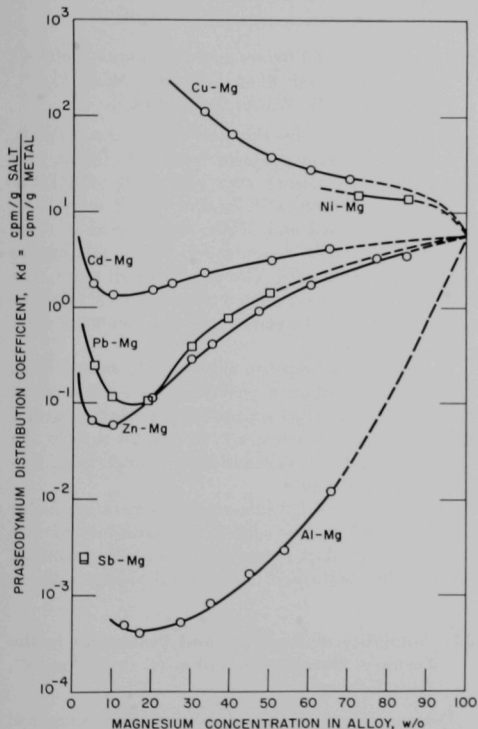
\* Co-op Student, University of Detroit.

perature, the solubility of lanthanum became retrograde.

These results indicate that lanthanum has a sufficiently low distribution coefficient (see Figure I-9) and a sufficiently high solubility (Figure I-8) in Al-Mg alloy at 700°C to permit its consolidation into this alloy at reasonably high concentrations. Further studies are in progress on the behavior of yttrium, cerium, and praseodymium.

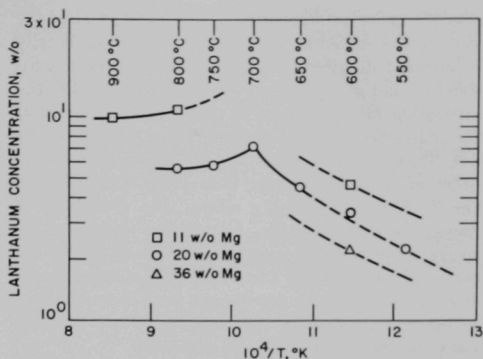
(d) *Distribution of Plutonium Between 30 m/o NaCl-20 m/o KCl-50 m/o MgCl<sub>2</sub> and Cu-Mg Alloys*  
(J. B. KNIGHTON, AND J. W. WALSH)

The strong tendency of praseodymium distribution to favor the salt phase in a 30 m/o NaCl-20 m/o KCl-50 m/o MgCl<sub>2</sub>/Cu-Mg system (Fig. I-7) sug-



108-8542  
FIG. I-7. Distribution of Praseodymium between 30 m/o NaCl - 20 m/o KCl - 50 m/o MgCl<sub>2</sub> and Magnesium Alloys at 600°C.

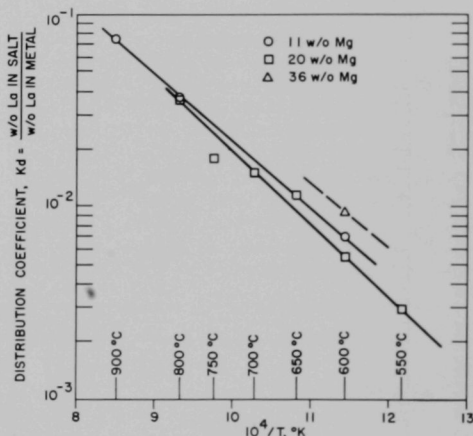
Mixing Rate: 300 rpm  
Crucible: tantalum  
Atmosphere: argon



108-8720, Rev. 1

FIG. I-8. Solubility of Lanthanum in Al-Mg Alloy.

Mixing Rate: 300 rpm  
Crucible: tantalum  
Atmosphere: argon



108-8719, Rev. 1

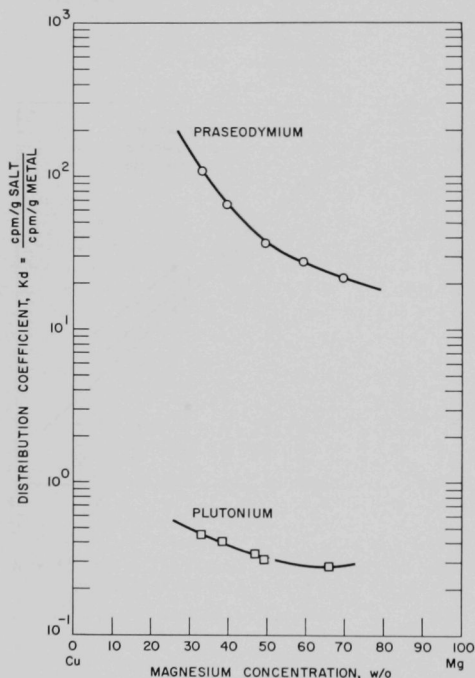
FIG. I-9. Distribution of Lanthanum between 30 m/o NaCl - 20 m/o KCl - 50 m/o MgCl<sub>2</sub> and Al-Mg Alloy.

Mixing Rate: 300 rpm  
Crucible: tantalum  
Atmosphere: argon

gested the possibility that this system might offer larger separation factors for a plutonium-rare earth separation than those available with Zn-Mg or Cd-Zn-Mg alloys. Therefore, the distribution behavior of plutonium between 30 m/o NaCl-20 m/o KCl-50 m/o MgCl<sub>2</sub> and Cu-Mg alloys was investigated. The liquid metal and molten salt were contained in a tantalum

crucible under an argon atmosphere at 600°C, and the system was stirred at a rate of 300 rpm. Individually determined distribution coefficient curves for praseodymium and plutonium are shown in Figure I-10. The separation factors (ratios of distribution coefficients) for praseodymium and plutonium are listed in Table I-9. These separation factors are approximately one order of magnitude larger than those obtained with the Zn-Mg or Cd-Zn-Mg alloys. The possibility of increasing the separation factors by decreasing the temperature and the magnesium concentration in the metal phase is being examined. Preliminary results from a codistribution experiment with plutonium and praseodymium show no significant difference from the data obtained with the single elements.

The higher separation factors obtained with the



108-8711

FIG. I-10. Distribution of Praeseodymium and Plutonium between 30 m/o NaCl-20 m/o KCl-50 m/o MgCl<sub>2</sub> and Cu-Mg Alloy.

Temperature: 600°C  
 Mixing Rate: 300 rpm  
 Crucible: tantalum  
 Atmosphere: argon

TABLE I-9. SEPARATION FACTORS FOR PLUTONIUM AND PRAESEODYMIUM BETWEEN 30 m/o NaCl-20 m/o KCl-50 m/o MgCl<sub>2</sub> AND Cu-Mg ALLOYS AT 600°C

Mg Concentration in Cu Alloy (w/o)	Separation Factor, S.F. = $\frac{Kd(Pr)}{Kd(Pu)}$
33	239
40	174
50	118
60	98
70	76

Cu-Mg system may permit an adequate removal of rare earth fission products from plutonium by a single-stage extraction with the molten salt. Alternatively, only a few stages would be needed for a high-decontamination rare earth-removal step, provided adequate phase separation methods are available.

(e) *Distribution of Yttrium and Californium Between LiCl-MgCl<sub>2</sub> and Zn-6 w/o Mg Alloy* (J. B. KNIGHTON, J. W. WALSH, J. D. SCHILB)

In order to determine the feasibility of a separation of rare earth fission products from californium, two distribution experiments were performed with LiCl-MgCl<sub>2</sub> salt mixtures and Zn-6 w/o Mg alloy. The proportions of LiCl and MgCl<sub>2</sub> were varied to show the effect of MgCl<sub>2</sub> concentration in the salt on the distribution coefficients. Yttrium, although not a rare earth metal, was used as a representative of the rare earth fission products, since it offers a somewhat more difficult separation.

The results, presented in Figure I-11, indicate that the optimum distribution coefficients for a californium-yttrium (or rare earth) separation are obtained with a MgCl<sub>2</sub> concentration between 10 and 20 m/o in the salt phase. Under these conditions, the separation factor is approximately 8.

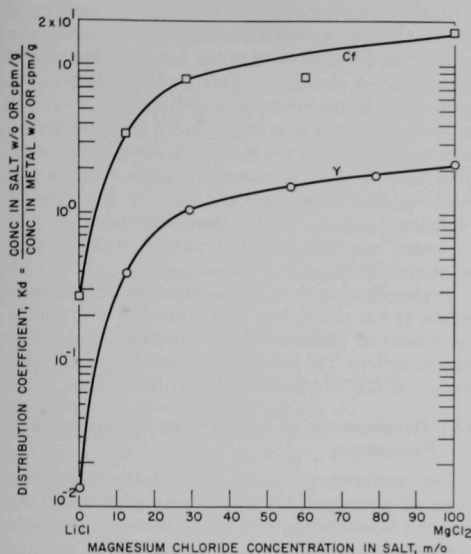
Although the californium-yttrium separation factor is rather small, it does suggest the possibility of rare earth fission product separations from transplutonium elements by multistage liquid metal-molten salt extraction.

### (3) Solubility of Uranium and Plutonium in the Ternary System, Cd-Mg-Zn (R. VON AMMON\*, J. B. KNIGHTON)

Determinations of the solubilities of uranium and plutonium in the ternary liquid alloy Cd-Mg-Zn were reported previously (ANL-6800, p. 94; ANL-6900, p. 65). Chemical analyses of a series of samples of the delta-phase U<sub>2</sub>Zn<sub>17</sub> that were isolated from quenched U-Cd-Mg-Zn alloys were also reported previously

\* Kernforschungszentrum, Karlsruhe, Germany.

(ANL-6900, Table I-6, p. 69). X-ray data have subsequently been obtained on these delta-phase samples to yield the results shown in Table I-10. There appears



108-5710

FIG. I-11. Distribution of Californium and Yttrium between Zn-6 w/o Mg and LiCl-MgCl<sub>2</sub>.

Temperature: 800°C  
 Mixing Rate: 300 rpm  
 Crucible: tantalum  
 Atmosphere: argon

TABLE I-10. LATTICE PARAMETERS OF THE U<sub>2</sub>Zn<sub>17</sub> DELTA PHASE AS A FUNCTION OF THE AMOUNT OF SUBSTITUTIONAL SOLUTION BY CADMIUM AND MAGNESIUM

Composition of Solvent (a/o)			Composition of Crystals (a/o)				Lattice Parameters (Å)		c/a	Volume of Elementary Cell (Å <sup>3</sup> )
Zn	Mg	Cd	U	Zn	Mg	Cd	a <sup>a</sup>	c <sup>b</sup>		
- U <sub>2</sub> Zn <sub>17</sub> -			10.53	89.47	0	0	8.9810	13.1610	1.4654	919.28
20	10	70	10.56	86.17	0.28	3.08	8.9998	13.1875	1.4652	924.92
6	20	74	10.35	85.90	0.30	3.46	9.0187	13.2181	1.4656	931.06
20	13	67	10.53	85.12	0.45 <sup>c</sup>	4.09 <sup>c</sup>	9.0204	13.2205	1.4656	931.60
20	20	60	10.52	84.00	1.13 <sup>d</sup>	4.20	9.0239	13.2296	1.4660	933.08
30	10	60	10.89	83.93	0.71 <sup>e</sup>	4.29 <sup>e</sup>	9.0215	13.2286	1.4664	932.40
7	16	77	10.32	84.39	0.32	4.97	9.0252	13.2226	1.4650	932.72
13	13	74	10.74	83.28	0.45	5.53	9.0306	13.2358	1.4657	934.78
10	10	80	10.27	81.84	0.58	7.31	9.0359	13.2423	1.4658	936.26
13	10	77	10.53	82.28	0.36 <sup>e</sup>	7.51 <sup>e</sup>	9.0345	13.2428	1.4658	936.05

<sup>a</sup> Error  $\pm 0.0002$  Å, based on 95% confidence limit.

<sup>b</sup> Error  $\pm 0.0005$  Å, based on 95% confidence limit.

<sup>c</sup> These values differ slightly from those reported in ANL-6900, Table I-6, p. 69, since the analyses have been repeated and corrected.

<sup>d</sup> Questionable value.

to be no definite correlation between substitution of cadmium for zinc within the hexagonal lattice of the delta-phase crystals and the cadmium concentration in the liquid metal solvent. A correlation is evident, however, between the cadmium content of the delta-phase crystals and their lattice parameters. Both the a and c parameters increased with increasing cadmium content, but the axial ratio c/a remained nearly constant.

#### (4) Stability of Plutonium in Cd-Zn-Mg Solutions Toward Container Materials (J. B. KNIGHTON, J. W. WALSH)

Cadmium-magnesium-zinc alloys are being investigated as liquid metal solvents for the reprocessing of fast breeder reactor fuels (ANL-6900, p. 65). Experiments have been conducted on the stability of metallic plutonium solutions in 70 a/o Cd-15 a/o Mg-15 a/o Zn toward the following materials: (1) type 304 stainless steel, (2) 1020 mild steel, (3) type 405 stainless steel, and (4) Croloy-2¼. Solutions of plutonium in the Cd-Mg-Zn alloy were held in contact with 30 m/o NaCl-20 m/o KCl-50 m/o MgCl<sub>2</sub> for 100 hr at 600°C in crucibles fabricated from each of the four materials. Filtered samples of the metal solution were withdrawn after 1, 4, 25, 50, 75, and 100 hr. Filtered salt samples were taken after 25, 50, 75, and 100 hr.

Analytical results from the tests with type 304 stainless steel, 1020 mild steel, and type 405 stainless steel are presented in Table I-11. Final results from the test with Croloy-2¼ are not yet available. In the three container materials tested, the plutonium, magnesium, and zinc concentrations remained constant

TABLE I-11. STABILITY OF PLUTONIUM SOLUTION IN Cd-Mg-Zn ALLOY CONTAINED IN THREE TYPES OF STEEL CONTAINER MATERIALS

Liquid Metal Phase:	Cd 70 a/o (85.4 w/o)
	Mg 15 a/o (4.0 w/o)
	Zn 15 a/o (10.6 w/o)
Molten Salt Phase:	NaCl 30 m/o (21.9 w/o)
	KCl 20 m/o (18.6 w/o)
	MgCl <sub>2</sub> 50 m/o (59.5 w/o)
Temperature:	600°C
Mixing Rate:	200 rpm
Atmosphere:	Argon
Weight of Pu Charged:	Expt. 1 (type 304 stainless steel) 3.7 g
	Expt. 2 (1020 steel) 3.1 g
	Expt. 3 (type 405 stainless steel) 3.0 g

Time (hr)	Concentration in Metal (w/o)			Concentration in Salt (w/o)	Distribution Coefficient, $K_d(\text{Pu})^a$
	Mg	Zn	Pu	Pu	
Expt. 1: type 304 stainless steel					
0 (nominal)	3.97	10.6	0.613	—	—
1	3.94	11.4	0.584	—	—
4	3.89	11.2	0.582	—	—
25	3.85	11.6	0.586	0.0236	$4.03 \times 10^{-2}$
50	3.91	11.2	0.576	0.0244	$4.23 \times 10^{-2}$
75	3.85	11.7	0.583	0.0252	$4.33 \times 10^{-2}$
100	3.85	11.4	0.579	0.0256 <sup>b</sup>	$4.43 \times 10^{-2}$
Expt. 2: 1020 mild steel					
0 (nominal)	3.97	10.6	0.513	—	—
1	3.91	11.0	0.329	—	—
4	3.97	—	0.327	—	—
25	3.91	—	0.333	0.0130	$3.99 \times 10^{-2}$
50	3.81	—	0.320	0.0124	$3.89 \times 10^{-2}$
75	3.97	—	0.327	0.0138	$4.22 \times 10^{-2}$
100	3.97	10.6	0.327	0.0132 <sup>b</sup>	$4.05 \times 10^{-2}$
Expt. 3: type 405 stainless steel					
0 (nominal)	3.97	10.6	0.498	—	—
1	3.94	11.3	0.492	—	—
4	3.96	—	0.513	—	—
25	3.90	—	0.497	0.0211	$4.24 \times 10^{-2}$
50	3.95	—	0.502	0.0120 <sup>c</sup>	$3.89 \times 10^{-2}$
75	3.85	—	0.485	0.0193	$3.98 \times 10^{-2}$
100	3.92	11.4	0.482	0.0205 <sup>b</sup>	$4.25 \times 10^{-2}$

$$^a K_d(\text{Pu}) = \frac{\text{w/o Pu in salt}}{\text{w/o Pu in metal}}$$

<sup>b</sup> Plutonium material balances as follows: Expt. 1, 96.8%; Expt. 2, 65%; Expt. 3, 98.7%.

<sup>c</sup> Questionable value.

throughout the period between 1 and 100 hr. Plutonium material balances based on the amount of plutonium added initially, however, were 96.8% for the type 304

stainless steel, 65% for 1020 steel, and 98.7% for type 405 stainless steel.

The low plutonium material balance obtained with 1020 steel, together with the subsequent constancy of the plutonium concentration, suggests that some form of reaction occurred early in the run removing part of the dissolved plutonium. This result indicates that 1020 steel is probably an unsatisfactory container material. The data also imply that a small plutonium loss might have occurred in the type 304 stainless steel. The 98.7% plutonium material balance for type 405 stainless steel indicates that little, if any, loss of plutonium occurred under these conditions. Of the container materials tested, type 405 stainless steel seems to offer the most promise.

During the course of the solution stability experiments, it was convenient to measure the distribution coefficients of plutonium in the molten chloride/Cd-Mg-Zn system. The distribution coefficient of the plutonium at 600°C remained essentially constant.

### (5) Development of Engineering Equipment and Procedures

The engineering feasibility of continuous pyrochemical procedures for the recovery of nuclear fuels is being investigated. Continuous processes generally require less space and less direct manipulation than batch processes. These advantages may be especially important in shielded facilities where space is expensive and any handling of the equipment must be done remotely.

The initial objective of this program is the construction and operation of a countercurrent packed extraction column in which the two solvent phases will be a cadmium-base metal alloy and a low melting mixture of 50 m/o MgCl<sub>2</sub>, 30 m/o NaCl, and 20 m/o KCl. Uranium and rare earths will be the distributing solutes. A twofold purpose will be served by this study: (1) to demonstrate the performance of various components of the equipment, such as valves, pumps, and flowmeters, and (2) to determine the capability of an extraction column to extract and separate actinides and rare earths which are required for any flow process.

#### (a) Design of Metal-Salt Extraction Equipment and Components

##### High Temperature Extraction Facility

(T. R. JOHNSON, V. G. TRICE)

A conceptual design has been made of a prototype extraction facility which will be placed in the resistance furnace previously used for the cadmium distilla-

tion unit (ANL-6800, p. 127). This facility consists of: a 1-in. dia., 18-in. long packed column, four tanks to hold the salt and metal feeds for the column and to contain the effluents from the column, constant-head tanks to control feed rates to the column, and centrifugal pumps to circulate the fluids. Valves, flowmeters, liquid level detectors, and column interface controllers are also required. Construction drawings of the feed tank, pump, and constant-head tank for the metal phase have been completed. However, construction of the high temperature extraction facility awaits getting additional information about the corrosion resistance of materials of construction (as is described below) and the mass transfer rate between salt and metal. Meanwhile, development of other components for high-temperature service is continuing.

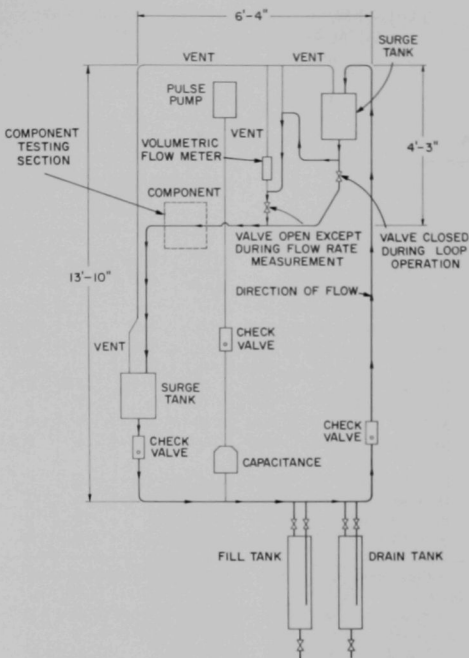
### Engineering Test Loop

(W. J. WALSH, V. G. TRICE, L. F. DORSEY)

A facility has been constructed for the purpose of testing components for eventual use in the high temperature extraction unit. A drawing of the test loop is shown in Figure I-12. Liquid metal or salt is circulated by a pulse pump from the lower surge tank to the upper tank. The liquid flows by gravity from the upper tank into the lower tank to complete the circuit. The two bottom tanks (fill tank and drain tank) are used only in filling or draining the system. The facility was designed to allow isothermal operation at temperatures ranging from 450 to 650°C, using resistance heaters thermally bonded to the pipe with Thermon T-63\* over the entire loop. The temperature is controlled automatically using 30 variable transformers, 57 thermocouples, and 14 temperature controllers. The loop has been designed to allow the insertion of various items of equipment to test their performance in liquid metal and molten salt use. Construction of the facility has been nearly completed. Initial runs have been started with the piping empty to determine the heater voltage settings that will produce isothermal conditions around the loop.

The first high temperature test with the system filled with liquid will involve the circulation of a 50 m/o  $MgCl_2$ -30 m/o  $NaCl$ -20 m/o  $KCl$  ternary salt (m.p., 396°C) to determine the reliability of the heating technique, various valves, a flowmeter, and a pulse pump. Construction has begun on a 4-ft (1-in. dia.) prototype packed column to be installed in the loop for the contacting of countercurrent streams of metal and salt. The purpose of this test is to demon-

\* Manufactured by Thermon Manufacturing Company, Houston, Texas.



108-8102 Rev.

FIG. I-12. Engineering Test Loop.

strate the removal of rare earths from a cadmium-base alloy on a large scale (50 to 100 lb alloy treated) using fused salt extraction.

### Corrosion Testing

(M. L. KYLE, W. PEHL)

*Corrosion of Ferrous Alloys by Molten Metal-Halide Flux Systems.* A cadmium-magnesium-zinc solution and a molten halide flux are the two phases which will be contacted in the continuous countercurrent extraction column of the High Temperature Extraction Facility. Since little corrosion information is available on a system of this type, a corrosion program has been initiated to evaluate various materials of construction for use in this system.

Corrosion of four ferrous alloys†—types 304 and

† Nominal alloy compositions (w/o) as follows:

Alloy	Fe	Ni	Cr	C	Mn	Other
1019 Carbon Steel	98+	—	—	0.19	0.85	0.09
Croloy 2¼	95+	—	2.25	0.15	0.45	1.6
304 SS	66+	8-11	18-20	0.08	2.0	1.1
405 SS	82+	—	11-15	0.08	1.0	1.4

TABLE I-12. CORROSION OF FERROUS ALLOYS BY  
 Cd-Mg-Zn-U/CHLORIDE FLUX SYSTEMS

 Time of each test: 200 hr  
 Static conditions  
 Flux\*: 35 m/o NaCl  
 25 m/o LiCl  
 40 m/o MgCl<sub>2</sub>

Metal Phase (w/o)				Temp (°C)	Maximum Observed Depth of Corrosion (mils)			
Zn	Mg	Cd	U		1019 Carbon Steel <sup>b</sup>	Croloy 2¼ <sup>c</sup>	304 SS <sup>c</sup>	405 SS <sup>c</sup>
0	80	20	0	600	2	0.4	1	<0.1
0	60	40	0	600	—	0.4	0.4	<0.1
0	40	60	0	600	<0.1	0.6	—	<0.1
15	10	72	3	600	0.4	0.4	2.5	0.4
15	15	67	3	600	<0.1	2	2	2
20	10	69	1	600	2	1	4	2
10	15	74	1	600	>2	0.5	5	0.5
15	10	72	3	650	1	2	5	0.5
15	15	67	3	650	2	1	6	2
20	10	69	1	650	>2	2	>12	2
10	15	74	1	650	>2	1	>8	4

\* Flux dried by liquation in an argon atmosphere at 600°C for 1 hr.

<sup>b</sup> Specimens were 4 mils thick. Values reported as >2 indicate corrosion across entire specimen thickness.

<sup>c</sup> Nominal thickness—30 mils.

405 stainless steel, type 2¼ Croloy, and type 1019 carbon steel—by the Cd-Mg-Zn-U/halide flux system has been investigated. Seven metal phase compositions were used. Prior to being charged, the salt was dried by liquation at 600°C for 1 hr under a flowing argon atmosphere. The flux composition (Table I-12) was selected before a decision was made to use a salt consisting of 50 m/o MgCl<sub>2</sub>, 30 m/o NaCl, and 20 m/o KCl in the prototype extraction facility. Corrosion characteristics of the two salts are not expected to be very different, but corrosion by the salt will have to be measured. The halide flux chosen for this work was 35 m/o NaCl-25 m/o LiCl-40 m/o MgCl<sub>2</sub> (m.p. about 475°C). The tests were conducted under static conditions at 600 and 650°C for 200 hr.

Results obtained in the corrosion tests are shown in Table I-12. Both type 1019 carbon steel and 304 stainless steel were attacked to a greater extent than either Croloy 2¼ or 405 stainless steel. Attack in the case of the 1019 carbon steel was mostly by embrittlement with corrosion rates increasing with increase in temperature. The effect of zinc concentration could not be determined because of the small number of samples tested. In the case of the type 304 stainless

steel, metallographic examination indicated extensive nickel leaching by all liquid metals containing zinc. Previous experience has shown that the water content of the flux plays a major role in determining corrosion rates, and it is suspected that a more efficient salt drying system could probably reduce these corrosion rates somewhat. However, the tests show that a nickel-containing steel cannot be used.

Preliminary tests were subsequently made at 650°C for 200 hr to test further the corrosion resistance of type 405 stainless steel to a system with a metal phase composed of 81.4 w/o Cd-5.4 w/o Mg-10.9 w/o Zn-2.3 w/o U and a flux phase of 50 m/o MgCl<sub>2</sub>-30 m/o NaCl-20 m/o KCl. This metal-salt system was chosen as an approximation to the probable system for use in the high temperature extraction facility now being designed (previously discussed, this section). These tests were conducted by fabricating the specimens into agitator blades rotating in the solvent media. One specimen was located in each of the liquid phases, one at the metal-salt interface, and one in the vapor phase. An alumina crucible was used in these tests. In the first of these tests, made with salt previously exposed to the atmosphere for about 1 hr, the coupons in the metal phase and near the interface showed little corrosion while the coupons in the salt and vapor phases were corroded and embrittled, especially the one in the vapor phase.\* Because it was suspected that the salt had taken up water in the 1-hr exposure to air, a second test was made with salt flux purified by contacting it with Cd-Mg metal and filtering to remove oxide impurities. Use of this salt (which contained 0.13 w/o oxygen\*\*) in the subsequent test reduced the corrosion rate of the vapor phase specimen to less than 1 mil in 200 hr. It is evident that the water content of the salt flux greatly influences the corrosiveness of the flux on ferrous alloys. All future runs will be conducted with purified salt which will be handled only in dry argon or helium atmospheres.

*Oxidation Rates of 405 Stainless Steel and Croloy 2¼.* The High Temperature Extraction Facility now being designed is expected to operate in air at temperatures near 600°C. Tests have been performed to evaluate the oxidation resistance of two promising materials of construction, type 405 stainless steel and Croloy 2¼. For these tests, the sample metal was heated in air for 200 hr at 600°C for Croloy 2¼ and at 650°C for 405 stainless steel. After 200 hr, the specimens were

\* Measured corrosion as follows:

In vapor phase: >5 mils  
 In salt phase: >2 mils

Near interface: >2 mils  
 In metal phase: 1 mil

\*\* Determined by fluorination with BrF<sub>3</sub> and analysis of evolved noncondensable gases for oxygen.

TABLE I-13. OXIDATION RATES OF TYPE 405 SS AND CROLOY 2¼

Air exposure of ¼-in. plate. Values presented are averages for 8 samples.

Metal	Temperature (°C)	Weight Change (mg/cm <sup>2</sup> )	
		200-hr Exposure	400-hr Exposure
405 SS	650	+0.10	+0.10
Croloy 2¼	600	+43.0	+54.0

cooled, and the amount of oxidation determined by weighing the specimens. The samples were then reheated for an additional 200 hr under identical conditions to determine if the oxide film previously formed would significantly limit further oxidation. Data obtained are shown in Table I-13. Type 405 stainless steel oxidized slightly in the first 200-hr period with no significant additional oxide formed during the additional 200 hr. Croloy 2¼ oxidized significantly during the first 200 hr, and although the rate was substantially less during the second 200 hr, significant oxidation rates still prevailed.

Based on the superior air oxidation resistance of type 405 stainless steel and its good corrosion resistance to process solutions (molten metal and salt), type 405 stainless steel has been selected as the material of construction for the High Temperature Extraction Facility.

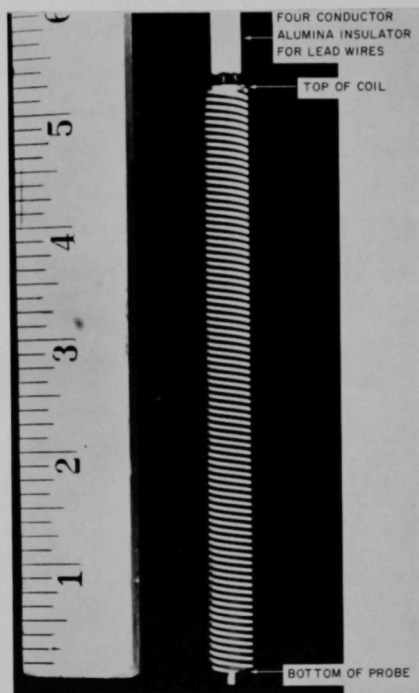
#### Eddy Current Induction Probe for Liquid Level Measurements

(T. R. JOHNSON, F. G. TEATS)

An accurate and reliable method of measuring the depth of liquid metals is required for continuous processes and is desirable for the batch processes currently being developed for the EBR-II Skull Recovery Process. The development of an eddy current induction probe to measure levels of liquid metals and to detect the interface between metals and salts is nearly complete. The probe consists of a bifilar winding of nichrome wire placed around an alumina form and encased in a corrosion-resistant well which extends into the liquid. When a high-frequency voltage is applied to one coil, the voltage induced in the second coil is sensitive to the presence of an electrical conductor in the medium surrounding the coil, and therefore, to the extent that the coil is surrounded by liquid metal. When there is liquid metal around the coil well, the induced voltage is reduced as a result of the eddy currents induced in the liquid metal. The relation of

the reduction of induced voltage to liquid metal depth may be determined by calibration for each liquid metal. The probe, its mode of operation, and the circuit diagram are presented in ANL-6800, p. 118.

The work reported earlier was performed using a probe consisting of dual wound coils of nichrome wire wrapped around an alumina rod and insulated by means of a ceramic adhesive. The tendency of this adhesive at high temperatures to lose its insulating properties and to flake away, exposing the coils, made this type of probe unreliable. To avoid the use of any adhesive, an alumina form having helical grooves was fabricated. The wires were wound in the grooves to insulate them and to insure uniform coil spacing (see Figure I-13). One such probe has given reproducible readings (maximum deviation equivalent to  $\pm 1/8$  in. of cadmium) over a three-month period. During this time, it was at temperatures above 350°C for more than 300 hr and was cycled between 700°C and room



108-7898A

FIG. I-13. Sensing Coil of Eddy Current Liquid Level Probe. (Primary and secondary coils of nichrome wire wound on an alumina form.)

temperature at least thirty times. This probe had a maximum drift of 0.05 mv (equivalent to  $\frac{1}{32}$  in. of cadmium) when it was held at 450°C for 16 hr. The drift caused by shutting-down and restarting was 0.2 mv which is equivalent to  $\pm\frac{1}{8}$  in. It is felt that this reproducibility will be acceptable for most applications.

Typical calibration data are shown in Figure I-14. The eddy current probe was placed in a stainless steel well (0.032-in. wall) with the bottom of the well resting on the bottom of the stainless steel crucible. The position of the probe was kept constant, since the location of the crucible bottom with respect to the coil was found to influence the output signal slightly. The depth of liquid metal was changed by adding increments of cadmium. To calibrate the eddy current probe, the metal-gas interface was located with a movable resistance probe.

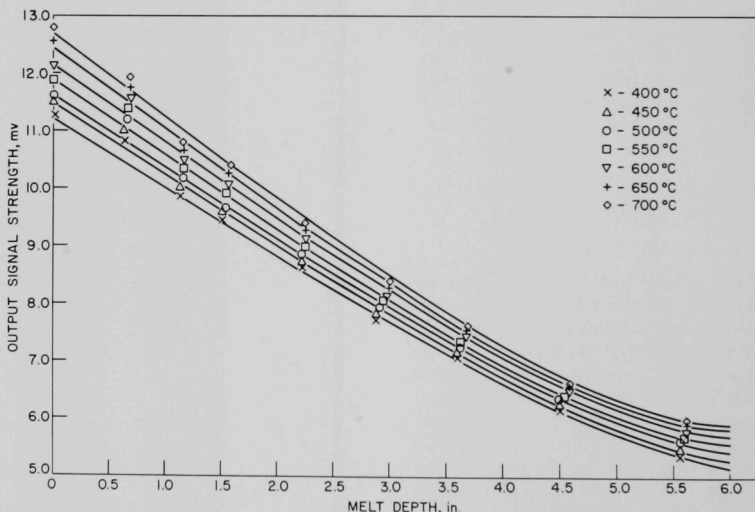
The central portions of the curves in Figure I-14 are nearly straight lines. As would be expected, there is some curvature in those portions of the curves representing melt depths for which the metal-gas interface is near the end of the coil. In this set of calibrations,

a melt depth of  $5\frac{1}{4}$  in. coincided with the top of the winding.

The signal strength was a function of temperature because the resistances of the nichrome wire, the well, and the liquid metal changed with temperature. This temperature effect had a negligible dependence on the melt depth and could be conveniently corrected by changing the bias voltage, as shown in Figure I-15, to make the isotherms of Figure I-14 coincide with a 625°C curve. The bias voltage was subtracted from the output signal to shift it to values which could be conveniently recorded.

The high frequency coils were relatively insensitive to the geometry of the surroundings, because of the small depth of penetration of the induced eddy currents. For materials having resistivities of the order of 10 to 100  $\mu\text{ohm-cm}$ , the calculated effective depth of penetration is less than  $\frac{3}{8}$  in. if the input frequency is 50 kc. Stainless steel crucibles having inside diameters greater than  $1\frac{1}{2}$  in. had no detectable effect on the output signal. Therefore, a probe calibration made in one geometry should be applicable to other situations.

The presence of a molten salt, composed of either



108-8707

FIG. I-14. Effect of Melt Depth on Output Signal of Eddy Current Liquid Level Probe.

Input Frequency: 50,000 cps  
 Input Voltage: 7.0 volts  
 Bias Voltage: 4.64 mv  
 Crucible: 304 S.S.  
 10-in. high by  $5\frac{5}{8}$ -in. ID  
 Liquid Metal: Cd  
 Length of Winding: 5 in.

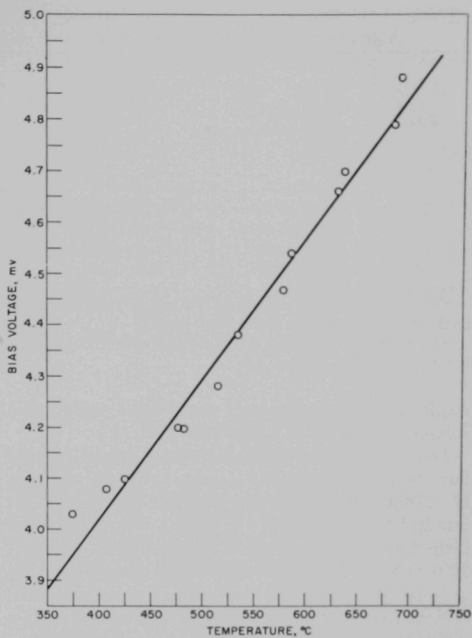
50 m/o  $MgCl_2$ -30 m/o  $NaCl$ -20 m/o  $KCl$  or 50 m/o  $MgCl_2$ -50 m/o  $CaCl_2$ , had no detectable effect on the output signal. In a two-phase system, the salt-metal interface could be detected, but the depth of the molten salt could not be measured with the present arrangement. It should be possible to detect the salt level if the equipment is changed by using (1) a protection well having a resistivity higher than that of the molten salt, (2) a larger input voltage, and (3) a higher frequency signal.

For the measurement of liquid levels in systems containing volatile, corrosive molten metals, the eddy current induction probe has proved to be superior to any other types of liquid level instruments which could be used at high temperatures. The induction probe has been reliable and its reproducibility and accuracy are adequate for most applications. The instrument should be easily adaptable to remotely operated high-temperature equipment since there are no moving parts. Future work will be directed toward the application of the instrument to specific process equipment.

(b) *Preliminary Extraction Studies* (T. R. JOHNSON, W. J. WALSH, F. G. TEATS, K. R. TOBIAS)

Attempts are being made to measure the rate of transfer of uranium and rare earths between chloride salts and cadmium-base alloys. This information will then be used to predict the performance of counter-current liquid-liquid extraction columns and to judge the feasibility of using columns to separate actinides from rare earths. Other investigations using similar liquid metal-salt systems have shown that the mass transfer rate is reasonably rapid. Studies have been made at Brookhaven of the transfer of a rare earth solute from single drops of metal into salt<sup>2</sup> and in counter-current extraction columns.<sup>3</sup> A metal phase of bismuth-magnesium and a salt phase consisting of 50 m/o  $MgCl_2$ , 30 m/o  $NaCl$ , and 20 m/o  $KCl$  were used in these studies. The reported results indicate that published mass transfer coefficients for aqueous-organic systems based on the two-film theory<sup>4</sup> yield reasonable approximations of mass transfer rates in metal-salt systems and support the hypothesis that a packed extraction column is practical for cadmium-base alloy systems, although it is not possible to predict reliably the performance of a column.

Preliminary results suggest that good agitation of the metal phase will be required if practical extraction rates are to be achieved. In most process applications



108-8702

FIG. I-15. Bias Voltage Settings for Eddy-Current Level Probe. (Bias voltages required to make output signal strengths from 400 to 700°C coincident with the output signal strengths at 625°C with the eddy current probe immersed in cadmium from 0 to 5.5 in.)

Basic

Output Signal:	Independent of temperature
Crucible:	Stainless steel, 5½-in. ID
Well:	Stainless steel, 30-mil wall

envisioned for metal-salt columns, the metal will be the discontinuous phase. In ordinary situations, the discontinuous phase would be expected to be less turbulent than the continuous phase. However, motion pictures of a packed column in which Wood's metal (50 w/o bismuth, 27 w/o lead, 13 w/o tin, and 10 w/o cadmium, melting point, 70°C) was passed counter-currently to water at 90°C have shown that there was a high degree of turbulence in the discontinuous phase owing to the pools of metal being struck by falling metal droplets. The metal tended to collect in pools at specific sites in the packing. When struck by drops, the pools tended to vibrate and break into smaller droplets which then fell to pools below. It would thus appear that a high degree of agitation in the falling drops resulted from their mode of formation. These

<sup>2</sup> Katz, H. M., Hill, F. B. and Speirs, J. L., *Trans. Met. Soc. AIME* **218**, 770 (October 1960).

<sup>3</sup> Hill, F. B. and Kukačka, L. E., Jr., *BNL-791*, January 1963.

<sup>4</sup> Handlos, A. E. and Baron, T., *A. I. Ch. E. J.* **3**: 129 (1957).

TABLE I-14. DYNAMIC EXTRACTIONS OF URANIUM BETWEEN MOLTEN HALIDE SALT AND CADMIUM-MAGNESIUM ALLOYS  
*Molten Cd-Mg alloy poured into a packed column containing molten 50 m/o MgCl<sub>2</sub>-30 m/o NaCl-20 m/o KCl salt*

Run	Direction of U Extraction	Packing	Temperature (°C)	Final Composition			Calc. Equilib. Salt Conc.
				Metal		Salt	
				Mg (w/o)	U (w/o)	U (w/o)	U (w/o)
1 <sup>a</sup>	Metal to Salt	1/8-in. dia. quartz spheres	450-500	3.7	0.51	0.014	0.02
2 <sup>a</sup>	Metal to Salt	1/4-in. dia. quartz cylinders	630	3.2	0.45	0.090	0.063
3 <sup>a</sup>	Metal to Salt	1/8-in. dia. SS spheres	600	3.6	0.42	0.069	0.042
4 <sup>b</sup>	Salt to Metal	SS rings	550	4.8	0.156	0.032	0.010

<sup>a</sup> Extraction column was a 1-in. OD quartz tube with a packing depth of 5 1/2 in. Initial metal composition essentially equal to final metal compositions; initial Salt: no U.

<sup>b</sup> Extraction column was a 1-in. OD SS tube with a packing depth of 11 in. Initial metal composition: Cd-4.85 w/o Mg—no U; initial Salt: 1.41 w/o U.

results and a description of the Wood's metal-water column were given in ANL-6900, p. 81.

Four preliminary high-temperature extraction runs have been made in order to estimate the transfer rate of uranium in a countercurrent packed column. Two hundred fifty g of Cd-3 w/o Mg-0.5 w/o U alloy was poured into a static column of molten 50 m/o MgCl<sub>2</sub>-30 m/o NaCl-20 m/o KCl salt which was contained in a 7/8-in. ID quartz tube in each of three runs. The central 6-in. section of the tube was loaded with a different packing (Table I-14) in each run. When most of the metal had fallen through the packing and collected in the bottom of the tube, the tube was cooled rapidly to minimize transfer across the metal-salt interface at the bottom. The metal was in contact with molten salt for two to five minutes. The final uranium concentrations in the salt and metal were determined by dissolving each entire phase separately. In a similar run, 380 g of salt containing 7.7 g of UCl<sub>3</sub> was charged to a stainless steel column packed with wire rings. The tube was then heated to 550°C, and about 800 g of a Cd-4.8 w/o Mg alloy was transferred from a second container into the top of the packed section. When all of the metal had been transferred (~5 min), the extraction column was cooled as rapidly as possible. For analysis, the salt phase was completely dissolved in water and drillings were taken of the metal that had fallen through the packing.

The conditions and results of these four runs are summarized in Table I-14. The amount of uranium required to saturate the salt phase at equilibrium is negligible with respect to the uranium charged initially. The best performance attainable by these transient columns would be to saturate the salt with respect to the uranium in the metal. In the three runs in which uranium was charged in the metal phase, the salt approximately reached equilibrium. The salt con-

centration appeared to exceed equilibrium in runs 2 and 3. This may have been caused by inaccuracies in measuring the uranium content of the salt or the temperature during the extraction, or by oxidizing impurities in the salt. In the last run, a large amount of uranium was transferred from the salt into the metal and the final uranium concentration in the salt approached equilibrium. However, the uranium material balance was poor in run 4. These experimental results are encouraging, but the experiments will be refined before any quantitative conclusions are made.

### c. SUPPORTING CHEMICAL INVESTIGATIONS (L. BURRIS, R. K. STEUNENBERG)

Supporting chemical studies of liquid metals and molten salts are being pursued to supply data of process importance and to elucidate the chemical aspects of various process steps. During the reporting period, this work has been devoted principally to determinations of pertinent phase diagrams, to salt purification studies, and to the possibility of performing ion exchange separations in molten salt solutions.

#### (1) Liquidus Temperatures of the System LiCl-KCl-MgCl<sub>2</sub> (N. R. CHELLEW, J. T. FEENEY)

The molten salt systems LiCl-NaCl-MgCl<sub>2</sub> and LiCl-KCl-MgCl<sub>2</sub> appear promising for the extraction of rare earth fission products from liquid metal solutions of uranium and plutonium. In order to select temperatures and suitable salt compositions for process use, it is necessary to know the liquidus temperatures as a function of composition. The LiCl-NaCl-MgCl<sub>2</sub> system was investigated initially and a diagram of its liquidus surface was presented in the above report (ANL-6900, p. 90). Measurements have since been made to determine the melting points of various compositions of the LiCl-KCl-MgCl<sub>2</sub> system, since no

TABLE I-15. LIQUIDUS TEMPERATURES FOR THE SYSTEM LiCl-KCl-MgCl<sub>2</sub>

Section I Starting Mixture (m/o) MgCl <sub>2</sub> -89.6 LiCl-10.4		Section II Starting Mixture (m/o) MgCl <sub>2</sub> -79.8 LiCl-20.2		Section III Starting Mixture (m/o) MgCl <sub>2</sub> -69.2 LiCl-30.8		Section IV Starting Mixture (m/o) MgCl <sub>2</sub> -60.2 LiCl-39.8		Section V Starting Mixture (m/o) MgCl <sub>2</sub> -50.0 LiCl-50.0		Section VI Starting Mixture (m/o) MgCl <sub>2</sub> -39.9 LiCl-60.1		Section VII Starting Mixture (m/o) MgCl <sub>2</sub> -19.9 LiCl-80.1	
KCl (m/o)	Temp. (°C)	KCl (m/o)	Temp. (°C)	KCl (m/o)	Temp. (°C)	KCl (m/o)	Temp. (°C)	KCl (m/o)	Temp. (°C)	KCl (m/o)	Temp. (°C)	KCl (m/o)	Temp. (°C)
0	688	0	670	0	644	0	619	0	600	0	591	0	597
19.7	613	17.5	591	9.2	604	7.8	582	20.2	498	7.9	564	10.0	556
33.9	455	26.0	528	17.5	552	14.5	540	30.1	426	19.0	500	20.1	503
43.2	472	32.1	440	25.0	484	21.8	489	39.7	392	30.2	425	29.8	447
50.7	469	41.2	457	31.4	431	29.5	424	48.0	376	38.3	384	35.8	411
60.7	429	48.6	446	37.2	440	36.8	420	54.0	372	46.0	351	41.7	359
71.5	502	58.0	417	46.5	434	45.1	404	60.0	401	54.9	367	49.7	341
		63.2	412	53.0	408	54.8	385	70.1	560	63.0	480	55.0	433
		67.2	442	57.8	401	67.0	489			70.0	544	60.2	501
		70.2	498	65.2	437					71.3	566	64.5	542
		79.6	636	75.2	509							69.7	604
				85.0	692							74.9	639
												84.9	704

information on the liquidus temperatures of this ternary system was found in the literature.

Reagent grade KCl and LiCl, and anhydrous MgCl<sub>2</sub> were used to prepare the salt mixtures. The MgCl<sub>2</sub> was purified by vacuum sublimation. The LiCl was purified by a method similar to that described by Maricle and Hume,<sup>5</sup> in which chlorine was passed through the molten salt. The KCl was heated to about 825°C and cast into rods.

Conventional thermal analysis techniques were used. The liquidus temperatures were measured with a stainless steel-sheathed chromel-alumel thermocouple immersed in the salt. The apparatus was calibrated with standard reference materials: recrystallized NaCl, m.p. 800.4°C, and National Bureau of Standards lead, m.p. 327.4°C. The precision of the temperature measurements was ±1°C.

The liquidus temperature data were taken along composition lines radiating from the KCl corner of the ternary system. Accurately weighed amounts of KCl were added incrementally to a fixed ratio of MgCl<sub>2</sub>:LiCl. The salts were kept under a helium atmosphere and were not exposed to air until the thermal analysis measurements had been completed.

Melting point data for compositions along seven lines radiating from the KCl corner of the diagram are given in Table I-15. A diagram of liquidus isotherms for the ternary system (Figure I-16) was constructed from quasi-binary diagrams in which KCl was one component and the second component was the initial mixture of MgCl<sub>2</sub> and LiCl to which the KCl was

added. Liquidus temperatures for the isothermal intersections at the edges of the ternary diagram were obtained from literature data on the binary systems, LiCl-MgCl<sub>2</sub> (ANL-6596, p. 78), LiCl-KCl,<sup>6</sup> and KCl-MgCl<sub>2</sub>.<sup>7</sup>

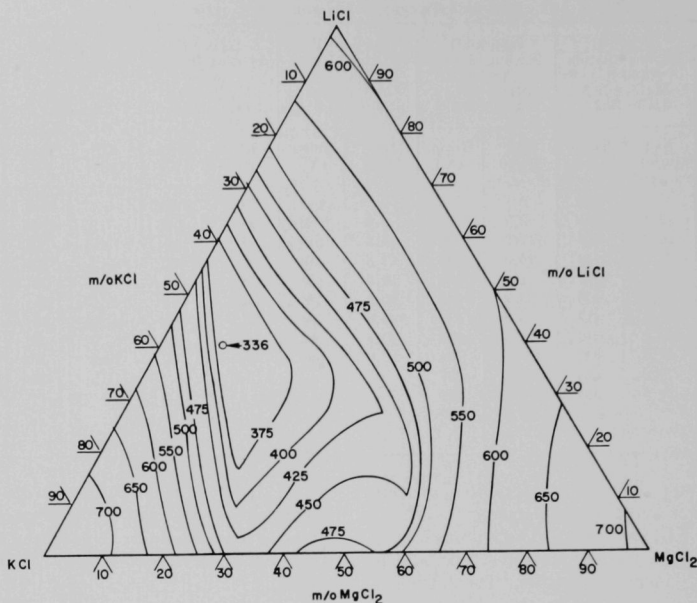
In general, the ternary diagram shows that liquidus temperatures below 500°C exist in a wide belt of compositions extending from 29 to 60 m/o MgCl<sub>2</sub> on the KCl-MgCl<sub>2</sub> edge of the diagram to 23 to 55 m/o KCl on the LiCl-KCl edge. The minimum liquidus temperature in the ternary system, 336°C, lies at about 40 m/o LiCl, 50 m/o KCl, and 10 m/o MgCl<sub>2</sub>.

A discussion of the selection of a molten salt system for process use appeared previously in ANL-6596, p. 64 and ANL-6648, p. 46. For systems consisting of MgCl<sub>2</sub> diluted with two alkali metal chlorides, the compositions most useful for the separation of fission products from uranium and plutonium are those which have (a) a high MgCl<sub>2</sub> content, and (b) a larger proportion of the alkali chloride diluent with lower molecular weight (LiCl in this case). A liquidus temperature below 500°C is also desirable. Figure I-16 indicates that LiCl-KCl-50 m/o MgCl<sub>2</sub> mixtures containing up to 28 m/o LiCl can exist completely molten at temperatures of 500°C and lower. By comparison, when NaCl is substituted for KCl in the above system, the maximum amount of LiCl which can be added so that the mixture can still exist completely molten at temperatures of 500°C and lower is reduced to 13 m/o.

<sup>5</sup> S. D. Gromakov and L. M. Gromakova, Zh. Fiz. Khim. **27**, 1545 (1953).

<sup>7</sup> A. I. Ivanov, Sbornik Statef Obschei Khim., Akad. Nauk SSSR **1**, 754 (1953).

<sup>5</sup> D. L. Maricle and D. N. Hume, J. Electrochem. Soc. **107**, 354 (1960).



108-8104

FIG. 1-16. Liquidus Isotherms in the System  $\text{LiCl-KCl-MgCl}_2$ . (Temperatures in  $^{\circ}\text{C}$ .)

Thus, substitution of  $\text{KCl}$  for  $\text{NaCl}$  in the ternary mixture permits lower processing temperatures to be used with melts containing relatively high  $\text{MgCl}_2$  and  $\text{LiCl}$  concentrations.

## (2) Liquid Immiscibility in the System Pu-Mg (J. D. SCHILB, R. K. STEUNENBERG)

The binary system Pu-Mg is of interest in the processing of plutonium-bearing reactor fuels in liquid metal solvents that contain magnesium, as in the EBR-II blanket process (ANL-6875, p. 23). It has been reported<sup>8</sup> that a region of liquid immiscibility exists in the Pu-Mg phase diagram, but the immiscibility curve has not been determined experimentally. The liquidus curves outside the immiscibility region are also considered to be tentative. The purpose of the present study is to define the immiscibility curve and the liquidus curves in the Pu-Mg system. Although this information is of considerable process interest, it should also be useful for extending thermodynamic correlations of the activity coefficients of plutonium and magnesium in the binary system to high temperatures. See discussion in Section IA2b(2) (a).

<sup>8</sup> F. W. Schonfeld and F. H. Ellinger, *Binary Alloys of Plutonium*, LADC-2656, 1956.

The equipment and technique used in the initial investigation of the immiscibility curve of the Pu-Mg system were developed by using the Pb-Zn system as a stand-in. Experimental results for the immiscibility curve obtained with the Pb-Zn system showed good agreement with the information in the literature.<sup>9</sup> The apparatus consisted of a 1¼-in. dia. by 3-in. deep cylindrical tantalum crucible which, after being loaded with a Pu-60 a/o Mg alloy, was heated under an argon atmosphere in a resistance-heated, stainless steel tube furnace. Melt temperatures were measured by means of two chromel-alumel thermocouples protected by tantalum thermocouple wells that were immersed in the melt. The individual liquid phases were sampled simultaneously using ¼-in. dia. tantalum tubes which were welded shut and tapped at the top and fitted with tantalum filter frits pressed into the bottom. These sample tubes were attached to threaded stainless steel rods and inserted into the furnace through two air locks in the furnace head. The sample tubes were lowered into position in the melt, and when the system had reached the desired temperature, filtered samples of the two liquid metal phases were with-

<sup>9</sup> M. Hansen and K. Anderko, *Constitution of Binary Alloys*, McGraw-Hill Book Co., Inc., New York, 1958, p. 1119.

drawn by increasing the argon pressure to about 2 atm. The samples were raised and frozen in the upper, cool part of the furnace, and then moved into the glove box atmosphere (nominally dry nitrogen). Next, the outsides of the sample tubes were cleaned with emery cloth, and the lower halves of the tantalum frits and the welds at the top were cut off and discarded. The samples were then dissolved out of the tantalum tubes by acid and the solutions were analyzed for plutonium.

The experimental data were obtained between 660 and 948°C. The curve derived from these preliminary data (see Figure I-17) shows a liquid immiscibility region extending from about 8.5 to 84 a/o magnesium at 625°C. The consolute temperature appears to be in the vicinity of 975°C. The marked disagreement between two of the experimental points and the curve is attributed to faulty sampling. Further measurements are being made in order to improve the reliability of the data.

### (3) Ion Exchange Reactions in Molten Salt Media (R. VON AMMON\*)

The possible use of ion exchange materials for separations such as the removal of fission products from molten salt solutions is being investigated in an exploratory study. The solid ion exchange materials used thus far include Molecular Sieves,\*\* potassium hexatitanate, zirconium phosphate, zirconium molybdate, zirconium tungstate, zirconia, and alumina. The molten salt media have included  $\text{AlBr}_3$  and mixtures of  $\text{AlBr}_3$  and  $\text{KBr}$  to produce solvents of varying polar character.

Batch-type equilibrations were performed in which the solid was contacted with the melt under an inert atmosphere for periods up to 10 hr. The melts contained the metal cations  $\text{Cu}^{2+}$ ,  $\text{Fe}^{2+}$ ,  $\text{U}^{4+}$ , or  $\text{Ba}^{2+}$  in concentrations of about 0.01M. The  $\text{Ba}^{2+}$  was spiked with trace amounts of  $^{133}\text{Ba}$ .

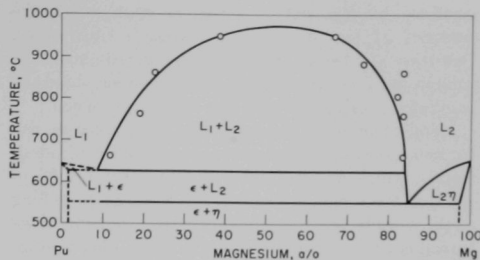
Preliminary experiments showed that the cations in solvents with a  $\text{KBr}:\text{AlCl}_3$  molar ratio less than unity could not be exchanged nor adsorbed on the solids. This probably results from the melt being strongly covalent, i.e., having a low dielectric constant, which prevents dissociation of the dissolved salts and the ion exchange material, but favors the formation of ion pairs. Such ion pairs involving transition metal ions have been identified in  $\text{KCl}:\text{AlCl}_3$ <sup>10, 11</sup> melts by infrared spectroscopy.

\* Kernforschungszentrum, Karlsruhe, Germany.

\*\* A synthetic dehydrated zeolite (sodium-aluminum-silicate) manufactured by the Linde Company.

<sup>10</sup> H. A. Oye and D. M. Gruen, *Inorg. Chem.* **3**, 836 (1964).

<sup>11</sup> D. M. Gruen and H. A. Oye, 148th National Meeting of the American Chemical Society, Chicago, Aug. 30 to Sept. 5, 1964, Div. of Inorg. Chem., Paper 14.



108-8701

Fig. I-17. Liquid Immiscibility Gap in the Binary System Magnesium-Plutonium.

The experimental results were much more encouraging with a solvent having a  $\text{KBr}:\text{AlBr}_3$  molar ratio of unity. At this ratio, the melt is ionic and  $\text{K}^+$  and  $\text{AlBr}_4^-$  ions are present instead of  $\text{AlBr}_3$ . In one case, with potassium hexatitanate as the solid phase and  $\text{Ba}^{2+}$  as the exchanging ion, a distribution coefficient ( $K_d = \text{cpm/g of solid phase / cpm/g of melt}$ ) of  $10^3$  was obtained. Work is currently in progress to determine whether similar results can be obtained with molten salt solutions that are of more direct process interest.

### d. SUPPORTING ENGINEERING STUDIES (L. BURRIS, R. D. PIERCE)

During the past reporting period, engineering studies were conducted in three areas: (1) determination of the critical constants of alkali metals, (2) examination of nonturbulent vaporization of mercury, and (3) determination of the viscosity of liquid metal alloys.

#### (1) Determination of the Critical Constants of Alkali Metals (I. G. DILLON,† P. A. NELSON††)

Thermodynamic properties of alkali metals are of particular interest because of the use of these metals as heat exchange media in nuclear reactors. For most alkali metals, vapor pressures and liquid and vapor densities are generally known up to the vicinity of the boiling point. While many estimates have been made of the critical constants of alkali metals, no actual measurements of the critical constants, vapor pressure, vapor density, and liquid density are known which cover the entire range of temperature from the boiling point to the critical point. To supply this missing data, measurements of the vapor and liquid densities of the alkali metals, sodium, potassium, rubidium, and cesium are being made from room temperature up to the critical point or to as close to the critical point as

† Ph.D. candidate from Illinois Institute of Technology.

†† Argonne advisor.

possible. As the critical point is approached, the densities of the two phases approach each other. Densities are being determined by measurement of gamma radiation from the liquid and vapor phases of irradiated alkali metal held in a high pressure cell.

*Installation of Equipment.* The high pressure cell for measurement of the critical temperature of alkali metals, which was described in ANL-6900, pp. 96 to 100, has been installed and tested. Seizing and galling of the capsule and the threaded capsule holding plugs turned out to be a serious problem above 1300°C since this made it impossible to remove the capsules without destroying them. Use of various lubricants in the capsule chamber and in the threaded plugs was only partially successful. Therefore, a new high pressure cell was designed to alleviate the capsule removal problem. The salient new design feature is the split, tapered center piece held in place by a 3-in. OD sleeve (see Fig. I-18). This split center piece should make possible easy removal of the capsule after heating to high temperatures. The construction material is molyb-

denum-30 w/o tungsten, which was satisfactory from both a strength and corrosion standpoint when used in the earlier design. The complete furnace assembly is shown in Figure I-18.

The counting equipment for measuring vapor and liquid densities consists of two 1-in. by 1-in. NaI, thallium-activated crystals with preamplifiers, positive high voltage sources, a recorder, count meter, scaler, single-channel analyzer, and amplifiers. The assembled equipment has been checked in separate tests with irradiated standards of  $\text{CsNO}_3$ ,  $\text{NaNO}_3$ ,  $\text{KNO}_3$ , and rubidium metal. Satisfactory spectra and counting rates were obtained.

*Preliminary Runs.* Initial measurements are being made on cesium and rubidium since their estimated critical temperatures (1700 to 1800°C) are much lower than those estimated for sodium and potassium (2200 to 2500°C). Preliminary runs were made with unirradiated cesium and rubidium to test the reliability of the molybdenum-30 w/o tungsten capsules. No failures were encountered up to 1900°C. Amounts of

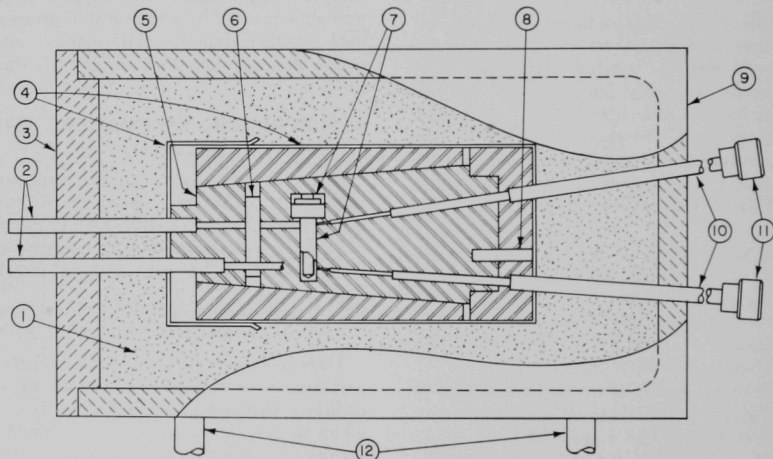


FIG. I-18. Revised Furnace Assembly for Critical Temperature Apparatus.

108-8548

1. Insulation
2.  $\frac{1}{4}$ -in. tantalum tubes connecting to temperature measurement holes in tapered Mo-30 w/o W cylinder
3. Fiberfrax lid
4. Tantalum can and lid
5. Tapered Mo-30 w/o W cylinder in 3-in. OD Mo-30 w/o W sleeve
6. Locating pin
7. Mo-30 w/o W capsule containing alkali metal in  $\frac{3}{16}$ -in. ID narrow section 1-in. long by 30-mil wall
8. Locating pin
9. Silicon carbide crucible ( $6\frac{1}{2}$ -in. OD by 11 in. high by  $\frac{1}{2}$ -in. wall)
10.  $\frac{1}{4}$ -in. OD tantalum tubes connecting to collimation holes in Mo-30 w/o W cylinder
11.  $\frac{1}{2}$ -in. Veeco fittings in wall of vacuum tank
12. Ceramic supports

material considerably less than the critical amount (amount needed to fill the capsule completely with dense phase at the critical density and critical temperature) were used in the majority of these tests. However, some capsule failures occurred after extensive thermal cycling. One failure occurred at 1715°C when more than the estimated critical amount was present. This failure may have been caused by a pressure fracture which was due to a very high pressure from both vapor pressure and hydrostatic pressure. Another failure occurred at 1850°C, again after extensive thermal cycling, when somewhat less than the critical amount of material was present. Since the critical temperatures of cesium and rubidium are both expected to be less than 1850°C, containing them up to the critical temperatures should not be a serious problem when there is less than the critical amount of material present.

Several runs have also been made with irradiated cesium. The preliminary data from these runs indicate a critical temperature of about 1660°C. Further runs are needed in the neighborhood of the critical temperature to firm up the data. Liquid densities obtained in the lower temperature regions (<1200°C) agreed with literature data. This is additional evidence that the counting equipment is operating satisfactorily.

### ERRATA

The graphs for Figs. I-32 and I-33 in the Chemical Engineering Division Research Highlights Report, May 1964–April 1965, ANL-7020, Argonne National Laboratory were, through error in make-up, interchanged. The graph of Figure I-32, p. 69 should appear in Figure I-33, p. 70 and the graph of Figure I-33, p. 70 should appear in Figure I-32, p. 69. The titles of the two figures are correctly located.

### (2) Study of Mechanisms of Liquid Metal Boiling and Entrainment (J. WOLKOFF)

The vaporization of pure mercury during convective boiling has been under study. No vapor bubble nucleation within the liquid occurs with this mode of vaporization and it has been referred to as "nonturbulent vaporization" during the present study. Vaporization occurs only at the free liquid surface. Since there are no vapor bubbles, there are no liquid droplets formed at the liquid-vapor interface and, consequently, there is no entrainment of liquid by the vapors. It has previously been shown that vaporization rates equivalent to heat fluxes as high as 115,000 Btu/(hr) (sq ft) through the vaporizing surface could be attained under vacuum when good liquid mixing was provided (ANL-6687, p. 58).

The measurement of the surface temperature of the

mercury during vaporization was difficult experimentally since a large temperature gradient existed within the liquid near the surface (ANL-6800, p. 133; ANL-6900, p. 93). Two techniques for this measurement were used: (1) extrapolation of vertical temperature traverses to zero depth, and (2) use of a surface temperature probe. The surface temperature probe consisted of a fine wire which penetrated the vaporizing surface from above to form a thermocouple with the liquid metal (ANL-6900, p. 95). Agreement between the two methods was fair. Slightly higher temperatures were obtained by the surface probe than by extrapolation of vertical temperature traverses. Although the probe was primarily sensitive to the surface temperature, some sensitivity to the higher temperatures below the surface existed.

A mathematical analysis of the surface thermocouple probe was made to clarify the limitations of the method and to provide a rational means for designing such a probe.

A thermoelectric potential is generated at the interface between the wire and the liquid metal, the potential varying along the wire-liquid metal interface because the temperature varies. At steady state, the Laplace equation can be written for the voltage distribution in each metal. A simplified mathematical model of the thermocouple system (based on a step change in temperature rather than a smoothly varying change) was solved to give the following equation:\*

$$\frac{e}{s} = 1 - V - \frac{4}{\pi^2 U} \sum_{n=1}^{\infty} \frac{\sin n\pi V}{n^2} \cdot \frac{I_1(n\pi U)K_1(n\pi U)}{I_0(n\pi U)K_1(n\pi U) + WI_1(n\pi U)K_0(n\pi U)}$$

where

$e$  = error in the surface temperature, in °C,

$s$  = step change in temperature, in °C, at the wire-liquid metal interface. This occurs immediately below the surface temperature region  $t_0$ ,

$V$  = fraction of the immersed wire length that is at the surface temperature  $t_0$ ,

$U$  = wire radius/depth or wire immersion,

$W$  = electrical resistivity of liquid metal/electrical resistivity of immersed wire,

$n = 1, 2, 3, \dots, \infty$

$I_0, I_1$  = modified Bessel functions of the first kind of order 0 and 1, respectively,

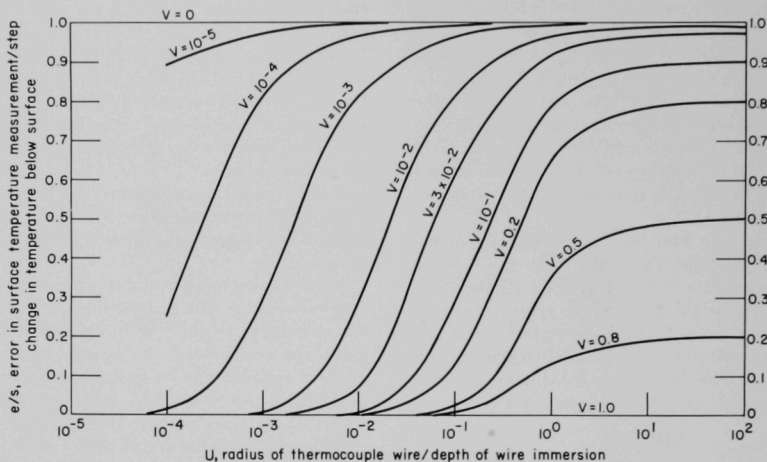
$K_0, K_1$  = modified Bessel functions of the second kind of order 0 and 1, respectively.

\* The help of D. A. Woodward and A. J. Strecek of the Applied Mathematics Division in solving the equation and in programming the computations is gratefully acknowledged.

A step temperature change was assumed to occur at various positions along the immersed portion of the thermocouple wire, and the magnitudes of the error in the surface temperature measurements were calculated as a function of the ratio of wire radius to depth of immersion.

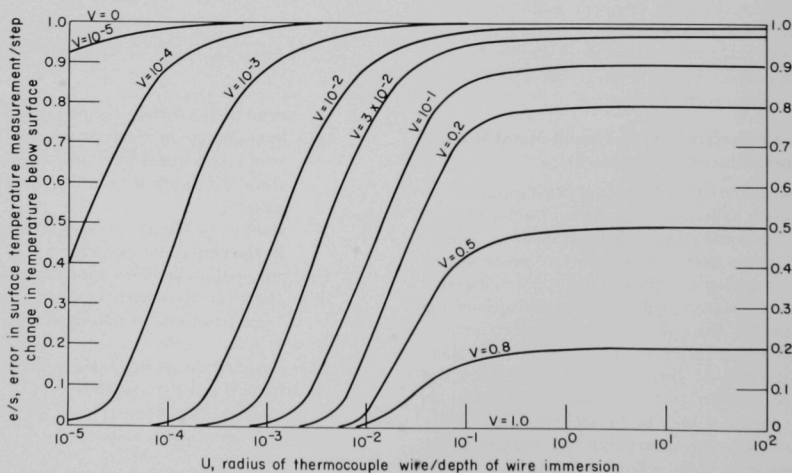
The calculated values of the equation are plotted in Figure I-19 for  $W = 1.5$ . This is the resistivity ratio

for the liquid metal mercury and the thermocouple wire chromel at  $180^\circ\text{C}$ , the temperature used in the mercury vaporization studies. As the wire radius decreases, it is evident that the error in reading the surface temperature decreases. For any finite value of  $V$ , a value of  $U$  can be found below which the error will be low. Figure I-20 is a similar plot for a resistivity ratio of  $W = 100$ . It can be seen that, under otherwise



108-8704

Fig. I-19. Error Parameters for Surface Temperature Thermocouple:  $W = 1.5$ . (Symbols defined in text.)



108-8705

Fig. I-20. Error Parameters for Surface Temperature Thermocouple:  $W = 100$ . (Symbols defined in text.)

similar conditions, measurements with high resistivity liquid metals tend to be more in error than measurements with low resistivity liquid metals.

The error in surface temperature measurement for the 10-mil thermocouple that was used in the mercury boiling studies was estimated from Figure I-20. At a temperature gradient of 165°C/in. (the maximum measured), the error in the surface temperature measurement was about +1°C.

A topical report of this work will appear as ANL-6957.

### (3) Determination of the Viscosity of Liquid Metals and Fused Salts (B. MISEK,\* R. D. PIERCE)

The viscosities of liquid metal and liquid salt solutions are of interest in interpreting mass transfer and fluid dynamics results obtained in some of the pyrochemical processing studies. For this reason, apparatus has been constructed for the determination of these viscosities. The equipment consists of a cup suspended by a torsion wire, and instrumentation to measure the

damping of the rotational oscillations of the cup. The damping is caused by the viscous shear of the liquid under study which is contained in the cup. A mathematical analysis for such an oscillating cup viscometer has been made by Shvidkovskiy.<sup>12</sup>

The major advantages of the selected method are (1) high sensitivity resulting from an extended period of viscous damping, (2) relatively small sample size, and (3) nonrequirement of direct observation of the fluid. The cup is suspended in a furnace and has only an extension visible for the amplitude and period-of-oscillation measurements. He derived an expression which allows the calculation of absolute kinematic viscosity if the system parameters are known.

Construction of the viscometer has been completed. Preliminary measurements have been made on mercury and on cadmium-base alloys.

<sup>12</sup> Ye. G. Shvidkovskiy, Certain Problems Related to the Viscosity of Fused Metals, NASA-TT-F-88 (March 1962). [Translation of Document Published by State Publishing House for Technical and Theoretical Literature (Moscow) 1956.]

\* Co-op Student from Northwestern University.

## B. FUEL PROCESSING FACILITIES FOR EBR-II (J. H. SCHRAIDT, M. LEVENSON, L. F. COLEMAN)

A direct-cycle fuel reprocessing plant (Fuel Cycle Facility) based on compact pyrochemical processes was designed and constructed as part of the Experimental Breeder Reactor No. II (EBR-II) Project. Melt refining, liquid metal extraction, and processes involving fractional crystallization from liquid metal systems are methods being examined for the recovery and purification of EBR-II fuels. Based on these studies, process equipment is being designed and tested.

The results of operations being carried out in the Fuel Cycle Facility are presented in Section I-C of this Report. This section (I-B) of the report describes the efforts of the Chemical Engineering Division in providing technical assistance for problems arising in the operation of the Fuel Cycle Facility and in developing equipment for compact pyrochemical processes which will subsequently be operated in the Fuel Cycle Facility.

### 1. Technical Assistance and Service Equipment Development

#### MANIPULATOR AND CRANE DEVELOPMENT

(J. GRAAE, P. KELSHEIMER, T. DENST†)

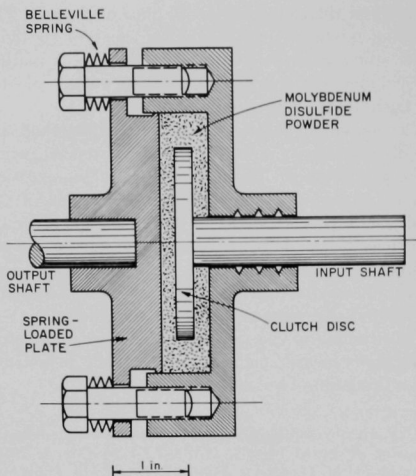
##### (1) Multiple Disc Type Slip Clutch

Multiple disc type slip clutches of Chemical Engineering Division design are being added to the hoist motors for the in-cell manipulators at the EBR-II Fuel Cycle Facility in order to protect the hoist mechanisms and cables from damage due to mechanical

overloads (see ANL-6900, pp. 108-109). The slip clutch includes a Maxitorq Disc-Pac No. 22†† which is kept under compression with Belleville disc-springs. The slip clutch is mounted inside the housing of the hoist motor gear-reducer and is so compact in size that no modification to the housing was necessary. The disc-pack, which is operated in oil, is set to slip at 50% overload. After initial slipping, the transmitted torque

†† Manufactured by Carlyle Johnson Machine Corporation, Manchester, Conn.

† Central Shops.



108-8722 Rev.

FIG. I-21. Dry Powder Slip Clutch.

(slip-torque)\* drops to about one-half the break-away torque.\*\*\* The break-away torque is adequate for all normal operations including acceleration of loads.

These slip clutches have been installed in four of the eight operating manipulators. The hoist units were shipped to Argonne, Illinois, one or two at a time, for the installation work. By modifying two spare hoist units first, it was possible to perform the required modifications without interrupting the use of in-cell manipulators. Before each modified hoist unit was returned to Idaho, it was subjected to two tests. One test consisted of first blocking the hoist in the "UP" position and then operating the hoist motor at various speeds in order to observe the slipping of the clutch and to measure the resulting armature current of the hoist motor. In first speed (32-volt tap), the clutch would not slip; the motor would stall and the armature current would be 10 amp. In second and third speeds (72- and 105-volt taps), the clutch would slip. A newly installed clutch would initially slip at an armature current of 15 to 20 amp. However, after a short conditioning period of starting and stopping (to prevent overheating a motor or blowing a fuse), the armature current at which the clutch slipped would drop to 8 to 9 amp. The full load (dc) rating of the motor is

\*\*\* Break-away torque is the torque at which the components of the clutch first start to slip relative to each other. Slip-torque is the torque transmitted between the driver and the driven shaft when the components of the clutch are slipping relative to each other.

8 amp. The second test consisted of lifting a 920-lb load (the rated load of the manipulator hoists is 750 lb) at each hoisting speed, measuring the resulting armature current, and observing clutch slippage. In the first speed (32-volt tap) the motor stalled, drawing a current load of 9 to 10 amp. In second and third speeds (72- and 105-volt taps), the load was lifted without the clutch slipping; the current load was 8 to 9 amp. These tests indicate that the clutches will operate as intended.

## (2) Dry Powder Slip Clutch

Although conventional clutches will satisfy many applications, there is a need for a clutch which would display a steady torque response. Conventional clutches do not slip at the same steady torque for a given torque setting. Rather, the torque transmitted while slipping varies after repeated operations and is different than the break-away torque. The multiple disc type slip clutch which is used for the manipulator has a break-away torque that is about twice the torque transmitted while slipping.

A new type of slip clutch (Figure I-21) has, therefore, been designed, built, and tested by the Chemical Engineering Division. The clutch consists of two parts: (1) a cylindrical housing that is filled with molybdenum disulfide powder† and is attached to one shaft, and (2) a clutch disc that is enclosed in the housing and driven by a second shaft. All parts of the slip clutch (other than powder) are made of mild steel without surface hardening or special machining, such as grinding. The powder forms a ¼-in. layer between the faces of the clutch disc and the adjacent faces of the housing and is compressed by a Belleville spring-loaded plate which forms one end of the housing. Friction between the molybdenum disulfide powder and the disc determines the torque transmitted. By varying the compression of the Belleville spring, this torque can be varied.

The clutch was tested by rotating the input shaft at 9 rpm and holding the output shaft stationary, thus slipping the clutch continuously. The transmitted torque was determined by measuring the force exerted at the end of a bar clamped to the output shaft. The torque initially transmitted was 350 in.-lb. It then dropped slowly to 200 in.-lb over a 2-hr period, after which the torque remained at this value for another 2 hr. Following this test, the direction of rotation was reversed, which caused the transmitted torque to drop to 180 in.-lb which within a few minutes increased to 250 in.-lb and remained at this value for the next ¾ hr when the test was terminated. No special shaft seals

† Alpha Molycoote Powder, Type 2; a product of the Alpha Molycoote Corp., Stanford, Conn.

were used and no leakage of powder was observed in these tests.

Apart from the gradual change in transmitted torque, the torque remained at a steady value without momentary fluctuations. Furthermore, there was no difference between break-away torque and torque transmitted while slipping. Subsequent tests have demonstrated that if the molybdenum disulfide powder is precompacted in the clutch housing, further compacting during operation is minimized, and the change in transmitted torque is largely eliminated.

Following the above tests, the dry powder slip clutch was installed on the bridge drive motor of the prototype manipulator in the Division's mock-up facility. The powder was compacted in the clutch prior to operation by drawing up tight the spring-loaded bolts. The bolts were then adjusted so that the clutch would slip at a torque of 880 in.-lb.

The clutch was first tested by operating the bridge drive motor while the end truck of the manipulator bridge was against a dead stop. The clutch did not slip (the motor stalled) at the low speed setting (32-volt tap); the clutch slipped, however, at the intermediate and high speed settings (72- and 105-volt taps). A Dillon dynamometer\* placed between the bridge end-truck and the rail stop showed that a force of 200 lb was being exerted while the clutch was slipping at the two higher speeds. The clutch slipped at this torque without an initial run-in period. The value of the slipping torque did not change during the tests which were repeated several times.

With a wheel diameter for the end truck of 8 in., the torque resulting from the 200-lb horizontal thrust is 800 in.-lb. The difference of 80 in.-lb between this torque and the initial torque setting of 880 in.-lb serves to overcome friction and other resistances in the drive mechanisms. The 880 in.-lb torque represents an overload of 50% on the motor. There was no difficulty in

backing the bridge away from the stop. (Since bridge drives are not equipped with slip clutches, spring-loaded bumpers are used to prevent a bridge drive from locking when a bridge hits the stop.)

The bridge and the lead-shielded carriage on it are very heavy, and operating experience at Idaho has shown that large forces (see ANL-6800, pp. 158-159) are involved when the bridge drive is engaged. The slip clutch was tested to determine if it would provide protection for the bridge drive mechanism during starting. For this test, the bridge was made free to move by backing it away from the dead stop. The clutch would initially slip even when the bridge motor was started at the low speed setting (32-volt tap). After the initial slipping, the clutch supplied sufficient torque to move the bridge.

The results of these tests show that this clutch does provide adequate protection for the bridge drive mechanism. The clutch promises to be radiation- and heat-resistant, maintenance-free, and inexpensive.

### (3) Prototype Manipulator

In order to provide the Fuel Cycle Facility with a means for checking out maintenance work that has been performed on manipulator carriages and for training personnel, the prototype manipulator (presently installed in the mock-up area of the Chemical Engineering Division, at Argonne, Illinois) will be dismantled and shipped to Idaho. Before this is done, however, the bridge and carriage will be modified. The rails on the bridge will be raised  $1\frac{1}{16}$  in., and the spring-loaded sliding collector assemblies will be replaced with new ones identical to those used in the Fuel Cycle Facility (see ANL-6900, p. 107). These two changes will make it possible to operate the prototype manipulator carriage on the bridges in the Air and Argon Cells and to operate the carriages from Air and Argon Cells on the prototype bridge.

## 2. Process Equipment Development

### a. SERVICE EQUIPMENT (J. O. LUDLOW, W. E. MILLER, J. V. NATALE)

It has become evident from operating experience in the Fuel Cycle Facility and in argon atmosphere gloveboxes that there were a number of problems uniquely associated with the operation of equipment in a dry argon environment. The lubricating and wetting properties of certain materials are changed markedly when their environment is changed from air to dry argon. Heat transfer rates for natural or forced

convection, under otherwise identical conditions, are less in argon than in air. The electrical strength of argon is much less than that of air.

In order to carry out a meaningful investigation of these problems, new environmental facilities utilizing an inert atmosphere were required. The establishment of these facilities (in Building 310) is being carried out in two steps. The first step, which has been completed, involved the installation of two gloveboxes and an associated argon gas purification system (see ANL-6900, pp. 115-116). The gloveboxes will be used for equipment and process development. The second step

\* A product of the W. C. Dillon Corp., Van Nuys, Calif.

is the construction of a large inert atmosphere enclosure and the modification of the existing argon purification system for use with the new enclosure. Plant-scale equipment for skull reclamation and blanket processing will be tested in this enclosure prior to installation in the Argon Cell of the Fuel Cycle Facility.

**(1) Large Inert Atmosphere Enclosure (Bldg. 310)** (J. O. LUDLOW, R. MALECHA,\* J. V. NATALE, J. H. SCHRAIDT, M. A. SLAWECKI)

Construction of the large inert atmosphere enclosure in Building 310 is nearing completion. Figure 1-22 shows the enclosure during a late stage of construction. The enclosure is about 24 ft long, 12 ft wide, and 14 ft high. The metal shell has been fabricated, and the windows have been installed. A major portion of the service piping and electrical work has been completed. Twelve windows are installed in the north side of the enclosure, eleven in the south side, four in the west side, and two in the east side; each window contains four glove ports. The southeast corner of the enclosure is provided with a niche which is at floor level and is 4 ft wide by 4 ft deep by 6 ft high. A 35-in. ID by 69-in. high cylinder, closed at the bottom and open at the top, is used as a lock for the transfer of large items into the enclosure. A hydraulic lifting device, which is a part of the enclosure, is attached to the transfer lock and is used to lift the lock to seal it against a capped opening at the top of the niche. Means for evacuating the lock and subsequently filling it with argon are being provided. A small transfer lock, 7 $\frac{3}{4}$ -in. ID by 28 $\frac{1}{2}$ -in. long, is installed in the east side of the enclosure and is used for the routine transfer of small-sized objects. The small transfer lock is provided with means for evacuating and refilling the lock.

The inert atmosphere enclosure is being provided with a 1-ton bridge crane which travels the length of the enclosure. All crane operations are remotely controlled.

The roof of the enclosure contains windows without glove ports. Fluorescent lights mounted above the roof windows furnish general interior lighting for the enclosure. A removable section of the roof, 7 $\frac{1}{2}$ -ft wide and 11 $\frac{1}{2}$ -ft long, is located at the east end of the enclosure. The removable section allows the introduction of very large pieces of experimental apparatus, including new crane bridges and trolleys.

Ports for introducing service and control lines into the enclosure are provided in the sides and ends below the windows and in the roof. The ports are the same

size as the glove ports in the windows and can be used as glove ports, if desired.

The enclosure is equipped with three 3-ton Freon cooling systems to control the temperature. The compressors are located in the basement service area. The direct expansion cooling coils and circulating fans are located above the top row of windows along the north wall of the enclosure.

After the installation of supporting equipment is completed, additional leak-testing of the enclosure will be performed. When all leaks are repaired, the installation of the skull reclamation equipment will be carried out.

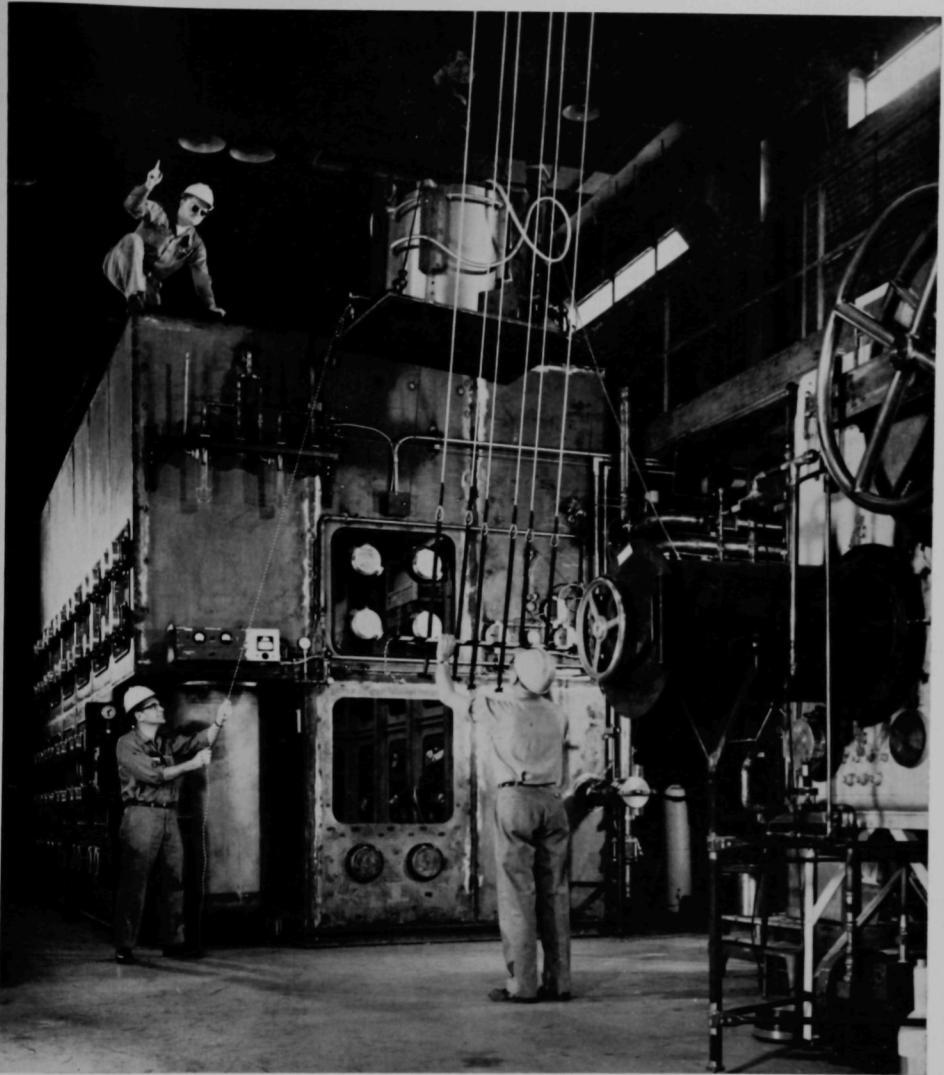
**(2) Operation of Argon Purification System (Bldg. 310)** (J. V. NATALE, A. CHANDLER, J. HARAST)

A purification system (see ANL-6900, pp. 116-117) has been installed in Building 310 to provide argon containing low concentrations of oxygen and water for the gloveboxes and similar inert atmosphere enclosures. The essential components of the purification system are a palladium catalyzer, a Molecular Sieve $\ddagger$  dryer and a centrifugal compressor that is installed in a gas-tight container. Gas from an enclosure is passed through the purification system and then returned to the enclosure. The oxygen in the flowing stream is catalytically converted with added hydrogen to water and this water, along with any water initially present in the gas stream, is removed by the dryer.

The argon purification system has been operating with only one glovebox connected to the system. The glovebox is maintained at a pressure of plus 0.7 in. of water, and only the gasketed container for the compressor and a small portion of the system piping are at a negative pressure. The rate of air leakage therefore is small (<1.2 cc/min). The oxygen concentration in the glovebox is controlled by adding hydrogen to the flowing stream over a 15 to 30-min period at the beginning of each workday. Moisture is controlled by passing gas through the system (without hydrogen addition) continually during each workday and occasionally overnight. The average oxygen concentration in the system, measured after the period of hydrogen addition, has been 5 ppm and the average moisture concentration at the end of each workday has been 15 ppm. The nitrogen concentration in the system was originally reduced to 0.1% and maintained at this concentration by purging with tank argon; however, the nitrogen concentration is now maintained at 5% (by periodic nitrogen additions) to simulate conditions in the Argon Cell of the Fuel Cycle Facility.

\* Central Shops.

$\ddagger$  Product of Linde Air Products Co., New York.



108-8351

FIG. I-22. Inert Atmosphere Enclosure during Construction. (This view shows the east side of the large inert atmosphere enclosure during a final construction stage. The large transfer lock is shown in its niche in the southeast corner of the enclosure. The small transfer lock is shown near the northeast corner. The operators are preparing to install a process furnace through a large hatch opening in the roof of the enclosure. One inert atmosphere glovebox and the vacuum transfer lock of a second are shown in the right foreground.)

Regeneration of the dryer bed has been necessary following each 500 hr of operation. The present regeneration procedure and equipment are only adequate for the one glovebox that is connected to the purification system. However, a second glovebox and the large inert atmosphere enclosure (see preceding subsection) will soon be connected to the system. In order to maintain the present regeneration interval and moisture content with this increased load, a predryer\* for the air in the regeneration step has been installed and is being tested. The use of predried room air during the course of regeneration will reduce the residual moisture content and increase the capacity of the dryer bed to a greater level than was possible in previous regenerations. The room air will be predried before it is passed through the dryer bed only during the final 2 hr of the 8-hr heating period of the regeneration procedure.

In addition to the installation of the predryer, other modifications have been made to the argon gas purification system which would make possible the attachment of the large inert atmosphere enclosure. These changes include the following: (1) extension of the existing supply and return headers for the argon gas, (2) installation of pressure controls for the overall system, (3) installation of an additional electrolytic oxygen analyzer, (4) relocation of existing analytical instruments, and (5) installation of an argon supply manifold for 3000-cu ft cylinders. These modifications and additions are in the process of being tested.

## b. SKULL OXIDE PROCESSING EQUIPMENT

(G. BERNSTEIN, T. ECKELS, J. GRAAE, D. GROSVENOR, J. LUDLOW, W. MILLER, M. SLAWECKI, E. JOHNSTON, P. KELSHEIMER, R. MALECHA,\*\* R. VREE\*\*)

At the conclusion of the EBR-II fuel melt refining operation, a residue (skull) remains in the processing crucible. The skull is converted to a free-flowing oxide powder in a skull oxidation furnace (see ANL-6900, pp. 116-120). A skull oxidation furnace has been installed in the Fuel Cycle Facility. A skull reclamation process is being developed for recovering the fuel material from the skull oxide and separating it from the associated fission products (see ANL-6800, p. 61). The skull reclamation process includes (1) extraction of noble metal fission products from the skull oxide, (2) reduction of the uranium oxide, (3) precipitation of a uranium-zinc intermetallic compound, (4) decomposition of the intermetallic compound, (5) dissolution of the uranium cake formed from the decomposition step, and (6) retorting of the uranium solution to yield a

uranium ingot. Equipment for processing skull oxides in the Fuel Cycle Facility is being built and tested by this Division.

The primary components of the processing equipment consist of the following: (1) a skull reclamation furnace, (2) a material transfer line, (3) transfer receiver equipment, and (4) a retorting furnace for recovery of the uranium product. The development status of the first three items is described below and the status of the fourth item, the retorting furnace, is discussed in subsection 2 c.

### (1) Skull Reclamation Furnace (M-2)

The reduction of uranium oxide to uranium metal and the gross separation of the uranium metal from fission products are to be carried out in one processing furnace. Tungsten appears to be the only suitable crucible material of construction which will resist the corrosive effects of the molten halide salts and molten zinc used in the skull reclamation process. A pressed-and-sintered tungsten crucible has been procured (see Figure I-23) for tests of the full-scale plant equipment. This crucible has an inside height of approximately 23¼ in. and an inside diameter of 14 in. It is designed to process approximately 5 kg of skull oxide as  $U_3O_8$ .

The operations to be conducted in the skull reclamation furnace (M-2) require several heating and cooling steps. To overcome the effects of fission product heating and to reduce the time necessary for cooling the crucible, a furnace design was required which would enhance the rate of heat dissipation (see ANL-6900, pp. 120-123). The construction of the M-2 furnace is based upon a Hastelloy C† open top cylinder which fits closely around the tungsten crucible. The furnace is to be heated by a close-fitting 20-kw resistance heater in the form of a vertically split cylinder. The cylinder halves are externally insulated and are held closed around the furnace during heating cycles. When the furnace is to be cooled, the cylinder halves are opened to expose the wall of the furnace.

The stainless steel furnace cover, which is hollow and filled with Fiberfrax insulation, contains openings for a stirrer assembly, a transfer line, and a charging port. The cover can be sealed to the furnace body by a fusible metal seal.

### (2) Agitator and Shaft Seal

In the skull reclamation process, the efficiency of noble metal extraction and the rate of reduction of uranium oxide are directly related to the effectiveness of the mixing in the crucible (see ANL-6725, pp. 45-46 and ANL-6900, pp. 58-59). In the pilot plant pro-

\* A product of the Pittsburgh Leetrodryer Division, McGraw-Edison Company, Elgin, Illinois.

\*\* Central Shops.

† Product of Haynes Stellite Company.

ess equipment as described in ANL-6687, p. 35, satisfactory results were obtained by using a crucible with four baffles and a double-bladed agitator. For the plant-scale operation, a large, unbaffled tungsten crucible (14-in. ID) with a hemispherical bottom will be used. The baffles were eliminated to simplify the fabrication of such a large size crucible. Tests were made to evaluate the mixing effectiveness of a proposed impeller in an unbaffled crucible and the performance of a special shaft seal and bearing assembly. The information was needed in order to design these components for the M-2 furnace. The limited space on the cover of the M-2 furnace requires that the agitator be mounted with its shaft located near the inside wall of the crucible. This limits the impeller diameter to 4 in. A pitched-blade impeller was selected for testing. The impeller (4-in. dia. by 1½-in. high) has four straight blades set at a 45° angle and was operated with downward discharge. The mixing tests were performed using the base from the M-1\* furnace and a steel vessel similar in shape to the tungsten crucible, but slightly larger (15½-in. ID). The impeller constructed of steel was mounted on a 1-in. dia. vertical steel shaft (the plant impeller and shaft are to be fabricated of Mo-30 w/o W). A bearing assembly for the impeller shaft and a variable-speed drive motor were supported on a frame above the M-1 furnace base. The variable-speed motor was adapted by appropriate sheaves and a belt drive to deliver speeds from 60 to 1000 rpm. Two mixing tests were made in which molten lead at 350°C was used as a stand-in for the molten zinc to be used in the skull reclamation process. The bottom edge of the impeller was located 4 in. above the crucible bottom and the impeller cleared the sides by 1½ in. The liquid lead level was ¾ in. and 2 in. above the top edge of the impeller in the first test and second test, respectively. In the first test, vortexing occurred at about 400 rpm; in the second test, at about 600 rpm. In the second test, good circulation and much turbulence was observed at 775 rpm. It is assumed that the vortexing would aid in combining the lighter flux with the metal phase. At 775 rpm, the power input to the motor was ¾ hp.

The agitation observed in these tests was sufficiently vigorous to indicate that an impeller of the same design should be tested in the M-2 furnace. On the basis of the power input observed (¾ hp) at 775 rpm, a 3-hp variable-speed d-c motor was selected for tests with the M-2 furnace. This size motor will permit operation at the maximum speed of the agitator drive (900 rpm),

\* The M-1 skull reclamation furnace is an early design of a plant-scale induction heated furnace. It has been superseded by the M-2 design. However, it is still being used for component testing while the M-2 furnace is under construction.



108-7344

FIG. 1-23. Plant-Size Pressed-and-Sintered Tungsten Crucible for Skull Reclamation Process. (Crucible size: 14-in. ID by 23¾-in. inside height. Crucible charge: 5 kg U<sub>2</sub>O<sub>5</sub>.)

even when derated for operation in an argon atmosphere (see ANL-6900, pp. 103-104).

An integral part of the mixing system is the bearing and shaft seal assembly. The assembly must be capable of operating at elevated temperatures, and the shaft seal must be able to hold system pressures up to 20 psi. A preliminary design was developed and various candidate bearing and packing materials were tested in the M-1 furnace. The assembly was operated under no load conditions (no mixing) and was not subjected to salt or metal fumes during the tests. Three tests were made in which the approximate temperatures at which components of the assembly will operate and the effectiveness of the packing and bearings for the test conditions were determined. A short stub-shaft, extending 6 in. beyond the bearing and seal assembly, was used in the test because a full length steel shaft (27 in.) would not be strong enough

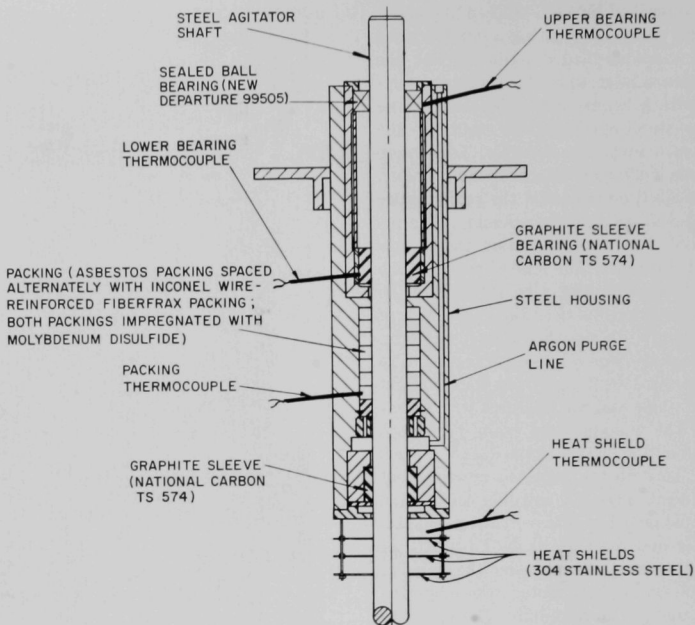


FIG. I-24. Agitator Bearing and Shaft Seal Assembly.

108-8700 Rev.

to withstand the forces of dynamic unbalance at the operating temperature ( $800^{\circ}\text{C}$ ) of the test.

In the first test, two conventional, unsealed ball bearings (ND-3205)\* were used with lubrication supplied with the bearing. The shaft seal was packed with asbestos packing (No. 811SP)\*\* impregnated with molybdenum disulfide in a wax carrier. The relative location of the bearings and the packing is shown in Figure I-24. After 33 hr of operation at an agitator shaft speed of 450 rpm and at a furnace temperature of  $800^{\circ}\text{C}$ , the lower bearing, which was at  $150^{\circ}\text{C}$ , failed. Examination showed that the cause of failure was loss of lubrication. For the second test the upper and lower ball bearings were replaced with new ones which were duplicates of those used in the first test, except that they were first degreased and then lubricated with a dry lubricant (tungsten disulfide). In this test, which was carried out under conditions similar to those of the first test, both bearings failed after  $\frac{1}{2}$  hr of operation.

In the third test, the lower ball bearing was replaced with a sleeve bearing made of a graphite material (National Carbon TS-574).† The upper ball bearing was replaced with a new ball bearing (ND 99505) which is a sealed type but otherwise similar to the bearings used in the two previous tests. Prior to use, the bearing was degreased and lubricated with NRRG-159,†† a radiation-resistant lubricant suitable for temperatures up to  $175^{\circ}\text{C}$ . The packing for the stuffing box was replaced with two types of packing rings which were alternately spaced. The first was a woven asbestos packing impregnated with molybdenum disulfide, and the second was a material made of woven Fiberfrax reinforced with Inconel wire and impregnated with molybdenum disulfide. This modified Fiberfrax material is a very hard packing and acts as a supplementary bearing. The agitator stuffing box assembly was mounted on the M-1 furnace and three stainless steel heat shields were positioned below the packing housing in order to simulate the design

\* Product of New Departure Division, General Motors Corp., Bristol, Connecticut.

\*\* Product of Crane Packing Co., Morton Grove, Illinois.

† Product of National Carbon Co., Division of Union Carbide Corp., New York, New York.

†† Product of Standard Oil Company of California.

planned for the M-2 skull reclamation furnace. A sketch of the assembly is shown in Figure I-24. Thermocouples were located at the top ball bearing, at the lower graphite bearing, in the lowest packing ring, and above the top heat shield. The furnace was maintained under 1 to 3 psi argon pressure during the test. Gas leakage from the entire furnace assembly was less than 1 cu ft/hr.

The operating conditions for this test and the temperatures attained by the bearings, packing, and top heat shield during the run were as follows:

Test Period, hr	109
Agitator Shaft Speed, rpm	750
Furnace Pressure (argon atmosphere), psi	1 to 3
Furnace Temp., °C	800
Upper Bearing Temp., °C	135
Lower Bearing Temp., °C	185
Lower Packing Ring Temp., °C	230
Top Heat Shield Temp., °C	315

The two bearings and the packing performed satisfactorily in this test. No lubricant was lost from the upper bearing. However, as noted above, the steel test shaft was not subjected to lateral deflection, a condition which would exist during mixing of molten metals, and the bearing and shaft seal assembly was not subjected to the action of metal and salt fumes. In order to evaluate performance under processing conditions, the assembly will be tested with a molybdenum-30% tungsten shaft and impeller in mixing tests using molten zinc and molten flux at 800°C in the M-1 furnace.

### (3) Transfer Line

The design of the transfer line to be used with the M-2 furnace was developed from information obtained in pilot plant studies that are described in ANL-6900, pp. 59-60. The transfer line for the M-2 furnace was made using two 3/4-in. OD rods of molybdenum-30% tungsten in which 1/2-in. ID holes were gun-drilled. The two lengths of drilled rod were joined by a threaded coupling and then formed to a J-shape by hot bending over a jig. The portion of the tubing (drilled rod) external to the furnace is wound with resistance heaters (1/8-in. OD) which are insulated with swaged magnesia and encased in Inconel. By using the heaters to maintain a temperature of about 800°C within the tubing, solidification of molten metal or molten flux during transfer is prevented. The wound section is insulated with Fiberfrax and potassium titanate powder and enclosed in a stainless steel jacket. The jacket protects the heaters, the insulation, and the tubing against mechanical damage and oxidation.

The transfer line will be fastened to the M-2 furnace cover and the waste receiver by means of solder seals. An external bellows is incorporated in the waste receiver seal to allow for thermal expansion of the line.

The transfer line is being adapted for temporary use with the M-1 furnace in order to carry out planned stirring and transfer tests.

### (4) Transfer Receiver Equipment

Flux and metal wastes from the skull reclamation furnace will be collected in 8-gal pails for disposal. These pails will fit the standard 6-ft waste container used for disposal of solid wastes (see ANL-6900, pp. 112-113). The design of the transfer receiver equipment, which is in the form of a fume hood, is complicated by the requirement that it provide for purging the transfer line, weighing the waste, and collecting the fumes which accompany the transferred material. (Purging of the transfer line is required to prevent plugging during normal furnace operations. Accurate weights of materials transferred are required at each process step in order to maintain close control of alloy composition. Contamination of the Argon Cell atmosphere by halide fumes may poison the atmosphere purification catalyst.)

The main components of the transfer receiver equipment will include (1) a secondary container for the waste pail, (2) a movable platform scale, (3) an elevating mechanism to raise the secondary container, and (4) a rugged fume hood which encloses the other components. A centrifugal blower will draw cell gas through the hood and through a large filter to remove metal and salt fumes before returning the gas to the cell. The filter will consist of a 4-in. deep layer of glass fibers with an 18-in. square cross section. The discharge end of the transfer line will enter the top of the hood and discharge into the waste pail. The waste pail will be held in the heavy secondary steel container which will rest upon the movable platform scale. After the platform scale has been rolled into position under the hood, the elevating mechanism will engage the secondary steel container. The container will then be elevated by a screw mechanism until it forms a seal against the top of the hood around the discharge end of the transfer line. An argon pressure line that is connected to and passes through the top of the hood will supply argon for purging the transfer line back to the furnace. When material is to be transferred from the furnace, the secondary container (holding a waste pail) will be lowered until it rests upon the scale platform. In addition to providing accurate weights of materials transferred, the scale will indicate the start and completion of the transfer operation. A separate waste

pail will be used for collecting each waste stream to be removed.

The design of the transfer receiver equipment is complete and final drawings are being prepared. Fabrication of components will begin in January 1965.

**c. RECOVERY OF URANIUM PRODUCT** (W. MILLER, J. LENC, J. HARAST, A. CHANDLER, R. PAUL)

In the current flowsheet for the EBR-II skull reclamation process, the process stream from the uranium-zinc intermetallic decomposition step is a solution which has the following approximate composition: Zn-12 w/o Mg-10 w/o U (see ANL-6800, Figure I-8, p. 61). Development work is being conducted on recovering uranium from this solution in a form suitable for use as a supplementary make-up feed material for the melt refining process. This work has included distillation of Zn-Mg alloy from the uranium product,

evaluation of beryllia crucibles, and uranium-hydriding experiments in tungsten crucibles.

**(1) Retorting-Distillation Runs**

Work is being continued on the recovery of uranium from zinc-magnesium-uranium by retorting. Recent retorting experiments have been conducted with a 7-kg charge of nominal Zn-12 w/o Mg-10 w/o U. (This scale of operation is about 17% of the plant scale and about 45% of the pilot plant scale.) The experiments are being conducted in a glovebox containing purified argon. The glovebox with the retorting furnace installed is shown in ANL-6900, p. 123, Fig. I-33. The assembly of internal components of the retorting unit is illustrated in Figure I-25 of the present report.

A series of 15 retorting runs was conducted to recover the uranium present in the Zn-12 w/o Mg-10 w/o U (nominal) ingots from the uranium dissolution step of seven pilot-scale demonstration runs of the skull

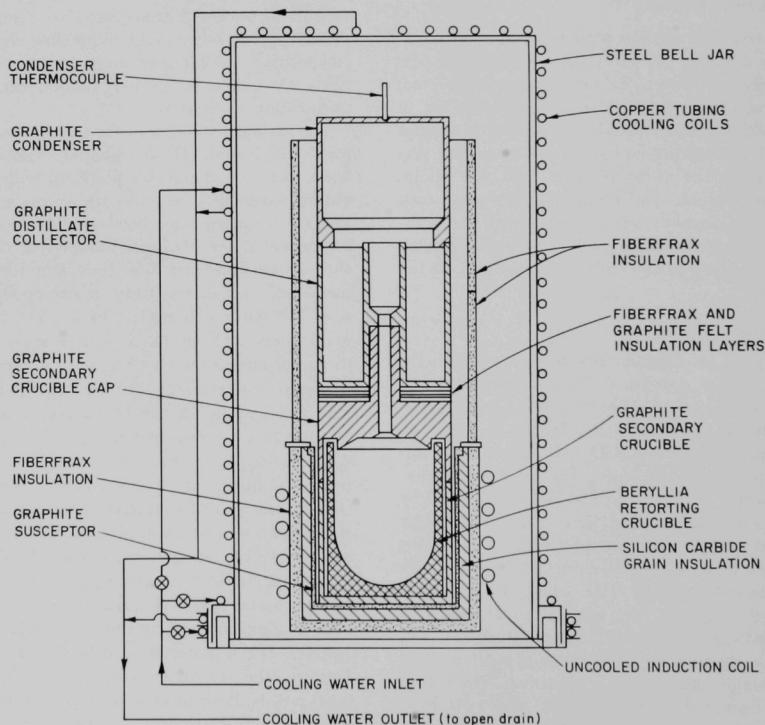


FIG. I-25. Apparatus for Retorting Zinc-Magnesium-Uranium Installed in Water-Cooled Bell Jar.

reclamation process (see section I-A-2-a-(1), this report). Since each ingot weighed from 10 to 13 kg, a minimum of two retorting runs was required to recover the total uranium product from one process demonstration run.

In addition to uranium product recovery, these retorting runs had two further objectives: (1) to reveal any major deficiencies in equipment design and (2) to evaluate the performance of beryllia retorting crucibles produced by various techniques by different vendors.

The same general experimental procedure was used in all 15 retorting runs. The Zn-Mg-U charge was first placed in a beryllia crucible. The crucible and other components of the retorting apparatus (see Fig. I-25) were then assembled. After the bell jar enclosure was sealed, the system was evacuated overnight. On the following day, the charge was inductively heated with about 6 kw power output from a 10 kc generator for ½ hr at pressures below 0.01 torr to remove water vapor and other sorbed gases from the apparatus and the charge (calibration runs had shown that a 6 kw input for ½ hr heated the charge to approximately 300°C). Next, the valve to the vacuum pump was closed and pressure of the retorting unit was increased to 30 to 40 torr with argon. Heating of the charge at the 6 kw power level was continued at this higher pressure. The progress of the distillation was followed by observing the graphite condenser temperature. The temperature initially increased as the distillation proceeded and then decreased after the bulk of the volatile metal in the charge had been vaporized. This step took 4 to 5 hr. At this stage, the power output from the generator was increased to about 7.5 kw in order to distill off any volatile material remaining in the beryllia crucible and to melt and consolidate the residual uranium product at a crucible temperature of 1250°C. The crucible was maintained at this temperature for 1 hr, after which the run was terminated. (Calibration runs which had been made with a thermocouple located in the retorting crucible had indicated that a crucible temperature of about 1250°C was attained in less than 1 hr with a 7.5-kw power output from the 10-kc generator.) The retorting unit was then allowed to cool under a partial vacuum (40 to 50 torr) for ½ hr before increasing the pressure to one atmosphere with argon. Following overnight cooling to room temperature, the unit was disassembled the next day, and the uranium product was recovered from the beryllia retorting crucible.

The weight of uranium product recovered in each of 15 retorting runs is presented in Table I-16. A photograph of a typical retorted uranium product which consists of a small solid button (or ingot) and some

TABLE I-16. RECOVERY OF URANIUM PRODUCT FROM RETORTING OF ZINC-MAGNESIUM-URANIUM INGOTS FROM URANIUM DISSOLUTION STEP OF EBR-II SKULL RECLAMATION PROCESS DEMONSTRATION RUNS<sup>a</sup>

Skull Reclamation Process Demonstration Run No.	Retorting Run No.	Zn-12 w/o Mg-10 w/o U (nominal) Retorting Charge (g)	Weight of Retorted Uranium Product		Uranium in Charge <sup>b</sup> (w/o)
			Button (g)	Fines (g)	
SKR-13	GBD-2 GBD-3	5,709 5,577	542 560	19 24	9.85 10.50
SKR-14	GBD-12 GBD-13	6,420 5,497	509 <sup>c</sup> 372 <sup>c</sup>	17 <sup>c</sup> 14 <sup>c</sup>	8.20 <sup>c</sup> 7.05 <sup>c</sup>
SKR-15	GBD-4 GBD-5	6,462 6,461	675 654	16 22	10.70 10.50
SKR-16	GBD-7 GBD-8	6,915 6,225	647 584	13 15	9.50 9.60
SKR-17	GBD-9 GBD-10	6,770 6,400	— 452	601 53	8.90 7.90
SKR-20	GBD-17 GBD-18	5,771 5,681	— 636	— 601	11.00 10.60

<sup>a</sup> See section I A 2 a (1), this report.

<sup>b</sup> Analysis of typical distillates showed uranium carryover to be insignificant. See section I A 2 a (1) of this report.

<sup>c</sup> These figures do not include a portion of the retorted uranium product that leaked through cracks in the beryllia retorting (or primary) crucible into the graphite secondary crucible.

fine powder is shown in Figure I-26. The button consisted of uranium and residual fission products (for analyses, see section I-A-2-a-(1), this report). X-ray diffraction analyses of the powder showed it was predominantly beta- $\text{UH}_3$ . This hydride was presumably formed by the reaction of the uranium with residual gases (from out-gassing) during the cool-down period at the end of the run. With few exceptions, the solid button comprised about 96 to 98 w/o of the total retorted uranium product recovered in each run.

In Table I-17 a composite material balance is given for the zinc-magnesium volatilized in this series of runs. Examination of the data in Table I-17 indicates that the retorting assembly was very effective in containing the metal vapors. An average of 96.8 w/o of the volatilized zinc-magnesium in the retorting charge was contained in the graphite distillate collector designed for this purpose. An average of only 0.8 w/o of the zinc-magnesium was unaccounted for. This amounted



108-7477

FIG. I-26. Typical Uranium Product Remaining after Retorting Zinc-Magnesium Ingots from EBR-II Skull Reclamation Process Demonstration Runs.\* (Major portion of product is in the form of a button; remainder is in the form of a fine powder.)

TABLE I-17. COMPOSITE MATERIAL BALANCE FOR ZINC-MAGNESIUM VOLATILIZED IN 15 RETORTING RUNS<sup>a</sup>

Total weight of volatile metal from all run charges:<sup>b</sup> 78,499 g

Location <sup>c</sup> of Condensed Metal after Run	Total Weight (g)	Percent of Volatile Metal in Charge (w/o)
In Graphite Collector	75,987	96.8
On Fiberfrax Insulators	1,648	2.1
On Graphite Secondary-Crucible Cap	79	0.1
On Graphite Condenser	157	0.2
Material unaccounted for	628	0.8
<b>TOTAL</b>	<b>78,499</b>	<b>100.0</b>

<sup>a</sup> Weights shown represent total weights for the 15 retorting runs. The charge material for these runs was from seven skull reclamation process demonstration runs (No. SKR-12, -13, -14, -15, -16, -17, and -20, see section I A 2 a (1) of this report).

<sup>b</sup> Equivalent to the total charge weight (86,465 g) less the total weight of retorted product (7,966 g) for the 15 retorting runs.

<sup>c</sup> See Figure I-25.

to a total weight of 628 g of Zn-Mg. The density of the condensed Zn-Mg was 4.7 g/cc; hence, the volume of material which had escaped from the internal assembly of the retorting apparatus into the bell jar enclosure was approximately 134 cc. This material generally condensed on the inner surfaces of the enclosure as a fine

powder that could be easily removed by means of a vacuum cleaner. No visible deterioration of the enclosure as a result of this material condensing on its surfaces has occurred.

A second bell jar enclosure (similar to the one being used for the present retorting apparatus) is being modified to accommodate a plant-scale retorting assembly. Installation of this retorting apparatus unit in Building 310 has begun. This unit will have a capacity for retorting a 50-kg charge of Zn-12 w/o Mg-10 w/o U from the uranium dissolution step of the plant-scale EBR-II skull reclamation process. In initial tests of the retorting apparatus which will be performed with the enclosure in an air atmosphere, 40-kg charges of Zn-14 w/o Mg (no uranium) will be distilled. The atmosphere in the enclosure will be argon at low (20 to 40 torr) pressure. After the performance of the unit has been satisfactorily demonstrated, the unit will be relocated in the Inert Atmosphere Enclosure now under construction in Building 310.

## (2) Performance of Beryllia Crucibles in Retorting Experiments

Thus far, four different beryllia crucibles have been used in retorting experiments in which uranium was recovered from charges having a nominal composition of Zn-12 w/o Mg-10 w/o U. These 5¼-in. OD, 9-in. high crucibles were produced by different fabricating techniques and manufacturers. Three of the crucibles were formed by thixotropic casting; they had hemispherical bottoms internally and a wall thickness of

\* See section I-A-2-a-(1), this report.

about  $\frac{3}{8}$  in. Two of the thixotropically cast crucibles were purchased from the Brush Beryllium Company of Elmore, Ohio, and the third was purchased from the Coors Porcelain Company of Golden, Colorado. The fourth crucible was formed by isostatic pressing; it had a conical bottom and a wall thickness of  $\frac{1}{8}$  in. This crucible was received as a test sample from Coors.

The first thixotropically cast crucible (Brush) performed satisfactorily for nine runs. Several cracks were visible in the crucible sidewall after seven runs. These cracks became more pronounced after each of the two remaining runs. After the ninth run, the crucible broke in handling. The broken crucible is shown in Figure I-27.

Three retorting runs have been completed in the second thixotropically cast crucible made by Brush. Although some hairline cracks are visible on the external surface of the crucible, it has performed satisfactorily in retorting runs made to date. Additional runs are to be conducted in this crucible to determine its useful life.

The third thixotropically cast crucible (Coors) was deemed unfit for further use after four retorting runs. During the last three runs conducted with the crucible, some of the molten charge leaked through visible cracks located in the lower 2 to 3 in. of the crucible sidewall. The severity of these cracks is illustrated in Figure I-28.

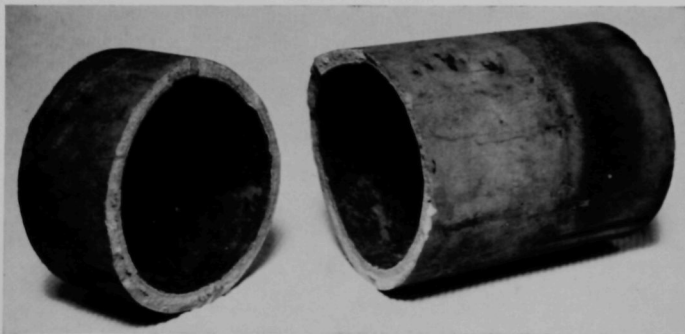
The isostatically pressed crucible (Coors) with a conically shaped bottom failed after one retorting run. A 3-kg charge of Zn-14 w/o Mg (no uranium) was used in this run; at the end of the run numerous cracks were apparent in the crucible. The lower tip of the conical bottom was easily broken away from the remainder of the crucible (see Figure I-29). Another

Coors isostatically pressed crucible (hemispherical bottom and  $\frac{3}{8}$ -in. sidewalls) has been obtained for testing.

### (3) Hydriding of Uranium in Tungsten Crucibles

In view of the rather limited useful life of the beryllia retorting crucibles tested to date, tungsten crucibles are being considered as alternatives for use in the retorting step of the EBR-II skull reclamation process. Tungsten crucibles are more readily available in the relatively large size (11 liters) required for plant-scale operations, and are not only initially stronger than beryllia crucibles but do not deteriorate with use. However, tungsten crucibles cannot be substituted for beryllia crucibles without some modification of the skull reclamation process. The need for the modification is brought about by the fact that the uranium product remaining in the crucible after the zinc and magnesium have been distilled off at 800 to 900°C adheres to the bottom of the crucible. Moreover, during consolidation of the uranium product by liquation (1150 to 1250°C), the tungsten crucible is attacked by the molten uranium. A possible means for overcoming these difficulties might be the hydriding of the uranium product at 250 to 330°C after the distillation of zinc and magnesium had been completed to convert the retorted uranium product to a free-flowing powder that could be transferred from the tungsten crucible.

To test this procedure, a number of hydriding experiments have been carried out in a 4-in. OD by 6-in. high tungsten crucible installed in the 7 kg-scale retorting apparatus. The first experiment was designed to demonstrate that uranium alone could be satisfactorily hydrided. The charge of 200 g of natural uranium and 100 g of depleted uranium-5 w/o fission alloy was



108-7595

FIG. I-27. Broken Thixotropically Cast Beryllia Crucible. (Failure of the crucible occurred after nine retorting runs in which uranium was being recovered from zinc-magnesium-uranium ingots.)



108-8011

FIG. I-28. Severely Cracked Thixotropically Cast Beryllia Crucible. (The cracks resulted from four retorting runs in which uranium was being recovered from zinc-magnesium-uranium ingots.)



108-7598

FIG. I-29. Broken Isostatically Pressed Beryllia Crucible. (Failure of the crucible occurred after one retorting run in which the charge was zinc-14 w/o magnesium; no uranium was present.)

heated to 1200°C under vacuum to consolidate the metal. After the charge had cooled to 250°C, the furnace was filled with hydrogen (1-atm pressure) and the charge was maintained at 250 to 330°C for 2 hr. Spectrographic analyses of the poured material

showed traces of tungsten, showing that liquation of the uranium alloy at 1200°C had caused corrosion of the tungsten crucible. The hydride was successfully produced and dumped from the crucible. The hydrided product was then charged to a beryllia crucible and

liquated (1200°C) under full vacuum to produce a clean-looking button of metallic uranium.

The second experiment was designed to demonstrate hydriding of the product from the uranium-zinc intermetallic decomposition step of the skull reclamation process. The Zn-Mg-U alloy added to the tungsten crucible weighed 2260 g; its composition was Zn-12 w/o Mg-8 w/o U. To this charge was added 194 g of natural uranium. The zinc and magnesium were distilled off at temperatures to 950°C and an argon pressure of 30 to 39 torr. The uranium remaining in the crucible was hydrided at 275 to 320°C and one-atm hydrogen pressure for 2½ hr. Once again, the uranium product was completely hydrided and easily dumped. As in the first experiment, the hydrided material was then charged to a beryllia crucible and melted under full vacuum; a clean, high-density button of metallic uranium was produced.

Two experiments were performed to determine whether the hydriding technique could be applied to the removal of the material which remains in the tungsten crucible after the intermetallic decomposition step has been carried out and the zinc-magnesium supernatant (Zn-50 w/o Mg) removed from the crucible (see ANL-6800, p. 61, Fig. I-8). This procedure would have the advantage of eliminating the uranium cake dissolution step which is now used as a means for transferring the product of the intermetallic decomposition step from a tungsten to a beryllia crucible. By eliminating the dissolution step, the solvent (Zn-12 w/o Mg) required to carry out this step would also be eliminated. Thus the volume of material transferred to the beryllia crucible would be decreased substantially and the need for large beryllia crucibles would be eliminated.

In the first of these experiments, the charge was prepared from 200 g uranium by first simulating the zinc-uranium intermetallic formation and precipitation step of the skull reclamation process, then decomposing the intermetallic compound and subsequently precipitating metallic uranium and decanting the Zn-50 w/o Mg solution. The 346 g product of these steps was metallic uranium dispersed in zinc-50 w/o magnesium. This Zn-Mg-U material, in the tungsten crucible in which it was prepared, was loaded into the retorting apparatus for the hydriding experiment. The charge was exposed to 1 atm hydrogen pressure for 4 hr at 280 to 320°C. The hydrided product (fine powder and some larger metallic pieces) poured easily from the crucible. Colorimetric uranium analysis of a sample of the large metallic pieces showed the uranium content to be 29.8 w/o. X-ray diffraction analysis of the fine powder indicated the presence of beta-UH<sub>3</sub> and the possible presence of a Mg-Zn intermetallic compound

and alpha-UH<sub>3</sub>. No UO<sub>2</sub>, UC, or alpha-U was detected.

The hydrided product was transferred to a beryllia crucible which was installed in the retorting apparatus. This hydride charge was decomposed at 500 to 600°C and one torr (hydrogen) or less. The charge was then heated to 1200°C to melt and consolidate the uranium product. The consolidated product weighed 128 g, 37 w/o of the product of the uranium precipitation and Zn-50 w/o Mg decanting step. This average concentration is greater than that (29.8 w/o) determined for a sample of one of the large metallic pieces in the hydrided material, indicating that a high Zn-Mg alloy concentration hinders the hydriding process.

In the second experiment a 516 g charge of Zn-Mg-U was prepared from 202 g uranium by the method previously described. The tungsten crucible containing this charge was hydrided in the retorting apparatus for 4½ hr at a 1 atm hydrogen pressure and 270 to 305°C. After hydriding, only 215 g of material poured from the crucible. The poured material was returned to the tungsten crucible, and the hydriding step was repeated. After the second hydriding step, 315 g of material poured from the crucible. The material remaining in the crucible was concentrated at the bottom and in that portion of the crucible from which the Zn-Mg solution had been decanted after the uranium precipitation step of the charge preparation. The material in the crucible was of two forms: (1) a brittle material covering the crucible bottom and (2) a continuous metal phase which covered the brittle material and extended up the crucible sidewall. The continuous metal phase was difficult to remove from the crucible. The brittle material, exposed after removal of the continuous metal phase, was easy to remove from the crucible. The appearance and location of the continuous metal phase indicated that it was zinc-magnesium remaining from the final step of the charge preparation.

The 503 g of material recovered from the hydriding step was loaded into a beryllia crucible in the retorting apparatus. The hydride was decomposed and the uranium product was consolidated as in the previous experiment. The consolidated product weighed 173 g, 34 w/o of the charge which had been hydrided.

These two experiments indicate that precipitated uranium enveloped in zinc-magnesium can be freed from a tungsten crucible by hydriding the uranium to disintegrate the metallic structure. The ease with which the material may be freed from the crucible appears to depend upon the distribution of the uranium in the Zn-Mg and the thickness of the Zn-Mg coating. Additional information is necessary to determine whether a hydriding procedure would permit eliminating the

uranium cake dissolution step of the skull reclamation flowsheet.

A limited number of additional hydriding experi-

ments are planned in order to evaluate the potential application of a hydriding step to the skull reclamation process.

## C. FUEL CYCLE FACILITY OPERATIONS (C. E. STEVENSON, D. C. HAMPSON, M. J. FELDMAN, D. M. PAIGE)\*

The first pyrochemical process being tested in the EBR-II Fuel Cycle Facility is melt refining. Installation of equipment for this process and for the refabrication of fuel elements is substantially complete and start-up operations with irradiated fuel have commenced.

Following tests and modifications to improve the performance of the interbuilding fuel transfer coffin, the dismantler, and the decanner, tracer studies were carried out to determine the path followed by iodine in the melt refining and oxidation furnaces. Extensive process development work has been conducted on the injection casting furnace, the pin processing and

welding machines, the bonder and bond tester, and the final assembly machine. Several hundred fuel elements have been remotely manufactured from unirradiated, enriched uranium scrap, and a number of EBR-II subassemblies have been fabricated, using fuel pins reclaimed from fuel material disassembled at Argonne National Laboratory, Argonne, Illinois. Fuel elements from the first discharged, irradiated EBR-II core subassembly have been processed through the preparation of acceptable castings. The Argon Cell atmosphere control systems have been maintained in satisfactory operation, and techniques have been developed for remote work with the cranes and manipulators.

### 1. Operations and Investigations with Equipment for Recovery of Irradiated Fuel

(D. C. HAMPSON, R. M. FRYER, D. L. MITCHELL)\*

#### a. INTERBUILDING FUEL TRANSFER COFFIN AND TRANSFER GRAPPLE

An interbuilding coffin (see ANL-6934) provides for the shielded transfer of a fuel subassembly containing spent or reconstituted fuel between the EBR-II Reactor Building and the Air Cell of the Fuel Cycle Facility. In addition to providing cooling of the subassembly during transfer by means of an integral blower and heat exchanger, the coffin serves as a reaction vessel for the removal of the thin film of sodium that is retained on the external surfaces of the subassembly after discharge from the EBR-II reactor.

Several modifications have recently been made on the coffin:

1. One of the insert tubes, which supports and locates a subassembly in the coffin, has been shortened to provide for more clearance ( $\frac{3}{8}$  in. total clearance) between the top of a subassembly in the coffin and the lower surface of the sliding top shielding plug. All (three) insert tubes have been modified so that the grapples for the assembly machine and the dismantling machine (see ANL-

6875, p. 62, Figure I-27) can be used for subassembly transfer in the Air Cell.

2. The sliding top shielding plug has been motorized to provide for safer, easier operation of this plug.
3. A mercury dump tank has been installed on the side of the coffin to provide an emergency cooling system for removing fission product heat. In case of failure of the argon circulation blower, the mercury can be introduced into the coffin cavity. The 0.71-cu ft capacity of the dump tank will provide enough mercury to submerge the subassembly in the coffin. The mercury prevents a subassembly meltdown by transferring the fission product heat from the subassembly to the coffin body.

Tests were conducted to determine a suitable method of drying the coffin cavity to prepare it for return of a refabricated subassembly to the reactor. The tests showed that both vacuum and air drying methods are adequate, although the air drying method is faster.

The dismantling machine transfer grapple has been received, installed in the Air Cell and tested. This grapple provides forced air cooling of a subassembly during transfer between the interbuilding coffin and the dismantling machine or the storage pits in the Air

\* Idaho Division.

Cell floor. The cooling air is drawn through the sub-assembly by means of dismantler cooling blowers. The grapple is handled by means of the Air Cell crane.

#### b. SUBASSEMBLY DISMANTLER

The Fuel Element Removal Machine (FERM), which was developed by the Remote Control Division at Argonne, Illinois, is an attachment to the subassembly dismantling machine and provides a semi-automatic method for separating fuel elements from the subassembly. At present, fuel elements are removed individually from the cluster, using a master-slave manipulator. The FERM was received, tested in the mockup area, and then remotely installed on the dismantler, where its operability was demonstrated. It was then removed and transferred again to the mockup area to allow technicians to be trained in its operation, while out-of-cell wiring and controls were being installed.

#### c. FUEL ELEMENT DECANNING

A considerable number of tool bit failures were encountered during initial operation of the fuel element decanning (and pin chopping) machine.\* These failures were determined to be a result of improper heat treatment of the tools by the supplier. (When another group of these tool bits, which had been properly heat treated, was tested at a later date, they performed satisfactorily.) While the causes of these failures were investigated, several new tool steels were tested. One of these, a high-speed steel tool material containing cobalt, was found not to be as brittle, and, thus, did not chip as readily as the tool material now being used.

High-speed motion pictures (1000 frames/sec) were taken to investigate difficulties caused by the interaction of the spiral decanner and fuel pin chopper. These films showed that the action of the chopper does momentarily stop the forward motion of a fuel pin during the decanning operation. This stoppage can cause excessive wear on the drive rolls and tool bits. This phenomenon was not observed when the decanner speed was reduced by one-half. Consequently, the decanner was modified to operate at one-half its original speed. The reduction in speed does not markedly increase the operating time per subassembly.

#### d. IODINE TRACER EXPERIMENTS

A series of  $^{131}\text{I}$  tracer experiments were conducted to aid in determining the fate or disposition of iodine in the melt refining equipment, skull oxidation equipment,

\* Fuel elements are placed in the spiral decanner (and pin chopper) (see ANL-6605, p. 59) where the stainless steel cans are removed and the fuel pins are cut to proper length for use in the melt refining furnace.

injection casting equipment, and associated off-gas handling equipment.

The systems designed to handle the off-gas from the melt refining furnaces and the skull oxidation furnace are shown in Figure I-30. The in-cell filters (see ANL-6687, p. 69) used in these systems consist of two sections: (1) a 2-in. layer of activated carbon through which the gas first passes, and (2) a high-efficiency glass media filter section; both sections are contained in a canister approximately 9 in. OD by 11 in. high. The melt refining furnace off-gas first passes through the in-cell filter and then through a vacuum pump and an oil separator, which are located in the subcell, to a shielded hold-up tank (500 cu ft) containing approximately 1000 lb of activated carbon. When meteorological conditions are favorable, the gas in the hold-up tank will be discharged through a heated (430°F) bed of silver nitrate-coated packing (silver nitrate tower), an exhaust pump, a bank of high-efficiency filters for removal of submicron particles, and then to the atmosphere through a 200-ft high stack. The nominal flow of air through the stack is 70,000 cfm, whereas the discharge rate from the hold-up tank ranges from 1 to 5 cfm. The various instruments used to monitor off-gas activity ( $^{133}\text{Xe}$ ,  $^{131}\text{I}$ , and other radioactive gases) are located immediately after the exhaust pump and at the base of the stack.

The skull oxidation furnace off-gas system is somewhat different and is separate from the melt refining furnace system. The oxidation furnace gases also pass through an in-cell filter and then to a separate hold-up tank (12 cu ft) in the subcell. When meteorological conditions are favorable, the gas is discharged through the bank of AEC filters and out the 200-ft high stack. The gases from the oxidation furnace are not passed through the off-gas system for the melt refining furnaces because of the possibility of any unused oxygen reacting with the activated carbon in the large hold-up tank. However, if the activity level in the oxidation furnace off-gas is too high, provision is made to allow the gas to be passed through the off-gas system for the melt refining furnaces.

The injection casting furnace, which is used to cast fuel pins from the ingot resulting from melt refining, also has a separate off-gas system. The gas from the bell jar first goes through an in-cell sintered stainless steel filter, then to the bank of high-efficiency filters and the 200-ft high stack, either directly from the furnace, when the furnace is vented after casting, or via a vacuum pump and ceramic pore filter, when the furnace is evacuated during the melting operation or purged prior to or at the completion of a run.

The first two  $^{131}\text{I}$  tracer experiments were performed in the melt refining furnaces, where, in each case, one

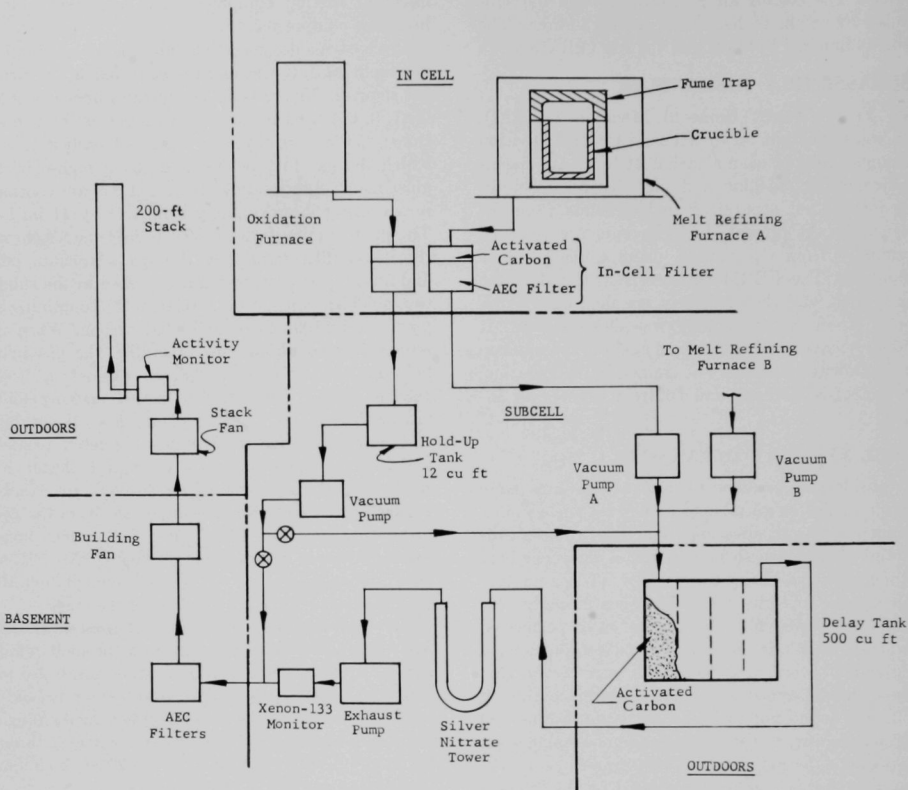


FIG. I-30. Melt Refining and Oxidation Furnace Off-Gas Systems.

curie of  $^{131}\text{I}$  (as palladium iodide which decomposes at  $350^\circ\text{C}$ ) was volatilized. In the first test, which was conducted in melt refining furnace A, the  $^{131}\text{I}$  was charged to a stainless steel beaker. The beaker was then placed in a melt refining zirconia crucible and this assembly was heated to  $850^\circ\text{C}$  and held for 45 min. No fume trap was used in this run. In the second test, which was carried out in melt refining furnace B, the  $^{131}\text{I}$  and 8270 g of unirradiated, depleted uranium-fissium pins were charged to a melt refining crucible. The crucible was heated to  $1400^\circ\text{C}$ , and held at this temperature for 3 hr. The melt was then poured from the crucible into a mold, leaving a skull of uranium-fissium in the crucible. The crucible during this run was covered with a fume trap which had been previously coated with sodium to simulate conditions in a melt refining run using sodium-bonded fuel pins. Table

I-18 summarizes the disposition of the  $^{131}\text{I}$  after each run. In the cases where a direct sampling technique could not be used, the iodine activity was estimated by using a Geiger-Mueller (G-M) counter inside the Argon Cell. The activity of an object was measured by holding the G-M instrument at a distance of greater than four times the object's major dimension. (Precautions were taken in order to eliminate as much background error as possible.) The measured activity was then assumed to emanate from a point source, and the appropriate calculations were made to determine the total activity. This method was estimated to be accurate within  $\pm 10$  to  $15\%$ . All other activity measurements were made by counting samples in a multi-channel gamma-ray spectrometer. All the values in Table I-18 are time-corrected for decay to the assay date of the charged  $^{131}\text{I}$ .

The results show that most of the  $^{131}\text{I}$  liberated was retained within the furnace and the in-cell filter, whereas only a small fraction of the original charge escaped to the off-gas system. In test 2, the two thief samples of the furnace off-gas were taken at a point in the subcell piping immediately following the 1-in. vacuum line feedthrough. The first sample was taken  $\frac{1}{2}$  hr after reaching a melt temperature of  $1400^\circ\text{C}$ , whereas the second sample was taken 3 hr after reaching the melt temperature. All of the gas removed from the system was passed through a caustic scrubber and a separate activated carbon filter prior to being pumped to the holdup tank.

The crucible and skull from test 2 were charged to the skull oxidation furnace. An estimate that the skull contained approximately 22 mc of  $^{131}\text{I}$  (see Table I-18) was based on an in-cell reading with the G-M tube counter. Following the oxidation step, a sample of the skull oxide was transferred out of the Argon Cell and analyzed for  $^{131}\text{I}$ . The analysis, when corrected for decay, showed that 27.9 mc of  $^{131}\text{I}$  was contained in the total skull oxide collected in the oxidation run. Analysis of samples of the oil from the skull oxidation furnace vacuum pump, the gas from the oxidation furnace holdup tank, and the solution used to scrub all gas discharged from the holdup tank revealed no detectable amounts of  $^{131}\text{I}$ .

Two additional experiments were performed in melt refining furnace B to determine if the residual radioactive iodine could be displaced either by the addition of inactive iodine or removed by sublimation with heat. In the first test, in which no fume trap was used, approximately one gram of inactive, crystalline iodine was charged to a stainless steel beaker which was then placed in a zirconia crucible. This assembly was heated in the furnace to  $850^\circ\text{C}$  and held at this temperature for 3 hr. The purpose of the second test was to determine if the  $^{131}\text{I}$  could be sublimed by the application of heat and was performed in conjunction with the first enriched uranium run (EUF-1) made in furnace B. In this run, in which a new fume trap was used, the furnace was heated to  $1400^\circ\text{C}$  and held at this temperature for  $\frac{1}{2}$  hr. Oil samples from the vacuum pump for furnace B were taken before and after each run. The results of the analysis of these samples showed that the oil had gained  $0.607 \mu\text{c}$  of  $^{131}\text{I}$  during run EUF-1 as compared with  $0.332 \mu\text{c}$  gained in the inactive iodine test. From these experiments, heating at elevated temperatures appears to be the more effective technique for displacing  $^{131}\text{I}$ ; however, buildup factors and migration rates cannot be evaluated on so few experiments. Iodine behavior will be followed in future processing operations.

Following each of the iodine experiments in the

TABLE I-18. DISTRIBUTION OF IODINE-131 IN COMPONENTS OF MELT REFINING FURNACES AND OFF-GAS SYSTEM

*Test 1 (melt refining furnace A).* One curie of  $^{131}\text{I}$  charged as palladium iodide to a stainless steel beaker (placed inside a melt refining zirconia crucible) and heated to  $850^\circ\text{C}$  for  $\frac{3}{4}$  hr. No fume trap was used in this test.

*Test 2 (melt refining furnace B).* One curie of  $^{131}\text{I}$  as palladium iodide charged with 8270 g of unirradiated, depleted uranium-fissium pins to a melt refining zirconia crucible and then heated to  $1400^\circ\text{C}$  and held at this liquation temperature for 3 hr. The crucible was covered with a fume trap which had been previously coated with sodium to simulate conditions in a melt refining run using sodium-bonded fuel pins.

Item	Test 1		Test 2	
	$^{131}\text{I}$ Retained <sup>a</sup> (mc)	Percent of Charge	$^{131}\text{I}$ Retained <sup>a</sup> (mc)	Percent of Charge
Fume Trap <sup>b</sup>	—	—	800	80
Bell Jar <sup>b</sup>	700	70	150	15
Base Plate <sup>b</sup>	150	15	80	8
Crucible Plus Skull <sup>b</sup>	—	—	22	2
Stainless Steel Beaker <sup>b</sup>	10	1	—	—
In-cell Filter <sup>b</sup>	3.5	0.5	0.3	0.05
Ingot <sup>c</sup>	—	—	0.07	0.007
Off-gas Thief Sample No. 1 <sup>e-d</sup>	$8 \times 10^{-5}$	—	$2 \times 10^{-4}$	—
Off-gas Thief Sample No. 2 <sup>e-d</sup>	—	—	$5 \times 10^{-7}$	—
Vacuum Pump Oil <sup>e</sup>	$7 \times 10^{-3}$	—	$8 \times 10^{-4}$	—
Caustic Scrubber <sup>e</sup>	$8 \times 10^{-4}$	—	$5 \times 10^{-5}$	—
Activated Carbon Filter <sup>e</sup>	—	—	$5 \times 10^{-6}$	—

<sup>a</sup> Corrected for decay.

<sup>b</sup> Activity estimated by in-cell monitor (Geiger-Mueller tube) reading. All readings are accurate to  $\pm 15\%$ .

<sup>c</sup> Activity measured on multichannel gamma-ray spectrometer<sup>f</sup>.

<sup>d</sup> Sampling point located at bottom of vacuum line feedthrough in the subcell (see Figure I-30).

<sup>e</sup> Off-gas from system passed through scrubber and separate activated carbon filter prior to discharge to delay tank. The scrubber and carbon filter are not ordinarily part of the off-gas system and were used in these tests for analytical purposes only.

melt refining furnaces, samples of Argon Cell gas were analyzed for  $^{131}\text{I}$  content ascribable to iodine from open melt refining furnaces (see below). A sample of the cell gas was taken five days after the first iodine experiment in furnace A. The  $^{131}\text{I}$  concentration amounted to less than  $1.5 \times 10^{-7} \mu\text{c/ml}$ . Two cell-gas samples were also taken on the sixth and ninth days following the first experiment in furnace B. The  $^{131}\text{I}$  concentrations were approximately  $1.1 \times 10^{-6} \mu\text{c/ml}$  and  $9.1 \times 10^{-7} \mu\text{c/ml}$ , respectively. These values, time corrected for decay, amount to approximately 0.1% of the iodine charge. These results would indicate that  $^{131}\text{I}$  is released very slowly from furnace compo-

nents and fume trap at ambient in-cell temperature ( $\sim 90^\circ\text{F}$ ).

The melt refining furnaces were open (bell jar removed) for most of the time after the iodine runs were completed. Furnace A was open continuously after the first iodine test ended. During the three-day span between the times the cell-gas samples were taken after the second iodine experiment, melt refining furnace B was open for two days and was used one day for the first iodine displacement test.

The off-gas from the iodine runs was discharged to the stack from the holdup tank. A sample stream from the discharge of the tank was scrubbed with sodium sulfite solution, and no detectable amounts of  $^{131}\text{I}$  were found in the scrubber solution.

The fuel pins resulting from an injection casting run on the melt-refined ingot (see Test 2, Table I-18), as well as the heel material from this injection casting run, showed substantially the same concentrations of iodine as the charge ingot. About 1½% of the iodine contained in the ingot was found in the oil of the vacuum pump from the injection casting furnace. The off-gas from the vacuum pump was not sampled.

One additional iodine experiment was performed in order to test the holdup efficiency of the off-gas holdup tank. One curie of elemental  $^{131}\text{I}$  was volatilized and introduced into the off-gas line about 50 ft from the inlet to the holdup tank; a flow of argon gas was provided to carry the iodine to the holdup tank, which contained activated carbon.

During the volatilization step, a monitor was placed on the pipe at the inlet to the off-gas holdup tank. The activity reading increased from essentially zero to 120 mr/hr (almost instantaneously) when the flow of argon carrier gas was started. Subsequent calculations, based on the activity level readings taken at the holdup tank, indicate that approximately one-fourth of the original one curie of  $^{131}\text{I}$  which had been volatilized reached the off-gas holdup tank.

During the three days following introduction of iodine into the system, the gas from the tank was pumped out daily through the silver nitrate tower and a sample of gas from the tank was taken during each pumpout. The tank was filled with fresh argon prior to the second and third pumpouts. The analytical results from the sample taken during the first pumpout, corrected for decay, showed that the estimated total  $^{131}\text{I}$  activity in the gas pumped from the tank to the silver nitrate tower was  $0.14 \mu\text{c}$ . The iodine concentrations in the gas from the second and third pumpouts were less than the limits of detection. Based on the estimated amount of  $^{131}\text{I}$  reaching the holdup tank (0.25 curie), the iodine removal efficiency for the

activated charcoal in the tank was calculated to be greater than 99.99%.

#### e. SKULL OXIDATION

A skull oxidation furnace (ANL-6900, pp. 116-123) and a control system for oxidizing the skull material that remains in the melt refining zirconia crucible after the purified metal has been poured has been installed and tested in the Argon Cell. Oxidation of the skull has the following objectives:

(a) to provide a free-flowing powder, allowing removal of the otherwise tightly adhering skull from the crucible,

(b) to oxidize all of the skull material and thereby eliminate problems of pyrophoricity during storage or future handling,

(c) to prevent nitridation of the skull by the nitrogen (up to 5% nitrogen) in the Argon Cell atmosphere, which would yield a material more difficult to process by the proposed skull reclamation process (ANL-6818),

(d) to reduce the volume for storage of the skull by removing it from the crucible.

The installation and shakedown of the equipment (furnace, oxide dumper, control system) proceeded without difficulty, and the equipment has been used for the routine processing of skulls from the melt refining runs. The skulls have come from the melt refining of unirradiated, enriched fuel,  $^{131}\text{I}$  tracer runs (see *Iodine Tracer Experiments* earlier in this report section), and irradiated fuel (see below).

#### f. INSPECTION AND PROCESSING OF IRRADIATED FUEL

Three irradiated subassemblies were received from the EBR-II reactor: an oscillator rod (OSR-1), an inner blanket (A-718), and a core (C-115). These subassemblies were removed from the reactor after the core subassembly had attained about a 0.1 a/o burnup. Sodium was removed from each of the subassemblies while each was contained in the interbuilding coffin. No problems were encountered in the sodium removal step. The activity level of the removed sodium was low since the reactor had been shut down for a week prior to transfer of the subassemblies. (At the time of transfer to the Air Cell, the blanket and core subassemblies had been cooled for 9 and 10 days, respectively.) The self-heating of the core subassembly, which was calculated to be 380 watts, masked the heat effect (chemical) of the sodium reaction steps. This indicated that the design of the sodium cleanup system, which is based on slow conversion of sodium to sodium hydroxide, was adequate in this respect. After the sodium re-

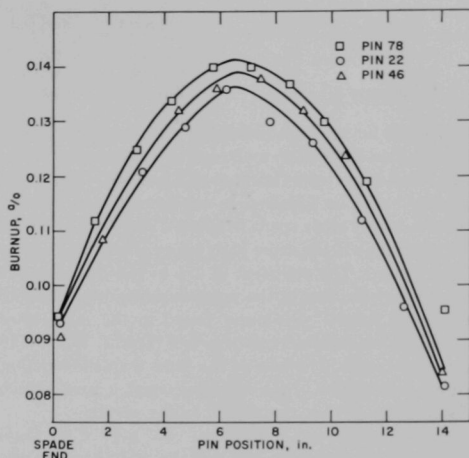
removal step, the oscillator rod subassembly was returned to the reactor building, and the inner blanket subassembly and the core subassembly were transferred to the Air Cell for dismantling operations.

Considerable difficulty was encountered in removing the inner blanket subassembly (A-718) from the interbuilding coffin. This difficulty was later determined to be a result of the upper pole piece being bent approximately  $\frac{1}{4}$  in. from the subassembly centerline. It is not known where the bending took place. After removal from the interbuilding coffin the inner blanket subassembly was dismantled and five of the 19 rods were inspected for swelling. No evidence of swelling was noted. The 19 rods were then transferred to the Argon Cell.

The core subassembly (C-115) was grappled and removed from the coffin with no difficulty. Radiation from the core subassembly when it was introduced into the Air Cell was approximately  $10^5$  r/hr at 1 ft. The core subassembly was then dismantled. All of the fuel elements were checked and were found acceptable for bow and tip condition.\* Eleven fuel elements, representing a cross section of fuel elements through the subassembly, were segregated for sampling and inspection and eight of these were transferred to the Argon Cell for future dimensional checks. (The remaining eighty elements were also transferred to the Argon Cell.) Three of the segregated fuel elements [representing the shortest (Pin No. 78), average (Pin No. 22), and maximum (Pin No. 46) radii from the center of the core subassembly] were decanned, and  $\frac{1}{4}$ -in. long samples were taken at approximately  $1\frac{1}{2}$  in. intervals along the pins and submitted for analysis. Figure I-31 represents the relative burnup (horizontal and vertical patterns) of these three pins. These data are based on the  $^{140}\text{La}$  concentration in the samples which was determined by multi-channel gamma analysis. Analysis of the pins also indicated that, at the reactor operating temperatures (maximum cooling outlet temperature of  $443^\circ\text{C}$ ), about 0.2% of the fission product cesium formed in the fuel was found in the bonding sodium. Because of this migration of cesium to the bonding sodium, cesium is not used for burnup determinations of the EBR-II fuel.

The core fuel elements, inner blanket rods, and sub-

\* If a fuel element is bowed too much, i.e., greater than 1-in. bow over its entire length, it may jam or bend in the decanning machine. The first step of decanning is to shear the spade end tip (see ANL-7020, p. 4) from the element at the juncture of the spade and the fuel. This shear position is gauged from the spade end. If the tip is bent or shortened, the shear point would then be into the fuel.



108-8748

FIG. I-31. Axial and Radial Burnup Distribution for Core Subassembly C-115. (Burnup data obtained by determining  $^{140}\text{La}$  concentration in fuel pin segments.)

assembly hardware, which were surveyed for activity, exhibited the following radiation levels:

Item	Radiation Reading (r/hr at 1 ft)	Time (days) After Reactor Shutdown
<i>Core Subassembly C-115</i>		
91 Fuel Elements	$8.3 \times 10^4$	12
Upper Blanket Elements	190	12
Lower Blanket Elements	215	12
Lower Fixture	0.450	12
$\frac{1}{2}$ -in. long Sample—taken next to spade end of pin No. 46	40	16
<i>Blanket Subassembly A-718</i>		
Blanket Rods	3000	9
Hex Tube	50	9

After transfer to the Argon Cell, the eighty core fuel elements were decanned, chopped, and charged to the melt refining furnace for the first melt refining run (MR-1) with irradiated uranium. The charge (8.6 kg) to the furnace consisted of chopped pins (5.4 kg), injection casting scrap (2.9 kg) and re-enrichment uranium (0.3 kg). The charge was liquated for 3 hr at  $1400^\circ\text{C}$ . The resulting ingot (Figure I-32) weighed 7.95 kg for a yield of 92.7%. Two samples were obtained from the ingot and transferred to the analytical caves for analysis.

Analytical results of the fission product removal obtained in the melt refining run are as follows:

Element	% Removal	Element	% Removal
Cerium	99	Barium	99.9
Iodine	99	Cesium	99.99
Lanthanum	99.9	Zirconium	50

Except for the high zirconium removal, these results are in good agreement with results previously obtained in small-scale experiments (ANL-6696). Zirconium removal will be followed in subsequent melt refining processing of other spent irradiated core subassemblies to determine if the same high removal continues to be experienced. The retention of 1% of the initial iodine content of the fuel in the ingot is substantially higher than the 0.007% previously found in the ingot after a palladium iodide tracer run (see Test 2, Table I-18 of this report). Analysis of the fume trap showed that it contained 80% of the iodine charged, a value which is consistent with the tracer iodine results.

The furnace was allowed to cool over a weekend immediately following the run. Prior to opening the furnace, the following temperature readings were obtained:

Cell Ambient	37°C
Mold Reference	48°C
Crucible (base reference)	70°C
Fume Trap (top reference)	97°C

The above-ambient temperatures of the mold, cru-

cible and fume trap are assumed to be due to the self-heating effects of the fission products.

The melt refining crucible containing the skull from Run MR-1 was transferred to the oxidation furnace (ANL-6900, pp. 116-120), and oxidation (Run SO-1) of the irradiated skull was carried out. The skull charge weight was 632 g and the oxide product weight was 750 g, indicating complete conversion of the uranium to  $U_3O_8$ . The crucible failed structurally when it was dumped into the waste can (ANL-6800, pp. 168-175).

Eleven grams of the skull oxide was removed from the cell for various analyses, including an analysis for zirconium, to determine the behavior of certain fission elements during melt refining and skull oxidation. The zirconium analysis was made in an effort to determine if an excessive amount of zirconium from the zirconia melt refining crucible was being picked up by the oxide product. These results show that approximately 3½ g of zirconia was added to the oxide as a result of spalling or other action of the crucible. This quantity of zirconia resulted in an increase in the zirconium content of the skull oxide of approximately ½%.

There was no indication of partitioning of molybdenum between the ingot and skull.

The ruthenium content of the skull oxide was about 20% lower than expected. This does not indicate a partition of the ruthenium since there was no buildup of ruthenium in the ingot. No ruthenium was found in

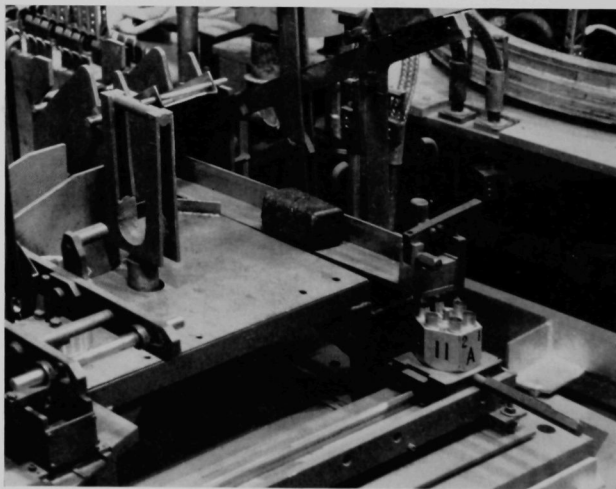


FIG. I-32. Ingot Produced from Melt Refining of Irradiated EBR-II Fuel. (Ingot weight: 7.95 kg.)

a sample from the melt refining furnace fume trap. Some ruthenium may have volatilized as the tetroxide during the skull oxidation; however, no ruthenium was found in the off-gas stream during skull oxidation.

The ingot resulting from Run MR-1 was injection cast into fuel pins, as is described later in this section. The amount of iodine retained by the cast metal in this run differs markedly from that retained in the  $^{131}\text{I}$  tracer run described earlier in this report section. For the tracer run, approximately 98% of the iodine was retained in the cast metal and, within the limits of experimental determination, the iodine material balance was complete. For the irradiated fuel run (Run 3001), however, only 0.6% of the iodine was found in the cast metal. Less than 0.01% was found in the vacuum pump oil and less than  $10^{-5}\%$  was found in the vacuum pump off-gas, which was scrubbed with a sodium sulfite solution. The overall material balance accounts for less than 1% of the iodine initially contained in the ingot.

After completion of work in the Air Cell, the core subassembly fuel elements, all radioactive scrap and blanket material were transferred from the Air Cell to the Argon Cell. The Air Cell was then carefully cleaned by vacuuming, after which it was entered and surveyed for radioactive contamination. Little contamination was found, other than a few stainless steel chips on the dismantler.

The decanning and melt refining operations introduced radioactive contamination into the Argon Cell atmosphere. The major areas where localized activity was detected were on the cooling coils of the Argon Cell cooling system, in the oil and oil separator of the melt refining vacuum pump, and in the holdup tank. Remote monitoring heads from the gamma detectors (Geiger-Mueller tube and Juno) which are located in each of the subcells were positioned at the cooling coils and at the vacuum pumps. These instruments were not calibrated for the longer detector cords used, but the readings did show relative changes in activity levels. During the decanning operation, the readings at the cooling coils increased by a factor of 10. When the melt refining furnace was opened after the irradiated fuel run, the cooling coil reading increased by an additional factor of 15 to 20. During the melt refining run, the activity level of the oil in the off-gas vacuum pump gradually increased to a final radiation reading of two to three times that before the run. When the furnace was pumped down after the cooldown at the conclusion of the melt refining run, the activity level at the vacuum pump increased by about a factor of 30.

Readings obtained with Geiger-Mueller tubes and Juno (ionization chamber instruments) during and after the melt refining run are as follows:

	Radiation Reading (mr/hr) During Run	After Pumpdown of Furnace
At outside of shielding on holdup tank	0.1	2
At outside of ventilation housing on vacuum pump	1.1	35
Cooling coil-cell gas recirculation system	2.5	55 <sup>a</sup>
Filter-cell gas recirculation system	1.3	7 <sup>a</sup>
Oil separator—melt refining vacuum system	—	950 at 2 in.

<sup>a</sup> Melt refining furnace open.

The activity level at the outside of the holdup tank shielding decreased from 2 mr/hr to 1.4 mr/hr after approximately 24 hr. Analysis of a gas sample from the Argon Cell revealed the presence of  $^{131}\text{I}$ ,  $^{140}\text{La}$ ,  $^{103}\text{Ru}$ , and  $^{58}\text{Co}$ . The  $^{58}\text{Co}$  is believed to have originated from the stainless steel jackets removed from the fuel elements during decanning.

The radiation level at the surface of a 10-ml oil sample obtained from the vacuum pump for melt refining furnace B was found to be 180 mr/hr. A radiochemical analysis of the oil showed that it had picked up approximately 675  $\mu\text{c}$  of  $^{131}\text{I}$  during the run. However, the major activity detected was xenon, both  $^{131}\text{Xe}$  and  $^{133}\text{Xe}$ . A calculated value for  $^{131}\text{I}$  in the pump oil (based on the amount of  $^{131}\text{I}$  in the irradiated fuel charged to the furnace and the decontamination factors obtained in the  $^{131}\text{I}$  tracer runs) agreed within a factor of two with the quantitatively determined amount of  $^{131}\text{I}$  in the oil. These results indicate that the decontamination factors obtained in the tracer runs are reasonably valid for calculation of iodine removal.

Analysis of a gas sample removed from the skull oxidation holdup tank following skull oxidation run SO-1 revealed no detectable amounts of  $^{131}\text{I}$ . Based on the activity level of the Argon Cell circulation filter system, the amount of contamination of the cell atmosphere did not change when the oxide was dumped; however, it did increase by a factor of 2 to 3 when the crucible was dumped. A baffle has been installed on the dumper (see ANL-6800, pp. 170-176 for a description of this equipment) to attempt to reduce the spread of activity when the crucible is dumped into the waste can.

### g. BEARING MATERIALS TESTS (with G. A. BENNETT\*)

A program has been initiated to investigate the effects of atmosphere (within the range of that anticipated for the Fuel Cycle Facility Argon Cell) on the life of bearing materials. In previous work on this subject (ANL-5973), the low levels of oxygen encountered in the Argon Cell were not investigated and the moisture content of the experimental environment was not controlled as closely as can be done in the gloveboxes utilized for this program. In addition to extending the range of investigation on these two variables (oxygen content and water content), it is also intended to investigate the effect of nitrogen content on bearing wear. Also, new materials, recommended or developed since the previous investigation, will be evaluated.

The overall purpose of this investigation will be threefold:

1. to determine impurity levels ( $O_2$ ,  $N_2$ ,  $H_2O$ ) in the Argon Cell atmosphere that will be acceptable with regard to bearing wear.
2. to test new bearing materials.
3. to develop an understanding of the causes of bearing wear in inert atmospheres.

The same equipment is being utilized for this experiment as was used in the earlier work. A test consists of contacting a test material against a rotating polished steel cylinder in a glovebox containing the desired test atmosphere.

Initial runs were made which repeated the tests of Carson and Morris (ANL-5973) in order to obtain base line confirmatory data.

Wear rate tests of selected graphitic-base materials were carried out in argon atmospheres containing oxygen, water vapor (35 ppm) and nitrogen (~1%). Preliminary results indicate that lowering the oxygen

\* Chemical Engineering Division.

content to 10 ppm greatly increases the wear rate as compared with similar tests conducted at oxygen contents of 50 to 1000 ppm.

The investigation of materials was extended to very low concentrations of oxygen and water (3 ppm and 1 ppm, respectively) in argon. These conditions resulted in the greatest wear on bearing materials yet experienced. Whether this is an effect of low oxygen content, of low water content, or of both has not yet been ascertained.

The limited amount of available data indicates the following:

(a) Carbon graphites are better base materials than fully graphitized materials. However, unimpregnated materials wear rapidly under the test conditions regardless of whether they are primarily carbon or fully graphitized.

(b) The addition of silver, molybdenum disilicide, resins, or molten salts† as impregnants to the graphitic-base materials is an effective means of reducing bearing wear.

(c) Cadmium, copper, and Babbitt metal are ineffective impregnants under the test conditions.

Future experiments will be carried out for these purposes:

(a) to differentiate quantitatively between various impregnated carbon-base bearing materials,

(b) to compare metallic bearing materials with the carbon-base materials,

(c) to ascertain whether low concentrations of oxygen, low concentrations of water, or both are the primary reasons for the high wear encountered in a very high-purity argon atmosphere, and

(d) to ascertain the effect of radiation on the wearability of selected bearing materials.

† The composition of these salts was not revealed by the bearing manufacturer. This is considered proprietary information.

## 2. Operations with Equipment for Fuel Fabrication (M. J. FELDMAN,

J. P. BACCA, V. G. ESCHEN, D. E. MAHAGIN)‡

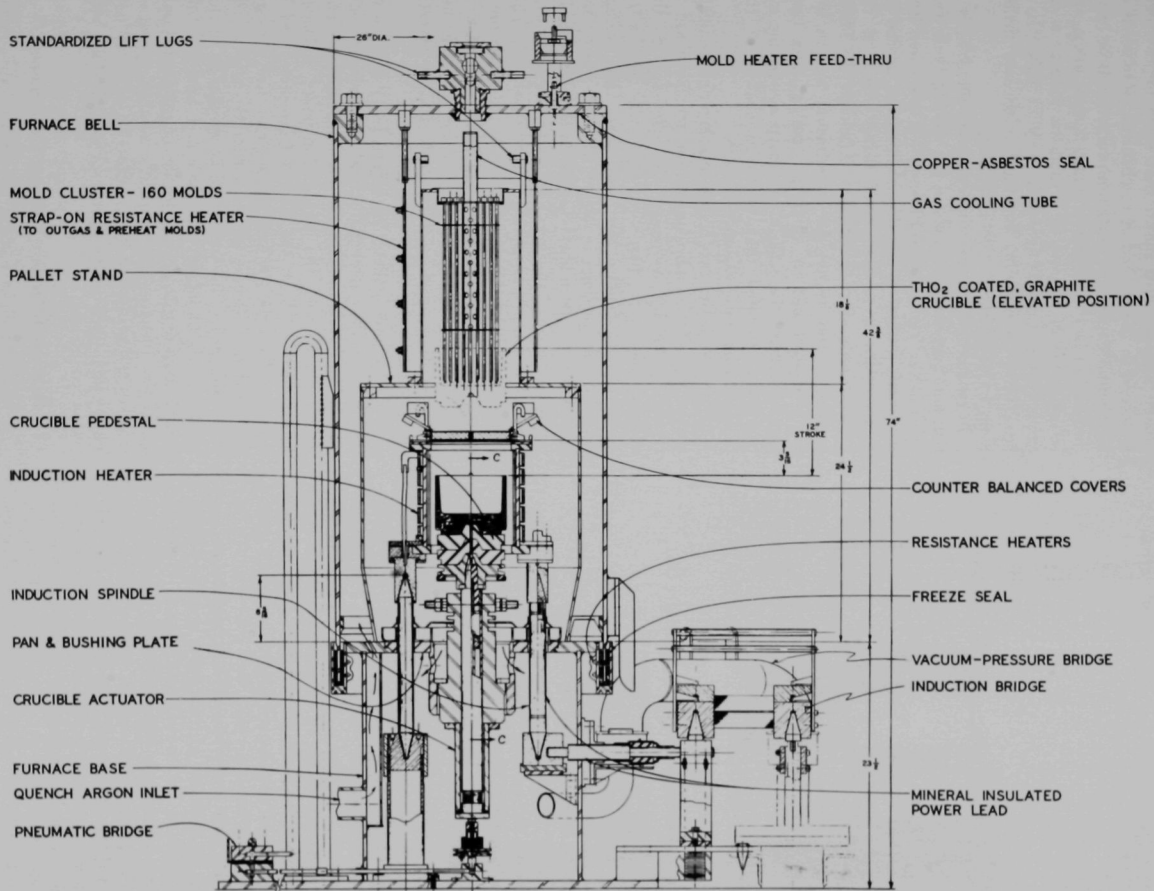
### a. INJECTION CASTING

The basic method of this process is injection or pressure casting of molten fuel into precision-bore Vycor†† (silica) tubes or molds to produce fuel-pin castings of finished diameter but of excess length. In this casting operation, the fuel is melted in a crucible

† Idaho Division.

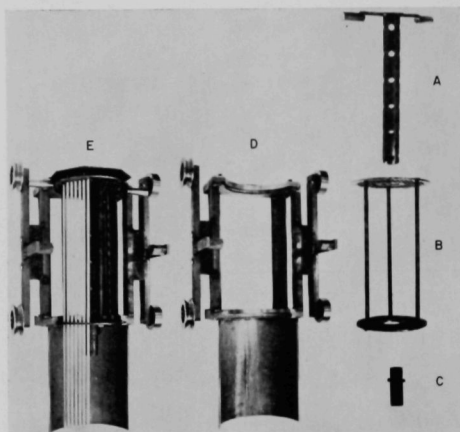
†† Vycor is the trade name for high-silica glass manufactured by Corning Glass Company.

inside a closed furnace (see Figure I-33). Above the crucible, the Vycor molds are suspended vertically in a pallet. The tube molds are open at their lower ends and closed at their upper ends. When the melt is at the casting temperature (about 1300 to 1400°C), the furnace is evacuated, and then the crucible is raised until the molten fuel covers the lower ends of the molds. The furnace is then pressurized to about 25 psia, which forces the molten fuel up into the molds where it solidifies to form the castings. The crucible is



106-5743

FIG. I-33. Injection Casting Furnace.



103-F5374

FIG. I-34. Disposable Pallet and its Transfer Cart.

- A. Center Tube (permanent)
- B. Disposable Pallet Section
- C. Center Tube Lock (permanent)
- D. Special Transfer Cart
- E. Pallet in Special Transfer Cart

lowered before the residual fuel or heel in the crucible freezes to the ends of the molds.

### (1) Equipment Status

The basic injection casting equipment was installed and placed in operation. It is operating as described in a report (ANL-6605) and a journal article.<sup>13</sup> Modifications have been made in the loading and casting operations and equipment. These have included the addition of an immersion thermocouple, the use of a disposable pallet for the molds, and the use of helium (replacing argon) as the pressurizing-quenching gas.

Initially, the casting cycle was controlled on a timed basis, with a thermocouple housed below the crucible as an indicator of the casting sequence. Since some variation in the heating and cooling cycles of the casting sequence is expected with variation in burnup, charge size, and charge composition, it was felt that a direct thermocouple indication of the melt temperature is necessary. To this end, a thermocouple in a tantalum protection tube has been inserted in the center tube of the mold pallet. Operating experience to date has verified the value of this ap-

proach and has also shown that some improvement is needed in the method of mechanical attachment of the thermocouple. The tantalum protection tube has a limited life in the molten uranium-fission alloy, and investigation of the use of a tungsten tube or a ceramic-coated tube is planned. Beryllia tubes have been used successfully, but their brittleness makes them undesirable for remote handling.

In an attempt to control more closely the solidification and quenching portions of the casting cycle, two experimental runs (Run 0.29 described below and Run 3001 with irradiated fuel described earlier in this report section) have been made using helium as the pressurizing and quenching gas. Although the initial purpose of the helium gas experiments was to improve control of the castings' cooling rate (and thereby control the ratio of phases present), the experiments indicated that improved control of the pressurization rate was also possible.

Results from the two helium casting runs indicate that more of the high-temperature gamma phase is retained (thereby increasing the efficiency of the shearing operation) than when argon was used as the pressurizing-quenching gas and that the average length of the castings is longer (thus increasing the probability of obtaining a usable casting length). In the second of the two runs (Run 3001), there was evidence that the pressurization rate was too high. This is an encouraging development, since the argon pressurization cycle, of necessity, had been operated with the control valves fully open up to this time. The use of helium thus provides the opportunity for investigation of an optimum pressurization rate.

The disposable pallet (see Figure I-34) consists of two match-drilled steel plates and three spacer rods. The rods are used to maintain the proper distance and orientation between the plates. The pallet is loaded with coated molds in the Thoria Laboratory and is transferred via the Air Cell to the Argon Cell through the small lock (by means of a special cart) to the work table inside the Argon Cell at window 9. At this location, it is combined with the center tube and lifting bar assembly to allow insertion of the loaded pallet in the furnace. The remote assembly operation requires approximately ten minutes. To date, the pallet has been used for ten runs, and no difficulties have been encountered.

### (2) Remote Injection Casting Experience

A series of eight casting runs with unirradiated, enriched fuel material was carried out remotely in the Argon Cell. The results of these injection casting runs are shown in Table I-19. Experience in the fabrica-

<sup>13</sup> Jelinek, H. F. and G. M. Iverson, Equipment for Remote Injection Casting of EBR-II Fuel, *Nucl. Sci. Engr.* **12** (3), 405-411 (1962).

tion of Core I of the EBR-II reactor indicates that a casting batch efficiency of 80% (good castings  $\times$  100/total molds cast) is the maximum to be expected.

## b. PIN PROCESSING

The purpose of the pin-processing operations is to produce finished fuel pins ready for the cladding operation. In the transition from raw castings to finished pins, the metal is removed from its mold, sheared to length, inspected for length, diameter, weight, and porosity and stacked in an assembly-loading magazine (see Figure I-35). The byproducts of the process are waste molds and chopped fuel. The chopped fuel comes from both reject castings and the shearing operation.

### (1) Equipment Status

The original concept of the pin processing operation as described in a report (ANL-6605) and a journal article<sup>14</sup> has been modified and somewhat simplified by the introduction of a sealed master-slave manipulator (Model A) for use with one of the pin processing stations (at window 5 of the Argon Cell).

During the initial checkout of the pin processing machine, each of the operating modules (shearing, weight measurement, length measurement, etc.) was operated successfully, but transport between operations as designed could not be successfully accomplished. In particular, the two feed trays, which were designed to transport pregnant molds into the demolder and to transport demolded pins to the shear, did not operate consistently.

To overcome these feeding difficulties, the demolder module of the pin processor was removed and mounted separately. Since this module was separated, feeding of both the demolder module and the shear module has been accomplished by means of the manipulator. Design concepts were investigated for refinement of the two automatic feed operations. Although it is believed that these operations can be improved to a point where remote automatic operation is possible, no immediate additional effort is contemplated.

### (2) Pin Processing Machine Calibration

Both the accuracy and precision of the measurements made by means of the pin processor are highly important. These were analyzed by two sets of comparative measurements.

In the first series of determinations, the precision was investigated by measuring two fuel pin standards

<sup>14</sup> Carson, Jr., N. J. and S. B. Brak, Equipment for the Remote Demolding, Sizing, and Inspection of EBR-II Cast Fuel Pins, Nucl. Sci. Engr. **12**, 412-418 (1962).

TABLE I-19. SUMMARY OF INJECTION CASTING RUNS WITH UNIRRADIATED, ENRICHED URANIUM FUEL MATERIAL

*Equipment remotely operated*

Injection Casting Run No.	Charge (kg)	Cast Metal Produced (kg)	Number of Castings	Number of Castings 15 in. or Longer	Number of Acceptable Castings <sup>a</sup>
0.21	10.1	8.1	100	99	86
0.22	11.6	8.4	110	84	62
0.23	11.2	8.2	110	86	71
0.24	9.5	6.5	89	67	52
0.25	10.2	7.2	95	71	48
0.26	8.1 <sup>b</sup>	4.9	75	13	9
0.28	8.5	5.6	76	70	50
0.29 <sup>c</sup>	7.2	4.4	56	54	50

<sup>a</sup> The acceptable casting data are from the pin processing operation. These castings are within tolerance for diameter, weight, length, and porosity.

<sup>b</sup> The charge for injection casting run 0.26 had a high scrap and dross content.

<sup>c</sup> First run in which helium was used as the pressurizing-quenching gas.

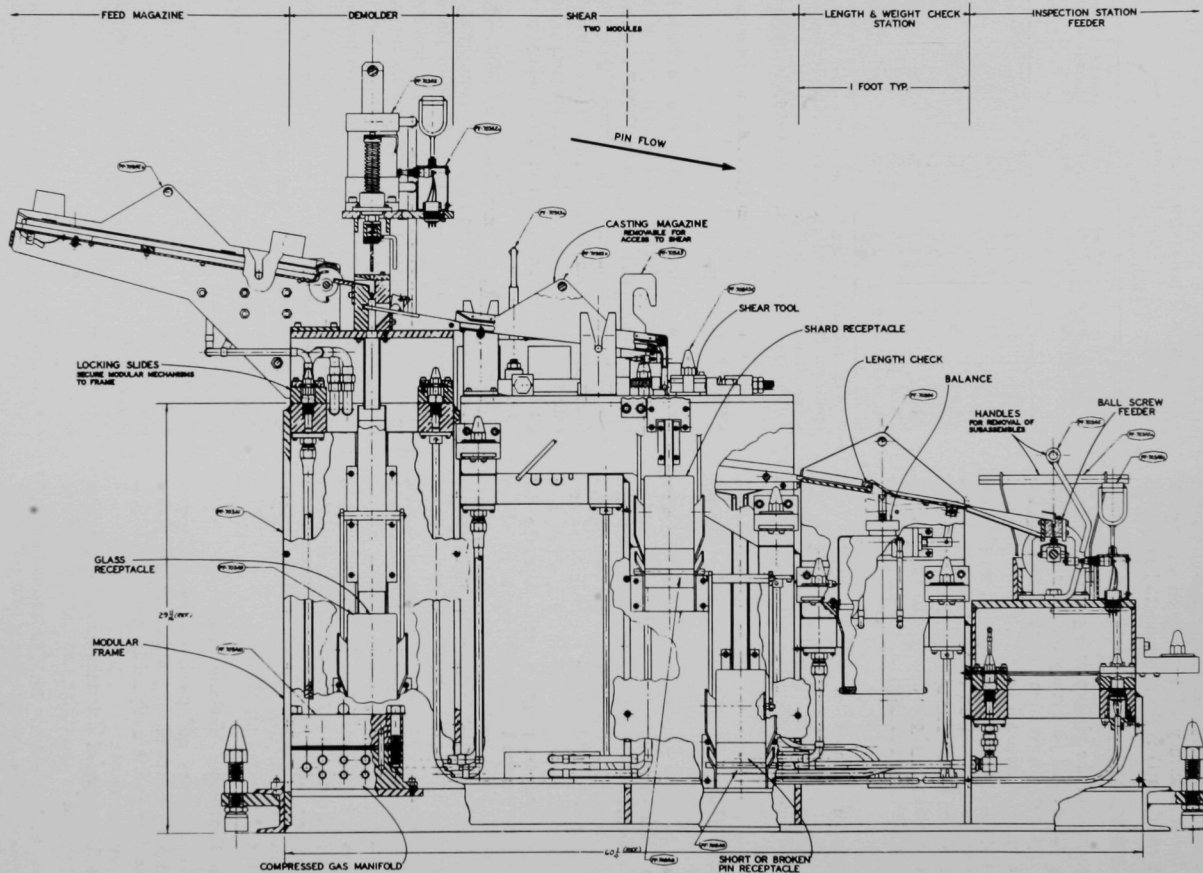
for a total of 25 times each. These two standards had been carefully calibrated in the laboratory to at least one significant figure more than was determined with the pin processing machine. The results of these determinations are shown in Table I-20. The results indicate that the precision of the measurements is adequate for the determination of acceptability of the fuel.

A second series of comparisons was made, whose purpose was to determine the relative accuracy of the pin processor measuring devices. A pin-by-pin and batch comparison of data from six pin processing machine runs (Batches 21, 23-26, and 28-29) with duplicate laboratory measurements has been made in order to determine the batch and individual precision of the data. The mean and the standard deviation for each batch were determined and are compared in Table I-21. In addition, the correlation coefficient,  $r$ ,<sup>\*</sup> was determined for each batch.

From the data presented in Table I-21, the following conclusions can be drawn:

*Length measurements.* Comparison of the means and the standard deviations for the laboratory and pin processing machine measurements indicates that in general the same population is being described. The  $r$  values indicate that with 95% assurance a correla-

<sup>\*</sup>  $r = \frac{\sum (x - \bar{x}) \sum (y - \bar{y})}{\sum (x - \bar{x})^2 \sum (y - \bar{y})^2}$ ; from G. W. Snedecor, Statistical Methods, Iowa State College Press, Ames, Iowa.



106-5742

FIG. I-35. Machine for Fuel-Pin Manufacture.<sup>14</sup>

tion exists between the laboratory and pin processing machine values. With one exception (batch 21 for which  $r$  is 0.323), there is a 99.9% indication of correlation.

*Weight measurements.* As in the length measurements, comparison of the means and the standard deviations for the weight measurements performed in the laboratory and in the Argon Cell indicates that the two sets of measurements describe the same population. The correlation coefficients for these sets of measurements are higher than those for the other three parameters. The correlation coefficient,  $r$ , is designed so that a value of 1 indicates perfect correlation whereas zero indicates random variation.

*Volume.* This dimension is not *per se* a criterion for acceptance or rejection of fuel pins, but it plays an important part in the control of sodium level in the fuel element. Comparison of means and standard deviations indicates that the same populations are being measured. The key to successful sodium level control is indicated by the relatively narrow spread of the values encountered.

*Density.* The spread in values for the density measurements was not expected to indicate good correlation of duplicate populations since the method utilized by the pin processing machine is subject to three separate measurement errors. This parameter is not a criterion for pin acceptance but may have statistical value in radiation damage studies where a large number of pins have been examined.

### (3) Data Handling System

An addition to the data display system which has been described in the literature<sup>14</sup> is an IBM card system. As the data are displayed for an accept-

TABLE I-20. PRECISION OF PIN PROCESSING MACHINE MEASUREMENTS

Parameter	Fuel Pin Sample No.	Mean Value, Laboratory	Mean Value, Pin Proc. Machine <sup>a</sup>	Std. Dev., Pin Proc. Machine <sup>a</sup>
Weight (g)	4	68.7689	68.765	0.010
	15	69.0009	68.944	0.014
Length (in.)	4	14.209	14.209	0.007
	15	14.205	14.201	0.005
Volume (cc)	4	3.8334	3.835	0.010
	15	3.8554	3.843	0.009
Density (g/cc)	4	17.939	18.04	0.055
	15	17.897	18.05	0.045

<sup>a</sup> Based on 25 measurements.

TABLE I-21. COMPARISON OF LABORATORY AND PIN PROCESSOR DATA FOR BATCHES 21, 23, 24, 25, 26, 28, AND 29

Batch	No. of Pins	Mean Value, Laboratory	Mean Value, Pin Processing Machine	Std. Dev., Laboratory	Std. Dev., Pin Processing Machine	Correlation Coefficient, $r$
Weight (g)						
21	85	68.27	68.27	0.247	0.245	0.734
23	67	68.18	68.25	0.248	0.192	0.876
24	51	68.20	68.26	0.359	0.326	0.971
25-26	57	68.25	68.24	0.216	0.215	0.982
28	50	68.29	68.17	0.238	0.185	0.361
29	50	67.70	67.73	0.166	0.163	0.974
Length (in.)						
21	85	14.205	14.206	0.021	0.020	0.323
23	67	14.216	14.212	0.006	0.005	0.865
24	51	14.217	14.214	0.015	0.004	0.369
25-26	57	14.228	14.226	0.014	0.014	0.993
28	50	14.238	14.231	0.006	0.007	0.900
29	50	14.238	14.232	0.003	0.004	0.589
Volume (cc)						
21	85	3.805	3.794	0.014	0.017	0.442
23	67	3.809	3.806	0.010	0.027	0.292
24	51	3.811	3.811	0.014	0.012	0.749
25-26	57	3.811	3.810	0.011	0.018	0.527
28	50	3.823	3.825	0.012	0.013	0.745
29	50	3.811	3.812	0.009	0.021	0.718
Density (g/cc)						
21	85	17.94	17.93	0.067	0.087	0.459
23	67	17.91	17.90	0.119	0.056	0.290
24	51	17.89	17.92	0.086	0.097	0.829
25-26	57	17.91	17.88	0.035	0.047	0.285
28	50	17.85	17.76	0.018	0.041	0.259
29	50	17.76	17.70	0.025	0.070	0.239

reject decision by the operator, the data are also recorded on a standard IBM card.

If the fuel pin being processed is accepted, the card that is generated follows that length of fuel through all of the succeeding fabrication steps. When the fuel pin, after being clad, is used in the manufacture of a subassembly, its position in that subassembly is noted on the IBM card and the card filed. Upon return of the subassembly from the reactor to the Fuel Cycle Facility, the individual clad fuel pin can be position-identified, and any parameters of interest can be compared with preirradiation data.

#### (4) Remote Pin Processing Experience

The products of the eight injection casting runs described in Table I-19 were processed with the pin processing machine. Table I-22 shows the pertinent results of these operations. In general, these acceptance rates are higher than those expected for the initial stages of remote operation.

In order to have data for future comparison, a time study was conducted of one of the pin processing runs (0.24). The results are shown below:

Step	Time (min)
1. Demolding	70
2. Calibration of Physical Measurements	70
3. Processing* (72 castings)	195
4. Data Card Handling	45
5. Scrap Handling	30
Total Operating Time	410
6. Machine Downtime (repair)	120
Total Time for 72 Castings	530

\* Processing refers to shearing and measuring the fuel pin.

#### (5) Reclamation of Fuel Alloy Scrap

In the demolding operation, varying amounts of metal (fuel alloy) scrap are collected along with the crushed glass mold material. Initially, a study was undertaken to ascertain the amount of scrap metal present in the broken glass for Runs 0.21 to 0.29. Table I-23 shows the result of this study.

On the basis of the information in Table I-23, a scrap reclamation step is believed to be necessary. Since the metal scrap in the broken glass is a mixture of short pin castings and metal adhering to the outside of the mold, the general approach chosen was to grind the mixture in a ball mill and then to screen it. In the initial attempts to grind and screen the mixture,

TABLE I-22. PIN PROCESSING RUNS WITH ENRICHED REACTOR FUEL

Casting Batch No.	Castings Received		Fins Accepted	Number Rejected			
	Number	Weight (kg)		Short Castings <sup>a</sup>	Length	Diameter	Porosity
0.21	100	8.1	86	1	13	—	—
0.22	99	8.4	62	15	22	—	—
0.23	96	8.2	71	10	15	—	—
0.24	72	6.5	52	5	13	1	1
0.25	95	7.2	48	24	23	—	—
0.26	75	4.9	9	62	4	—	—
0.28	76	5.6	50	6	20	—	—
0.29	56	4.4	50	2	2	2	—

<sup>a</sup> Castings less than 15 in. in length will not shear correctly and are termed short castings. Castings over 15 in. in length do not always shear to a size within the specification of 14.21 ± 0.030 in. and are rejected then as length rejects.

TABLE I-23. ALLOY METAL PRESENT WITH GLASS SCRAP FROM THE DEMOLDER OPERATION IN PIN PROCESSING

Batch No.	Injection Cast Metal Produced (kg)	Estimated Weight of Uranium-bearing Metal in Scrap Mixture <sup>a</sup> (g)
0.21	8.1	450
0.22	8.4	86
0.23	8.2	506
0.24	6.5	649
0.25	7.2	261
0.26	4.9	779
0.28	5.6	285
0.29	4.4	28

<sup>a</sup> Weight estimated by weight difference between injection cast metal produced and pin processing product.

TABLE I-24. SCRAP METAL RECOVERY FROM CRUSHED AND BALL-MILLED GLASS MOLDS

Batch No.	Estimated Weight of Uranium-bearing Metal in Scrap Mixture <sup>a</sup> (g)	Metal Recovered with Air-Type Separator (g)	Metal in Fines <sup>b</sup> (g)	Recovery (%)
0.21	450	448	9	98.0
0.22	86	57	1	98.3
0.23	506	354	9	97.5
0.26	779	593	4	99.3

<sup>a</sup> Weight estimated by weight difference between injection casting product (see Table I-23) and pin processing product.

<sup>b</sup> By chemical analysis.

it was obvious that the fine silica dust produced by ball milling would be a problem in in-cell handling. In current work, the product of the ball mill has been processed through an air-type separator. The results of four runs for the recovery of metal scrap are shown in Table I-24. Chemical analysis of the reclaimed metal to determine the amount of silica carry-over is underway.

#### c. FUEL ELEMENT ASSEMBLY AND WELDING

In the assembly and welding operations the accepted fuel is placed in the sodium-loaded stainless steel jacket. The partial assembly is then heated to liquify the sodium, and a restrainer is added and welded in place.

#### (1) Equipment Status

The fuel element assembly operation is a simple one and is carried out by means of a master-slave manipulator. The addition of the restrainer-cap to

the fuel element, which was at one time a mechanized operation<sup>15</sup> is now also done by means of the master-slave manipulator.

### (2) Argon Shroud Gas for Fuel Element Welding

A shroud gas is used during welding of the end caps on fuel element cans. The shroud gas was changed from helium to argon when preliminary results by the Chemical Engineering Division indicated that helium contamination of the argon atmosphere was a potential source of difficulty with electrical systems in the Argon Cell. The change to argon required an increase in the power to the welder. This was accomplished by the addition of two 17,000  $\mu$ f, 150-volt electrolytic capacitors to the ten already in the circuit (ANL-6605), making a total of twelve.

Welds made at the increased power and with argon shroud gas have been acceptable as leak-tested. There has been a minor problem of a slumping or off-center weld bead, which is discussed below in the section on leak detection.

### (3) Sodium Level Control

In the fuel element assembly operation, the amount of sodium needed to produce the required sodium level ( $0.65 \pm 0.05$  in. above a fuel pin in its cladding can) is determined from the volumes of the cladding can and the fuel pin. Data on the control of sodium level are discussed below in the section on bonding and bond testing.

## d. LEAK DETECTION

### (1) Equipment Status

The leak detection stations are operating basically as described in a report (ANL-6605) and a journal article.<sup>16</sup> The leak detection method involves sealing the top one-half inch of a fuel element in a test chamber of known volume. This top one-half inch contains the weld, the fuel cans having been leak tested before they were placed in the cell. A metered amount of gas (helium) is forced into the known volume, and the resulting pressure is recorded. If the weld is tight, the metered volume of gas in the calibrated cavity produces a known pressure which remains constant. If the element has a defective weld, the pressure drops below the original value to one corresponding to the

sum of the volumes of the cavity and the gas void in the element.

### (2) Operating Experience

A total of 400 fuel elements which utilized acceptable fuel pins from previously described runs 0.21 to 0.29 were remotely welded and leak detected. Of the 400 welded elements, 28 were rejected for leaks.

As previously mentioned in the section on welding, the off-center welds on the end caps constituted a minor problem. The head (top hat) of the leak detector restricts the overall size of the weld diameter to 0.180 in. (the tubing diameter is 0.176 in.). Thus, an off-center or slumped weld would not, in all cases, enter the leak detectors. To correct these potentially rejectable elements, a small pneumatically operated swaging station was added to the leak detector station. The swage is capable of correcting welds that are less than 10 mils over tolerance (to the time of writing, all of the off-center welds have been less than 10 mils over tolerance).

## e. BONDING AND BOND TESTING

The purpose of bonding and bond-testing operations is to insure the quality and quantity of the sodium heat transfer envelope. The bonding operation is a high temperature (500°C) vibrating impaction step which removes voids in the sodium. The testing operation utilizes an eddy current detection system which measures the integrity of the bond and the sodium level.

### (1) Equipment Status

Initial experience with solenoid-powered, cyclic, impact bonders indicated that inadequate energy for successful sodium bonding was being imparted to the fuel elements. Attempts to increase the impact energy were not successful. The basic bonding machine<sup>15</sup> was modified by replacing the electrically energized system with a pneumatically actuated system. This change provided adequate energy to achieve successful bonding.

A study was made of the effect on bonding efficiency of the major parameters, impact energy and number of impacts. The impact energy (measured as amplitude of element rise) was varied between  $\frac{3}{4}$  and  $1\frac{1}{4}$  in. The number of impacts was varied from 100 to 1000. (Earlier work by the Reactor Engineering Division, ANL-6724, had fixed the optimum bonding temperature at 500°C.) As a result of this work, an amplitude of  $1\frac{1}{4}$  in. and a total of 1000 impacts were chosen as the operating parameters for the sodium bonding operation.

<sup>15</sup> Cameron, T. C. and N. F. Hessler, Assembling, Sodium Bonding, and Bond Testing of EBR-II Fuel Rods, Nucl. Sci. Engr. **12**, 424-431 (1962).

<sup>16</sup> Grunwald, A. P., Leak Testing of EBR-II Fuel Rods, Nucl. Sci. Engr. **12**, 419-423 (1962).

## (2) Effectiveness of Eddy Current Devices for Detecting Sodium Level and Defects in Sodium Bonding

Interpretation of the eddy-current signals of the bond tester for the determination of sodium level and sodium bonding efficiency was an integral part of the startup of the bonding operation. Sodium levels determined by X-radiography (X-ray) of fuel elements were correlated with levels determined with the bond testing machine. These correlations showed interpretation of the eddy-current trace to be accurate to  $\pm 0.030$  in.

Voids or bubbles (a bubble is a large void above the fuel pin and below the restrainer) in fuel elements indicated by eddy-current traces were correlated with the voids or bubbles found by stripping the cladding from the same fuel elements and observing the cladding-sodium interfaces. Approximately 100 elements were stripped. In all cases, a void was observed at the point indicated by the eddy-current trace; conversely, close inspection of the interface revealed no voids ( $\frac{1}{16}$ -in. dia. or larger) that had not been detected by the test coil.

## (3) Operating Experience

Table I-25 summarizes the bonding and bond testing effort on the enriched material (36 kg) which was remotely processed in the Argon Cell. Experience in fabrication of Core I indicated approximately 10% rejections for defects and 15% rejection for level. These runs (omitting 0.22) indicate 1½% rejection for level and 13% rejection for defects.

In other work, a group of 2500 fuel elements from the initial manufacture of core subassemblies for the EBR-II reactor were transferred to the Fuel Cycle

Facility. A large portion of these fuel elements had been made into special backup subassemblies for dry and wet critical tests in the EBR-II reactor. These backup subassemblies had subsequently been dismantled to free the fuel elements for reactor use. A sampling of these fuel elements indicated that the subassembly and the dismantling operations had altered the sodium bond to an extent that rebonding and bond testing were necessary before these fuel elements could be used for reactor subassemblies. Table I-26 summarizes the results of this reclamation work.

## (4) Control of Sodium Level

It is apparent from Table I-25 that, with the exception of one run (0.22), little difficulty in obtaining an acceptable sodium level has been encountered. Statistical analysis of the data from each of the runs has indicated the quality of the operational control. As an example, the results for Run 0.23 indicated a mean sodium level of 0.72 in. and a standard deviation of 0.085. From the data, the predicted acceptance level was 81%. The actual acceptance level was 90%. For batch 0.24, the mean sodium level was 0.651 in. and the standard deviation was 0.068. The predicted acceptance level was 97% and the actual acceptance level was 97.5%.

## f. FINAL ASSEMBLY AND TESTING

The function of the final assembly and testing operations is to combine completed fuel elements into a core subassembly that is acceptable for insertion into the reactor. The feed material consists of accepted elements from the bond and sodium-level inspection station, as well as the externally produced

TABLE I-25. SUMMARY OF SODIUM-BOND TESTING FOR FUEL ELEMENTS MANUFACTURED IN THE EBR-II FUEL CYCLE FACILITY

Batch No.	Initial Bonding			Rebonding			Total			
	Accept	Reject		Accept	Reject		Accept	Reject		
		Level	Void		Bubble	Level			Void	Bubble
0.21	55	0	6	6	0	0	4	61	7 <sup>a</sup>	
0.22	11	37	3	—	—	—	—	11	40	
0.22A <sup>b</sup>	26	4	3	4	0	1	2	30	7	
0.23	50	1	11	1	8	3	0	2	58	5
0.24	36	1	0	12	4	1	0	8	40	9
0.25-0.26	38	0	7	7	5	0	7	2	43	9
0.28	31	0	10	2	3	0	7	2	34	9
Recycle I <sup>c</sup>	12	0	12	0	5	0	6	1	17	7
0.29	Data Incomplete									

<sup>a</sup> Includes 3 damaged fuel elements.

<sup>b</sup> Level rejects from Batch 0.22 were stripped of cladding and recanned.

<sup>c</sup> Rejects from Batches 0.21 to 0.24.

TABLE I-26. RECLAMATION OF NONIRRADIATED FUEL ELEMENTS FROM EBR-II SUBASSEMBLIES  
Subassemblies from initial core manufacture.

Group No.	Number of Elements	Number of Reclamation Cycles <sup>a</sup>	Accepted	Rejected <sup>b</sup>
350	91	2	84	7
351	91	2	88	3
352	91	2	83	8
353	91	2	86	5 (1)
354	91	2	91	0
356	91	2	91	0
357	91	2	89	2
358	91	2	86	5 (2)
360	91	2	87	4 (2)
362	91	2	86	5 (2)
364	91	2	88	3
365	91	2	89	2
366	91	2	89	2 (1)
367	91	2	81	10 (7)
368	89	1	82+	N/A
369	91	2	86	5 (1)
370	91	2	86	5
371	91	1	78+	N/A
372	91	1	82+	N/A
373	91	1	81+	N/A
C-100	89	1	79+	N/A

<sup>a</sup> A normal, first reclamation bonding cycle consists of a total of 1000 impacts at 500°C followed by a room-temperature bond test, with the rejects subjected to a 130°C bond test. A second reclamation cycle follows the same pattern as the first, except that the number of impacts is reduced to 750 at 500°C.

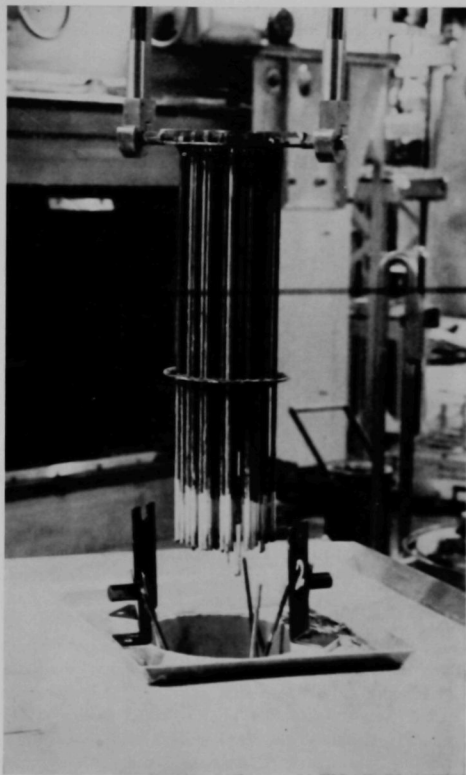
<sup>b</sup> The numbers in parentheses are the numbers of fuel elements rejected because of physical damage during remote handling. N/A means "not available".

components (blanket ends and hexagonal tubing). These materials are fabricated into a subassembly for the reactor. The actual assembly and final welding operations are preceded by an inspection and sizing operation. The final step of the remote refabrication operation is a tensile and straightness test on the complete subassembly.

### (1) Equipment Status

The assembly machine,<sup>17</sup> with very minor modification, was installed and is operating in the Fuel Cycle Facility Air Cell. A second machine (described in ANL-6605), whose function is to tensile test and gauge the straightness of the subassembly, has not proved to be as successful; its tensile testing capabilities have been satisfactorily demonstrated, but the straightness testing portion of the machine has not

<sup>17</sup> R. H. Olp, Remote Assembly of Reprocessed Fuel Subassemblies for EBR-II, in Proceedings of the Eighth Hot Laboratories and Equipment Conference, San Francisco, Calif. Dec. 13-15, 1960, American Nuclear Society, USAEC Report TID-7599, Vol. 2, p. 429.



103-F5456

FIG. I-36. Castings Produced in First Injection Casting Run of Irradiated EBR-II Fuel Material (Run No. 3001).  
108-8546

been adequate. Since it is also intended to straighten a subassembly that is not within specification (0.080-in. T.I.R.\*), a new machine has been designed and is being tested which will function as a straightness tester and straightener. Tensile test capabilities are being added to the assembly machine.

### (2) Operating Experience

Twenty-two subassemblies have been fabricated and tested by remote methods. All 22 passed the tensile test, but only four were indicated to be straight within the requirements of the test machine. Since this fuel had not been irradiated, it was possible to check the straightness of each subassembly in the labora-

\* T.I.R. represents Total Indicator Reading upon rotation about a fixed axis.

tory. The results of the laboratory inspection indicated that the T.I.R. of rejected subassemblies ranged from 0.035 to 0.065 in. Our present testing machine, which was designed to reject subassemblies which deviate from straightness by  $\pm 0.040$  in., has been accepting with a conservative bias.

### g. INJECTION CASTING AND PIN PROCESSING OF IRRADIATED EBR-II FUEL

As described earlier in this report section, an irradiated EBR-II core subassembly (C-115) has been dismantled, decanned, and melt refined. The resulting ingot (MR-1) was transferred to injection casting. The injection casting run (No. 3001) had a charge of 7.95 kg and used 65 molds. The metal cast weighed 5.04 kg. Figure I-36 shows the castings as they were removed from the furnace.

## 3. Fuel Surveillance Program (M. J. FELDMAN, D. E. MAHAGIN, D. C. HAMPSON, D. L. MITCHELL)\*

### *EBR-II Fuel and Blanket Material*

The first two of a series of irradiated surveillance subassemblies were examined. The two, one core subassembly (C-115) and one blanket subassembly (A-718) had been irradiated in the EBR-II reactor to the equivalent of 0.1 a/o burnup. (Transfer of these subassemblies from EBR-II to the Fuel Cycle Facility, dismantling of the subassemblies, and processing of the core subassembly are described earlier in this report section.) The blanket subassembly (A-718) was visually inspected and no deterioration of the chromium and the stainless steel surfaces was noted. No straightness test was attempted since the upper pole piece had been damaged. Five of the individual blanket rods were visually examined; their diameters were checked with a "go no-go" gage, and all rods were accepted by the gage.

The core subassembly (C-115) was visually examined, and no surface degradation was noted. This

\* Idaho Division.

## 4. Performance of Process Auxiliaries (D. M. PAIGE, W.F. HOLCOMB, J. O. KLEFFNER)\*

### a. CONTROL OF TEMPERATURE AND PRESSURE OF ARGON CELL ATMOSPHERE; CELL ATMOSPHERE PURIFICATION

Because radioactivity has been introduced into the Argon Cell, control of the cell pressure at a pressure

\* Idaho Division.

The 65 castings were transferred to the pin processing station. The 65 molds yielded 56 castings which were suitable for processing. Of the 56 castings processed, 36 were accepted, 2 rejected as short castings, 6 rejected for length, 10 rejected for diameter (surface defects), and 2 rejected for internal porosity. This injection casting run was the second of two runs in which helium was used as the pressurizing and quenching gas in the casting sequence. It is believed that the relatively low yield of acceptable castings is due to the high pressurization rate used.

Both the casting and pin processing operations proceeded normally. With the low burnup (approximately 0.1 a/o), no effects of radiation or self-heating were noted, except that the glass molds were darkened appreciably. This is not known to have any effect on the process.

subassembly passed the straightness test (less than  $\pm 0.040$  in. deviation).

Eleven fuel elements (constituting a diametrical row on a core radius) were visually examined; their diameters were checked, their sodium and bonds and levels tested. No hot spots or sodium leaks were noted in the visual examination. In the diameter check, a 0.176-in. "go" gage (0.1765-in. hole) accepted all eleven elements. The bonding and sodium level test indicated some minor void formation and a small statistical increase in sodium level. These effects do not indicate any serious change in the fuel elements, but they do establish the initial points of possible trends.

Eight fuel elements of the eleven have been stored to await further examination. (Three were decanned to provide radiochemical analysis samples, as is described earlier in this section.) Equipment is being prepared to allow determination of the pressure, volume, and composition of the gas in the fuel elements and for the measurement of length, diameter, and weight of the fuel pins.

below atmospheric is required at all times. The system<sup>18</sup> for argon pressure control has operated excep-

<sup>18</sup> Schraidt, J. H., L. F. Coleman, W. F. Holcomb, M. Lewenson and J. O. Ludlow, Establishing and Maintaining a High Purity Atmosphere in EBR-II Fuel Cycle Facility Argon Cell, *Proceedings of the Eleventh Hot Laboratories and Equipment Conference, New York, Nov. 18-21, 1963*, pp. 181-190.

tionally well over the past six-month period. The control has been mainly effected by supplying more or less cooling of the cell atmosphere as demanded by the pressure sensing system. Several times, however, the temperature sensing system took control, in part owing to high cell temperature ( $>100^{\circ}\text{F}$ ), and operated very satisfactorily.

Several samples of cell gas have been taken for mass spectrometric and chemical analyses to determine the concentrations of impurities in the Argon Cell atmosphere. Table I-27 shows some of the values from a recent typical sample.

At approximately the same time that the gas samples were taken, the readings of the gas analyzer instruments on the cell system were 8.56 v/o nitrogen and 40 ppm oxygen. The high reading on the nitrogen instrument can be explained if it is assumed that the instrument is eight times as sensitive to helium as it is to nitrogen (this is the ratio of the thermal conductivities of the two gases as compared to argon).

An in-cell experiment was run to determine the effectiveness of Linde 5A Molecular Sieves\* for removing  $\text{CO}_2$  from the Argon Cell atmosphere (see ANL-6900, p. 103). Carbon dioxide may be introduced from the radiolytic decomposition of organic materials (lubricants, etc.) in the Argon Cell. The adsorbent was first completely regenerated to remove all water. About two cell volumes of gas were then passed through the bed, and gas samples for  $\text{CO}_2$  analysis were taken before and after the run. Analytical results showed  $\text{CO}_2$  concentrations of 74 ppm before and 24 ppm after the run, representing approximately 2.5 cu ft of  $\text{CO}_2$  removed. Since water will displace the  $\text{CO}_2$  on the bed, another regeneration of the bed is required before it can be used for water adsorption. The cell gas will be periodically sampled to determine whether the  $\text{CO}_2$  concentration is increasing.

Since the last argon fill (February 1964), it was determined that the Argon Cell atmosphere can be maintained at levels as low as 5 ppm water and 8 ppm oxygen. However, because a high rate of wear of carbon bearings and motor brushes was assumed to be the result of operation at this low moisture level, the water and oxygen concentrations in the cell atmosphere were increased to and purposely maintained at  $40 \pm 20$  ppm each. Thus far, operation at these new water and oxygen concentrations has worked out very satisfactorily; however, some higher levels of water and oxygen have occurred over weekends when the purification system has been shut down.

Only one item of mechanical difficulty has been

\* Linde 5A Molecular Sieves is used in desiccant bed of argon purification system.

TABLE I-27. CONCENTRATION OF IMPURITIES IN A SAMPLE FROM THE ARGON CELL ATMOSPHERE

Contaminant	v/o
$\text{N}_2$	5.85
He	0.40
$\text{H}_2$	<0.001
$\text{CO}_2$	0.0019 (chemical analysis)

noted in the purification system since the last argon fill in February 1964. A ball bearing on the turbo-compressor became overheated because of excess lubrication. Inspection of the bearing showed that the grease chamber was completely filled. Because of the use of remote grease connections and long fill pipes, it is difficult to use normal lubrication techniques. Removal of this excess appears to have solved the problem.

In general, the minimum air in-leakage rate observed (calculated from oxygen buildup) has been in the range of 0.003 scfm at a cell pressure of minus 3 in. of  $\text{H}_2\text{O}$ . Higher rates have usually been traced to air leaking through lock gaskets or through process equipment piping outside the cell. If it were not for these occasional higher rates, it would be possible gradually to reduce the nitrogen content of the cell atmosphere by dilution with fresh argon as required for lock transfers or pressure adjustments. A short test of this nitrogen dilution approach was made using 1810 cu ft of fresh argon; the nitrogen content was reduced from 6.86% to 6.58% or 0.015% per 1000 cu ft added argon in the 6% nitrogen range. Since the test was short (<1 hr), no correction was made for the air in-leakage rate of 0.3 cfh. This indicates that approximately 400 cu ft of fresh argon per day would be required to keep up with a minimum leak rate (0.3 cfh). This is the amount of fresh argon that is required when making a large lock transfer, and presumably argon added in amounts greater than this would reduce the nitrogen content.

## b. CRANES AND MANIPULATORS

Table I-28 summarizes the total hours of usage of the motor drives of the cranes and manipulators for 6 months (May through October 1964). The manipulator bridge drive was the most used component, average usage per manipulator being in the range 40 to 70 hr. The next most used unit was the manipulator hoist drive (30 to 50 hr per manipulator), followed by the manipulator carriage drive (about 25 hr per manipulator). Crane bridge drive and manipulator grip and rotate drive usage was of the order of 5 to 25 hr each.

TABLE I-28. IN-CELL CRANE AND ELECTROMECHANICAL MANIPULATOR COMPONENT USAGE  
May through October 1964

Type of Unit	Number of Units	Total Hours of Use for Each Type of Unit				
		Grip	Rotate	Hoist	Carriage	Bridge
Argon Cell Manipulators	6 <sup>a</sup>	90	45	160	130	210
Air Cell Manipulators	2	10	10	100	50	135
Argon Cell Cranes	2	—	—	40	16	50
Air Cell Cranes	1	—	—	35	10	12

<sup>a</sup> One unit out of service for 2½ months.

### (1) Cranes

One five-ton crane is installed in the Air Cell, and two are installed in the Argon Cell. Once reprocessing of radioactive fuel has commenced, radioactive contamination is expected to make direct personnel access to these cells impossible. Therefore, a considerable effort has been spent on making the cranes (and all other mechanical equipment in the cells) reliable and remotely maintainable.

Since the preceding semiannual report (ANL-6900), a new lifting tool for the crane-bridge drive unit has been designed and built. The lifting hooks are spring-loaded and are provided with indicators to warn operators of interference or binding during removal or installation of a drive unit. This feature is desirable because the drive units are located in lead-shielded boxes on the crane-bridges close to the ceiling of the cells and it is rather difficult to observe the removal or replacement operation.

The cranes have been operating with no discernible difficulties, except that the up-limit switch on the Air Cell crane was thought to have failed several times. On careful study, the trouble was traced to the brush contact on the Air Cell bus bars. These bars had been corroded by water leaking through the roof at various locations. This corrosion was not severe enough to effect the 220-volt lines, but the 24-volt lines were not making adequate contact at several points. Cleaning the bars and coating them with a conductive graphite seems to have solved the problem (the roof leaks are being repaired also). The slip clutches installed between the gear motor and the main hoist reducer approximately one year ago appear to have protected the mechanical parts from damage to a significant degree.

The manipulators have operated without difficulties, except for an accident due to an operational error.

On July 23, 1964, a manipulator carriage in the Air Cell was accidentally dropped while being removed for transfer into the Argon Cell as part of a maintenance operation. The removal was done remotely with the jib-crane located on the Air Cell roof and involved dropping the jib-crane hook through one of the roof penetrations. Apparently, the hook engaged one of the outer lifting lugs on the lifting beam adapter for the manipulator carriage. These lugs are intended only for transportation of the unloaded beam when using a manipulator dual hook and are not designed for lifting the beam with a carriage attached. The jib-crane hook should engage a heavy cross-bar in the center of the beam adapter. However, it is very difficult to observe the hook when it is located above a manipulator carriage on a bridge. The operator, who attempted to get the best possible view of the operation under a simulated remote transfer condition, thought the hook was properly engaged. The assumption that the hook was properly engaged was supported by the fact that the carriage was lifted clear of the bridge. It was not until the bridge had been removed and the lowering of the carriage had started that the outer lug of the lifting beam adapter broke off. The carriage and beam dropped about 12 ft and fell onto one of the collapsible service stands situated on the transfer cell hatch cover in the Air Cell. It dented the cell hatch cover, twisted the stand, and came to rest on the floor tilted at a 45° angle.

The impact drove the telescoping arm up through the carriage, tilting the lifting beam so that the lifting lugs on the carriage were sheared off. The mounting plate for the manipulator hoist mechanism was torn loose and bent, and there was other damage such as sheared bolts, bent shafts, broken mineral-insulated cables, etc. However, it appears that most of the major components of the manipulator carriage can be reused and that the damage was surprisingly light considering the distance of fall. A large portion of the impact energy was undoubtedly absorbed by the Air Cell hatch cover and the service stand. Other equipment in the Air Cell was not damaged. The carriage has been dismantled, new parts ordered, and repairs of the damaged parts initiated. One of the six manipulator carriages in the Argon Cell has been transferred to the Air Cell to help carry the work load there. (When this was done, it was discovered that the carriage motion was the reverse of that indicated by the control box. Necessary corrections consisted of reversing the two leads to the field of the Air Cell carriage motor and reversing the armature leads in the control cabinets for the Air Cell manipulators.)

### e. DRY ARGON COMPRESSORS

Two horizontal 2-stage dry compressors are used to supply compressed argon at 100 lb/sq in. for the various in-cell pneumatic equipment items (see ANL-6800, p. 154). Because of the very dry atmosphere, the piston ring (horizontal pistons) wear has been excessive.

The compressors were originally supplied with piston rings of carbon-filled Teflon. The wear rate for these piston rings is shown in Figure I-37 as a function of piston-to-cylinder clearance. The data show a reliable service life of only 1700 hr. Piston rings of carbon- and glass-filled Teflon were tried and wore to the minimum clearance in 500 hr of operation, which was unsatisfactory service life. For future testing, a different formulation of carbon-glass-Teflon is being obtained. Piston rings of this material should provide increased service life if the increase is as great as that obtained by the Metallurgy Division, Argonne, Illinois, with the same material installed in a similar compressor operating with helium.

### d. CELL VIEWING DEVICES

The periscope in the Air Cell has been used to take several detailed pictures of irradiated fuel subassemblies removed from the EBR-II reactor. Very good pictures can be obtained if the object is held station-

ary; approximately 10-min exposures are required with fast film.

A closed-circuit television monitor system was set up and tested in the Air Cell (no activity present in the cell). A very good picture was obtained on the monitor, especially with an auxiliary light mounted on the camera. The system appears to be useful for special maintenance jobs or for finding items lost under equipment. For use in the Air Cell, the leads could be brought through one of the floor conduits. For use in the Argon Cell, a special feed-through would be required with coaxial cable for the one lead. It is recognized that normally the system could be used only for short periods because of the high radiation levels expected in both cells.

### e. HIGH-LEVEL-ACTIVITY SOLID WASTE HANDLING

Plans are now well formulated for handling the high-level-activity solid wastes generated in the Air and Argon Cells (see ANL-6900, p. 112). The primary container will be a steel pail, 10-in. dia. by 11 or more in. deep, similar to those used for paint, that can be sealed remotely. Up to five or six of these pails will be placed in a 6-ft high steel can, after which it will be sealed. The sealed can will be loaded into a shielded cask (8½ in. of lead) through the floor shielding plug at the west end of the Air Cell. The

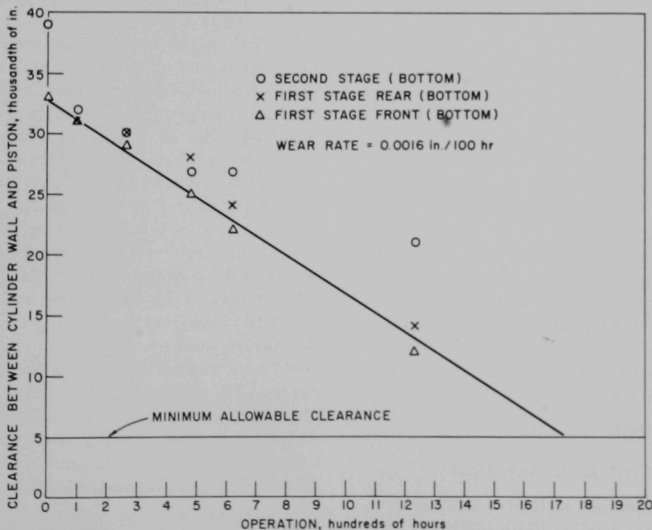


FIG. I-37. Wear Rate for Carbon-Filled Teflon Piston Rings in Dry-Argon Compressor No. 1.

cask (18 tons) will be transported to the nearby burial ground by means of a special low-bed trailer being fabricated.

Final disposal will be in a 12-ft deep hole lined with steel pipe ( $\frac{1}{4}$ -in. thick wall by 16-in. dia.). After the cask is positioned over one of these holes, the 6-ft can will be dropped from the bottom of the cask. Gravel can then be added as backfill to a depth of 6 ft to form a shield. To seal the hole, a cover will be welded to the hole liner; the waste will then be doubly contained. The holes will be suitably marked, and records will

be kept of the material (estimated) in each hole.

To date, the primary containers and the 6-ft tall cans have been handled very satisfactorily within the cells. (Several, containing active waste, are stored in the Argon Cell pits.) The shielded cask has been received and set up, but has not been loaded at the Air Cell yet. Construction of the special trailer has been completed. Work is completed on the burial ground and the road servicing it. Approximately 30 of the 2500 holes planned have been drilled and liners with covers installed.

## D. CHEMISTRY OF LIQUID METALS (I. JOHNSON, H. M. FEDER)

The chemistry and thermodynamic properties of liquid metal systems and metallic alloys are being investigated to provide basic data for the pyrochemical processing of nuclear fuels and for liquid alkali metal

technology. The results of these studies also provide data for the testing of theories of liquid metal solutions.

### I. Liquid Sodium Chemistry

The increasing utilization of liquid alkali metals as heat transfer media in high power-density, nuclear reactors and other power sources makes essential a continuing advancement of alkali metal technology. To insure the soundness of such an advance the support of fundamental research is needed. A program to elucidate the chemistry of the reactions that occur in liquid alkali metal solutions has been undertaken; special emphasis will be given to liquid sodium because its practical importance is greatest.

Sodium of known, high purity is needed for significant research. Therefore studies are being made in the closely related areas of purification, analysis, and contamination during handling. Three common contaminants in sodium—oxygen, hydrogen, and carbon—appear to be particularly important with regard to its corrosive properties. An understanding of the major reactions involving these contaminants in liquid sodium will furnish a basis for a better understanding of corrosion mechanisms and possibly lead to new methods for corrosion control.

#### a. SODIUM ANALYSIS

##### (1) Oxygen (G. LUTZ,\* K. E. ANDERSON)

A fast-neutron activation method (ANL-6800, p. 189) which involves the reaction  $^{16}\text{O}(n,p)^{16}\text{N}$  has been chosen for the analysis of total oxygen in sodium (ap-

prox. 1-g samples). A major obstacle to the realization of this method is the requirement of a sample encapsulation material which does not interfere because of its own oxygen content. Two approaches have been applied to this problem.

The first approach was the conventional one of using an encapsulation material with as low an oxygen content as possible. Two samples of 2S aluminum and one of OFHC (oxygen-free high conductivity) copper were examined. The 2S aluminum samples were formed into capsules whose oxygen blanks were 10 and 30 ppm. After repeated irradiation (to obtain adequate counting statistics for samples low in oxygen) and counting of the aluminum capsules, no appreciable buildup of long-lived activity was found within the energy range used for counting  $^{16}\text{N}$ . There is reason to believe that if capsules were made of aluminum which has been vacuum liquated and bottom poured, the oxygen content would be low enough to permit analysis of sodium samples containing about 10 ppm oxygen. The protective oxide layer which forms on aluminum can be kept to about 20 Å thickness if the surface is cleaned properly and protected from subsequent contamination, particularly by chlorides. Such a surface layer would contribute only one to two micrograms of oxygen to the blank.

Capsules made from OFHC copper indicated oxygen contents equivalent to about 30 ppm. However, repeated irradiations gave rise to the buildup of a long-

\* Post-doctoral Fellow, now at U.S. Bureau of Standards.

lived activity which counted in the same energy range as  $^{16}\text{N}$ . The impurity in copper responsible for this induced activity has not been identified.

The second approach was to irradiate the sodium at one end of an 8-in.-long polyethylene tube and then to transfer the sodium to the other end for counting. An estimate based on ideal geometry alone indicated that counting of sodium at the unirradiated *vs.* the irradiated end of the tube would decrease the blank due to oxygen by a factor of three. Only a 30% reduction was actually found. The polyethylene- and copper-encapsulation techniques were abandoned after finding that 2S aluminum capsules gave significantly lower oxygen blanks.

Routine analysis for oxygen in sodium by fast-neutron activation has been turned over to the Chemistry Division. Samples of sodium which contain 50 ppm oxygen or more (i.e., a majority of the samples) can be analyzed using the apparatus and 2S aluminum capsules now available. Further improvements in quality of the capsule materials, higher neutron fluxes, and more reproducible irradiation and counting geometries should make this method suitable down to 10 ppm oxygen in sodium.

## (2) Carbon (C. LUNER, C. CLIFTON)

Various current studies require a method for the determination of carbon in sodium. Most of the analytical techniques described in the literature<sup>19-22</sup> are based on the oxidation of carbon to carbon dioxide and subsequent measurement of the quantity of evolved gas. The principal variations occur in the oxidant used and the method of liberating and measuring carbon dioxide. For example, the oxidation of carbon may be carried out by direct combustion with oxygen or by use of a strong oxidizing agent, such as Van Slyke reagent. Some of these techniques were recently tested<sup>23</sup> in a cooperative study by various laboratories. The results were highly scattered, and it is not clear whether they afford a valid comparison of the analytical methods or, in fact, reflect differences attributable to variations in sampling and sample preparation techniques.

In the light of this uncertainty, it was felt necessary

to pursue further the problem of reliability of analytical and sampling techniques. Two variants of the so-called "dry" oxidation method have been tried. The sample is first burned in low-pressure (150 torr), purified oxygen to form a residue of mixed sodium oxide and carbonate. The combustion tube is loaded in a helium-filled glovebox to avoid exposure of the sample to air. The oxygen used in the reaction is of ultra high purity and is further purified by passage through two furnaces containing both platinum and copper oxide at 950°C, two ascarite traps, and a cold finger kept at -180°C by liquid oxygen.

In the first variant the residue is heated in a silica boat to 1100°C in oxygen. The carbon dioxide liberated by the reaction of sodium carbonate and silica is collected in a cold trap (liquid oxygen coolant) and subsequently measured manometrically. Reagent blanks of 4  $\mu\text{g}$  or less have been consistently obtained. After each analysis, the reaction tube is treated with phenolphthalein solution to determine whether any sodium oxide has deposited in the cold zone where it might reabsorb carbon dioxide.

In the second variant, which is a modification of the method reported by Kallman and Liu,<sup>21</sup> the sodium is burned as in the "dry" oxidation, but carbon dioxide is released from the residue by the addition of dilute sulfuric acid. The liberated gas is then measured by gas chromatographic techniques. The reagent blanks in this method have consistently been 1.5 to 2  $\mu\text{g}$ .

A comparison of the two variants was made with various samples withdrawn over a short interval of time from a pot of liquid sodium. The results of this comparison are shown in Table I-29. The fairly good agreement between the average results of the two methods indicates their general equivalence. However, the rather large spread of apparent carbon contents points to the likelihood that there is a sampling problem. This problem is further discussed in part c, below.

TABLE I-29. APPARENT CARBON CONTENTS (PPM) OF LIQUID SODIUM AT 158°C BY THE "DRY" OXIDATION METHOD

High Temperature Reaction	Acidification Reaction
88	47
106	87
55	112
71	48
72	62
63	
Average 76 $\pm$ 18	71 $\pm$ 27

<sup>19</sup> L. P. Pepkowitz and J. T. Porter, II., KAPL-1444, Nov. 28, 1955.

<sup>20</sup> J. Herrington, AWRE-O-62/62, November 1962.

<sup>21</sup> S. Kallman and R. Liu, Anal. Chem. **36**, 590 (1964).

<sup>22</sup> T. G. Mungall, J. H. Mitchen and D. E. Johnson, Anal. Chem. **36**, 70 (1964).

<sup>23</sup> R. W. Lockhart and W. W. Sabol, in letter to AEC, "Results of the First Round Robin Analysis for Carbon in Sodium," General Electric Co., Atomic Products Equipment Department, San Jose, Cal., Feb. 23, 1962.

## b. SODIUM PURIFICATION (C. LUNER, C. CLIFTON)

One of the principal requirements of the experimental program is a supply of ultrapure sodium. Such sodium would be an aid in the development of the methods for analysis of carbon and oxygen in the parts per million range. Ultrapure sodium is also required for experiments designed to examine various reactions of liquid sodium. Three methods for the purification of sodium are now being examined.

Vacuum distillation has been frequently mentioned in the literature as the method of choice. Accordingly, a stainless steel still has been constructed and operated. Spectroscopic analysis of sodium distilled in this apparatus indicates that the metallic impurity content has been decreased; however, carbon contents below about 50 ppm have not been achieved. Because this may have been due to contamination by back diffusion of pump oil, the pumping system has been modified to include a trap containing Linde Molecular Sieves, Type 13X. Further work on the vacuum distillation method will be carried out.

Centrifugation has not been previously applied to sodium as a method of purification. Carbonaceous particulate matter capable of passing through a 5 $\mu$ -porosity filter has been found in all samples of sodium that we have examined. (Such particles may also be entrainable in distillation.) Calculations indicate that particles larger than 1 $\mu$  should be removable by centrifugation at reasonable speeds and temperatures. A high temperature centrifuge (500°C maximum) capable of operating in a helium-filled dry box has been designed and is now being constructed.

Zone refining of sodium has not been reported in the literature although the technique has been used extensively for the purification of other metals. In principle, the method depends on the difference in solubility of an impurity between the solid and liquid phases of the material being refined. Zone refining may also provide removal of particulate impurities by their segregation to a moving liquid-solid interface. Simple zone refining equipment has been ordered to test the feasibility of purifying sodium by this technique.

## c. "SOLUBILITY" OF CARBON IN LIQUID SODIUM (C. LUNER, C. CLIFTON)

It has been established that various metals may be significantly carburized or decarburized when in contact with liquid sodium. This phenomenon presents a potentially serious problem relative to the use of liquid sodium in nuclear reactors. Undesirable changes in the mechanical properties of structural materials, such as steel, may result from small changes in carbon content.

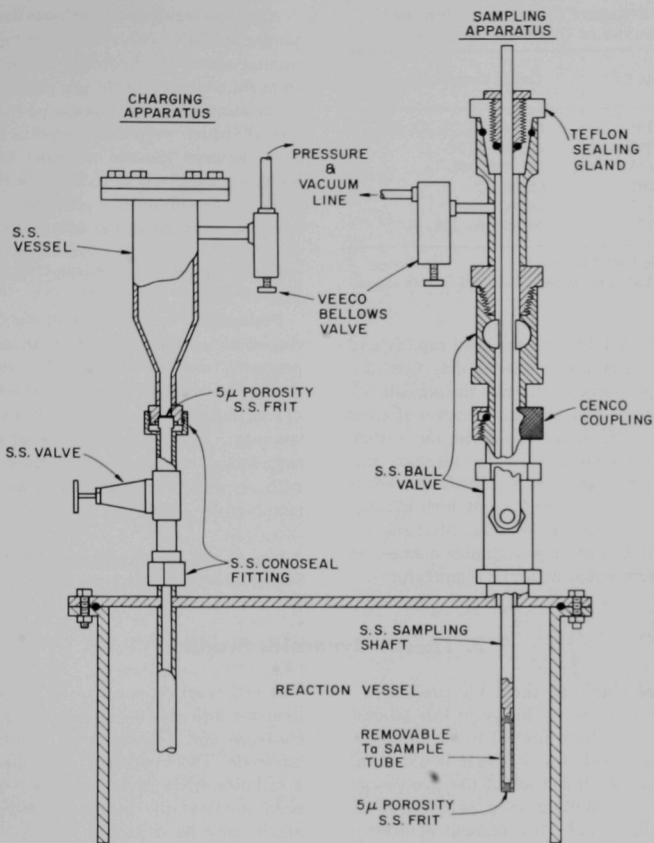
Various mechanisms of carbon transport have been proposed in the literature but the problem remains unresolved. A study of the transport of carbon in sodium must commence with understanding the chemical nature of carbon in sodium. The present study has been directed toward the determination of whether or not a true solubility of carbon in sodium exists.

A cross-section of the solubility apparatus is shown in Figure I-38. Distilled sodium was added to the charging vessel under a helium atmosphere; it was then pressured into the reaction vessel through a 5 $\mu$ -porosity stainless steel (S.S.) frit. The filtered sodium was held at various temperatures in a graphite crucible which had been previously outgassed at 1000°C in vacuum. Samples were taken by lowering a tantalum sample tube whose lower end was closed by a 5 $\mu$ -porosity S.S. frit into the melt and pressurizing to about 3 atm with purified helium. The sample tube was isolated by means of the two ball valves, and the sampling apparatus was then disconnected at the Cenco coupling and removed to a helium-filled glovebox without exposure to the atmosphere.

The analyses were performed by the high temperature "dry" oxidation method. All the individual analyses of replicate experiments are given in Table I-30. Noticeable in the data are their tendency to scatter erratically. If there is, in fact, any significant increase in carbon content with temperature, it is concealed by other sources of variability. These results suggested that the original sodium contained carbonaceous particulate matter capable of passing through a 5 $\mu$ -porosity S.S. filter.

To check the particulate hypothesis, graphite which had been pulverized in the dry box was intentionally added to sodium in a graphite crucible and the previous experiment was repeated at a constant temperature of 316°C. The results were revealing. Although the starting sodium (sampled as a solid) had a carbon content of 220 ppm, the first filtered sample obtained after eight days of contact, one hour of stirring, and one hour of settling contained 760 ppm of carbon. After six days of settling, two samples contained 70 and 230 ppm of carbon. It is evident from these experiments that particles of graphite were readily dispersed in sodium, that some of these particles were small enough to pass through 5 $\mu$ -porosity filters, and that the degree of aggregation of the dispersion depended in some complex way on its previous history. Briefly, this study does not appear to support the existence of a readily measurable equilibrium in the graphite-sodium system, such as that reported by Gratton.<sup>24</sup> Further work is required to clarify this situation.

<sup>24</sup> J. G. Gratton, KAPL-1807, June 30, 1957.



108-8709

Fig. I-38. Solubility Apparatus for Determination of Carbon in Sodium.

#### d. SODIUM-GAS REACTIONS (J. G. SCHNIZLEIN, R. A. BLUMQUIST)

Impurities can be introduced into sodium by reactions with contaminants present in cover gases. Because such reactions are important with respect to sodium technology for nuclear reactors, the reactions of sodium with various gases are being investigated. Helium containing various contaminants has been bubbled through liquid sodium and the extents of the reactions have been qualitatively determined by mass spectrometric analysis. More detailed studies of the kinetics of reactions of pure gases at low pressure are being made in a static system.

The apparatus for bubbling contaminated helium through sodium consists of a Toepler pump, sampling

bulbs, a S.S. 304 reactor, and an associated vacuum system. The sodium is supported on a S.S. frit of  $5\mu$ -pore size in a  $1\frac{3}{8}$ -in.-ID reactor. The frit disperses the gas, thereby assuring good contact with the sodium. The Toepler pump recirculates the gas at a flow rate of 100 cc/min (10 cm/min linear velocity).

In preliminary experiments the helium was contaminated with 1000 to 2000 ppm each of the following gases: oxygen, nitrogen, carbon dioxide, carbon monoxide, hydrogen and methane. The concentrations of the contaminants in the gas were determined by mass spectrometric analyses of samples collected at various times up to 6 hours. Experiments were conducted at 190, 300, 385 and 455°C.

In all experiments, as was expected, oxygen and

TABLE I-30. APPARENT CARBON CONTENTS OF SODIUM CONTAINED IN GRAPHITE CRUCIBLES

Order of Sampling	Temp. (°C)	Carbon Content (ppm)
1	158	88, 106, 55, 71, 72, 63 <sup>a</sup>
2	307	41, 56, 58, 57
3	455	101, 116, 108
4	291	61, 80, 47
5	157	74, 66, 130
— <sup>b</sup>	375	59, 127, 96, 130, 45

<sup>a</sup> Taken from Table I-29, Column 1.

<sup>b</sup> A second master batch of sodium was used in this experiment.

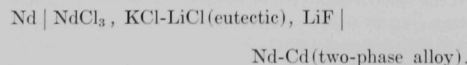
carbon dioxide were found to be consumed rapidly and completely within analytical limits of detection. Although the mass spectrometer did not distinguish between carbon monoxide and nitrogen because of their coincidence at mass 28, in all likelihood the carbon monoxide reacted completely while the nitrogen was unaffected. Hydrogen contents decreased to levels which were, presumably, in equilibrium with unsaturated solutions of hydrogen in sodium. Methane reacted rapidly at 455°C, but only negligible changes in its concentration were noted at lower temperatures.

## 2. Thermodynamics Studies

Three methods of obtaining thermodynamic information on metallic systems are in use in this laboratory. (a) Galvanic cells have proved to be especially useful for the measurement of activities in liquid metal solutions and for the determination of the free energy of formation of the equilibrium solid phase in solid-liquid two-phase alloys. (b) Measurement of decomposition pressures by the Knudsen effusion method has been effective for the two-phase regions of systems composed of several well-defined intermetallic phases. (c) A vapor phase optical absorption method is being employed for certain systems in which the components have appreciable vapor pressures but only small differences in electrochemical potential.

### a. THERMODYNAMICS OF NEODYMIUM-CADMIUM SYSTEM (EMF STUDIES) (I. JOHNSON, R. YONCO)

The thermodynamics of the cadmium-rich portion of the neodymium-cadmium system has been studied by emf measurements using galvanic cells of the type



After the reaction of methane with sodium at 455°C, purges at 300°C with either pure helium or helium containing about 1% hydrogen did not liberate methane from the sodium into the gas phase. These observations are not consistent with some recently reported experiments<sup>25</sup> which were interpreted in terms of an equilibrium between gaseous methane and the carbon and hydrogen dissolved in sodium. Further studies will be made to determine if equilibrium can be established between methane in the cover gas and carbon in sodium and, if such an equilibrium exists, whether the presence of sodium influences the equilibrium  $\text{C} + 2\text{H}_2 \rightleftharpoons \text{CH}_4$ .

Preliminary experiments in the static system were conducted at 150 to 350°C with carbon monoxide at pressures from 0.3 to 9 torr. The reaction kinetics appear to be very complex. The results so far indicate: (1) an induction period or a minimum temperature for reaction; (2) a strong influence of sodium purity; (3) considerable variation of the kinetic order of reaction with respect to carbon monoxide; and (4) a small temperature coefficient of reaction.

<sup>25</sup> D. L. Johnson, Chromatographic Analysis of Gases over Sodium, NAA-SR-848, Sept. 15, 1964.

The cell reaction consists of the dissolution of neodymium into the fused salt at the pure neodymium electrode and deposition of neodymium at the alloy electrode. The two-phase alloy electrode consisted of a cadmium-rich liquid phase in equilibrium with the solid intermetallic compound  $\text{NdCd}_{11}$ . The cell reaction may be written



Thus the emf,  $E$ , of the cell gives directly the activity of neodymium,  $a_{\text{Nd}}$ , in the saturated solution:

$$RT \ln a_{\text{Nd}} = -3 \text{ FE.}$$

The free energy of formation of  $\text{NdCd}_{11}$  may be computed from the equation

$$\Delta G_f^\circ = RT \ln a_{\text{Nd}} + 11 RT \ln a_{\text{Cd}}$$

where the two activities refer to the saturated liquid solution. The small term  $11 RT \ln a_{\text{Cd}}$  was estimated from the cadmium content of the saturated solution and the activity coefficient of cadmium. This latter quantity was computed using the Gibbs-Duhem equation and the assumption that the dependence of the activity coefficient of neodymium on concentration is of the form  $\log \gamma_{\text{Nd}} = A x_{\text{Cd}}^2$ , where  $A$  is a temperature-

TABLE I-31. FREE ENERGY OF FORMATION, LANTHANON-CADMIUM INTERMETALLIC COMPOUNDS OF THE TYPE  $MCd_{11}$  400°C

Compound	$-\Delta G_f^\circ$ (kcal/mole)
$LaCd_{11}$	43.1
$CeCd_{11}$	40.5
$PrCd_{11}$	39.0
$NdCd_{11}$	37.4

dependent constant and  $x_{Cd}$  in the atom fraction of cadmium in solution. The free energy of formation of  $NdCd_{11}$  may be represented by the equation

$$(352 \text{ to } 504^\circ\text{C}) \Delta G_f^\circ \text{ (cal/mole)} \\ = -62,610 + 37.29 T.$$

These measurements complete this phase of our study of lanthanon-cadmium systems using the emf method. The free energies of formation of the cadmium-richest intermetallic compounds in the four systems which have been studied are compared in Table I-31. The decrease in the negative free energy of formation as one proceeds from  $LaCd_{11}$  to  $NdCd_{11}$  parallels the corresponding increase in the solubility of these rare earth metals in liquid cadmium.

#### b. THERMODYNAMICS OF BINARY ALKALI METAL SOLUTIONS (F. CAFASSO, V. KHANNA,\* R. MURRAY)

The thermodynamic properties of binary alkali metal solutions are being determined by a vapor pressure method which utilizes the principles of absorption spectrophotometry. In this method, light of characteristic frequency (resonance radiation) is passed through the vapors above either a pure alkali metal or its alloys. The quantity of resonance radiation which is absorbed is a measure of the concentration of an alkali metal in the vapor. Comparison of the absorption by an alloy to that by a pure alkali metal is, in principle, a direct measure of the thermodynamic activity of that metal in the solution.

The thermodynamic activity of sodium in several liquid Na-K solutions was determined in the range 135 to 150°C. Over this short range, no temperature variation of the activity outside of the expected experimental error could be observed. Therefore, the results are given in a single figure, Figure I-39, which shows the variation of the sodium activity with solution composition. It is evident that sodium and potassium form solutions which exhibit positive departures from ideality.

\* Post-doctoral Fellow.

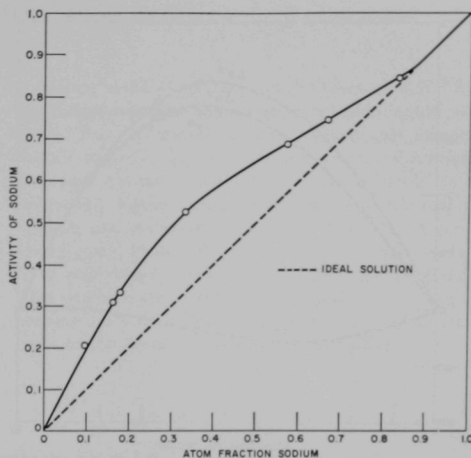


FIG. I-39. Variation of Sodium Activity in Sodium-Potassium Solutions at 414°K. 108-8550

A clearer exhibition of the thermodynamic properties of the Na-K system is shown in Figure I-40. On this plot are given the Gibbs excess free energy of mixing,  $\Delta G^{ex}$  (derived by Gibbs-Duhem integration of the present results), the heat of mixing,  $\Delta H^M$  (measured<sup>26</sup> at 111°C but assumed to be valid at 141°C), and the excess entropy of mixing (from  $T\Delta S^{ex} = \Delta H^M - \Delta G^{ex}$ ). Inspection of Figure I-40 shows that even for this very simple system (1) the curves of  $\Delta G^{ex}$  and  $\Delta H^M$  vs. atom fraction are asymmetric, and (2) except for dilute solutions of potassium in sodium, the system is not regular, i.e.,  $\Delta S^{ex} \neq 0$ . Tentative conclusions have been drawn from the data; namely, that the size effect may predominate over the electronic effect in the system, and that calculations involving both may be required to fit the data.

#### c. EUTECTIC TEMPERATURES IN THE $LnCd-Ln$ FIELDS OF THE LANTHANON-CADMIUM SYSTEMS (E. VELECKIS, E. VAN DEVENTER)

The standard free energies of formation of intermetallic phases in a binary system can be obtained from a knowledge of the corresponding partial molar free energies of one of the components in each two-phase field of the phase diagram. Such information is presently being obtained for various lanthanon-cadmium ( $Ln-Cd$ ) alloys by a recording effusion bal-

<sup>26</sup> T. Yokokawa and O. J. Kleppa, *J. Chem. Phys.* **40**, 46 (1964).

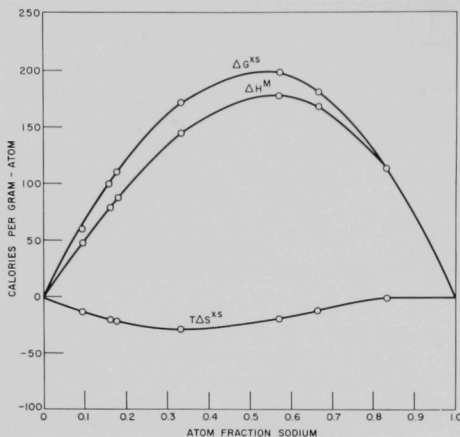


FIG. 1-40. Thermodynamic Functions for the Sodium-Potassium System at 414°K.  
108-S553

ance.<sup>27</sup> Optimum experimental conditions for this method are realized when the alloy sample is solid and the partial pressure of cadmium is in the range 0.001 to about 1 torr. In order to ensure the presence of solid alloys for effusion experiments in the LnCd-Ln fields, upper temperature limits, namely, the eutectic temperatures, were determined by differential thermal analysis using apparatus described elsewhere.<sup>28</sup>

The eutectic temperatures measured for eight systems are listed in the upper part of Table I-32. With the exception of lanthanum, europium and ytterbium (which were expected to show anomalous behavior), the results show an upward trend with increasing atomic number. Continuation of this trend would indicate that the eutectic temperatures for the remaining systems would be well above the range in which the effusion measurements are normally performed.

It was of interest, however, to estimate the eutectic temperatures of the remaining systems by the following procedure. The eutectic compositions in the LnCd-Ln regions of the first eight systems of Table I-32 were

<sup>27</sup> E. Veleckis, C. L. Rosen and H. M. Feder, *J. Phys. Chem.* **65**, 2127 (1961).

<sup>28</sup> A. F. Messing, M. D. Adams and R. K. Steunenberg, *Trans. Quarterly, A.S.M.* **56**, 345 (1963).

TABLE I-32. MEASURED AND ESTIMATED EUTECTIC TEMPERATURES IN THE LnCd-Ln REGIONS OF THE LANTHANON-CADMIUM SYSTEMS

System	$T_e$ (°K)	$T_m^a$ (°K)	$\Delta H_m$ (kcal/mole)	$f_{Ln}$
	Measured			
La-Cd	749	1193	1.6	0.670
Ce-Cd	690	1070	1.24	0.726
Pr-Cd	708	1208	1.65	0.615
Nd-Cd	759	1297	1.71	0.625
Sm-Cd	827	1345	2.06	0.617
Eu-Cd	712	1099	2.0	0.608
Gd-Cd	992	1585	2.1	0.672
Yb-Cd	731	1097	1.8	0.664
	Estimated			
Tb-Cd	951-1043	1629	2.2	0.650 ± 0.033 <sup>b</sup>
Dy-Cd	1179-1258	1680	3.8	
Ho-Cd	1233-1312	1734	4.1	
Er-Cd	1252-1333	1770	4.1	
Tm-Cd	1294-1376	1818	4.3	
Lu-Cd	1364-1453	1925	4.5	
Y-Cd	1038-1136	1775	2.4	

<sup>a</sup> K. A. Schneider, Jr., *Rare Earth Alloys*, D. Van Nostrand Co., Inc., 1961, p. 24.

<sup>b</sup> Average of first eight values.

approximated from the ideal freezing point lowering equation<sup>29</sup>

$$\log f_{Ln} = -\frac{\Delta H_m(T_m - T_e)}{2.3 RT_m T_e},$$

in which:  $f_{Ln} = x_{Ln} / (x_{Ln} + x_{LnCd})$ ;  $\Delta H_m$  is the heat of fusion of Ln;  $T_m$  and  $T_e$  are the melting point of pure Ln and the eutectic temperature, respectively, in °K; and  $R$  is the gas constant. The eutectic compositions thus calculated were averaged to give  $f_{Ln} = 0.650 \pm 0.033$ . Conversely, this same value was used to estimate the eutectic temperature ranges of the remaining lanthanon-cadmium systems. Results of these calculations, which are shown in the bottom half of Table I-32 support the expectation that the eutectic temperatures would increase with atomic number.

### ERRATA

Equation (3), p. 132, ANL-6900 should read:

$$\Delta G_f^{n,n} = -\sum_{i=1}^n \Delta G_{i,(i-1)} = RT \sum_{i=1}^n \Delta r \ln \frac{P_{i,(i-1)}}{P^0} \quad (3)$$

<sup>29</sup> See K. Denbigh, "The Principles of Chemical Equilibrium," The University Press, Cambridge, 1961, p. 259.

## E. PREPARATION OF FUELS FOR FAST REACTORS (A. D. TEVEBAUGH)

Refractory compounds of the actinide elements, such as uranium monocarbide and uranium mononitride, show promise as fast reactor fuels capable of withstanding high temperatures and large burnups. Methods are being investigated for the preparation of these refractory fuels. The more promising methods are being used to prepare sufficient quantities of these fuels for use in fuel element fabrication and irradiation tests. The major problems encountered in these studies are the control of stoichiometry and purity. In the case of the mixed uranium-plutonium ceramic, which is a highly desirable fuel for fast breeder reactors, one encounters the additional problem of preparing a solid solution of the ceramic.

### 1. Preparation of Uranium Monocarbide by a Liquid-Metal Process (E. J. PETKUS, M. A. BOWDEN)

The liquid-metal process for the preparation of uranium monocarbide (UC) involves the following steps:

- (1) dissolution of metallic uranium in a zinc solution containing 14 to 18 w/o magnesium,
- (2) addition of a degassed carbonaceous material (usually activated charcoal) at about stoichiometric quantities for UC formation,

- (3) reaction of the constituents with stirring for 8 to 19 hr at 800°C,
- (4) a phase separation to remove the bulk of the supernatant liquid metal (Zn-Mg) from the precipitated UC, and
- (5) vacuum distillation to remove the residual magnesium and zinc from the UC product.

The first four operations were performed in the trans-

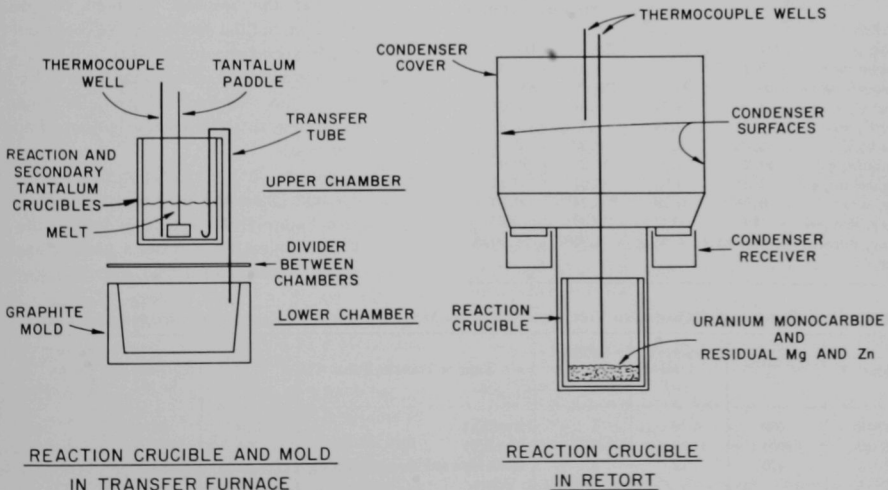


FIG. I-41. Equipment for Uranium Monocarbide Preparation by the Liquid-Metal Method.

fer furnace (see Figure I-41), and the vacuum distillation was done in the retort. Both the transfer furnace and the retort are attached to a vacuum-helium glovebox (ANL-6725, p. 80) when being used through a flange in the floor of the box.

After the phase transfer (step 4), the reaction crucible was moved into the vacuum-helium glovebox. The transfer furnace was removed, and the retort was attached to the glovebox for loading of the reaction crucible. After retorting, the reaction crucible containing the finely divided UC powder was moved into the glovebox for unloading into a Mason jar for storage.

Twelve normal UC production runs and two runs with fully enriched UC have been completed on a 500- or 1000-g scale of uranium metal; these runs were made to prepare UC having a carbon content near the theoretical value of 4.80 w/o and as low an oxygen content as possible. The UC prepared was sent to the

Metallurgy Division for fabrication and irradiation tests. Results of the Metallurgy Division tests are not yet available. Preliminary studies have indicated that the UC products are easily compacted to a high-density material. The current series of runs has been completed and the equipment placed in storage.

Data for runs UC-11 through UC-14 are shown in Table I-33. Data for runs UC-2 through UC-7 and UC-10, UC-11, and UC-12 were reported in ANL-6900, p. 136. Runs UC-13 and UC-14 were runs with 93% <sup>235</sup>U. Samples of UC from the runs in Table I-33 have been mounted and polished for detailed viewing by an electron probe. These studies will be completed and reported at a later date.

Material with an oxygen content of 0.2 w/o or less probably can be produced consistently in any future preparations. The source of most of the oxygen is the degassed activated charcoal. The higher oxygen content of run UC-14, (0.56 w/o) was due to the UC powder being inadvertently unloaded in an air contaminated glovebox. In later runs (UC-12, UC-13, and UC-14) the carbon content of the product was consistently near the maximum of 5.2 w/o desired by the Metallurgy Division.

The yield of UC product was increased from 61.6% to 83.5% (see Table I-34) in the latter runs. This was done by the following modifications in procedure and equipment:

- (1) an increase in reaction time from 8 hr to 19 hr so that the reaction between the dissolved uranium and the activated charcoal would more nearly approach equilibrium,
- (2) an increase in settling time from 1 hr to 3.75 hr so that the fine UC particles would have more time to settle on the bottom of the reaction vessel,
- (3) a change in the transfer tube so that the opening faced upward toward the Zn-Mg melt (see Figure I-41) instead of toward the settled UC particles. Thus, when a phase transfer was made, a sweeping action over the settled UC

TABLE I-33. ANALYTICAL AND PROCESS DATA FOR URANIUM MONOCARBIDE (UC) PREPARED BY THE LIQUID-METAL METHOD

Run	UC-11	UC-12	UC-13	UC-14
Scale (uranium charge)	1000 g	1000 g	500 g	500 g
Reaction Time, hr	8	12	12	19
C/U Atom Ratio in Charge	0.90	1.02	1.02	1.02
Phase Separation	Pressure-Siphon	Pressure-Siphon	Pressure-Siphon	Pressure-Siphon
<i>UC Product</i>				
Yield, g	444	714	388	471
Oxygen, w/o	0.29	0.18	0.24	0.56
Nitrogen, ppm	20	190	230	300
Total C, w/o	4.56	5.24	5.34	5.04
Free C, w/o	0.36	0.74	1.5	1.6
Free C/U	0.08	0.16	0.32	0.34
Uranium, w/o	94.2	93.0	94.2	92.9
Magnesium, w/o	0.01	0.08	0.07	0.11
Zinc, w/o	0.08	0.20	0.14	0.20
X-ray, Species	UC	UC	UC	UC
X-ray, Parameter	4.960Å	4.960Å	4.960Å	4.960Å

TABLE I-34. PROCESS VARIABLES AND YIELDS FOR URANIUM MONOCARBIDE (UC) PREPARATION BY LIQUID-METAL METHOD

Run	U Charge (g)	Reaction Time (hr)	Settling Time (hr)	Type of Transfer Tube	UC Yield (g)	% U (by analysis) in UC	% Yield ( $\frac{\% \text{ U in UC}}{\text{U Charge}} \times 100$ )
UC-10	503	8	1	Straight	343	90.4	61.6
UC-12	1004	12	1.5	Straight	714	93.0	66.2
UC-13	470	12	1	Bent Upward Toward Zn-Mg Melt	388	94.2	77.8
UC-14	524	19	3.75	Bent Upward Toward Zn-Mg Melt	471	92.9	83.5

was prevented and the amount of entrained UC particles present in the transferred supernatant liquid was decreased.

The largest increase in yield occurred when the

transfer tube tip was bent upward. The yield in run UC-13 was 11.6% greater than the yield in run UC-12, although both runs had similar reaction and settling times.

## 2. Preparation of Uranium Monocarbide by a Fluid-Bed Process (E. J. PETKUS, C. C. PAYNE, J. P. BARTOS)

The work on a fluid-bed process for the preparation of uranium monocarbide (UC) (ANL-6900, p. 139) has been continued. The process steps are:

- (1) formation of uranium hydride ( $\text{UH}_3$ ) particles by reacting uranium metal with hydrogen at 10 psig for 2 to 5 hr at 250–300°C,
- (2) heating of the  $\text{UH}_3$  particles to the reaction temperature (500–700°C) while fluidizing the particles with a mixture of hydrogen and a hydrocarbon gas at atmospheric pressure (during the heatup period, the  $\text{UH}_3$  particles are converted to uranium metal particles), and
- (3) continuation of fluidization at 500 to 700°C for 2 to 6 hr to convert the uranium to uranium monocarbide.

The 1-in. dia. fluid-bed reactor used in the runs is shown in Figure I-42. There is a 6-in. long heated zone and a 3-in. dia. particle deentrainment section which contains a porous stainless steel filter. Isolation valves at the top and bottom protect the pyrophoric UC from contamination by the atmosphere during transfer to an inert-atmosphere glovebox. A U-tube prevents the powder from pouring out of the heated zone. Runs UCF-1 through UCF-3 were made with the stainless steel column in the air atmosphere; however, loading and unloading of the materials were done in a glovebox. All the runs after UCF-3 were made with the stainless steel column in a vacuum-helium glovebox (ANL-6725, p. 80).

First attempts at the synthesis of near-stoichiometric UC were not successful because the gas fluidizing velocity was such that most of the uranium particles were entrained by the gases and removed from the heated reaction zone. In these initial experiments, a fluidizing velocity greater than 1.0 ft/sec was believed necessary to prevent sintering of the unreacted uranium metal particles. Subsequent work showed that sintering could be prevented by a hydrogen-hydrocarbon gas fluidizing velocity as low as 0.25 ft/sec, if the fluid bed was initially operated at 0.75 ft/sec for 15 min and then at 0.50 ft/sec for an additional 15 min; this diminished the problem of particle entrainment to the cold zone of the fluid bed. When the fluidizing velocity was decreased to 0.75 ft/sec and lower, uranium monocarbide was easily made (see Table I-35).

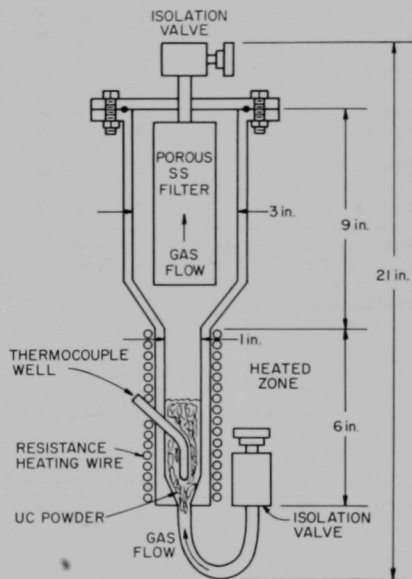


FIG. I-42. Fluid-Bed Reaction Vessel.

A low fluidizing velocity is also desirable because the total volume of gases passing through the bed and the amount of impurities introduced into the UC product from the gases are decreased. The fluidizing properties of  $\text{UH}_3$  and UC with helium at 0.25 ft/sec and room temperature were visually observed in a glass column. The material appeared to be fluidized at this low velocity.

On the basis of literature data,<sup>30-32</sup> it appeared

<sup>30</sup> A. D. Tevebaugh and E. J. Cairns, Saturated Hydrocarbon Fuel Cell Program, ARPA, Order No. 24761, December 31, 1962, Table 6, p. 108.

<sup>31</sup> H. S. Kalish *et al.*, NYO-2688, The Development of UC as a Nuclear Fuel, First Annual Report, May 1, 1959 to April 30, 1960, also NYO-2690 (October 1960), ORO-366 (September 1960).

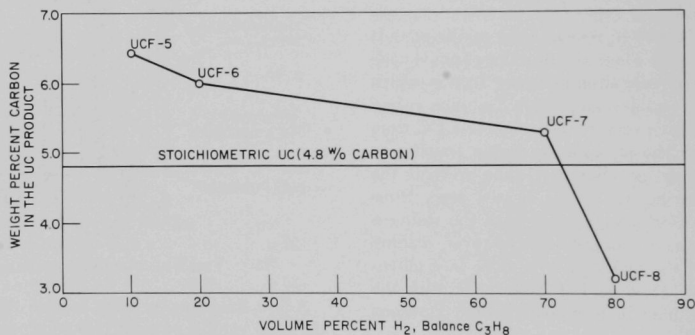
<sup>32</sup> E. J. Cairns and A. D. Tevebaugh, CHO Gas Phase Compositions in Equilibrium with Carbon, and Carbon Deposition Boundaries at One Atmosphere, *J. Chem. Eng. Data* **9**, 453 (1964).

TABLE I-35. PREPARATION OF URANIUM MONOCARBIDE (UC) BY THE FLUID-BED METHOD  
100-g scale

Run No.	Temp (°C)	Time (hr)	Reactant Gases <sup>a</sup>		Analysis of Product		Phases Determined by X-ray Diffraction	
			C <sub>3</sub> H <sub>8</sub> (v/o)	H <sub>2</sub> (v/o)	Total C (w/o)	Oxygen (w/o)	Major	Minor
UCF-2	600	5	80	20	4.4	1.5	UC	$\beta$ UH <sub>3</sub> Possible UO <sub>2</sub>
UCF-4	600	5	90	10	6.5	2.2	UC	Possible UC <sub>2</sub>
UCF-5	600	5.5	90	10	6.4	2.1	UC	Probable UC <sub>2</sub>
UCF-6	600	5.5	80	20	6.0	2.0	UC	Probable UC <sub>2</sub> Possible UO <sub>2</sub>
UCF-7	600	5	30	70	5.3	0.90	UC	Probable UC <sub>2</sub> Possible UO <sub>2</sub>
UCF-8	600	5	20	80	3.2	1.0	UC and $\beta$ UH <sub>3</sub>	UO <sub>2</sub>
UCF-9	700	3	20	80	5.4	0.70	$\beta$ UH <sub>3</sub> <sup>b</sup>	Possible UO <sub>2</sub> UC
UCF-10	700	2	20	80	3.3	0.55	UC	$\beta$ UH <sub>3</sub> (UO <sub>2</sub> and UC <sub>2</sub> very minor)
UCF-11	500	2	20	80	2.1	0.80	UC and $\beta$ UH <sub>3</sub>	Unknown

<sup>a</sup> Fluidizing gas velocity initially 0.75 ft/sec for 15 min, then 0.50 ft/sec for 15 min, and then 0.25 ft/sec for balance of each run except runs UCF-2 and UCF-4. In run UCF-2, the velocity was initially 1.00 ft/sec, and then 0.75 ft/sec; in run UCF-4, it was initially 0.75 ft/sec, and then 0.50 ft/sec.

<sup>b</sup> Possible sample mix-up.



108-8706

FIG. I-43. Preparation of Uranium Monocarbide (UC) by the Fluid-Bed Method. (w/o C in UC Product versus v/o H<sub>2</sub> in the H<sub>2</sub>-C<sub>3</sub>H<sub>8</sub> Fluidizing-Gas Mixture).

Charge: 100 g U  
 Fluidizing Gas Velocity: 0.25 ft/sec  
 Reaction Time: 5-6 hr  
 Bed Temperature: 600°C

probable that the carbon content of UC could be controlled by the proper choice of the variables: the hydrogen-to-hydrocarbon ratio in the gas, the reaction temperature, and the reaction time. Carbon deposition due to decomposition of the hydrocarbon can be prevented at equilibrium in a hydrogen-hydrocarbon gas mixture by proper adjustment of the H/C ratio.<sup>30, 32</sup> The atom percent of hydrogen at equilibrium to prevent free carbon deposition at 600°C is 90.70 (C = 9.30 a/o).

This is a gas concentration of 91.4 v/o hydrogen and 8.6 v/o C<sub>3</sub>H<sub>8</sub>. In a fluid bed and at the temperature of 500 to 700°C, equilibrium conditions probably are not established since the gases rapidly pass through the bed; however, the equilibrium data are useful as a guide in the choice of experimental conditions.

Table I-35 and Figure I-43 show the results of producing UC on a 100-g scale in a fluid-bed apparatus consisting of a 1-in. stainless steel column. Figure I-43

shows the decrease in total carbon content of UC with increasing hydrogen content of the reactant gases at 600°C. Hyperstoichiometric UC was produced when the hydrogen content was about 70 v/o or less. Above 70 v/o hydrogen, there was a sharp decrease in total carbon content such that at 80 v/o hydrogen only 3.2 w/o carbon was present in the product. Gas mixtures containing 70 to 80 v/o hydrogen will be studied in runs at 600°C.

A few runs were made at 700°C, and these had a higher reaction rate than at 600°C. For example, in run UCF-9 (Table I-35) at 700°C, there was 5.4 w/o carbon in the UC product after 3 hr at 80 v/o hydrogen whereas in run UCF-8 at 600°C, there was only 3.2 w/o carbon in the UC product after 5 hr at 80 v/o hydrogen. It would be advantageous to operate at a higher reaction rate (higher temperature) in order to decrease the total amount of fluidizing gases used and thereby decrease the amount of impurities introduced by the reactant gases. Further runs will be made at 700°C and at higher temperatures.

The effect of reaction time on the total carbon content of the UC will be investigated further. In run UCF-10 (Table I-35), there was 3.3 w/o carbon

in the UC after 2 hr at 700°C and 80 v/o hydrogen, while in run UCF-9 after 3 hr at 700°C there was 5.4 w/o carbon in the UC.

The existence of UC (Table I-35) in the products from the fluid bed experiments has been verified by X-ray diffraction analysis. Products with a carbon content of about 2.1 w/o or greater have consistently shown UC to be present as a major phase, except in run UCF-9. In run UCF-9, there exists the possibility that the discrepancy between the X-ray data and percent carbon content of the sample may be due to a mix-up of samples. Product having a carbon content of about 3 w/o or less has had  $\beta$  UH<sub>3</sub> as a major phase.

To remove oxygen and moisture from the hydrogen and propane, a Deoxo unit is used followed by a Lectrodryer unit. The Deoxo unit is a palladium catalytic unit which converts oxygen to water in the presence of hydrogen while the Lectrodryer unit is a molecular sieve bed for moisture removal. In the most recent runs, the oxygen content of the UC product (Table I-35) has varied from 0.55 to 1.0 w/o. It is thought that this impurity level can be reduced in future runs by having a purer atmosphere in the glovebox and by making the run time as short as possible.

### 3. Homogeneous Precipitation of UC and (U-Pu)C from Fused Salts (S. VOGLER, J. PAVLIK)

Most of the methods described in the literature for the preparation of UC are heterogeneous reactions between two or more solid phases or between a liquid phase and a solid phase. In a search for better methods for the preparation of carbides, the idea of homogeneous precipitation of uranium monocarbide from salt solutions was developed (ANL-6725, p. 80). The early experiments demonstrated that magnesium sesquicarbide is soluble in molten salts and that addition of magnesium sesquicarbide to a 35 m/o LiCl - 65 m/o MgCl<sub>2</sub> molten salt mixture containing UF<sub>4</sub> results in uranium monocarbide precipitating from solution. In similar experiments (ANL-6800, p. 145) the metals in the compounds UF<sub>4</sub>, U<sub>3</sub>O<sub>8</sub>, MgUO<sub>4</sub>, ZrO<sub>2</sub>, SiO<sub>2</sub>, NaWO<sub>3</sub>, V<sub>2</sub>O<sub>5</sub>, V<sub>2</sub>O<sub>2</sub>Cl<sub>4</sub>, TaO<sub>2</sub>, and NaMoO<sub>4</sub> were converted to the following carbides, UC, U<sub>2</sub>C, ZrC,  $\beta$ -SiC, WC,  $\alpha$ -W<sub>2</sub>C, VC, TaC, and Mo<sub>2</sub>C. In these initial studies, the pure carbides were not isolated and the product yields were not determined.

In other early experiments (ANL-6800, p. 146; ANL-6900, p. 139), the homogeneous reaction of PuCl<sub>3</sub> with Mg<sub>2</sub>C<sub>3</sub> in fused salts was studied. X-ray diffraction data indicated that the product was primarily Pu<sub>2</sub>C<sub>3</sub>, and no evidence could be found for PuC in the product. These results were disappointing since

it is known that UC forms a solid solution with PuC but not with Pu<sub>2</sub>C<sub>3</sub> whereas the primary interest in the homogeneous reaction process was its anticipated use for the preparation of a uranium-plutonium monocarbide solid solution. In spite of these discouraging data, the method appeared worthy of further study to determine if simultaneous precipitation of the uranium and plutonium carbides would yield the desired solid solution, [U<sub>2</sub>Pu<sub>(1-x)</sub>]C. These studies are described below.

Because of plutonium toxicity, all experiments were carried out in CENHAM gloveboxes.<sup>33</sup> A one-module box with a purified helium atmosphere (ANL-6652) was used to handle all materials and to load and unload the reaction vessels. This box, referred to as the drybox, was connected by means of a vacuum lock to a larger box with a nitrogen atmosphere. During routine operation, the drybox atmosphere was found to contain 12-20 ppm water.

The experimental procedures used for the preparation of fused salts containing plutonium and uranium and the subsequent reaction of the fused salt with

<sup>33</sup> R. F. Malecha *et al*, Low Cost Gloveboxes, Eighth Hot Laboratory and Equipment Conference, San Francisco, December 1960, Trans. Am. Nucl. Soc. 3 (2), 485 (1960).

Mg<sub>2</sub>C<sub>3</sub> were the same as those reported previously (ANL-6800, pp. 145-147; ANL-6900, pp. 139-141). Briefly, the process is as follows: Uranium and plutonium metals are dissolved in liquid zinc, which is then contacted with molten salt (e.g., MgCl<sub>2</sub> - 35 m/o LiCl). The molten salt contains sufficient ZnCl<sub>2</sub> to oxidize the uranium and plutonium to UCl<sub>3</sub> and PuCl<sub>3</sub>. The oxidized compounds are then transferred to the molten salt phase. After the transfer of all of the uranium and plutonium from the zinc phase to the salt phase, the liquid phases are cooled. The solidified salt and metal phases are then mechanically separated, and Mg<sub>2</sub>C<sub>3</sub> is added to the salt phase. The salt phase is then reacted with the added Mg<sub>2</sub>C<sub>3</sub> at 625 to 650°C (in a tantalum crucible) for approximately 1 hr. The salt phase is then removed from the carbide product by volatilization under vacuum at 850°C. The residue contains the carbides of uranium and plutonium. This carbide product was weighed and analyzed.

TABLE I-36. SUMMARY OF URANIUM CARBIDE-PLUTONIUM CARBIDE PRECIPITATION EXPERIMENTS

	Experiment				
	1	2	3	4	5
	Conditions				
U (g)	9.10	10.58	10.62	8.70	9.02
Pu (g)	2.30	2.27	2.31	2.30	2.30
Zinc (g)	300	300	300	200	200
LiCl (g)	19.3	19.3	53.3	73.5	74
MgCl <sub>2</sub> (g)	80.7	80.7	25	—	—
ZnCl <sub>2</sub> (g)	10.24	14.45	14.25	13.79	13.76
Mg <sub>2</sub> C <sub>3</sub> (g) <sup>b</sup>	4.9	3.6	9.7	7.4	4.2
	Product				
Wt. (g)	8.60	9.48	11.88	—	—
U (w/o)	84.5	89.0	67.6	38.4	63.9
Pu (w/o)	6.4	3.3	11.5	10.2	12.1
C (w/o)	4.12	4.46	7.69	<sup>a</sup>	5.81
O (w/o)	1.34	1.0	0.94	<sup>a</sup>	2.20
Insoluble (w/o)	~3	1.1	6.7	1.2	~10
Free Carbon (w/o)	~2	0.9	4.8	1.0	1.2
Phases shown by X-ray Diffraction <sup>c</sup>					
Major	FCC	FCC	FCC	FCC	FCC
	4.96	4.959	5.47	4.96	4.959
			FCC	BCC	
			4.96	8.09	
Minor					BCC
					8.13

<sup>a</sup> Not determined.

<sup>b</sup> Mg<sub>2</sub>C<sub>3</sub> plus unreacted magnesium.

<sup>c</sup> Lattice parameters of pertinent phases are: UO<sub>2</sub>, 5.468; PuO<sub>2</sub>, 5.396; PuO, 4.96; PuC, 4.959-4.973; UC, 4.961; U<sub>2</sub>C<sub>3</sub>, 8.088; Pu<sub>2</sub>C<sub>3</sub>, 8.129.

In four of the five experiments (see Table I-36), the ratio of the plutonium to uranium in the carbide product was much less than the corresponding ratio in the fused salt prior to the reaction with Mg<sub>2</sub>C<sub>3</sub>. In run 4, the ratio in the carbide product was essentially the same as in the fused salt prior to the addition of the Mg<sub>2</sub>C<sub>3</sub>. The overall yield of carbide product, based on the weight of the uranium plus the weight of the plutonium used, varied from 70 to 88 w/o for the three experiments where weight data are available. The carbide product was found to contain 90 w/o or more of the uranium used in the experiment; after precipitation of the carbides, the salt phase was found to contain less than 10<sup>-2</sup> w/o of the uranium and plutonium. After removal of the salt phase from the carbide product by vacuum distillation, however, the salt phase was found to contain approximately 20-50 w/o of the plutonium used in the experiment. These data indicate that the fused salt reacted with the plutonium carbide during the vacuum sublimation step to form PuCl<sub>3</sub>, which distilled along with the LiCl-MgCl<sub>2</sub> salt mixture. A similar reaction has been observed between UC and LiCl-MgCl<sub>2</sub> at 650°C; the color of the salt phase indicated the presence of UCl<sub>3</sub>, and a metallic film (presumably Mg) sublimed to a cold section of the reaction vessel.<sup>34</sup> The reaction was apparently:



Such a reaction was not observed at the same temperature when the salt phase was LiCl-KCl.<sup>34</sup> On the basis of these data, LiCl was used as the salt phase in the last two experiments (runs 4 and 5, Table I-36) in place of the LiCl-MgCl<sub>2</sub> mixture used in the previous experiments. At 1000°K the  $\Delta F_f^0$  for LiCl is -79 kcal per mole and for MgCl<sub>2</sub> it is -58 kcal per gram atom of chlorine (1/2 MgCl<sub>2</sub>). Thus, the greater stability of LiCl than of MgCl<sub>2</sub> was expected to prevent the reaction of the carbides with the LiCl during the vacuum sublimation step. In the fourth experiment, where only LiCl was used as the salt phase, the plutonium content of the sublimed salt phase was very low (at least a factor of 100 less than in previous experiments); however, in the fifth experiment the plutonium content of the sublimed salt phase was once again high. No explanation can be offered for these latter results.

For the carbide product from the first two experiments (Table I-36), examination by X-ray diffraction techniques indicated that the dominant phase exhibited face centered cubic crystal symmetry with a lattice parameter of 4.960Å. This is the lattice param-

<sup>34</sup> M. Adams, Argonne National Laboratory, Private Communication.

eter for UC and is the value to be expected for solid solutions of (Pu-U)C up to approximately 15 to 20 a/o plutonium.<sup>35</sup> Possible very minor phases in experiment 1 were PuOCl, UO<sub>2</sub>, or Mg.

In later experiments, X-ray results revealed the presence of a body centered cubic crystal symmetry with a lattice parameter of 8.09Å and 8.13Å. These values are the lattice parameters of U<sub>2</sub>C<sub>3</sub> and Pu<sub>2</sub>C<sub>3</sub>. In these later experiments, the plutonium content of the precipitate was greater than in the first two experiments.

From the results, it is difficult to say that a true solid solution of UC-PuC had formed, since the plutonium contents of the carbide products from the first two experiments were low and if plutonium had been present as the sesquicarbide, it might not have been detected by X-ray diffraction analysis. In the last two experiments (runs 4 and 5) in which the plutonium content of the precipitate was higher, the sesquicarbide phases were observed to be present.

The total carbon contents of the U-Pu carbide products were determined by combustion of individual samples in oxygen and measurement of evolved CO<sub>2</sub>. This method measures the total carbon present as carbide and as occluded free graphite. The data in Table I-36 indicate a wide variation in the total carbon content of the precipitated carbide products. Free carbon was also measured (Table I-36), and varying amounts were found in the U-Pu carbide products. This free carbon is probably formed as a product of the precipitation reaction and by thermal decomposition of the Mg<sub>2</sub>C<sub>3</sub>. Although the stoichiometry of the precipitation reaction has not been established, the following reaction appears reasonable.



<sup>35</sup> S. Rosen, M. V. Nevitt, and A. W. Mitchell, *J. Nucl. Mater.* **9**, 137-142 (1963).

#### 4. Studies of Mobile Blanket Fuels for Fast Reactors

Mobile blanket fuels for fast breeder reactors show promise of reducing reactor down-time for fuel shuffling, improving sodium coolant utilization and, thus, power conversion efficiency, and decreasing fuel processing and refabrication costs. Experimental work has been initiated to develop a paste blanket fuel consisting of a uranium-containing ceramic fuel dispersed in a liquid metal. Currently, the most attractive of the mobile blanket fuels which have been considered is a paste of uranium mononitride (UN) in sodium.

Free carbon is also an end product for a similar reaction with magnesium dicarbide (MgC<sub>2</sub>).

The major impurity measured other than free carbon was oxygen. The results in Table I-36 show that the oxygen contamination was at least 1%. Since uranium and plutonium carbides are known to be sensitive to moisture, it was thought possible that the carbide product had reacted with moisture in the drybox atmosphere. A crude experiment demonstrated this: a portion of the product of an experiment was allowed to stand in the drybox (box atmosphere ~20 ppm water) for two days. The oxygen content of the carbide rose from 0.94 to 1.3%. Thus, although it is difficult to evaluate the magnitude of the increase in oxygen level, it is probable that substantial oxygen contamination occurred during sampling of the recovered product. In the early experiments, the oxygen impurity was attributed to inadequately purified salts. In the last two experiments, the oxygen content of the LiCl was below the detectable limits (<0.02 w/o oxygen). Thus, even if all the oxygen in the LiCl had been transferred to the product, the oxygen content of the product should not have exceeded about 0.1%.

No further work is planned on the homogeneous precipitation method (using Mg<sub>2</sub>C<sub>3</sub>) for the preparation of a solid solution of uranium and plutonium monocarbide for the following reasons:

1. Pu<sub>2</sub>C<sub>3</sub> was apparently formed instead of the desired solid solution of (U-Pu)C.
2. Large amounts of free carbon were found in the carbide products, and the bound carbon contents were variable.
3. Magnesium sesquicarbide was difficult to prepare in pure form, and the yields were low (40 to 50%) (see ANL-6800, p. 145). Another metal carbide such as lithium carbide or sodium carbide might be a better choice than Mg<sub>2</sub>C<sub>3</sub>, but no experiments with these carbides are planned at this time.

##### a. REACTOR REQUIREMENTS FOR MOBILE FUEL BLANKETS (P. NELSON)

If reactors with mobile fuel blankets are to have an economic advantage over reactors with solid fuel blankets, the advantages must be gained without great changes in the core design. The nuclear characteristics of the core, the ease of removal of the core fuel, and the core fuel cycle costs have much greater effects on the overall economics of the reactor than do blanket characteristics. Since core characteristics are optimized

for minimum power costs consistent with safety, gross changes in the core to accommodate a mobile blanket would negate the potential economic advantages of a mobile blanket fuel. Accordingly, it is believed that a mobile fuel would not be suitable for axial blankets since removal of the core fuel would be complicated by such blankets, particularly the top blanket. Mobile blanket fuel appears to be best suited for reactors requiring large radial blankets and producing a high fraction of the breeding in the radial blanket.

#### b. PROPERTY REQUIREMENTS OF PASTE BLANKET FUELS (P. A. NELSON, M. G. CHASANOV)

The nuclear requirements for blanket fuels are less stringent than for core fuels because most of the nuclear interactions, particularly the fissions, take place in the core. However, a high uranium density in the blanket fuel can be beneficial in providing high neutron capture efficiency for a relatively thin blanket. For this reason, pastes with liquid-metal vehicles containing at least 50 v/o solid fertile material appear to be more attractive blanket fuels than dilute slurries or molten uranium salt solutions.

The shift of a given amount of fuel in the blanket has a smaller effect on reactor reactivity than a shift of the same amount in the core. However, even in the blanket, shifts in uranium density are undesirable. This consideration again favors low-mobility settled pastes, since these appear to be more stable than slurries, owing to the fact that the latter depend on fluid motion to maintain an even distribution of solid particles.

Although a static paste fuel contained in sealed tubes in much the same way as solid fuel might be feasible, the present experimental effort is being directed toward developing a paste fuel which could be circulated. The advantages of a circulating paste fuel are as follows:

1. Fission product gases can be continuously separated from the fuel by circulating the fuel through a separating device.
2. Fuel in a circulating blanket system may be frequently or even continuously removed for reprocessing without reactor shut-down.
3. The build-up of plutonium to high concentrations in the region of the core and the associated heat removal problem which is common to reactors with stationary fuel may be avoided by circulation of the fuel.

These advantages can be gained by having a flow velocity of only a few feet per hour, a velocity that is easily obtainable with a heavy paste. Good paste flow characteristics may require finely ground solid

particles with a narrow size range. In order to maintain these flow characteristics, the particles must be nonsinterable under reactor conditions. Low solubility of the solid particles in the liquid metal vehicle is also a necessity, since mass transfer effects, i.e., growth of the particles and deposition of material, might result in stopping of the flow of blanket paste. Another phenomenon which would stop paste flow and also result in overheating of the fuel would be sudden dewetting of the solid particles by the liquid metal. This might result from (1) a gradual change in the composition of the solid or liquid phases of the paste, or (2) gas evolution from the solid.

It would be impractical to remove the heat developed in paste blanket fuel by circulating it to an external heat exchanger because the pumping rate required would be too high for a viscous paste. Therefore, it would be necessary to contain paste blanket fuel in tubes and to remove the heat from the tubes by a coolant such as sodium, as is done in solid-fueled fast reactors. The rate of heat removal (which equals heat generation at equilibrium) from a paste contained in a tube is given by the following relationship for heat transfer from a rod with uniform internal heat generation:

$$q = 4 k \Delta T / r^2$$

where

$q$  = heat generation rate per unit volume,

$k$  = thermal conductivity of fuel,

$\Delta T$  = temperature differential between the center line and the periphery of the fuel rod, and

$r$  = radius of fuel rod.

It is apparent that the boiling point of the vehicle of paste fuels, which controls the maximum allowable center-line temperature, and the thermal conductivity of the fuel are important fuel characteristics. A sodium-vehicle paste would require a center-line temperature limitation set safety below the 1621°C boiling point of the sodium vehicle. Alloy vehicles with a lead or bismuth base would have an advantage over sodium since they have higher boiling points. However, this advantage would be partially offset by the relatively low thermal conductivity of bismuth, lead, and their alloys.

Compatibility of the fuel with the container material is a stringent requirement because the expensive circulating system must endure for five to ten years to be economical. It would seem easier to meet this goal with a sodium vehicle than with a vehicle of bismuth or lead alloys which are more corrosive than sodium to stainless steel, the probable container material. It is also possible that tubing containing the paste would be attacked by decomposition products from a ceramic

fertile material constituting the solid phase of a blanket paste. In uranium carbide-sodium pastes, carbon which is transferred from hyperstoichiometric UC through sodium may cause failure of the tubing by carburization.<sup>36</sup> In uranium dioxide-sodium pastes, sodium may reduce the oxides of fission products<sup>37</sup> to form sodium oxide which would render the sodium more corrosive to stainless steel tubing.<sup>38</sup> Since UN is compatible with sodium<sup>39</sup> and stainless steel,<sup>40</sup> it appears that a paste of UN in sodium would be innocuous for use with stainless steel.

In summary, the following characteristics are desirable for the components and the paste fuel to be used in the blanket of a fast reactor:

#### A. Fertile Particle Characteristics

1. Nonsinterability
2. Low solubility in vehicle
3. Chemical stability relative to vehicle, fission products, and container
4. High bulk density
5. Fine, uniform particle size
6. High thermal conductivity

#### B. Vehicle Characteristics

1. Noncorrosiveness
2. High thermal conductivity
3. High boiling point

#### C. Paste Characteristics

1. Stable wetting of particles by vehicle
2. Uniform high uranium density
3. Compatibility with container
4. Stable fluidity
5. High thermal conductivity

A paste consisting of UN suspended in sodium appears to fulfill many of the requirements listed above better than the other pastes considered. Experiments are underway to prepare and test the selected paste to determine whether it can meet the exacting requirements of paste blanket fuel.

### e. PREPARATION OF URANIUM MONONITRIDE

(P. A. NELSON, C. F. LEHMANN)

Uranium mononitride powder was prepared by reaction of nitrogen with uranium turnings at 900 to 1350°C and subsequent grinding of the product. The method developed in this work produces UN powder of unusually high bulk density.

Several methods for preparing UN are described by Katz and Rabinowitch.<sup>41</sup> The standard procedure is

first to prepare mixed crystals of  $U_2N_3$  and  $UN_2$  by a method similar to the following:

- (1) Direct reaction of uranium with nitrogen at 800 to 1000°C.
- (2) Reaction of  $UH_3$  with nitrogen at 250 to 350°C.
- (3) Reaction of  $UH_3$  with  $NH_3$  at 200°C.

The product of these preparations is then decomposed to UN and  $N_2$  by heating to 1300°C or higher under reduced pressure. These methods yield products with bulk densities of 3 to 7 g/cc.

The object of the present work was to shorten the time of preparation by carrying out the reaction at a temperature high enough to avoid formation of the higher nitrides. In addition, it was reasoned that such a preparation might yield a product of high bulk density. Uranium, in the form of turnings, was nitrided at 200 to 400 torr pressure. The temperature was maintained at 900 to 1050°C for several hours. Before a nitrogen-to-uranium ratio of one was reached, the temperature was gradually increased to about 1300 to 1350°C. The higher temperature was maintained until nitriding was complete.

In an experiment with 90 g of uranium turnings, 40% of the nitrogen reacted at temperatures above 1100°C. The reaction stopped after 20 min at the final reaction temperature of 1300°C. (The nitride coating on the turnings contained the molten uranium, m.p. 1132°C, during the last step of this process.) The pressure was reduced to  $5 \times 10^{-5}$  torr in a period of 15 min with no evidence of nitrogen evolution from the reaction product. The product was dark gray and in the form of the original turnings. It was easily ground into a coarse (~100 mesh) powder having a bulk density of 8.0 g/cc, which is higher than is usually obtained for uncompact UN powder. X-ray analysis of a sample of -400 mesh powder indicated a major phase of UN with a minor phase of the  $U_2N_3$  of hexagonal structure<sup>42</sup> and a lesser amount of UO. The lattice constant for the UN phase was 4.890 Å, which is in good agreement with a recent literature value.<sup>43</sup> Analysis of the product for nitrogen by combustion to  $U_3O_8$  and correction for the oxygen content (0.095%) of the sample yielded a nitrogen content of 5.60%. (The nitrogen content of stoichiometric UN is 5.557%.)

In a second UN preparation by this general procedure, the reaction terminated before the temperature reached 1300°C. Nitrogen was evolved as the pressure was reduced, thereby indicating that higher nitrides had formed during nitridation. The bulk density of the powdered product, 6.1 g/cc, was considerably less than

<sup>36</sup> B. A. Webb, NAA-SR-6246, May 1963.

<sup>37</sup> L. F. Epstein and J. Nigriny, AECD-3709, 1948.

<sup>38</sup> E. G. Brush, Corrosion **11**, p. 229t, 1955.

<sup>39</sup> R. A. Wullaert *et al.*, DMI-1638, June 1963.

<sup>40</sup> S. Katz, J. Nucl. Mater. **6**, 172, 1963.

<sup>41</sup> J. J. Katz and E. Rabinowitch, *The Chemistry of Uranium*, Doven Publications, Inc., New York, 1951.

<sup>42</sup> D. A. Vaughan, X-ray Diffraction Study of the Nitrides of Uranium, J. Metals **8**, AIME Trans. **206**, 78, (1956).

<sup>43</sup> P. E. Evans and T. J. Davies, Uranium Nitrides, J. Nucl. Mater. **10** (1), 43 (1963).

the value of 8.0 g/cc obtained in the first run (in which less of the higher nitrides were formed).

#### d. WETTING OF CERAMIC FUEL MATERIALS BY LIQUID SODIUM (M. G. CHASANOV)

The wetting properties of liquid sodium for ceramic fuel materials are of importance in the choice and operation of a mobile blanket system based on slurries or pastes of these materials. In order to make a preliminary survey of the wetting properties of liquid sodium for uranium ceramics, an apparatus for the determination of contact angles by the sessile drop method was installed in a helium glovebox. The equipment employed was quite simple. A plaque of the ceramic material was heated on a hot plate in the glovebox; a drop of distilled sodium was placed on the plaque and then photographed by means of a camera and a low-power telescope. The image was captured on Type 55 Polaroid film. Sample temperature was measured using a chromel-alumel thermocouple in contact with the hot plate surface next to the plaque; temperature control was about  $\pm 10^\circ\text{C}$ . While the atmosphere in the glovebox was quite good (oxygen  $< 10$  ppm, nitrogen  $< 20$  ppm, moisture  $\sim 1$  ppm or less), a drop of molten sodium would nevertheless become heavily coated with oxide in six or seven minutes.

Experiments were carried out with plaques of  $\text{UO}_2$ , UP, US, UC, and UN. The contact angles were determined by visual examination of the photographs. For those cases where the ceramic surfaces were reasonably flat, the contact angle was calculated from the drop parameters, using a method developed for surfaces of revolution by Mack and Lee.<sup>44</sup> The results of these studies are presented in Table I-37. For our initial evaluations, these preliminary data were sufficiently accurate. These values should be regarded as tentative because of the relative crudity of the experiments; use of a more refined apparatus such as that employed by Bradhurst and Buchanan<sup>45</sup> would probably lead to more exact data.

The data in Table I-37 indicate poor wetting of the ceramic fuel by liquid sodium at the temperatures investigated. Interestingly, all these data fall within the limits observed by Bradhurst and Buchanan<sup>45</sup> for

TABLE I-37. SUMMARY OF CONTACT ANGLES DETERMINED BY SESSILE DROP METHOD FOR LIQUID SODIUM AND U CERAMICS

Ceramic <sup>1</sup>	Temperature (°C)	Contact Angle $\theta$ , degrees	
		visual observation	calculated
$\text{UO}_2$	210	$130 \pm 2$	130.6
UP	260	$130 \pm 2$	129.9
US	240	$150 \pm 4$	—
UC	250	$144 \pm 1$	143.6
UN	255	$157 \pm 8$	—
Data of Bradhurst and Buchanan <sup>46</sup>			
$\text{UO}_2$ (oxygen-saturated sodium)	250	130	—
$\text{UO}_2$ (oxygen-free sodium)	250	160	—

$\text{UO}_2$  and sodium of varying oxygen content; these data are included in Table I-37 for comparison. Another technique of determining contact angles, the vertical plate method,<sup>46</sup> gives quite different results for  $\text{UO}_2$  and sodium; good wetting is indicated at these temperatures.<sup>47</sup> In this approach, the ceramic is first completely immersed in liquid sodium and then the force required to raise the sample from the sodium bath is measured; from the known dimensions of the sample and the surface tension of sodium, one can then calculate the contact angle. This contact angle would probably be more meaningful for a mobile blanket system in which the ceramic particles are completely immersed in molten liquid metal than would the sessile drop values obtained in our experiment, which represent the advancement of a molten metal over a porous surface covered with a foreign gas. At present, no additional sessile drop studies on these systems are planned.

The indications are that sodium has about the same wetting properties for UN as for  $\text{UO}_2$ . Since sodium- $\text{UO}_2$  slurries and pastes have already been successfully made, no problems are anticipated in making a sodium-UN paste.

<sup>44</sup> G. L. Mack and D. A. Lee, *J. Phys. Chem.* **40**, 169 (1936).

<sup>45</sup> D. H. Bradhurst and A. S. Buchanan, *Australian J. Chem.*

**14**, 397 (1961).

<sup>46</sup> C. C. Addison, D. H. Kerridge, and J. Lewis, *J. Chem. Soc.* 2861 (1954).

<sup>47</sup> B. R. T. Frost, *J. Nucl. Mater.* **7** (No. 2), 100 (1962).

## II. Fuel Cycle Applications of Volatility and Fluidization Techniques\* (A. A. Jonke)

### INTRODUCTION

Development work was continued on fluid-bed fluoride volatility processes for the recovery of uranium and plutonium from spent nuclear fuels. These processes are based on the ability to convert the uranium and plutonium to volatile hexafluorides which can be readily separated from associated fuel materials (cladding, fission products) and purified by established techniques. These processes are considered applicable to a wide variety of fuels and are currently being developed for two main types of fuel which are of interest. One is low-enrichment uranium dioxide-plutonium dioxide clad in either Zircaloy or stainless steel. The other is highly enriched uranium fuels which are alloyed and clad with Zircaloy or aluminum.

A conceptual flowsheet for a process for  $UO_2$ - $PuO_2$  fuels was presented in ANL-6800, p. 197. A number of alternative flowsheets have been considered and some are under investigation. Some of these alternative flowsheets are reviewed below.

Major process steps, shown in Figure II-1, are: decladding, fluorination, distillation, thermal decomposition, and conversion to final products. As outlined, several of the steps are combined in series for alternative routes, depending on the desired form of the products. The fuel elements, after removal of extraneous hardware, are charged as bundles to a fluid-bed reactor where they are immersed in a bed of high-fired alumina. Decladding of both Zircaloy and stainless steel are accomplished through the use of gaseous reactants at elevated temperature.

*Decladding of Zircaloy.* Zircaloy is readily attacked by HCl at temperatures above the sublimation point of  $ZrCl_4$  (331°C at 14.7 psia) as has been demonstrated in the studies with the highly enriched uranium alloy fuels (ANL-6900, p. 194). This step results in a separation of the cladding from the uranium and plutonium dioxides, which remain unattacked and are in the form of pellets or pellet fragments on the fuel support plate. The  $ZrCl_4$  may be pyrohydrolyzed to a solid oxide waste by reaction with steam in a second fluid-bed reactor and the HCl may be recycled if desired.

The  $UO_2$ - $PuO_2$  pellets may be pulverized chemically by reaction with an HF-oxygen mixture as in the case

of decladding schemes discussed below. This step is beneficial since partial fluorination to uranyl fluoride ( $UO_2F_2$ ) and  $PuF_4$  is achieved with a reagent that is appreciably less costly than fluorine; moreover, some decontamination is achieved such as that obtained by the formation of volatile molybdenum compounds.

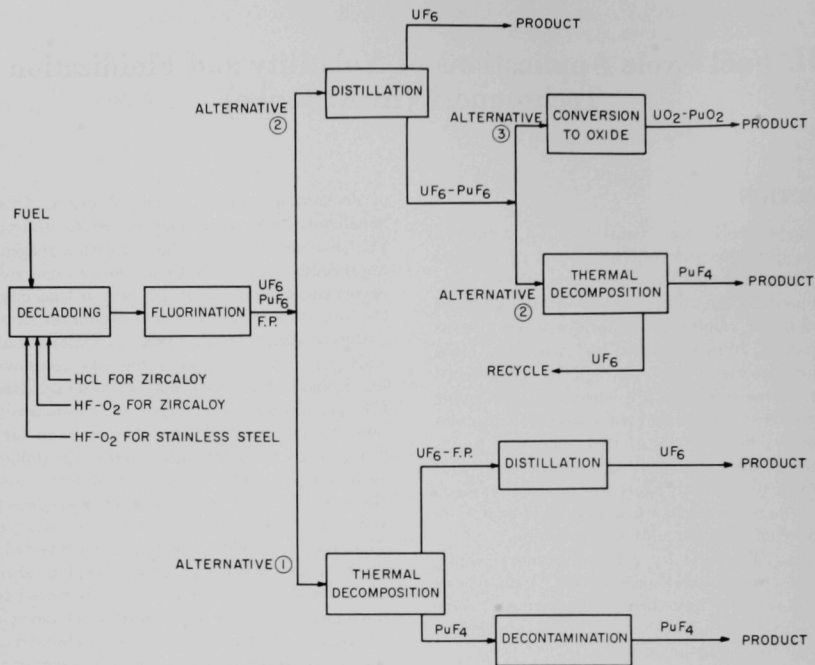
Recent studies at Brookhaven National Laboratory (BNL) and ANL indicated that an alternative scheme for decladding Zircaloy may be feasible. Mixtures of HF and oxygen attack Zircaloy at practical rates at temperatures above 550°C. The reaction products in this case are solid  $ZrO_2$  and  $ZrOF_2$ , the proportions of each apparently depending on the duration of the reaction step. The oxide fuel also reacts with these mixtures and the fuel is pulverized as the decladding proceeds. The uranium and plutonium are converted, respectively, to  $UO_2F_2$  and  $PuF_4$ . Some  $UF_4$  may also form. In the reaction, fission products are converted to oxides, oxyfluorides, or fluorides, some of which are volatile and are separated. The uranium and plutonium fines, the remaining fission products, and the cladding scale mix with the alumina and are reacted further in a subsequent fuel recovery step, the fluorination step.

*Decladding of Stainless Steel.* Stainless steel also was found to suffer destructive oxidation with HF- $O_2$  mixtures (about 30 mils/hr at 550°C with 40 v/o HF-60 v/o  $O_2$ ). The iron is converted mainly to  $\alpha$ - $Fe_2O_3$ , and the  $UO_2$ - $PuO_2$  pellets are again pulverized as described above. The remaining cladding constituents, mainly chromium and nickel, react and appear to remain in the bed as solids.

Work has been done on mechanical decladding schemes, but, in general, these appear to be more complicated than the chemical decladding methods outlined above.

*Fluorination.* After the decladding step and after all of the fuel has been reacted to form the compounds indicated above, the fuel mixture is reacted with fluorine that is diluted with a suitable fluidizing gas such as nitrogen. The fluorination reactions of the fuel result first in the formation of  $UF_6$  which is volatilized from the heated reactor. Several of the volatile fission product fluorides also volatilize from the reactor, along with the  $UF_6$ . After much of the uranium has been converted to the hexafluoride,  $PuF_6$ , formed by the reaction of  $PuF_4$  and fluorine, volatilizes from the

\* A summary of this section is given on pages 7 to 12.



108-8751

FIG. II-1. Fluid-Bed Fluoride Volatility Process Flowsheet for  $\text{UO}_2\text{-PuO}_2$  Fuel.

reactor, leaving the nonvolatile fission product fluorides in the bed. Recycle of fluorine is being considered for this latter fluorination period because the efficiency of fluorine utilization on a once-through basis is expectedly low.

*Decontamination and Conversion to Final Products.* The hexafluorides, together with the fission products whose fluorides are volatile at the temperature of the reaction, are collected in a condenser, thus separating the bulk of the uranium and plutonium from the fluorine and possibly certain of the very volatile fission product fluorides. At this point, several alternative procedures are possible. The mixture of hexafluorides could be passed from the condenser to a vessel in which the less stable  $\text{PuF}_6$  is decomposed to the nonvolatile  $\text{PuF}_4$  (Alternative 1 in Fig. II-1). It is likely that the  $\text{PuF}_4$  product from this step would require additional treatment to produce a fully decontaminated product. The  $\text{UF}_6$  and the remainder of the fluorides could then be introduced to a distillation column which provides for a separation of the fission product fluorides from the  $\text{UF}_6$ , resulting in a highly decontaminated uranium

product. Another alternative is the direct distillation of the  $\text{UF}_6\text{-PuF}_6$  mixture collected in the condenser (Alternative 2 in Fig. II-1). This distillation would produce a  $\text{UF}_6$  stream which is highly decontaminated but which would not contain all of the  $\text{UF}_6$ . The remainder of the  $\text{UF}_6$ , together with all of the  $\text{PuF}_6$ , would be removed from the column near the bottom and would be free from fission products. Should a plutonium product completely free from uranium be desired, this mixture of  $\text{UF}_6$  and  $\text{PuF}_6$  could be passed through a thermal decomposition vessel where the  $\text{PuF}_6$  is converted to  $\text{PuF}_4$ .

On the other hand, if the product from the separations process is to be an oxide, both the pure  $\text{UF}_6$  stream and the  $\text{UF}_6\text{-PuF}_6$  stream could be converted to the respective oxides by reaction with steam-hydrogen mixtures in a fluid bed (Alternative 3 in Fig. II-1). Adjustment of the composition of the  $\text{UF}_6\text{-PuF}_6$  stream by variations in the operating characteristics of the distillation step would permit any desired composition of the oxide mixture to be attained.

## PROCESS DEVELOPMENT STUDIES ON $UO_2$ - $PuO_2$ FUELS

The main steps in the fluid-bed fluoride volatility reprocessing scheme for  $UO_2$ - $PuO_2$  fuels are to be investigated in an engineering-scale alpha facility. Equipment for the processing of batches of pellets to a mixed hexafluoride product has been installed and shakedown work on this unit started. A unit for studies on the conversion of the mixed hexafluorides to dense mixed oxide particles by reaction with steam and hydrogen is also nearly complete.

Development engineering investigations aimed at establishing conditions for processing batches of unclad pellets and related decladding work are in progress. Studies on the behavior (reactions) of  $PuF_6$  with simulated glovebox atmospheres is continuing. Information on the kinetics of these  $PuF_6$  reactions is expected to facilitate the design of clean-up systems for glovebox exhaust streams.

Laboratory support work is continuing. Laboratory-scale fluid-bed fluorinations of  $UO_2$ - $PuO_2$  combined with simulated fission product mixtures and decladding reaction products are being performed in 1½-in. dia. and 2-in. dia. fluid-bed units. Equipment for basic studies on solid-liquid equilibria in the system  $UF_6$ - $PuF_6$  has been installed and is being tested. Studies on vapor-liquid equilibria with this system are to start soon.

Studies on the chemical behavior of  $PuF_6$  are continuing. An investigation of the  $PuF_6$  sorption capacity of selected solid materials is being made. Concluding studies on the decomposition of gaseous  $PuF_6$  to  $PuF_4$  and fluorine by alpha radiation have been made.

Corrosion work is also continuing. A survey of the unclassified literature concerning the corrosion of nickel by  $UF_6$ ,  $PuF_6$ , and fluorine has been completed.

Application of volatility methods to the recovery of plutonium from solid scrap materials produced at the Rocky Flats Division of the Dow Chemical Company has been investigated.

A study of the chemistry of neptunium hexafluoride has been initiated. Other work included a study of the reaction of molybdenum oxides with fluorine.

## PROCESS DEVELOPMENT STUDIES ON HIGHLY ENRICHED URANIUM-ALLOY FUELS

Development work on a fluid-bed fluoride volatility process for recovering highly enriched uranium from uranium-alloy fuels was continued. The overall objectives of this work are to develop and demonstrate an economical, high-decontamination, and high (greater than 99%) uranium recovery process that is applica-

ble to a variety of fuels. At present, applicability of the process to both zirconium-based and aluminum-based fuels is being established.

The process consists of two main chemical reactions conducted in a single vessel. The first is a separation step in which the alloying materials are volatilized by reaction with gaseous hydrogen chloride; the second is a recovery step in which the uranium, after reaction with gaseous fluorine, is recovered as the hexafluoride. The reactions are conducted in a bed of inert alumina granules fluidized by reagent gases and nitrogen; the use of fluidized beds facilitates dissipation of reaction heat as well as the heat due to the fission products in the spent fuel. The progress of the reactions can be followed continuously by measuring the concentration of key components in the off-gas stream by the use of in-line thermal conductivity cells.

Hydrochlorination is carried out at temperatures greater than the sublimation point of the chloride of the alloying element (sublimation points at 1 atm for  $ZrCl_4$  and  $AlCl_3$  are 331 and 180°C, respectively). Since the uranium is converted into particulate uranium chlorides, separation of the fuel constituents is achieved. The uranium chlorides remain, for the most part, associated with the fluid-bed material. A portion of the uranium chlorides is entrained in the gas stream and is collected on a packed bed of alumina which serves as a high-temperature filter. The uranium chloride that passes through the filter is one source of uranium loss. After the fuel charge has been completely reacted, the bulk of the solid chlorides are converted to fluorides by reaction with HF at 350°C. (This step was used in development work to avoid the production of gaseous chlorine and interhalogen compounds which would be expected to form in the direct reaction of the uranium chlorides with elemental fluorine. However, it may not be necessary to include this processing step in the commercial application of the process.) The system is then fluorinated with elemental fluorine and the uranium recovered as the volatile hexafluoride (sublimation point for  $UF_6$  at 1 atm is 56.6°C). The uranium retained by alumina beds, which are discarded as solid wastes, is a second source of uranium loss.

Initial process development work, conducted in a bench-scale unit with unirradiated fuel materials, has now been concluded. The main objective of this work, the establishment of optimum conditions for achieving recoveries of greater than 99% of the uranium in the fuel charge, was attained. A final analysis of the data is presented in this report.

Demonstration of the process on a practical engineering level (~20 kg of fuel) with unirradiated uranium-aluminum and uranium-Zircaloy subassem-

blies is continuing in a pilot-scale unit. The initial seven runs were described previously (ANL-6900, pp. 194-200).

Studies with irradiated fuel materials were initiated after completing shakedown work in the new bench-scale facility installed in the Senior Cave of the Chemical Engineering Division.

An exploratory corrosion program in support of the fluid-bed volatility program was concluded. In-process corrosion work is continuing. Major emphasis is

on the evaluation of nickel as a material of construction.

Fundamental fluidization studies in support of the applied program are continuing. An equation for predicting heat transfer coefficients from surfaces to gas-fluidized beds has been derived. In order to use the equation it is necessary to have experimental data on the average residence time of fluidized particles at the heat transfer surface. A study has been initiated to obtain these data.

## A. LABORATORY INVESTIGATIONS (M. J. STEINDLER)

### 1. Fluid-Bed Fluorination of $U_3O_8$ - $PuO_2$ Mixtures (R. JARRY, W. GUNTHER, W. SHINN, J. STOCKBAR, T. BAKER, G. REDDING, T. GERDING, R. WAGNER, J. SAVAGE)

Laboratory-scale fluid-bed fluorinations of mixtures of uranium oxide, plutonium oxide, and fission product element oxides are being performed in support of studies on the fluid-bed fluoride volatility process. In this process the spent fuel element, after chemical decladding, is contacted with fluorine in a fluidized bed at temperatures from 450 to 550°C to convert the uranium and plutonium oxides to their respective hexafluorides. The laboratory support work is being performed to determine the optimum reaction conditions under which the retention of plutonium on the alumina fluid-bed material is minimized, and to obtain general information which will be useful in the operation of the fluid-bed fluoride volatility process pilot plant (see ANL-6569, p. 110 and ANL-6800, p. 242).

The results of several fluid-bed fluorination experiments which were reported in the preceding semiannual report (ANL-6900, p. 144) indicated the following:

(a) In experiments performed to determine the feasibility of reusing the alumina bed for several addition-fluorination cycles, it was shown that high plutonium recovery was achieved only by incorporating an extensive recycle-fluorination period after each addition-fluorination. Using this scheme, several addition-fluorination cycles can be accomplished without retaining more than 0.02 w/o plutonium on the alumina.

(b) It was observed in these experiments that the quantity of plutonium retained on the alumina increased with an increase in the amount of either plutonium or fission products in the feed to the reactor.

(c) It was observed in experiments involving fluorination of plutonium-free feed material (alumina), that the residual plutonium concentration on the alumina

was dependent on the quantity of plutonium fed to the reactor in the previous experiment. The residual concentration of plutonium in these "blank" experiments varied from less than 0.001 to 0.007 w/o. A plutonium concentration in the alumina of 0.003 w/o was considered to be the background level for this reaction system.

(d) Autoradiographic analysis of alumina particles showed that the plutonium was located on the surface of the particles and that no plutonium was present in the interior of the particles.

This report presents the results obtained for the following types of experiments: (1) Experiments performed to determine plutonium retention in the alumina bed with reuse of the bed for several additions and fluorinations of a  $U_3O_8$ - $PuO_2$ -fission product mixture. The procedure for these experiments was based on the results obtained in a preliminary alumina reuse experiment which has been previously reported (ANL-6900, p. 151, Table II-3). (2) The evaluation of the effect of the use of a nonfluidized static bed on plutonium retention in the alumina bed. (3) A series of experiments performed to show the effect of flow rate of fluorinating gas during the recycle-fluorination period on plutonium retention on the alumina bed. (4) Experiments were performed in which iron oxides were added to show effect upon plutonium retention in the alumina. (5) And finally, an experiment was performed to evaluate Alcoa Type T-61 tabular alumina for use as the fluidized material.

For the experiments in Items 2-5, a modified fluorination procedure was incorporated wherein the entire charge of feed material was contained in the fluid bed at the start of fluorination. This modification was dictated by the development of a decladding process in

which stainless steel or Zircaloy cladding is converted to particulate oxides by reaction with a gaseous mixture of hydrogen fluoride and oxygen. In this decladding step, the oxide fuel material is converted to a mixture of oxyfluorides and fluorides.

The modified fluorination procedure involves two steps: (1) an initial period with dilute fluorine during which the bulk of the uranium reacts, followed by (2) a recycle-fluorination period using 100% fluorine.

#### a. MATERIALS, APPARATUS, AND GENERAL PROCEDURE

The preparation of the  $U_3O_8$ -PuO<sub>2</sub>-fission product (F.P.) mixtures was described in a previous report (ANL-6800, pp. 200 and 201). In a single experiment, 300 g of the  $U_3O_8$ -PuO<sub>2</sub>-F.P. mixture, containing about 0.4 w/o plutonium, 84 w/o uranium, and 0.85 w/o fission product oxides, was used. The fission product mixture used for one of the alumina reuse experiments and all other experiments described in this report contained the 10 fission product element oxides listed in Table II-1, footnote c. For the other alumina reuse experiments, the fission product mixture used contained MoO<sub>3</sub>\* in addition to those listed in Table II-1, footnote c.

Prior to use, commercial grade fluorine was passed through a sodium fluoride trap at 100°C to remove hydrogen fluoride from the fluorine. Nitrogen, which was used as the fluidizing gas and also as diluent for the fluorine, was passed through a trap containing molecular sieves to remove water.

Two types of alumina were used in these experiments, Type RR, a high-purity fused alumina produced by Norton Co., and Type T-61, produced by Alcoa. Two mesh designations of Type RR alumina were employed: (1) nominal 120 mesh having a median particle size of 90 $\mu$  and a particle range of 50 to 140 $\mu$ , and (2) nominal 60 mesh having a median particle size of 200 $\mu$  and a particle size range of 150 to 250 $\mu$ . The Type T-61 alumina had a median particle size of about 150 $\mu$  and a particle size range of 80 to 250 $\mu$ .

Other materials used in these experiments were UO<sub>2</sub>F<sub>2</sub>, PuF<sub>4</sub>, Fe<sub>2</sub>O<sub>3</sub>, and a mixture of fission product element fluorides. The UO<sub>2</sub>F<sub>2</sub> contained 77.3% uranium (theor. 77.3%), and the PuF<sub>4</sub> contained 77.02% plutonium (theor. 75.9%). Ferric oxide from two different sources was used. Reagent grade material of 99% purity was used in the first experiment. The second material was prepared by the HF-promoted oxidation of type 304 stainless steel. The mixture of fission product element fluorides was prepared by fluorination of a portion of a

mixture of fission product oxides which did not contain MoO<sub>3</sub>.

The fluid-bed apparatus used in this work has been previously described (ANL-6725, p. 115, and ANL-6763). The entire apparatus is contained within an alpha box, and manipulation of the apparatus is accomplished through gloveports. Photographs of the alpha box and of the fluid-bed reactor are presented in a previous report (ANL-6800, pp. 202-203).

The general operating procedure for these experiments was as follows:\*\* The feed material for the alumina reuse experiments consisted of 300 g of U<sub>3</sub>O<sub>8</sub>, 1.4 g of PuO<sub>2</sub>, and 2.0 or 2.6 g of fission products, which was mixed with 150 g of 120 mesh alumina and fed into the fluid-bed reactor by the fluidizing nitrogen stream. The mixture was contacted in the fluid bed with a separate stream of 20 v/o fluorine in nitrogen. This portion of the reaction, designated as the feeding-fluorination period, was performed at 450°C.

For the other experiments, the charge of plutonium and uranium compounds and fission products, and in some cases iron oxide, was mixed with the alumina bed (60 mesh, T-61 alumina), placed in the reactor, and fluorinated. During the initial fluorination carried out for about 1 hr, the gas phase contained 5 to 20 v/o fluorine in nitrogen and the reaction temperature was 300, 350, or 450°C. During this portion of the reaction, the gas phase was passed through the reactor and a series of cold traps to remove the UF<sub>6</sub> and PuF<sub>6</sub>. The remaining gases were then passed through an activated alumina trap to dispose of the fluorine, and the nitrogen was vented to the box atmosphere.

After the initial reaction period, the system was put on total recycle and the gas phase was changed to 100% fluorine. During this portion of the reaction, designated the recycle-fluorination period, the gas was passed from the reactor through the cold traps to remove UF<sub>6</sub> and PuF<sub>6</sub>. A remote-head Lapp diaphragm pump was employed to recycle the fluorine gas stream to the fluid-bed reactor. One or more recycle-fluorination periods were used at temperatures of 450, 500, and 550°C. Samples of the starting material and the bed remaining after the experiment were analyzed for uranium and plutonium.

#### b. RESULTS AND DISCUSSION

##### Effect of Reuse of Alumina on the Retention of Plutonium

Experiments were performed in which an alumina bed was used for the fluorination of several additions of U<sub>3</sub>O<sub>8</sub>-PuO<sub>2</sub>-fission product mixture. The procedure

\* See ANL-6800, p. 201, for the proportions of the fission products in the mixtures.

\*\* A detailed description of the procedure was given previously in ANL-6800, p. 199.

for these experiments was as follows: In each addition, 300 g of  $U_3O_8$ -PuO<sub>2</sub>-F.P. mixture blended with 150 g of 120 mesh alumina was injected into the 400 g alumina bed at 450°C and there contacted with 20 v/o fluorine in nitrogen. Following the feeding-fluorination period, fluorination was continued for three recycle-fluorination periods, the first at 450°C for 5 hr, the second at 500°C for 5 hr, and the third at 550°C for 10 hr. In each experiment 20 g of fresh alumina was added through the powder feeder at the end of the feeding-fluorination period as a "wash" for the feed line. At the end of each of the addition-fluorination cycles, the alumina bed, which weighed about 570 g, was removed from the reactor and sampled. Analyses for plutonium, uranium, fluoride, and surface area were carried out. A small amount of solids (about one gram) remained in the disengaging chamber of the reactor and was removed by rapping the outer wall of the chamber; this residue was returned to the bed for subsequent fluorination. The alumina bed was then divided into two parts, 400 g for the bed of the next experiment and 150 g for mixing with 300 g of the  $U_3O_8$ -PuO<sub>2</sub>-F.P. mixture to make up the next feed material.

The data obtained and the experimental conditions used in these experiments are listed in Table II-1. The results for the reuse series in which the fission product mixture did not contain MoO<sub>3</sub> are listed in Section A of Table II-1. For the first seven addition-fluorination cycles, the  $U_3O_8$ -PuO<sub>2</sub>-F.P. mixture contained about 0.4 w/o plutonium, while for the eighth cycle the  $U_3O_8$ -PuO<sub>2</sub>-F.P. mixture contained about 3 w/o plutonium. The fission product content in the eighth addition was also increased proportionately.

In Section B of Table II-1, the fission product mixture contained 22 w/o MoO<sub>3</sub>. For all of these cycles, the  $U_3O_8$ -PuO<sub>2</sub>-F.P. mixture contained about 0.4 w/o plutonium.

The results obtained for the reuse series in which the fission product mixture did not contain MoO<sub>3</sub> (Table II-1, Section A) showed 0.0046 w/o plutonium in the alumina after the first addition-fluorination cycle and 0.0036 w/o plutonium in the alumina after the second addition-fluorination cycle. These values of plutonium retention on the alumina corresponded to volatilization of 97.4 and 99.0% of the total plutonium charged to the reactor, respectively. After the third addition-fluorination cycle, the alumina bed contained 0.193 w/o plutonium. This high level of retention was considered to be due to malfunctioning of the reactor filter blow-back system. The high level of plutonium in the alumina bed was rectified with subsequent addition-fluorination cycles, and after the seventh cycle the plutonium content of the alumina was 0.0088 w/o, corresponding to volatilization of

99.4% of the plutonium. After the eighth cycle, during which the quantity of plutonium fed to the reactor slightly exceeded the total quantity fed in the previous seven cycles, the plutonium content of the alumina bed was 0.025 w/o, corresponding to volatilization of 99.2% of the total plutonium fed to the reactor.

The results for the alumina reuse series in which the F.P. mixture contained 22 w/o MoO<sub>3</sub> are listed in Section B of Table II-1. After the first addition-fluorination, the alumina bed contained 0.003 w/o plutonium. The concentration of plutonium in the alumina rose to 0.03 w/o after the second addition-fluorination, and then fell gradually to a value of 0.014 w/o after the fifth addition-fluorination. The concentration of 0.014 w/o plutonium on the alumina after the fifth and last addition-fluorination corresponded to volatilization of greater than 98% of the plutonium charged to the reactor. If the plutonium level of the alumina bed remained at 0.014 w/o for two additional addition-fluorinations, the alumina would contain 1% or less of the plutonium charged to the reactor. These results show a significant increase in plutonium retention on the alumina which may be due to the presence of MoO<sub>3</sub> in the fission product mixture. Although the presence of MoO<sub>3</sub> appears to affect the course of plutonium volatilization, a higher degree of plutonium removal may be achieved by incorporating seven reuse cycles; this is not only economically attractive but also appears feasible on a process basis.

The fluoride content and surface area of the alumina bed shown in Table II-2 were determined after each addition-fluorination cycle for the series of experiments listed in Section B of Table II-1. The fluoride content of the alumina bed showed an average increase of about 0.5% per addition-fluorination cycle after the 1.4% level was reached in the first addition-fluorination cycle. Surface area measurements by the BET method showed a value of 0.08 m<sup>2</sup>/g after the first addition-fluorination cycle\* and a value of 0.13 m<sup>2</sup>/g after the second addition-fluorination. After the third cycle, the surface area was 0.20 m<sup>2</sup>/g and remained relatively constant for the fourth and fifth cycles. These data indicate that these secondary reaction effects do not seriously hamper the reuse of the alumina bed by the production and accumulation of fines.

Analysis of the bed for molybdenum after the second addition (Table II-1, Section B) indicated that less than 3% of the molybdenum fed to the reactor remained in the alumina bed. The analysis, carried out by a colorimetric method, indicated that the molybdenum content of the bed was less than 0.004 w/o. It is likely that the molybdenum content of the bed is

\* Original surface area of the 120-mesh alumina was 0.011 m<sup>2</sup>/g.

TABLE II-1. FLUID-BED FLUORINATION OF  $U_3O_8$ - $PuO_2$ -FISSION PRODUCT MIXTURES: THE EFFECT OF REUSE OF ALUMINA FOR SEVERAL ADDITIONS AND FLUORINATIONS ON PLUTONIUM RETENTION BY THE ALUMINA

## Feeding-Fluorination Period

Temperature:	450°C
Total Gas Flow Rate:	12 liters/min (1.6 ft/sec at 500°C)
Fluorine Concentration in Total Flow:	20 v/o
Alumina in Bed:	400 g (120 mesh)
Alumina in Feed Material:	150 g plus 20 g wash (120 mesh)

## Recycle-Fluorination Periods

Temperature, Time:	450°C, 5 hr; 500°C, 5 hr; 550°C, 10 hr
Total Gas Flow Rate:	8 liters/min (1.2 ft/sec at 500°C)
Fluorine Concentration:	100%

Addition-Fluorination Cycle	Feed Material <sup>a</sup>			Feed Rate (g $U_3O_8$ - $PuO_2$ per minute)	Pu and U in Alumina Bed after Addition-Fluorination Cycle				Cumulative % of Total Pu Volatilized <sup>b</sup>
	Pu (g)	U (g)	F.P. (g)		Pu (w/o)	Pu (g)	U (w/o)	U (g)	
A. Experiments in which fission product mixture did not contain $MoO_3$ <sup>c</sup>									
1	0.986 (0.986) <sup>d</sup>	250	1.99	1.6	0.0046	0.026	0.010	0.057	97.4
2	1.182 (2.168)	254	2.56	3.3	0.0036	0.021	0.009	0.051	99.0
3	1.182 (3.350)	254	2.56	2.2	0.193	1.175	3.60	21.92	65.0
4	1.162 (4.512)	248	2.54	1.8	0.012	0.070	0.042	0.245	98.4
5	1.198 (5.710)	254	2.60	2.2	0.010	0.058	0.039	0.226	99.0
6	1.194 (6.904)	254	2.60	1.5	0.0093	0.054	0.025	0.145	99.2
7	1.223 (8.127)	256	2.60	1.5	0.0088	0.051	0.043	0.250	99.4
8	8.647 (16.774)	234	16.00	1.1	0.025	0.150	0.004	0.024	99.2
B. Experiments in which the fission product mixture contained $MoO_3$ <sup>c</sup>									
1	0.990 (0.990) <sup>d</sup>	254	2.58	2.22	0.003	0.017	0.009	0.052	98.3
2	1.209 (2.199)	254	2.58	2.27	0.030	0.171	0.006	0.034	92.2
3	1.213 (3.412)	254	2.58	2.25	0.028	0.161	0.105	0.604	95.3
4	1.225 (4.637)	257	2.62	2.30	0.018	0.105	0.070	0.403	97.7
5	1.218 (5.855)	254	2.58	2.50	0.014	0.082	0.005	0.028	98.6

<sup>a</sup> Composed of about 300 g of a  $U_3O_8$ - $PuO_2$ -fission product mixture containing about 0.4 w/o Pu, 84 w/o U, and 0.85 w/o F.P. oxides (for the proportion of the individual oxides in the fission product oxide mixture see ANL-6800, p. 201, Table II-1) mixed with 150 g of nominal 120 mesh alumina.

<sup>b</sup> Based on the quantity of plutonium retained in the alumina bed and that fed to the fluid-bed reactor.

<sup>c</sup> The fission product mixture contained the following oxides:  $La_2O_3$ ,  $CeO_2$ ,  $Pr_6O_{11}$ ,  $Nd_2O_3$ ,  $Sm_2O_3$ ,  $Eu_2O_3$ ,  $Gd_2O_3$ ,  $Y_2O_3$ ,  $BaO$ , and  $ZrO_2$ .

<sup>d</sup> Figures in parentheses are the cumulative quantity of plutonium fed to the fluid-bed reactor.

<sup>e</sup> The fission product mixture contained those oxides listed in footnote c plus 22 w/o  $MoO_3$ .

actually significantly less than 0.004 w/o since an X-ray fluorescent scan of a sample of the bed (purported to be quite sensitive to small concentrations of molybdenum) showed no detectable molybdenum. For com-

parison, it may be noted that one addition of the fission product mixture would result in a molybdenum concentration of 0.06 w/o if none of the molybdenum were removed from the bed. The apparent absence of

TABLE II-2. SURFACE AREA OF ALUMINA BED AND PERCENT CONVERSION OF ALUMINA TO ALUMINUM FLUORIDE<sup>a</sup>

Addition-Fluorination Cycle	Fluoride Concentration in Alumina			% of Al <sub>2</sub> O <sub>3</sub> Conv. to AlF <sub>3</sub>	Surface Area of Bed (m <sup>2</sup> /g) <sup>e</sup>
	F (%)	Total F (g)	g F as AlF <sub>3</sub> <sup>b</sup>		
1	1.74	10.02	8.95	1.41	0.08
2	2.68	15.30	13.13	2.06	0.13
3	3.60	20.74	17.34	2.72	0.20
4	3.90	22.46	18.09	2.84	0.19
5	4.60	26.08	20.78	3.26	0.18

<sup>a</sup> For experiments listed in Section B in Table II-1.

<sup>b</sup> This value obtained by subtracting fluoride due to U and Pu content of bed and fluoride combined with fission product elements from the total fluoride as determined by analysis.

<sup>c</sup> Surface areas obtained by BET method. Surface area of untreated 120-mesh alumina is 0.011 m<sup>2</sup>/g.

significant concentrations of molybdenum in the bed after fluorination makes the effect of molybdenum on the retention of plutonium somewhat difficult to explain.

The results obtained in these alumina reuse experiments show that such multiple use of an alumina bed is feasible and that the plutonium content of the alumina can be held to a value of less than 1% of that fed to the reactor. It further shows that under these reaction conditions, larger quantities of plutonium can be fed to the reactor (Cycle 8, Section A, Table II-1) without increasing the plutonium content of the alumina to an excessive value as previously experienced (ANL-6900, p. 151, Table II-3) when this amount of plutonium was fluorinated in a new alumina bed. These data also show that the presence of MoO<sub>3</sub> in the fission product mixture increases the retention of plutonium on the alumina. In the case in which no MoO<sub>3</sub> was present, the plutonium content of the alumina was reduced to 1% of the total charged to the reactor after the second addition-fluorination (Cycle 2, Section A, Table II-1), whereas in the case in which MoO<sub>3</sub> was present, the 1% plutonium level would not be expected to be reached until the seventh addition-fluorination cycle had been carried out.

### Effect of the Use of a Nonfluidized Static Bed on Plutonium Retention

Several experiments were performed, during which the alumina bed was not fluidized, to determine if fluorination under static bed conditions would result in efficient removal of plutonium. In these experiments, the solid charge of PuO<sub>2</sub> (1.4 g) and fission product oxides (2.0 g; no MoO<sub>3</sub>) was mixed with 570 g of 60 mesh alumina from which the -170 mesh fraction had

been removed. This mixture was placed in the reactor prior to fluorination rather than feeding the mixture into the bed during the initial fluorination period. Three reaction periods were employed using 100% fluorine: 450°C for 5 hr, 500°C for 5 hr, and 550°C for 10 hr. The fluorine flow rate was approximately 0.5 liter/min, equivalent to a linear velocity in the reactor of 0.05 ft/sec. The plutonium concentration of the alumina bed after these fluorination periods averaged 0.075 w/o plutonium. Related experiments in which a fluidized bed was used (Table II-3) resulted in plutonium concentrations in the alumina of from 0.002 to 0.004 w/o (equivalent to volatilization of 98 to 99% of the plutonium). These results indicate that use of this static bed fluorination technique would not result in adequate removal of plutonium.

### Effect of Fluorinating Gas Flow Rate on Plutonium Retention

A series of experiments was made to determine the effect of fluorinating gas flow rate on plutonium retention in the alumina bed. These experiments were performed in a manner similar to that used in the static bed experiments and employed the same quantities of solid reaction charge. A gas phase of 100% fluorine was recycled through the alumina bed at flow rates of 4 to 8 liters/min. The results obtained for these experiments are listed in Table II-3. At a gas flow rate

TABLE II-3. FLUID BED FLUORINATION OF PuO<sub>2</sub>-FISSION PRODUCT MIXTURES: EFFECT OF FLUORINE FLOW RATE ON PLUTONIUM RETENTION ON ALUMINA BED

<i>Solid Charge to Reactor:</i>	1.4 g PuO <sub>2</sub> (1.25 g Pu) 2.0 g Fission Product Mixture <sup>a</sup> 570 g 60 mesh Alumina (+170 mesh) <sup>b</sup>
<i>Gas Phase:</i>	100% Fluorine
<i>Recycle-Fluorination Periods:</i>	450°C, 5 hr; 500°C, 5 hr; 550°C, 10 hr

Fluorine Flow Rate (liters/min)	Gas Velocity (ft/sec) <sup>c</sup>	Alumina Bed Analysis		% of Pu Volatilized
		Pu (w/o)	Pu (g)	
4	0.43	0.026	0.148	88.2
4	0.43	0.019	0.108	91.4
6	0.66	0.0038	0.022	98.2
7	0.77	0.0038	0.022	98.2
8	0.87	0.0022	0.013	99.0
8 <sup>d</sup>	0.87	0.0022	0.013	98.0

<sup>a</sup> Fission product mixture contains the following oxides: La<sub>2</sub>O<sub>3</sub>, CeO<sub>2</sub>, Pr<sub>6</sub>O<sub>11</sub>, Nd<sub>2</sub>O<sub>3</sub>, Sm<sub>2</sub>O<sub>3</sub>, Eu<sub>2</sub>O<sub>3</sub>, Gd<sub>2</sub>O<sub>3</sub>, Y<sub>2</sub>O<sub>3</sub>, BaO, and ZrO<sub>2</sub>. (See ANL-6800, p. 201, Table II-1, for proportion of each oxide in mixture.)

<sup>b</sup> Nominal 60 mesh Type RR (manufacturer's designation) from which -170 mesh fraction has been removed.

<sup>c</sup> At 500°C, atmospheric pressure.

<sup>d</sup> Solid reaction charge contained 0.63 g plutonium.

TABLE II-4. FLUID BED FLUORINATIONS OF MIXTURES OF  $UO_2F_2$ ,  $PuF_4$ , FISSION PRODUCT FLUORIDES, AND FERRIC OXIDE

## Fluorination Periods:

1st Period: 450°C, 1 hr, 5-20 v/o  $F_2$  in nitrogen  
4 hr, 100%  $F_2$   
2nd Period: 5 hr, 500°C, 100%  $F_2$   
3rd Period: 10 hr, 550°C, 100%  $F_2$   
Gas Flow Rate: 8 liters/min

Addition-Fluorination Cycle	Solid Reaction Charge <sup>a</sup>				$Al_2O_3^d$ (g)	U and Pu in Alumina Bed after Addition-Fluorination Cycle				Percent of Total Pu Volatilized <sup>e</sup>
	Pu (g)	U (g)	F.P. <sup>b</sup> (g)	$Fe_2O_3^c$ (g)		Pu (w/o)	Pu (g)	U (w/o)	U (g)	
1	1.252	254	2.28	45.0	570	0.0087	0.053	0.041	0.240	95.8
1	0.943	191	1.71	33.8	428	0.010	0.048	0.012	0.056	94.9
2	0.943 (1.886) <sup>f</sup>	191	1.71	45.0	455	0.014	0.069	0.033	0.165	96.3

<sup>a</sup> Mixture of  $PuF_4$ ,  $UO_2F_2$ , fission product fluorides, iron oxides, and alumina.

<sup>b</sup> Prepared by fluorination of a mixture of 10 oxides (see footnote c, Table II-1).

<sup>c</sup> Prepared by the HF- $O_2$  reaction with type 304 stainless steel.

<sup>d</sup> Type T-61 alumina having a median particle size of about 150  $\mu$  and a particle size range of 80 to 250  $\mu$ .

<sup>e</sup> Calculated from quantity of plutonium remaining in alumina bed and total quantity of plutonium fed to reactor.

<sup>f</sup> Cumulative plutonium added in this experiment.

of 4 liters/min, the final plutonium concentration in the alumina bed averaged 0.022 w/o, while at gas flow rates of 6 to 8 liters/min the plutonium content of the alumina bed ranged from 0.002 to 0.004 w/o. These results clearly indicate that a gas flow rate of 6 liters/min or greater is necessary for effective removal of plutonium from the fluidized alumina bed.

#### Effect of Addition of $Fe_2O_3$ on Plutonium Retention

The use of the HF-promoted oxidative decladding of stainless steel would result in the formation of a considerable amount of iron oxides in the alumina bed, in addition to uranium and plutonium oxyfluorides and lower fluorides. As much as 5 to 10% of the resulting bed would be an iron oxide such as  $Fe_2O_3$ . Experiments were performed to determine if the presence of  $Fe_2O_3$  in the reaction mixture would affect the plutonium retention in the alumina bed. The usual three recycle-fluorination periods (see Table II-4) were employed, using a gas phase of 100% fluorine.

Two scouting experiments were made, using reagent grade  $Fe_2O_3$  as a stand-in for the product that would be formed in the decladding step. The solid reaction charge, containing 1.4 g  $PuO_2$ , 2.0 g fission products (no  $MoO_3$ ), and 45 g of reagent grade  $Fe_2O_3$ , was mixed with 570 g of 60 mesh alumina. The plutonium content of the alumina beds after fluorination averaged 0.021 w/o. This greater retention of plutonium with  $Fe_2O_3$  present\* may have been biased by the relatively

greater fines transport from the alumina bed. A significant portion of the finely divided  $Fe_2O_3$  or the iron fluoride was present in the disengaging chamber of the reactor, and some interaction might have occurred between the iron compounds and the  $PuF_6$  in the gas phase. After the fluorination was completed, it was observed that the color of the alumina bed was reddish-brown rather than the light green which was expected from the reported color of the iron fluorides. Analysis of a portion of the fines, however, showed that 96 to 100% of the iron oxide had been converted to ferric fluoride.

In order to approximate more closely the use of material obtained by a decladding step, three experiments were performed using a solid reaction mixture simulating that expected from the decladding step. The mixture contained  $UO_2F_2$ ,  $PuF_4$ , fission product fluorides, and material produced by the reaction of type 304 stainless steel with an HF- $O_2$  mixture. Two experiments involved the fluorination of single batches of feed simulating declad fuel. In a separate experiment to demonstrate reuse of alumina bed material, the final alumina bed from the previous batch fluorination experiment was used as the starting bed for the fluorination of an additional batch of the same feed material. Type T-61 alumina\*\* was used in these experiments. This type of alumina is being used in current pilot plant work in place of Type RR high-purity alumina. The reaction procedure used in these experiments was the same as for those described in a pre-

\* Comparison can be made with a similar experiment without  $Fe_2O_3$  (see Table II-3).

\*\* See the following section of this report for an experimental evaluation of type T-61 alumina.

ceding section, *Effect of Fluorination Gas Flow Rate on Plutonium Retention*, with one difference. In the initial 450°C fluorination period, the concentration of fluorine was increased to 20 v/o during the first hour of operation in which the greater part of the uranium was fluorinated. During this first hour, the gas flow was once-through. The remainder of the 450°C period was then completed under recycle, using 100% fluorine as the gas phase.

The process parameters and results of the experiments are listed in Table II-4. For the two experiments involving fluorination of single batches of fuel, the alumina beds contained 0.0087 and 0.010 w/o plutonium and 0.041 and 0.012 w/o uranium, respectively. The data listed for the last entry in Table II-4 are from the experiment involving reuse of the alumina bed resulting from the second experiment listed in Table II-4. The plutonium and uranium concentrations in the alumina bed after this experiment were 0.014

and 0.033 w/o, respectively. This modest increase in plutonium concentration on the alumina indicates that multiple use of an alumina bed for this type of solid charge could be successfully accomplished.

### Evaluation of Alcoa T-61 Tabular Alumina

Present pilot plant operation involves the use of Alcoa T-61 tabular alumina in place of the high purity Type RR alumina previously used. The use of Type T-61 alumina rather than high purity alumina, Type RR, would result in lowered cost for the fluid-bed material. One experiment was performed using the same solid reaction charge and reaction conditions as were used for the experiments listed in Table II-3. The fluorine flow rate was 8 liters/min. The alumina bed after this fluorination contained 0.0026 w/o plutonium. This result is similar to those obtained, under the same reaction conditions, using the high purity Type RR alumina and indicates that type T-61 is as suitable as Type RR alumina.

## 2. Fluorination of $UO_2$ - $PuO_2$ Pellets in a 2-inch Diameter Fluidized-Bed Reactor (L. J. ANASTASIA, P. G. ALFREDSON,\* J. G. RIHA)

A 2-in. dia. fluidized-bed reactor has been constructed to investigate the decladding and fluorination of  $UO_2$ - $PuO_2$  pellets which are clad in stainless steel or Zircaloy. Decladding and fluorination are two (of four) major steps (ANL-6800, pp. 197-198) in a fluid-bed fluoride volatility process under development for the recovery of uranium and plutonium from spent uranium dioxide fuels. The objective of experiments carried out in the 2-in. dia. reactor is to determine reaction conditions for  $UO_2$ - $PuO_2$  pellets which will insure that a minimum of the uranium and plutonium is retained by the inert alumina particles of the fluidized bed. This work will be performed in support of the fluid-bed volatility process pilot plant.

The decladding step involves separation of the fuel from the metallic cladding. Two alternative methods for removal of fissionable values from stainless steel cladding are of interest: (1) mechanical broaching of the cladding followed by oxidation of the  $UO_2$  to  $U_3O_8$  which forms as a fine powder and readily separates from the cladding, and (2) chemical destruction of the stainless steel by oxidation with oxygen in the presence of hydrogen fluoride. Removal of  $UO_2$  from stainless steel cladding by oxidation to  $U_3O_8$  has been successfully demonstrated on a pilot-plant scale (ANL-6800, pp. 227-234). In recent tests of chemical destruction by fluoride-promoted oxidation of the stainless steel,

reaction rates of 30 mils/hr were observed for types 304 and 347 stainless steel specimens which were oxidized at 550°C by a gas mixture of 40 v/o hydrogen fluoride in oxygen while the specimens were immersed in a fluidized bed of alumina (ANL-6923, p. 69).

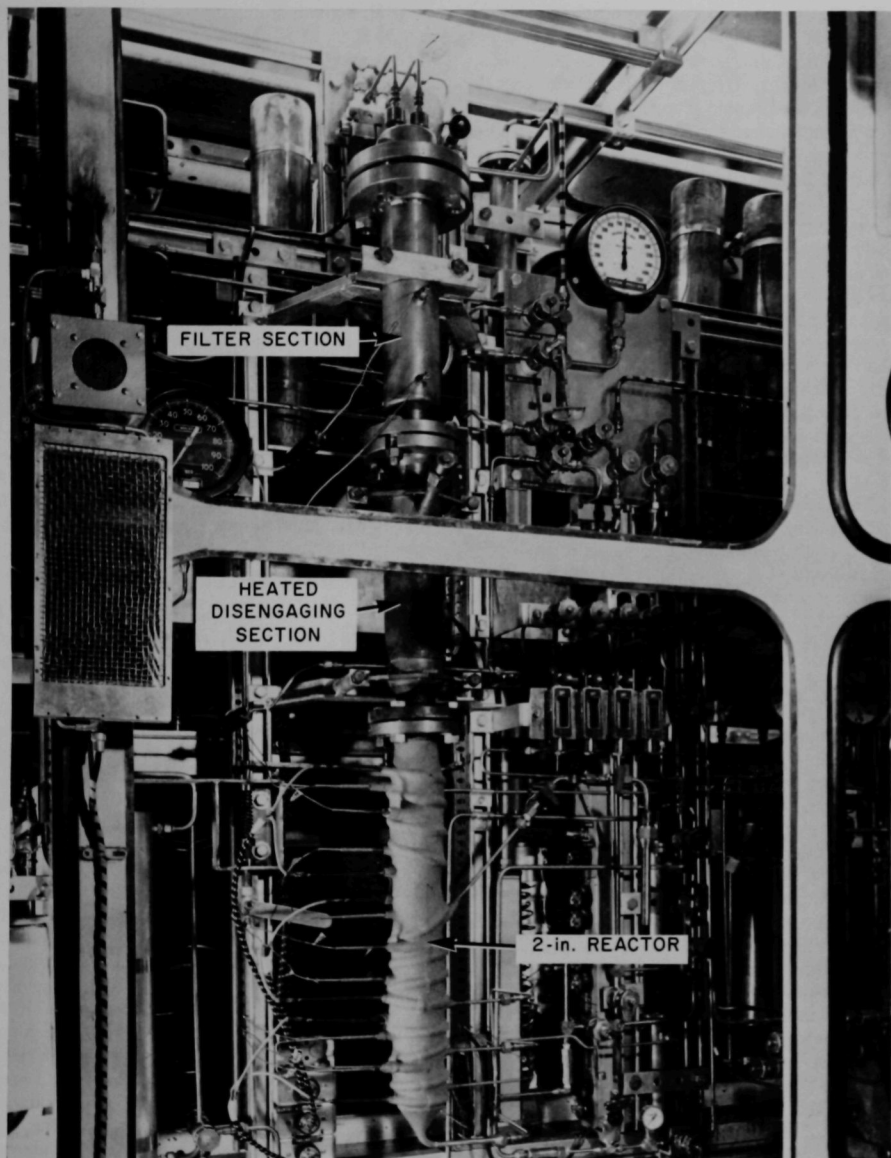
The 2-in. dia. reactor has been equipped to study the removal of  $UO_2$ - $PuO_2$  pellets from cladding by oxidation (using the two-zone oxidation-fluorination technique), and the chemical destruction of cladding by oxidation with  $HF-O_2$  mixtures. The experimental program will be directed toward this latter approach, with emphasis placed upon the reaction of fluorine with the uranium and plutonium fluorides resulting from the decladding step, and the cleanup of residual uranium and plutonium from the fluidized-bed of solids by recycle-fluorination.

### a. EQUIPMENT AND PROCEDURE

The entire reactor system is contained in an alpha glovebox with overall dimensions, 10-ft width by 3.5-ft depth by 6.7-ft height. The major components of the system are located in the glovebox; these items include the fluid-bed reactor, reactant gas disposal traps, hexafluoride collection vessels, a remote-head positive displacement pump, and a thermal conductivity cell.

The fluid-bed reactor is fabricated in 3 sections from Schedule 40 nickel pipe; a 2-in. dia. by 27.5 in. fluidized-bed section, a 3-in. dia. by 17 in. disengaging section, and a 3-in. dia. by 15.4 in. filter section. The reactor assembly is shown in Figure II-2.

\* Guest Scientist, Australian AEC.



108-7817A

FIG. II-2. Two-Inch Fluidized-Bed Reactor.

The  $\text{UO}_2\text{-PuO}_2$  charge, in the form of unclad pellets or clad segments of simulated fuel rods, is supported by nickel balls in the fluidized-bed section above the conical gas distributor. Several heating zones and several gas inlets have been provided so that either two-zone oxidation-fluorination or fluoride-promoted oxidative-decladding of pellets can be studied. Individually controlled Calrod heaters provide two heating zones for the lower half of the fluid-bed section and one zone for the upper half. Seven interior thermowells are spaced along the length of the reactor to provide temperature measurement and control. The fluidizing gas enters at the bottom of the column. Fluorine can be fed through the bottom or through ports located 2 and 5 in. above the conical gas distributor. Pulsing of the fluid bed can be provided by nitrogen supplied independently of the fluidizing gas; the frequency and duration of pulsing are controlled by electric timers and a solenoid valve. The fluid bed can be sampled through a  $\frac{1}{4}$ -in. OD tube which enters the wall of the reactor at an angle of  $45^\circ$ ; the sampling point is located 7 in. above the top of the gas distributor.

The disengaging section of the reactor is heated by a system of shell heaters, and the temperature of the section is sensed and controlled by a thermocouple. The disengaging section of the reactor is also provided with a  $\frac{3}{4}$ -in. OD charging port through which pellets or alumina can be added without dismantling the reactor.

The filter section of the reactor contains two bayonet-type, 10- $\mu$  pore size, sintered nickel filters,  $1\frac{3}{4}$  in. wide and 12 in. long, which remove solids entrained in the reactor effluent gas. Solids collected on the filters are removed by reverse flow of nitrogen gas; the frequency and duration of this blowback for each filter is controlled by electric timers and a solenoid valve. A secondary, nonblowback, sintered nickel filter,  $1\frac{3}{4}$  in. by 6 in. long, housed in a separate unit, is connected in series with the process filters.

Pressure drop measurements across the filters and the fluidized bed are obtained by signals from differential pressure transmitters which are indicated on instruments inside the glovebox and also continuously recorded on a millivolt recorder outside the glovebox. The pneumatic signal from the transmitters is converted to an electrical signal by a potentiometer-type pressure transducer.

Unreacted hydrogen fluoride or fluorine is removed from the reactor effluent by chemical reaction with reactive solids in traps 4-in. OD by 24 in. high. A minimum of two traps in series are used for this purpose. Fluorine is removed by reaction with activated alumina. The hydrogen fluoride removal scheme has not been fixed; however, soda lime [10%  $\text{Ca}(\text{OH})_2$  in

$\text{NaOH}$ ], activated alumina, or a combination of both can be used, as is discussed in a following section (c. Hydrogen Fluoride Disposal).

During fluorination, the hexafluoride products are collected in a series of three cold traps 4-in. OD by 12 in. high maintained at  $-80^\circ\text{C}$  by a trichloroethylene-dry ice bath; a back-up trap of sodium fluoride at  $100^\circ\text{C}$  is in series with the cold traps. During the initial period of the fluorination step when most of the uranium and plutonium charge is present in the reactor, the fluorine-containing off-gas from the hexafluoride cold traps is disposed of directly in the activated alumina traps. The concentration of fluorine in the gas stream during this part of the fluorination step is limited to 20 v/o. Fluorine concentration is measured during this part of the fluorination step by passing 50 cc/min of the effluent gas from the hexafluoride collection traps through the thermal conductivity cell system (ANL-6725, pp. 135-137).

When more than 80% of the charge has reacted, recycle-fluorination with high concentrations of fluorine is used. During this part of the fluorination, fluorine is circulated through the fluid-bed system by a remote-head positive displacement pump.

## b. EQUIPMENT CHECK-OUT RUNS

A series of preliminary experiments with unclad  $\text{UO}_2$  pellets has been started. The objectives of these runs have been to check out the operation of all equipment components and to demonstrate the reaction of unclad  $\text{UO}_2$  pellets with  $\text{HF-O}_2$  mixtures followed by fluorination of the product with fluorine diluted with nitrogen. Unclad  $\text{UO}_2$  pellets were used to obtain the uranium compounds which would be present in a fluidized bed reactor following the fluoride-promoted oxidative-decladding of stainless steel- or Zircaloy-clad fuel rods.

The  $\text{UO}_2$  pellets used in these runs were hydrogen-fired, reactor grade pellets (ANL-6287, p. 149). The hydrogen fluoride and fluorine were obtained from commercially available vendor's cylinders, and the alumina was a high-purity, refractory grain Alundum.\*

In each of two runs (Sure-1 and Sure-2) completed thus far, a 2-in. deep bed of  $\text{UO}_2$  pellets and a 10-in. deep bed (static conditions) of  $-40+170$  mesh alumina were charged to the reactor. The weights of pellets and alumina were 660 g and 990 g, respectively. The complete conversion of this quantity of  $\text{UO}_2$  would yield a fluid bed consisting of  $\sim 40\%$  fines after the  $\text{HF-O}_2$  treatment. The pellet beds were supported above the bottom cone of the reactor by a packed bed of nickel balls.

A temperature of  $550^\circ\text{C}$  was used for both the HF-

\* A product of the Norton Co., Worcester, Mass.

O<sub>2</sub> step and the fluorination step in the two runs. During an interval of 2 hr between the HF-O<sub>2</sub> step and the fluorination step, the reactor was maintained at temperature and the bed was fluidized with nitrogen to purge residual HF and H<sub>2</sub>O from the system. During the fluorination, nitrogen was fed to the pellet bed to avoid fluorination of unreacted UO<sub>2</sub>; fluorine was fed to the reactor above the pellet bed. In this way the effects of the HF-O<sub>2</sub> reaction on the pellets could be observed after fluorination of fines from the fluidized alumina. The operating conditions for Runs Sure-1 and Sure-2 are given in Table II-5.

Several observations during Run Sure-1 suggested virtually no reaction occurred during the HF-O<sub>2</sub> step. These observations included no visible uranium oxides and/or fluorides in fluid-bed samples, the uniformity of bed temperatures, and the constancy of pressure drop values across the fluid-bed and sintered metal filters. When the pellets were removed from the reactor following the fluorination step, a tightly adherent, dark-green layer which covered ~80 to 90% of the pellet surface areas was the only evidence of chemical reaction. Apparently, UF<sub>4</sub> which had formed on the surface of the pellets had inhibited further reaction. It was concluded that the ratio of HF to O<sub>2</sub> (see Table II-5) had been too high. This ratio, as well as the superficial fluidization velocity, was higher than anticipated because HF polymers, rather than the monomer, were metered through the HF rotameter. According to McBride,<sup>1</sup> the specified metering conditions of 5 psig and 38°C on the HF rotameter calibration were not sufficient to prevent polymerization. In subsequent runs, HF polymerization was prevented by increasing the temperature of the supply line from 50°C, as in Run Sure-1, to 85°C.

Significant chemical reaction was evident in Run Sure-2 when the HF-O<sub>2</sub> step was carried out at 550°C with 42 v/o HF in oxygen (see Table II-5). Samples of the fluid bed taken after 0.5, 1.5, and 3.0 hr of operation contained black uranium reaction products in the form of fine particles and discrete flakes which were slightly larger than the 40 mesh alumina. Material balances based on analysis of the uranium, fluoride, and UO<sub>2</sub>F<sub>2</sub> content in these samples indicated: (1) the UO<sub>2</sub>F<sub>2</sub>/UF<sub>4</sub> ratio increased from 0.3 after 0.5 hr of reaction to 0.7 after 3.0 hr and (2) the total uranium in the fluid bed increased during the interval 0.5 to 3.0 hr from 7.4 to 10.3 w/o of which 3 w/o uranium was as an oxide after 0.5 hr of reaction and, within the limits of the analyses, no uranium oxides remained unconverted after 3.0 hr of reaction.

The change in the reactor off-gas flow from the HF

TABLE II-5. AVERAGE OPERATING CONDITIONS FOR RUNS SURE-1 AND SURE-2

<i>Equipment:</i>	2-in. dia. fluid-bed reactor		
<i>UO<sub>2</sub> Pellets:</i>	0.5-in. dia. by 0.5 in. right cylinders		
Weight:	660 g		
Bed Depth:	2 in.		
Bed Support:	nickel balls		
<i>Alumina Fluid Bed:</i>	Norton RR Alundum		
Weight:	990 g		
Size Limits:	-40+170 mesh		
Static Bed Depth:	10 in.		
<i>Temperature:</i>	550°C		
	Pellet Fluorination with HF-O <sub>2</sub>	Run Sure-1	Run Sure-2
Process time (hr)		0-3.0	0-3.0
Reactor pressure (mm Hg)		920	900-1060
Total gas flow to fluid bed (liters/min) <sup>a</sup>		25-28	15.0-16.4
Superficial velocity (ft/sec) <sup>b</sup>		1.4-1.7	0.9
Reactant concentrations to pellet bed:			
HF (v/o)		47	42
O <sub>2</sub> (v/o)		12	58
N <sub>2</sub> (v/o)		41	—
	Fluorination with F <sub>2</sub>		
Process time (hr)		3.0-5.0	3.0-8.0
Reactor pressure (mm Hg)		1120	1230-1575
Total gas flow to fluid bed (liters/min) <sup>a</sup>		18.9	9.9
Superficial velocity (ft/sec) <sup>b</sup>		0.9	0.4
Fluorine concentration in fluid bed (v/o)		2.7-5.3	6.4-11.6
Diluent		N <sub>2</sub>	N <sub>2</sub>

<sup>a</sup> 1 atm, 27°C.

<sup>b</sup> Based on cross-sectional area of the 2-in. column and calculated for operating conditions.

disposal lines to the hexafluoride cold trapping and fluorine disposal lines results in an increase in reactor pressure of ~200 mm Hg. In Run Sure-2, the reactor pressure continued to increase as the fluorination with fluorine was continued (see Table II-5). The increased pressure was due to accumulated solids in the backup filter. Analysis of these solids by X-ray diffraction indicated that they were similar in composition to products obtained in a study of the UO<sub>2</sub>F<sub>2</sub>/H<sub>2</sub>O/HF system.<sup>2</sup> Thus, the solids accumulation in the backup filter was attributed to reaction of UF<sub>6</sub> with HF and H<sub>2</sub>O which had condensed at ambient temperature in the filter chamber. Heat tracing of the filter chamber and of HF disposal lines was scheduled but not completed for Run Sure-2; consequently, condensation in these lines is not expected to be a major problem in the future.

<sup>2</sup> L. H. Brooks, E. V. Garner, and E. Whitehead, Chemical and X-ray Crystallographic Studies on Uranyl Fluoride, IGR/CA-277, 1956.

<sup>1</sup> R. H. McBride, Metering of HF and Fluorine, AECD-3690, Oct. 29, 1945.

Although the fluidized-bed reactor operated quite smoothly during Run Sure-2, only 42.5% of the expected  $UF_6$  (880 g) was collected in the cold traps and the sodium fluoride trap. About one-half of the pellet bed remained in the reactor after fluorination. This portion of the pellet bed had expanded and was packed in the reactor just above the nickel balls. Several holes were visible in the packed section; evidently, fluidizing nitrogen could pass through these holes with relatively low pressure drop. The packed section was friable and easily removed from the reactor. Qualitatively, there appeared to be definite zones of  $U_3O_8$ ,  $UO_2F_2$ , and  $UF_4$  formation. Since back diffusion of fluorine from inlets above the pellet bed was insignificant in Run Sure-1, it appears that these uranium compounds are the products of the  $HF-O_2-UO_2$  reaction at 550°C.

### c. HYDROGEN FLUORIDE DISPOSAL

Two dry methods of hydrogen fluoride removal from reactor effluent have been investigated. Removal by reaction with soda lime was used in Run Sure-1 and removal by reaction with activated alumina was used in Run Sure-2.

The HF-soda lime reaction is exothermic and occurs along a narrow reaction front; therefore, consumption of the soda lime is easily monitored by temperature measurement. However, 0.9 kg of water vapor must be condensed or vented to the box atmosphere per kilogram of HF reacted.

The reaction of HF with activated alumina releases 0.45 kg water vapor per kilogram of HF reacted; however, this water is adsorbed on unreacted alumina. Since both the reaction and the adsorption are exothermic, consumption of the alumina is difficult to monitor. Therefore, a third system of HF disposal will be tested in subsequent runs. This system will consist of a series of two soda lime traps, a water vapor condenser, and an activated alumina trap. It is hoped that this system will prove suitable for long-term use in this work.

### d. FUTURE PROGRAM

It is proposed that preparation for plutonium studies will begin after two additional preliminary runs with  $UO_2$  pellets are completed. These latter runs will be concerned with fluorination of the uranium products present in a fluidized bed after a decladding step at 550°C with 40 v/o HF in oxygen. Since exposure of the pellets to the  $HF-O_2$  atmosphere is limited by the amount of cladding actually removed, it is believed that a packed bed of pellets may not be representative of the declad pellets under production conditions. Therefore, nickel baskets  $\frac{3}{16}$ -in. ID by 8-in. long with large open areas have been constructed to support the pellets vertically in the reactor. It is expected that similar lengths of clad, simulated, fuel rod segments will be used in actual decladding studies with  $UO_2$ -PuO<sub>2</sub> pellets.

## 3. Phase Studies

The program of experimental studies of the vapor-liquid equilibria and the solid-liquid equilibria in the system  $UF_6$ -PuF<sub>6</sub> has been briefly outlined (see ANL-6875, p. 114). The results of these studies will be useful in the choice of process conditions for the separation of PuF<sub>6</sub> and UF<sub>6</sub> in the fluid-bed fluoride volatility process and will contribute to the understanding of the fundamental chemistry of this system.

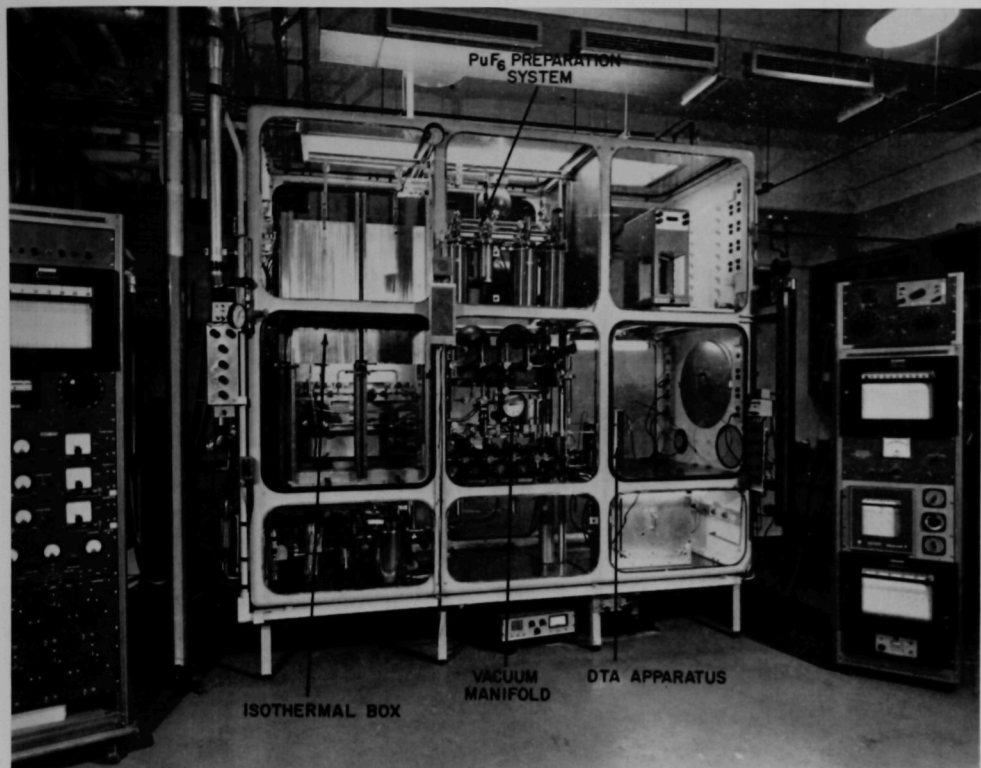
Apparatus has been constructed for determining (1) the liquid-vapor equilibria of the system PuF<sub>6</sub>-UF<sub>6</sub> (i.e., the phase composition and pressure data as a function of temperature) and (2) the temperature-composition diagram of solid-liquid equilibria in the system PuF<sub>6</sub>-UF<sub>6</sub>. The apparatus has been installed in a CENHAM 3-module, 2½-tier glovebox<sup>3</sup> (Figure II-3). The major items in the glovebox are an iso-

thermal box containing apparatus for the determination of vapor-liquid equilibria, a nickel manifold for the vacuum manipulation of volatile fluoride compounds, a tube furnace and trap system capable of preparing PuF<sub>6</sub> by the fluorination of PuF<sub>4</sub> in 50-g batches, a sample holder assembly for thermal analysis, and a 1-kg capacity Mettler balance. All thermocouples to be used in precision measurements have been calibrated against a platinum resistance thermometer. Vacuum valves, originally equipped with brass bellows, were found to be unsuitable for fluorine work, and Monel replacement bellows have been installed.

### a. SOLID-LIQUID EQUILIBRIA IN THE SYSTEM PuF<sub>6</sub>-UF<sub>6</sub> (L. TREVORROW, J. SAVAGE)

For the study of solid-liquid equilibria by thermal analysis, mixtures of UF<sub>6</sub> and PuF<sub>6</sub> will be prepared by filling calibrated ballast tanks at room temperature with the vapors. The vapors of both components will

<sup>3</sup> Malecha, R. F., Smith, H. O., Schraidt, J. H., Natale, J. V., Ross, N. E., and Brown, H. O. Jr., Low Cost Gloveboxes, *Proceedings of the Eighth Conference on Hot Laboratories and Equipment*, TID-7599, pp. 485-493, 1960.



108-7534A

FIG. II-3. Apparatus for Phase Studies of Fluoride Mixtures Containing  $\text{PuF}_6$ .

then be condensed into a nickel sample tube attached to a special valve assembly. The sample tube and valve assembly can be disconnected from the vacuum manifold and weighed to determine the quantity of each compound. The sample tube and valve assembly will be placed in a cylindrical nickel sample holder assembly positioned in a large stainless steel Dewar. The sample holder is wound with a double helix of  $\frac{3}{16}$ -in. dia. copper tubing. Cooling gas is blown through one helix, and asbestos-covered Nichrome heating wire is threaded through the other helix. Proportioned, d-c electrical power is supplied to the heating wire by a strip chart, recording controller fitted with timer-interrupters in conjunction with an electric control unit and a silicon-controlled rectifier. The temperature of the sample holder assembly can be programmed as a linear function of time with this equipment.

Two thermocouples will be used in the thermal analysis work. One thermocouple will indicate the temperature of the sample mixture, and its signal will be read either on a strip chart recorder with a 1-mv span and a variable suppression, or by a Leeds and Northrup type K-3 potentiometer. The other thermocouple will be a reference which is electrically opposed to the sample thermocouple. The result is a differential signal which is amplified by a Leeds and Northrup d-c amplifier, and the amplified signal is recorded on a zero-center strip chart recorder with a span of  $-5$  to  $+5$  mv. The thermal analysis apparatus is currently being tested with pure  $\text{UF}_6$ .

#### b. LIQUID-VAPOR EQUILIBRIA IN THE SYSTEM $\text{PuF}_6\text{-UF}_6$ (L. TREVORROW, D. STEIDL)

The fluoride separations process has included fractional distillation as a means for the separation of mix-

tures of plutonium hexafluoride ( $\text{PuF}_6$ ) and uranium hexafluoride ( $\text{UF}_6$ ). This operation requires the handling of these compounds in both the condensed and vapor phases. The planned study of the vapor-liquid equilibria in the system  $\text{PuF}_6$ - $\text{UF}_6$  will provide information useful in the choice of process conditions for the separation of  $\text{UF}_6$  and  $\text{PuF}_6$  as well as data of more fundamental interest. Phase composition and pressure data as a function of temperature between 70 and 90°C for  $\text{PuF}_6$ - $\text{UF}_6$  are to be determined. This temperature range is limited by the triple point of  $\text{UF}_6$  (64°C) and the high vapor pressure of  $\text{UF}_6$  at 90°C (2400 mm Hg). Experimental determinations in this temperature range should permit prediction of the distillation behavior of mixtures of  $\text{PuF}_6$ - $\text{UF}_6$  in the pressure-temperature range of practical interest. The study of

liquid-vapor equilibria will be carried out with an equilibrium still of the type in which the vapor phase is recirculated through the liquid phase with a mechanical pump. After equilibrium has been reached, samples of the liquid and vapor phases will be withdrawn and analyzed for uranium and plutonium.

A preliminary discussion of this study, as well as a description of the apparatus to be used, have been published (ANL-6875, p. 114). Construction of the apparatus has been completed (Fig. II-2). Equilibria for a number of ethanol-water mixtures have been determined using this equipment, and the results agree satisfactorily with the literature values. Measurements of the properties of  $\text{UF}_6$  in the vapor phase are proceeding prior to experiments with mixtures of  $\text{UF}_6$  and  $\text{PuF}_6$ .

#### 4. Reactions of $\text{PuF}_6$ (G. PIERINI,\* R. WAGNER, W. SHINN)

Investigations of the chemical behavior of  $\text{PuF}_6$  are continuing. This study will provide information which will permit a comparison of  $\text{PuF}_6$  with other volatile fluoride compounds. Such comparisons will lead to the selection of alternative chemical methods for the separation of  $\text{PuF}_6$  from other volatile fluorides.

Recent investigations at the Oak Ridge National

investigated in the present work, using larger quantities of  $\text{PuF}_6$ . Attempts are also being made to prepare, isolate, and characterize  $\text{PuF}_6$ -metal fluoride complex compounds similar to  $\text{NaF}\cdot\text{UF}_6$ .

Two types of experiments were carried out. One consisted of static experiments in which a metal fluoride was placed in a nickel container and exposed to  $\text{PuF}_6$

TABLE II-6. EXPOSURE OF  $\text{PuF}_6$  VAPOR TO GROUPS IA AND IIA METAL FLUORIDES

Type of Experiment	Metal Fluoride <sup>a</sup>				Metal Fluoride Temperature (°C)	$\text{PuF}_6$ Used	$\text{PuF}_6$ -MF Contact Time (hr)	$\text{PuF}_6$ /MF mole ratio
	MF	Mesh Size	Surface Area ( $\text{m}^2/\text{g}$ )	Amount (moles $\times 10^{-3}$ )				
Static	NaF	-325	0.94	6.22	25	125 mm <sup>b</sup>	8	0.0057
Static	NaF	-325	0.94	43.5	100	109 mm <sup>b</sup>	12	0.014
Static	LiF	—	3.11	5.25	25	125 mm <sup>c</sup>	96	
					100		1	0.024
Flow	$\text{CaF}_2$	-10+40	<sup>d</sup>	109	100	4.4 g	0.75	0.000021

<sup>a</sup> NaF and LiF were reagent grade materials;  $\text{CaF}_2$  was optical grade.

<sup>b</sup>  $\text{PuF}_6$  vapor in equilibrium with solid  $\text{PuF}_6$  at ambient temperatures.

<sup>c</sup> Average  $\text{PuF}_6$  pressure.

<sup>d</sup> Low surface area.

Laboratory<sup>4</sup> (ORNL) indicated that small amounts of  $\text{PuF}_6$  are completely sorbed on calcium fluoride ( $\text{CaF}_2$ ), lithium fluoride (LiF), and sodium fluoride (NaF). A maximum of 67 mg of  $\text{PuF}_6$  was used. Since the adsorption of  $\text{PuF}_6$  on these metal fluorides is being proposed as a means of separating  $\text{PuF}_6$  from  $\text{UF}_6$ , the sorption capacity of these solids for  $\text{PuF}_6$  has been in-

vapor. After a period of time, the vapor was removed and the solid was analyzed for plutonium. In the other experiments, a flow system was used, which more nearly represented process conditions and provided better contact of the  $\text{PuF}_6$  with the metal fluoride.

Data for the initial experiments are listed in Table II-6. The quantities of  $\text{PuF}_6$  used were much larger than those used in the ORNL experiments. In the static experiments, the  $\text{PuF}_6$  used is reported as the partial pressure of  $\text{PuF}_6$  initially above the solid. The  $\text{PuF}_6$  vapor was in equilibrium with solid  $\text{PuF}_6$  at room

\* Guest Scientist, EURATOM, CEN, Mol, Belgium.

<sup>4</sup> G. I. Cathers and R. L. Jolley, Recovery of  $\text{PuF}_6$  by Fluorination of Fused Fluoride Salts, ORNL-3298, Sept. 24, 1962; Annual Report ORNL-3452, p. 43, Sept. 20, 1963; Annual Report ORNL-3627, May 31, 1964.

temperature in all cases except the 96-hr exposure to LiF.

In the flow experiment, the  $\text{CaF}_2$  was placed in a  $\frac{3}{8}$ -in. OD prefluorinated nickel U-tube. The  $\text{PuF}_6$  was transferred through the bed by a dead-end sublimation to a weighable nickel can cooled to  $-196^\circ\text{C}$ . During the transfer, a gas, not condensable at  $-196^\circ\text{C}$ , was formed. The unidentified gas was removed by pumping through an activated alumina tower to permit further passage of  $\text{PuF}_6$  through the bed.

The retention of  $\text{PuF}_6$  by NaF, LiF, and  $\text{CaF}_2$  is low. The results of the present experiments are compared in Table II-7 with those obtained at ORNL. Since particles of different sizes and surface areas were used in the experiments, the results were compared on the basis of moles  $\text{PuF}_6/\text{m}^2$  of particle surface area. It appears, since the ORNL values are lower than those obtained in the present work, that the latter results are more nearly saturation values of  $\text{PuF}_6$  on the metal fluorides.

## 5. Alpha Radiation Decomposition Rate of Plutonium Hexafluoride

(R. WAGNER, W. SHINN)

Studies of the decomposition of gaseous plutonium hexafluoride ( $\text{PuF}_6$ ) to fluorine and solid plutonium tetrafluoride ( $\text{PuF}_4$ ) by alpha radiation from the plutonium have been continued. These studies are part of an investigation of the radiation behavior of  $\text{PuF}_6$  and of means to handle and store  $\text{PuF}_6$ .

The nature of the dependence of  $\text{PuF}_6$  decomposition rate on such parameters as duration of decomposition, initial  $\text{PuF}_6$  pressure, storage container volume, temperature, surface to volume ratio of the storage container, nature of container surface, and additives such as fluorine, oxygen, nitrogen, helium, krypton, and  $\text{PuF}_4$  is being determined. Results of previous experiments are reported in ANL-6800, p. 216 and ANL-6900, p. 156. Results of short-duration (0.5 to 16.0 days) experiments are given in the present report.

### a. PROCEDURE

Thirty-one  $127 \pm 2$  cc hollow nickel spheres, containing Hoke 1479 valves attached to the spheres with silver solder were prefluorinated in two batches. The nickel spheres were prefluorinated to provide a protective nickel fluoride film on the inner surfaces of the spheres. Prefluorination of each batch consisted of a  $\frac{1}{2}$ -hr treatment with 1200 mm Hg of  $\text{ClF}_3$  at  $26^\circ\text{C}$ , followed by a  $\frac{1}{2}$ -hr treatment with 500 mm Hg of fluorine at  $40^\circ\text{C}$ , then with 620 mm Hg of fluorine at  $100^\circ\text{C}$  for 24 hr.

All 31 vessels were weighed, randomly attached to a vacuum-gas manifold, and filled simultaneously with purified  $\text{PuF}_6$  from a common source. The  $\text{PuF}_6$  pres-

sure was observed by means of a Booth-Cromer pressure transmitter and a mercury-in-glass manometer. Attempts were made to adjust the  $\text{PuF}_6$  pressure in all spheres to 100 mm Hg, but determination of the  $\text{PuF}_6$  content of the spheres by weighing showed that 178.1 to 219.1 mg  $\text{PuF}_6$  was contained in the spheres. The differences in volume of the spheres ( $127 \pm 2$  cc) and the variation in ambient temperature in the glovebox ( $24$  to  $25^\circ\text{C}$ ) are not sufficient to account for the spread in  $\text{PuF}_6$  content based on the weights of the empty and filled spheres.

Metal Fluoride	Moles $\text{PuF}_6/\text{m}^2$ of Material Used	
	Argonne	ORNL
NaF	0.367	0.002
LiF	0.298	0.00024
$\text{CaF}_2$	0.0013	0.002*

\* Specific surface area was not reported. An approximate specific surface area was calculated assuming an average particle size of 18 mesh.

Prior to dissolution of a sphere, its outer surface was etched in warm 6N  $\text{HNO}_3$  to remove any plutonium contamination. Analysis of the etchant indicated that the spheres had acquired negligible plutonium contamination while in the glovebox. After the sphere surfaces were etched, the valves were removed from the spheres which had contained  $\text{PuF}_6$  by bending the

spheres which had contained  $\text{PuF}_6$  by bending the

valves by hand several times. The valves were easily separated from the spheres at the silver-soldered connection between the valve downleg and the spheres. The silver solder joint was sufficiently weak, even on the spheres which had been filled with  $\text{PuF}_6$  for only 0.5 day, to permit breaking the connection. Valves could not be removed by hand from spheres which had been used for blanks (blanks were prefluorinated and treated similarly to other spheres used in the  $\text{PuF}_6$  study except that they were not filled with  $\text{PuF}_6$ ). These observations qualitatively illustrate the corrosive effect of  $\text{PuF}_6$  on silver solder.

After the valve of the vessel used in a short-term experiment was separated from the sphere, the valve legs and the inside surface of the phosphor-bronze bellows of each valve were leached four or five times with acid solution, and this solution was added to the solution used to dissolve the corresponding sphere. In one case (a two-day experiment), however, the wash solution from the valve was submitted separately for a radiochemical plutonium analysis.

The amount of  $\text{PuF}_6$  lost by chemical reaction within the valve should be nearly constant for each  $\text{PuF}_6$  filling and emptying cycle. This assumption was tested by dissolving, separately, the spheres and the corresponding valves used in four of the 571-day experiments with 50 mm  $\text{PuF}_6$ . The valve and sphere of a vessel used for three experiments with  $\text{PuF}_6$  were dissolved separately to determine the amount of  $\text{PuF}_6$  corrosion in the valve as a function of a longer exposure time. A valve from a vessel from a 75-day experiment

was also analyzed for plutonium to determine corrosion of the valve.

## b. RESULTS

Data for the amount of  $\text{PuF}_6$  decomposed in the nickel spheres and in the Hoke 1479 valves are presented in Table II-8. The geometrical surface area of the sphere is greater by a factor of about forty than the surface area in the valve. The data show that 5 to 30% of the decomposed  $\text{PuF}_6$  was found in the valves. Since the material with the largest surface area in the valve is the phosphor-bronze bellows, most of the  $\text{PuF}_6$  must have decomposed on it; the surface area of the nickel downleg constitutes only a small fraction of the total surface area and is similar to the material of the downleg. However, the bellows are exposed to  $\text{PuF}_6$  only during the filling and emptying of the vessels. The exact durations of exposure during filling of the spheres were not determined, but the exposure time ranged from 15 min to 2 hr. The exposure time during emptying of the vessels was less than 2 min and can be neglected.

The data for the short-term decomposition of  $\text{PuF}_6$  must be corrected for the  $\text{PuF}_6$  decomposed by corrosion of the phosphor-bronze. Since only one value is available for the amount of  $\text{PuF}_6$  decomposed in the valve of a vessel used for the short-term experiments, this value (1.98 mg  $\text{PuF}_6$ ) has been used as a correction for all of the short-term experiments. This correction has been subtracted from both the initial quantity of  $\text{PuF}_6$  put into the vessels and the total amount of  $\text{PuF}_6$  decomposed.

Data for the short-term  $\text{PuF}_6$  decomposition experiments are listed in Table II-9 and shown in Figures II-4 and II-5. The rate of  $\text{PuF}_6$  decomposition in the spheres is high for short durations but decreases rapidly with increasing storage time. For 100 mm of  $\text{PuF}_6$  stored at  $26 \pm 2^\circ\text{C}$ , the average decomposition rates (percent per day) are 2.20 (0.5 day), 1.12 (1.0 day), 0.92 (2.0 days), 0.50 (5.0 days), 0.35 (8.0 days), 0.29 (12.0 days), and 0.27 (16.0 days).

Since past experience had indicated significant retention of either  $\text{F}_2$  or  $\text{PuF}_6$  on finely divided  $\text{PuF}_4$ , some spheres from tests at some of the durations were heated to  $60^\circ\text{C}$  after the major portion of the undecomposed  $\text{PuF}_6$  and the fluorine was removed from the sphere. When the spheres were heated, the pressure rose from a value of  $15\mu$  to a value of  $70\mu$  while the spheres were being pumped out. This behavior is indicative of gases adsorbed on the vessel walls and/or on the  $\text{PuF}_4$ . It was not possible to determine if the adsorbed gas was fluorine or  $\text{PuF}_6$ . The  $\text{PuF}_6$  decomposition rates obtained in the spheres which were heated were not significantly different from the  $\text{PuF}_6$  rates

TABLE II-8. DISTRIBUTION OF  $\text{PuF}_6$  DECOMPOSITION PRODUCT IN 127-CC VESSELS

Duration of Experiment (days)	Initial $\text{PuF}_6$ Pressure (mm of Hg)	Wt of $\text{PuF}_6$ Introduced (mg)	Wt. (mg) $\text{PuF}_6$ Decomposed	
			In Sphere	In Valve
571	50	118.4	47.7	3.9
571	50	115.6 <sup>a</sup>	49.8	5.0
571	50	116.5 <sup>a</sup>	43.1	4.1
571	50	118.2 <sup>a</sup>	45.2	5.2
			4.6 $\pm$ 0.6 <sup>b</sup>	
75	100	218.6	26.4	2.9
2	100	193.7	4.36	1.98
5.6	100	232.9	88.0	6.7
176	100	229.4		
75.6	100	234.9		

<sup>a</sup> These spheres were filled simultaneously from a common  $\text{PuF}_6$  source; therefore, their phosphor-bronze bellows were exposed to  $\text{PuF}_6$  for nearly equal times.

<sup>b</sup> Error is  $\pm 2\sigma$ .

TABLE II-9. ALPHA DECOMPOSITION OF GASEOUS PLUTONIUM HEXAFLUORIDE

Spherical Nickel Vessels: 125 to 129 cc  
 Storage Temperature:  $26 \pm 2^\circ\text{C}$   
 Initial  $\text{PuF}_6$  Pressure: 100 mm  
 Prefluorination Conditions: 1200 mm  $\text{ClF}_3$  at  $26^\circ\text{C}$ ,  $\frac{1}{2}$  hr;  
 then 500 mm  $\text{F}_2$  at  $40^\circ\text{C}$ ,  $\frac{1}{2}$  hr;  
 then 620 mm  $\text{F}_2$  at  $100^\circ\text{C}$ ,  
 24 hr.

Initial Weight <sup>a</sup> of $\text{PuF}_6$ (mg)	Duration of Decomposition (days)	Average Rate of $\text{PuF}_6$ Decomposition <sup>a,b</sup> (percent per day)
212.3	0.5	1.60
210.8 <sup>c</sup>	0.5	2.06
192.3	0.5	1.94
209.8 <sup>c</sup>	0.5	2.58
177.7 <sup>c</sup>	0.5	2.84
210.2	1.0	0.86
203.1	1.0	1.04
207.6	1.0	1.08
190.8 <sup>c</sup>	1.0	1.51
209.9	2.0	0.66
210.2	2.0	0.74
217.1	2.0	0.88
191.7 <sup>c</sup>	2.0	1.14 <sup>c</sup>
180.8 <sup>c</sup>	2.0	1.19
216.1	5.0	0.35
191.8	5.0	0.43
210.6	5.0	0.52
205.8	5.0	0.55
186.6	5.0	0.65
207.9	8.0	0.30
203.7 <sup>c</sup>	8.0	0.30
210.4 <sup>c</sup>	8.0	0.32
201.3	8.0	0.41
208.1	8.0	0.42
195.8 <sup>c</sup>	12.0	0.26
196.3	12.0	0.27
210.3 <sup>c</sup>	12.0	0.29
184.8	12.0	0.31
199.6	12.0	
212.8 <sup>c</sup>	16.0	0.20
176.3	16.0	0.34

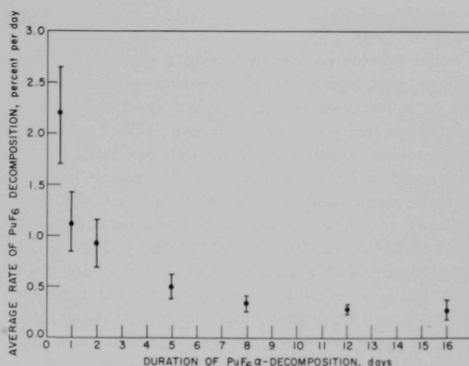
<sup>a</sup> A correction of 1.98 mg of  $\text{PuF}_6$  was made on all initial weights of  $\text{PuF}_6$  and on all values of  $\text{PuF}_6$  decomposed.

<sup>b</sup> The plutonium of the  $\text{PuF}_6$  decomposition product was determined by alpha-counting methods after the sphere was dissolved in 6N  $\text{HNO}_3$ , 0.1M  $\text{Al}(\text{NO}_3)_3$  solution. The interior of the valve was leached with a similar acid solution, and the wash solution was added to the solution containing the sphere.

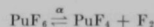
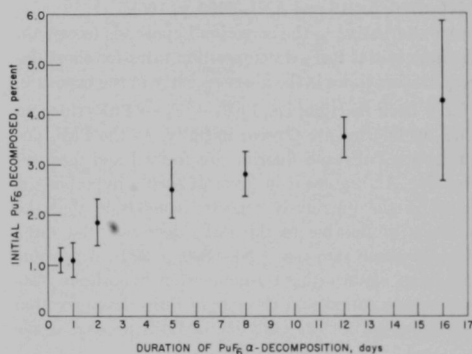
<sup>c</sup> These spheres were heated to  $60^\circ\text{C}$  to facilitate removal of undecomposed  $\text{PuF}_6$  during the emptying of the spheres.

<sup>d</sup> Uncertainties are  $\pm 2\sigma$ .

<sup>e</sup> In this experiment the solution used to leach the interior of valve was analyzed for plutonium separately from the solution in which the sphere and its contents had been dissolved. The valve contained 1.34 mg of plutonium, which indicates



108-8744

FIG. II-4. Average Rate of  $\text{PuF}_6$  Decomposition versus Duration of Decomposition.Volume of Nickel Spheres:  $127 \pm 2$  ccInitial  $\text{PuF}_6$  Pressure: 100 mmStorage Temperature:  $26 \pm 2^\circ\text{C}$ 

108-8732

FIG. II-5. Percent  $\text{PuF}_6$  Decomposition versus Duration of Decomposition.

obtained in spheres which were not heated during the  $\text{PuF}_6$ -fluorine removal.

A plot of the data expressed as the percent of the initial  $\text{PuF}_6$  decomposed versus the decomposition time (Fig. II-4) shows that the decomposition must proceed very rapidly during the first 12 hr. It appears, by extrapolation of the curve toward zero time, that from 0.5 to 1.5% of the original  $\text{PuF}_6$  is lost by chemical corrosion of the sphere walls.

that 1.98 mg of  $\text{PuF}_6$  had decomposed in the valve. Since all the valves had equal exposure to  $\text{PuF}_6$ , 1.98 mg of  $\text{PuF}_6$  has been assumed to have decomposed in each valve.

## c. DISCUSSION

Some previously reported results support the hypothesis that high initial decomposition rates may be due to a corrosion reaction. When experiments were carried out under similar conditions (127-cc prefluorinated nickel vessels containing 100 mm PuF<sub>6</sub> for 75 days at 26 ± 2°C), the first use of the vessels resulted in PuF<sub>6</sub> decomposition rates of 0.19% per day, and reuse of the vessels resulted in PuF<sub>6</sub> decomposition rates of 0.14% per day (see ANL-6800, p. 219). These data suggest that a pretreatment of the vessel walls with PuF<sub>6</sub> is essentially completed by the time the sphere is used for a second experiment or that the PuF<sub>6</sub> reaction with the vessel wall is proceeding at a rate which changes too slowly with time to be detected.

Further evidence in favor of the corrosion hypothesis was previously reported for experiments in which spheres were packed with nickel wool. It was observed that, upon initial exposure to the packed spheres, the PuF<sub>6</sub> decomposition proceeded at a relatively high rate (0.30% per day). Upon reuse of two spheres, the decomposition rates dropped to 0.18 and 0.13% per day (see ANL-6800, p. 218 and ANL-6900, p. 160).

An alternative to the corrosion hypothesis to explain the high initial PuF<sub>6</sub> decomposition rates for short decomposition times is the absence, early in the exposure, of any back reaction, i.e.,  $\text{PuF}_4 + \text{F}_2 \xrightarrow{\alpha} \text{PuF}_6$  since no PuF<sub>4</sub> or fluorine are present initially. As the PuF<sub>6</sub> decomposes, PuF<sub>4</sub> and fluorine are formed and may recombine. An argument in favor of such a hypothesis is found in the previously reported conclusion that the addition of fluorine to the PuF<sub>6</sub> decreases the PuF<sub>6</sub> decomposition rate (see ANL-6800, p. 220). A possible argument against this recombination hypothesis rests in the observation that the rate of PuF<sub>6</sub> decomposition is independent of the quantity of PuF<sub>4</sub> present at the

start of the PuF<sub>6</sub> decomposition (see ANL-6800, p. 219).

Finally, it has been shown that plutonium hexafluoride decomposes at a higher rate at 80 to 83°C than at 26 ± 2°C (see ANL-6900, p. 159). Since these were the only two temperature ranges studied, it is not certain that at 26 ± 2°C the thermal decomposition of PuF<sub>6</sub> can be neglected.

## d. SUMMARY

In summary, studies of the gas-phase, alpha-induced decomposition of PuF<sub>6</sub> have been hampered by inability to isolate the alpha-induced decomposition from other modes of decomposition (such as chemical reaction with the vessel and thermal decomposition). Lack of information on the adsorption behavior of PuF<sub>6</sub> and fluorine on PuF<sub>4</sub> and the nickel fluoride walls of the vessels makes determination of the amount of PuF<sub>6</sub> present as a gas uncertain. No way has been found to determine experimentally the amount of the alpha energy absorbed in the gas phase or to determine the nature of the absorbing species.

Considerable effort would be required to overcome these difficulties, and, for the present, no further experiments on the alpha decomposition of PuF<sub>6</sub> are planned.

The data obtained thus far do provide some practical information on the handling and storage of gaseous PuF<sub>6</sub>. During the first eight days of PuF<sub>6</sub> storage in a prefluorinated nickel vessel, PuF<sub>6</sub> will decompose at a rapid rate (from 2.2 to 0.35% per day) whereas the rate should decrease from 0.35% per day to 0.07% per day over the next 563 days. Reuse of the vessel would result in less PuF<sub>6</sub> decomposition. These data indicate that a certain plutonium inventory will be held in the equipment used to handle PuF<sub>6</sub>. This plutonium can be recovered by fluorination of the process vessels and lines at 300°C.

## 6. Corrosion of Materials (W. GUNTHER)

The fluoride volatility program is designed to develop processes for the recovery of uranium and plutonium from partially spent nuclear reactor fuels by the formation of the volatile hexafluorides of uranium and plutonium, which are subsequently separated from the fission product fluorides by distillation. Nickel or nickel alloys such as Monel are commonly used as the material of construction for process equipment which is to be exposed to fluorine and to corrosive fluorides at elevated temperatures, since extensive attack on these materials is prevented by the buildup of a protective nickel fluoride scale which limits further reaction. In

order to make estimates of the expected useful lifetimes of equipment exposed to UF<sub>6</sub>, PuF<sub>6</sub>, fluorine, and the volatile fission product fluorides at temperatures up to 550°C, a knowledge of the corrosion rates by these fluorides, either in combination or individually, is required.

A corrosion program in support of the fluoride volatility program has been initiated. Two types of experiments are planned to determine the rate of corrosion of nickel-200: (a) small-scale static experiments conducted in a tube furnace wherein nickel coupons will be exposed to the volatile fission product fluorides and

(b) exposures of nickel coupons to process gases under actual operating conditions in the 2-in. dia. fluid-bed reactor.

A survey of the unclassified literature has revealed very little useful information concerning the corrosion of nickel or Monel at temperatures up to 550°C by the volatile fission product fluorides. However, some data on the corrosion of nickel and nickel alloys by  $UF_6$  and fluorine have been published.

Corrosion of numerous metals including nickel and Monel by  $UF_6$  gas from 500 to 1000°C has been studied by Langlois.<sup>5</sup> It was observed that the rate of corrosion of nickel at 550°C and 700°C was approximately 10 mils/yr. However, at 640°C a maximum corrosion rate was reached which approached 1400 mils/yr. A sharp decrease in the corrosion rate was observed in the temperature interval 640 to 700°C, followed by a linear increase in corrosion rate from 700 to 1000°C. The corrosion rate of Monel by  $UF_6$  is linear over the temperature range investigated, being about 350 and 1400 mils/yr at 550°C and 800°C, respectively.

Hale and associates<sup>6</sup> have reported the results of a study of the reaction of nickel with  $UF_6$ . At 816°C with an initial  $NiF_2$  scale of 37,000 Å a rate of 3.0 mils/yr is reported, while at 982°C with an initial  $NiF_2$  scale of 74,000 Å, a rate of 3.2 mils/yr is observed.

Very little information on the corrosion of nickel by  $PuF_6$  is available. Steindler<sup>7</sup> reported that a nickel crucible which had been exposed to plutonium fluorides and fluorine for 2 hr at 700°C showed appreciable corrosion including some intergranular attack.

Several investigations of the rate of corrosion of nickel by fluorine have been reported. Hale et al.<sup>6</sup> found the rates at 593°C and 705°C to be 18 and 130 mils/yr, respectively, on a nickel surface having an initial  $NiF_2$  scale thickness of  $10^5$  Å. Jarry et al.<sup>8</sup> determined the rate of nickel-200 corrosion by elemental fluorine at 500 and 600°C to be 17 and 60 mils/yr on a fresh nickel surface. Steindler and Vogel<sup>9</sup> found the corrosion rate of nickel-200 by fluorine at 650 and 750°C to be 314 and

816 mils/yr, respectively, and the corrosion rate of Monel to be 3500 mils/yr. The conflict in these data is not readily resolved.

Work has begun on the construction of an all-metal system to be used to study the corrosive effects of the volatile fission product fluorides on commercially available nickel-200 at temperatures up to 550°C. The volatile fission products to be examined in small-scale static tests include  $GeF_4$ ,  $AsF_5$ ,  $SeF_6$ ,  $NbF_5$ ,  $MoF_6$ ,  $RuF_5$ ,  $RhF_5$ ,  $SbF_5$ ,  $TeF_6$ , and possibly at a later date  $BrF_3$ ,  $BrF_5$ ,  $IF_5$ , and  $IF_7$ . Due to the difficulty in handling technetium compounds in the present system,  $TeF_6$  corrosion will not be investigated at this time. The fission product fluorides that are commercially available will be purchased; other fluorides will be made by the direct fluorination of the metal or the oxide. Purity checks of the volatile fluorides will include vapor density and infrared spectral measurements.

It is planned to insert nickel-200 coupons into the 2-in. dia. fluid-bed reactor to obtain corrosion data for typical processing environments. Sample coupons will be placed in both the fluid bed and the disengaging chamber sections of the reactor, and corrosion rates will be evaluated after the completion of one or more process runs. The 2-in. dia. reactor is designed to investigate HF-promoted oxidative dechlorination of spent nuclear fuels, followed by fluorination to volatilize the uranium and plutonium as hexafluorides. This apparatus will afford an opportunity to obtain controlled corrosion data in an  $HF-O_2-F_2$  system. Corrosion data will be calculated from weight and/or dimensional changes.

Corrosion data will also be obtained on coupons welded with nickel-200 welding rods (high purity) and nickel-61 welding rods (containing 2.0-3.5% titanium). There are indications that corrosion rates in fluorinating atmospheres are much higher when nickel-61 metal filler rods are used than when nickel-200 filler rods because of the presence of titanium in the former.

The corrosion rate of INOR-8 metal will be briefly studied in both the fluid-bed and static tube furnace experiments, and the rates of corrosion of INOR-8 and nickel-200 will be compared.

Autoradiographic examination of selected coupons will be made in an attempt to find out if any uranium or plutonium is present in the intergranular areas of the metal. Microscopic examinations will be carried out to determine the amount of intergranular attack both in the base metal and in the welded areas. If possible, a correlation between rate of corrosion and the amount of intergranular attack will be made.

<sup>5</sup> Langlois, G., Corrosion de materiaux metalliques par l'hexafluorure a Joule temperature, CEA-2385, 1963. (Available in translation as USAEC Report ANL-trans-82.)

<sup>6</sup> Hale, C., Barber, E., Bernhardt, H. and Rapp, K., High Temperature Corrosion of Some Metals and Ceramics in Fluorinating Atmospheres, USAEC Report K-1459, 1960.

<sup>7</sup> Steindler, M., USAEC Report ANL-6753, 1963.

<sup>8</sup> Jarry, R., Gunther, W. and Fischer, J., The Mechanism and Kinetics of the Reaction between Nickel and Fluorine, USAEC Report ANL-6684, 1963.

<sup>9</sup> Steindler, M. and Vogel, R., Corrosion of Materials in the Presence of Fluorine at Elevated Temperatures, USAEC Report ANL-5662, 1957.

## 7. Fluorination of Waste Samples from Rocky Flats Plant (R. P. WAGNER, W. A. SHINN, M. J. STEINDLER)

At the request of the Rocky Flats Division of the Dow Chemical Company, the possibility of applying volatility methods to the recovery of plutonium from waste stream materials was investigated. Interest on the part of the Rocky Flats Division stemmed from the potential savings which may be attained by using a simple, direct method of plutonium removal from a variety of waste materials. The procedure used was to fluorinate samples with elemental fluorine in a boat reaction vessel at 500°C or 550°C to produce volatile plutonium hexafluoride. Data on the degree of removal of plutonium from waste materials and estimates of rates of reaction were to be obtained. Impurity content of the collected plutonium hexafluoride was not determined.

### a. MATERIALS

Three types of plutonium-containing waste materials were obtained from Rocky Flats. These wastes are classified according to their source at Rocky Flats. The particular samples used for the present experiments are not necessarily typical of what would be handled during routine operations. The materials used, together with the corresponding plutonium analyses (by Rocky Flats), are (1) skull oxide, 87.13 w/o Pu; (2) incinerator ash, 11.6 w/o Pu; (3) sweepings, 58.8 w/o Pu. The skull oxide is relatively pure  $\text{PuO}_2$ . The sample of sweepings, mainly  $\text{PuO}_2$ , is abnormally low in carbon (0.39%) and silicon (1%) for this type of material. The samples of incinerator ash and sweepings had been oxidized and hydrofluorinated at Rocky Flats prior to shipment because of their high initial carbon and silicon content. Impurities present at a concentration of one percent or more are C, Ca, Cu, K, Na, and Pd for the incinerator ash; Ni, Si, and Ti for the sweepings; and Al, Fe, and Mg for both. The skull oxide and sweepings samples appear similar to  $\text{PuO}_2$ , while the incinerator ash is very light in color (gray-white) and has a bulk density considerably lower than those of the other two materials.

### b. EQUIPMENT

Fluorinations of samples were performed in a 2-in. OD nickel reaction tube heated by a 1400-watt Hevi Duty Furnace. The samples were placed in shallow boats (4 by 1 by 0.2 in.) constructed from 0.015-in. thick nickel sheet. The boat rested on a track, machined from nickel rod, which acted as a heat sink and allowed convenient handling of the sample. A lip on the edges of the track supported a hemi-cylindrical piece of fused alumina tubing placed over the sample to keep out of

the boat any nickel fluoride which might spall from interior surfaces of the nickel reaction tube. The temperature of the furnace was controlled by a Gardsman controller and two Variacs connected to a chromel-alumel thermocouple.

A 6-lb (400 psi) fluorine cylinder supplied by Allied Chemical Company, a Matheson Company fluorine regulator, and another fluorine cylinder used as a low-pressure ballast tank were used as the fluorine supply system. A Kel-F rotameter (Brooks-Mite, 0-500 ml  $\text{F}_2/\text{min}$ ) was used to measure fluorine flow, which was on a once-through basis. The gas leaving the reaction tube flowed through two 3/4-in. dia. nickel test tube traps in which the plutonium hexafluoride product was collected. The traps were cooled by a mixture of trichloroethylene and solid carbon dioxide. Unreacted fluorine was disposed of in an activated alumina tower constructed of 4-in. dia. copper pipe. Teflon was used as a gasket material, and permanent joints were either silver-soldered or nickel Heliarc welded. Valves constructed of nickel and Monel with silver-soldered diaphragms (Hoke 413) were used.

### c. PROCEDURE

A weighed sample of plutonium-containing waste was placed in the boat so as to cover the bottom of the boat as evenly as possible. Two- to four-gram samples were used to limit the extent of any unexpected reaction. The sample was heated to the operating temperature while the reaction tube was evacuated. Fluorine flow was then started, and when the system pressure reached one atmosphere (in approximately 5 min), the gas exit valve connected to the alumina tower was opened. Fluorination was continued for at least 5 hr at temperature (500 or 550°C) with a fluorine flow rate of 200 ml/min. At the end of the experiment, the system was evacuated through the cold traps.

After fluorination, the residue from the sample was examined, and the sample and the boat were placed in a plastic bottle. The sample and boat were dissolved in 250 ml of 4N  $\text{HNO}_3$  containing  $\text{Al}(\text{NO}_3)_3$  and a trace of HF, and the plutonium was determined by alpha counting. This treatment, as well as treatment with such reagents as HCl,  $\text{HClO}_4$ , HF, and  $\text{H}_2\text{SO}_4$ , failed to dissolve all the nickel fluoride formed by the fluorination of the nickel reaction boat. Some plutonium was found by leaching the undissolved residue, but not enough to materially affect the results. Samples of the original waste materials were fused with ammonium bifluoride and radiochemically analyzed to check the analysis of the starting materials.

## d. RESULTS AND OBSERVATIONS

Plutonium removal data are based on alpha counting of the starting material and of the fluorinated residue. The plutonium removal, Table II-10, was 99 percent or better except for the 5-hr experiment on the incinerator ash which gave a plutonium removal of 82.2%. This experiment was repeated, and satisfactory plutonium removal (98.4%) was achieved. No reason for the low result is known. A temperature excursion of 40°C was noted for incinerator ash at the beginning of fluorine flow, while a 20°C rise was observed for the sweepings and even less for the skull oxide. The residues contained various amounts of  $\text{NiF}_2$ , which is expected under these experimental conditions. Corrosion of the nickel boat was severe in tests with incinerator ash, while considerably less corrosion was observed during processing of sweepings and skull oxide. The residue from fluorination of skull oxide was predominately  $\text{NiF}_2$  and also contained small amounts of red  $\text{PuF}_4$ .

Rate-of-reaction data were obtained for the fluorination of skull oxide at 500°C and 550°C by weighing the plutonium hexafluoride collected after successive intervals of time. Cumulative  $\text{PuF}_6$  collection as a function of time for 500°C and 550°C tests is shown in Figure II-6. The reaction appears to proceed through the formation of intermediate  $\text{PuF}_4$ .

An attempt to measure product ( $\text{PuF}_6$ ) purity was

unsuccessful. Large amounts of nickel introduced into the product from the hydrolysis of  $\text{PuF}_6$  in the nickel test tube traps did not allow spectrographic analysis of plutonium by the methods currently used.

TABLE II-10. PLUTONIUM REMOVAL FROM WASTE MATERIALS  
Fluorinating gas: fluorine

Material	Sample Weight (g)	Pu in Sample (mg)	Reaction Time (hr)	Temp (°C)	F <sub>2</sub> Flow (ml/min)	Pu in Residue (mg)	Plutonium Removal (%)
Skull Oxide	2.0795	1812	9	500 <sup>a</sup>	100 <sup>a</sup>	3.4	99.8
Skull Oxide	4.1120	3583	10	500	200	25.5	99.3
Skull Oxide	3.6811	3207	5	550	200	35.3	98.9
Incinerator Ash	2.2087	256	5	550	200	45.5	82.2
Incinerator Ash	2.2103	256	10	550	200	1.7	99.1 <sup>b</sup>
Sweepings	2.151	1265	5	550	200	0.6	99.9
Sweepings	2.1365	1256	10	550	200	0.4	99.9
Incinerator Ash	2.2677	263	5	550	200	4.3	98.4 <sup>b</sup>

<sup>a</sup> The fluorination procedure for this sample was: 1 hr at 370 to 510°C, F<sub>2</sub> flow rate of 100 ml/min; 4 hr at 510°C, F<sub>2</sub> flow rate of 100 ml/min; 4 hr at 490°C, F<sub>2</sub> flow rate of 500 ml/min.

<sup>b</sup> Includes plutonium recovery by leaching of dissolution residue.

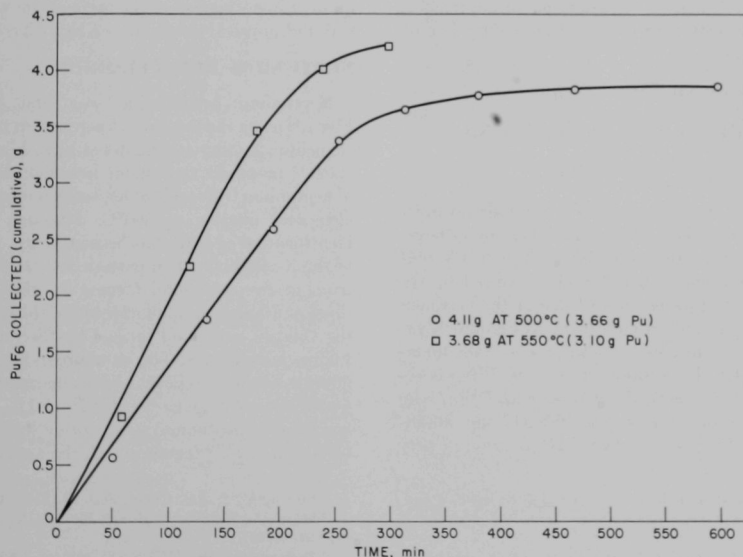


FIG. II-6. Cumulative  $\text{PuF}_6$  Collection for Fluorination of Skull Oxide.

### c. CONCLUSIONS

Fluorination of waste samples containing plutonium resulted in removal of essentially all of the contained plutonium by the conversion of plutonium to the hexafluoride and its subsequent volatilization. Both temperatures and rates of reaction appear to be relatively favorable for process application.

The data obtained in the present set of exploratory experiments should be applied with caution. It has been recognized that the samples fluorinated in the experiments reported here may be atypical; if so, the degree of removal as well as the rate of removal of plutonium may not be typical of those achievable for routine waste samples. Further, the purity of the plutonium hexafluoride has not been checked. Those impurities which form volatile fluorides will certainly contaminate plutonium hexafluoride volatilized from the mixtures. Also, the reactivity of impurities will determine to some extent the peripheral problems encountered in the fluorination by influencing the heat of reaction, the rate of plutonium volatilization, the optimum operating temperature, and other factors.

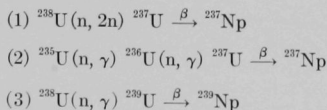
Since a recovery process would be designed to con-

vert plutonium in waste material to plutonium tetrafluoride suitable for conversion to metal, the reduction of plutonium hexafluoride is an important step in the process. No answers to questions on the choice of reduction method (thermal, chemical), the purity of the product, the physical state of the product, etc. have been provided in the present study, although some information on several of these points may be available from the literature. The impurity content of the initial samples may become an important consideration in the choice of variable for the reduction step.

Finally, extrapolation of the rate data obtained on samples held in reaction boats to other types of process equipment is often difficult. Of particular note in this regard is the extrapolation of rate data from boats to fluid beds. Hence, information on the behavior of waste samples in fluid-bed equipment would be needed before such reactors could be employed. While the results of the present experiments appear to be encouraging regarding the application of fluoride volatility methods to the recovery of plutonium from waste materials, additional work both in the laboratory and on an engineering scale is indicated before firmer conclusions can be drawn.

## 8. Neptunium Chemistry (T. GERDING)

Neptunium (element 93) is produced during irradiation of uranium with neutrons by at least three important mechanisms.



Neptunium\* can be expected as a contaminant in irradiated uranium fuel.<sup>10</sup> The volatile neptunium hexafluoride can be expected as a contaminant in the plutonium and/or uranium hexafluoride produced by the fluoride volatility process. Knowledge of the pertinent chemical and physical properties of neptunium hexafluoride will be of interest to both process and fundamental chemistry. In addition, interest in <sup>237</sup>Np is related to one of the methods of producing <sup>238</sup>Pu,<sup>11</sup> by neutron irradiation of mixtures <sup>237</sup>NpO<sub>2</sub> and aluminum. <sup>238</sup>Pu is of interest to the SNAP program. A pro-

gram of investigation of the preparation and the chemical and physical properties of NpF<sub>6</sub> has been started.

### NEPTUNIUM HEXAFLUORIDE

Neptunium hexafluoride was first prepared by Florin<sup>12</sup> using the reaction of neptunium trifluoride and elemental fluorine at bright red heat. Malm and associates<sup>13</sup> prepared neptunium hexafluoride by reaction of neptunium trifluoride or neptunium tetrafluoride with elemental fluorine at 500°C. Although no chemical identification of NpF<sub>6</sub> has been reported, the similarity of the X-ray diffraction pattern and the infrared spectrum of the compound formed by this procedure to those of uranium hexafluoride led to the conclusion that the volatile compound formed by the reaction is neptunium hexafluoride. The structure of neptunium hexafluoride has been reported by Zachariassen.<sup>14</sup> Structure parameters are given in Table II-11. The infrared spectrum of neptunium hexafluoride has been reported by Malm et al.<sup>15</sup> together with the assignments of the

\* Owing to the short half life of <sup>239</sup>Np (2.34 d) little, if any, of this isotope will be present at the time fuel material is processed.

<sup>10</sup> Vondy, D. R., Lane, J. A., and Gresky, A. T., *Ind. Eng. Chem. Process Design Develop.*, **3**(4), 293-296 (October 1964).

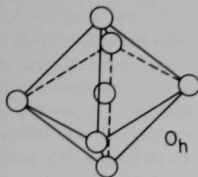
<sup>11</sup> *Chem. Eng. News*, **41**, 47 (Aug. 5, 1963).

<sup>12</sup> Florin, A., *J. Am. Chem. Soc.* **70**, 2147 (1948).

<sup>13</sup> Malm, J., Weinstock, B. and Weaver, E., *J. Phys. Chem.* **62**, 1506 (1958).

<sup>14</sup> Zachariassen, W., *NNES IV*, 14B, p. 1462.

<sup>15</sup> Malm, J., Weinstock, B. and Claassen, H., *J. Chem. Phys.* **23**, 2192 (1955).

TABLE II-11. STRUCTURE PARAMETERS FOR UF<sub>6</sub>, NpF<sub>6</sub> AND PuF<sub>6</sub>

	UF <sub>6</sub>	NpF <sub>6</sub>	PuF <sub>6</sub>
Symmetry (solid)	ortho-rhombic	ortho-rhombic	ortho-rhombic
<i>Lattice Parameters</i> <sup>a</sup>			
a <sub>0</sub> (Å)	9.900	9.91	9.91
b <sub>0</sub> (Å)	8.966	8.97	8.94
c <sub>0</sub> (Å)	5.207	5.21	5.21
Density (g cm <sup>-3</sup> )	5.060	5.00	5.08
M-F distance (Å)	1.994	1.980	1.972
M-F stretching force constant (md/Å)	3.78	3.71	3.59

<sup>a</sup> See ANL-6900, Table II-8, p. 164.

TABLE II-12. INFRARED AND RAMAN SPECTRAL DATA FOR UF<sub>6</sub>, NpF<sub>6</sub>, AND PuF<sub>6</sub> (CM<sup>-1</sup>)

	UF <sub>6</sub>	NpF <sub>6</sub>	PuF <sub>6</sub>
ν <sub>1</sub> Raman	667	648	628
ν <sub>2</sub> Raman	535	528	523
ν <sub>3</sub> Infrared	623	624	615
ν <sub>4</sub> Infrared	181	200	203
ν <sub>5</sub> Raman	202	206	211
ν <sub>6</sub> Inactive	140	164	171

TABLE II-13. PHASE TRANSITION DATA FOR THE HEXAFLUORIDES OF URANIUM, NEPTUNIUM, AND PLUTONIUM

	UF <sub>6</sub>	NpF <sub>6</sub>	PuF <sub>6</sub>
Boiling Point (°C)	56.54	55.18	62.16
Triple Point (°C)	64.052	55.10	51.50
(mm Hg)	1139.6	758.0	533.0
Vapor Pressure (mm Hg) 0°C	17.65	20.8	17.9
25°C	111.85	127.17	105.45
75°C	1592	1425	1136
Heat of Fusion (cal mole <sup>-1</sup> )	4588	4198	4456
Entropy of Fusion (cal mole <sup>-1</sup> deg <sup>-1</sup> )	13.61	12.79	13.72

fundamental frequencies. The absorption spectrum of neptunium hexafluoride in the visible region is mentioned by Malm et al.<sup>13</sup> but no data are given. Goodman<sup>16</sup> shows a tracing of the absorption spectrum of neptunium hexafluoride, but failed to give values for extinction coefficients. The positions of some of the major peaks were identified. Spectral data are presented in Table II-12. Neptunium hexafluoride is said to be quite photosensitive;<sup>13</sup> hence, the absence of Raman data is not surprising.

Phase transition data for neptunium hexafluoride are presented in Table II-13. Weinstock et al.<sup>17</sup> determined the vapor pressure of neptunium hexafluoride, and the following equations were fitted to the data:

$$(0 \text{ to } 55.10^\circ\text{C}) \log P_{\text{mm}} = \frac{-2892.0}{T(^{\circ}\text{K})} - 2.6990 \log T + 18.48133$$

$$(55.10^\circ\text{C} \text{ to } 76.82^\circ\text{C}) \log P_{\text{mm}} = -\frac{1191.1}{T(^{\circ}\text{K})} + 2.5825 \log T + 0.01023$$

A computer program was set up, and the vapor pressure of neptunium hexafluoride has been tabulated from  $-10^\circ\text{C}$  to  $100^\circ\text{C}$ .<sup>18</sup>

Little information on the chemical properties of neptunium hexafluoride is available. Owing to the lower alpha activity of <sup>237</sup>Np compared to <sup>239</sup>Pu, neptunium hexafluoride does not decompose by radiation to the extent observed for plutonium hexafluoride. Further, neptunium hexafluoride is considerably more stable toward thermal decomposition than is plutonium hexafluoride. A sample of neptunium hexafluoride at 900 mm Hg was heated to 500°C for 3 hr in a nickel vessel without showing any evidence of thermal decomposition.<sup>13</sup> Neptunium hexafluoride is hydrolyzed by water and yields the NpO<sub>2</sub><sup>2+</sup> ion.

A program of research on the chemistry of neptunium fluorides has started. Initial studies will be devoted to the chemistry of the formation of neptunium hexafluoride by fluorination of neptunium tetrafluoride (or neptunium trifluoride) and characterization of the solid residues. It is also planned to obtain data on the absorption spectrum of neptunium hexafluoride and to study the equilibrium in the system NpF<sub>6</sub>-NpF<sub>4</sub>-F<sub>2</sub>. Apparatus for this work has been constructed.

<sup>16</sup> Goodman, G., Thesis, Harvard University (1959).

<sup>17</sup> Weinstock, B., Weaver, E. and Malm, J., J. Inorg. Nucl. Chem. **11**, 104 (1959).

<sup>18</sup> Steindler, M. J., Private Communication.

## 9. Fission Product Chemistry: Behavior of MoO<sub>3</sub>, MoO<sub>2</sub>, and SnF<sub>4</sub> Under Fluorination Conditions (G. PIERINI\*)

During experiments on the fluid-bed fluorination of U<sub>3</sub>O<sub>8</sub>-PuO<sub>2</sub>-fission product mixtures, the presence of MoO<sub>3</sub> in the fission product mixture is believed to have contributed to plugging of valves in the cold trapping system (ANL-6900, p. 150). A series of short exploratory experiments were carried out to determine the volatility of MoO<sub>3</sub>, MoO<sub>2</sub> and SnF<sub>4</sub> in a fluorine or a fluorine-nitrogen-oxygen stream. These experiments were carried out in a 1½-in. OD horizontal nickel tube reactor. The starting material was placed in a nickel boat and the products were collected in traps cooled to -80°C. Total flow rates of 1400 cc/min were found to be too high, as evidenced by frequent plugs in the line to the traps. Hence total flow rates of 250 to 400 cc/min were employed.

### a. THE VOLATILITY OF MoO<sub>3</sub> AND MoO<sub>2</sub> IN A FLUORINE STREAM

Reactions with MoO<sub>3</sub> were carried out at 450°C. In two experiments in which fluorine was diluted with nitrogen and oxygen and in two experiments in which a fluorine-nitrogen stream was used, only 3 to 5% of the product was collected in the cold traps. This material was identified as MoF<sub>6</sub> by vapor pressure measurements. The remainder of the product, found in the cooler portions of the tubular reactor, was a white needle-like crystalline solid which is probably a mixture of MoOF<sub>4</sub> and MoF<sub>5</sub>.

In order to determine if the low yield of MoF<sub>6</sub> was due to a reaction of MoF<sub>6</sub> with oxygen at 450°C, MoF<sub>6</sub> and oxygen were simultaneously fed into the heated reactor. No reaction was observed.

\* Guest Scientist, EURATOM, Mol, Belgium.

A gas mixture which consists of 40 v/o HF, 40 v/o oxygen, and 20 v/o nitrogen is being used for the destructive oxidation of stainless steel cladding. The volatility of MoO<sub>3</sub> at 550°C in such a gas stream was tested. It was necessary to stop the reaction after 30 min of intermittent feeding of HF because the slightly volatile product which was formed (probably MoO<sub>2</sub>F<sub>2</sub>, sublimation point 270°C) condensed in the outlet zone of the reactor and plugged the line. About 30% of the MoO<sub>3</sub> charged reacted. No MoF<sub>6</sub> was observed.

When MoO<sub>2</sub> was treated at 450°C with a fluorine-oxygen-nitrogen mixture, only an insignificant quantity of MoF<sub>6</sub> was collected. The behavior of MoO<sub>3</sub> and MoO<sub>2</sub> is similar under these fluorination conditions.

From these experiments it may be tentatively concluded that molybdenum would be volatilized from the fluid bed on treatment of oxide fuel pellets with HF-O<sub>2</sub>. Further, the low yield of MoF<sub>6</sub> would indicate that the uranium and plutonium hexafluoride product formed during fluorination may be only slightly contaminated with MoF<sub>6</sub>.

### b. THE VOLATILITY OF SnF<sub>4</sub> IN A FLUORINE STREAM

Tin is a minor constituent of Zircaloy-2, which is commonly used as a cladding in power reactor fuels. A 30-min treatment of 200 mg of SnF<sub>4</sub> at 500°C with a 400 cc/min flow of a fluorine-nitrogen mixture resulted in a removal of 185 mg of SnF<sub>4</sub> from the heated zone. A white sublimate was found on the wall of the reactor in the cold zone near the gas exit. Therefore, tin, being both a fission product and a constituent of Zircaloy cladding, would be at least partially volatilized during fluorination of the fuel.

## B. ENGINEERING-SCALE INVESTIGATIONS OF FLUID-BED FLUORIDE VOLATILITY PROCESSES (A. A. JONKE)

### 1. Development of Fluid-Bed Fluoride Volatility Processes for the Recovery of Uranium and Plutonium from Uranium Dioxide Fuels

#### a. DESIGN AND CONSTRUCTION OF AN ENGINEERING-SCALE ALPHA FACILITY (N. LEVITZ, G. J. VOGEL, E. L. CARLS, I. KNUDSEN, W. MURPHY, M. JONES, B. KULLEN, A. RASHINSKAS, R. KINZLER, J. HEPPELRY)

An engineering-scale alpha facility has been installed to permit the study of the main steps in the fluid-bed

fluoride volatility reprocessing scheme for UO<sub>2</sub>-PuO<sub>2</sub> ceramic oxide fuels (see Figure II-1). The facility consists of two large alpha boxes, the larger box containing the main processing equipment, the other containing auxiliary equipment such as scrubbers and inlet gas distribution manifolds. Fluorination equipment for processing batches of UO<sub>2</sub>-PuO<sub>2</sub> pellets to hexafluorides

and a converter system for the preparation of dense mixed uranium-plutonium oxide particles from mixed hexafluorides has been installed. The converter will be used also to study the thermal decomposition of  $\text{PuF}_6$  to  $\text{PuF}_4$  as a means of separating plutonium from uranium.<sup>19</sup> Both the converter and fluorinator systems are described in a recent topical report.<sup>20</sup> Space remains in the large processing equipment box for a distillation unit that is now in a preliminary design stage and from which separations data on mixed uranium-plutonium hexafluoride systems will be obtained. Windows are expected to be installed soon in both boxes.

In a parallel effort, shakedown work has started on the fluorinator (see below) and converter systems as the mechanical and electrical work approach completion. Testing of overall facility components is also near completion. Several additional shakedown experiments with uranium materials will be carried out as a final check on system operability. These latter tests are also needed to allow final detailing of the operating procedures before the addition of plutonium to the systems. Corrosion specimens will be added to the process units when this main phase of the work starts.

### (1) Testing of Components Associated with Overall Facility Operation

Final tests of general facility systems, such as the process and ventilation scrubbers, were made, and development of special operating procedures, such as that for vertically bagging large equipment in an out of the boxes, were continued. Safety evaluation of systems and procedures is near completion.

**Scrubber Tests.** From a safety standpoint, complete containment of plutonium and uranium hexafluoride in the alpha facility is necessary. Hexafluorides contained in the ventilation air which might pass through the larger alpha box as a result of an inadvertent release, and trace amounts of hexafluoride in the fluorinator process off-gas will be trapped by a fluorinator process scrubber-filter combination. The gas stream is humidified in the scrubber, where, upon contact with water, the hexafluorides react to form particulate oxyfluoride solids capable of being trapped by absolute filters. Performance tests were carried out on the fluorinator process scrubber in which the mass transfer coefficients of water vapor-to-air were determined.

<sup>19</sup> Trevor, L. E., J. Fischer and J. G. Riha, Laboratory Investigations in Support of Fluid-Bed Fluoride Volatility Processes, Part III. Separation of Gaseous Mixtures of Uranium Hexafluoride and Plutonium Hexafluoride by Thermal Decomposition, ANL-6762, August 1963.

<sup>20</sup> Vogel, G. J., E. L. Carls and W. J. Mechem, Engineering Development of Fluid-Bed Fluoride Volatility Processes, Part 5. Description of a Pilot-Scale Facility for Uranium Dioxide-Plutonium Dioxide Processing Studies, ANL-6901, December 1964.

From this information an estimate was made of the quantity of hexafluoride that could be handled. The possible problem of the filters becoming wetted (and inoperable) by the humidified air stream was also evaluated in these tests, even though a steam reheat coil is provided upstream of the filters to minimize this occurrence.

The scrubber consists of a vertical column, 18 in. in dia. and 8 ft long, and operates with countercurrent liquid and gas flows. Two in-series, spray nozzles (Sprayco  $\frac{3}{8}$ , 1155 M, hollow-cone) are located in the lower half of the column. In the gas exit region above these nozzles are a demister for removing entrained water and a finned, steam coil for superheating the saturated air to reduce the chance of wetting and plugging the filters.

Ventilation air flow rates of 402, 510, and 560 cfm were used in the separate tests. Air flows were measured by a vane anemometer. The water circulation flowrate to the nozzles was 2100 lb/(hr) (sq ft). The dewpoint of the entering air was calculated from wet and dry bulb temperatures. Mass transfer coefficients were calculated on the basis of the quantity of make-up water added to the system to compensate for the amount lost through transfer. Mass transfer coefficients of 167, 245, and 192 lb moles/(hr) (atm), were obtained for the three cases. During actual operations, the make-up water will be provided by the condensate from the steam reheat coil. On the basis of preliminary tests, the quantity of water produced is adequate to maintain the desired constant-inventory system. Overall performance of this unit is expected to be satisfactory without modification.

**Vertical Bagout.** Initial tests of the vertical bagout system were completed. Thirty-inch diameter bagout openings are provided at the top of each alpha-box module along with a hoist outside the box to handle objects which, because of their bulk or weight, cannot be transferred through the 8-in. and 22-in. dia. horizontal openings at the ends of the alpha box. The main problem in bagging proved to be the collapse of the bag around the object being withdrawn when the bag was in the extended position outside the box. Movement of the object within the bag was then virtually impossible. A solution was found by design of collapsible rings which could be fixed inside the bag to keep it expanded. These rings are reusable.

**Gas Recycle Pump.** Performance of the fluorine recycle pump proved satisfactory; a flow rate of 2.3 scfm at 15 psig discharge pressure was achieved. The rated capacity was 2 scfm at 10 psig.

### (2) Shakedown Work in the Fluorinator

A shakedown experiment (Run UO-1) was completed in the fluorinator system using the two-zone

TABLE II-14. OPERATING CONDITIONS FOR URANIUM OXIDE FLUORINATION RUN UO-1

Equipment:	3-in. dia. nickel fluorinator								
Reactor Charge:	UO <sub>2</sub> pellets: 3-in. bed depth, 2.2 kg, 1/2-in. dia. by 1/2-in. right cylinders								
Alumina:	24-in. static bed depth, 5.52 kg (High Purity Blue Label, Norton Co.), -60 +170 mesh								
Pellet Support:	Nickel balls								
	Run Time (hr)								
	1	2	3	4	5	6	7	8	9
Bed Temperature (°C)	450				515				
Fluorine Conc. (v/o)	5	→10				→15, 30, 60		→	
Oxygen Conc. (v/o)	3	→4.5				→off		→	
Velocity (ft/sec) at Column Conditions	1.0				0.62, 0.32,	0.16			

oxidation-fluorination method of processing UO<sub>2</sub> pellets (ANL-6687, pp. 112-124). In the two-zone method, there are two distinct reaction zones: the first is a bed of UO<sub>2</sub> pellets with high-fired alumina particles in the voids; the second is a bed of alumina particles placed over the UO<sub>2</sub> pellet bed. In the pellet-bed zone, U<sub>3</sub>O<sub>8</sub> fines are produced by contacting the UO<sub>2</sub> with an oxygen-nitrogen stream which also serves to fluidize the alumina particles. The U<sub>3</sub>O<sub>8</sub> fines are carried from the lower zone by the oxygen-nitrogen gas stream and are reacted in the upper zone with fluorine, which is admitted to the fluidized bed of alumina just above the UO<sub>2</sub> pellet bed. The major objectives of the shake-down experiment were: (a) to investigate the performance of the various equipment components, (b) to achieve satisfactory removal of uranium from the reactor, (c) to demonstrate completeness of hexafluoride product collection, and (d) to show that satisfactory material balances can be obtained.

#### Equipment, Procedure and Conditions

A shallow bed (3-in. bed depth, 2.2 kg) of UO<sub>2</sub> pellets and a 24-in. bed (static height) of -16+170 mesh alumina were used as the charge. Equipment items included the fluorinator (3-in. dia.), auxiliary filter, the hexafluoride collection system, and off-gas cleanup system. Once-through fluorine was used; thus the recycle pump was not tested at this time.

The conditions and sequence of operations for the run are listed in Table II-14. The run was divided into four parts: (a) normal two-zone operation until approximately 90% of the UF<sub>6</sub> was collected, (b) switching of the fluorine introduction point from the side inlet to the bottom of the reactor and turning off the oxygen, (c) increasing the reaction temperature, and

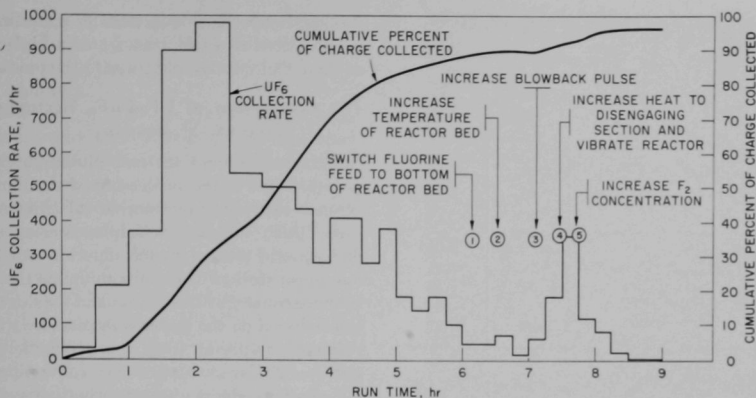
(d) increasing the fluorine concentration by decreasing the nitrogen diluent flow.

The UF<sub>6</sub> was collected in a single condenser backed up by a NaF trap. During the UF<sub>6</sub> collection period the cold trap was operated at an outer wall temperature of 25 to 50°C while the coolant temperature ranged from -64°C to -78°C. The condenser exit gas was monitored continuously for fluorine content via a thermal conductivity cell apparatus. Uranium hexafluoride collection was continuously recorded utilizing an automatic chain-balancing scale equipped with a remote weight-readout device. Sensitivity to weight changes of ±10 g was achieved by connecting the process lines to the condenser in an extended torsion-lever arm arrangement.

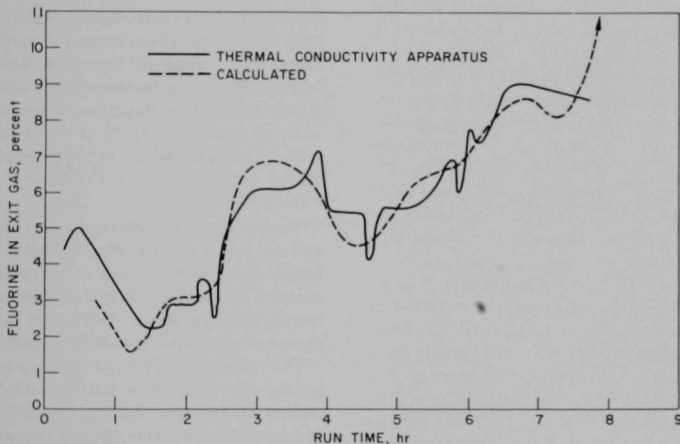
From the total amount of fluorine used, the concentration of fluorine in the off-gas, and the amount of UF<sub>6</sub> produced, the percentage of fluorine consumed in the conversion of U<sub>3</sub>O<sub>8</sub> to UF<sub>6</sub> and the percentage used in the production of UO<sub>2</sub>F<sub>2</sub> fines could be calculated. The oxygen and fluorine rates were regulated in such a way that the buildup of fines in the alumina bed was minimized. Ideally, the U<sub>3</sub>O<sub>8</sub> fines produced by the oxidation should react immediately upon contact with the fluorine. Automatic blowback of filters to return fines accumulated on the filters to the reaction zone and gas pulsing to aid in fines transport from the lower (pellet) zone to the fluorination zone were employed.

#### Results

**UF<sub>6</sub> Collection Rate.** Figure II-7 shows the UF<sub>6</sub> collection rate and percent of charge collected versus time. The collection curve is typical of previous pilot-plant operations in which a period of high collection rate is followed by a period in which the collection rate declines. Introduction of fluorine at the bottom of the reactor (Point 1, Figure II-7) as well as increasing the head to the bottom of the unit (Point 2) did little to increase the rate of recovery of hexafluoride. The peak in the collection rate obtained during the latter stages of the run was due to a combination of factors: increasing the blowback pulse, mechanical jarring of the upper sections of the unit (see Points 3 and 4), and also increasing the temperature of the disengaging section to 350°C. (During the earlier parts of the run the disengaging section was kept at 250 to 275°C. The filter chambers were kept at 150°C throughout the run.) Increasing the concentration of fluorine in the inlet gas stream by cutting back on the flow of diluent nitrogen (Point 5) seemed to have no beneficial effect on the rate of UF<sub>6</sub> formation. The peak production rate of UF<sub>6</sub> of 975 g/hr in the 3-in. dia. reactor corresponds to a rate of 42 lb/(hr) (sq ft).



108-8545 Rev. 2

Fig. II-7.  $UF_6$  Collection Rate and Percent of Charge Collected during Run UO-1.

108-8750

Fig. II-8. Fluorine Concentration in the Cold Trap Exit Gas.

*Residual Uranium Content of the Alumina Bed.* After 9 hr, the residual uranium content of the alumina bed was 0.03 w/o, equivalent to about 0.08% of the uranium charged to the reactor. Subsequent refluorination of a portion of the alumina bed under static-bed conditions in a bench-scale (1½-in. dia.) reactor at 500°C and 550°C for consecutive 1-hr periods reduced the uranium content to less than 0.01 w/o.

*Fluorine Utilization.* The overall fluorine efficiency for this preliminary run was 32%. During peak production periods, efficiencies of fluorine in the conver-

sion to hexafluoride of 72 to 73% were observed. Future work will aim toward overall efficiencies of 50% or greater. Figure II-8 is a plot of the fluorine concentration in the cold trap exit gas versus time. The results as obtained by the thermal conductivity apparatus are compared with the calculated values based on fluorine input and hexafluoride production rate. The close agreement would indicate that little if any accumulation of intermediate uranium fluoride fines occurred during the run.

*Uranium Hexafluoride Material Balance and Cold*

TABLE II-15. URANIUM MATERIAL BALANCE—RUN UO-1

Uranium Charged 2200 g	UF <sub>6</sub> Equivalent 2868 g	% 100
<i>Uranium Collected</i>		
Uranium Collected in Cold Trap	2770	96.62
Backup NaF Trap	55	1.91
<i>Uranium Remaining in the Reactor</i>		
Final Alumina Bed 0.03 w/o U	2.4	0.08
+40 Fraction (Unreacted Pellets)	6.0	0.21
Fines from Filters and Filter Chambers	34	1.18
	2867	99.97

*Trap Performance.* The UF<sub>6</sub> material balance for the run is shown in Table II-15. From weight changes and analysis of bed residues, a material balance of 99.97% was achieved. The efficiency of the cold trap for UF<sub>6</sub> collection was 98% based on the amount of material collected in the cold trap and the amount collected in a NaF backup trap downstream of the cold trap.

*Uranium Hexafluoride Transfer from the Cold Trap.* Subsequent to the fluorination run the material collected in the cold trap was transferred to a product receiver pot. This transfer involved: (1) evacuation of the cold trap and warm product receiver pot, (2) chilling of the product receiver pot to -60°C and heating of the closed cold trap to 75 to 80°C to liquify the UF<sub>6</sub>, (3) a closed-system vapor transfer of the UF<sub>6</sub> to the chilled product receiver pot.

In a 2-hr period, 2587 g out of a possible 2770 g\* were transferred out of the cold trap and collected in the product receiver. At this point the exit line from the cold trap was connected to a vacuum pump via a NaF trap. Pumping on the warm cold trap in this manner for 3 hr transferred an additional 112 g of UF<sub>6</sub> out of the cold trap, giving a total of 2699 g. The percent transferred for the two steps was therefore 97.4%.

#### Discussion

Aside from minor difficulties with the remote-reading scale mechanism, the operation of the equipment, the gas control systems, the air-water reactor cooling system, and the thermal conductivity gas analysis apparatus was excellent.

Future work will be concerned with improving product collection. This can be accomplished by a combination of utilizing two cold traps in series to collect the UF<sub>6</sub>, and optimizing of fluorination con-

\* The amount of UF<sub>6</sub> collected during the fluorination period according to the scale readout.

ditions. Improvements in transfer operating conditions are expected to effect transfer of a higher percentage of the UF<sub>6</sub> from the cold traps to the product receivers.

### (3) Conversion of UF<sub>6</sub>-PuF<sub>6</sub> Mixtures to Oxides (I. KNUDSEN, M. JONES)

Mixtures of uranium and plutonium hexafluorides are produced in the processing of uranium-plutonium ceramic oxide fuels by fluoride volatility methods. Because PuF<sub>6</sub> suffers from alpha decomposition<sup>21</sup> producing solid plutonium tetrafluoride and fluorine gas, long-term storage of the plutonium as the hexafluoride is undesirable. For this reason and for safety considerations (based on the increase in pressure within storage cylinders resulting from the production of fluorine gas), a fluid-bed reactor for converting the mixed UF<sub>6</sub>-PuF<sub>6</sub> products of the fluorination step to a stable oxide powder form is being installed in the alpha facility. As a converter, this unit will also be used to investigate the effects of process variables in the production of high-density mixed-oxide particles for compacted fuels, work similar to that carried out with UF<sub>6</sub> alone.<sup>22</sup> Recycling of the converter product to the fluorinator is being considered in the program. A means of separating the plutonium fraction from the bulk uranium stream by thermal decomposition<sup>23</sup> of PuF<sub>6</sub> to PuF<sub>4</sub> will also be studied in this unit.

#### Equipment

The converter process equipment includes gas supply sources, a gas preheater, a fluid-bed reactor with integral filter section, a secondary filter, an off-gas analysis system, an exit gas scrubber and dry chemical traps. The reactor is fabricated of Inconel; other equipment and lines are of nickel and Monel.

The reactor is composed of three sections connected by flanges: a 60° cone bottom, a 2-in. dia. fluid-bed section and a 4-in. dia. cooling-filtering section (see Figure II-9). The cone bottom (shown in better detail in Figure II-10) has an opening at the apex for the gas feed; the hexafluoride mixture enters through a 0.125-in. ID nozzle extending 2½ in. into the cone;

<sup>21</sup> Steindler, M. J., D. V. Steidl and Jack Fischer, Laboratory Investigations in Support of Fluid Bed Fluoride Volatility Processes. Part V. The Radiation Chemistry of Plutonium Hexafluoride, USAEC Report ANL-6812, December 1963.

<sup>22</sup> Knudsen, I. and N. M. Levitz, Engineering Development of Fluid-Bed Fluoride Volatility Processes. Part 6: The Fluid-Bed Conversion of Uranium Hexafluoride to High-Density Uranium Dioxide, USAEC Report ANL-6902, 1964.

<sup>23</sup> Trevorrow, L., J. Fischer and J. Riha, Laboratory Investigations in Support of Fluid Bed Fluoride Volatility Processes. Part III. Separation of Gaseous Mixtures of Uranium Hexafluoride and Plutonium Hexafluoride by Thermal Decomposition, USAEC Report ANL-6762, August 1963.

the fluidizing nitrogen or steam and hydrogen reactants enter through the annulus around the hexafluoride nozzle. The side opening in the cone bottom is for product take-off and sampling.

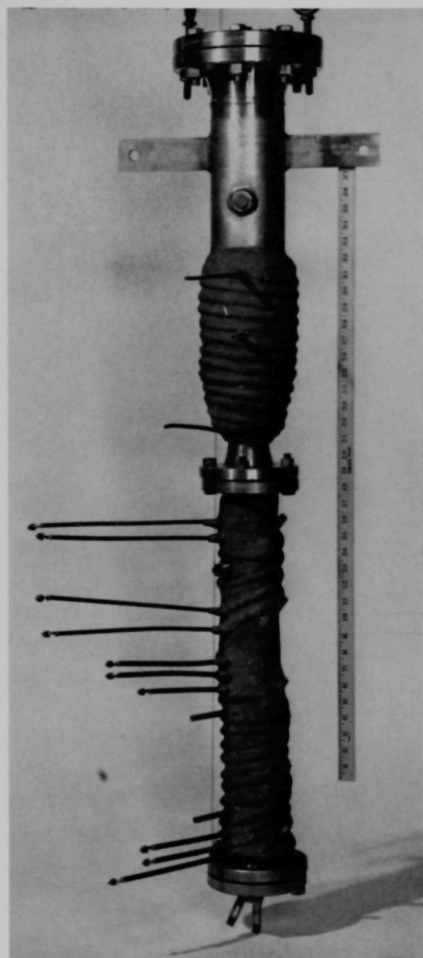
The fluid-bed section, 2.07-in. ID, is 24 in. long. Three 1500-watt and two 750-watt alloy-sheathed tubular electric resistance heaters (includes one spare of each size) are bonded to the outside wall with a coating of copper and a cover coating of stainless steel. Thermocouples are inserted through side inlets which also serve as pressure taps. One side inlet is available for adding seed particles to the fluid bed. Other openings include a solids overflow pipe and a port, normally plugged, through which a borescope can be inserted for examination of the interior of the reactor. Two thermowells are located on the lower half of the wall of the fluid-bed section for measuring skin temperatures.

The cooling and filtering section of the reactor is 26 in. in length, 4.03 in. ID, and is tapered at the bottom to join to the fluid-bed section. The lower half of the cooling and filtering section is wrapped with cooling coils which are bonded in the same way that the coils are bonded to the main reaction section. A two-phase air-water mixture is the coolant. In the middle of this section, a port is provided for viewing the interior of the reactor. The cover flange is provided with a center opening for a thermowell and four couplings for the four bayonet filters, 1 $\frac{3}{4}$  in. by 12 in. long, of porous nickel.\* Filter blowback devices (jet-pumps), utilizing high-pressure nitrogen, are provided for each filter (see Figure II-11).

The secondary (backup) filter vessel, 21-in. long and 3.55-in. ID, is wrapped with a 1500-watt tubular heater. A single cylindrical filter 18-in. long and 2 $\frac{3}{4}$  in. in dia., of a similar grade porous nickel serves as a backup to the primary filters (see Figure II-12).

The UF<sub>6</sub>-PuF<sub>6</sub> mixture is fed from 4-in. dia. cylindrical vessels, 31-in. long, which are heated by two 200-watt band heaters. Cooling coils are provided for emergency cooling. Air, nitrogen, and hydrogen are supplied from high pressure cylinders and pass through driers. Steam is supplied by a constant-pressure, electrically heated steam generator. All gas flow rates are metered and automatically controlled by orifice-differential pressure systems. The gases entering the converter (nitrogen, steam, hydrogen, or oxygen) are preheated in a 33-in. long, 1 $\frac{1}{2}$ -in. dia. pipe section packed with  $\frac{1}{2}$ -in. nickel Raschig rings; heat is supplied by clamshell heaters that are automatically controlled.

The off-gas from the secondary filter vessel passes to a scrub tower for HF removal. The scrubber is a

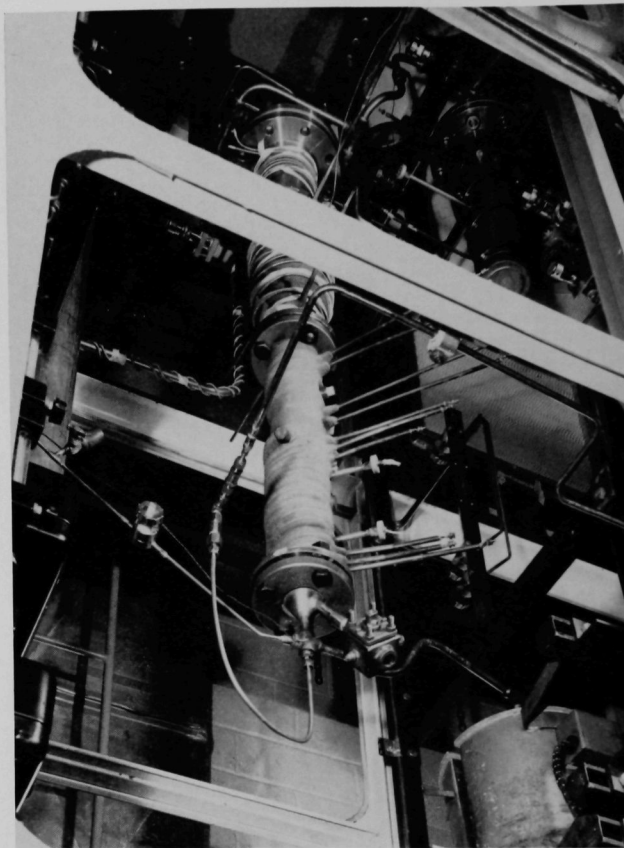


108-7578

FIG. II-9. Assembled Fluid-Bed Conversion Reactor.

countercurrent, packed tower constructed from 4-in. dia. pipe of Monel alloy 400 in which caustic is circulated. The packed section, containing  $\frac{1}{2}$ -in. dia. Monel Raschig rings, is 3 ft long and is finned on its outer surface for heat dissipation. Caustic solution is pumped from the hold tank and sprayed onto the top of the packing; the off-gas enters the bottom of the tower and passes through the packed section to a liquid deentrainment vessel and then is discharged into the ventilation-air treatment system.

\* Grade G (mean pore opening 10 $\mu$ ), a product of Aircraft Porous Media, Inc., Glen Cove, New York.



108-7889

FIG. II-10. Fluid-Bed Converter Installed in Alpha Facility.

Gas evacuated from the process lines is passed successively through traps containing NaF and activated alumina before entering the vacuum pump. Discharge from the pump is to the ventilation-air treatment system.

Control, indicating, and recording instruments are mounted on a panelboard which is outside the cell area. A hydrogen detection system is provided to monitor the air environment of the converter installation. Detectors are located in the large and the small alpha boxes with individual indication and alarm signal at the panelboard of the presence of hydrogen. The HF content of the process off-gas is measured by a thermal conductivity cell and recorded continuously.

#### *Program*

*Conversion of Hexafluorides to Dioxides.* For the processing of hexafluorides to oxides for storage or reuse, the converter will be operated at 650°C with a 3.6-kg fluid bed and hexafluoride feed rates of 11 to 22 g/min [42 to 84 lb U, Pu/(hr) (sq ft reactor cross section)]. The production of high-density particles will require steam-to-hexafluoride mole ratios near a value of 2 with larger quantities of steam to be used during the cleanup period to achieve adequate fluoride removal. Alternate 30-min periods of hexafluoride feed and product cleanup will be used with product removal at the end of the cleanup period. Further tests will be made of the oxidation-reduction procedure (see ANL-

6900, pp. 175–181) for adjusting the particle size in the bed.

**Thermal Decomposition of  $\text{PuF}_6$ .** Studies of the thermal decomposition of  $\text{PuF}_6$  and  $\text{PuF}_4$  are also to be made in this unit. Initial experiments have been carried out on a laboratory scale. For the proposed tests, provision will be made for effluent gas from the reactor to be routed to the condenser of the fluorinator system. Conversion of product  $\text{PuF}_4$  to  $\text{PuO}_2$  by a pyrohydrolysis reaction may be carried out *in situ*.

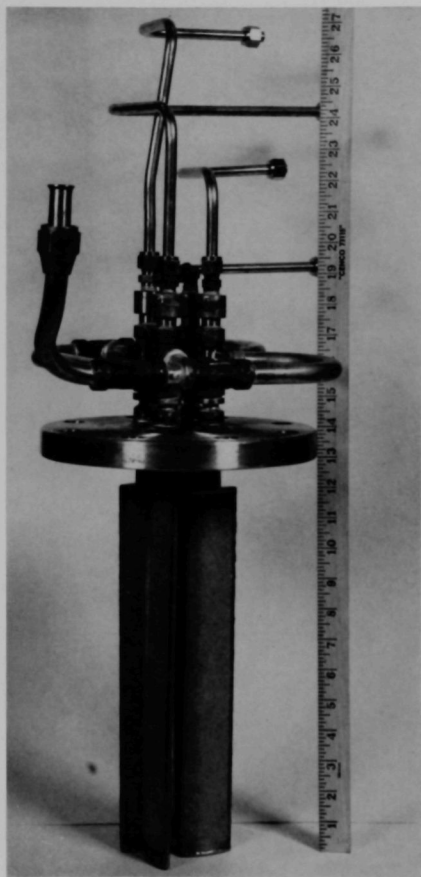
#### b. DECLADDING AND FLUORINATION OF URANIUM DIOXIDE FUELS (D. RAMASWAMI, J. GABOR, D. RAUE, J. STRAND)

Studies on the decladding and fluorination of  $\text{UO}_2$  fuels are being made to optimize the processing conditions for the fluid-bed fluoride volatility process for recovery of fissionable values from spent nuclear reactor fuel of the  $\text{UO}_2$ - $\text{PuO}_2$  type.

Stainless steel (SS) and Zircaloy are commonly used as the cladding materials for the  $\text{UO}_2$  fuels. Several methods for decladding these fuels have been studied. In an oxidative decladding method, the  $\text{UO}_2$  pellets are oxidized to  $\text{U}_3\text{O}_8$  fines which are separated from the cladding. Previous studies with SS tubing (see ANL-6800, pp. 227–242) established operating conditions for this method; however, mechanical operations, broaching of the cladding or shearing of the fuel into short lengths are required. These operations are costly to perform in radioactive environments.

Experimental work on solely chemical decladding methods which do not require mechanical operations have also been initiated. For SS cladding, the following decladding methods appear feasible: (1) chemical destruction with aqueous hydrochloric acid in an air-fluidized bed and (2) catastrophic oxidation catalyzed by solid fluorides (see BNL-806, pp. 75–76). For Zircaloy decladding, treatment with HCl as in the enriched alloy reprocessing scheme is probably directly applicable. Recent tube-furnace experiments at ORNL<sup>24</sup> showed that destructive oxidation of SS is promoted by gaseous HF at lower temperatures. Penetration rates of 67.5 mils/hr were observed at 650°C with 40 v/o HF in oxygen. These results indicate that HF-promoted destructive oxidation is a potential decladding method that might be incorporated into the fluid-bed fluoride volatility process for SS-clad fuels. An investigation was initiated at Argonne to explore the range of conditions for which HF-promoted destructive oxidation in a fluidized bed of granular alumina might be satisfactory. Work at Argonne is also concerned with the processing of declad fuel. Stud-

<sup>24</sup> Oak Ridge National Laboratory, April 6, 1964 (Unpublished).



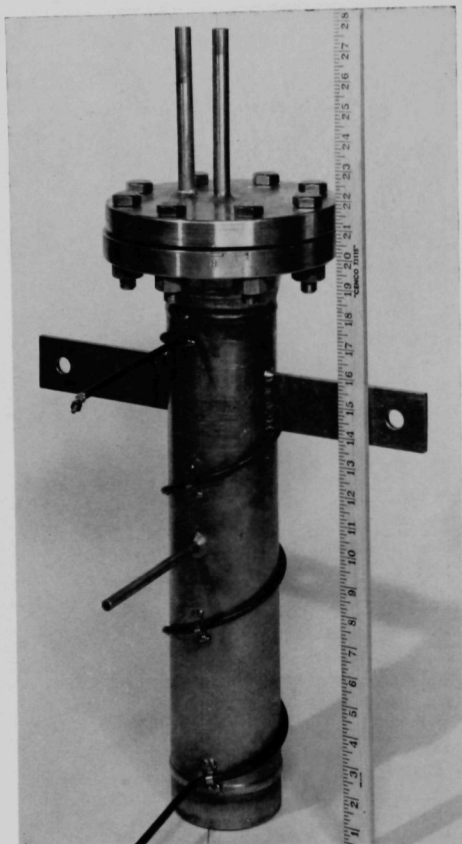
108-7891

FIG. II-11. Converter Top with Cluster of Sintered Metal Filters and Filter-Blowback Piping.

ies aimed at optimization of the HF-oxygen decladding process are being conducted at Brookhaven. Feasibility of processing  $\text{UO}_2$ -SS cermet fuels by the HF-oxygen, fluorine cycle was also investigated. The results of the various studies at Argonne are outlined in the following.

#### (1) Destructive Oxidation of Stainless Steel

Four exploratory runs were made in a bench-scale fluid-bed reactor (described in ANL-6569, p. 114) to determine the optimum fluid-bed temperature for the HF-oxygen reaction with stainless steel. Two runs were



108-7576

FIG. II-12. Backup Filter Housing for the Converter.

made in a pilot-scale fluid-bed reactor (described in ANL-6725, pp. 134 to 135). The operating conditions and results in terms of penetration rates are listed in Table II-16. The fluid-bed temperatures were maintained in the range 500 to 600°C. Sintered alumina was used as the inert fluid-bed material.

The penetration rates increased with temperature from about 2 mils/hr at 500°C to about 33 mils/hr at 600°C for type 304 SS with 40 v/o HF, 40 to 60 v/o oxygen (plus nitrogen) in the feed gas stream. A practical operating temperature was found to be about 550°C which gave a penetration rate of about 30 mils/hr. Penetration was markedly higher for the portion of the specimen immersed in the fluidized bed than

for the section of the specimen exposed to the gas phase above the bed as shown in Figure II-13. Also, in the fluidized bed itself, the rates were highest at the portion of the specimen which was contacted by the entering gases and decreased in the direction of gas flow. The treatment with HF-oxygen resulted in the conversion of a major fraction of the iron to  $\alpha$ -Fe<sub>2</sub>O<sub>3</sub> and a minor fraction to Fe<sub>3</sub>O<sub>4</sub>. The results from the pilot-scale studies confirmed the results from the bench-scale tests.

## (2) Destructive Oxidation and Fluorination of Stainless Steel-Clad UO<sub>2</sub>—Processing of a Fuel Bundle

A run was made in the pilot-scale reactor to demonstrate the processing of a simulated type 304 SS-clad UO<sub>2</sub> fuel bundle. The fuel bundle, which simulated the fuel elements employed in the Vallecitos Boiling Water Reactor,<sup>25</sup> consisted of six 3-ft long tubes containing UO<sub>2</sub> pellets (see Figure II-14). End plugs, force-fitted into the ends of the tubes, held the UO<sub>2</sub> pellets in place. The bed of sintered alumina grain\* extended approximately 4 in. above the fuel bundle when fluidized. The main process conditions are detailed in Table II-17.

*Destructive Oxidation.* The destructive oxidation period was of 3-hr duration. After ½, 1, and 3 hr of the decladding phase the residual fuel fragments and bed were removed from the column for examination. The temperature of the fluid bed was maintained at 550°C during the first hour but only at 450°C during the last two hours of operation because of heater failure.

After the first ½ hr of the decladding step the length of the fuel bundle was reduced by approximately one-fourth. After the first hour the length of the bundle was reduced somewhat over a half. Figure II-14 shows a fuel bundle before reaction and after one hour of reaction. After 3 hr the entire fuel bundle was completely disintegrated; the reaction products were found to be well mixed with the alumina bed. The bed consisted of the alumina grain, UO<sub>2</sub>F<sub>2</sub> fines (-325 mesh), partially reacted UO<sub>2</sub> pellets, and Fe<sub>2</sub>O<sub>3</sub> scale from the tubing. The uranium fines constituted 22% of the bed material. Eleven percent of the bed was larger than 45 mesh and consisted of scale and partially reacted pellets in about a 3:1 weight ratio. Most of the pieces of scale were about ⅜ by ⅜ in. and a few were on the order of ⅜ by 3 in. The bed material was satisfactorily fluidizable for further processing.

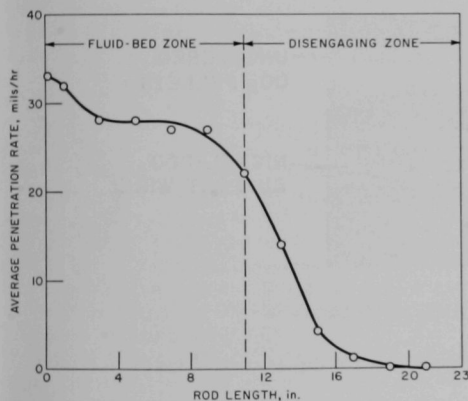
\* Tabular Alumina, type T-61, manufactured by Aluminum Company of America.

<sup>25</sup> Fowler, W. D. and J. W. Lingafelter, Design and Fabrication of High Power Density Fuel Assemblies for VBWR Irradiation Testing, GEAP-3609, November 1, 1962.

TABLE II-16. DESTRUCTIVE OXIDATION OF STAINLESS STEEL IN FLUIDIZED BEDS OF ALUMINA

	Bench-scale Studies				Pilot Plant Studies	
	Run Number					
	HF-6	HF-7	HF-2	HF-1	SSOX-1	SSOX-2
Type of Stainless Steel	304	304	304	304	304	304, 347
Mesh Size of Granular Alumina <sup>a</sup>	48-100	48-100	-30+50	-30+50	48-100	48-100
Gas Velocity (ft/sec)	0.63	0.63	0.63	0.63	0.9	0.9
Feed Gas Composition (v/o)						
HF	40	40	45	45	43	43
Oxygen	40	40	32	32	57	57
Nitrogen	20	20	23	23	—	—
Time (hr)	3	3	3	3	2	2
Temperature of the Fluid Bed (°C)	500	550	550	600	500	550
Penetration Rates (mils/hr)	2	25	30	33	1.3	30 for type 304 SS 13 for type 347 SS

<sup>a</sup> Sintered alumina, type T-61, manufactured by Aluminum Company of America.



108-8543

FIG. II-13. Penetration Rates at 550°C of Type 304 Stainless Steel by HF-Oxygen Mixture.

Equipment: 1½-in. dia. fluid-bed reactor  
 Initial Dimensions: ½-in. dia. and 23 in. long rod  
 Initial Weight: 583.9 g  
 Final Weight: 392.4 g  
 Run Time: 3 hr  
 Composition of Feed Gas: 40 v/o HF, 40 v/o oxygen, 20 v/o nitrogen  
 Fluid-bed Material: Sintered alumina

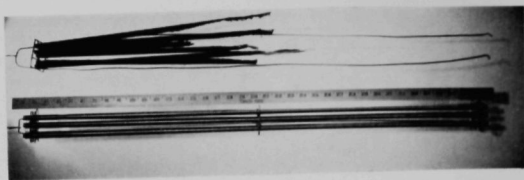
**Fluorination.** In the fluorination phase of the run, the entire bed including SS oxidation products as well as the UO<sub>2</sub>F<sub>2</sub> fines and residual pellets were reacted with fluorine. The temperature of the fluid bed was maintained initially at 400°C. During the first 6 hr of operation, nitrogen at a rate of 0.5 cfm (25°C and 1 atm) was introduced at the bottom of the reactor to

fluidize the bed and fluorine (0.05 cfm) diluted with recycled off-gas (0.5 cfm) was introduced into the reactor at approximately the middle of the fluid bed. This procedure facilitates control over the fluorination of the large quantities of uranium fines (~22 w/o UO<sub>2</sub>F<sub>2</sub> fines in the alumina grain), since, in the middle portion of the bed and above, the fluidizing gas bubbles are fully developed and the solids movement most vigorous. Dilute fluorine was fed when the bulk of the uranium fines was present. During the second part (from 6 to 11 hr) of the fluorination step, fluorine and recycle gas were introduced at the bottom of the reactor and the nitrogen was completely cut off (except for purges) to complete the cleanup. This allowed the fluorine concentration to build up to the order of 90%. Because of heater limitations, the bed temperature did not exceed 450°C during the cleanup phase of the run, although final temperatures of 550°C were intended.

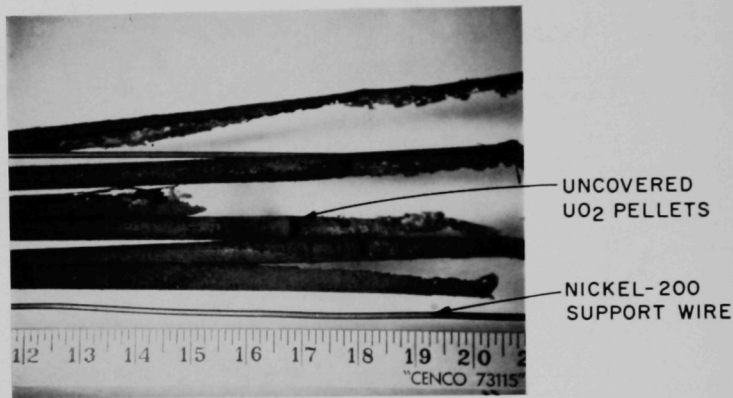
During the first part of the fluorination period, 82% of the UF<sub>6</sub> was collected. The Fe<sub>2</sub>O<sub>3</sub> was fluorinated to FeF<sub>3</sub> fines. The fluorine efficiency for the entire run based on the reaction of fluorine with both the UO<sub>2</sub>F<sub>2</sub> and Fe<sub>2</sub>O<sub>3</sub> was 67%. The concentration of uranium at the end of fluorination was 0.05 w/o indicating a recovery of about 99.9% of the uranium in the charge. The bed at the end of the run was free flowing, and no caked material was found in the bed.

### (3) Destructive Oxidation and Fluorination of SS-Clad UO<sub>2</sub> Cermet Fuel Elements

An exploratory run was made in the bench-scale fluid-bed reactor to determine the feasibility of processing UO<sub>2</sub>-SS cermet fuel by the HF-oxygen, fluorine cycle. Cermet fuels are currently being used in medium power plants and contain highly enriched uranium.



Comparison of original bundle with bundle after 1 hr of exposure



Close-up view showing exposed  $UO_2$  pellets

108-7769B

FIG. II-14. Destructive Oxidation of a Simulated SS-Clad Fuel Bundle after 1 hr Exposure to 40-60 v/o HF-O<sub>2</sub> at 550°C.

The fuel for this test consisted of a 90-g miniature fuel subassembly of 18 w/o  $UO_2$ -SS (type 304) cermet fuel. The subassembly, which simulated those used<sup>26</sup> in the Stationary Medium Power Plant, SM-1, consisted of four plates, approximately 8 $\frac{3}{8}$ -in. long, 1 $\frac{1}{16}$ -in. wide, and 0.03-in. thick, held together by  $\frac{1}{16}$ -in. dia. nickel-200 wire with a plate spacing of  $\frac{1}{8}$  in. The subassembly was submerged in a fluid bed of sintered alumina. Details of the processing conditions are presented in Table II-17. The reaction cycle comprised a HF-promoted destructive oxidation step and fluorination of the resultant oxides. The first step was conducted at 550°C for 4 hr with 40 v/o HF, 40 v/o

oxygen, and 20 v/o nitrogen. The second step was initiated at 250°C with 2 v/o fluorine in the feed gas stream, and completed at 550°C with 95 v/o fluorine. The total time of fluorination was 11 hr.

High recovery (>99%) of the uranium in the charge was indicated by the low quantities of uranium retained by the alumina at the end of fluorination. The concentration of uranium was 0.005 w/o of the bed at the end of fluorination which corresponds to 0.2% of the uranium in the charge. The material in the fluid-bed zone was fluidizable throughout the run and was free flowing at the end of the run. The subassembly was completely disintegrated at the end of the destructive oxidation. These initial results show the applicability of this processing scheme to a variety of SS fuels. A few more runs are planned to optimize the operating conditions.

<sup>26</sup> Directory of Nuclear Reactors, Vol. IV, Power Reactors (Revised and Supplemented Edition of Vol. I), International Atomic Energy Agency, Vienna, 1962, pp. 9 to 14.

#### (4) Decladding Stainless Steel-Clad Fuel with Aqueous Hydrochloric Acid in an Air-Fluidized Bed

Tests on the decladding of SS-clad fuel by aqueous hydrochloric acid in an air-fluidized bed were concluded this period. The purpose of this investigation was to develop a SS-decladding process that would be compatible with the overall scheme of the fluid-bed fluoride volatility process for reprocessing UO<sub>2</sub> fuel.

Results from initial tests in a 1½-in. dia. glass column revealed that decladding rates increased with increasing liquid content in the fluidized bed (see ANL-6900, pp. 173-175). However, fluidization of the bed was satisfactory only when small amounts of liquid were used, quantities corresponding to about 2.7 w/o of the bed. Data reported by Leva<sup>27</sup> on the effect of column diameter on fluidization quality suggested that work with higher liquid contents might be facilitated by operation in larger diameter equipment. On the basis of these data, further tests have been conducted in a 3-in. dia. glass column.

#### Current Work

Current tests were made in a 3-in. dia. glass column, 3 ft in length. The necessary temperatures (80 to 100°C) were maintained with heating tape consisting of nichrome wire wrapped around the column. Thin sheets of mica were placed between the heating tape and the exterior column wall to provide uniform heat distribution. A Teflon disk perforated with 0.025-in. dia. holes served as a gas distributor. The fluidized bed consisted of 1800 g of -30+50 mesh alumina grain (expanded bed height about 1 ft).

Hydrochloric acid (37 w/o HCl in H<sub>2</sub>O) was fed from a constant-head tank and was injected into the bed through a hypodermic needle inserted through the Teflon flange at the bottom of the column. The effective concentration of HCl in the acid in the bed was assumed to be about 20 w/o, the equilibrium value for HCl in hydrochloric acid at the nominal operating temperature (90°C). A glass rotameter with a sapphire float indicated the hydrochloric acid feed rate. At the beginning of each run, 95 g of hydrochloric acid was injected into the bed giving an initial liquid content of 5 w/o in the bed. Although a portion of the acid was lost by evaporation to the fluidizing gas, steady-state acid contents in the bed were maintained by adjusting both the acid and air flow rates. A sample port was installed at the top of the column to allow passage of a long-handled dipper for bed sampling. The liquid

TABLE II-17. CONDITIONS FOR DECLADDING AND FLUORINATION OF URANIUM DIOXIDE FUELS

	Pilot-scale Studies	Bench-scale Studies
	Run No.	
	SSOX-3	HF-13
Type of Fuel	Fuel Bundle <sup>a</sup>	SS-UO <sub>2</sub> cermet
UO <sub>2</sub> Charge (kg)	4.5	0.016
Type 304 Stainless Steel Charge (kg)	1.6	0.074
Alumina Charge <sup>b</sup> (kg)	7.7	0.48
<i>Destructive Oxidation</i>		
Temperature (°C)	550 <sup>c</sup>	550
Time (hr)	3	4
Feed Gas Composition (v/o)		
HF	43	40
Oxygen	57	40
Nitrogen	—	20
Gas Velocity (ft/sec)	0.7	0.75
<i>Fluorination</i>		
Initial Period		
Temperature (°C)	400	250
Time (hr)	6.5	6
Concentration of Fluorine in Nitrogen (v/o)	5	2 to 90
Gas Velocity	0.77	0.25 to 0.6
Final Period		
Temperature (°C)	450	550
Time (hr)	5	5
Concentration of Fluorine in Nitrogen (v/o)	90	95

<sup>a</sup> Cylindrical UO<sub>2</sub> pellets (0.432-in. long × 0.425-in. dia.) in 0.43-in. ID tubes (wall thickness, 0.02-in.).

<sup>b</sup> Tabular Alumina, type T-61, nominal 48-100 mesh, manufactured by Aluminum Company of America.

<sup>c</sup> Temperature was 450°C during the last 2 hr as a result of heater failure.

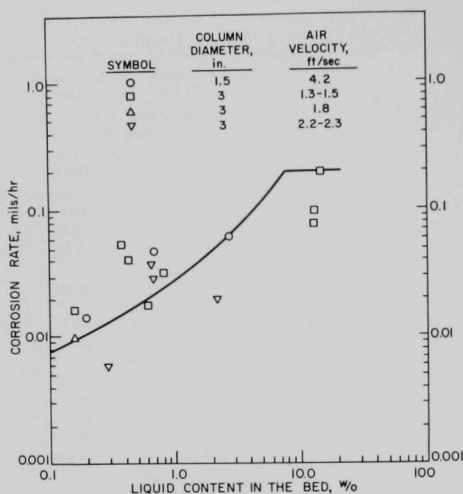
content in the bed was determined by measuring the weight loss of samples dried in an oven.

A ½-in. dia. type 304 SS rod, 12 in. in length, was used as the test specimen. Penetration rates were calculated from the rod weight loss by assuming uniform attack along the length of the rod. The penetration rate for the run with the highest liquid content (15 w/o) was great enough to be measured directly.

#### Results and Discussion

The results of the current tests with the 3-in. dia. column and of previous tests with the 1½-in. dia. column are plotted on Figure II-15 in terms of mils/hr corrosion versus liquid content in the bed. The trend of increasing corrosion rate with increasing liquid con-

<sup>27</sup> Leva, Max, *Fluidization*, McGraw-Hill Book Co., New York, 1959, p. 24.



108-8749

FIG. II-15. Dependence of Stainless Steel Corrosion Rates on Liquid HCl Content in Air-Fluidized Beds.

Test Specimen: Type 304 SS rod,  $\frac{1}{2}$ -in. dia., 12-in. long  
 Acid Concentration

of Feed to Bed: 20 w/o HCl in water

tents in the bed appears to be similar for both columns. Better operation was obtained with the 3-in. dia. unit than that obtained earlier with the smaller column, operations with liquid contents up to 15 w/o being feasible in the larger column. However, corrosion rates remained low, the highest rate achieved being about 0.1 mil/hr.

#### Future Work

It appears from the current work that still greater liquid contents in the bed would be necessary before satisfactory decladding rates could be achieved. Improvement in the method of liquid introduction so as to provide uniform distribution of the liquid throughout the bed might permit the use of larger quantities of liquid in the bed. Another possibility is increasing the amount of liquid so that a slurry is formed. In an earlier test (ANL-6900, p. 264), a slurry was used which contained 26 w/o liquid in the bed. With this slurry a corrosion of 8.7 mils/hr was obtained. However, information pertaining to the use of slurries is meager. Because of this lack of information, work on the decladding of SS-clad fuels by aqueous hydrochloric acid in gas-fluidized bed has been suspended in favor of the technique of fluoride-promoted destructive oxidation. As described above, the latter scheme has obvious advantages in that it involves gaseous re-

actants and allows both the decladding and fluorination steps to be carried out in a single reactor fabricated of nickel. This is not possible with the aqueous system since nickel is attacked by aqueous HCl.

#### c. CLEANUP OF CELL EXHAUST AIR CONTAMINATED WITH PLUTONIUM HEXAFLUORIDE (R. KESSIE, D. RAMASWAMI, L. MAREK)

A program investigating the hydrolysis and filtration of airborne  $\text{PuF}_6$  is in progress. The program is directed toward the evaluation and design of exhaust air treatment methods for facilities handling  $\text{PuF}_6$ . Extremely efficient removal of plutonium from the ventilation air is necessary due to its low permissible concentration in air ( $3 \times 10^{-8}$  mg of  $^{239}\text{Pu}$  per cubic meter of air<sup>28</sup>).

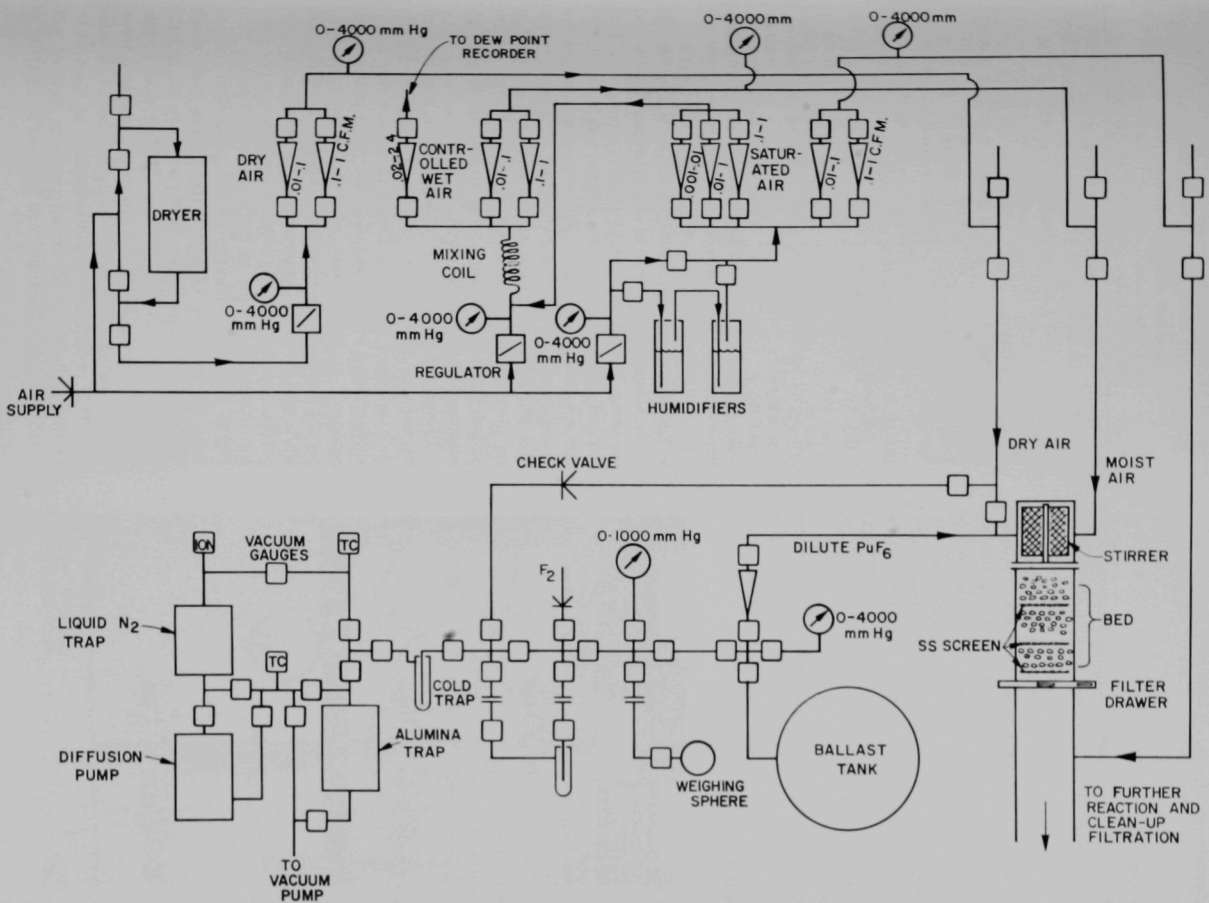
Previous experiments (ANL-6725, p. 157) indicated that when pure  $\text{PuF}_6$  (or  $\text{UF}_6$ ) is released into an atmosphere of ordinary moisture content, the hydrolysis reaction,  $\text{PuF}_6(\text{g}) + 2 \text{H}_2\text{O}(\text{g}) \rightarrow \text{PuO}_2\text{F}_2(\text{s}) + 4 \text{HF}(\text{g})$ , proceeds rapidly in the gas phase resulting in a fume (particles with a diameter of  $<0.1\mu$ ) of plutonyl fluoride ( $\text{PuO}_2\text{F}_2$ ). With an excess of water present, the hydrolysis reaction is complete, resulting in the formation of a particulate material that is retained by the AEC-type filters. Two filters in series reduced the plutonium concentration to between  $10^{-6}$  to  $10^{-9}$  of the entering concentration.

Dilute  $\text{PuF}_6$  gas streams, in fluid-bed fluoride volatility processes, may leak into the ambient air and require cleanup of plutonium. Therefore, studies of the hydrolysis and filtration of dilute  $\text{PuF}_6$  gas streams were initiated. To facilitate the design of such experiments, runs were made with dilute  $\text{UF}_6$  gas streams (ANL-6900, pp. 166-172). These experiments indicated that when the  $\text{UF}_6$  concentration in the gas stream was lower than 100 ppm before being mixed with atmospheric air of normal moisture content, the hydrolysis reaction occurred preferentially on any solid surface contacted by the gas and did not occur in the gas phase to a significant extent.

#### Current Work

The major effort during this report period was directed toward construction of new experimental facilities for handling  $\text{PuF}_6$  gas streams. The equipment is similar to that used in the previous studies with dilute  $\text{UF}_6$  gas streams except for the preparation system for

<sup>28</sup> U.S. Department of Commerce National Bureau of Standards Handbook 69, "Maximum Permissible Body Burdens and Maximum Permissible Concentrations of Radionuclides in Air and in Water for Occupational Exposure", Washington, D. C. (1959), p. 87.



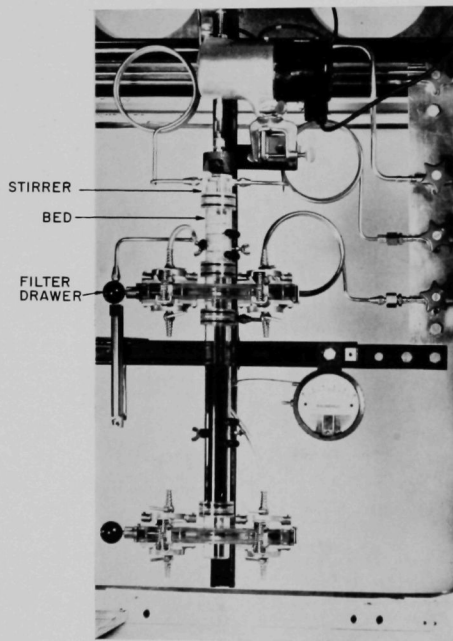
108-8753

Fig. II-16. Schematic Drawing of  $\text{PuF}_6$  Hydrolysis Apparatus.

the hexafluoride gas stream. Work with  $\text{PuF}_6$  was initiated.

### Experimental

In order to estimate the plutonium escaping from the system in dilute  $\text{PuF}_6$  releases, its hydrolysis rates are determined by mixing dilute  $\text{PuF}_6$  with moist air, and passing the mixed gas stream over a packed bed of glass spheres. Air dried to about 0.1 ppm of moisture is used as a carrier for  $\text{PuF}_6$ . Air with a controlled moisture content between 0.1 and 10 mm Hg (0.6 to 60% relative humidity at 68°F) is mixed with the  $\text{PuF}_6$  carrier stream for studying the hydrolysis rates. Another air stream saturated with moisture is combined with the mixed stream after it passes through the packed bed of glass spheres and AEC filter discs. This final addition of moisture insures the complete hydrolysis of unreacted hexafluoride and facilitates final cleanup of the gas before discharge. The equipment for supplying these three streams is shown schematically in the top half of Figure II-16.



108-7654A

FIG. II-17. Equipment for the Hydrolysis of Plutonium Hexafluoride.

TABLE II-18. COMPARISON OF  $\text{UF}_6$  AND  $\text{PuF}_6$  HYDROLYSIS EXPERIMENTS

	Run No.		
	UM-14	SUR-2	PM-1
Hexafluoride ( $\text{MF}_6$ )	$\text{UF}_6$	$\text{UF}_6$	$\text{PuF}_6$
$p^{\circ}\text{MF}_6$ (mm Hg)	0.00310	0.00244	0.00150
$p^{\circ}\text{H}_2\text{O}$ (mm Hg)	0.42	0.42	0.54
Feed Rate (mg of M/hr)	15.9	12.5	7.84
Run Time (min)	58.4	60.0	60.0
<i>Wt of M Collected per Bed Segment (mg)</i>			
0- $\frac{1}{2}$ in.	4.3	3.0	2.31
$\frac{1}{2}$ -1 in.	1.3	1.45	0.506
1-2 in.	0.70	0.94	0.139
2-3 in.	0.07	0.08	0.0438
1st Filter	0.048	—	0.0515
2nd Filter	0.006	—	0.00152
3rd Filter	0.0014	—	0.00237

The remaining equipment, shown in the lower half of the schematic, includes hexafluoride purification and metering items, and the hydrolysis apparatus. This part of the equipment was constructed in duplicate; one set in a glovebox for  $\text{PuF}_6$  experiments and the other set in a vacuum frame hood for  $\text{UF}_6$  experiments. The  $\text{PuF}_6$  hydrolysis equipment is shown installed in the glovebox in Figure II-17. A detailed cross section of the hydrolysis apparatus was included in the last summary report (ANL-6900, p. 168).

Plutonium hexafluoride, in solid form, was purified by vacuum pumping at  $-80^\circ\text{C}$ . The solid  $\text{PuF}_6$  was then sublimed and recondensed to release any impurities trapped within the solid. The vapor pressure was measured at temperatures slightly below room temperature and compared with reported values<sup>29</sup> for pure  $\text{PuF}_6$  as a check of the purity of the hexafluoride. The purification process was repeated until the vapor pressure became constant at the value reported for pure  $\text{PuF}_6$ . A weighed quantity of  $\text{PuF}_6$  was then charged from the weighing sphere to the ballast tank which was pressurized to 1900 mm Hg with dry air and the contents were allowed to mix. Mixing was accomplished by maintaining a temperature gradient across the ballast tank, the bottom being  $5^\circ\text{C}$  hotter than the top. This gradient was maintained for at least 16 hr. During a run the  $\text{PuF}_6$ -air mixture was metered with a rotameter at a constant rate between 50 and 100 ml

<sup>29</sup> Steindler, M. J., The Properties of Plutonium Hexafluoride, ANL-6753, August 1963.

per min. This mixture was then further diluted with dry air to produce the feed to the hydrolysis equipment.

### Results

The results of the first  $\text{PuF}_6$  experiment, Run PM-1, in the new equipment are presented in Table II-18 with the results of similar experiments (Runs UM-14, SUR-2) in which  $\text{UF}_6$  was used. Run UM-14 is one of twelve experiments reported in ANL-6900, pp. 166-172 and is the most similar to the current  $\text{PuF}_6$  experiment. Run SUR-2 is a  $\text{UF}_6$  experiment used to check out the new  $\text{PuF}_6$  equipment. Probably the best analysis of the hydrolysis rates of  $\text{UF}_6$  and  $\text{PuF}_6$  may be made by comparing the values of the constants in the rate equation. However, more information is required before rate constants can be determined; this informa-

tion will become available as additional runs are made.

A preliminary comparison of the runs in Table II-18 indicates that the rate of hydrolysis of  $\text{PuF}_6$  was not more than twice nor less than the rate with  $\text{UF}_6$ . Additional experimental data are needed before more definitive conclusions can be reached.

### Future Work

A series of experiments is planned with  $\text{PuF}_6$  covering the range of variables used in experiments with dilute  $\text{UF}_6$  to get further comparative data on uranium and plutonium systems. Following this, experiments will be designed to explore conditions which determine whether the reaction proceeds in the gas phase (fume-forming) or on solid surfaces.

## 2. Process Studies on the Recovery of Uranium from Highly Enriched Uranium Alloy Fuels (A. A. JONKE)

### a. BENCH-SCALE HYDROCHLORINATION AND FLUORINATION STUDIES ON HIGHLY ENRICHED URANIUM-ALLOY FUELS AND EVALUATION OF PACKED-BED FILTERS (D. RAMASWAMI AND J. STRAND)

A fluid-bed fluoride volatility process for recovering enriched uranium from uranium-Zircaloy and uranium-aluminum alloy fuels is under development. Studies carried out using a bench-scale unit with unirradiated fuel materials were concluded during this period.

The studies were performed in a 1½-in. dia. fluid-bed reactor system. Recoveries of uranium equivalent to greater than 99% of the uranium in the fuel charge were consistently achieved under a wide variety of process operating conditions. The conditions for processing both types of fuels are similar except that, in the case of the aluminum-alloy fuels, lower temperatures possibly can be used during hydrochlorination and deeper packed-bed filters are needed. Recommended operating conditions for processing a uranium-Zircaloy-2 alloy charge are:

Bed Material:	High-fired alumina (fused or sintered)
Fluid Bed:	Sufficient quantity of nominal 40 mesh alumina to cover the element (a multi-plate assembly)
Packed-Bed Filter:	-14+20 mesh alumina, 6 in. deep
Hydrochlorination:	Temperature of fluid bed: 350 to 450°C
	Temperature of packed-bed filter: 330 to 350°C

Time: ~8 hr per charge

Gas Velocity: 0.5 to 0.7 ft/sec in the fluid bed and packed-bed filter (down flow of gases)

Quantity of HCl: ~2.5 stoichiometric amounts

Concentration of HCl: 5 to 75 v/o as required to maintain high reaction rates

#### Fluorination:

Gradual increase in temperature from 250°C to 500°C while fluidizing with 5 to 10 v/o fluorine in nitrogen, then gradual increase in fluorine concentration to 90 v/o

Total time about 4 to 8 hr depending on the quantity of uranium charge.

These conditions may be used for processing uranium-aluminum alloys, except that packed-bed filter depths of 8 to 12 in. are required and filter-bed temperatures of 180 to 200°C are desirable; the temperature of the fluid bed may be maintained in the range of 200 to 400°C.

Uranium losses for both types of fuels were due to two causes: (a) containment in the gas stream exiting from the packed-bed filter during hydrochlorination and (b) retention by alumina at the end of fluorination. In order to establish the effects of all the processing conditions on the uranium losses a stepwise multiple regression analysis<sup>30</sup> was performed.

<sup>30</sup> Davies, O. L., *Statistical Methods in Research and Production*, Hafner Publishing Company, New York, 1958, p. 191.

The analysis (based on data from 27 runs) of the effects of the operating conditions on uranium losses through the packed-bed filter during hydrochlorination of uranium-Zircaloy-2 alloy fuels showed that uranium losses decreased when the following changes in experimental conditions (listed in order of decreasing importance) were carried out:

- (1) The filter-bed depth was increased from 0 to 12 in.; deeper beds gave better filtration of particulate species and provided additional surface for greater condensation of volatile species.
- (2) The average partial pressure of HCl was lowered (in the range 0.88 to 0.17 atm); this probably affected the quantity of volatile species formed.
- (3) The average particle size of alumina in the packed-bed filter was decreased from  $\sim 1.4$  mm (nominal 14 mesh) to 0.125 mm (nominal 120 mesh); smaller particles gave better filtration and allowed greater condensation.
- (4) The temperature attained by the gas stream between the fluid bed and the outlet of the filter bed was lowered from 400 to 320°C; greater condensation of the volatile species was effected (see ANL-6725, pp. 180-182).
- (5) The average particle size of alumina in the fluid bed was decreased from 0.42 mm (nominal 40 mesh) to 0.125 mm (nominal 120 mesh); possibly a combination of all four effects listed above contributed: the production and filtration of particulate species and the formation and condensation of volatile species.
- (6) The average hydrochlorination rate of uranium was decreased from 0.268 to 0.016 kg/(hr) (sq ft of fluid-bed reactor cross section); the relative amounts and the physical characteristics of uranium chlorides formed were affected.

The analysis also indicated that the use of those operating conditions which tended to decrease the partial pressure of  $UF_6$  in the gas stream resulted in less uranium retention by the alumina in the beds after fluorination. This effect of partial pressure of  $UF_6$  suggested that if the fluorine is to be recycled it may be desirable to recover the  $UF_6$  completely from the gas stream before recycle. The conditions which appear to result in low uranium retention are: (1) operating at a low bed temperature during the initial fluorination period, (2) operating with low mass velocities in the gas stream during both the hydrochlorination and fluorination steps, and (3) operating the hydrochlorination step in such a manner as to produce a low reaction rate between uranium metal and HCl. The data also indicated that the effects of the fluorination conditions are more significant than those of hydrochlorination. The following

empirical relationship was derived from the analysis and seems to represent the experimental data with an average error of  $\pm 40\%$ .

$$U = 0.0000573 t \frac{e^{\frac{122.8}{T}} p_{UF_6}^{1.78}}{r^{0.56} p_{F_2}^{0.70}}$$

where

- $U$  = w/o of uranium in the alumina fluid bed after fluorination,  
 $t$  = time in hours in which the major amount (90%) of  $UF_6$  was recovered,  
 $T$  = bed temperature ( $^{\circ}K$ ) during the high temperature fluorination period in the two part fluorination schemes,  
 $p_{UF_6}$  = average partial pressure (mm Hg) of  $UF_6$  during time  $t$ ,  
 $r$  = rate of uranium recovery (lb/(hr) (lb of alumina) for the total fluorination time,  
 $p_{F_2}$  = maximum partial pressure (atm) of fluorine that the alumina was exposed to.

This proposed relation is intended for process scale-up and is applicable in the following ranges of operating conditions:

$$\begin{aligned} U &= 0.002 \text{ to } 0.006 \text{ w/o} \\ t &= 0.02 \text{ to } 4.0 \text{ hr} \\ T &= 350 \text{ to } 500^{\circ}C \\ p_{UF_6} &= 1.1 \text{ to } 26 \text{ mm Hg} \\ r &= 0.0016 \text{ to } 0.028 \text{ lb of } U/(\text{hr})(\text{lb of alumina}) \\ p_{F_2} &= 0.6 \text{ to } 1.2 \text{ atm} \end{aligned}$$

The data from the pilot-scale reactor (6-in. dia.) and the bench-scale reactor being used with irradiated fuels appear to confirm this relation.

Data relating the effects of particle size to the overall efficiency of HCl utilization are given in Table II-19. Utilization appears to increase with a decrease in the ratio of plate spacing to average particle size and an increase in the particle size distribution of alumina. These effects are made apparent by examining the data obtained in the following runs: Run Zr-39, Run Zr-41, and Run Zr-40. In these runs, uranium-Zircaloy-2 alloy subassemblies of similar dimensions were processed. In Run Zr-39 the ratio of plate spacing to particle size was 12.0 and the alumina mesh size was  $-80+100$ . In Run Zr-41, the ratio of plate spacing to particle size was 4.7 and the alumina mesh size was  $-30+60$ . The quantity of HCl needed to complete the reaction was much higher (9 times stoichiometric requirement) in Run Zr-39 than in Run Zr-41 (2.9 times stoichiometric requirement). In Run Zr-40, the ratio of plate spacing to particle size was 8.2 and the alumina used was a mixture of  $-40+60$  and  $-80+100$  mesh. The HCl requirement was 4.6 times the stoichiometric amount. The improvement in HCl utilization efficiency in Run Zr-40 as compared

with Run Zr-39 may be due to the better quality of fluidization resulting from the use of particles of mixed sizes rather than particles having a narrow size distribution. A similar tendency was noted in the processing of uranium-aluminum alloy fuels.

#### Future Work

Since the objectives of this bench-scale study on the processing of uranium-alloy fuels have been achieved, further work on this phase of the program has been suspended. Development studies are continuing in the present 1½-in. unit on the decladding and fluorination of UO<sub>2</sub> fuels and related processes.

#### b. PILOT-PLANT DEMONSTRATION OF THE FLUID-BED VOLATILITY PROCESS FOR ENRICHED URANIUM-ALLOY FUELS (J. T. HOLMES, H. STETHERS, C. SCHOFFSTOLL, W. KREMSNER)

A pilot-plant facility is being used to demonstrate a fluid-bed volatility process for the recovery of uranium from enriched uranium-alloy fuels. The facility consists of a 6-in. dia. halogenation reactor, a 9-in. dia. packed-bed filter for retaining particulate uranium chlorides, a 6-in. dia. fluid-bed reactor for converting the volatile alloy chlorides to solid oxide waste with steam, and traps for UF<sub>6</sub> product collection. Equipment details are reported in ANL-6800, p. 282 and ANL-6900, p. 194. The facility is being operated with unirradiated fuel charges which simulate Shippingport PWR Core I seed assemblies (Zircaloy-2-uranium alloy), and MTR or ETR assemblies (aluminum-uranium alloy). The processing capacity of the pilot plant is about 30 kg per batch of Zircaloy fuel and 14 kg per batch of aluminum fuel. The current work has been concentrated on the processing of unirradiated uranium-aluminum fuel charges.

Prior experiments (ANL-6800, p. 282 and ANL-6900, pp. 194-200) with both aluminum and zirconium fuels have demonstrated: (1) excellent control of the highly exothermic hydrochlorination reaction using a fluidized-bed heat transfer medium, (2) high processing rates for batch charges of either aluminum- or zirconium-based fuels, (3) high HCl utilization without recycle (about 50%), and (4) satisfactory conversion of the waste metal chlorides to solid oxides in a fluid-bed pyrohydrolysis reactor.

The overall aims of the current work were to demonstrate: (1) improved filtration of uranium particulate from the gas streams using the packed-bed filter, (2) over 99% removal of uranium from the reactor and filter system as UF<sub>6</sub> in the fluorination step, and (3) increased average reaction rate and HCl utiliza-

TABLE II-19. EFFECT OF RATIO OF SUBASSEMBLY PLATE SPACING TO AVERAGE PARTICLE DIAMETER ON HYDROGEN CHLORIDE EFFICIENCIES

Equipment Used: 1½-in. dia. fluid-bed reactor unit  
Height of Fuel Element: 5 in.

Run No.	Previous Report	Granular Alumina		Plate Spacing <sup>21</sup> (in.)	Ratio of Plate Spacing to Av. Particle Diameter <sup>a</sup>	Quantity of HCl (× Stoichiometric)
		Mesh Size	Type			
Zr-39	ANL-6800, pp. 271-282	-80+100	38 <sup>b</sup>	½₆₄	12.0	9.0
Zr-38	ANL-6725, pp. 178-182	-80+100	38 <sup>b</sup>	½₆₄	12.0	8.7
Zr-37	ANL-6725, pp. 178-182	-40+60	RR <sup>b</sup>	⅓₈	9.5	5.0
Zr-40	ANL-6800, pp. 271-282	-40+60 50 w/o -80+100 50 w/o	38 <sup>b</sup>	½₆₄	8.2	4.6
Al-2	ANL-6800, pp. 271-282	-80+100	38 <sup>b</sup>	½₂₀	7.8	3.6
Al-3	ANL-6800, pp. 271-282	-40+120	T-61 <sup>c</sup>	½₂₀	5.0	3.0
Zr-41	ANL-6900, pp. 188-193	-30+60	T-61 <sup>c</sup>	½₆₄	4.7	2.9
Zr-42	ANL-6900, pp. 188-193	-40+60	T-61 <sup>c</sup>	⅓₁₆	4.7	2.9
Al-4	ANL-6800, pp. 271-282	-40+120	T-61 <sup>c</sup>	½₂₀	4.7	2.5

<sup>a</sup> Average particle diameter was calculated from the mesh size and not particle size distribution.

<sup>b</sup> Fused alumina, manufactured by Norton Company.

<sup>c</sup> Sintered alumina, manufactured by Aluminum Company of America.

tion by using a multicharge hydrochlorination procedure before performing the fluorination steps.

#### Experimental Procedure and Conditions

A series of five experiments was successfully completed using uranium-aluminum fuel charges (ETR type). Three of the runs were made with single charges and two of the runs involved three fuel elements each (see Table II-20). In every case the end fittings of the fuel elements were removed leaving an assembly with nineteen 0.055-in. thick fuel plates and two 0.25-in. thick side plates. Each assembly was about 38 in. long, weighed about 6.0 kg, and contained about 280 g of uranium.

Prefluorinated alumina (Alcoa type T-61) has been used in all runs for both the reactor and filter-bed material. The reactor bed weighed about 40 kg and

<sup>21</sup> *The Shippingport Pressurized Water Reactor*, Addison-Wesley Publishing Company, Reading, Massachusetts, 1958, p. 586.

TABLE II-20. CONDITIONS AND RESULTS FOR PROCESSING ALUMINUM-BASED FUELS

Run Number	8	9	10	11	12
Fuel Element (kg)	6.060	6.195 6.150 6.166 18.511	6.030 6.080 5.971 18.081	5.880	5.962
Uranium (g)	273.6	841.3	828.7	280.4	280.5
<i>Hydrochlorination Data</i>					
Average Rate (kg/hr)	1.09	1.48	1.26	0.86	0.92
Maximum Rate (kg/hr)	1.6	3.0	1.6	1.3	2.8
Reaction Time (hr)	5.6	12.5 (4.2 per element)	14.4 (4.8 per element)	6.8	6.5
Average HCl Utilization (%)	40.0	48.3	52.6	37.2	37.4
Maximum HCl Utilization (%)	60	90	65	56	65
<i>Temperatures (°C)</i>					
A. Hydrochlorination					
Reactor Bed Av.	369	356	351	350	360
Max.	395	419	380	385	366
Element Channel Av.	—	351	393	383	—
Max.	—	470	460	500	—
Reactor Wall	350	340	330	330	350
Packed Bed Filter	296	183	190	190	197
Pyrohydrolyser Bed	313	327	348	306	326
B. Hydrofluorination of 2 hr					
Reactor Bed (°C)	350	364	360	—	360
Filter Bed (°C)	350	257-377	350	—	350
C. Fluorination					
Reactor Bed and Filter					
(1) Reactor Fluidized	250-500 (2.0 hr)	250-500 (2.8 hr)	250-500 (5.9 hr)	—	250-500 (7.5 hr)
(2) Reactor Static	500 (2.0 hr)	500 (2.1 hr)	500 (2.0 hr)	—	500 (2.0 hr)
<i>Reactant Concentrations (v/o)</i>					
A. HCl in N <sub>2</sub>	78	98	95	98	91
B. HF in N <sub>2</sub>	8	26	27	—	21
C. F <sub>2</sub> in N <sub>2</sub>					
(1) Reactor Fluidized	5.5	2.0	2.0	—	5
(2) Reactor Static	40	40-60	30-50	—	68
<i>Reactor Velocity (ft/sec)</i>					
A. Hydrochlorination	0.54	0.48	0.40	0.39	0.39
B. Hydrofluorination	~0.5	~0.5	~0.5	—	0.41
C. Fluorination					
(1) Reactor Fluidized	~0.6	~0.55	~0.50	—	0.39
(2) Reactor Static	~0.05	~0.04	~0.04	—	0.04

was about 48 in. deep. The nominal particle size was 28 to 100 mesh. The final reactor bed from the first run was reused in successive runs; however, a fresh bed was used in one run in which only the hydrochlorination step was performed. The packed-bed filter weighed about 16 kg in each run and was about 12 in. deep on a support of nickel balls. The nominal particle size was 14-28 mesh in the first run and 14-48 mesh in the other runs. The smaller size (14-48 mesh) was used to improve the filtration efficiency. The filter bed material was not reused from run to run. The starting bed for

the pyrohydrolysis reactor was the final bed from the previous run, and contained about 5 kg of 28-100 mesh type T-61 alumina, and about 5 kg of -200 mesh pyrohydrolysis product.

The hydrochlorination steps were conducted using conditions prescribed in earlier pilot plant experiments (ANL-6800, p. 287 and ANL-6900, pp. 195-196). The reactor wall temperature was controlled between 330 and 350°C in each run. The remainder of the system that was exposed to AlCl<sub>3</sub> was maintained at 180 to 200°C. The input concentration of HCl in nitrogen was

about 78 v/o in the first run and about 98 v/o in the other four runs. Multicharge hydrochlorinations were made in two runs wherein three fuel elements were reacted, one at a time, after about 60 to 80% of the previous element had been hydrochlorinated. This procedure was used to eliminate the period of low reaction rate and low HCl utilization which occurs at the end of a batch hydrochlorination.

The purpose of the hydrofluorination step is to convert the residual chlorides in the reactor and filter vessel to fluorides in order to minimize the formation of chlorine fluorides when fluorine is used to recover the uranium as  $UF_6$ . The hydrofluorination was carried out using 10 to 30 v/o HF in nitrogen for 2 hr at about 350°C.

The fluorination step was performed to remove the uranium from the system as  $UF_6$  using the two-temperature fluorination scheme developed in the bench-scale work (ANL-6900, p. 193). A two-temperature, fluid-bed refluorination of the filter beds from two of the runs was also conducted in order to reduce the uranium retention. Fluorination was initiated using 1 to 5 v/o fluorine in nitrogen while the beds were heated from 250 to 500°C. When 500°C was attained, the fluorine concentration was raised to 30 to 60 v/o by reducing the nitrogen diluent. The reactor bed became static as the total flow was reduced. Fluorine recycle was not used. The process times for the 250 to 500°C part of fluorination ranged from 2.0 to 7.5 hr and the process times at 500°C ranged from 2.0 to 2.2 hr. Two sodium fluoride (NaF) traps in series, each containing 7 kg of 1/8-in. pellets, were used to collect the  $UF_6$  product. To prepare NaF pellets of high surface area sodium bifluoride pellets\* were decomposed to NaF at 300°C. The traps were operated at a temperature of 100 to 125°C at the inlet to the first trap and about 30 to 60°C at the outlet of the second trap. At the end of the run, the entire amount of pellets was ground in a disk mill and sampled for analyses.

### Results and Discussion

In general, the operation of the pilot-plant facility was highly satisfactory. The results and some minor problems are discussed in the following sections.

**Hydrochlorination.** The times required for complete hydrochlorination of the total fuel charges were 5.6, 6.8, and 6.5 hr for those runs where single fuel elements were processed (Table II-20). The hydrochlorination times were reduced to average values of 4.2 and 4.8 hr per element in the runs where the multicharge technique was used. The temperatures were well controlled

in all runs; the reactor bed temperatures averaged about 355°C and the maximum bed temperature was 420°C. The maximum temperature, measured in the channels between the fuel plates, was about 500°C. The overall hydrochlorination utilization was about 40% in those runs where single fuel elements were charged and increased to about 50% in the multicharge runs where three fuel elements were used (see Table II-20). A corresponding increase in the average reaction rate, therefore a decrease in the hydrochlorination time per element, resulted from the use of the multicharge procedure. The characteristics of the multicharge runs are similar to those reported in ANL-6648, p. 162 for the bench-scale work. Using this technique, the hydrochlorination time for a typical ETR, aluminum fuel element can be reduced by about 25% and the HCl utilization can be increased by a like amount, which is important in reducing the overall hydrochlorination time and may be sufficient to eliminate the need for HCl recycle.

The reaction rates and HCl utilization achieved in the current runs with uranium-containing fuel are on the order of 10 to 20% lower than the values reported for similar runs made earlier with elements which did not contain uranium. With uranium present, non-volatile uranium chlorides form and these may inhibit the reaction of HCl with the aluminum.

During the hydrochlorination step of the current runs the packed-bed filter operated satisfactorily, although in each run the pressure drop across the filter increased from initial values of about 2 psig to final values of 4 to 6 psig. The total system pressure drop, including the reactor, packed-bed filter, pyrohydrolysis reactor and 8-ft-gas scrubbers, remained less than 12 psig in all runs. Inspection of the top surface of the packed-bed filter, after each hydrochlorination step, revealed a black layer about 1/4- to 1/2-in. thick. In one run, where only the hydrochlorination step was performed, the caked material was found to be self-supporting; that is, when the filter-bed particulate material was drained from the bottom of the vessel, the cake remained as a layer bridged between the walls and the heat transfer fins of the filter vessel and had to be mechanically removed. The surface of the filter was black; this was probably due to the formation of uranium oxides, possibly as a result of oxygen in the reagents. The free-flowing portion of the filter bed was not significantly discolored.

The operation of the pyrohydrolysis reactor which is used to convert the volatile metal chlorides to solid oxide wastes has been routine in this series of runs. Water solubility data are being obtained to determine the suitability of the oxide product for waste storage.

A number of generalizations can now be made con-

\* Sodium bifluoride (NaF-HF) pellets were obtained from the Harshaw Chemical Company, Cleveland, Ohio.

cerning the hydrochlorination characteristics when processing aluminum-uranium fuels:

- 1) The reaction rate is virtually independent of temperature in the range studied during intervals in which the HCl utilization is high.
- 2) Higher reaction rates, with no concomitant decrease in HCl utilization efficiencies, were observed at high fluidizing gas velocities ( $\sim 0.6$  ft/sec) than were observed in tests with gas velocities of 0.4 ft/sec.
- 3) A satisfactory combination of high reaction rate along with high HCl utilization can be achieved by use of 80 v/o HCl in  $N_2$  as the feed gas to the reactor.
- 4) Successive charging of fuel elements to the reactor results in a significant increase in HCl utilization and overall reaction rate.
- 5) The packed-bed filter operated satisfactorily even though a self-supporting surface layer was formed during the hydrochlorination step.
- 6) The operation of the pyrohydrolysis reactor in series with the halogenation reactor and packed-bed filter to convert the volatile chloride to solid oxide was entirely satisfactory.

*Hydrofluorination.* Residual chloride concentrations in the reactor bed after hydrofluorination for 2 hr at 360°C using 25 v/o HF in nitrogen were less than 0.05 w/o, which corresponds to about 20 g of chlorine in the entire system.

*Fluorination.* The fluorination step was carried out without using fluorine recycle. The fluorine requirement was 6.9 g of fluorine per gram of uranium removed from the beds. This value is in agreement with the data obtained in the bench-scale studies (see ANL-6840, p. 74). It implies that the reagent cost of fluorine\* would be as low as three cents per gram of uranium. Since the fluorine requirement is quite low, a fluorine recycle procedure may not be required for plant-scale operation.

In the fluorination step of each aluminum run, temperature excursions were encountered at the surface of the packed-bed filter during the later part of the run when the fluorine concentration was increased from about 2 v/o to about 50 v/o. The excursions started about 20 to 60 min after the fluorine concentration was increased. The temperature excursions were limited to less than 50°C (500 to 550°C) by reducing the fluorine concentrations from about 50 v/o to about 30 v/o.

After each fluorination, there was a 1/2- to 1-in. thick layer of gray material caked on top of the free-flowing portion of the original filter bed. The caked layer was

found to be self-supporting and had to be mechanically removed. Visual inspection indicated that the cake was mainly fines, agglomerated with a layer of the filter-bed particulate material. Chemical analysis of this layer showed that aluminum fluoride was the major compound present; up to 11 w/o uranium and 4 w/o iron were also found.

There are a number of possible causes for the temperature excursions and related caking problems:

- (1) Alumina fines from reactor bed attrition or from the oxidized surface of the fuel elements fluorinate at higher rates than the larger filter-bed particulate material;
- (2) Alloy constituents, such as iron,† or corrosion products may, upon fluorination, cause sintering or act as a binder for the bed material;
- (3) The uranium chlorides may adsorb significant quantities of aluminum chloride which does not fluorinate completely with HF, but does fluorinate rapidly when the fluorine concentration is increased during the later part of the run; and
- (4) Uranium compounds concentrated at the filter surface may fluorinate rapidly when a high (critical) fluorine concentration is reached.

Another factor affecting the caking problem may be associated with the behavior of the fuel elements during the hydrochlorination step. The aluminum-uranium fuel elements float in the fluid bed reactor owing to their low density. When the upper part of a fuel element protrudes from the surface of the fluidized bed, particulate material spouts‡ through the fuel channels and may be completely entrained in the gas stream and collected on the packed-bed filter. The fluorination behavior of aluminum fuels could be accounted for if a large quantity of particulate chlorides are carried to the filter by this spouting mechanism. The spouting phenomenon can be minimized if the fuel element is completely submerged in the fluidized bed by mechanical means. A method of fixing the elements in the bed will be investigated in the final studies in this program.

A number of tests and analyses are still pending which should reveal the causes of the temperature excursions with aluminum fuels and suggest solutions to them. One obvious solution is the redesign of the system so that the packed-bed filter can be fluorinated as a fluidized bed. With improved heat removal, more nearly isothermal conditions could be maintained. The problems discussed above seem to pertain only to

† The ETR assemblies contain about 0.7 w/o iron which is equivalent to about 40 g of iron per element.

‡ Spouting has been visually observed and is the sporadic ejection of fluid-bed material from the channels of a fuel element partially submerged in a fluidized bed.

\* Based on a cost of \$2.00/lb for fluorine.

TABLE II-21. PILOT-PLANT URANIUM BALANCE

	Run 8			Run 9			Run 10			Run 12			Overall		
	Weight (g)	Total Wt. (g)	(%)	Weight (g)	Total Wt. (g)	(%)	Weight (g)	Total Wt. (g)	(%)	Weight (g)	Total Wt. (g)	(%)	Weight (g)	Total Wt. (g)	(%)
<i>Total Uranium Charge</i>		273.6	100		841.3	100		827.6	100		285.7	100		2223.0	100
<i>U Recoverable</i>		255.2	93.3		834.5	99.2		743.7	89.9		276.1	96.6		2109.5	94.9
In NaF Traps	254.8			829.2			616.7			226.0			1926.7		
In F <sub>2</sub> Disposal System	0.32			2.17			126.6 <sup>a</sup>			49.8			178.9		
In Bed Samples	~0.1			3.13			0.4			0.3			3.9		
<i>U Lost</i>		14.9	5.4		6.2	0.7		13.2	1.6		2.8	1.0		27.0	1.2
To Pyrohydrolyser	8.60			3.17			4.45			0.13			16.3 <sup>b</sup>		
To Reactor Bed <sup>c</sup>	0.35			0.62			5.24			2.27			2.27		
To Filter Bed	5.9			2.36 <sup>d</sup>			3.49 <sup>d</sup>			0.39			8.4 <sup>e</sup>		
To Scrub System	0.0			0.001			0.007			0.01			0.02		
<i>U Accounted For</i>		270.1	98.7		840.7	99.9		756.9	91.5		278.8	97.6		2136.5	96.1

<sup>a</sup> This value is high due to leakage of gas through a bypass and into the activated alumina traps. The total recovery is low due to the low trapping efficiency of activated alumina for UF<sub>6</sub>.

<sup>b</sup> This value is high due to the loss in Run 8 where coarser particles were used in the packed-bed filter.

<sup>c</sup> Reactor bed material reused for Runs 8, 9, 10 and 12.

<sup>d</sup> Refluorination (250 to 500°C for 4.0 additional hours) of these beds, as a fluidized bed, removed 63% (3.7 g) of the uranium retained after the initial fluorinations.

<sup>e</sup> Can be reduced further by reuse of the packed-bed filter or by fluorination as a fluidized bed.

aluminum fuels, since temperature excursions did not occur while processing uranium-zirconium fuels.

*Uranium Disposition and Material Balance.* Table II-21 gives the uranium material balances for the current runs. The balance was exceptionally good in Run 9 where more than 99% of the uranium was recoverable and 99.9% was accounted for.

The reactor bed particulate material was reused for Runs 8, 9, 10, and 12. The final uranium retention was 2.27 g or only 0.1% of the total amount of uranium charged in the four runs. Reuse of the filter-bed alumina would probably have reduced these net losses significantly.

The high retention of uranium by the filter bed in the first three runs can probably be attributed to the temperature excursions and filter-bed caking which occurred in these runs. It should be noted, however, that refluorination of the filter beds from Runs 9 and 10 as fluidized beds effected removal of an additional 63% (3.7 g) of the uranium which remained after the first fluorination.

The uranium loss to the pyrohydrolysis reactor was relatively high (3.1%) in Run 8 where 14-28 mesh filter bed particulate material was used. With the use of finer mesh material, 14-48 mesh, losses were reduced considerably—to less than 0.6% in the remaining runs.

The loss in Run 12 was only 0.14%. It is expected that these losses could be reduced further by increasing the bed depth to greater than 12 in., which is the maximum depth attainable in the existing equipment.

The uranium accountability was relatively good in Runs 8 and 9 (over 98.5%). The uranium balances in Runs 10 and 12 were unsatisfactory; this may have resulted from leakage of product gas through a bypass into the fluorine disposal towers. The total recoveries were low possibly as a result of poor trapping efficiency of activated alumina for UF<sub>6</sub> in the presence of fluorine. Even though the uranium loss was high to the pyrohydrolysis reactor in Run 8 and filter-bed caking caused relatively high uranium retention, the overall loss for all runs was less than 1.2%. The remaining 98.8% should be recoverable. The overall material balance for these four runs is relatively inaccurate because of the poor filtration efficiency in Run 8 and the loss of UF<sub>6</sub> to the fluorine disposal system in Runs 10 and 12.

In order to determine the distribution of uranium in the system before fluorination, a run was made in which only the hydrochlorination step was performed. The uranium content of the free-flowing reactor bed corresponded to about 20% of that in the charge as compared to a previous run with zirconium fuel where

>70% of the uranium was in the reactor bed. Analysis showed the black material which was deposited on the top of the packed-bed filter contained uranium equal to about 10% of that in the charge. The amount of uranium in the free-flowing filter bed was about 5% of that in the charge. The remaining 65% was recovered from the fuel element basket and walls of the equipment in a subsequent fluorination of the empty equipment. The low uranium content of the reactor bed may be a result of elutriation promoted by the spouting mechanism which was described previously.

**Bed Attrition Tests.** An experiment was made to determine the effect of process reagents, flow rates, and temperatures on attrition of type T-61 Alcoa alumina. The run was made without a fuel element, but included a 2.6-hr prefluorination step at 250 to 500°C, a 6.0-hr hydrochlorination at 325 to 335°C, a 1.7-hr hydrofluorination at 350°C, and a 3.6-hr fluorination at 250 to 500°C. Fresh alumina was used at the start of the run for the reactor bed and the packed-bed filter.

Less than a ¼-in. depth of fines was visually observed on the top surface of the packed-bed filter after each process step. The run was smooth and no temperature excursions were encountered throughout the test. The beds were removed at the end of each step and a screen analysis was performed on a representative fraction of the bed. The beds were then returned to the reactor and filter vessel. The screen analysis showed that there is little attrition of the reactor bed and no significant buildup of fines in the packed-bed filter. The filter contained less than 0.32 w/o of -230 mesh particles at the end of the reaction cycle. This quantity is significantly less than the approximately 1.0 to 6.0 w/o of -230 mesh material found on the filter after Runs 8, 9, 10, and 12 in which aluminum-uranium fuel charges were processed. It is possible that these fines are aluminum oxide from the fuel plates or are produced by localized high temperatures at the surface of the fuel element during hydrochlorination, or by the reaction and temperature excursions at the surface of the packed-bed filter in the fluorination step.

#### Summary

In general, the operation of the pilot-plant facility with the aluminum-based fuels has been satisfactory. The uranium filtration efficiency of the packed-bed filter during the HCl step has been improved by increasing the bed depth to 12 in. and decreasing the nominal mesh size of the particulate solids to -14+48 mesh. Over 99% of the uranium was removed from the reactor and filter beds in the overall uranium material balance for four runs, and over 99% was recovered as UF<sub>6</sub> on beds of NaF in one of the runs. An increase in reaction rate and HCl utilization of about 25% was

demonstrated using a multicharge technique. The temperature excursions which were encountered in the fluorination step while processing aluminum fuels can probably best be eliminated by designing the system so that the filter-bed particulate material can be fluorinated as a fluidized bed and thereby allow efficient heat removal.

#### Future Work

The future work will be directed at obtaining satisfactory operation and uranium recovery for a multicharge zirconium fuel element run. Techniques will be sought for eliminating the packed-bed filter temperature excursions encountered while processing aluminum fuels. These studies, to be completed during the next report period, will conclude the pilot-plant program on the processing of enriched uranium-alloy fuels.

#### c. HIGH-ACTIVITY-LEVEL STUDIES ON ENRICHED URANIUM-ALLOY FUELS (A.

CHILENSKAS, K. TURNER\*, J. KINCINAS, G. L. POTTS, W. GOTTFALD\*\*)

A program of fluid-bed volatility studies with irradiated fuel materials on a bench-scale level (1½-in. dia. reactor) has commenced. Irradiated fuels of various types including high enrichment uranium-Zircaloy and uranium-aluminum alloys and low enrichment ceramic uranium oxides will be processed. The aims of the program are to obtain data on (1) the distribution of fission products throughout the various process steps, (2) decontamination factors that may be realized, and (3) the effects, if any, of irradiation and the presence of fission products on uranium recovery and reaction rates.

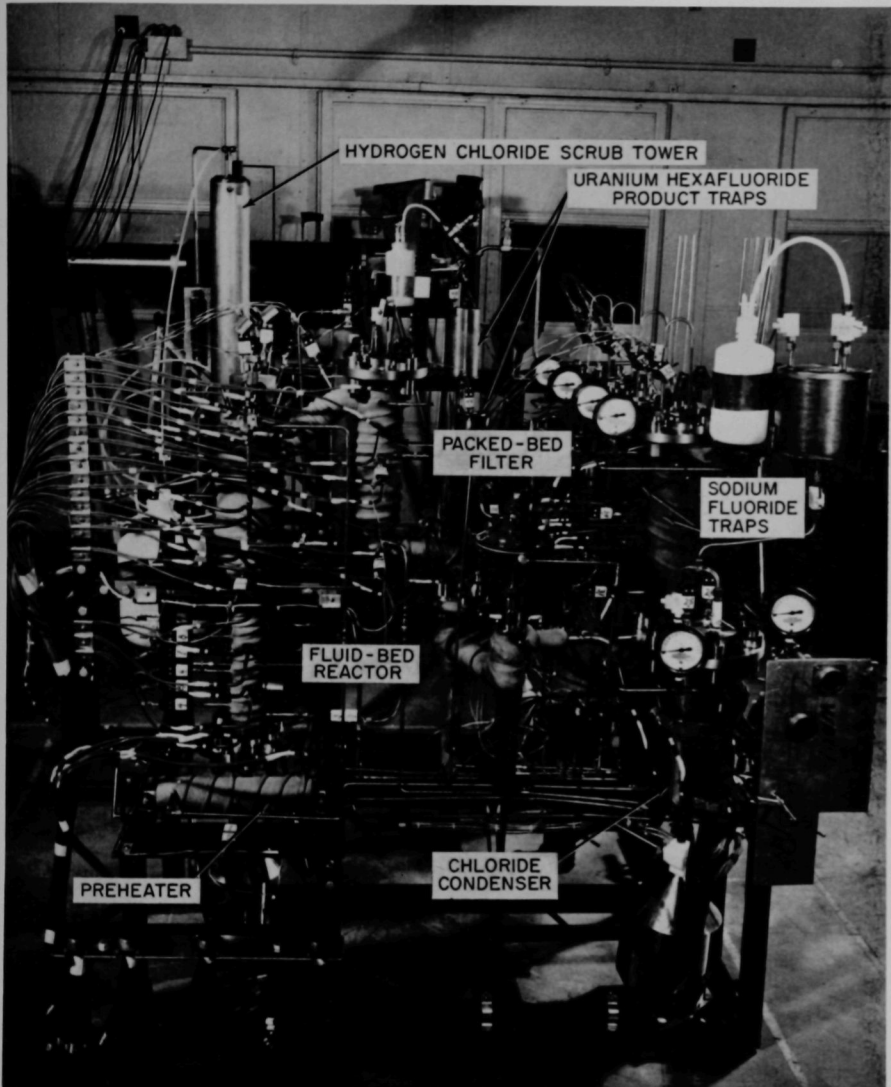
During the current period, the processing equipment was assembled in a mock-up area and tested with a series of eight experiments using unirradiated fuel materials. These tests, described in detail below, provided a complete check of equipment performance and the means for developing operating procedures and techniques to be used in experiments with irradiated fuel. After these tests the equipment was installed in the Senior Cave Facility of the Chemical Engineering Division and the first experiment, using 5-yr-cooled uranium-Zircaloy alloy, was completed. Operationally the run was highly satisfactory. Further evaluation awaits completion of analytical work.

#### Apparatus

A photograph of the equipment, immediately prior to its installation in the cave, is shown in Figure II-18.

\* Guest Scientist, Australian Atomic Energy Commission.

\*\* Central Shops machinist, attached to the Chemical Engineering Senior Cave Facility.

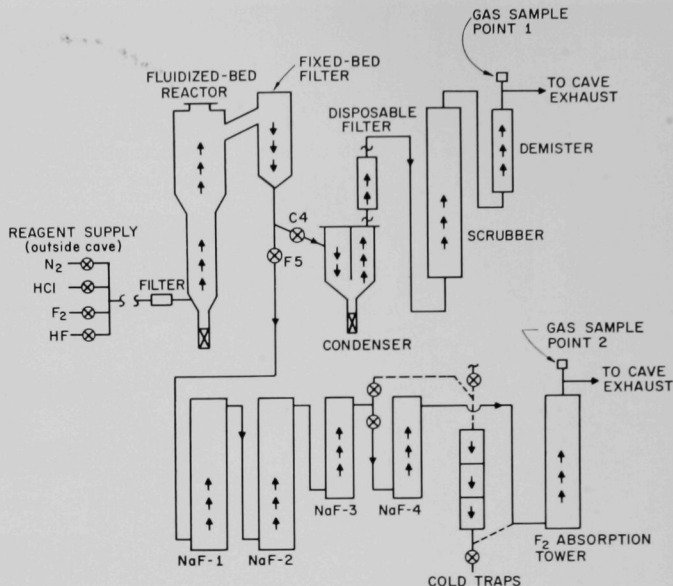


108-7239A

FIG. II-18. Fluoride Volatility Apparatus used in the High-Activity-Level Studies on Irradiated Fuel.

A schematic flow sheet for the apparatus is shown in Figure II-19. The hydrochlorination step is performed with valve F5 closed and valve C4 open. This procedure directs the gas flow from the fixed-bed filter

to the condenser, through the disposable condenser-filter to the HCl scrubber and then to the atmosphere via the cave stack. The  $ZrCl_4$  (or  $AlCl_3$ ) generated in the reactor is removed from the gas stream in the con-



108-8561 Rev.

FIG. II-19. Schematic of Equipment for Fluid-Bed Fluoride Volatility Studies with Irradiated Fuel.

denser (cooled by natural convection) and from the condenser by washing with dilute HCl. Experience with the unirradiated fuels showed that a filter is required behind the condenser to remove chloride fines which cause plugging of the line to the scrubber. The filter consists of a small section of 3-in. pipe, packed with glass wool, which can be removed and replaced remotely each run. The gas stream leaving the filter passes to a scrubber where HCl is removed from the nitrogen diluent gas. The scrubber consists of a tower packed with Raschig rings through which H<sub>2</sub>O is circulated. The resultant dilute HCl solution (approximately 16 liters) is solidified with Portland cement and discarded. A demister is provided to remove entrained scrub solution from the gas stream prior to discharge of the gas to the cave exhaust duct. A gas sampling point is situated at the exit from the demister, and an off-gas sample is continuously withdrawn during the hydrochlorination step for hydrogen analysis in a thermal conductivity cell located in the cave isolation room. The thermal conductivity cell provides a continuous record of the hydrogen concentration in the off-gas which in turn provides a means of calculating HCl reaction rate and utilization efficiency.

When the hydrochlorination step has been com-

pleted, the high-temperature valves are reversed (F5 is opened, C4 is closed) and the gas stream leaving the packed-bed filter is directed to the system of NaF traps or cold traps. During the fluorination step, UF<sub>6</sub> is generated in the fluid-bed reactor and passes through traps NaF-1 and NaF-2 (maintained at 400°C for removal of certain fission products) and is collected on trap NaF-3 which is maintained at 100°C. A fourth NaF trap (at room temperature) serves as a backup for NaF-3 trap. The gas flow continues to a fluorine absorption tower containing ¼-in. dia. activated alumina balls and then to the cave exhaust. When required, trap NaF-3 may be heated to 400°C and the UF<sub>6</sub> desorbed in a stream of fluorine and collected in dry ice cold traps. The UF<sub>6</sub> is removed from the cold traps by hydrolysis with 20 v/o nitric acid.

Sealing of the reactor and fixed-bed filter flanges is accomplished with copper O-rings which are nickel plated for corrosion resistance. The gaskets are annealed before use. The NaF traps and condenser flanges are sealed with flat Teflon gaskets. The cave atmosphere is continuously sampled and monitored for HCl or fluorine. The monitor is an M.S.A.\* Billion-Aire Analyzer situated in the isolation room adjoining

\* Mine Safety Appliance Co.

TABLE II-22. CONDITIONS DURING THE FLUORIDE VOLATILITY PROCESSING OF UNIRRADIATED URANIUM ALLOY FUELS

	SCIZ <sup>a</sup> -1		SCIZ-2		SCIZ-4		SCIA <sup>b</sup> -1		SCIA-2	
	Start	Final	Start	Final	Start	Final	Start	Final	Start	Final
<b>HCl STEP</b>										
Process Time (hr)	13½		9½		0-2 2-6¼		6		0-3½ 3½-4½	
Av. Bed Temp (°C)	400		390		395 505		210		220 250	
Av. Wall Temp (°C)	385		375		375 485		200		195 240	
Av. Filter Temp (°C)	355		350		350 350		220		210 210	
Inlet HCl Conc (v/o)	42-89		41-85		42-82		22-39		19-29	
Av. Superficial Gas Vel. in Reactor (ft/sec)	0.5		0.5		0.6		0.6		0.6 0.4	
Reaction Rate <sup>c</sup> (g/hr)	55		44		10 71		d		49 *	
HCl Utilization Eff. <sup>d</sup> (%)	27		22		4.5 28		d		100 *	
<b>F<sub>2</sub> STEP</b>										
Bed Temp (°C)	270	540	250	525	250	520	275	520	260	515
Wall Temp (°C)	255	500	250	500	240	490	255	495	240	490
Filter Temp (°C)	305	510	255	510	230	510	280	500	260	495
F <sub>2</sub> Conc (v/o)	8	63	8	78	8	66	8	83	8	56
Superficial Gas Vel. in Reactor (ft/sec)	0.6	0.1 <sup>f</sup>	0.5	0.1 <sup>f</sup>	0.5	0.1 <sup>f</sup>	0.5	0.1 <sup>f</sup>	0.5	0.1 <sup>f</sup>

<sup>a</sup> Senior Cave Inactive Zircaloy.

<sup>b</sup> Senior Cave Inactive Aluminum.

<sup>c</sup> The reaction rate varied considerably during the course of the experiment. The values shown represent steady rates obtained for significant portions of the time period under consideration. They do not represent overall average values.

<sup>d</sup> Erratic reaction rate.

<sup>e</sup> Constantly decreasing reaction rate and HCl utilization efficiency.

<sup>f</sup> Bed in static condition.

the cave operating area, calibrated for 0-25 ppm HCl and 0-25 ppm fluorine.

#### Experiments with Unirradiated Fuel Materials

Experiments with unirradiated fuel materials consisted of three runs with 4 w/o uranium-Zircaloy, two runs with 4 w/o uranium-aluminum, one each with Zircaloy alone and aluminum alone, and one with UO<sub>2</sub> pellets. For the alloy charges the experimental conditions were similar to those developed in other bench-scale (see ANL-6800, pp. 271-282) and pilot-plant work on highly enriched alloy fuels. These conditions were: (1) hydrochlorination at approximately 400°C for Zircaloy and approximately 220°C for aluminum, and (2) fluorination between 250°C and 500°C using a fluorine-nitrogen concentration starting at approximately 10 v/o and gradually increasing to a final concentration of approximately 70 v/o. The conditions used in all of the current uranium-alloy runs are summarized in Table II-22.

Uranium is collected as UF<sub>6</sub> during the fluorination on a NaF trap operated at 100°C. The UF<sub>6</sub> may then be desorbed from the NaF at 400°C and collected in cold traps held at approximately -80°C. When runs are made with irradiated materials additional NaF traps will be installed upstream of the UF<sub>6</sub> sorption

column for the collection of some of the fission products volatilized from the reactor. These will be operated at 400°C.

For the UO<sub>2</sub> run, the charge was reacted initially with 40 v/o HF in oxygen for 2 hr. This period was followed by a fluorination step similar to that used for the alloy charges.

#### Results and Discussion

Samples of the various beds, zirconium or aluminum chloride hydrolyzate and the uranium hexafluoride hydrolyzate solutions were analyzed to follow the movement of uranium throughout the equipment. The analyses for five of the inactive runs are shown in Table II-23. The significant results may be summarized as follows:

(a) The retention of uranium by the reactor bed and the filter bed for all the runs with the exception of Run SCIZ-4 totalled less than one percent of the uranium charged. The high retention of uranium in the bed material in Run SCIZ-4 is believed to be the result of incomplete reaction of the alloy charge during hydrochlorination. The hydrochlorination time was reduced to 6¼ hr, a considerably shorter time than the hydrochlorination time for Run SCIZ-1 (13.7 hr) and in Run SCIZ-2 (9.3 hr).

TABLE II-23. URANIUM DISTRIBUTION FOLLOWING FLUORIDE VOLATILITY PROCESSING OF UNIRRADIATED URANIUM-ALLOY FUELS

	Uranium Concentration as Percent of Original Charge				
	SCIZ-1	SCIZ-2	SCIZ-4	SCIA-1	SCIA-2
Reactor Bed: 700 g Alcoa T61 alumina, 28-100 mesh					
Filter Bed: 380 g Alcoa T61 alumina, 14-28 mesh, for all runs except Run SCIZ-4					
900 g Alcoa T61 alumina, 14-28 mesh, for Run SCIZ-4					
Charge	100	100	100	100	100
Reactor Bed	<0.45	0.46	2.2	0.22	0.13
Filter Bed	<0.22	0.11	4.1	0.04	0.10
Condenser	N.A. <sup>a</sup>	3.8	0.20	10.4	0.30
NaF Trap 1	0.12 <sup>b</sup>	0.13 <sup>b</sup>	0.49	0.20	0.12
NaF Trap 2	0.40 <sup>b</sup>	0.42 <sup>b</sup>	<sup>c</sup>	0.11	<sup>c</sup>
NaF Trap 3 (Before desorb.)	N.A. <sup>a</sup>	N.A. <sup>a</sup>	92.2	N.A. <sup>a</sup>	N.A. <sup>a</sup>
NaF Trap 3 (After desorb.)	0.07	0.19	(0.23) <sup>d</sup>	0.33	0.16
NaF Trap 4	13.9 <sup>b</sup>	14.5 <sup>b</sup>	0.28	2.34	0.04
Cold Traps	38.2	69.2	(84.5) <sup>d</sup>	60.6	90.3
F <sub>2</sub> Absorption Tower	4.3	7.6 <sup>c</sup>	(5.6) <sup>d</sup>	9.3 <sup>e</sup>	9.4 <sup>e</sup>
U Balance	58	96	99.5	84	101

<sup>a</sup> Not analyzed.

<sup>b</sup> Analyzed following SCIZ-2. Represents an average result for 2 runs.

<sup>c</sup> NaF Trap 2 not charged for these runs.

<sup>d</sup> These values are results after desorption of NaF Trap 3 and are not included in the uranium balance listed as Percent of Original Charge.

<sup>e</sup> Analyzed following SCIA-2. Represents an average result for 3 runs.

(b) The uranium loss to the condenser during hydrochlorination was reduced significantly by redesigning the fixed-bed filter and increasing the bed depth from 4½ in. to 7 in. The changes were completed prior to Run SCIZ-4, the last run in the series, and in this run the uranium loss was only 0.2% of the charge.

(c) The uranium balances achieved were considered satisfactory in that the final run (SCIA-2) resulted in high uranium recovery and essentially complete accountability of the uranium.

### 3. The Corrosion of Nickel-200 in Fluoride Volatility Process Environments (A. A. CHILENSKAS, G. GUNDERSON)

Corrosion studies in support of the fluoride volatility program have been completed. Two types of tests were used in these studies: (1) small-scale laboratory tests conducted in tube furnaces and (2) in-plant exposure tests. The laboratory tests were designed to

examine the effect upon nickel of short-term and long-term exposures of selected gaseous environments representative of those found in fluoride volatility processing. The in-plant tests consisted of exposing specimens within various pieces of pilot-plant equip-

ment. The efficiency of the cold traps was somewhat less than had been obtained in other studies. This can be seen from the significant amounts of uranium that were collected in the fluorine absorption tower (activated alumina) which is a backup for the cold traps during desorption of the UF<sub>6</sub> from trap NaF-3. Since the uranium balance for the active runs will be obtained only from the NaF trap analyses, this procedure is considered satisfactory for the purpose of determining any additional decontamination that may be obtained from a desorption step.

Uranium in the Backup NaF Trap (NaF-4). The NaF pellets are contained in a removable cartridge within the NaF traps. To minimize bypassing of the cartridge by the UF<sub>6</sub>, a seal between the cartridge and the trap body was made by partly filling the annular space between the cartridge and the trap with solids of a much finer mesh size than that of the NaF pellets. However, it was not possible to obtain a perfect seal by this means, and approximately 10% of the gas was found to bypass the cartridge. In Runs SCIZ-1, SCIZ-2, and SCIA-1, the solid used for the seals was -20+40 mesh CaF<sub>2</sub>, which does not sorb UF<sub>6</sub>, and hence significant quantities of uranium bypassed the NaF pellets in trap NaF-3. The bulk of the uranium that bypassed the NaF pellets in Trap NaF-3 was trapped on the NaF pellets in Trap NaF-4. In subsequent runs, uranium bypassing was virtually eliminated by substituting -25+60 mesh NaF for the CaF<sub>2</sub>.

#### Future Work

Further work with irradiated fuels of both the highly enriched uranium-alloy and low enrichment UO<sub>2</sub> fuel types is planned. Immediate experiments will involve 5-yr-cooled uranium-Zircaloy alloy fuel. Subsequently, uranium-aluminum alloy fuels that have been cooled for relatively short periods, 6 months and 3 months, will be used in a study of iodine behavior during the process steps.

ment and evaluating the corrosion rates after the completion of one or more process cycles.

### The Long-Term Corrosion of Nickel-200 Plate and Welded Nickel-200 Plate in Static Gas Environments

The results of long-term corrosion studies with nickel-200 plate are summarized below. These results were previously reported in ANL-6900, pp. 201-202, and are included in the present report because they are pertinent to the discussion of results that follows.

The corrosion rate of nickel-200\* plate was found to be 0.9 mil/yr for an atmosphere of 50 v/o fluorine in nitrogen when the specimens were held at about 475°C. The corrosion rates for the fluorine-HCl cycles and fluorine-oxygen cycles were found to be somewhat higher than those obtained with a 50 v/o fluorine environment alone, but since the overall range of values (0.9 to 4.1 mils/yr) was relatively narrow, these apparently higher rates are believed not to be significant. Metallographic examination of the specimens after exposure disclosed no evidence of intergranular penetration.

A comparison of the values for the corrosion rate of nickel-200 specimens welded with weld filler metal 61\*\* and nickel-200 specimens welded with nickel-200 filler shows clearly that the welds made with nickel-200 filler have superior corrosion resistance in every instance (1 to 4 mils/yr compared with 67 to 1315 mils/yr).

A comparison of the corrosion rates for all nickel-200 welded and nonwelded plate specimens indicates that very slightly higher corrosion rates are obtained with the welded specimens (1 to 5 mils/yr compared with 1 to 4 mils/yr). Both welded and nonwelded specimens were examined metallographically for evidence of intergranular penetration and of localized attack in areas where high-stress concentration would be expected. No such evidence was found.

### The Corrosion Rate of Nickel-200 from In-Plant Tests

The corrosion rates of nickel-200 specimens exposed to the high-enriched pilot-plant environment or to process gases in the bench-scale apparatus for high-activity-level studies are shown in Table II-24. The corrosion rates ranged from 12 to 40 mils/yr; speci-

TABLE II-24. CORROSION RATE OF NICKEL-200 SPECIMENS FROM IN-PLANT TESTS

Test Designation	Exposure Run Conditions	Corrosion Rate (mils/yr)		
		Total Time (hr)	In Bed	Out of Bed
1	High-enriched pilot plant Runs 1, 2, 6 with Zircaloy subassemblies and Runs 3, 4, 5 with aluminum subassemblies (no uranium present); 47 hr with HCl at 440°C and 12 hr with HF at 310°C.	59	40	35
2	Above 6 runs plus Runs 7 and 8 (one each with uranium-Zircaloy and uranium-aluminum subassemblies); 16.5 hr with HCl at 440°C, 4 hr with HF at 310°C, and 12.5 hr with F <sub>2</sub> at 250-500°C.	92*	37	27
3	High-enriched pilot plant Run 10 with uranium-aluminum subassemblies; 14.4 hr with HCl at 370°C, 2 hr with HF at 360°C, and 11.6 hr with F <sub>2</sub> at 250 to 500°C.	28	—	12
4	Above Run 10 plus attrition run performed without fuel charge; 4.6 hr with HCl at 330°C, 2 hr with HF at 355°C, and 8 hr with F <sub>2</sub> at 250 to 500°C.	43*	35	—
5	Shakedown Run 2 on bench-scale equipment for high-activity-level studies; no fuel charge; 8 hr with HCl at 370°C and 8 hr with F <sub>2</sub> at 250 to 500°C.	16	23	16

\* Cumulative values.

mens immersed in the fluid-bed exhibited the higher rates.

### The Effect of a Fluidized Bed of Alumina upon the Corrosion Rate of Nickel

Two runs have been conducted in the Senior Cave bench-scale equipment in which the effect of a fluidized bed of alumina upon the corrosion rate of nickel-200 plate was examined. The results and conditions of these runs are given in Table II-25.

The data in Table II-25 indicate that a fluid bed of alumina effects a significant increase in the corrosion rate of nickel-200 (11 mils/yr without a bed, 23 mils/yr with a bed). The presence of the alumina under nonfluidized conditions did not appear to have much effect upon the corrosion rate as may be seen by comparing the rate obtained in the fixed-bed filter with

\* Manufactured by the International Nickel Co., Inc., nominal composition in percent: Ni, 99.5; C, 0.06; Mn, 0.25; Fe, 0.15; S, 0.005; Si, 0.05; and Cu, 0.05.

\*\* Manufactured by the International Nickel Co., Inc., nominal composition in percent: Ni, 93.0; C, 0.15; Mn, 1.0; Fe, 1.0; S, 0.01; Si, 0.75; Cu, 0.25; Al, 1.50; Ti, 2.0 to 3.5; other, 0.50.

TABLE II-25. THE EFFECT OF A FLUIDIZED ALUMINA BED UPON THE CORROSION RATE OF NICKEL-200

- Run 1: Prefluorination at 25 to 450°C for 2 $\frac{3}{4}$  hr, HCl at 370°C for 8 hr, fluorination at 250 to 500°C for 4 hr, duplicate specimens exposed in the zones listed above, no alumina bed in the reaction zone of the reactor, alumina bed present in the fixed-bed filter section.
- Run 2: Conditions similar to Run 1 except an alumina bed was added to the reaction zone of the reactor. Gas velocities were such as to maintain the alumina fluidized except for the latter part of the fluorination step.

Specimen Location	Corrosion Rate (mils/yr)	
	Run 1 No Bed in Reaction Zone	Run 2 Fluid Bed in Reaction Zone
Reaction zone of reactor	11	23
Disengaging section	18	16
Fixed-bed filter	12	9

TABLE II-26. THE EFFECT OF THERMAL CYCLING UPON THE CORROSION RATE OF WELDED AND NONWELDED NICKEL-200 IN FLUORINE

Temperature: 550  $\pm$  10°C  
 Reagent Gas: 50 v/o fluorine in nitrogen  
 Flow Velocity: About 0.002 ft/sec

Type of Specimen	Corrosion Rate (mils/yr)	
	Constant Temp	Thermal Cycled
Nonwelded	2.6	3.9
Welded	6.2	4.6

TABLE II-27. THE EFFECT OF AIR EXPOSURE UPON THE CORROSION RATE OF NICKEL-200 EXPOSED TO HCl AND FLUORINE

Test Cycle: 50 v/o HCl in nitrogen at 375°C for 6 hr  
 50 v/o fluorine in nitrogen at 375-500°C for 3 hr

Flow Velocity: 0.002 ft/sec

	Air-Exposed		N <sub>2</sub> Blanket	
	(mils/cycle)	(mils/yr) <sup>a</sup>	(mils/cycle)	(mils/yr) <sup>a</sup>
Nonwelded	0.011	10	0.010	8
Welded	0.015	13	0.010	8

<sup>a</sup> Based upon one calendar year exposure (8750 hr).

that obtained in the reaction zone of the reactor (12 mils/yr as compared with 11 mils/yr). The corrosion rate (18 mils/yr) exhibited in the disengaging section of the fluid-bed reactor was somewhat higher than expected. During a run, temperatures in the disengag-

ing section were about 25°C higher than those in the reaction zone, and these higher temperatures may be, at least in part, the reason for the higher corrosion rate.

### The Effect of Thermal Cycling Upon the Corrosion Rate of Welded and Nonwelded Nickel-200 in a Static 50 v/o Fluorine Environment

In this test, the tube furnace containing control samples was maintained continuously at 550  $\pm$  10°C and was fed a mixture of 50 v/o fluorine in nitrogen at 5  $\pm$  1 psig for 8 hr each day. For the remainder of each day a purge of nitrogen only was maintained. A second tube furnace in series with the first received the same reactants for the same times but the temperature was maintained at 550  $\pm$  10°C only during the 8-hr exposure to fluorine, following which it was cooled to room temperature and reheated to 550°C prior to the next cycle.

Two types of specimens were used:  $\frac{3}{16}$ -in. nickel-200 plate and  $\frac{3}{16}$ -in. nickel-200 plate with a machined "V" notch fitted with nickel-200 weld metal. The weld metal was laid down by the TIG welding procedures and the beads were ground flush. Triplicate specimens were included in each tube furnace. Both tube furnaces received 10 cycles (80-hr total exposure to fluorine). After exposure, the specimens were defilmed in an equimolar bath of KNO<sub>3</sub>-NaNO<sub>3</sub> at 500°C for 15 min and weighed. The results of this test are shown in Table II-26.

The effect of thermal cycling upon the corrosion rate under these conditions appears to be negligible for practical purposes.

### The Effect of Air Exposure Upon the Corrosion Rate of Welded and Nonwelded Nickel-200 Plate Exposed to HCl and Fluorine

A test has been completed which examined the effect of exposing nickel-200 corrosion coupons to the air atmosphere after they had been exposed to HCl and fluorine at process temperatures. Specimens were exposed in two furnace tubes to three cycles of reagents and temperatures as shown in Table II-27. Between cycles each furnace tube was allowed to cool to room temperature overnight under nitrogen. While at room temperature, room air flowed through one tube furnace for one hour while the other tube furnace was maintained under nitrogen. The conditions and results of this test are shown in Table II-27.

As shown by the values in the table, the specimens which were exposed to air exhibited slightly higher corrosion rates than those kept under nitrogen. For all practical purposes, this difference is not considered significant.

### Discussion of Results and Conclusions

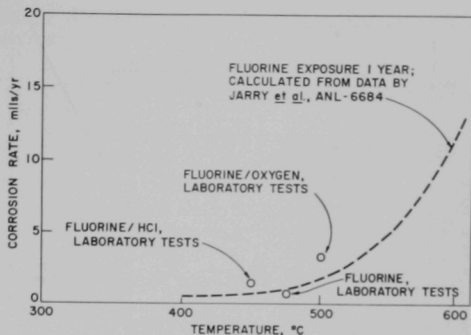
In an attempt to understand the corrosion process and to evaluate the relative importance of particular parameters under study in the laboratory tests, it is useful to compare the results of the laboratory tests with the results of the in-plant tests and with kinetic data<sup>32</sup> when such data are available.

Laboratory test data obtained for fluorine, fluorine alternated with HCl, and fluorine alternated with oxygen, are compared with corrosion values calculated from a kinetic study of nickel with fluorine in Figure II-20. The laboratory values shown are the average values obtained from the three exposure periods, 240, 480, and 960 hr. The comparison shows that the rates obtained in the laboratory tests are in close agreement with the values found for pure fluorine in the kinetic study. It is important to note that the comparison is made for specimens which have been exposed to the reactants for a long period of time under conditions of quiescent reagent supply which permit protective films to form. The rate of change of the reaction rate between nickel and fluorine with time after an exposure of 33 hr becomes small<sup>32</sup> and the comparison made in Figure II-20 (exposures of 240 hr and higher) should be valid. Under these conditions the conclusion may be drawn that alternating a fluorine environment with HCl or with oxygen does not significantly increase the corrosion rate.

The protective nature of the nickel fluoride film is illustrated in Figure II-21. The corrosion rate is very rapid initially but decreases rapidly as the film of nickel fluoride increases in thickness. The corrosion rate is highly dependent upon the thickness of the film which exists at any particular time. In process equipment where fairly high gas velocities occur or a fluidized bed of alumina is present, films which would form under quiescent conditions may be removed. Experimental work has shown that the corrosion rate is increased by the action of a fluidized bed indicating that some film removal may have occurred by attrition.

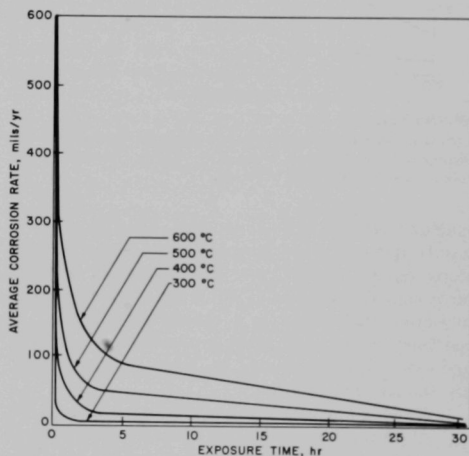
A summary of corrosion results from in-plant tests is shown in Table II-24. For purposes of comparison these results are plotted in Figure II-22 along with the corrosion rate of nickel by fluorine for short exposures. As would be expected from the hypothesis that the protective film may be removed by the action of the fluid bed or by the high gas velocity in process equipment, the corrosion values for in-plant specimens are higher than would be predicted from static tests.

<sup>32</sup> Jarry, R. L., W. H. Gunther, and J. Fischer, The Mechanism and Kinetics of the Reaction between Nickel and Fluorine, ANL-6684, August 1963.



108-8743 Rev.

FIG. II-20. Long-Term Corrosion of Nickel-200 in Static Gaseous Environments.



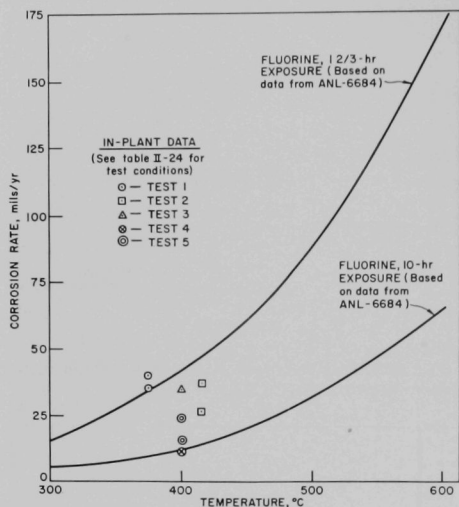
108-8747

FIG. II-21. Corrosion of Nickel in Fluorine as a Function of Temperature and Time.

(Based on data by Jarry et al., ANL-6684)

Temp, °C	Corrosion Rate, mils/yr	
	Initial Rate Exposure 1 min	Final Rate Exposure 1 yr
300	112	—
400	324	0.7
500	790	1.5
600	1550	13

The in-plant specimens behave as though they are protected by a thin fluoride film equivalent to that which would be produced by static fluorine exposures



108-8745 Rev.

FIG. II-22. Comparison of the Corrosion Rates of Nickel-200 Obtained from In-Plant Tests with Rates Obtained from Short-Term Exposures to Fluorine.

ranging from 1 to 10 hr in duration. Thus the in-plant results appear to be reasonable when compared with static results obtained for short exposures. The in-plant corrosion values fall within an acceptable range indicating that nickel is a satisfactory material of construction for many plant applications. The results and conclusions which may be drawn from this study are summarized below.

1. Under static conditions or conditions of very low gas flow rates, which allow protective films to form easily, the corrosion rate of nickel by (a) fluorine alternated with HCl and (b) fluorine alternated with oxygen is low (1 to 4 mils/yr) and is in close agreement with the rate exhibited by nickel for fluorine alone (see Figure II-20).
2. Under conditions which do not allow films to form readily (high gas velocities) or which lead to the removal of films, (fluid-bed action) the corrosion rate has been found to be significantly

higher than that found under static conditions, but less than the rate which would occur if no protective film formed. Experimental evidence of the effect of a fluidized bed upon the corrosion rate of nickel has been obtained which shows that the rate is considerably increased (from 11 mils/yr to 23 mils/yr) due to the presence of the bed (see Table II-25). For the range of conditions studied thus far, the corrosion values in plant equipment would be expected to range between 12 to 40 mils/yr (see Table II-24) with the lower values existing in most of the components while the higher values would be expected for those components in contact with the fluid bed.

3. A comparison of the corrosion rate obtained under static conditions for long-term exposure of two types of nickel welds has been made. Nickel welds made with nickel-200 metal filler have been shown to be clearly superior to welds made with nickel-61 filler metal. The corrosion rates of welds made with nickel-200 ranged from 1 to 5 mils/yr (comparing closely with the corrosion rate of 1 to 4 mils/yr for nonwelded nickel plate) whereas the welds made with nickel-61 filler metal ranged from 67 to 1315 mils/yr. Some evidence has been obtained which indicates that the presence of a small amount of titanium in the nickel filler metal-61 is the cause of the high corrosion rates exhibited.
4. Metallographic examination of specimens exposed to both the laboratory-scale and in-plant environments have exhibited no evidence of sub-surface (intergranular) attack.
5. Several parameters which were believed to have a possible effect upon the integrity of the protective film were studied for their effect upon the corrosion rate of nickel. The effect of thermal cycling on the corrosion of nickel specimens exposed to process environments was shown to be negligible (see Table II-26). The effect of exposing a specimen to air after each process cycle (see Table II-27) was shown to be small, the corrosion rate increasing from 8 to about 12 mils/yr. This increase is not regarded as being significant.

## 4. Basic Studies of Fluidized-Bed Behavior Related to Process Operations

(D. RAMASWAMI)

### Particle Residence Times at Surfaces of a Gas-Fluidized Bed (L. B. KOPPEL)\*

Experimental and theoretical investigations have been initiated to measure the statistical distribution of particle residence times at solid surfaces in contact with a gas-fluidized bed. The objective of this work is to utilize the residence time distributions to predict heat transfer coefficients, using an equation developed previously:<sup>23</sup>

$$\frac{hD_p}{k_g} = \frac{4\pi/\sqrt{3}}{\left[1 + \frac{12k_g \bar{\theta}}{\rho_s C_s D_p^2 (\alpha + 1)}\right] (\alpha + 1)}$$

where

- $h$  = bed-to-surface heat transfer coefficient
- $D_p$  = particle diameter
- $k_g$  = gas thermal conductivity
- $\rho_s$  = solid density
- $C_s$  = solid specific heat
- $\bar{\theta}$  = average residence time of particles at the heat transfer surface
- $\alpha$  = shape factor in statistical distribution of particle residence times at the surface, to be discussed below.

This equation has been shown to compare favorably with heat transfer data, regarding the qualitative dependence of  $h$  on the thermal properties  $k_g$  and  $C_s$ , but cannot be used as an independent predictor of heat transfer coefficients without quantitative knowledge of the parameters  $\bar{\theta}$  and  $\alpha$ .

In the previous studies the statistical distribution of residence times had been assumed to be of the gamma form,

$$f(\theta) = \frac{1}{\alpha! \bar{\theta}^\alpha} \left[ (\alpha + 1) \frac{\theta}{\bar{\theta}} \exp\left(-\frac{\theta}{\bar{\theta}}\right) \right] (\alpha + 1)$$

where  $f(\theta) d\theta$  is the fraction of surface particles which reside at the surface for a time between  $\theta$  and  $\theta + d\theta$ . The parameter  $\alpha$  characterizes the shape of the distribution. The current investigations have been directed toward correlation of parameters  $\bar{\theta}$  and  $\alpha$  as functions of the physical and flow properties of the system. The advantage of this approach is that there should be no effect of thermal properties on these parameters and,

therefore, the necessary correlation effort is significantly reduced.

Three possible techniques for measurement of  $\bar{\theta}$  and  $\alpha$  have been investigated. The surface studied was a small test area on the wall of a  $5\frac{1}{2}$ -in. dia. Lucite column containing nominal 60 mesh, alumina particles (Type 38 Alundum, manufactured by Norton Co.) fluidized with air. A small fraction, 0.3%, of the particles was dyed with India ink for easy observation. The techniques were:

(1) *Direct photographic observation of individual black particles in the test area.* The individual particles were observed in successive frames, a new frame being exposed every 0.3 sec. By noting the number of frames between the appearance and disappearance of a particle at the test area, its residence time may be estimated. A histogram of these residence times, taken for several particles, yields the distribution, and, hence, fitted estimates of  $\alpha$  and  $\bar{\theta}$ . This technique was demonstrated to yield good results, but is tedious and time-consuming. It is believed unlikely that sufficient data can be obtained in this manner without expenditure of an unreasonable experimental effort.

(2) *Photographic observation of transients in the total count of black particles in the test area.* In theory, one can release a quantity of black particles into the column and deduce the residence time distribution by differentiation of the transient rise in the total number of black particles in the test area. This technique eliminates the need for observation of individual particles. Furthermore, the total particle counts were determined directly from the film, with encouraging accuracy, by means of the CHLOE digital automatic data reduction technique.<sup>24</sup> However, practical experimental problems precluded use of this method for accurate measurement of residence times.

(3) *Calculation of the autocorrelation function of total particle counts.* It was demonstrated theoretically that the autocorrelation of the frame-to-frame statistical fluctuations in total black particle counts, at steady-state conditions, yields the average residence time,  $\bar{\theta}$ . Preliminary experimental verification has been achieved for a specific set of conditions. Here again, the films are processed automatically, which fact makes it possible to secure large quantities of data. Development work is still required to improve the accuracy of the CHLOE particle counts.

The autocorrelation technique was deemed to have

\* Consultant, Purdue University.

<sup>23</sup> Ziegler, E. N., L. B. Koppel and W. T. Brazelton, Ind. Eng. Chem. Fundamentals, **3**, 325 (1964).

<sup>24</sup> Private communication from Butler, J. W., Applied Mathematics Division, Argonne National Laboratory.

the greatest value in this work, and current plans are to concentrate on development of this method. The first step will be establishment of a method for the estimation of  $\alpha$ . To this end, calculations are in progress to generate simulated, random particle counts from known, assumed residence time distributions. The fluctuations in these counts will be examined for statistical inference of the known value of  $\alpha$ .

As soon as the two major problems, i.e., improvement of accuracy of CHLOE counts and development of an estimation of  $\alpha$ , are resolved, the autocorrelation method will be used to determine residence time distributions as functions of the physical and flow properties. The distributions so obtained will be used to predict heat transfer coefficients, and the predictions will be compared with experimental data.

# III. High Temperature Reactor Materials Development\*

(R. K. Edwards, H. M. Feder)

A program directed toward the development of high temperature nuclear reactor materials is under way. The objective is to build up a reservoir of basic data which may be used for screening and evaluation. The study will be concerned with the chemical stability of potential high temperature fuels, i.e., oxides, phosphides, sulfides, arsenides, and nitrides of uranium and their solid solutions; and with the reactions of these fuels with hydrogen, its contaminants, and supporting structural materials such as tungsten, rhenium, molybdenum, tantalum, and certain alloys. These studies will be done quantitatively to yield thermodynamic and phase-diagram information. Each selected fuel-

refractory metal-gas system is to be studied in an integrated way, using several methods of investigation that are mutually supporting.

The emphasis of current experimentation is on the determination of the phase diagram of the condensed state of the uranium-urania system and on the equilibria between the vapor and condensed phases of this system. Equipment being constructed for studies in the hydrogen-uranium-urania system is mostly completed and undergoing initial testing. Experimental work to determine phase relations in the tungsten-uranium-urania triangle is projected. The study of the uranium-uranium monosulfide phase diagram has also been initiated.

\* A summary of this section is given on page 12.

## A. CURRENT STATUS OF HIGH TEMPERATURE PHASE RELATIONS AND THERMODYNAMIC PROPERTIES IN THE URANIUM-URANIA SYSTEM

### I. Objectives, Experimental Plans, and Recent Experimental Results

The specific objective of the studies of the uranium-urania\*\* system is to obtain comprehensive thermodynamic data for compositions from pure uranium to slightly hyperstoichiometric urania.

The phase diagram for the condensed system is of importance in guiding and interpreting the thermodynamic experimentation. This work (Section III-B) has advanced to the point that considerable detail can be given; the results are presented in Figure III-1. As was considered probable (ANL-6800, pp. 297-300), it has been found that urania at high temperature can exist at compositions which are hypostoichiometric.

The thermodynamic properties of this system are to be determined by establishing the partial pressures of all the vaporizing species as functions of the temperature and composition of the condensed phases. Studies of the vaporization of the condensed phases through

Knudsen effusion orifices or into transpiration carrier gases are in progress. The Knudsen effusion method is inherently limited to low gaseous pressures; thus, the effusion studies will be restricted to below about 2200°C. The transpiration method may possibly be pursued to 2800°C with the apparatus on hand.

The significant gaseous species in this system are U, UO, UO<sub>2</sub>, UO<sub>3</sub>, O, and O<sub>2</sub>. Their relative partial pressures vary considerably with the composition of the condensed phase(s). Knudsen effusion measurements yield  $R$ , the total rate of effusion of uranium-bearing species in moles per unit orifice area:

$$R = R_U + R_{UO} + R_{UO_2} + R_{UO_3}. \quad (1)$$

The partial pressure of each species is related to its rate of effusion by

$$P_i = R_i \sqrt{2\pi k T M_i} = a R_i \sqrt{M_i}, \quad (2)$$

in which  $k$  is the Boltzmann constant,  $T$  is absolute temperature, and  $M_i$  is its molecular weight. The total pressure,  $P$ , of uranium-bearing vapor species is then,

$$P = a(R_U \sqrt{M_U} + R_{UO} \sqrt{M_{UO}} + R_{UO_2} \sqrt{M_{UO_2}} + R_{UO_3} \sqrt{M_{UO_3}}). \quad (3)$$

\*\* The term urania will be used in Section III to denote a phase of fluorite structure with composition unspecified; the symbol UO<sub>2</sub> will be used to denote stoichiometric uranium dioxide. The terms hyperstoichiometric and hypostoichiometric refer to the oxygen in UO<sub>2</sub>; the symbols UO<sub>2-x</sub> and UO<sub>2+x</sub> denote hypostoichiometric and hyperstoichiometric urania, respectively.

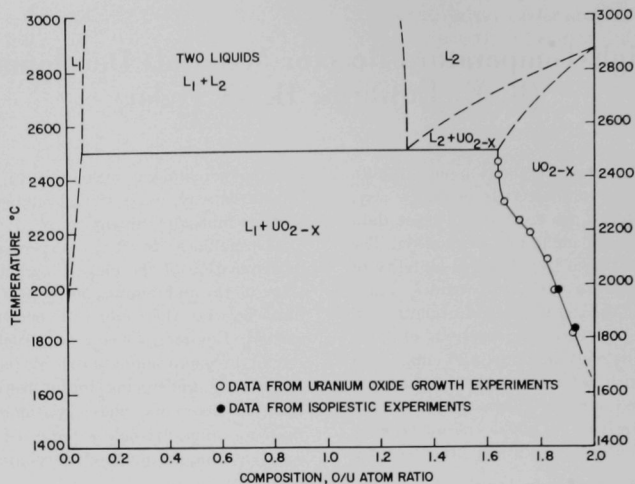


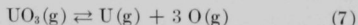
FIG. III-1. Uranium-Uranium Phase Diagram at Elevated Temperatures.

The transpiration method measures the total pressure of uranium-bearing vapor species:

$$P = P_U + P_{UO} + P_{UO_2} + P_{UO_3}$$

When this method is used it is generally desirable to employ a buffering carrier gas. In the present studies, the buffering carrier gas will consist of hydrogen and water vapors of measured concentrations, in order to render the system invariant by fixing the composition of the solid at each temperature. The invariance ensues from fixing the values of  $P_O$  and  $P_{O_2}$ , which are accurately calculable from well-established thermodynamic data for the  $H_2$ ,  $H_2O$ ,  $O$ , and  $O_2$  species.

Mass spectrometric determinations of the ratios of species emanating from Knudsen effusion cells are being carried out in order to obtain the information required to separate the variables in Equations 3 and 4. Such data are most conveniently summarized by equilibrium constants for the gaseous reactions; e.g.,



These constants should be carefully determined as functions of temperature so that they may be reliably extrapolated to the temperatures used in the transpiration measurements. Thus all the partial pressures in Equation 4 become explicitly calculable when a buffering carrier gas is used for the transpiration measurements.

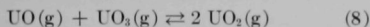
A nearly complete set of measurements of total rates of effusion has been collected for the two-phase system uranium (liquid, saturated with  $UO_{2-x}$ ) in equilibrium with  $UO_{2-x}$  (solid, saturated with uranium). Tentative values of the total pressures of uranium-bearing species were calculated by Equation 3 with the use of the approximation that the molecular weight of each species was the same as that of  $UO$ . The mass spectrometric results showed that this approximation was satisfactory to within a few percent. The results for the two-phase system are shown in Figure III-2. Also shown is the vapor pressure (total for uranium-bearing species) data for solid  $UO_{2.00}$  taken from the excellent study of Ackermann, Gilles, and Thorn.<sup>1</sup> Comparison of the curves shows that the vapor pressure over the two-phase system is a factor of from 10 to 4 higher than over  $UO_{2.00}$  in the range 1300 to 2000°C, respectively.

A considerable number of Bendix T-O-F (Time-Of-Flight) mass spectrometric observations of the relative concentrations of effusing species have been made for the two-phase system. However, problems have arisen which cast doubt on the quantitative results reported previously (ANL-6900, p. 35 and pp. 208-212); the data are being reevaluated for presentation in a later report. Qualitatively, it is clear that over the two-phase system the predominant species (by about a factor of 10) is  $UO(g)$ , that  $U(g)$  and  $UO_2(g)$  are

<sup>1</sup> Ackermann, R. J., P. W. Gilles and R. J. Thorn, *J. Chem. Phys.* **25**, 1089 (1956).

each present at conveniently measurable concentrations, and that  $\text{UO}_3(\text{g})$  is only barely measurable with the present sensitivity. When the data are evaluated and shown to be reliable, the species ratios will be used in Equation 3 to obtain partial pressure values.

In later experiments, hydrogen gas at low pressures will be passed over the two-phase system in an effusion cell within the mass spectrometer and the  $P_{\text{H}_2}/P_{\text{H}_2\text{O}}$  ratio in the effusate will be observed. When equilibrium is established, such a system is invariant at each temperature by virtue of the presence of the two condensed phases. If the partial pressures of the uranium-bearing species are known from the evaluation discussed above, the  $P_{\text{H}_2}/P_{\text{H}_2\text{O}}$  ratios fixed by the system permit the determination of the equilibrium constants for Equations 5 and 6. The available mass spectrometric data indicate that to obtain comparable information for Equation 7, the solid urania composition must be stoichiometric or hyperstoichiometric. At the stoichiometric composition, the partial pressures  $P_{\text{VO}}$  and  $P_{\text{VO}_2}$  are of nearly the same magnitude and  $P_{\text{VO}_2}$  is a factor of 50 to 100 times higher. However, rough calculations indicate that  $P_{\text{V}}$  is likely to be too small for measurement. The equilibrium constant for the reaction,

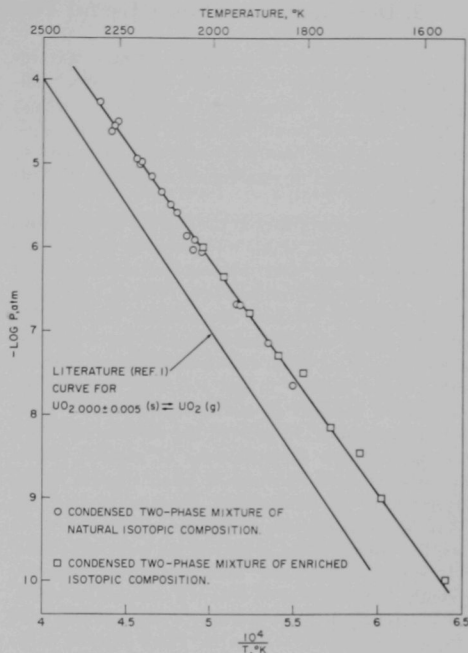


could be determined and, when used together with the constants for Equations 5 and 6, would yield the desired constant for Equation 7. Alternatively, it may be possible to achieve greater accuracy by using a buffering ratio of  $\text{H}_2/\text{H}_2\text{O}$  which fixes the solid phase at a composition  $\text{UO}_{2+x}$  such that  $P_{\text{VO}_2}$  and  $P_{\text{VO}_3}$  are nearly equal. In this case the equilibrium constant for the reaction



would be determined. It is clear from the thermodynamic analyses, and confirmed by the accumulated mass spectrometric data, that as the solid phase changes from  $\text{UO}_2$  to  $\text{UO}_{2+x}$ ,  $P_{\text{VO}_2}$  will decrease slowly,  $P_{\text{VO}}$  will decrease more rapidly, and  $P_{\text{VO}_3}$  will increase rapidly. Hence, the desired condition of  $P_{\text{VO}_2} \cong P_{\text{VO}_3}$  is probably attainable.

The two-phase system will also be studied by the transpiration method in order to extend the data of Figure III-2 to 2500°C, if possible. Either an inert carrier gas or hydrogen may be used for this system. The use of hydrogen together with determination of the  $\text{H}_2/\text{H}_2\text{O}$  ratio at the output end of the apparatus may make possible the evaluation of  $P_{\text{O}}$  and  $P_{\text{O}_2}$  over the two-phase system. However, the equilibrium pressure of  $\text{H}_2\text{O}(\text{g})$  must be reached and must be sufficient



108-8539

FIG. III-2. Total Vapor Pressure over the Uranium-Urania Two-Phase System. (Study of the equilibrium  $\text{U}(\text{liquid, saturated with } \text{UO}_{2-x}) + \text{UO}_{2-x}(\text{solid, saturated with U}) \rightleftharpoons \text{U}(\text{g}), \text{UO}(\text{g}), \text{UO}_2(\text{g})$ ; total pressure calculated assumes a mean molecular weight corresponding to that for  $\text{UO}$ .)

so that back reaction with the transported uranium-bearing species does not contribute an appreciable error to the observed  $\text{H}_2/\text{H}_2\text{O}$  ratio. If this approach is unsuccessful, the species ratio data from the mass spectrometer studies will be extrapolated to the required temperatures in order to separate the variables in Equation 4.

The vapor pressures over urania throughout its existence range will be studied using  $\text{H}_2\text{-H}_2\text{O}$  buffering mixtures in both the mass spectrometric and transpiration experimentation. In this work the buffering gaseous mixtures are to be equilibrated with the solid phase until constant compositions are reached. The compositions will then be established by chemical analyses.

The investigations discussed above should yield a family of isotherms of partial pressures of each of the species versus solid composition and thereby permit the calculation of the desired thermodynamic functions.

## 2. Development of Some Useful Theoretical Guidelines for Experimentation

Theoretical analysis of the results of mass spectrometric measurements of gaseous species over (unbuffered) solids of composition ranging from  $\text{UO}_{2.095}$  to  $\text{UO}_{1.995}$  has led to an important general principle not known to have been previously put forth, and to some consequences of significance in guiding the experimentation.

Considerable variability in the gaseous species ratios  $P_{\text{VO}_2}/P_{\text{VO}_2}$  and  $P_{\text{VO}_3}/P_{\text{VO}_2}$  was observed in the mass spectrometer when solid uranium dioxide samples of the same nominal composition ( $\text{UO}_{2.000 \pm 0.005}$ ) were studied. Also, at constant temperature and starting with the initial composition  $\text{UO}_{2.095}$ , a rapid decrease in the  $P_{\text{VO}_3}/P_{\text{VO}_2}$  ratio was observed simultaneously with a rapid increase in the  $P_{\text{VO}_2}/P_{\text{VO}_2}$  ratio as the composition changed in stoichiometry toward lower O/U atomic ratios. In general, the observations show that the relative concentrations of gaseous species are very sensitive functions of small changes in the stoichiometry of solid uranium. Because of this, the following thermodynamic arguments were used to establish criteria to aid in guiding the experimentation.

It appears established<sup>1</sup> that uranium vaporizes congruently (from an effusion cell) at a composition which, if not precisely  $\text{UO}_2$ , is probably within  $\pm 0.005$  units of the stoichiometric O/U ratio. There must be either a maximum or a minimum in the total pressure for the congruency condition to obtain. (The effusion condition causes only a minor effect in the system under discussion.) The data of Figure III-2 demonstrate that the total pressure of uranium-bearing species is about a factor of 10 lower over  $\text{UO}_2$  than over the hypostoichiometric composition at the uranium-rich phase boundary. The contribution from the species O and  $\text{O}_2$  can be shown to be negligible. Therefore, congruency occurs at a minimum pressure rather than at a maximum pressure. But the mass spectrometric results have shown that  $\text{UO}_2(\text{g})$  is the major species during congruent effusion and that  $\text{UO}(\text{g})$  and  $\text{UO}_3(\text{g})$  are each much lower in concentration.  $P_{\text{VO}_2}$  must reach a maximum at some composition of the condensed uranium-oxygen binary system. One might intuitively expect that this composition is in the vicinity of  $\text{UO}_2$ . There thus seems to be a possible conflict in the expected occurrence of a maximum  $P_{\text{VO}_2}$  at a solid composition near  $\text{UO}_2$  while the vapor above it, which consists predominantly of  $\text{UO}_2(\text{g})$ , reaches a minimum in total pressure. It seemed worthwhile to determine, if possible, through thermodynamic arguments the solid composition at which  $P_{\text{VO}_2}$  is a maximum.

The following general equation for a condensed binary A-B system at equilibrium with its gas phase

was developed by means of the Gibbs-Duhem relation and equilibrium relationships for the gaseous species:

$$\left(\frac{\partial \ln P_{A_a B_b}}{\partial \ln P_B}\right)_T - z + \left(\frac{V_c}{RT}\right)\left(1 + \frac{b}{a} + z\right) \left[ \left( \sum_{j=0}^{\infty} \sum_{i=0}^{\infty} j P_{A_i B_j} \right) - \frac{b}{a} \left( \sum_{i=0}^{\infty} \sum_{j=0}^{\infty} i P_{A_i B_j} \right) \right] = \frac{1}{a} \left[ 1 - \left(\frac{V_c}{RT}\right)\left(1 + \frac{b}{a} + z\right) \left( \sum_{i=0}^{\infty} \sum_{j=0}^{\infty} i P_{A_i B_j} \right) \right] \quad (10)$$

The symbols are identified as follows:

$P_{A_a B_b}$  = partial pressure in the gas phase of a particular species of the molecular formula  $A_a B_b$ ;

$P_B$  = partial pressure in the gas phase of the component B;

$z$  = composition variable representing the deviation of the condensed phase from the stoichiometric  $b/a$  ratio in the formulation  $A B_{b/a+z}$ ;

$V_c$  = molar volume of the condensed phase at the temperature  $T$ ;

$R$  = gas constant; and

$i, j$  = running indices representing the atoms per molecule for all possible gaseous molecules.

The equation is exact except for the assumption of ideal gas behavior. By setting the derivative equal to zero, one can show that for systems at high temperature and low pressure a maximum in  $P_{A_a B_b}$  occurs when  $z$  is an exceedingly small value, that is, the partial pressure of the  $A_a B_b$  species goes through a maximum when the solid phase has the stoichiometry of that gaseous species. A maximum with respect to  $\ln P_B$  also requires a maximum with respect to  $X_B$ , the gram-atom fraction of component B in the solid phase, since  $P_B$  must be a continuously increasing function of  $X_B$ . For the uranium-oxygen binary system, in the composition range encompassing the uranium phase, the result of the application of Equation 10 is

$$\left(\frac{\partial \ln P_{\text{VO}_2}}{\partial \ln P_{\text{O}_2}}\right)_T - z + \left(\frac{V_c}{RT}\right)(3 + z) = \frac{(P_{\text{VO}_3} + P_{\text{O}_2} + 2P_{\text{O}_2} - 2P_{\text{U}} - P_{\text{VO}_2})}{1 - \left(\frac{V_c}{RT}\right)(3 + z)(P_{\text{U}} + P_{\text{VO}_2} + P_{\text{VO}_3} + P_{\text{VO}_2} + P_{\text{VO}_3})} \quad (11)$$

The use of available order-of-magnitude data leads to  $z(\text{at max.}) \cong \pm 10^{-10}$  at 2000°K.

Except at values of  $z \cong \pm 10^{-10}$ , the very small terms involving the volume of the condensed phase in Equation 11 may be neglected and the equation may be rewritten,

$$\left( \frac{\partial \ln P_{\text{O}}}{\partial \ln P_{\text{UO}_2}} \right)_T = -\frac{1}{z}. \quad (12)$$

Similar equations may be derived for the other important species:

$$\left( \frac{\partial \ln P_{\text{UO}}}{\partial \ln P_{\text{UO}_2}} \right)_T = \frac{1+z}{z}, \quad (13)$$

$$\left( \frac{\partial \ln P_{\text{UO}_3}}{\partial \ln P_{\text{UO}_2}} \right)_T = -\frac{1+z}{z}, \quad (14)$$

$$\left( \frac{\partial \ln P_{\text{U}}}{\partial \ln P_{\text{UO}_2}} \right)_T = \frac{2+z}{z}. \quad (15)$$

The form of the derivatives in these expressions was chosen to permit inspection of the behavior of each species with reference to  $\text{UO}_2(\text{g})$ , a species whose partial pressure is known to be the least sensitive to changes in the composition of uranium (see estimates below). Equations 12 to 15 demonstrate that the partial pressures of all the other species, however, are highly sensitive to variations in the stoichiometry of the condensed phase. This is illustrated by some recent data obtained at 2100°C. On going from solid  $\text{UO}_{1.82}$  to solid  $\text{UO}_2$ , the partial pressures changed by the following factors:  $\text{UO}_2$ , 3.64;  $\text{UO}$ ,  $2.8 \times 10^{-3}$ ;  $\text{UO}_3$ ,  $4.7 \times 10^3$ ;  $\text{U}$ ,  $2.1 \times 10^{-6}$ ;  $\text{O}$ ,  $1.3 \times 10^3$ .

An extreme variability of ratios of gaseous species over the solid in the vicinity of  $\text{UO}_2$  is predicted by these equations and was observed in the mass spectrometer for different samples of nominal  $\text{UO}_2$ . The variations may arise from composition differences too small to be discerned by existing analytical procedures. (It is, of course, worth bearing in mind that small variations in sample contamination could also produce the same effects if the contaminants were of an oxidizing or reducing character.)

On one important point, the analysis given above leads to the same conclusion as do theoretical treatments<sup>2</sup> based on solid state models for nonstoichiometric compounds, namely, the partial pressure of oxygen is expected to be inordinately sensitive to small deviations in  $z$ . This factor greatly magnifies the difficulty of obtaining reliable thermodynamic data for those compositions of greatest interest to the testing of the theoretical models. The point is well

demonstrated in the paper by Hagemark *et al.*<sup>3</sup> which compares the results of several investigations on hyperstoichiometric uranium. Although generally good agreement is found for compositions  $z \gtrsim 0.001$ , gross disagreement, even to the extent of opposite signs, is found for the compositions  $z < 0.01$ .

The mathematical analysis and the observations to date have led to a better understanding of the experimental procedures which need special concern if reliable thermodynamic values are to be obtained for uranium and, particularly, for nearly stoichiometric uranium. First, it is important that compositions of solids be controlled to precise values during the collection of condensable vapors if the results are to be translated into equilibrium pressure values, as, for example, in transpiration measurements. Secondly, there is a need to know the composition of the solid phase with greater precision and accuracy than current limitations in chemical analysis permit.

With regard to the first of these considerations, the appropriate procedure is to make use of a buffering technique. This is one of the prime reasons for using  $\text{H}_2$ - $\text{H}_2\text{O}$  mixtures in the carrier gas in the transpiration measurements. Another equally important reason is that oxygen partial pressures are directly calculable from the  $\text{H}_2/\text{H}_2\text{O}$  concentration ratios used. As was noted earlier, some of the mass spectrometric measurements will also make use of this buffering gas.

The mass spectrometric, torsion, and continuous recording effusion techniques, which give essentially instantaneous observations, can circumvent the problem of composition change during the observation and may be used if there is a way of relating the observed values to the composition of the solid phase. The thermodynamic analysis suggests how this may, in principle, be done through the use of Equations 12 to 15. Consider mass spectrometric measurements on the vapor effusing from solid  $\text{UO}_{2+z}$  which has initially a value of  $z$  corresponding to a point on the hypostoichiometric phase boundary. It is known that at a given temperature the value of  $z$  will continuously shift until the congruently effusing composition (very near  $\text{UO}_2$ ) is reached. Thus if a continuous record of the ion intensities,  $I_i$ , of each of the two dominant species,  $\text{UO}(\text{g})$  and  $\text{UO}_2(\text{g})$ , were obtained for this composition range, the slope of a  $\log I_{\text{UO}}$  vs.  $\log I_{\text{UO}_2}$  curve would establish the composition of the solid phase for any pair of values of  $I_{\text{UO}}$  and  $I_{\text{UO}_2}$ . This follows from the fact that  $I_i$  is directly proportional to  $P_i$  and from Equation 13. The precision with which the data can be fitted with an analytical expression

<sup>2</sup> Anderson, J. S., "Nonstoichiometric Compounds," Advances in Chemistry Series, No. 39, American Chemical Society, Washington, D.C., 1963, Ch. 1, p. 6.

<sup>3</sup> Hagemark, K., KR-67, Institutt for Atomenergi, Kjeller Research Establishment, Kjeller, Norway, February 1964.

will determine the precision of the value of  $z$ . The accuracy of  $z$  will depend on how closely the proportionality constants (principally instrumentation parameters and temperature) between  $I_i$  and  $P_i$  can be held truly constant for a given set of data. There would be, of course, an error contributed by impurities in the sample, or by nonequilibrium within the effusion cell during measurement. The results from the chemical analysis procedure that is considered to be most reliable (oxidation of the  $\text{UO}_{2+z}$  sample to  $\text{U}_3\text{O}_8$ ) suffer from: (a) uncertainty in the absolute composition of  $\text{U}_3\text{O}_8$ , (b) uncertainty in the gram-atomic weight of uranium, (c) uncertainty due to sample contaminants, (d) uncertainty in weighing, particularly for small samples, and (e) possible oxygen pickup of the  $\text{UO}_{2+z}$  sample prior to the performance of the chemical analysis.

## B. EXPERIMENTATION IN THE URANIUM-URANIA SYSTEM

### I. Effusion Vapor Pressure Studies (M. S. CHANDRASEKHARAI AH, R. K. EDWARDS, P. M. DANIELSON)

Vapor pressure measurements in the range 1300 to 2000°C have been carried out by the effusion method for the two-phase system, uranium (liquid, saturated with  $\text{UO}_{2-x}$ ) in equilibrium with  $\text{UO}_{2-x}$  (solid, saturated with uranium). This study is being conducted in collaboration with R. J. Thorn and R. J. Ackermann of the Chemistry Division. The effusion apparatus and procedure that is being used have been described in a previous report (ANL-6900, p. 203). Some of the measurements carried out during the present report period employed enriched uranium-urania mixtures in order to increase the sensitivity of analysis of the effusates. In these cases no attempt was made to fabricate crucibles from the enriched urania; instead, contact between uranium and urania was established within a tantalum cup which was placed in the tungsten effusion cell. The data obtained to date are presented in Figure III-2. (Because of some minor corrections which are now being calculated, the series C measurements reported in Table III-1, p. 206 of ANL-6900 are not included in Figure III-2.) Another series

of effusion measurements for the low temperature region is in progress and, when completed, a report covering the entire study will be prepared.

It seems possible that by the thermodynamic approach outlined above the values of  $z$  can be determined to a higher degree of accuracy than that possible by chemical analysis. Edwards and Brodsky<sup>4</sup> were the first to apply this type of thermodynamic approach for the determination of compositions to effusion systems. In their work the error in the compositions of the gas phase, as determined by chemical analysis of very small collections of effusate, was considerably reduced by the thermodynamic evaluation.

The remainder of Section III presents the status of current experimentation, classified according to the different methods being utilized.

<sup>4</sup> Edwards, R. K., M. B. Brodsky, *J. Am. Chem. Soc.* **78**, 2893 (1956).

Two measurements were carried out by an isopiestic equilibration technique to obtain compositions at the hypostoichiometric boundary of the urania phase. A tantalum crucible with a tight-fitting lid was out-gassed by heating in vacuum at 2100°C for 2 hours. A thin-walled urania cup containing uranium metal was centered in this crucible. Small pellets of urania were placed in the annular space between the oxide cup and the tantalum crucible wall. The crucible assembly was evacuated ( $<10^{-6}$  torr) and heated slowly to the desired temperature for a few hours. After cooling in vacuum, the crucible lid was opened and the oxide pellets were carefully removed and analyzed for oxygen content. The results obtained are included in Figure III-1. Some additional isopiestic equilibrations with longer reaction periods will be carried out to evaluate whether true saturation was achieved.

## 2. Mass Spectrometric Effusion Studies (J. W. REISHUS, J. E. BATTLES, R. K. EDWARDS, P. M. DANIELSON)

Measurements of the relative concentrations of gaseous species in equilibrium with condensed phases of the uranium-urania system have been undertaken. In this study, a mass spectrometer (Bendix T-O-F) is being used to determine the concentrations of the various species in the vapor effusing from a Knudsen effusion cell.

During this report period, measurements have been

carried out on a number of solid urania samples having different O/U ratios. The results have helped to define optimum conditions for experimentation. Several instrumentation problems were also revealed and for this reason none of the data is being reported at this time. However, some of the qualitative results obtained and their theoretical implications have been discussed in Section III A-2.

## 3. Transpiration Studies of Vaporization (M. TETENBAUM, P. D. HUNT)

The essential features of the transpiration apparatus for vapor pressure measurement have been previously described (ANL-6900, p. 214). Assembly of the transpiration apparatus including the carrier gas manifold system has been completed. The system includes a moisture monitor (electrolytic cell type) attached to the manifold on both inlet and outlet sides of the transpiration chamber. An optical pyrometer is sighted through the condenser tube and is used to observe the sample temperature. The volume of carrier gas used during a measurement is measured by means of a wet test meter located at the exit side of the apparatus.

Exploratory experiments using argon as the carrier gas have been carried out with solid  $UO_2$  and with the two-phase system, uranium (liquid, saturated with urania) in equilibrium with urania (solid, saturated with uranium). The object of these experiments was

the testing of the operational characteristics of the apparatus. In particular, a preliminary evaluation was desired of the range of carrier gas flow rates suitable for the samples and experimental arrangement being used. The condensed uranium-bearing material which was collected in the tungsten condenser tube was dissolved by repeated elutions with hot concentrated nitric acid. The solutions were assayed for uranium by fluorophotometric analysis.

The preliminary work indicates that saturation of the carrier gas with vaporizing species is achieved at flow rates of 30 to 55 cc/min for the two-phase system and 60 to 120 cc/min for the solid  $UO_2$ . The most recently measured total pressures for solid  $UO_2$  fall very well on the appropriate curve of Figure III-2, thereby indicating that the apparatus is functioning properly. Additional testing will be conducted.

## 4. Uranium-Urania Phase Diagram Studies (A. E. MARTIN, F. C. MRAZEK, G. E. GUNDERSON)

As previously reported (ANL-6900, p. 215), the uranium-urania system was found to contain a very wide miscibility gap at elevated temperatures, thereby implying the existence of a monotectic. The monotectic reaction may be written as



where  $L_1$  is the uranium-rich liquid,  $L_2$  is the uranium oxide-rich liquid, (the monotectic liquid), and  $UO_{2-x_m}$  is the solid urania phase at the monotectic temperature. The monotectic reaction goes to the right on heating and to the left on cooling.

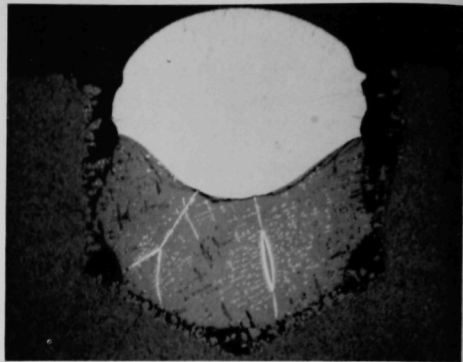
Additional experiments have been carried out to establish (a) the composition of the monotectic liquid, (b) the monotectic temperature, (c) the solidus line in the system below the monotectic temperature, i.e., the

hypostoichiometric boundary of the urania phase, and (d) the liquidus line in the system below the monotectic temperature, i.e., the solubility of urania in liquid uranium.

Previous examination (ANL-6900, p. 216) of arc-melted products had indicated the approximate composition of the monotectic, but these findings had been rendered somewhat questionable by the subsequent finding of uranium nitride as a minor contaminant phase. The source of the nitrogen in the arc melting process was found and eliminated so that recent preparations have been free of uranium nitride. The recent findings with nitride-free products are essentially the same as before. To date, the two arc-melted products which appear to have compositions closest to the monotectic composition correspond to O/U atomic

ratios of 1.25 and 1.35. The 1.25 product is obviously hypomonotectic since the microstructure contains globules of the uranium-rich phase in a monotectic-structure matrix; the 1.35 product is presumably hypermonotectic since it contains none of these globules. These observations indicate that the monotectic is at a composition with an O/U ratio of  $1.30 \pm 0.05$ .

The monotectic temperature in the uranium-urania system was established by a simple procedure. A small urania crucible, 0.5 in. in dia., was charged with an amount of uranium such that the overall composition corresponded to an O/U ratio of about 1.4. This crucible was placed on a urania support within a tungsten crucible. The tungsten crucible was fitted with a cover containing a hole through which reaction zone temperatures could be observed. Contact between the urania crucible and its support was held to a minimum by means of some coarse grains of urania. Assemblies of this type were heated with a tungsten resistance furnace in a helium atmosphere for half-hour periods at temperatures known from preliminary experiments to be near the monotectic temperature. After cooling to room temperature, the products were examined for evidence that the monotectic temperature had been reached. The highest temperature at which a uranium ingot was found within a still intact urania crucible was  $2475 \pm 20^\circ\text{C}$ , a temperature obviously below the mono-



108-8024

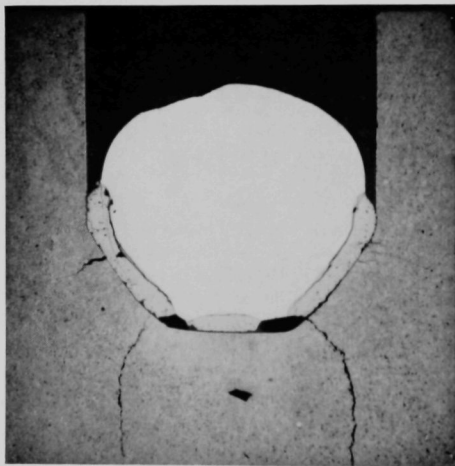
FIG. III-4. Growth Layer of Hypostoichiometric Urania between Liquid Uranium and Urania Crucible. (Growth at  $2300^\circ\text{C}$  after  $\frac{1}{2}$  hour.)

Specimen: as polished  
Crucible: 1 inch OD

tectic temperature. However, in an experiment at  $2495 \pm 20^\circ\text{C}$ , no uranium ingot was found. Apparently, the uranium liquid had reacted with the urania crucible to form the monotectic liquid which flowed down to the urania support. Thus the temperature of this experiment was above the monotectic temperature. The monotectic temperature, therefore, is indicated as being at  $2485 \pm 30^\circ\text{C}$ .

It was also observed in the experiments carried out below the monotectic temperature that the uranium ingots were separated from the urania crucibles by layers of oxide which presumably had grown by a diffusion process. These oxide growths formed at temperatures even as low as  $1800^\circ\text{C}$ . The thickness of the growths increased both with time and with temperature. Growths which formed in half-hour periods at  $1800$  and  $2300^\circ\text{C}$  are shown in Fig. III-3 and III-4, respectively. The oxide growths contain uranium metal as a dispersed phase both at grain boundaries and within the oxide grains. Obviously, the uranium phase had precipitated from solid solution during cooling. X-ray diffraction examinations of the growths at room temperature disclosed only  $\text{UO}_2$  as the major phase and alpha uranium as the minor phase. Except for microporosity due to tear-outs from the polishing operation and to shrinkage following precipitation and freezing of uranium, the growths are free of porosity. However, as shown in the photomicrographs, there is considerable porosity at the junction of the growths with the crucibles.

The oxide growths had formed in contact with the liquid uranium and, thus, were assumed to consist of



108-8023

FIG. III-3. Growth Layer of Hypostoichiometric Urania between Liquid Uranium and Urania Crucible. (Growth at  $1800^\circ\text{C}$  after  $\frac{1}{2}$  hour.)

Specimen: as polished  
Crucible: 1 inch OD

urania saturated with uranium at the temperature of the experiment. It appeared feasible, therefore, to establish the hypostoichiometric boundary of the urania phase by the chemical analysis of growths formed at various temperatures. Accordingly, similar experiments were carried out, but with larger crucibles (1-in. dia.) in order to obtain larger growths for analysis. The holding periods at temperature were varied by trial and error to achieve a useful amount of growth while still retaining the essential contact with the liquid uranium. In a few experiments at the lower temperatures, too short holding periods were employed with the result that insufficiently large growths were obtained; whereas in an experiment at about 2430°C, too long a holding period (2.5 hr) was used with the result that the uranium melt was ejected from the crucible by the growth. The results of the successful experiments are given in Table III-1.

Data for the hypostoichiometric boundary of urania are presented in the phase diagram given in Figure

TABLE III-1. DATA ON OXIDE GROWTH EXPERIMENTS AT TEMPERATURES BELOW THE MONOTECTIC IN THE URANIUM-URANIA SYSTEM

Temp. (°C)	Time at Temp. (hr)	Weight of Oxide Growth (g)	O/U Atom Ratio of Oxide Growth
1813	22	3.5	1.92
1978	7.5	2.9	1.85
2084	4	4.3	1.83
2188	4	4.0	1.76
2236	2	7.2	1.72
2306	2.5	8.4	1.67
2410	1	5.0	1.64
2455	1	6.7	1.64

III-1. These data are self-consistent to the extent that there is a progressive change in the composition with temperature. The data are also consistent at lower temperatures with two values obtained from isopiestic experiments.

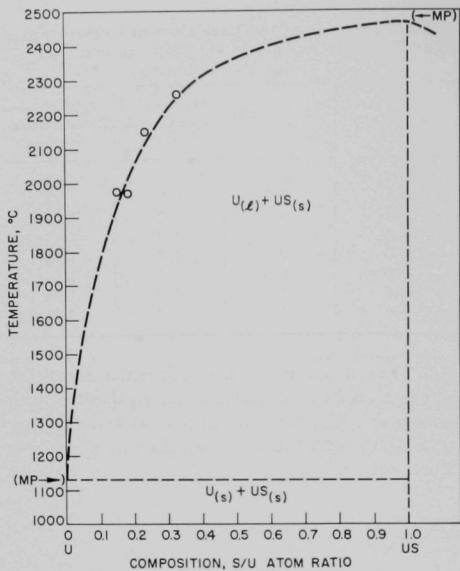
## C. URANIUM-URANIUM MONOSULFIDE PHASE DIAGRAM STUDIES (L. N. YANNOPOULOS)

Previous work (ANL-6900, p. 219) on uranium monosulfide was concerned with the study of its diffusion through tungsten. However, the diffusion rate was found to be too low to warrant further study and led to the conclusion that dense tungsten was well suited for containing uranium monosulfide at high temperatures. Current studies are directed toward delineation of the uranium-uranium monosulfide phase diagram. Thermodynamic investigations, similar to those under way for the uranium-urania system, will follow when the phase diagram studies are sufficiently advanced.

The liquidus boundary of the uranium-uranium monosulfide system is currently being determined. A series of arc melting experiments with pressed pellets of mixtures of uranium and uranium monosulfide has

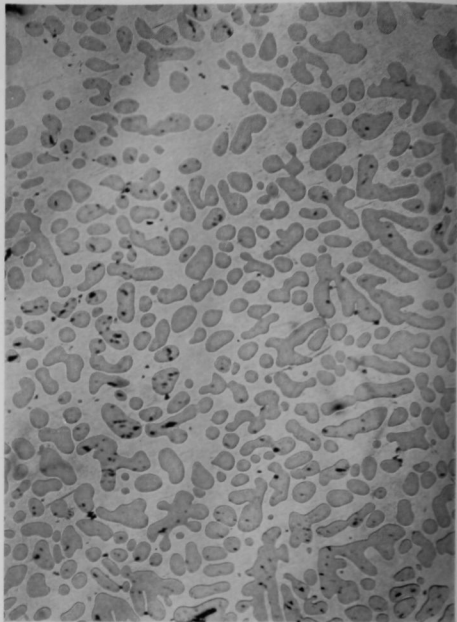
yielded no indication of a monotectic region. Measurements of the solubility of uranium monosulfide in liquid uranium were made by placing uranium metal in a uranium monosulfide cup which was held in a tungsten crucible, and inductively heating the crucible assembly in vacuum for 1½ hours at temperature. Then, the furnace power was turned off which dropped the temperature 600°C/min, thereby quenching the reaction. Compositions of the quenched liquid phase were determined by chemical analysis and gave the results shown in Figure III-5. A photomicrograph of a quenched liquid phase is given in Figure III-6 and shows the uranium monosulfide phase precipitated within the uranium matrix.

Further work on determination of the liquidus and solidus boundaries is planned.



108-8555

FIG. III-5. Tentative Phase Diagram for the Uranium-Uranium Monosulfide System.



108-8699

FIG. III-6. Typical Microstructure of Quenched Uranium-Uranium Monosulfide Liquid Phase. (US is precipitated within the continuous U matrix. Magnification about 54X.)

## IV. Calorimetry\* (W. N. Hubbard, H. M. Feder)

For many compounds of interest in high temperature chemistry, thermochemical data are either completely lacking or lack acceptable accuracy. This may be due to experimental difficulty in making the necessary measurements or to the difficulty of obtaining well-characterized samples. The present thermochemical program places equal emphasis on the procurement of well-characterized samples and the development of adequate experimental techniques.

The determination of standard enthalpies of formation of compounds is an essential foundation for further thermodynamic studies. Part of the program has been devoted to determinations of these enthalpies by oxygen bomb calorimetry. Many of the compounds of interest are difficult to burn in oxygen, however, and cannot be studied by this method. To study the compounds not amenable to oxygen bomb calorimetry, the techniques of the bomb calorimetric method, which has been developed to a high degree of precision and accuracy, have been modified so that fluorine can be used as the oxidant.

\* A summary of this section is given on pages 12 to 13.

### A. COMBUSTION OF PHOSPHORUS IN FLUORINE (P. A. G. O'HARE†)

The calculation of enthalpy of compound formation from enthalpy of combustion data requires that the enthalpies of formation of the various products of compound combustion be known with an accuracy commensurate with the precision of the combustion data. As an adjunct to the determination of the enthalpies of formation of the sulfides, phosphides, selenides and tellurides of uranium by combustion in fluorine, a program has been undertaken to establish the enthalpies of formation of sulfur hexafluoride, phosphorus pentafluoride, selenium hexafluoride and tellurium hexafluoride.

The combination of fluorine with sulfur, phosphorus, selenium and tellurium takes place vigorously and spontaneously and can be studied by the technique of fluorine bomb calorimetry. Because of the spontaneity of combustion, the fluorine must be isolated from the sample until initiation of the reaction is desired.

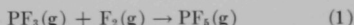
† Postdoctoral Fellow.

The accumulation of enthalpy-of-formation data for fluorides is both a necessary preliminary to the general use of fluorine bomb calorimetry for compounds and a valuable program on its own merit. To date, enthalpy-of-formation values have been determined for the following fluorides: the difluorides of cadmium, magnesium, and zinc; the trifluorides of boron and aluminum; the tetrafluorides of titanium, zirconium, hafnium, and silicon; the pentafluorides of niobium, tantalum, and ruthenium; and the hexafluorides of molybdenum and uranium. The enthalpies of formation of the following compounds have also been determined by fluorine bomb calorimetry: boron nitride, silicon dioxide, and the diborides of zirconium, hafnium and niobium.

To determine thermodynamic properties at high temperatures, values of enthalpies of formation at 25°C are combined with values of the enthalpy increments to the higher temperatures. A drop calorimeter system for making enthalpy increment measurements up to 1500°C has been assembled and is being tested.

An apparatus<sup>1</sup> which was previously developed for the combustion of spontaneously reacting substances, and which consists of a tank charged with fluorine connected to the combustion bomb, has been used in this study.

Preliminary experiments showed that a phosphorus sample supported on a 20-g nickel dish could be burned completely to phosphorus pentafluoride in fluorine at 4 atm pressure. The nickel dish showed an average increase in weight of  $1 \times 10^{-5}$  g from experiment to experiment. The reaction was rapid and resulted in gaseous products only. Formation of phosphorus trifluoride is considered extremely unlikely because the enthalpy of the reaction



is approximately  $-150$  kcal mole<sup>-1</sup> and the reaction

<sup>1</sup> R. L. Nuttall, S. S. Wise and W. N. Hubbard, *Rev. Sci. Instr.* **32**, 1402 (1961).

TABLE IV-1. COMBUSTION DATA FOR RED PHOSPHORUS

	Run No.				
	RP-1	RP-2	RP-3	RP-4	RP-5
$m'$ , g	0.39598	0.43068	0.44598	0.24311	0.56169
$p^i(F_2)$ , atm	2.811	2.733	2.701	3.147	2.447
$\Delta t_c$ , °C	1.42931	1.55088	1.60749	0.87931	2.02443
$\varepsilon(\text{Calor.})(-\Delta t_c)$ , cal	-4811.44	-5220.68	-5411.25	-2959.99	-6814.78
$\Delta E_{\text{contents}}$ , cal	-3.73	-4.05	-4.21	-2.27	-5.33
$\Delta E_{\text{imp}}$ , cal	-0.01	-0.02	-0.02	-0.01	-0.04
$\Delta E_{\text{gas}}$ , cal	-0.02	-0.02	-0.02	-0.01	-0.03
$\Delta E_{\text{blank}}$ , cal	8.0	8.0	8.0	8.0	8.0
$\Delta E^c/M$ , cal g <sup>-1</sup>	-12,140.0	-12,112.8	-12,125.0	-12,152.1	-12,127.9
Mean $\Delta E^c/M = -12,131.6 \pm 6.7$ cal g <sup>-1</sup>					

occurs spontaneously in excess fluorine. The gaseous products of reaction will be subjected to gas-solid chromatographic analysis as soon as a successful technique is established.<sup>2</sup>

Because of the possibility of phosphorus pentafluoride hydrolysis (and its associated large enthalpy of reaction) the bomb and fluorine chamber were pre-treated with 1000 torr commercial phosphorus pentafluoride and then pumped for 18 hr to a high vacuum prior to each run. All manipulations of bomb and sample (except the weighing of sample) were performed in an inert atmosphere dry box (~0.1 ppm H<sub>2</sub>O).

The 99.999 % pure sample of crystalline red phosphorus used for the experiments was analyzed spectrochemically and the following impurities (in ppm) were reported: Ag 10 (?), Al 2, Cu 2, Fe 8, Mg 10 and Si 3 (?).

The results of the combustion experiments are summarized in Table IV-1. Standard state corrections were applied in the usual manner.<sup>3</sup> The entries in the table are as follows:

(1)  $m'$ , masses of phosphorus, ranging from 0.24 to 0.56 g, burned in the experiments.

(2)  $p^i(F_2)$ , the fluorine pressure in the bomb after combustion. (The tank surrounding the bomb was charged to 125 psia for each run; this gave an expanded fluorine pressure,  $p^i(F_2)$ , of 3.8 atm.)

(3)  $\Delta t_c$ , the observed increase in the calorimeter temperature, corrected for heat exchanged between the calorimeter and its surroundings.

(4)  $\varepsilon(\text{Calor.})(-\Delta t_c)$ , the energy equivalent of the calorimetric system minus the contents of the bomb,

multiplied by the negative of the temperature increase. ( $\varepsilon(\text{Calor.}) = 3366.27 \pm 0.31$  cal deg<sup>-1</sup> C as determined by several benzoic acid combustions carried out immediately prior to and after the phosphorus combustions.)

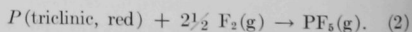
(5)  $\Delta E_{\text{contents}}$ , the energy absorbed by the contents of the bomb during the hypothetical isothermal process at 25°C.

(6)  $\Delta E_{\text{imp}}$ , the net correction for impurities in the sample.

(7)  $\Delta E_{\text{gas}}$ , the net correction for reducing the pressures of the bomb gases to standard state conditions. (The Berthelot equation of state was used to estimate the second virial coefficient for phosphorus pentafluoride.)

(8)  $\Delta E_{\text{blank}}$ , a correction which incorporates the heat of the Joule-Thomson effect and the heat of reaction of the expanded fluorine with the small amounts of water which were still adsorbed on the bomb walls despite the pretreatment previously described. (The net heat of these effects was measured in separate experiments in which the conditions for an actual combustion were exactly duplicated, except, of course, that the phosphorus sample was omitted. The blank correction is discussed further in section IV-E.)

(9)  $\Delta E^c/M$ , the energy evolved per gram of phosphorus for the reaction



The mean  $\Delta E^c/M$  was  $-12,131.6$  cal g<sup>-1</sup> with a standard deviation of the mean of  $\pm 6.7$  cal g<sup>-1</sup>. Thus, for the reaction given in Equation 2

$$\Delta E_f^\circ(PF_5, g) = -375.6 \text{ kcal mole}^{-1}, \text{ and}$$

$$\Delta H_f^\circ(PF_5, g) = -376.6 \pm 0.4 \text{ kcal mole}^{-1}.$$

The quoted uncertainty is twice the standard error (overall standard deviation) of the mean, all the un-

<sup>2</sup> This work is being done by Chemical Research Services, Inc., Addison, Illinois.

<sup>3</sup> W. N. Hubbard, "Experimental Thermochemistry," Vol. II, H. A. Skinner, Editor, Interscience Publishers, Inc., New York, N. Y., 1962, Ch. 6, pp. 95-127.

certainties in the auxiliary data and processes being included. This value for the enthalpy of formation of phosphorus pentafluoride is in close agreement with the value determined by Gross<sup>4,5</sup> by measurement of

<sup>4</sup> P. Gross, *et al.*, Fulmer Research Institute Report, R146/4/23, November 1960.

the heat of reaction of white phosphorus with fluorine. Analysis of Gross' work and correction to the standard state of red phosphorus gave  $\Delta H_f^\circ(\text{PF}_5, \text{g}) = -377.2 \pm 0.8 \text{ kcal mole}^{-1}$ .

<sup>5</sup> JANAF Thermochemical Tables, The Dow Chemical Co., Midland, Mich., June 30, 1963.

## B. COMBUSTION OF SULFUR IN FLUORINE (P. A. G. O'HARE,\* J. L. SETTLE)

Preliminary experiments on the combustion of sulfur in fluorine have shown that substantially the same techniques used for combustions of phosphorus in fluorine will be satisfactory for sulfur. Up to 0.6 g sulfur

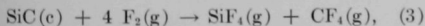
\* Postdoctoral Fellow.

burned completely in fluorine at a tank pressure of 170 psi. Investigations<sup>2</sup> are under way to determine the feasibility of detecting and determining the amounts of sulfur tetrafluoride and disulfur decafluoride should these gases be side-products of combustion. Calorimetric combustions have been started.

## C. COMBUSTION OF SILICON CARBIDE AND GRAPHITE IN FLUORINE (E. GREENBERG, C. A. NATKE, R. TERRY)

Discrepancies<sup>6,7,8</sup> among various literature values for the enthalpy of formation of silicon carbide could be resolved if accurate values of the energies of combustion of silicon carbide, silicon, and carbon in fluorine were available. The determination of the enthalpy of formation of silicon tetrafluoride has already been reported.<sup>8</sup>

The experimental technique developed for the combustion of silicon carbide in fluorine (15 atm pressure) according to the reaction



was described in ANL-6800, p. 313. Preliminary combustion data were reported in ANL-6900, p. 223. Four samples of SiC have been employed: Samples 1 and 2 are  $\alpha$ -SiC, Samples 3 and 4 are  $\beta$ -SiC. Samples 1, 3, and 4 are green. Sample 2 is yellow and is designated as "Golden Grain" by the Carborundum Co. The two  $\alpha$ -SiC samples were made by entirely different methods and are unrelated. Samples 3 and 4, however, are related in that Sample 4 was obtained by leaching a

portion of Sample 3 with acid in order to reduce metallic contamination.

Standard state calculations<sup>3</sup> have been carried out for 20 completed combustion experiments and the results are presented in Tables IV-2 and IV-3. The horizontal row headings are the same as in Table IV-1 except as noted below.

The mass of sample burned was determined by subtracting the mass of unburned material recovered after combustion from the mass of sample initially charged to the bomb.

$\Delta E_{\text{ignition}}$ , the electrical energy required to ignite the molybdenum fuse wire, was measured with an electronic power integrating circuit.

$\Delta E_{\text{Mo fuse}}$  is the energy supplied by combustion of the molybdenum fuse wire which was used to ignite the silicon carbide sample.

$\Delta E_{\text{C}_2\text{F}_6}$  and  $\Delta E_{\text{CF}_4}$  represent the respective thermal corrections for the small amounts of these side-products formed during combustion. These corrections represent the difference in energy involved in forming these side-products instead of  $\text{CF}_4$ .

The last line in the tabulation is the energy evolved per gram of silicon carbide burned and is obtained by summing the quantities from  $\epsilon(\text{Calor.})(-\Delta t_c)$  through  $\Delta E_{\text{imp.}}$  and dividing by the mass of sample burned. It is evident that almost all of the measured energy

<sup>6</sup> J. Chipman, *J. Am. Chem. Soc.* **83**, 1762 (1961).

<sup>7</sup> J. C. d'Entremont and J. Chipman, *J. Phys. Chem.* **67**, 499 (1963).

<sup>8</sup> S. S. Wise, J. L. Margrave, H. M. Feder and W. N. Hubbard, *J. Phys. Chem.* **67**, 815 (1963).

TABLE IV-2. COMBUSTION DATA FOR ALPHA SILICON CARBIDE

	Combustion No.											
	1a	2a	3a	1	2	6	7	10	12	15	16	17
Sample No.	1	1	1	2	1	1	2	2	1	2	1	1
Mass, g	0.49153	0.47841	0.47179	0.48120	0.48435	0.50894	0.50310	0.49608	0.49657	0.69995	0.29630	0.48779
$\Delta t_c$ , °C	2.04356	1.99169	1.95567	1.99999	2.00687	2.11012	2.08182	2.04678	2.05975	2.89281	1.22914	2.02882
$\xi(\text{Calor.})(-\Delta t_c)$ , cal	-7238.88	-7055.14	-6927.55	-7081.98	-7106.35	-7471.96	-7371.75	-7247.67	-7293.60	-10,243.47	-4352.40	-7173.45
$\Delta E_{\text{contents}}$ , cal	-8.12	-7.91	-8.27	-8.46	-8.49	-8.82	-8.70	-8.66	-8.60	-12.18	-5.10	-8.46
$\Delta E_{\text{ignition}}$ , cal	0.29	0.41	0.31	0.84	0.12	0.43	0.07	0.17	0.22	0.22	0.19	0.19
$\Delta E_{\text{gas}}$ , cal	0.21	0.25	0.24	0.21	0.25	0.27	0.26	0.27	0.27	0.33	0.17	0.26
$\Delta E_{\text{Mo fuse}}$ , cal	18.61	26.46	18.72	27.66	9.40	14.55	6.89	15.78	10.41	8.67	11.88	15.09
$\Delta E_{\text{C}_2\text{F}_6}$ , cal	-5.15	-2.84	-10.47	-7.73	-10.92	-19.01	-12.39	-20.33	-20.71	-22.76	-6.38	-7.00
$\Delta E_{\text{C}_2\text{F}_4}$ , cal	-3.21	—	-8.84	-4.67	-6.42	-13.19	-9.82	-17.45	-11.87	-20.00	-5.48	-6.51
$\Delta E_{\text{imp.}}$ , cal	-2.18	-2.12	-2.09	-4.02	-2.15	-2.26	-4.20	-4.14	-2.20	-5.84	-1.32	-2.17
$\Delta E_c^\circ/M$ , cal g <sup>-1</sup>	-14,726.32	-14,717.27	-14,705.59	-14,709.37	-14,709.53	-14,736.49	-14,708.09	-14,679.14	-14,753.37	-14,708.24	-14,709.55	-14,723.65

TABLE IV-3. COMBUSTION DATA FOR BETA SILICON CARBIDE

	Combustion No.							
	3	4	5	8	9	11	13	14
Sample No.	3	4	3	4	4	3	3	4
Mass, g.	0.49780	0.50111	0.49790	0.50610	0.49499	0.49944	0.29974	0.70892
$\Delta t_c$ , °C	2.06471	2.07864	2.06623	2.10061	2.05564	2.07376	1.24470	2.94525
$\xi(\text{Calor.})(-\Delta t_c)$ , cal	-7311.16	-7360.49	-7316.54	-7438.28	-7279.04	-7343.20	-4407.50	-10,429.16
$\Delta E_{\text{contents}}$ , cal	-8.73	-8.79	-8.63	-8.78	-8.58	-8.66	-5.23	-12.40
$\Delta E_{\text{ignition}}$ , cal	0.12	0.24	0.07	0.17	0.19	0.17	0.22	0.14
$\Delta E_{\text{gas}}$ , cal	0.27	0.26	0.27	0.26	0.26	0.26	0.18	0.33
$\Delta E_{\text{Mo fuse}}$ , cal	19.11	12.42	10.83	12.53	8.36	12.88	16.67	15.94
$\Delta E_{\text{C}_2\text{F}_6}$ , cal	-5.54	-5.32	-4.59	-5.96	-3.71	-2.00	-8.06	-5.03
$\Delta E_{\text{C}_2\text{F}_4}$ , cal	-4.11	-3.71	-2.96	-3.92	-1.99	—	-4.97	-3.15
$\Delta E_{\text{imp.}}$ , cal	-11.67	-5.41	-11.68	-5.47	-5.35	-11.71	-7.03	-7.66
$\Delta E_c^\circ/M$ , cal g <sup>-1</sup>	-14,708.14	-14,708.95	-14,728.32	-14,719.32	-14,727.29	-14,721.01	-14,731.83	-14,728.02

was liberated by the primary combustion reaction under consideration.

Table IV-4 summarizes the data of Tables IV-2 and IV-3 by listing the standard energies of combustion per gram,  $\Delta E_c^\circ/M$ , their means, and their standard deviations. On the basis of the additional experiments completed during this report period and refinements of the corrections involved, the preliminary conclusions given in ANL-6900, p. 224 have been modified as follows.

The results obtained with the  $\beta$ -SiC samples are in excellent agreement despite the difference in impurity contents. It is reasonable to pool the combustion results and to derive therefrom a value of the enthalpy of formation of  $\beta$ -SiC.

The results for the two  $\alpha$ -SiC samples are in disagreement by an amount which is greater than the combined uncertainties. The difference in impurity levels between Samples 1 and 2 is less than that between the two  $\beta$ -SiC samples. Hence, the disagreement between  $\alpha$ -SiC samples should not be attributed to impurity content.

A careful analysis of the data reveals the following facts:

1. Except for one experiment the corrections for side-reaction products in the  $\beta$ -SiC combustions are all less than 10 calories, whereas five of the  $\alpha$ -SiC combustions have corrections ranging from 22 to 43 calories.
2. In all the  $\beta$ -SiC experiments 99.5 to 99.8% of the sample was burned; for the  $\alpha$ -SiC samples the range was 99.2 to 99.4%. In other words, the best  $\alpha$ -SiC combustion was not as complete as the poorest  $\beta$ -SiC combustion.

Although there is no direct correspondence between the incompleteness of combustion and the amount of higher fluorocarbons formed, it seems that some undefined process or source of error connected with these observations is involved in the combustion of the  $\alpha$ -SiC samples. The difference in combustion behavior is suspected to be connected with the particle size of the samples; the  $\alpha$ -SiC samples are much coarser than the  $\beta$ -SiC samples. A new sample of  $\alpha$ -SiC (green variety) which is much finer than Samples 1 and 2 has recently been received from the Carborundum Co.

Experiments with this sample will be undertaken in an effort to resolve the discrepancy between Samples 1 and 2.

Combining the combustion results for  $\beta$ -SiC with values of the enthalpies of formation of SiF<sub>4</sub> and CF<sub>4</sub>,  $-386.0^8$  and  $-221^9$  kcal mole<sup>-1</sup>, respectively, yields a value of  $-15.5$  kcal mole<sup>-1</sup> for the standard enthalpy of formation ( $\Delta H_f^{298}$ ) of  $\beta$ -SiC. This value is within the range of literature data summarized by d'Entremont and Chipman<sup>7</sup> and compares well with their value of  $-15.8 \pm 0.9$  kcal mole<sup>-1</sup> and the value of Rein and Chipman<sup>10</sup> of  $-15.6$  kcal mole<sup>-1</sup>.

The largest uncertainty in the derived enthalpy of formation of  $\beta$ -SiC is the uncertainty in the enthalpy of formation of CF<sub>4</sub>, which is probably about 1 kcal mole<sup>-1</sup>. There have been a number of recent determinations of the enthalpy of formation of CF<sub>4</sub> but none of these has been a direct determination. Because this value is an important basic thermochemical quantity, we are planning to carry out a direct determination of

<sup>8</sup> This is the value currently suggested by the National Bureau of Standards, Washington, D.C.

<sup>10</sup> R. H. Rein and J. Chipman, *J. Phys. Chem.* **67**, 839 (1963).

the enthalpy of formation of CF<sub>4</sub> by combustion of carbon in fluorine. The experimental problem of carrying out combustions of graphite in fluorine was discussed in ANL-6800, p. 314.

TABLE IV-4. RESULTS OF SILICON CARBIDE COMBUSTION EXPERIMENTS

Standard Energy of Combustion, $\Delta E_c/M$ (cal g <sup>-1</sup> )				
Sample 1 ( $\alpha$ -SiC, green)	Sample 2 ( $\alpha$ -SiC, Golden Grain)	Sample 3 ( $\beta$ -SiC, green)	Sample 4 ( $\beta$ -SiC, green)	
14,726.3	14,709.4	14,708.1	14,709.0	
14,717.3	14,708.1	14,728.3	14,719.3	
14,705.6	14,679.1	14,721.0	14,727.3	
14,709.5	14,708.2	14,731.8	14,728.0	
14,736.5				
14,753.4				
14,709.6				
14,723.7				
Mean	14,722.7	14,722.3	14,720.9	
Std. Dev. of mean	$\pm 5.7$	$\pm 7.4$	$\pm 5.2$	$\pm 4.4$

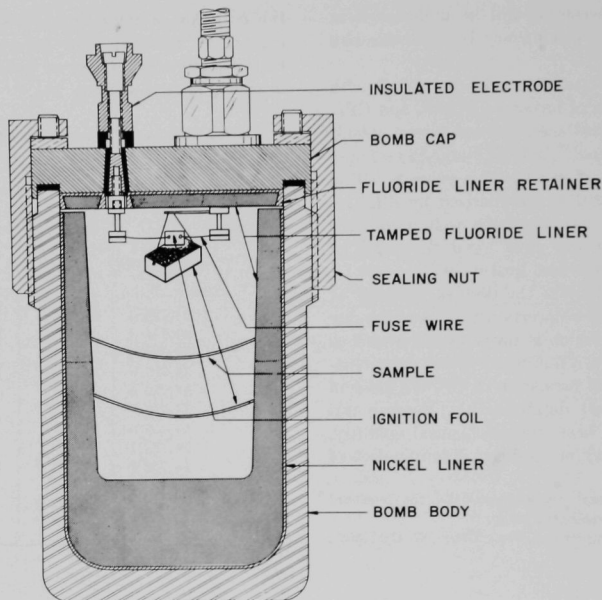
#### D. COMBUSTIONS OF MAGNESIUM, ALUMINUM, YTTRIUM, LANTHANUM, GADOLINIUM, AND HOLMIUM IN FLUORINE (E. RUDZITIS, E. VAN DEVENTER)

The accumulation of experience in fluorine bomb calorimetry has led to attempts to classify substances on the basis of their combustion characteristics in fluorine. The combustion behavior of a substance can be related to its physical and chemical properties and to the properties of its reaction product fluorides. Such relations can be helpful in the prediction of the combustion behavior of substances to be studied and in the design of appropriate combustion techniques.

Metals which form nonvolatile (ionic) fluorides constitute a typical group. Their combustion is characteristically accompanied by melting and sputtering. Therefore, they require a special support for the sample and an arrangement for the protection of the interior surfaces of the combustion bomb. The solution to this problem has been the use of a bomb lined with the pure fluoride of the metal to be burned. A more detailed discussion of the problem and of the development of the combustion technique for such metals has been given previously (ANL-6900, p. 227). The application of this technique has resulted in recent calorimetric combustions of magnesium, aluminum, nickel, yttrium, lanthanum, gadolinium and holmium in fluorine. The

combustions of magnesium and aluminum were re-determinations<sup>8</sup> in order to improve on earlier work (ANL-6596, p. 168; ANL-6648, p. 179).

The metals, in the form of sheet or foil, were suspended in the bomb and ignited by the usual wire-to-foil technique. Magnesium, aluminum, nickel, yttrium, and gadolinium were suspended by a fine wire of the respective metal from a heavily fluorinated nickel post. Suspension by the ignition wire alone was used for combustions of lanthanum and holmium. Ignition difficulties which were encountered with aluminum and nickel were overcome by forming 5-mil foil into a small basket (see Figure IV-1) into which filings or cuttings of the respective metals were placed. The sample was ignited by a cadmium fuse wire. It was found that burying molten droplets of nickel, gadolinium, and holmium contacted and melted small volumes of fluoride liner and submerged therein. This submergence caused premature termination of the combustions. This problem was partially alleviated by stacking part of the sample in the form of foils below the suspended basket. The stacked foils were supported by the protective fluoride liner. With this arrangement the ignited sample was pre-



108-7124 Rev.

FIG. IV-1. Sample Arrangement for Combustions in Fluorine.

TABLE IV-5. SOME PHYSICAL PROPERTIES AND COMBUSTION YIELDS OF METALS FORMING NONVOLATILE FLUORIDES

Metal	$\Delta d^a$ (g/cm <sup>3</sup> )	Metal M.P. (°C)	Metal B.P. (°C)	Fluoride M.P. (°C)	Fluoride B.P. (°C)	Com- bustion Yield (%)
Mg	-1.3	650	1107	1400	2240	>99
Y	-0.6	1550	3000	1150	2300	99
Al	-0.4	660	2450	— <sup>b</sup>	>2000	90-95
La	0.3	920	4500	1500	2300	>95
Gd	0.9	1350	3000	1230	2300	>90
Ho	1.1	1500	2700	1130	2200	>90
Zn	2.1	420	906	875	1500	80-90
Cd	2.3	321	765	1050	1750	>99
Ni	4.6	1450	2700	<1450	1700	~50
Th	5.6	1750	3850	1100	3850	~10

<sup>a</sup> Room temperature density difference between metal and its fluoride.

<sup>b</sup> Sublimes under ordinary conditions.

vented from falling directly onto the liner; instead, the burning proceeded in several steps as the stacked foils successively ignited.

The evaluation of the accumulated calorimetric combustion results from these studies is still in progress. The combustion yields have been examined in an

attempt to correlate this important parameter with some of the physical properties of the metals and their fluorides. For the sake of comparison cadmium, zinc, and thorium, which also belong to the group of metals forming nonvolatile fluorides, have been included in the correlation. Cadmium<sup>11</sup> and zinc<sup>12</sup> were burned earlier using similar techniques. Attempts to burn sufficient amounts of thorium failed because of severe submergence problems.

The correlation shown in Table IV-5 lists: the metal, the room temperature density difference between the metal and its fluoride, the melting and boiling points of the metal and its fluoride, and representative combustion yields in percent. Several observations can be made. The low combustion yield associated with submergence is directly related to the density difference. It also appears that the volatility of the metal and melting point of the metal fluoride affect the combustion yields. These observations are of a tentative nature and may be expanded and adjusted as new data become available.

<sup>11</sup> E. Rudzitis, H. M. Feder and W. N. Hubbard, *J. Phys. Chem.* **67**, 2388 (1963).

<sup>12</sup> E. Rudzitis, R. Terry, H. M. Feder and W. N. Hubbard, *J. Phys. Chem.* **68**, 617 (1964).

## E. COMBUSTION OF TANTALUM DIBORIDE IN FLUORINE (G. K. JOHNSON)

Experimental combustions of tantalum diboride have been completed using the combustion technique previously described (ANL-6596, p. 173) for the diborides of zirconium, hafnium, and niobium.

The results of 12 acceptable combustions out of 14 performed are presented in Table IV-6. The entries in the table are the same as in Table IV-1 except that:  $m'$  is the mass of tantalum diboride burned, obtained by subtracting the mass of unburned diboride (determined by boron analysis) from the mass originally charged to the bomb; and  $\Delta E_{\text{suflur}}$  is the energy supplied by the combustion of a small amount of sulfur used to insure reproducible ignition.

The twelve combustion results presented in Table IV-6 represent two series of combustions of portions of the same specimen of tantalum diboride. The second series, comprising the last five columns in the table, was conducted under conditions in which the  $\Delta E_{\text{blank}}$  correction was considerably smaller than in the first series. The second series was prompted by concern that the blank correction, which is measured by expansion of fluorine into a cold bomb, may not be the same as in the actual combustion when there is an exothermic reaction going on in the bomb. Attempts to eliminate adsorbed moisture from the bomb walls, and thus make the blank correction negligibly small, were not entirely successful. These attempts included handling the bomb in a dry box and various pretreatments with fluorine and boron trifluoride.

In the first series of combustions the average value

of six blank experiments conducted before, during, and after the calorimetric combustions was applied to all the combustions in the series because the blanks showed only experimental fluctuations and no trend. However, in the second series, in which one or more blank experiments were conducted between successive combustions, the value obtained for  $\Delta E_{\text{blank}}$  prior to any given combustion was applied to that combustion. This was necessary because of the different perfluorination methods used. The conclusion to be drawn from the good agreement of  $\Delta E_c/M$  (sample) between the two series and between the large and small sample masses within each series is that the  $\Delta E_{\text{blank}}$ , as measured by expansion of fluorine into a cold bomb, is applicable to actual calorimetric combustions.

The sample was analyzed for boron, tantalum, and impurities. The boron/tantalum ratio is 1.927 after correcting for the amounts of these elements assumed to be combined with impurities.

The experimental value of  $\Delta E_c/M$ , combined with a molecular weight of 201.781 for  $\text{TaB}_{1.927}$  and the enthalpies of formation of  $\text{BF}_3^{13}$  and  $\text{TaF}_5^{14}$  of  $-269.88$  and  $-454.98$  kcal mole $^{-1}$ , respectively, gives a tentative value of  $-40.8$  kcal mole $^{-1}$  for the enthalpy of formation of  $\text{TaB}_{1.927}$ .

<sup>13</sup> S. S. Wise, J. L. Margrave, H. M. Feder and W. N. Hubbard, *J. Phys. Chem.* **65**, 2157 (1961).

<sup>14</sup> E. Greenberg, C. A. Natke and W. N. Hubbard, "Fluorine Bomb Calorimetry. X. The Enthalpies of Formation of Niobium and Tantalum Pentafluorides," submitted for publication in *J. Phys. Chem.*

TABLE IV-6. COMBUSTION DATA FOR TANTALUM DIBORIDE

(1) $m'$ , g	1.25145	1.24870	1.25176	1.25062	0.60938	0.61245	0.61343	1.24608	1.24817	1.24507	0.61098	0.60929
(2) $\Delta t_c$ , °C	1.85213	1.84062	1.85648	1.84781	0.97047	0.97774	0.97383	1.81561	1.81808	1.81803	0.95925	0.95858
(3) $\xi$ (Calor.) ( $\Delta t_c$ ), cal	-6224.27	-6185.59	-6238.89	-6209.75	-3261.36	-3285.79	-3272.65	-6173.20	-6181.60	-6181.43	-3261.52	-3259.24
(4) $\Delta E_{\text{contents}}$ , cal	-11.86	-11.63	-11.88	-11.68	-6.17	-6.14	-6.19	-11.41	-11.43	-11.43	-5.99	-5.99
(5) $\Delta E_{\text{gas}}$ , cal	-0.23	-0.23	-0.23	-0.23	-0.10	-0.10	-0.10	-0.26	-0.26	-0.26	-0.13	-0.13
(6) $\Delta E_{\text{suflur}}$ , cal	445.11	423.34	459.78	437.10	445.11	452.85	435.58	427.93	433.69	444.03	444.93	444.30
(7) $\Delta E_{\text{blank}}$ , cal	12.58	12.58	12.58	12.58	12.58	12.58	12.58	4.62	-0.34	0.31	3.71	5.50
(8) $\Delta E_c/M$ (sample), cal g $^{-1}$	-4617.58	-4614.02	-4614.41	-4615.29	-4611.15	-4615.23	-4614.67	-4616.33	-4614.71	-4613.90	-4613.90	-4621.05
Mean $\Delta E_c/M$ (sample)	= $-4615.19 \pm 0.69$ cal g $^{-1}$											
Impurities	= $-4.43$ cal g $^{-1}$											
$\Delta E_c/M$	= $-4619.6 \pm 0.7$ cal g $^{-1}$											

## F. FLUORINE FLOW CALORIMETER: COMBUSTION OF URANIUM MONOSULFIDE IN FLUORINE (J. SETTLE)

Preliminary studies of the behavior of uranium monosulfide, US, in fluorine (ANL-6725, p. 192) showed that the extent of spontaneous reaction was so great that the monosulfide would have to be protected from exposure to fluorine before intentional ignition. These studies also showed that it was necessary to employ a high fluorine pressure and an auxiliary combustible substance in order to obtain complete conversion to uranium hexafluoride. The best combustions of US in a calorimetric bomb were obtained by using fluorine pressures in excess of ten atmospheres and by using a quartz dish both to support the sample and act as the auxiliary combustible substance. Although complete combustions of US were achieved, a large amount (1 to 2 g) of quartz reacted at the same time. The large thermal correction that would have to be made for the combustion of quartz would lead to an undesirably large uncertainty in the value for the energy of combustion of US.

These observations led to the consideration of using alternative equipment. A fluorine flow calorimeter was selected for trial. Some possible advantages of a flow system were: fluorine-sensitive compounds could be kept in an inert atmosphere until introduction of fluorine and initiation of the reaction were desired; the rate of reaction could be varied by controlling the total pressure in the vessel and the rate of flow of fluorine; the temperature in the reaction zone could be reduced by operating at low reaction rates, and corrosion of the sample support dish would be reduced; and the amount of sample to be burned could be varied over any desired range.

A simple flow reaction system was built. It consisted of a flow meter in series with a short inlet line for introducing gases, a Pyrex reaction vessel of about one-liter volume with attached pressure gauge, and a short outlet line connected to several traps and a vacuum pump. This system was used for preliminary combustions of US and it was demonstrated that all of the presumed advantages of a flow system could be obtained. Samples of US weighing 0.5 to 10 g were successfully burned. The reaction rate could be varied over wide limits. At reaction rates sufficiently low to avoid melting of the uranium tetrafluoride intermediate product, quantitative combustion of US was achieved. Reaction of the quartz support dish was an order of magnitude less than during bomb combustions, although still objectionably large (0.1 to 0.2 g) in the most favorable tests. With nickel support dishes, it was found possible to obtain 99.8 or greater percent

combustion of US, with no detectable attack on the nickel dish if melting of uranium tetrafluoride was avoided. The solid residual mixture of uranium tetrafluoride, black intermediate uranium fluorides, and uranium pentafluoride usually weighed less than 0.02 g. The thermal corrections made necessary by incomplete combustion of a sample held by a nickel dish would be about two orders of magnitude smaller than the thermal corrections made necessary by complete combustion of US held by a quartz dish.

The flow reaction system was then modified so that it more nearly simulated the apparatus which might be used in a flow calorimeter. A flow calorimeter must have heat exchangers on both the inlet and outlet lines. The heat exchanger on the inlet line must adjust the incoming gases to the temperature of the jacket surrounding the calorimeter; the heat exchanger on the outlet line must extract the heat produced by reaction and adjust the temperature of the outgoing gases to the temperature of the calorimeter. The flow rates, pressures and temperatures of these gases must be known so that their contributions to the heat capacity of the calorimetric system and to the heat exchanged between the calorimeter and its environment can be evaluated. The modified apparatus consisted of an inlet line in series with a pressure gauge, a flow meter, and a 1.8-meter length of 1/8-in. OD tubing which simulated the inlet line heat exchanger; a Pyrex reaction vessel of about 0.18-liter volume, with attached pressure gauge (Pyrex will not be used in an actual calorimetric vessel); and an outlet line consisting of a 1.8-meter long heat exchanger in series with a pressure gauge, traps, and a vacuum pump. Trial combustions were made of US supported on a nickel dish. The combustion characteristics were not significantly affected by the change in volume (1 to 0.18 liter) of the reaction vessel. Greater than 99% conversion to volatile fluorides was obtained consistently. Uranium hexafluoride is the only uranium fluoride that is volatile at room temperature, but all the sulfur fluorides are volatile. Infrared absorption spectrum analyses of the products of several combustions indicated that probably greater than 98% of the sulfur was in the form of sulfur hexafluoride, with disulfur decafluoride as the major side-product. No absorption bands attributable to other sulfur fluorides or sulfur oxyfluorides were observed. A method for the quantitative analysis of mixtures of sulfur fluorides is being developed by Chemical Research Services, Inc., of Addison, Illinois.

The analysis of the small amounts of solid uranium fluorides left after combustion presents no serious problems.

A nickel reaction vessel, which is believed suitable for use in a calorimeter, is now being used with the trial apparatus in place of the small Pyrex reaction vessel. Preliminary indications are that the procedures worked out with the Pyrex vessel can be used with the nickel vessel. Further trial combustions will be done with the nickel reaction vessel immersed in water in order to complete the simulation of a calorimetric system.

## G. HIGH TEMPERATURE ENTHALPY CALORIMETRY (J. E. BRUGGER, D. R. FREDERICKSON, A. T. HU,\* R. KLEB\*\*)

### I. 1500°C Drop Calorimeter

#### a. CONSTRUCTION

A somewhat simplified version of the vacuum, high precision, high temperature drop calorimeter has been assembled. The system is designed to determine enthalpy increments of samples up to 1500°C. The device is of the dropping type and consists of a drop control mechanism, a drop tube that rests on a furnace where the sample is heated while suspended by a wire, a gate system that is opened while the sample is falling, and a copper-block calorimeter proper where the heat given up by the sample is measured. (A drawing of the drop calorimeter is shown in ANL-6477, p. 165.)

The drop control mechanism has operated satisfactorily. Ultimately, it may be desirable to provide a means for obtaining point-by-point data on the actual distance travelled *vs.* time of fall of the sample from the furnace to the calorimeter. These data should improve the accuracy and precision of the correction for the heat loss of the sample during the drop. A 0.020-in. dia. tantalum wire served satisfactorily as the suspension wire. (Platinum-7% tungsten wire is available and will also be tested for suitability as a suspension wire.) Temperature control for the furnace was adequate. The copper-block calorimeter performed satisfactorily. A technique for adjusting the temperature of the copper block to a suitable initial value has been developed, but improved methods are under consideration. Incorporation of the above improvements should suffice for taking data of the desired precision and accuracy.

Serious consideration has been given to an alternative solution to the combustion problems mentioned at the outset. The use of a two-chambered system is proposed whereby the combustion sample is stored in a calorimetric bomb and fluorine is stored in an auxiliary tank. This system protects sensitive samples from exposure to fluorine prior to ignition. However, the two-chambered system presently available can not deliver more than eight atmospheres of fluorine pressure into the reaction vessel. Therefore, a second two-chambered system capable of delivering a higher pressure is being made for testing.

The furnace used for drops during the early part of this report period consisted of a high purity, recrystallized alumina core which was wound with tantalum heater wire, a double-walled tantalum can filled with 100-mesh alumina grains—the so-called “dust shield”, three molybdenum radiation shields, and eight stainless steel shields.

For later runs, the ceramic core was replaced by a molybdenum core (see ANL-6648, p. 184, Fig. 57). The core consists of four elements: bottom shield, outer shield, main shield, and floating shield. The function of the bottom shield, an 8-in. long, 3-in. OD cylinder with a 1-in. ID bore, is to reduce the radiative heat loss from the furnace chamber proper and to provide a region at furnace temperature through which the dropping sample can accelerate from rest without undergoing severe thermal radiation losses. The outer, main, and floating shields are nested, top-end-closed cylinders. The outer shield is 5 in. long by 3-in. OD; the cavity in the floating shield (for the sample) is 3 in. long by  $\frac{7}{8}$ -in. ID.

The original design of the furnace was such that the outer, main, and bottom shields could each be resistance heated. In the present assembly, tantalum wire heaters are installed in only the outer and bottom shields. The heater elements consist of 0.020-in. dia. tantalum wire looped through double-bore 0.125-in. dia. Morganite TC alumina tubing. Separate sets of twelve of these bifilar heater elements were equally spaced around the cylindrical outer surfaces of the outer and bottom shields. The top of the outer shield is heated by additional ceramic-encased heater wire.

Tantalum-sheathed and Morganite (Triangle RR

\* Postdoctoral Fellow.

\*\* Central Shops.

grade) alumina-sheathed Pt-10% Rh vs. Pt thermocouples have been inserted in the floating shield for intercomparison and for monitoring the furnace cavity temperature. A similar tantalum-sheathed thermocouple in the outer shield and a Morganite alumina-sheathed thermocouple in the bottom of the bottom shield are used for temperature control. The noise level of the tantalum-sheathed thermocouple is more than an order of magnitude smaller than that of the ceramic-sheathed thermocouple.

A tantalum spider, which was installed to center the core within the dust shield, failed to maintain alignment of the core along the suspension wire axis. Also, the bottom and outer shield heater elements were damaged during trial heatups. The furnace has been dismantled to replace these elements and to improve the installation of the thermocouples. The dust shield has been rebuilt to accommodate the push-pull core alignment rods provided for in the original design of the furnace. The rebuilt dust shield will be used as long as inward buckling does not occur. A substitute shield has been fabricated by rolling 0.003-in. molybdenum foil into a ten-turn spiral with successive turns spaced  $\frac{1}{16}$  in. apart by embossing. The spiral shield will be installed if necessary but, in any event, it will be tested in place at some convenient time.

## b. TEMPERATURE MEASUREMENTS

Accurate and precise determination of the temperature of an object suspended in the furnace is of prime importance. Consideration has been given to methods for calibrating the floating shield thermocouple in place so that it will give a true measure of the temperature. Inspection has revealed that the visible end of a suspended object is indistinguishable from the floating shield at 1000°C. The temperature of a suspended object can therefore be assumed to be the same as that of the floating shield. The interior of the floating shield seems to have all the qualities of a black-body cavity. An attempt will be made to determine whether any vertical temperature gradient exists in an object having the same size and shape as a sample capsule.

Methods so far considered for calibration and recalculation of the floating shield thermocouples *in situ* involve: (1) use of a calibrated optical pyrometer to obtain the temperature of a (black) body in the floating shield cavity, (2) calibration of the pyrometer from first principles<sup>15</sup> by determination of the gold point of a sample in the furnace cavity and by brightness matches between the radiative intensity of the

pyrometer filament at the gold point and of the attenuated intensity (using rotating sectored discs) of black bodies at higher temperatures, (3) calibration using the thermal halts of secondary standards (copper, nickel, cobalt) which have been allowed to cool in the furnace cavity, (4) permanent installation of an externally calibrated thermocouple, and (5) periodic removal of the thermocouple for external calibration. It is anticipated that methods (1) and (3) will be given active consideration.

In any case, there is doubt that the furnace temperature at the design maximum (1500°C) can be determined to less than  $\pm 1^\circ\text{C}$  by the best method, which is method (2). Use of a photoelectric brightness pyrometer could conceivably permit the determination to less than  $\pm 1^\circ\text{C}$ . The accuracy of the other methods would likely be  $\pm 1.5$  to  $\pm 2.0^\circ\text{C}$  at best.

At present, the temperature determination by the thermocouple is being checked against the temperature of the sample measured with an optical brightness pyrometer. The pyrometer has been calibrated against a standardized strip lamp. The calibration unit includes an optical bench for use in determining the correction for the optical elements (glass plate and prism) that are used when the temperature of the sample in the furnace is measured with the pyrometer.

## c. ERROR ANALYSIS

So far as can be determined at present, temperature control is better than  $\pm 0.1^\circ\text{C}$  at 1500°C, i.e.,  $\pm 0.007\%$ . If it is accepted that the absolute value of the furnace temperature at 1500°C is known to only  $\pm 1^\circ\text{C}$ , it can be expected that the error of a single enthalpy determination will be no less than  $\pm 0.07\%$ . There will be an additional uncertainty of a similar magnitude owing to the heat loss correction during a drop.

The temperature gradient in the sample capsule is unknown but is estimated to be small. A calculation indicates that the temperature at the top of the capsule might be 0.02°C below that of the floating shield owing to heat leak along the suspension wire; and that radiation from the capsule to the cold zone of the furnace might lower the temperature of the bottom of the capsule 0.04°C, or so. (Note that the bottom of the capsule was indistinguishable from the cavity at the temperatures so far checked, namely, up to 1000°C.) The uncertainty in the temperature of the capsule will be set principally by inaccuracy in the furnace temperature measurement; errors arising from temperature gradients may well be negligible.

The heat loss by the capsule during a drop is difficult to estimate; an educated guess leads to 1 to 2% at 1500°C. When experimental data are available for capsules of various sizes and masses at different drop

<sup>15</sup> H. J. Kostkowski and R. D. Lee, "Theory and Methods of Optical Pyrometry," NBS Monograph 41, U.S. Government Printing Office, 1962.

speed programs, it is anticipated that the true heat loss can be calculated semiempirically from these measurements so that the ultimate error in the enthalpy arising from error in estimating the heat loss correction will be of the order of  $\pm 0.05\%$ .

A series of drops of samples heated up to  $1000^\circ\text{C}$  was made with copper, with a tantalum rod, and with a heavy-walled cylinder of tantalum. To date, the reproducibility of the enthalpy measurements has been about  $\pm 0.2\%$ . In these drops, only moderate care was exercised to insure reproducibility. The precision of the calorimetry was an order of magnitude better ( $\pm 0.02\%$  for the electrical calibration runs of the copper-block calorimeter) and the precision of furnace temperature control was  $\pm 0.01\%$ . Hence, the major irreproducibilities appear to have been in the sequence of actions associated with the actual drops: opening the furnace-to-calorimeter gate and the calorimeter shutter, activating the drop mechanism to initiate the programmed drop, reengaging the clutch to close the shutter and gate, and adding heat transfer gas to the calorimeter to the desired pressure (helium, 15 torr absolute). Little difficulty is anticipated in increasing the reproducibility of this sequence.

In summary, the achievement of greater than  $\pm 0.1\%$  accuracy in an enthalpy determination will depend principally on the accuracy of the determination of the furnace temperature and only slightly less on the accuracy of the heat loss correction. The precision of enthalpy determinations should not be less than  $\pm 0.1\%$  and could be improved to  $1/3$  to  $1/2$  of this value when experience is gained in the use of the complete drop calorimeter and when the adiabatic calorimeter is used in place of the copper-block device.

#### d. CALORIMETRY

In computing the corrected temperature rise of the calorimeter block during an electrical calibration or by the drop of a heated sample, account must be taken of heat loss by the block to the water jacket and to the

external environment through the calorimeter access tube (see ANL-6800, p. 322, Fig. IV-1). In this computation use is made of Newton's cooling law,

$$-\frac{d\theta}{dt} = \alpha(\theta_c - \theta) + U, \quad (4)$$

where

$\theta$  = calorimeter block temperature,

$\theta_c$  = convergence temperature,

$\alpha$  = cooling constant in  $\text{sec}^{-1}$ ,

$U$  = constant heat exchange term in  $\text{deg/sec}$ ,

and

$t$  = time in sec.

The law states that the rate of temperature change of a body—in this case, the calorimeter block—is proportional to the thermal head. Both the cooling constant  $\alpha$  and the constant term  $U$  are determined from the data of the fore- and after-periods. In the data so far evaluated, the cooling constant and the constant term were parallel functions of the atmosphere maintained in the calorimeter well. The full significance of this observation is not clear, although it is certain that it reflects the effect of transfer of heat between the copper block and the jacket and between the block and the external environment. The calorimeter is to some degree connected thermally to the external environment through the calorimeter access tube by the pressurizing gas used.

A further effect of the thermal connection of jacket, copper block and external environment was noted on the energy equivalent of the calorimeter,  $\mathcal{E}(\text{Calor.})$ . Approximate values of  $\mathcal{E}(\text{Calor.})$  for vacuum, air, and 15 torr helium\* in the access tube were 1053, 1056 and 1057.5  $\text{cal/deg}^{-1}\text{C}$ . In effect, a different calorimeter is used during the fore-period of a normal drop (calorimeter evacuated) than during the period following the drop (15 torr helium in the calorimeter well and access tube). The complications introduced by the required addition of a conducting gas can be handled in the computation of the corrected temperature rise.

## 2. $2500^\circ\text{C}$ Drop Calorimeter

Because of the press of work on the  $1500^\circ\text{C}$  drop calorimeter, assembly of the electron-beam-heated  $2500^\circ\text{C}$  drop calorimeter was temporarily suspended. The specifications of high precision automatic photo-

electric brightness pyrometers are being evaluated with a view to the joint use of such a device with both the  $1500^\circ\text{C}$  and the  $2500^\circ\text{C}$  calorimeters.



## V. Reactor Safety\* (L. Baker, A. D. Tevebaugh)

The program on reactor safety comprises three areas of research: (1) the study of metal-water reactions,

\* A summary of this section is given on pages 13 to 15.

(2) recently initiated studies relating to the safety of fast reactors, and (3) the study of the oxidation and ignition processes of substances used in reactor technology.

### A. METAL-WATER REACTIONS

#### 1. Studies of Metal-Water Reactions by the High Pressure Furnace Method

(R. E. WILSON, C. BARNES)

A high temperature, high pressure furnace has been constructed in order to study the reaction of steam with stainless steel, zirconium, aluminum, and  $UO_2$ . The

basic furnace components were described in a previous report (ANL-6900, p. 242). The furnace, which is contained in a steel pressure vessel, consists of two zones:

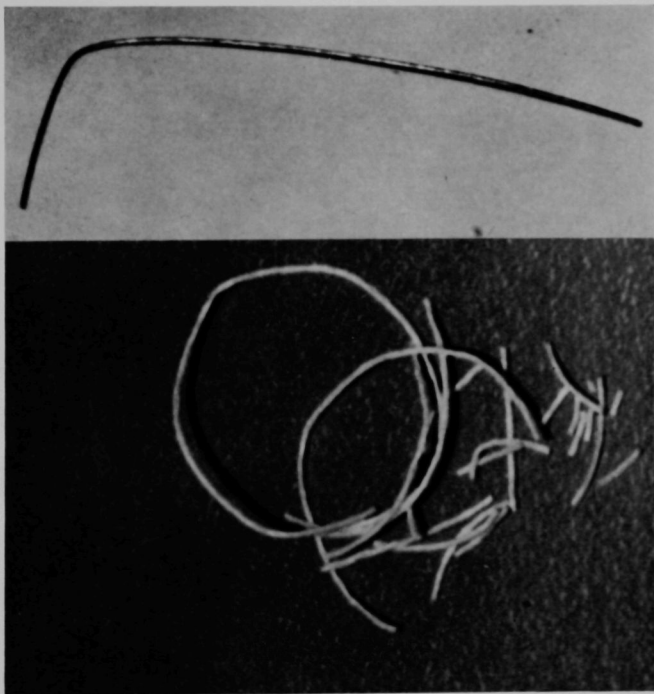
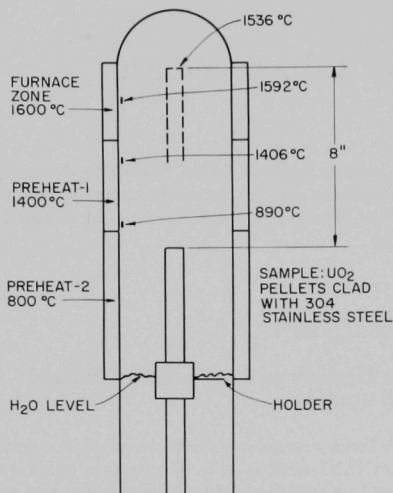


FIG. V-1. Appearance of Zirconium Wires (15 mil) Before and After Exposure to Steam at 1450°C and 15 psig.



108-8575

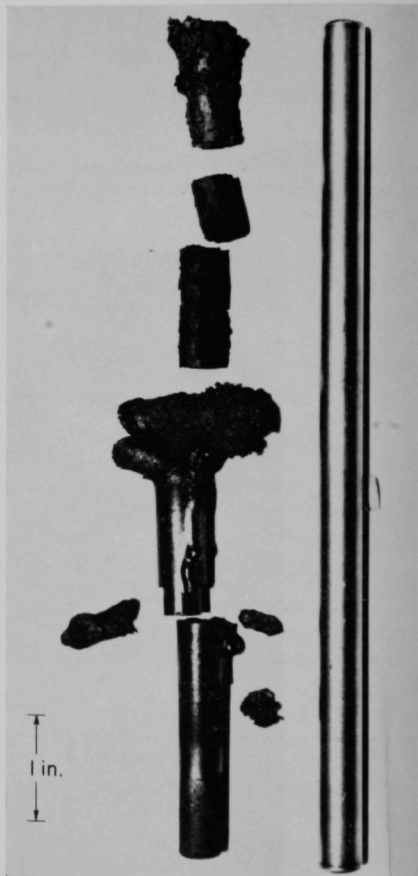
FIG. V-2. Temperature Distribution in the High Pressure Furnace during the Simulated Fuel Element Experiment.

an internal, steam-filled zone that is surrounded by an alumina tube, and an external zone that is argon-filled. The argon-filled zone contains molybdenum heater windings and insulation. The pressures in the two zones are automatically matched to avoid stresses on the alumina tube. Water is introduced into the lower part of the steam zone by a positive displacement pump and is converted to steam. Some unreacted steam and the hydrogen produced by metal-steam reaction are continuously removed from the upper part of the steam zone (high temperature section) through an outlet valve. The extent of reaction is determined by the amount of hydrogen collected. The pressure is controlled by a pressure regulator operating the outlet valve. The apparatus is designed for a maximum pressure of 1000 psig and sample temperatures as high as 1700°C. During the start-up period of an experiment, the sample is introduced into the lower (cooler) part of the steam-filled zone, the air is flushed out, and the furnace (already at the operating temperature) is brought up to the operating pressure. After conditions have stabilized the sample is raised into the upper (hottest) part of the steam zone by an external crank mechanism.

#### a. ZIRCONIUM WIRE

A shakedown experiment was performed with a sample consisting of 200 mg of 15-mil zirconium wire contained in an alumina crucible. The sample tempera-

ture was increased from 700°C to about 1450°C in a few minutes. The steam pressure was held at 15 psig in this experiment. The sample wire was converted into a thread of stoichiometric  $ZrO_2$ , shown in Figure V-1. A volume of hydrogen which corresponded to 99.2% completion of the zirconium-steam reaction was collected over a period of about 90 min. The sample residue was originally in one piece and was broken during handling after removal from the apparatus. The results indicated satisfactory furnace operation with quantitative hydrogen collection.



108-8018 Rev. 2

FIG. V-3. Simulated Fuel Element (304-Stainless Steel Clad,  $UO_2$  Core) Before and After Exposure to Steam at 1500°C and 15 psig.

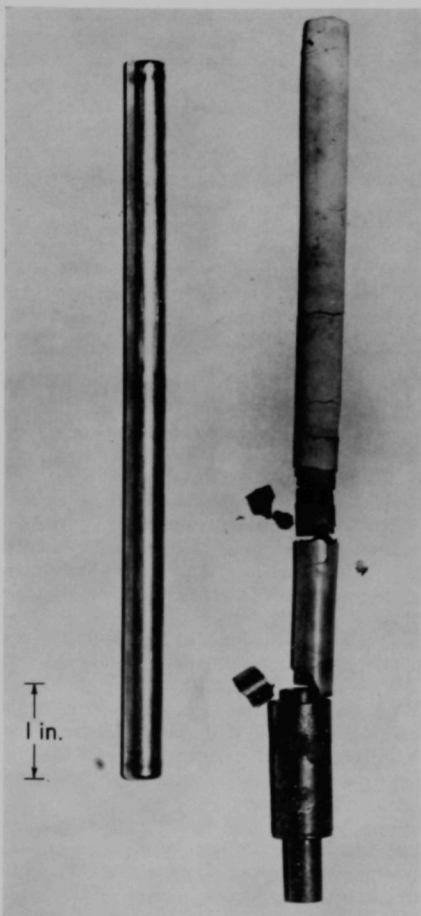
### b. STAINLESS STEEL-CLAD $\text{UO}_2$

The second experiment was designed to simulate the environment of the fuel in a water-cooled power reactor following a loss-of-coolant accident. In such a situation, the fuel would be subjected to a slowly rising temperature because of decay heat. Typical accident calculations have indicated that, in the absence of effective countermeasures, fuel temperatures would reach the melting point of the metal cladding in about 10 min. The steam pressure in this experiment was arbitrarily set at 15 psig.

The sample consisted of several high-density  $\text{UO}_2$  pellets clad with type 304 stainless steel tubing having a wall thickness of 27 mils. The top and bottom of the stainless steel tube were closed with  $\frac{3}{16}$ -in. thick welded plugs. The overall length of the sample was 8 in. The 2.5-mil radial gap between the  $\text{UO}_2$  and the cladding was filled with helium.

The temperature distribution of the furnace is shown in Figure V-2. The temperature of the center of the hot zone was  $1536^\circ\text{C}$  before the sample was raised into the upper position. At this time the top of the sample was at about  $800^\circ\text{C}$ . The sample was raised to the upper portion of the furnace at a rate of 1 in./min. After insertion of the sample, the temperature of the central portion of the hot zone dropped to  $1488^\circ\text{C}$  and then rose to  $1499^\circ\text{C}$  over a period of 12 min. The upper two thermocouples failed after 21 min. At this time the indicated temperature was  $1495^\circ\text{C}$  in the center of the hot zone.

The reaction was continued for 180 min from the time that the sample was first inserted. The sample was then lowered to its original position. About 9 liters (STP) of hydrogen was collected (mostly during the first 90 min). This amount of hydrogen corresponds to a reaction of about 62% of the stainless steel. The sample fuel element, after removal from the furnace, is shown along with an unreacted sample in Figure V-3. The appearance of the reacted sample shows that relatively little reaction occurred at the lower end of the sample which was maintained at about  $800^\circ\text{C}$ , and that extensive reaction of the stainless steel occurred in that portion of the sample which reached a temperature of above about  $1400^\circ\text{C}$ . The appearance of the fuel element after exposure to steam suggests that considerable foaming of the stainless steel occurred during the reaction. The cladding was almost completely removed from several of the  $\text{UO}_2$  pellets in the upper portion of the fuel element. The spongy mass at the top of the fuel element is probably the remains of the  $\frac{3}{16}$ -in. thick top end cap. The appearance of some of the  $\text{UO}_2$  pellets indicated considerable deterioration. Chemical and X-ray analyses of the pellets will be performed to determine the nature of the reaction.



108-8059 Rev. 2

FIG. V-4. Simulated Fuel Element (Zircaloy-2 Clad,  $\text{UO}_2$  Core) Before and After Exposure to Steam at  $1500^\circ\text{C}$  and 15 psig.

### c. ZIRCALOY-2-CLAD $\text{UO}_2$

A sample fuel element, identical with the stainless steel-clad element with the exception that the clad material was Zircaloy-2, was exposed to the same environment as the stainless steel-clad element.

The reaction was continued for a total of 270 minutes from the beginning of the insertion of the sample. The sample was then lowered to the original position. The total hydrogen collected corresponded to 73.6% reaction of the Zircaloy-2.

The sample residue and an unreacted fuel element are shown in Figure V-4. The  $\text{UO}_2$  showed some evidence of deterioration, but this effect was not as pronounced as in the first experiment with a stainless steel-clad element. The upper portion, i.e., hottest portion, of the Zircaloy-2 cladding appeared to be entirely converted to oxide, while the cooler end of the sample retained a metallic appearance. In the broken sections of the fuel element, the cladding residue consisted of two layers, a white outer layer and a yellow inner layer. The oxide appeared to have considerable strength. The original diameter of the fuel element (0.426 in.) increased upon complete oxidation to between 0.458 and 0.486 in.

## 2. Reaction of Refractory Metals with Steam (M. KILPATRICK, S. K. LOTT)

A brief study of the kinetics of reactions of refractory metals with steam was undertaken for two primary reasons:

1. to determine the suitability of high-melting metals for the fabrication of equipment for studies of metal-water reactions at high temperatures, and
2. to extend our knowledge of the kinetics and mechanisms of high temperature metal-steam reactions in general.

The metals studied included molybdenum (m.p. 2610°C), rhenium (m.p. 3100°C), tungsten (m.p. 3380°C), niobium (m.p. 2470°C), and tantalum (m.p. 2996°C). Because of the high melting points of these metals, it is possible to study metal-steam reactions at high temperatures while taking advantage of the greater simplicity and accuracy inherent in studies of solid, rather than liquid, metals.

In prior work, the oxides resulting from the metal-water reaction have not been volatile. Among the refractory metals, however, are some which form at least one oxide whose melting and boiling points lie below the melting and boiling points of the parent metal (see ANL-6800, p. 336). The study of the reaction of such metals, i.e., molybdenum, rhenium, and tungsten, with steam was expected to shed new light on the mechanisms and rate laws of metal-water reactions.

The experimental method consisted of passing steam over an inductively heated sample of metal, passing the products through a condenser to remove the aqueous solution, and collecting the gas evolved in a eudiometer. The apparatus has been described in previous reports (ANL-6800, p. 335 and ANL-6900, p. 244). Studies of the reaction of steam with molybdenum, rhenium, tungsten, niobium, and tantalum have now been completed by this method and are reported in separate sections below. It was concluded that the high reaction

## d. FUTURE STUDIES

The preliminary experiments described above have demonstrated the chemical and physical changes which a reactor fuel might undergo following a loss-of-coolant accident. Additional experiments will be performed with simulated fuel for shorter periods of exposure in order to check reaction rate calculations of the type described in Section VA-7 of this report. The furnace will also be used for isothermal studies of the aluminum-steam reaction at elevated pressures and the stainless steel-steam reaction at temperatures greater than 1400°C.

rates observed for all five metals precluded their use as materials of construction for high temperature metal-water studies. During these investigations, a brief study was made of the thermal decomposition of flowing steam on platinum, iridium, and nickel surfaces; these studies were reported in ANL-6900, p. 244.

## a. MOLYBDENUM (1100 to 1700°C)

Preliminary results of the reaction of molybdenum with steam were reported in ANL-6800, p. 335. Experiments conducted in the range 1100–1700°C showed that the reaction followed a linear rate law. The velocity constant, expressed in gram atoms  $\text{Mo}/(\text{cm}^2)(\text{min})$  varied from  $6 \times 10^{-4}$  at 1700°C to  $2 \times 10^{-8}$  at 1130°C.

To determine the effect of steam flow rate on the velocity constant, a series of experiments was performed in which quartz tubes of different diameters were used with specimens of various diameters. The data are presented in a plot of hydrogen evolved versus time for typical runs in Figure V-5. An Arrhenius plot in Figure V-6 shows that a tenfold change in flow rate causes a change of less than a factor of two in the velocity constant.

The Arrhenius equations for the velocity constants as gram atoms  $\text{Mo}/(\text{cm}^2)(\text{min})$  at three steam flow rates are as follows:

at 4.7 liters/ $(\text{cm}^2)(\text{min})$  steam flow

$$k = (6.58 \pm 1.54) \times 10^2 \exp \frac{-54,400 \pm 700}{RT}, \quad (1)$$

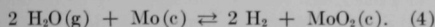
at 25 liters/ $(\text{cm}^2)(\text{min})$  steam flow

$$k = (12.18 \pm 1.79) \times 10^2 \exp \frac{-55,600 \pm 500}{RT}, \quad (2)$$

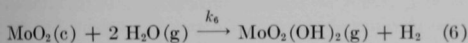
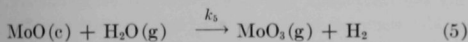
at 51 liters/ $(\text{cm}^2)(\text{min})$  steam flow

$$k = (28.0 \pm 16.2) \times 10^2 \exp \frac{-57,500 \pm 1,800}{RT}. \quad (3)$$

It is pertinent at this point to speculate on the mechanism of the molybdenum-steam reaction. In reactions between gases and solids, the usual sequence of processes is collision, sorption, and reaction. When steam is passed over a noble metal at temperatures above 1500°K, the products of the reaction are hydrogen and oxygen, and the equilibrium between water vapor, hydrogen, and oxygen is rapidly established at the temperature of the metal. The reaction of steam with readily oxidizable metals such as molybdenum, tungsten, and rhenium produces hydrogen and metal oxide, whereas the reaction with a less readily oxidizable metal such as nickel produces some oxygen along with hydrogen and metal oxide. It seems logical to assume that water vapor is dissociatively adsorbed on the metal and that the resulting adsorbed oxygen adds two electrons to form the oxide ion and subsequently the oxide. For the reaction of molybdenum with steam,



The  $\text{MoO}_2$  would offer a barrier to the diffusion of water vapor or oxygen to the metal and, if no other reactions took place, the rate law would be parabolic. However,  $\text{MoO}_2$  is rapidly oxidized to  $\text{MoO}_3$  and the trioxide is removed as a vapor of  $\text{MoO}_3$  or its polymers, or as the more volatile  $\text{MoO}_2(\text{OH})_2$ .



The amount of molybdenum present in the  $\text{MoO}_2$

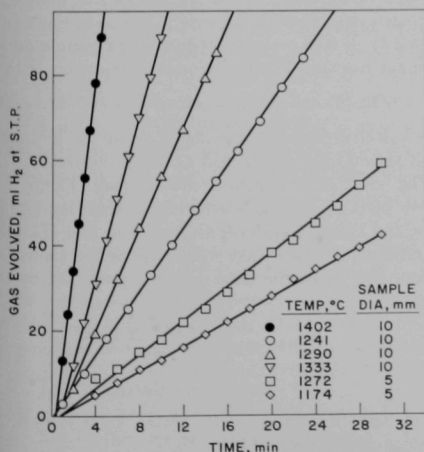
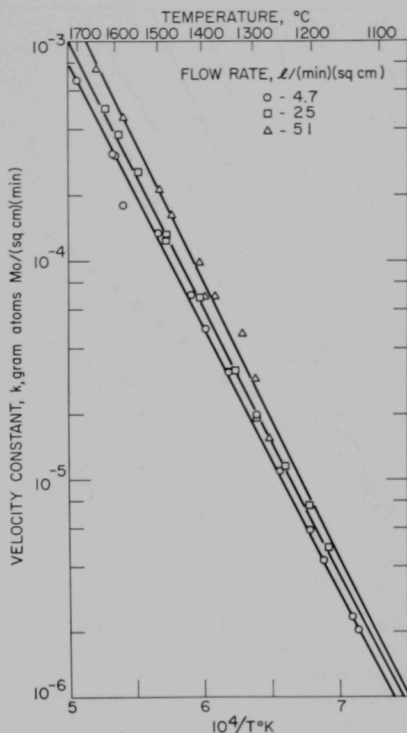


FIG. V-5. Reaction of Molybdenum with Steam.



108-7424 Rev.

FIG. V-6. Arrhenius Plot for the Molybdenum-Steam Reaction at Various Flow Rates.

film would depend on the relative rates of loss of dioxide by reactions 5 and 6 and of formation of dioxide by reaction 4. Letting  $x$  represent gram atoms  $\text{Mo}/\text{cm}^2$  fixed in the film at time  $t$ , we have, following Loria's<sup>1</sup>

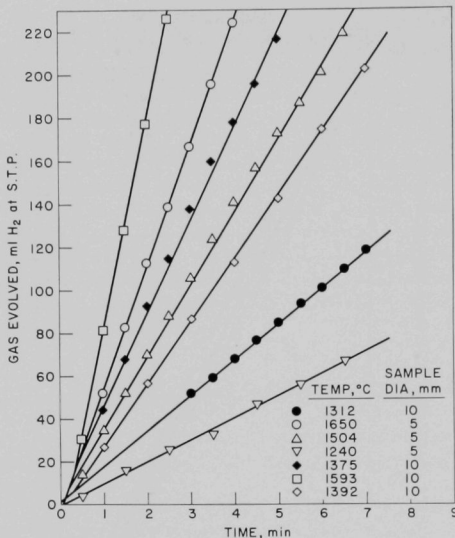
$$dx = \frac{k_p}{x} dt - k_t dt \quad (7)$$

where  $k_p$  is a parabolic rate constant and has units of  $(\text{gram atoms Mo}/\text{cm}^2)^2 \text{min}^{-1}$  and  $k_t$  is a linear rate constant in units of  $(\text{gram atoms Mo}/\text{cm}^2) \text{min}^{-1}$ . Since our experimental curves are straight lines passing through or close to the origin, it is clear that the steady state where

$$\frac{dx}{dt} = 0 \quad \text{and} \quad (x)_{\text{state}} = k_p/k_t \quad (8)$$

is reached practically at once, and that the amount of

<sup>1</sup> J. Loria, Compt. rend. **231**, 522 (1950).



108-7627

Fig. V-7. Reaction of Rhenium with Steam.

molybdenum stored as  $\text{MoO}_2$  film is negligible. Our observation of only a slight tarnish on the molybdenum metal supports this hypothesis. The measured rate of loss of molybdenum from the specimen under our conditions is then given by the linear rate constant,  $k_t$ , in (gram atoms  $\text{Mo}/\text{cm}^2$ )  $\text{min}^{-1}$  or ( $1/3$  moles  $\text{H}_2/\text{cm}^2$ )  $\text{min}^{-1}$ .

If the dioxide yields gaseous  $\text{MoO}_2(\text{OH})_2$  as well as gaseous  $\text{MoO}_3$  plus its polymers, the rate constant would be expected to be

$$k = [\text{MoO}_2(c)] (\text{H}_2\text{O}) [k_5 + k_6 (\text{H}_2\text{O})] \quad (9)$$

where  $[\text{MoO}_2(c)]$  represents the surface concentration of active sites.

The measured energy of activation has an average value of about 55 kcal/mole. It is of interest to compare this figure with the enthalpy changes accompanying reactions 5 and 6, respectively. Employing the heats of formation<sup>2</sup> of the species involved in reaction 5 one finds that  $\Delta H_5 = 61$  kcal/mole at 1500°C. The same calculation cannot be made for reaction 6 at this temperature because of lack of information about the hydrate; however, an estimate can be made of  $\Delta H_6$  at 1000°K. Glemser and v. Haesler<sup>3</sup> studied the reaction

at temperatures up to about 1000°K, and found  $\Delta H_{10} = 35.3$  kcal/mole,



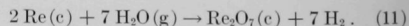
from which one obtains  $\Delta H_6 = 47$  kcal/mole at 1000°K.

## b. RHENIUM (350 to 1700°C)

Although the oxidation of rhenium has been studied in air,<sup>4,6</sup> no study of the reaction of steam with rhenium has been reported. The reaction of rhenium with oxygen produced  $\text{Re}_2\text{O}_7$ , which melts at 296°C and boils at 362°C under 1 atm pressure. The reaction occurs uniformly over the surface rather than preferentially at the grain boundaries.

For the present study rhenium metal with a quoted purity of 99.9% was obtained from the Rembar Company in the form of rods 5 and 10 mm in dia. The product metal had been sintered in hydrogen at 2700°C, compacted, cold swaged to finish size by 10% reduction per pass, and process annealed in hydrogen-nitrogen. The final annealing was carried out at 1650°C in a hydrogen atmosphere. Spectrographic analysis at Argonne showed only a faint trace of calcium (<0.0001%) and a trace of aluminum (<0.001%). Sample specimens were cut from the rods in 1-cm lengths, and  $1/10$ -in. dia. holes drilled by the Elox method for mounting the samples in the field of the induction furnace.

The rhenium specimens were heated inductively in flowing steam at temperatures from 850 to 1700°C. The rhenium at the end of a run was bright, but examination of the surface showed many small crystals of metal randomly oriented. Plots of the hydrogen evolved vs. time were linear. A comparison of the volume of hydrogen evolved with the weight loss of the specimen gave  $3.41 \pm 0.15$  moles of hydrogen per gram atom of rhenium reacted. The stoichiometric equation is thus



The velocity constants calculated from the hydrogen evolved and from weight loss agreed fairly well.

The effect of flow rate is rather small. Figure V-7 shows plots of hydrogen evolved vs. time for typical runs, and Figure V-8 shows an Arrhenius plot of all the data. Although two least squares lines are shown on Figure V-8, all of the data can be represented by the equation

$$k = (0.962 \pm 0.384) \exp \frac{-29,800 \pm 1,000}{RT} \quad (12)$$

gram atoms  $\text{Re}/(\text{cm}^2)(\text{min})$

<sup>4</sup> C. Agte, H. Alterthum, K. Becker, C. Heyne and K. Moers, Z. anorg. allgem. Chem. **196**, 129 (1931).

<sup>5</sup> C. Sims, C. M. Craighead and R. I. Jaffe, Trans. A.I.M.E. **7**, 168 (1955).

<sup>6</sup> W. L. Phillips, Jr., J. Less-Common Metals **5**, 97 (1963).

<sup>2</sup> C. E. Wicks and F. E. Block, Bulletin 605, U. S. Bureau of Mines, 1963.

<sup>3</sup> O. Glemser and R. v. Haesler, Z. anorg. allgem. Chem. **316**, 168 (1962).

This value of about 30 kcal/mole for the energy of activation may be compared with  $\Delta H_{\text{sublimation}} = 33.5 \pm 0.1$  kcal/mole for solid rhenium heptoxide at the m.p. 296°C.<sup>7</sup> This suggests the possibility that the rate-determining step is the desorption of the oxide.

### c. TUNGSTEN (1050 to 1700°C)

Although the reaction of flowing steam with tungsten is similar in some respects to the reaction with molybdenum over the temperature range concerned, there are important differences. The oxide products are relatively less volatile than the corresponding molybdenum compounds. The presence of a liquid phase around 1450°C complicates the kinetics. Two oxides,  $W_{20}O_{88}$  and  $W_{18}O_{49}$ , are formed which are less volatile and less readily oxidized to  $WO_3$  than is  $WO_2$ . Above 1530°C,  $WO_2$  disproportionates to W and  $W_{18}O_{49}$ .<sup>8</sup>

The oxidation of tungsten by water vapor at 38 torr has been reported by Farber,<sup>9</sup> who measured the change in electrical resistance with time over the temperature range 1700–2000°K and found a value of 14.5 kcal/mole for the energy of activation.

The tungsten used in these experiments was in the form of 5- and 10-mm dia. rods and was 99.9% pure. Both the 5- and 10-mm rods contained similar trace impurities, including Fe, Cr, and Mo. The tungsten specimens were heated inductively in flowing steam at temperatures from 1050 to 1700°C.

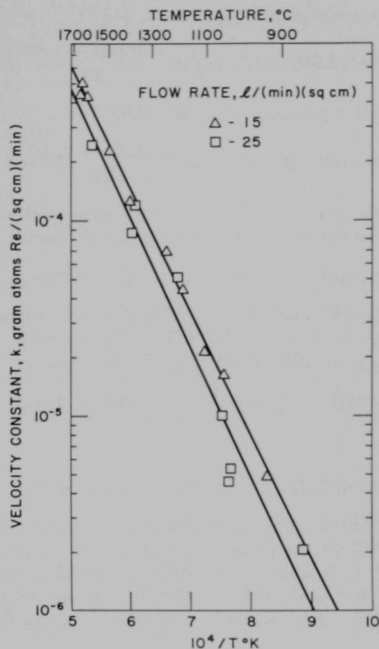
The stoichiometry of the reaction was established by comparing the moles of hydrogen evolved with the gram atoms of tungsten reacted as determined by weight loss. Although this ratio was  $3.02 \pm 0.04$ , the specimen at the end of a run was very seldom free of black oxide or nonadhering dark violet oxide. Filings from the surface of the specimen after a typical run near 1200°C were examined by X-ray diffraction and were found to contain  $WO_2$  with  $W_{20}O_{88}$  as a minor constituent in addition to tungsten. Filings from a specimen after a run just above 1500°C were found to contain  $W_{18}O_{49}$  as a minor constituent in addition to tungsten.

There is considerable heat evolved when the polished metal initially reacts with steam, but the temperature of the sample rapidly becomes constant. When a specimen is rerun without polishing, the initial rise in the temperature of the specimen above the control temperature is absent, and the rate of reaction is the same

<sup>7</sup> W. T. Smith, Jr., B. E. Line, Jr., and W. A. Bell, J. Am. Chem. Soc. **74**, 4964 (1953).

<sup>8</sup> B. Philip and L. L. Y. Chang, Trans. A.I.M.E. **203**, 1203 (1964).

<sup>9</sup> M. Farber, J. Electrochem. Soc. **100**, 751 (1959).



108-7634

FIG. V-8. Arrhenius Plot for the Rhenium-Steam Reaction at Various Flow Rates.

as that of a polished specimen after the initial perturbation. However, if the temperature of the specimen overshoots to 1500°C, with a very rapid evolution of hydrogen, the subsequent drop in temperature to about 1470°C causes the evolution of hydrogen to decrease sharply. This decrease is due to the fact that, as the molten oxide solidifies, the coating becomes impermeable to steam. Reaction does not continue normally unless the temperature is raised above the melting point of  $WO_3$  (1473°C).

In spite of the fact that not all of the product was converted to the volatile trioxide or its complex with water, the rate of evolution of hydrogen was constant, and the velocity constants, in gram atoms  $W/(\text{cm}^2)$  (min) calculated from the weight loss agreed well with the velocity constants calculated from hydrogen evolution.

Figure V-9 shows a plot of hydrogen evolved vs. time for typical experiments. All data are summarized in an Arrhenius plot in Figure V-10.

The Arrhenius equations for the velocity constants, in gram atoms  $W/(\text{cm}^2)$  (min) are as follows:

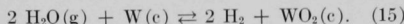
for the temperature range 1050 to 1450°C

$$k = (1.688 \pm 0.593) \exp \frac{-48,900 \pm 1,000}{RT} \quad (13)$$

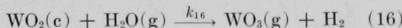
for the temperature range 1450–1700°C

$$k = (0.282 \pm 0.178) \exp \frac{-22,700 \pm 2,200}{RT} \quad (14)$$

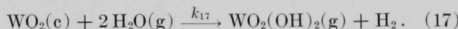
If the reaction of tungsten with steam follows the path for the reaction of molybdenum with steam, then



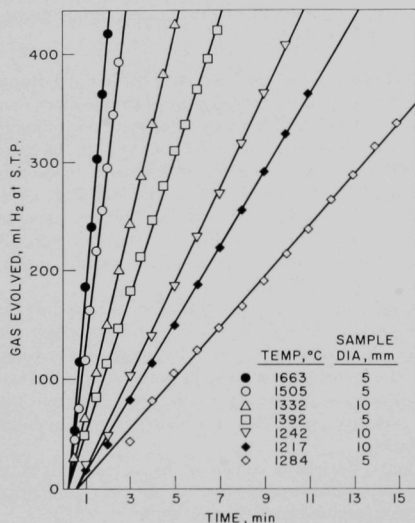
The dioxide would then be oxidized to  $\text{WO}_3$  and would be removed as a vapor of  $\text{WO}_3$  and its polymers, or as the more volatile  $\text{WO}_2(\text{OH})_2$ , via the reactions



and

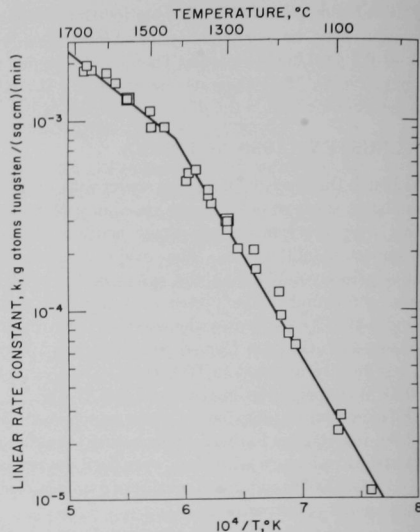


As in the case of molybdenum, the measured reaction rate follows the linear law, and shows (1) that the steady state would be reached very quickly under the conditions used, and (2) that the amount of metal stored as dioxide would be small. Assuming the dioxide



108-7632

FIG. V-9. Reaction of Tungsten with Steam.



108-7630

FIG. V-10. Arrhenius Plot for the Tungsten-Steam Reaction.

to be removed via both reaction 16 and reaction 17, the rate constant would be

$$k = [\text{WO}_2(\text{c})] (\text{H}_2\text{O}) [k_{16} + k_{17}(\text{H}_2\text{O})], \quad (18)$$

where  $[\text{WO}_2(\text{c})]$  represents the surface concentration of active sites.

The measured energy for the reaction of steam with tungsten over the range 1050 to 1450°C is 49 kcal/mole. It is of interest to compare this figure with the enthalpy changes accompanying reactions 16 and 17, respectively. Using the heats of formation<sup>10</sup> of  $\text{WO}_2(\text{c})$  and  $\text{WO}_3(\text{c})$ , and the heat of sublimation of the trioxide from Glemser and Völz,<sup>11</sup> one finds  $\Delta H_{16}$  at 1500°K to be 43 kcal/mole. For the reaction



$\Delta H$  is about 40 kcal/mole.<sup>3, 11, 12</sup> From this value and the heats of formation,  $\Delta H_{17}$  at 1500°K is estimated to be 41 kcal/mole. It may also be mentioned that Battles<sup>13, 14</sup> investigated the rate of volatilization of the

<sup>10</sup> J. P. Coughlin, Bulletin 542, U. S. Bureau of Mines, 1954.

<sup>11</sup> O. Glemser and H. G. Völz, Naturwiss. **43**, 33 (1956).

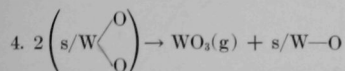
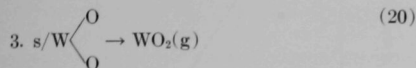
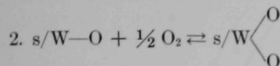
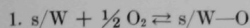
<sup>12</sup> G. R. Belton and R. L. McCarron, J. Phys. Chem. **68**, 1852 (1964).

<sup>13</sup> J. E. Battles, Doctoral Dissertation, Department of Metallurgical Engineering, Ohio State University, 1964.

<sup>14</sup> J. E. Battles, M. Sc. Thesis, Department of Metallurgical Engineering, Ohio State University, 1961.

trioxide in a flowing mixture of argon and water vapor and found the energy of activation to be 40 kcal/mole.

In a recent paper, Bartlett<sup>15</sup> has proposed that the reaction between oxygen and tungsten, below 2000°C, proceeds by the steps



where  $s/W$  indicates an uncovered surface site, and  $s/W-O$  indicates a covered site in a monolayer of chemisorbed oxygen atoms. At low pressures, about equal amounts of  $WO_2$  and  $WO_3$  would form, the proportion of the latter increasing with increasing pressure of oxygen. The activation energy for the oxygen-tungsten reaction found by Bartlett was 42 kcal/mole. Although there was discoloration of the tungsten rods in his experiments, he believed the surface film to have formed on cooling.

In view of the results in the present study, it appears that in the reaction of water vapor and tungsten there is an initial, rapid reaction with the bright metal, accompanied by evolution of heat. During this initial reaction a film of oxide is formed on the surface of the metal so that if the specimen is reused without polishing a steady rise of control temperature occurs, with no overshoot. This phenomenon is readily reproducible. The hypothesis that a thin layer of lower oxide is formed appears, therefore, to be more tenable in the case of the reaction of water vapor with tungsten than does the scheme proposed by Bartlett for the reaction of oxygen with tungsten.

#### d. NIOBIUM (1050 to 1500°C)

Blackburn<sup>16</sup> has shown that when niobium is oxidized by water vapor, beginning at 250°C a film consisting of  $NbO$  and  $Nb_2O_3$  grows on the surface of the metal, an outer scale of porous  $Nb_2O_5$  is formed up to 750°C, whereas  $Nb_2O_5$  begins to form between 750 and 900°C. Graphs of log weight loss vs. log time indicate a parabolic rate law,  $W^2 = k_{st}t$ , for the temperature range 250 to 350°C; between 400 and 750°C the data can be fitted to a cubic law,  $W^3 = k_{st}t$ ; and between 750 and

TABLE V-1. TRACE IMPURITIES IN NIOBIUM

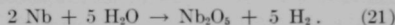
Element (ppm)	Element (ppm)	Element (ppm)	Element (ppm)
Ag <1.5	Cr 5	Mo ~8	Ta 15
Ba <0.3	Cu <2	Ni <1.5	U <5
Be <0.01	Ga <0.5	P <50	W 250
Cd <1.5	Hf <1.5	Ni <1.5	Zn <5
Co <5	Mn <0.2	Sn <5	Zr 5

900°C the slope of the plot does not indicate either category. Analogous observations have been made for the reaction of niobium with oxygen<sup>16,17</sup> except that the beginning of the  $Nb_2O_5$  formation takes place between 400 and 500°C as compared to 750-900°C for the reaction of niobium with water vapor.

$NbO$  and  $Nb_2O_3$  were prepared and treated with water vapor by Blackburn.<sup>16</sup> For  $NbO$  at 500°C, the oxidation followed a linear law, but  $Nb_2O_3$  showed no weight gain until heated to 900°C when oxidation took place with a rate that increased with time and finally became constant. This process was interpreted as the beginning of breakdown oxidation by the nucleation and growth of  $Nb_2O_5$  on  $Nb_2O_3$ , with the  $Nb_2O_5$  growing through the  $Nb_2O_3$ . Since the rate of growth for  $Nb_2O_5$  is greater than for  $Nb_2O_3$ , the latter phase is eventually oxidized to  $Nb_2O_5$ .

The purity of the metal used in the present investigation was 99.5% and the impurities observed by spectrographic analysis are listed in Table V-1. The niobium samples were cut in lengths of 1 cm from 5- and 10-mm dia. rods and polished by abrasion with 600 grit silicon carbide paper. Specimens were heated inductively in flowing steam at temperatures from 1050 to 1500°C.

Analysis of the gas evolved indicated hydrogen and water vapor; X-ray analysis of the coating showed only  $\beta$   $Nb_2O_5$ ; and a comparison of the moles of hydrogen evolved to the gram atoms of niobium reacted, as determined by the weight increase, was  $2.57 \pm 0.16$ . This corresponds to the stoichiometric equation



The rate law is essentially linear after a brief (~2 min) induction period during which time the gas evolution is somewhat low (Figure V-11). Figure V-12 gives the Arrhenius plot of the linear rates for both the 5- and 10-mm dia. samples. The corresponding equations for velocity constants as gram atoms  $Nb/(cm^2)$  (min) are as follows:

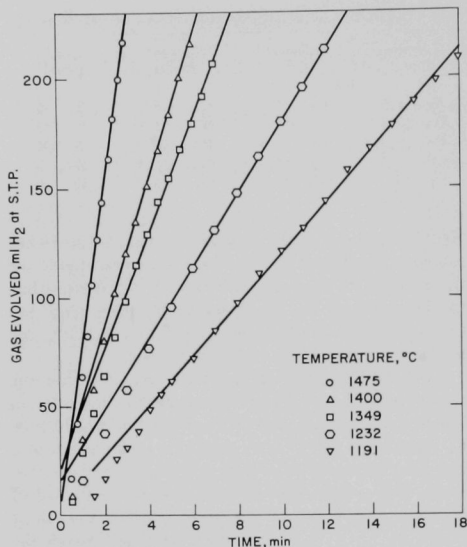
for 5-mm dia. rods and 15 liters/( $cm^2$ )(min) steam flow,

$$k = (0.714 \pm 1.114) \exp \frac{-29,400 \pm 4,000}{RT} \quad (22)$$

<sup>15</sup> R. W. Bartlett, Trans. A.I.M.E. **230**, 1100 (1964).

<sup>16</sup> R. E. Blackburn, J. Electrochem. Soc. **109**, 1142 (1962).

<sup>17</sup> T. Hurlen, J. Inst. Metals **89**, 273 (1961).



108-7779, Rev. 2

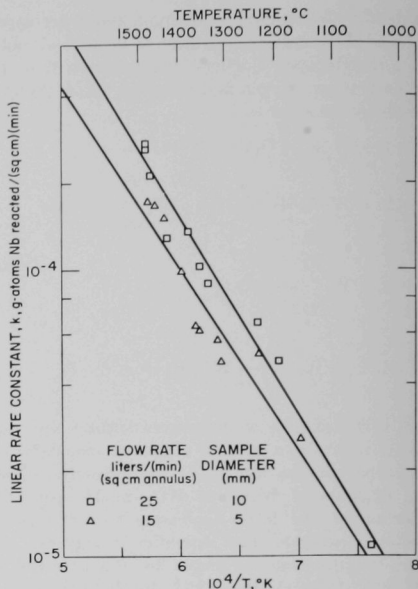
FIG. V-11. Reaction of Niobium with Steam.

and for 10-mm dia. rods and 25 liters/(cm<sup>2</sup>)(min) steam flow,

$$k = (2.000 \pm 1.200) \exp \frac{-31,500 \pm 1,800}{RT} \quad (23)$$

In the experiments conducted at temperatures between 1475 and 1500°C the oxide coating melted and there was some pitting of the specimens. When the melted oxide was resolidified, the evolution of hydrogen practically stopped. When the temperature was raised again above the melting range of Nb<sub>2</sub>O<sub>5</sub>, hydrogen was again evolved. Above 1500°C the rate of evolution of hydrogen was too fast for measurement under our experimental conditions.

The fact that NbO and NbO<sub>2</sub> are not found in these experiments is not a contradiction of the results of Blackburn.<sup>16</sup> Under our conditions NbO<sub>2</sub> would be completely oxidized, and the NbO film would be too thin for X-ray identification. During the induction period reactions, the formation of NbO and NbO<sub>2</sub> will have reached a steady state with very little if any NbO<sub>2</sub> remaining and only a thin coating of NbO. The rate determining step may be the nucleation and growth of Nb<sub>2</sub>O<sub>5</sub>. When the NbO<sub>2</sub> is completely reacted, the oxide coating will be more permeable to oxygen and the overall rate of the niobium-steam reac-



108-7777, Rev. 2

FIG. V-12. Arrhenius Plot for the Niobium-Steam Reaction.

TABLE V-2. TRACE IMPURITIES IN TANTALUM

Element (ppm)	Element (ppm)	Element (ppm)
Ag <1.5	Hf <1.5	Pb <1.5
Ba <0.3	In <1.5	Sb <15
Be <0.015	Zr <1.5	Sn <6
Co <1.5	Li <0.015	Ti 1
Cr 3	Nb 3	U <6
Cu <2	Ni <1.5	V 1.5
Fe 20	P <60	W <3
Ga <0.6		

tion will become constant. Since our experiments with water are at constant steam pressure, the oxygen concentration would also be constant at constant temperature.

### e. TANTALUM (950 to 1300°C)

Although an extensive study of the oxidation of tantalum by oxygen over the temperature range 300 to 1300°C has been carried out by Kofstad,<sup>18</sup> no data on the oxidation of tantalum by steam have been reported. In both cases, the oxide product is  $\beta$  Ta<sub>2</sub>O<sub>6</sub> below

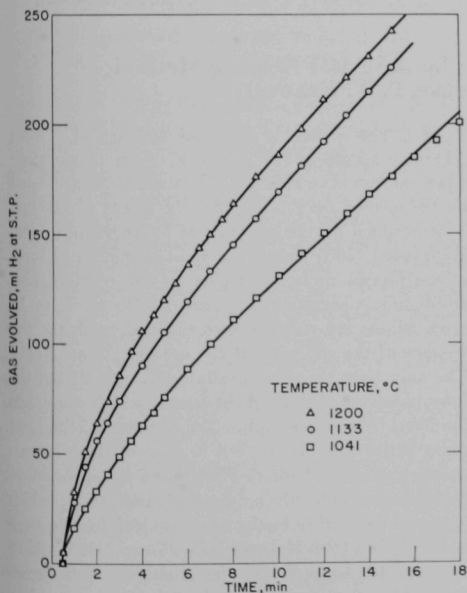
<sup>18</sup> P. Kofstad, J. Less-Common Metals 5, 477 (1963).

1200°C and  $\alpha$  Ta<sub>2</sub>O<sub>5</sub> above that temperature, and in both cases the reaction above 1300°C is too fast for measurement.

The specimens used in the present study were 1-cm long cylinders cut from 5- and 10-mm dia. rods of tantalum of 99.9% purity. Table V-2 lists the impurities found by spectrographic analysis. The specimens were descaled with 600 grit silicon carbide paper before being heated inductively in flowing steam at temperatures from 950 to 1300°C.

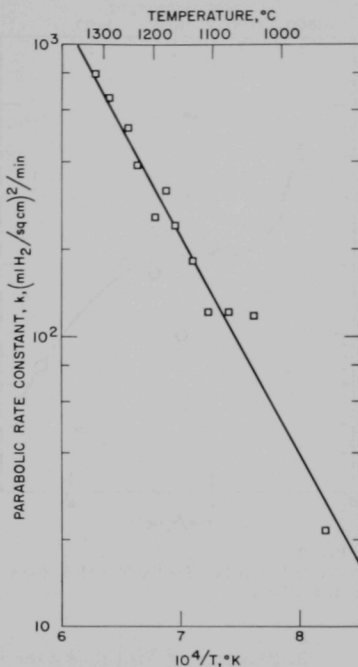
Although the only oxides identified by X-ray analysis were  $\beta$  Ta<sub>2</sub>O<sub>5</sub> (low temperature form) and  $\alpha$  Ta<sub>2</sub>O<sub>5</sub> (high temperature form) and the only gaseous product was hydrogen, it was not possible to establish the stoichiometry firmly from the ratio of the moles of hydrogen formed to the moles of Ta<sub>2</sub>O<sub>5</sub> calculated from the weight increase. The difficulty was due to the fact that tantalum reacted with the aluminum oxide support, and it was not always possible to remove the core of Al<sub>2</sub>O<sub>3</sub>. In some cases the oxide coating cracked off on cooling and a reliable weight could not be obtained. In a few cases, these difficulties were overcome and the ratio found was between 2.5 and 2.6.

Figure V-13 shows typical plots of the volume of



108-7775, Rev. 2

FIG. V-13. Reaction of Tantalum with Steam.



108-7774, Rev. 2

FIG. V-14. Arrhenius Plot for the Tantalum-Steam Reaction (Parabolic Portion).

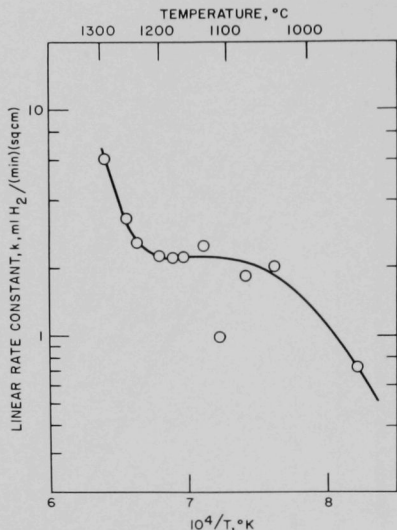
hydrogen evolved vs. time for the reaction of tantalum with steam. The reaction is para-linear, i.e., there is agreement with the parabolic rate law for the initial portion of the run, after which the reaction becomes linear. Figure V-14 presents an Arrhenius plot for the parabolic rate constant determined for the initial portion of the reaction in terms of the hydrogen evolved. The data fit the equation

$$k_p = (4.49 \pm 1.07) \times 10^7 \exp \frac{-34,700 \pm 2,500}{RT} \quad (24)$$

A similar plot for the linear portion is presented in Figure V-15. The similarity of this plot to the experimental plots of Kofstad<sup>19</sup> and the formulations of Ong<sup>20</sup> for the oxidation of tantalum in oxygen lead one to look on water vapor as a buffered source of oxygen,

<sup>19</sup> P. Kofstad, J. Electrochem. Soc. **110**, 491 (1963).

<sup>20</sup> J. N. Ong, Sr., Trans. A.I.M.E. **224**, 991 (1962).



108-7773, Rev. 2

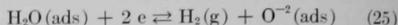
FIG. V-15. Arrhenius Plot for the Tantalum-Steam Reaction (Linear Portion).

### 3. Studies of Metal-Water Reactions by the Laser Heating Method (L. LEIBOWITZ, L. W. MISHLER, P. W. KRAUSE)

Experimentation is continuing on the application of laser beam heating to studies of rates of chemical reaction and heat transfer between individual metal particles and water. Using a simple lens, the beam from a ruby laser is focused on a small particle of metal submerged in water. The almost instantaneous heating of a metal particle simulates the rapid contacting of water with heated metal that would occur in a violent excursion in a water-cooled nuclear reactor. Analysis of reactor accidents requires information on the rate of exchange of both chemical and thermal energy between the metal and water. The laser heating technique was developed to allow the study of single metal particles of known size and the use of materials which cannot readily be examined by other methods.

Since the experimental procedure used in laser heating studies has already been described in detail (ANL-6800, p. 327), only an outline of the method is given here. A small square of metal foil (typically, 1 by 1 by 0.025 mm) is submerged in water in a quartz reaction cell which has optically flat windows on the top and

controlled by the hydrogen-to-water vapor ratio. The initial step in this process would be the dissociative adsorption of water vapor

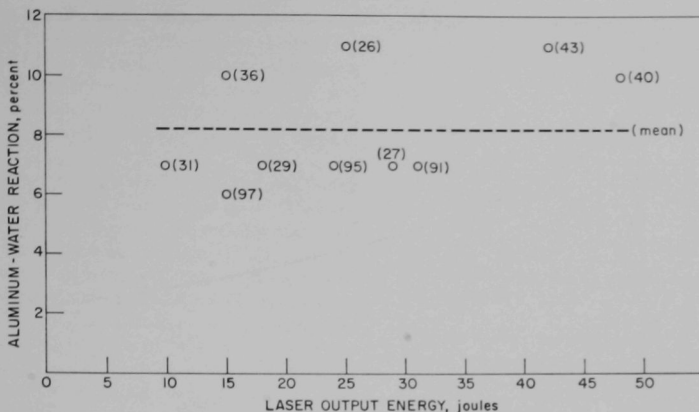


These reactions would be followed by nucleation, as postulated by Kofstad. The marked increase in rate of reaction near 1300°C may be associated with the transition of Ta<sub>2</sub>O<sub>5</sub><sup>21, 22</sup> from the low temperature to high temperature form. This transition is reported to occur at 1320 ± 20°C.<sup>22</sup> However, Kofstad<sup>18</sup> has found α Ta<sub>2</sub>O<sub>5</sub> at temperatures as low as 1200°C at an oxygen pressure of 0.01 torr. The oxygen pressure from the dissociation of water would be dependent on the hydrogen-water ratio and would be much lower than 0.01 torr if equilibrium with Ta<sub>2</sub>O<sub>5</sub> were established.

<sup>21</sup> S. Lagergren and A. Magneli, Acta Chem. Scand. **6**, 444 (1952).

<sup>22</sup> R. W. Wasilenski, J. Am. Chem. Soc. **75**, 1001 (1953).

bottom. The system is degassed and sealed. Unless otherwise specified, the cell is at room temperature when the run is carried out. The metal is then heated by the focused laser beam, and the extent of reaction is determined by the quantity of hydrogen produced. High speed (5000 frames per second) motion pictures of the process and examination of the residues give additional information. In much of the work to be reported, motion pictures were taken through the top window of the cell without the use of external lights. The only light that was available was that from the laser pulse and then from the sample which was made luminous by the laser pulse. The duration of the laser pulse varies with energy, but in most of these experiments was about 1 msec. From these films, measurements were made of the time of luminosity, which corresponds roughly to the time required for the sample to cool to 1500°K (see ANL-6257, p. 26). We have concentrated on studying the aluminum-water reaction and summarized below is the information now available. In all cases single particle residues were produced.



108-8536

FIG. V-16. Aluminum-Water Reaction: Variation of Percent Reaction with Laser Output Energy for Samples in Room Temperature Water. (Particle diameter:  $360\mu$ . Run numbers shown in parentheses.)

#### a. EFFECT OF LASER ENERGY

Using 1 by 1 by 0.025 mm pieces of aluminum foil ( $360\mu$  equivalent sphere diameter\*), experiments were carried out over a laser output range of 10 to 49 joules. The extent of aluminum-water reaction, calculated from hydrogen analyses, ranged from 6 to 11% with an average of 8.2%. The average deviation was about 20%.

Plotted in Figure V-16 are the data from these experiments. Although the data show considerable scatter, it is evident that in this energy range the extent of reaction is independent of laser beam energy. The numbers in parentheses are run numbers and indicate the order in which these experiments were carried out. It would, of course, be expected that at sufficiently low laser energies no reaction would occur. Although the threshold energy was not determined for the  $360\mu$  particles, a low energy threshold of 20 joules was observed in measurements with  $575\mu$  particles. Below an energy of 20 joules no reaction could be detected while above that energy roughly 10% reaction occurred. At energies greater than about 40 joules, sample breakup occurred with the  $575\mu$  particles.

#### b. EFFECT OF PARTICLE SIZE

The particle size range that could be investigated by the laser method was very narrow. With very small amounts of metal, difficulties in hydrogen analysis and sample handling were encountered; with very

large samples, insufficient laser power was available to achieve adequate heating. The results for the three particle sizes which could be studied are given in Figure V-17. The vertical lines through each point indicate estimated reliability ( $\pm 25\%$ ). The calculated line in the figure indicates percent reaction if one assumes that a  $7\mu$ -layer of aluminum reacts on each particle. The data are too limited to allow the general conclusion that the extent of reaction is equivalent to the reaction of a  $7\mu$  surface layer of aluminum, although this does describe the observed behavior over a limited particle size range within the accuracy of the data. Such a reaction is considerably greater than that expected from calculations based upon isothermal measurements at lower temperatures by the levitation method.\*\*

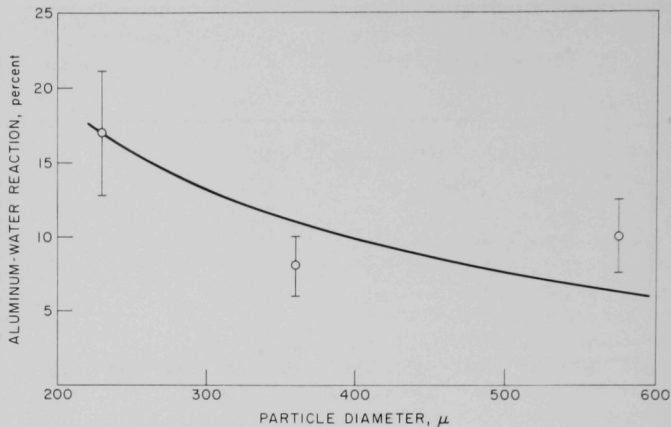
If the  $7\mu$  reaction hypothesis is correct, it would be necessary to use particles in the 50 to  $100\mu$  dia. range to achieve reactions extensive enough for results to be clearly outside experimental uncertainties. Extents of reaction predicted on this basis would be 55 and 40% for 50 and  $100\mu$  particles, respectively. Such small samples cannot be handled in the present experimental method.

#### c. EFFECT OF WATER PRESSURE

In addition to the effects of laser energy and specimen size, the effect of elevated water pressure (and temperature) on the aluminum-water reaction was

\* In the discussion that follows we will frequently refer to the sample size by the diameter of a sphere of equal volume. It should be remembered, however, that all samples were initially foil squares.

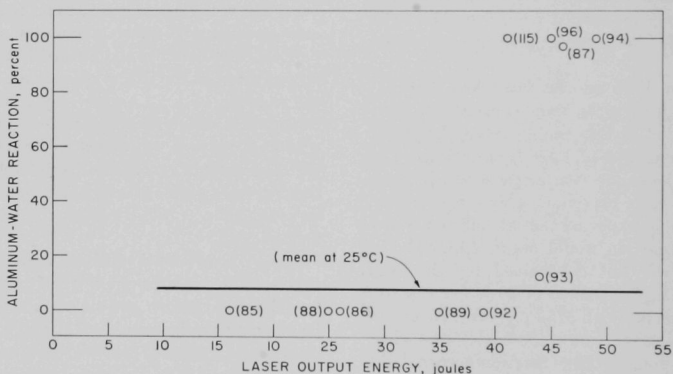
\*\* Unpublished calculation by L. Baker based on the kinetic studies of aluminum-steam reaction rates by R. E. Wilson (see ANL-6900, p. 233) indicate that less than 1% reaction would be expected in this range of particle sizes at temperatures below  $1750^\circ\text{C}$ .



108-8574

Fig. V-17. Aluminum-Water Reaction: Variation of Percent Reaction with Particle Size.

Water Temperature: 25°C  
 Percent Reaction Independent of Energy  
 Estimated 25% Average Deviation  
 Line Shows Calculated Values for the  
 Reaction of 7 $\mu$  Thickness of Aluminum



108-8535

Fig. V-18. Aluminum-Water Reaction: Variation of Percent Reaction with Laser Output Energy for Samples in 100°C Water. (Particle diameter: 360 $\mu$ . Run numbers shown in parentheses.)

examined. It was shown above that in the range of laser output energy between 10 and 49 joules an approximately constant extent of reaction was found in room temperature water. When similar experiments were carried out in a reaction cell heated to 100°C (1 atm water pressure) the results shown in Figure V-18 were obtained. The straight line at 8% reaction represents the average value for the runs in water at 25°C.

In water at 100°C, there was a sharp change in the character of the process at about 40 to 45 joules. Below 40 joules, the extent of reaction was negligible; above 45 joules, complete metal-water reaction occurred. These results indicate that there is a transition in the reaction mechanism between 0.03 atm water pressure (25°C) and 1 atm water pressure (100°C). Three runs were attempted at a water pressure of two

atmospheres (120°C) using 360 $\mu$  particles. In two runs at 15 and 26 joules energy input, no reaction occurred; in one run at 32 joules, the extent of reaction was 83% and particle breakup was observed. It was not possible to locate the threshold energy at 2 atm because of the complication introduced by particle breakup.

Four runs were carried out to test the possibility that heating the metal in water prior to the laser exposure might effect a change in the metal surface and thus reduce the extent of reaction at low energies. Cells containing aluminum specimens were heated to 100°C, held at that temperature for about five minutes, then cooled to room temperature before performing the experiments. The results of these experiments are listed in Table V-3. The average value for the extent of reaction is somewhat higher than the average value of about 8% reaction for runs in unheated water, but it is clear that preheating of the metal surface was not responsible for the effects observed in runs in 100°C water.

#### d. REACTION TIME OF ALUMINUM PARTICLES

From dark-field high-speed motion pictures of the reaction process, using 360 $\mu$  particles, the time interval was determined between the end of the laser pulse and the time that the aluminum sample cooled sufficiently so as not to be visible on film. The threshold of visibility on the high speed film is about 1500°K (see ANL-6257, p. 26). When the extent of the aluminum-water reaction was about 100%, the average time of sample luminosity was 166 msec (average deviation 6%). When the extent of reaction was low (in the range of 0 to 18%), the times of luminosity varied considerably, but a trend was observed which indicated that the time of luminosity increased with the extent of reaction. We have grouped the values for comparison as follows:

Percent reaction	0	6 to 7	12 to 18	100
Average time of luminosity (msec)	7	5	15	166
Number of runs	3	3	6	5

The long brightness time (~166 msec) observed for complete reaction is significant. A comparison of luminosity times suggests that a reaction which goes to completion is not necessarily more rapid, but merely longer. In the experiments conducted thus far, complete reaction has occurred only in 100°C water at high laser energies (>40 joules).

#### e. APPEARANCE OF RESIDUES

Figure V-19 shows the appearance of three 360 $\mu$ -dia. particles after reaction at 1 atm water pressure (100°C) at various laser energies. The sample in

TABLE V-3. EFFECT OF HEATING ALUMINUM PARTICLE IN WATER TO 100°C FOR FIVE MINUTES PRIOR TO PERFORMING LASER HEATING EXPERIMENT AT 25°C  
Particle size: 360 $\mu$

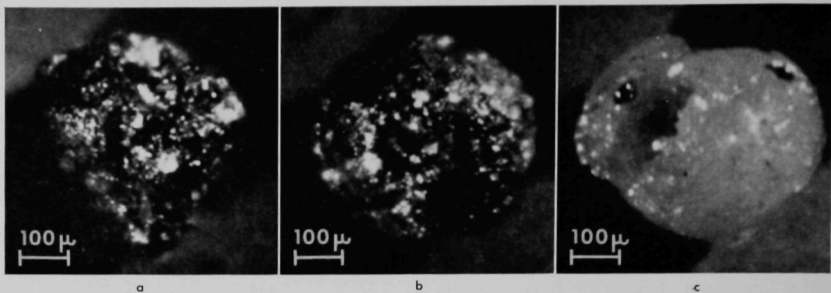
Run Number	Laser Output (Joules)	Percent Reaction <sup>a</sup>
101	33	16
102	33	4
103	24	18
104	24	14

<sup>a</sup> Extent of reaction for runs average at 25°C without prior heating: 8.2%.

Figure V-19a was exposed to a laser energy of 39 joules (no reaction); the sample in Figure V-19b, 44 joules (13% reaction); the sample in Figure V-19c, 46 joules (97% reaction). The appearances of all three residues are characteristic of samples having similar extents of reaction. Thus, we see at the lowest energy a sample which is not uniformly spherical; at the next higher energy, a sphere which is probably oxide coated; and at the highest energy a hollow, broken sphere of oxide. Occasionally, samples which have reacted to the extent of about 7 to 10% resemble the sample in Figure V-19a, but more often they resemble the sample in Figure V-19b. Several 575 $\mu$  samples showed a surface skin which was not completely continuous; metal could be seen in several places. An example of this is shown in Figure V-20. This observation supports the idea that there is actually an oxide film covering the samples. The sample shown in Figure V-20 had reacted to about 12% in 25°C water after a 41-joule laser pulse.

Another, more unusual, oxide formation is shown in Figure V-21. This sample, a 575 $\mu$  particle, gave 9% reaction in 25°C water after a 20-joule pulse. The oxide is formed, at least partially, in discrete mounds. Whether or not a continuous film also exists over the particle surface has not yet been determined.

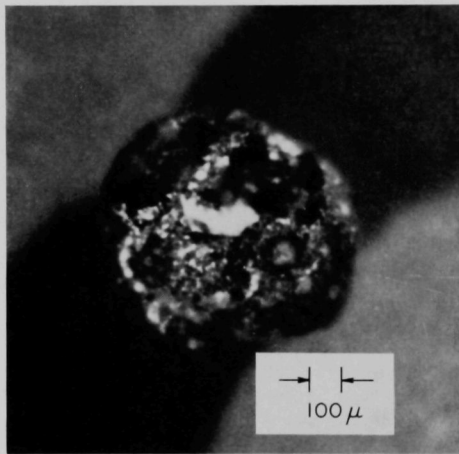
Microscopic examination of polished sections of aluminum samples which had undergone reaction with water failed to reveal any oxide film of the type found with zirconium (see ANL-6900, p. 252). Two examples of sections of 360 $\mu$  particles which had been reacted in 25°C water are shown in Figure V-22. The laser energies and extents of reaction are 29 joules, 7% reaction for Figure V-22a and 42 joules, 11% reaction for Figure V-22b. In preparation for microscopic examination the samples were polished with MgO and then treated with Keller's etch (1% HF, 1.5% HCl, 2.5% HNO<sub>3</sub> in water). Samples of partially reacted aluminum were frequently found to contain voids of varying size. However, it was not possible to distinguish an oxide film. Microscopic examination of sections of



108-8227, Rev. 2

FIG. V-19. Appearance of Aluminum Particles After Transient Laser Beam Heating in Water.  
(Nominal particle diameter:  $360\mu$ . Water temperature:  $100^{\circ}\text{C}$ .)

	Run No.	Laser Output Energy (Joules)	Percent Reaction
a	92	39	0
b	93	44	13
c	87	46	97

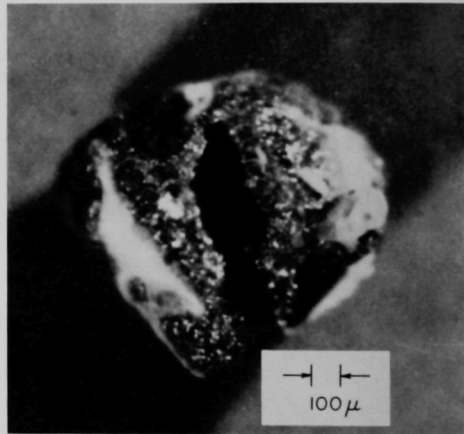


108-8576A

FIG. V-20. Residue from Aluminum-Water Reaction, Run No. 63.

Particle Diameter:  $575\mu$   
 Water Temperature:  $25^{\circ}\text{C}$   
 Laser Output: 41 Joules  
 Percent Reaction:  $\sim 12$

large aluminum samples which were obviously oxide-coated gave similar results, i.e., no distinguishable oxide film was observed. More elaborate techniques for revealing an oxide film, for example, techniques involving evaporation of an aluminum film on the



108-8577A

FIG. V-21. Residue from Aluminum-Water Reaction, Run No. 57.

Particle Diameter:  $575\mu$   
 Water Temperature:  $25^{\circ}\text{C}$   
 Laser Output: 20 Joules  
 Percent Reaction: 9

outer oxide surface before sample preparation, were not attempted.

Very careful microscopic examination of the surfaces of many samples revealed, in a number of cases, thin flakes of oxide-like material peeling from the metal surface.

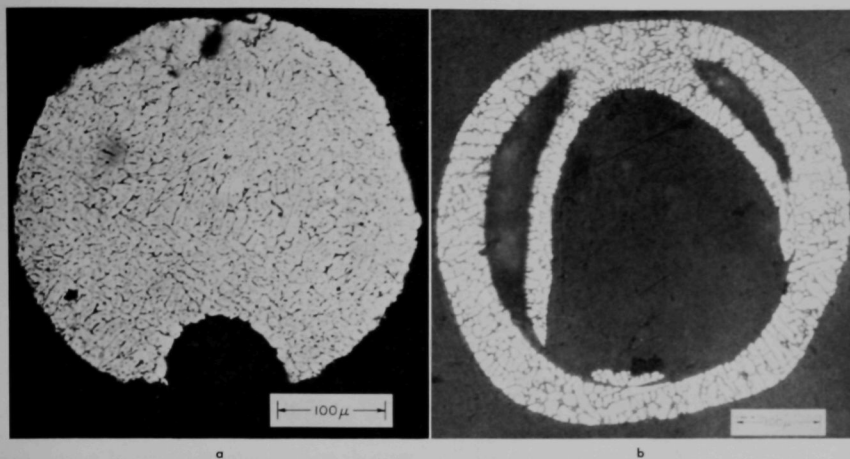


FIG. V-22. Sections of Residues from Aluminum-Water Reaction.

Particle Diameter:  $360\mu$   
Water Temperature:  $25^{\circ}\text{C}$

	Run No.	Laser Output (Joules)	Percent Reaction
a	27	29	7
b	43	42	11

In summary, typical results of aluminum-water reactions in which the metal specimens were heated by laser beams were as follows:

1. partial reaction ( $\sim 10\%$ ) produces spherical particles often with voids and with an oxide skin.
2. complete reaction produces hollow oxide shells.

#### f. DISCUSSION

During the period of heating by the laser beam, it would not be expected that the aluminum could be heated above its boiling point. In Figure V-23, the vapor pressure of aluminum is plotted as a function of temperature between 0.03 atm (the vapor pressure of water at  $25^{\circ}\text{C}$ ) and 1.0 atm (the vapor pressure of water at  $100^{\circ}\text{C}$ ). The vapor pressure plot was obtained by extrapolation of the vapor pressure equation of Brewer and Searcy,<sup>23</sup> who made measurements up to about  $1580^{\circ}\text{C}$ . Thus the boiling point of aluminum in  $25^{\circ}\text{C}$  water is about  $1900^{\circ}\text{C}$ , whereas the normal boiling point of aluminum (and the boiling point in  $100^{\circ}\text{C}$  water) is about  $2480^{\circ}\text{C}$ . The melting point of  $\text{Al}_2\text{O}_3$  is  $2030^{\circ}\text{C}$ . The information obtained from the extrapolated data suggests a reason for the differences

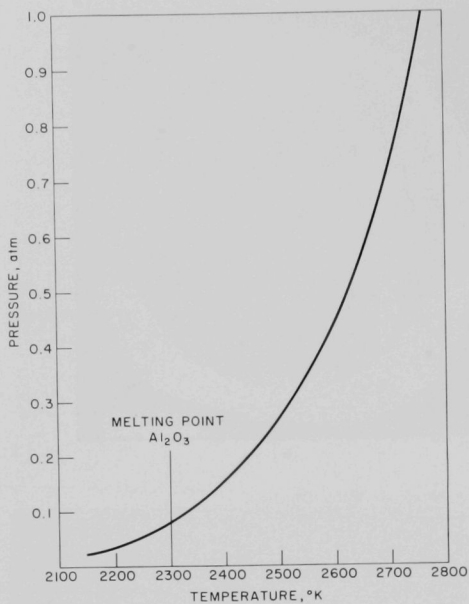
in results observed in experiments carried out with water at 25 and  $100^{\circ}\text{C}$ . If it is assumed that at high laser energy the metal is heated to the boiling point in both  $25^{\circ}\text{C}$  and  $100^{\circ}\text{C}$  water experiments, then in  $25^{\circ}\text{C}$  water there is a solid oxide film enclosing a mixture of aluminum and vapor, whereas in  $100^{\circ}\text{C}$  water the oxide film is a liquid. If the rate of reaction is controlled by a diffusion process through the oxide layer the rate of diffusion would be expected to be greater through the liquid oxide and hence the rate of metal-water reaction would also be greater.

The influence of the physical state of aluminum oxide has also been noted in other work. The importance of the oxide melting point to aluminum combustion in flames has been discussed previously.<sup>24, 25</sup> Freidman and Maček studied the ignition of 10 to  $74\mu$  dia. aluminum particles in flames and showed that the ignition temperature of  $2300^{\circ}\text{K}$  was not sensitive to changes in particle size. The ignition delay depended on the time needed to heat the particles to  $2300^{\circ}\text{K}$ . Bartlett et al. considered burning times in flames of 15 to  $50\mu$  dia. aluminum particles. For a model they

<sup>24</sup> R. Friedman and A. Maček, *Combustion and Flame* **6**, 9 (1962).

<sup>25</sup> R. W. Bartlett, J. N. Ong, Jr., W. M. Fassell, Jr., and C. A. Papp, *Combustion and Flame* **7**, 227 (1963).

<sup>23</sup> L. Brewer and A. W. Searcy, *J. Am. Chem. Soc.* **73**, 5308 (1951).



108-8579

FIG. V-23. Vapor Pressure of Aluminum Extrapolated from Data of Brewer and Searcy.<sup>23</sup>

assumed that molten metal at its boiling point is surrounded by an expanded shell of molten oxide, the rate of oxidation being determined by diffusion through the liquid oxide. It is likely that this model applies to our experiments at high pressure. Both groups of investigators found hollow spheres of oxide residues similar to those shown here in Figure V-19c. On the basis of the above model, the appearance of the particle shown in Figure V-21 can be understood. The discrete mounds of oxide could result from escape of aluminum vapor through cracks in the oxide layer. (The oxide layer was a solid in this particular experiment.) The low extents of reaction in 100°C water may be attributable to altered heat transfer characteristics at the higher pressure.

We are beginning to examine the molten oxide mechanism in quantitative terms. We are also considering how the proposed mechanism will effect (1) interpretation of data obtained by other experimental methods and (2) interpretations of reactor accidents.

Future studies by the laser method will investigate the effects of pressure on the aluminum-water reaction. Experiments will be performed in water at 25°C with an overpressure of 1 atm of inert gas to determine whether the reactions which occur at 1 atm water vapor are the result of water vapor pressure or total gas pressure. Experiments will also be performed in water at 181°C (vapor pressure, 150 psia) in a new metallic reaction cell which is now under construction.

#### 4. Studies in TREAT of Uranium Dioxide Fuel (R. C. LIIMATAINEN, F. J. TESTA)

Experiments were continued in TREAT to investigate the safety problems associated with the behavior

of unclad  $UO_2$  fuel specimens under conditions simulating a power excursion. Results of similar studies

TABLE V-4. RESULTS OF TREAT EXPERIMENTS WITH UNCLAD OXIDE FUEL PELLETS SUBMERGED IN WATER  
Water initially at room temperature  
Initial helium overpressure of 20 psia

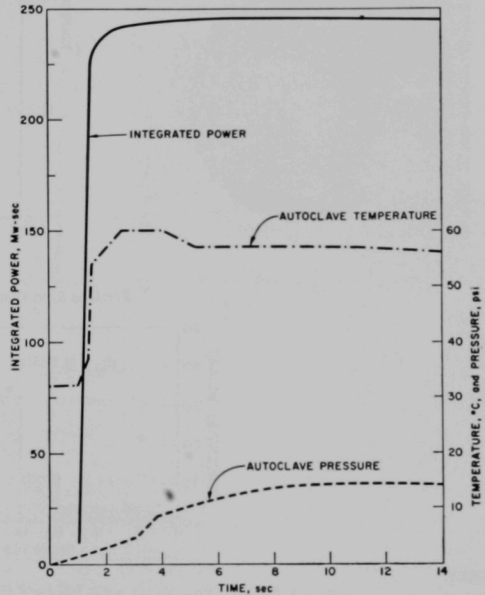
Fission Energy Input (cal/g)	Adiabatic Temp. (°C)	CEN Run No.	TREAT Characteristics		Results		
			Period (msec)	Int. Power (Mw-sec)	Appearance of Specimen after Transient	Mean Particle Diameter (mils)	Hydrogen Generated [ml(STP)/g $UO_2$ ]
(Pure $UO_2$ Fuel Pellets: 11.2% enriched, $\frac{3}{8}$ in. dia., $\frac{1}{2}$ in. long)							
223	2700	189	78	248	Fragmented	127	5.7
409	3300 <sup>a</sup>	188	74	327	Particles	14	17.7
775	3300 <sup>a</sup>	191	43	861	Fine particles	6	16.9
(Mixed Oxide Pellets: 81.5 w/o $ZrO_2$ , 9.1 w/o $CaO$ , 8.7 w/o $U_2O_8$ , 0.7 w/o $Al_2O_3$ , 93% enriched, $\frac{3}{8}$ in. dia., $\frac{1}{2}$ in. long)							
340	2250	190	71	424	Two large pieces	190	0

<sup>a</sup> Vaporization temperature.

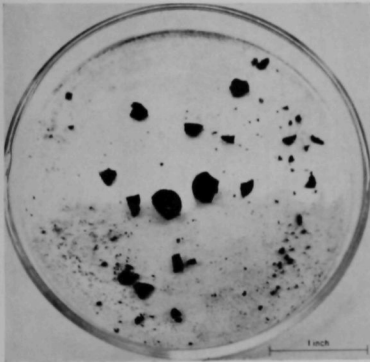
with Zircaloy-2 clad and stainless steel-clad oxide-core fuel pins were summarized in a previous report (ANL-6900, p. 254). As in previous studies, the unclad  $UO_2$  specimens were exposed to TREAT transients while submerged in water at room temperature. The objectives of the studies were to determine: (1) the extent of reaction of  $UO_2$  with water at temperatures in the range 2000 to 3300°C, and (2) the degree of

fragmentation of  $UO_2$ , in the absence of metal cladding, as a function of the integrated power of the reactor excursion to which the  $UO_2$  was subjected. The results of the experiments with unclad fuel specimens are summarized in Table V-4. Figures V-24 through V-27 show the oscillograph records of the transients, the appearance of the fuel after the transients, and the particle size distributions of the residues. The particle size determinations were accom-

## Oscillograph Record



## Fuel Pin after Transient



## Particle Size Distribution

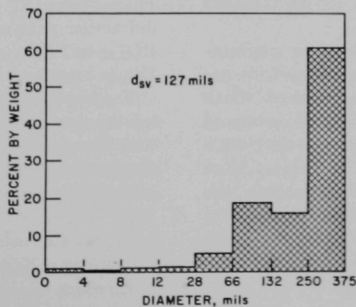
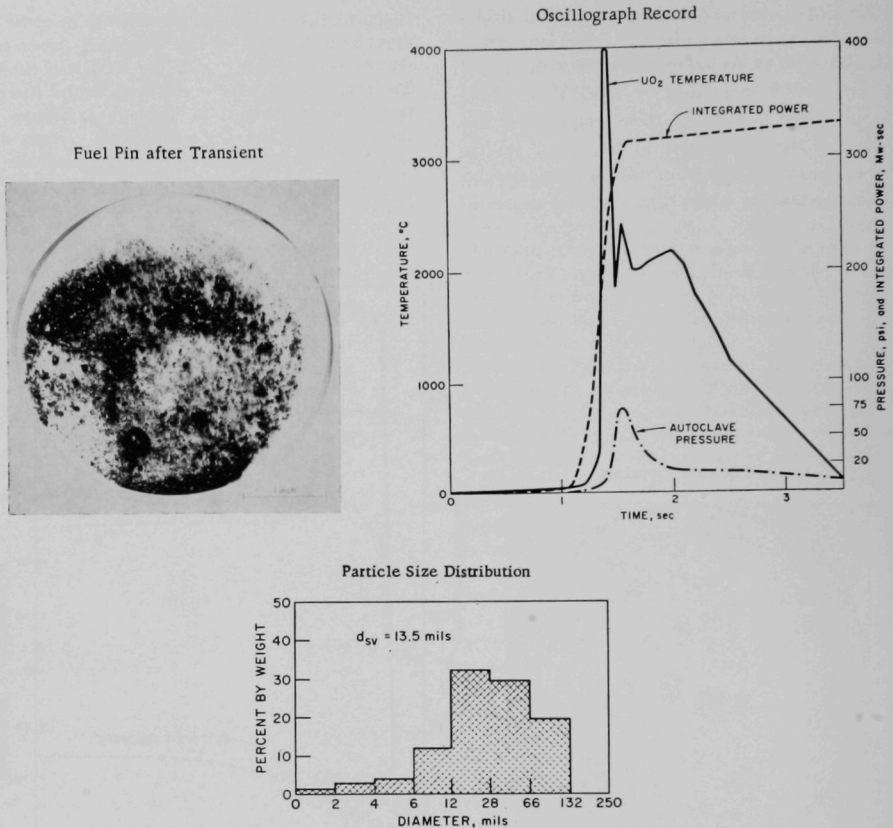


FIG. V-24.  $UO_2$  Fuel Pellet After TREAT Transient CEN-189. (223 cal/g  $UO_2$ .)



108-8581A

FIG. V-25.  $UO_2$  Fuel Pellet After TREAT Transient CEN-188. (409 cal/g  $UO_2$ .)

plished by sieving and the results reported as the Sauter mean diameter,  $d_{sv}$ .\*

The extent of reaction of  $UO_2$  with water was computed from the amount of hydrogen evolved, as determined mass spectrometrically. A transient which caused partial melting of  $UO_2$  (2700°C) produced about 6 ml  $H_2$  (STP)/g  $UO_2$ , corresponding to a calculated average final composition of  $UO_{2.07}$ . More energetic transients which brought  $UO_2$  into the vaporization region (3300°C) resulted in the evolution of about 17 ml  $H_2$  (STP)/g  $UO_2$  (calculated average

composition,  $UO_{2.19}$ ) as shown in Figure V-28. X-ray diffraction analyses indicating final compositions of  $UO_{2.12}$  to  $UO_{2.17}$  give support to the hypothesis that  $UO_2$  is reacting with water.

The results of the experiments with unclad  $UO_2$  have led to a reexamination of the data from previous studies with Zircaloy-2-clad and stainless steel-clad  $UO_2$ -core specimens. At this time, it appears likely that some of the hydrogen released in these experiments resulted from  $UO_2$ -water reaction rather than metal-water reaction. The extent of reaction of metal-clad  $UO_2$  with water is difficult to assess because of differences in exposure of the  $UO_2$  to water in the two types of experiments. In experiments with unclad  $UO_2$ , the specimens were in direct contact with water for ex-

$$*d_{sv} = \frac{\sum n_i d_i^3}{\sum n_i d_i^2} \text{ where } n_i$$

= number of particles with diameter,  $d_i$ .

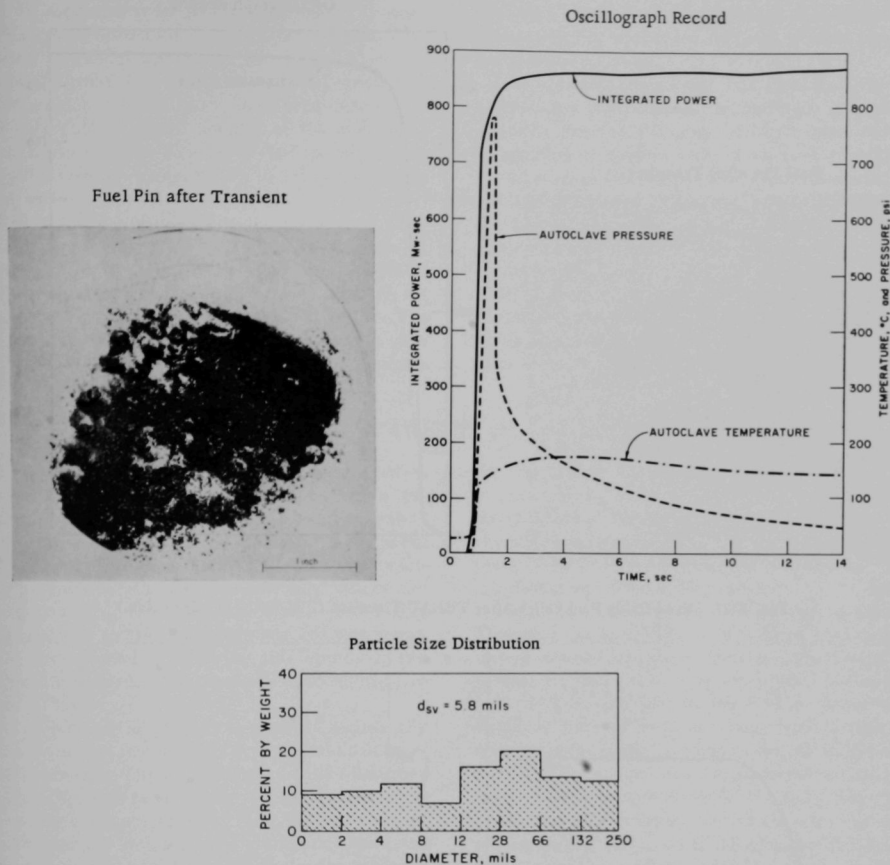


FIG. V-26.  $\text{UO}_2$  Fuel Pellet After TREAT Transient CEN-191. (775 cal/g  $\text{UO}_2$ .)

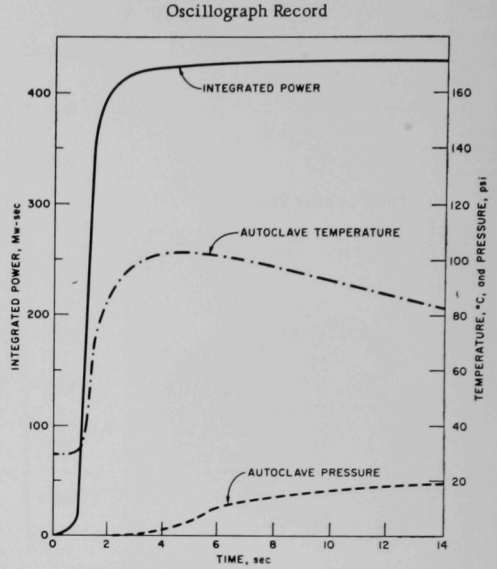
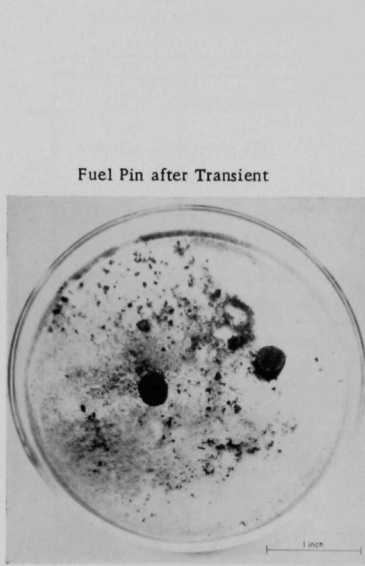
tended periods of time prior to the TREAT transient. Breakup probably occurred early in these experiments, and contact with water was continuous throughout the transient. In the experiments with metal-clad specimens, the oxide core contacted water only after the cladding material failed during the transient; in cases where the cladding remained intact, there was no contact of  $\text{UO}_2$  with water.

For purposes of evaluating the previously reported data (ANL-6900, p. 254), the experiments are divided into four general types, and the probable effect of the  $\text{UO}_2$ -water reaction on each type is discussed:

(1) In experiments at low energies, in which the

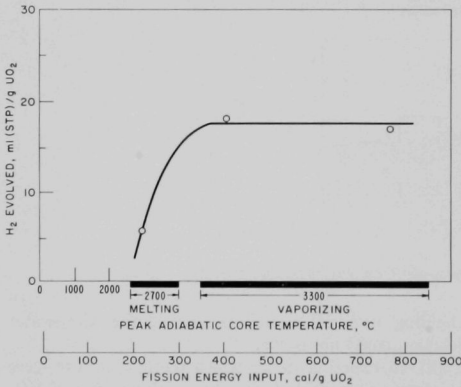
cladding material remained intact, the  $\text{UO}_2$ -water reaction could not occur.

(2) In experiments in which metal-clad  $\text{UO}_2$ -core specimens were heated into the melting region of  $\text{UO}_2$  (2700°C), it appears that the  $\text{UO}_2$ -water reaction did not occur to an appreciable extent, and the metal-water data, therefore, remained virtually unaltered. (Under the conditions of the experiments, contact of  $\text{UO}_2$  with water occurred only after cladding failure, and core breakup was incomplete.) This conclusion is supported by results of TREAT experiments with metal-clad, mixed oxide-core fuel pins heated to 2700°C. The mixed oxide core has the composition



108-8583A

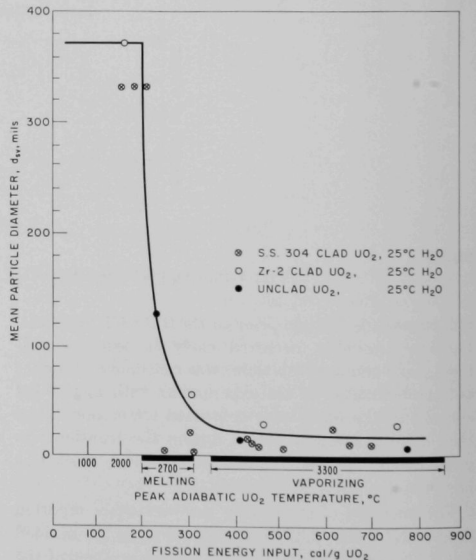
FIG. V-27. Mixed Oxide Fuel Pellet After TREAT Transient CEN-190. (340 cal/g oxide.)



108-8584

FIG. V-28. The Reaction of Unclad UO<sub>2</sub> Pellets with Water in TREAT: Hydrogen Evolved Versus Fission Energy Input.

81.5 w/o ZrO<sub>2</sub>, 9.1 w/o CaO, 8.7 w/o U<sub>3</sub>O<sub>8</sub>, 0.7 w/o Al<sub>2</sub>O<sub>3</sub>. All of these oxides are known to be inert to steam. With metal-clad mixed oxide-core pins, the extent of hydrogen evolution was similar to that of metal-clad, UO<sub>2</sub>-core specimens, thereby indicating that little or no hydrogen was generated by reaction of UO<sub>2</sub> with water under these conditions.



108-8585

FIG. V-29. Degree of Fragmentation of UO<sub>2</sub> Core Fuel Pins Subjected to a Reactor Pulse. (Fuel pins submerged in water.)

(3) In experiments in which metal-clad  $\text{UO}_2$ -core specimens were heated into the region of incipient  $\text{UO}_2$  vaporization (about 400 cal/g  $\text{UO}_2$ ), some  $\text{UO}_2$ -water reaction occurred. For stainless steel-clad specimens, the  $\text{UO}_2$ -water reaction may have been responsible for a maximum of about one-half of the amount of hydrogen evolved. For Zircaloy-2-clad specimens, the  $\text{UO}_2$ -water reaction was probably less than one-fourth of the total reaction.

(4) In experiments in which the metal-clad  $\text{UO}_2$ -core fuel pins were heated to the region of extensive vaporization of  $\text{UO}_2$  (700 cal/g  $\text{UO}_2$ ), the  $\text{UO}_2$ -water reaction was about the same as in the region of incipient vaporization (see Figure V-28). However, the  $\text{UO}_2$ -water reaction probably accounted for less than one-fourth of the hydrogen evolved from stainless

steel-clad specimens and less than one-eighth from Zircaloy-2-clad specimens because of the increased metal-water reaction.

It is apparent from these data that the  $\text{UO}_2$ -water reaction can contribute to the hydrogen generated in a reactor incident. Although hydrogen generation can be significant, there is little or no heat generated in the reaction of  $\text{UO}_2$  with water. From the particle size distributions shown in Figures V-24 to V-27, one can see that the  $\text{UO}_2$  was fragmented into a wide range of particle sizes. In Figure V-29, mean particle sizes obtained in the unclad  $\text{UO}_2$  experiments are compared with sizes obtained in previous experiments with stainless steel-clad and Zircaloy-clad fuel pins. The figure shows that the threshold of destruction is very close to the melting point of  $\text{UO}_2$ .

## 5. Scale-up Experiments in TREAT\* (R. C. LIIMATAINEN, F. J. TESTA)

During recent months, preparations have been in progress for conducting metal-water meltdown experiments on subassemblies which have approximately 100 times as much material as the previous single pin meltdowns conducted in TREAT during the metal-water program. The preparation included design and construction of the scale-up autoclaves (see Figure V-30) and the writing of a hazards analysis report which was approved. Following this approval, two experiments were run on 9-pin fuel subassemblies (see Figure V-31).

The purpose of this work is to simulate realistically a power excursion incident in a typical bundle of reactor fuel elements. The test subassembly is submerged in water; the primary container is a graphite crucible, enclosed by a Zircaloy-2 liner; these, in turn are contained within the stainless steel autoclave. Connected to the top of the autoclave is a valve for taking a sample of the gas for mass spectrometric analysis of the hydrogen evolved. A pressure transducer is also at the top of the autoclave.

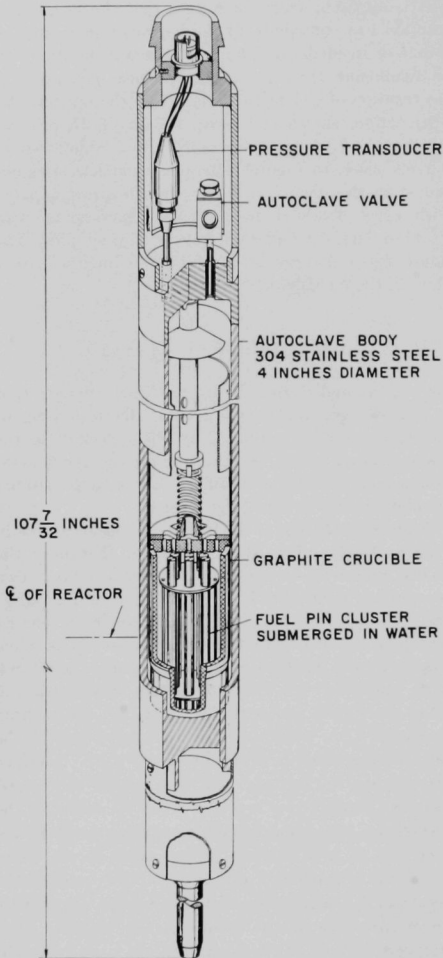
Table V-5 gives a summary of the data that are available to date from the two experiments which have been performed; Figures V-32 and V-33 show the oscillograph records of the transients. The significant point in Figure V-33 is the sudden inflection in the top of the reactor power-time curve near the peak of the transient; this inflection indicates a change in the reactivity of the TREAT reactor. It is believed that this perturbation was caused by a change in the reactivity of the nine-pin bundle when the geometry of the bun-

dle was altered during meltdown. This suggests that in these larger scale experiments, the beginning of meltdown may be indicated by the inflection in the reactor power curve. If this is the case, the reactor power record may be useful in fast reactor studies simulating meltdown of large clusters.

From examination of the two oscillograph records in Figures V-32 and V-33 it is evident that only the second power-time trace shows a perturbation. Two reasons are believed to have contributed to this difference. Firstly, the fuel in the first or lower energy transient slumped into two large masses plus some fragments and particles, whereas the fuel in the second, more energetic run was completely converted into small fragments and particles. Secondly, the melting in the first run occurred toward the very end of the reactor pulse (that is, all of the energy of the transient was required for melting) when the reactor power had already dropped to a very low level. However, in the second run there was enough energy imparted to the fuel pins to give melting at the peak of the pulse where the perturbation of the power was readily observable. A confirmation of these reasons is given by an examination of the record of the pressure as a function of time in the autoclave. In each case, the moment of breakup appears to be signaled by an abrupt rise in the pressure-time curve—in CEN-196S almost at the end of the transient, in CEN-197S in the middle of the transient.

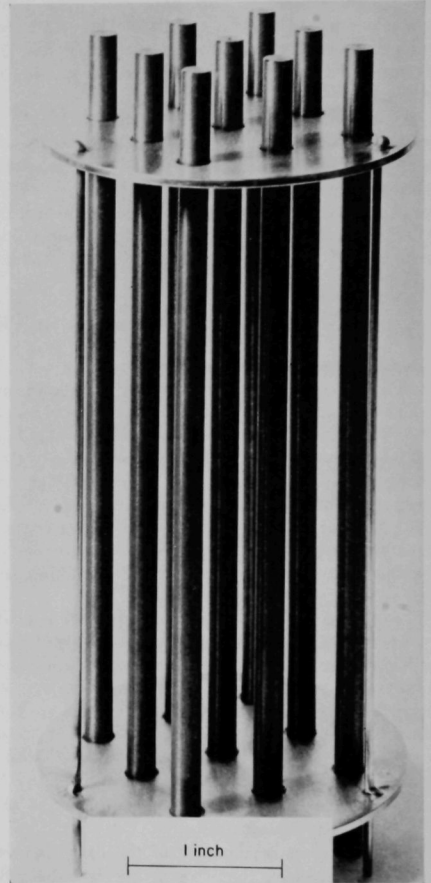
The original appearance of the subassembly of 9 uranium pins is shown in Figure V-31. The subassembly after meltdown in experiment CEN-196S is shown in Figure V-34. Examination of the residue from the more energetic transient, CEN-197S, showed that the

\* We gratefully acknowledge the cooperation and suggestions of James Boland and the TREAT personnel.



108-7467 Rev. 2

FIG. V-30. Capsule for 9 Pin Cluster Uranium-Water Experiments in TREAT.



108-8051A

FIG. V-31. Nine-Element Uranium Subassembly Before Meltdown in TREAT.

TABLE V-5. RESULTS OF METAL-WATER SCALE-UP EXPERIMENTS IN TREAT WITH URANIUM PINS

- Conditions: 1. Subassembly consisted of 9 uranium rods in a square cluster on  $\frac{5}{8}$ -in. centers with 3 rows of 3 elements per row. Each fuel pin was 0.2 in. in dia. by  $5\frac{1}{2}$  in. long and was 20% enriched with  $^{235}\text{U}$ . The total weight of the 9 element bundle was 490 g.
2. Fuel subassembly submerged in distilled water initially at ambient reactor temperature  $\sim 25^\circ\text{C}$ .
3. 20 psia helium atmosphere above the water.

	TREAT Transient No.	
	CEN-196S	CEN-197S
<i>Reactor Characteristics</i>		
Integrated Power, Mw-sec	91	222
Peak Power, Mw	255	361
Reactor Period, msec	157	140
<i>Results</i>		
Peak Pressure Rise, psi	65	570
Max. Rate of Pressure Rise, psi/sec	50	2150
Energy Input, Cal/g U	124	302
% of U Reacted with Water	10.7	$\sim 56$
Appearance of Cluster After Transient	Melted into two large irregularly shaped masses plus some fragments and particles.	Complete melt-down and conversion into relatively fine particles.

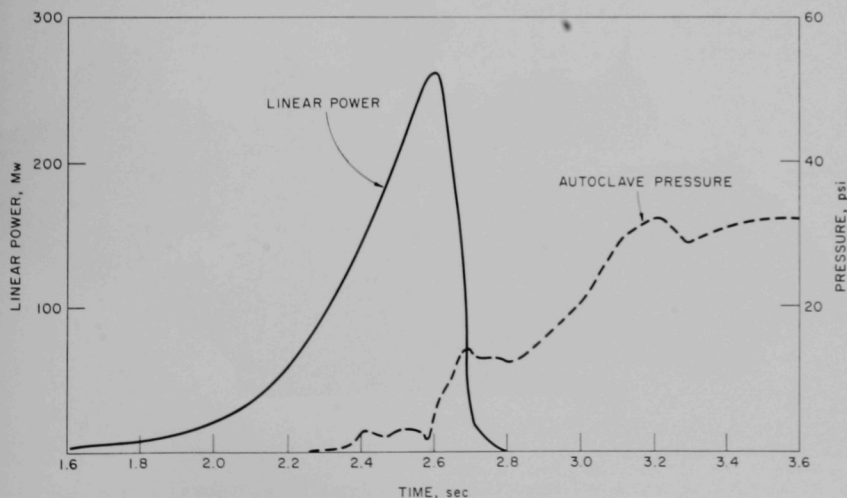
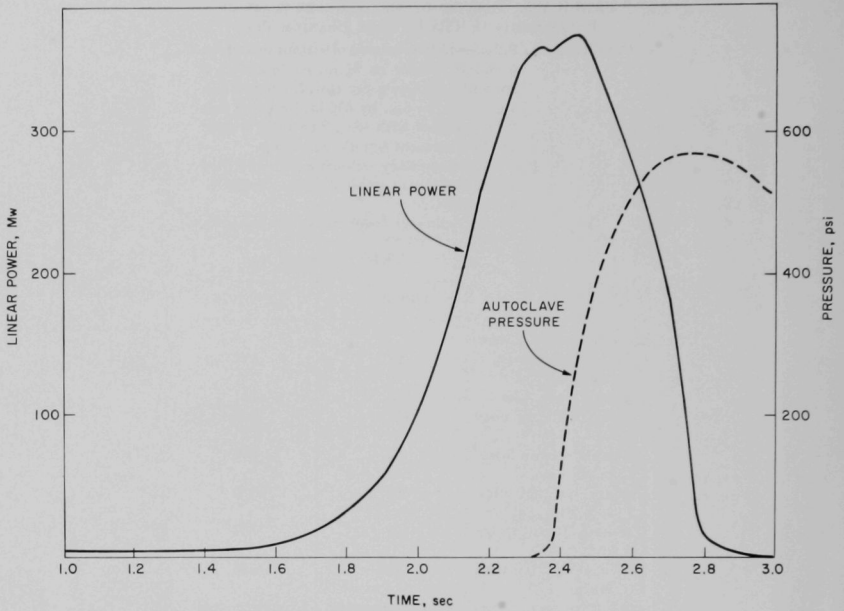
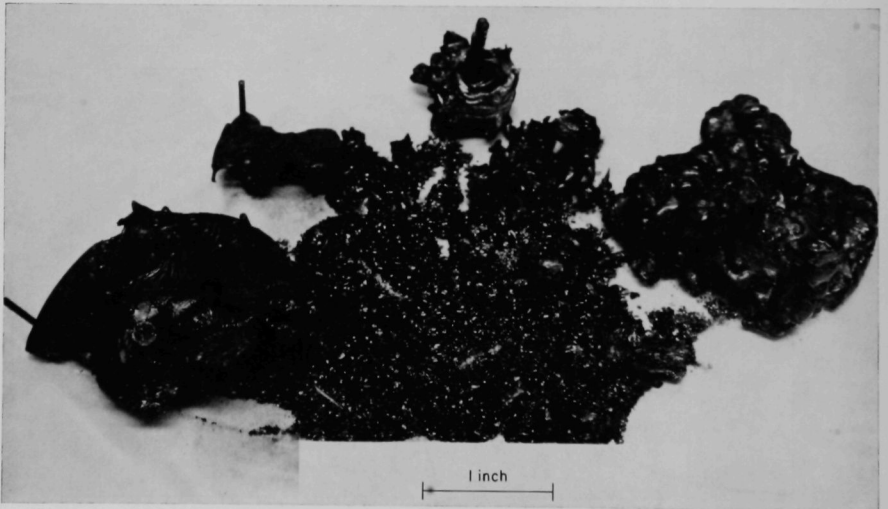


FIG. V-32. Oscillograph Record of Run CEN-196S.



108-8061

FIG. V-33. Oscillograph Record of Run CEN-197S.



108-8013A

FIG. V-34. View of Nine-Element Uranium Subassembly After Meltdown (CEN-196S).

fuel was completely melted and converted into relatively fine particles. Future experiments using the 9-

pin subassembly will be performed with stainless steel-clad and Zircaloy-clad  $\text{UO}_2$ -core fuel pins.

## 6. Water Hammer Evaluation (R. C. LIIMATAINEN)

During the hazards analysis for the scale-up experiment in TREAT, it became necessary to estimate the magnitude of a possible water hammer in the autoclave. A simple mathematical model was developed. The model was checked by applying it to the water hammer that occurred during the SL-1 accident.

A transient heat transfer and pressure generation model, developed and applied to the SPERT-1D destructive transient was discussed in the previous report (ANL-6900, p. 270). The model required assumptions concerning the details of the transient heat transfer process and also required a specification of the surface area of hot metal exposed to the water during meltdown. The present attempt is an effort to predict approximate water hammer pressures using gross assumptions concerning the total energy available for steam formation and time spread of the energy deposit in the water.

Three stages in an idealized water hammer are schematically illustrated in Figure V-35 for a reactor pressure vessel or autoclave containing a heat generating core submerged in water. Just after some arbitrary time, zero, when the water is at rest, the heat generation,  $Q$ , converts some of the water surrounding the core to steam. This force causes the water above the core to begin to accelerate upward at some velocity,  $V_1$ , at which time its position is  $x_1$ . Finally the driving steam pressure slams the water piston into the top heat of the vessel at some velocity,

$V_i$ . The impact of the water on the vessel produces an impulse pressure,  $P_i$ . The problem in hazards analysis, therefore, is to predict the velocity,  $V_i$ , and pressure,  $P_i$ .

Water hammers of the type pictured in Figure V-35 have been observed on widely different scales. In laboratory studies using laser heating of small metal foils in water, high speed motion pictures have shown an expanding steam bubble pushing up a water column in a glass tube (see ANL-6900, p. 250). Also, from the evidence accumulated during the post-incident examination of the SL-1 reactor, it was concluded that an accelerated slug of water was responsible for most of the damage.<sup>26</sup>

### a. DEVELOPMENT OF EQUATIONS

The mathematical model is based on Newton's second law and on the acoustic equation for the particle velocity of an ideal shock wave. From Newton's law, the product of the mass of the water column and its acceleration equals the sum of the forces acting upon it:

$$\frac{M}{g_c} \frac{d^2x}{dt^2} = P_D A - F_c - F_v - Mg \quad (26)$$

where

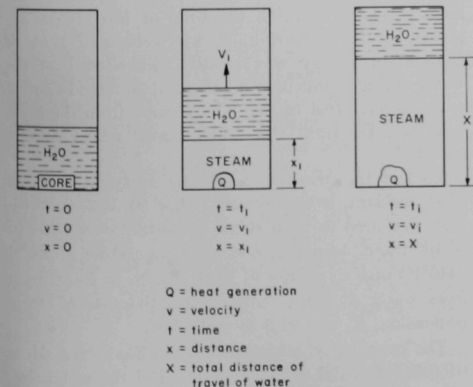
- $M$  = mass of water,
- $g_c$  = force/mass conversion constant,
- $x$  = displacement of water column,
- $t$  = time,
- $P_D$  = steam driving gas pressure,
- $A$  = cross-sectional area of water slug,
- $F_c$  = opposing force of cushion gas,
- $F_v$  = resisting frictional or viscous force, and
- $g$  = acceleration due to gravity.

In the application of Equation 26, the following assumptions were made:

- (1) Gravitational and frictional forces were neglected. Computer studies have shown these to be negligible in comparison with the steam driving force.<sup>27</sup>

<sup>26</sup> Final Report of SL-1 Recovery Operation, IDO-19311, 1962.

<sup>27</sup> E. C. Gay, C. F. Bohren, and E. Sank, Analysis of Impact Pressure Generated by a Metal-Water Reaction within a Closed Vessel, AMU-ANL Summer Engineering Practice School Report, July 6, 1964, R. C. Liimatainen, ANL Staff Advisor.



- (2) The presence of a gas cushion was ignored so that the calculation is conservative.
  - (3) The driving gas is generated at a constant rate.
  - (4) The driving gas obeys the ideal gas law.
  - (5) The temperature of the driving gas is constant.
- Equation 26 was therefore reduced as follows:

$$\frac{M}{g_c} \frac{d^2x}{dt^2} = P_{Di}A. \quad (27)$$

Using the ideal gas law,

$$P_{Di}Ax = nRT \quad (28)$$

where

- $n$  = moles of driving gas,
- $T$  = absolute temperature,
- $R$  = gas constant,

and assuming a constant rate of gas generation

$$n = Kt \quad (29)$$

where  $K$  = rate of gas generation, Equation 27 becomes

$$\frac{d^2x}{dt^2} = \left[ \frac{g_c R T K}{M} \right] \frac{t}{x}. \quad (30)$$

The equation has the following exact solution which satisfies the initial conditions that  $x = 0$  and  $dx/dt = 0$  at  $t = 0$ :

$$x = \left[ \frac{4g_c R T K}{3M} \right]^{1/2} t^{3/2}. \quad (31)$$

Evaluating Equation 31 at the moment of impact of the water slug with the top of the vessel yields:

$$X = \left[ \frac{4g_c R T K}{3M} \right]^{1/2} t_i^{3/2} \text{ or } t_i = \left[ \frac{3MX^2}{4g_c R T K} \right]^{2/3} \quad (32)$$

and

$$V_i = \left( \frac{dx}{dt} \right)_{t=t_i} = \left[ \frac{9g_c R T K X}{2M} \right]^{1/3} \quad (33)$$

where

- $X$  = total distance of travel of water slug,
- $t_i$  = time of impact, and
- $V_i$  = velocity of impact.

Using the acoustic equation for the impact pressure:<sup>25</sup>

$$P_i = \frac{\rho_c V_i}{g_c} \quad (34)$$

where

- $\rho$  = water density,
- $P_i$  = impact pressure,
- $c$  = velocity of sound in water, 5000 ft/sec,

and substituting  $V_i$  from Equation 33 gives

$$P_i = \rho_c \left[ \frac{9RTKX}{2g_c^2 M} \right]^{1/3}. \quad (35)$$

An expression of the driving gas pressure at the time of impact,  $P_{Di}$ , can be obtained by solving Equations 28, 29, and 32 to yield:

$$P_{Di} = \frac{1}{A} \left( \frac{3M}{4g_c} \frac{K^2 R^2 T^{2\alpha}}{X} \right)^{1/3}. \quad (36)$$

The average driving gas pressure over the time interval 0 to  $t_i$ ,  $\bar{P}_{Di}$ , can be shown to be equal to twice the driving gas pressure at impact.

$$\bar{P}_{Di} = \frac{2}{A} \left( \frac{3M}{4g_c} \frac{K^2 R^2 T^{2\alpha}}{X} \right)^{1/3}. \quad (37)$$

## b. COMPARISON WITH SL-1 ACCIDENT

The impact pressure of the water hammer produced in the SL-1 accident was sufficient to collapse some of the stainless steel tubes in the head of the reactor. Because the static yield pressure of these tubes was known to be about 7000 psi, and because a higher pressure is required to collapse a material under transient conditions, an actual impact pressure of 10,000 psi was estimated.<sup>26</sup> The following acoustic equation:

$$V_i = P_i \left( \frac{2\beta}{3\rho} \right)^{1/2} \quad (38)$$

where  $\beta$  = compressibility of water,  $5 \times 10^{-5} \text{ atm}^{-1}$ , was used to calculate a value of 159 ft/sec for the impact velocity,  $V_i$ . Of the total of 130 Mw-sec released by the excursion, it was estimated that 50 Mw-sec of energy was rapidly deposited into the water during a time interval of about 30 msec following peak power. Most of the energy came from the rapid heat transfer from those fuel plates which disintegrated.<sup>26</sup>

To test the proposed model by applying it to the SL-1 accident, it was assumed that 50 Mw-sec of energy was used to form steam uniformly over a period of 100 msec. Assuming a steam temperature of 500°K (440°F) and an energy of 1204 Btu/lb to form steam from water at room temperature, the rate of steam generation,  $K$ , was 21.8 lb moles/sec.

The quantity of water above the SL-1 core,  $M = 6460$  lb, the total distance of travel of the water slug,  $X = 3$  ft, and the cross-sectional area,  $A = 14.8$  sq ft, were used with Equation 32 for the impact time, with Equation 33 for the impact velocity, with

<sup>25</sup> R. H. Cole, "Underwater Explosions," Princeton University Press, 1948, pp. 19-20.

Equation 35 for the impact pressure, and with Equation 37 for the average driving gas pressure to yield:

impact time	$t_i = 35$ msec
impact velocity	$V_i = 126$ ft/sec
impact pressure	$P_i = 8500$ psi
average driving gas pressure	$\bar{P}_D = 340$ psi

The values calculated from the proposed model for the impact pressure (8500 psi) and impact velocity (126 ft/sec) agree very well with those estimated from the post-incident study of the SL-1 accident, i.e., 10,000 psi and 159 ft/sec.<sup>26</sup> An important result

is that a relatively modest driving pressure, 340 psi, is able to produce a very large impact pressure, 8500 psi.

The simplified water hammer model may be particularly useful in hazards analysis because the assumed steam generation rate,  $K$ , has a relatively small effect on the impact pressure and velocity. (The pressure and velocity are proportional to  $K^{1/3}$ .) Refinements to the model would include a transient heat transfer model that would give a more accurate picture of the rate of steam formation and would account for likely decreases in temperature of the driving gas as the water column rises.

## 7. Calculation of the Extent of Metal-Water Reaction During a Loss-of-Coolant Accident (L. BAKER, JR., R. O. IVINS, J. BINGLE)

A calculational study has been initiated to predict the extent of zirconium-water reaction that would occur during a loss-of-coolant accident in a water-cooled power reactor. The objective of this study is to demonstrate the application of metal-water reaction data to a reactor accident situation. The initial effort uses the reactor model conceived for the LOFT (Loss of Fluid Test) facility.<sup>29, 30</sup> The LOFT facility is being developed to conduct engineering tests to investigate the consequences of a loss-of-coolant accident with a pressurized-water power reactor. The reactor to be built is a 50 Mw(t) unit fueled with metal-clad  $UO_2$  pins. At present, a 15-mil stainless steel cladding is proposed for the core. For the purposes of this calculation, a 25-mil zirconium cladding was assumed.

The core is composed of 52 fuel assemblies each of which contains 64 cylindrical fuel pins (0.39-in. dia. by 36 in. long). Therefore, the core contains 3328 zirconium-clad fuel pins with a total weight of 366 kg (742 lb) of zirconium. The zirconium associated with the fuel pins would require 145 kg (320 lb) of water to react completely to form zirconium dioxide and hydrogen.

The analysis of the proposed final destructive experiments in the LOFT program<sup>29</sup> was used as far as possible as a basis for the metal-water reaction calculations. This analysis concerns the case of a break in the bottom inlet pipe (i.e., below the core) to the reactor vessel. The case of an upper-outlet pipe break was not treated. The blowdown following the lower pipe break was calculated to completely uncover the core in a

period of 10 sec. The core temperature would then rise as a result of decay heating and eventually core meltdown would occur.

In the preliminary analysis of such an incident the following assumptions were made:

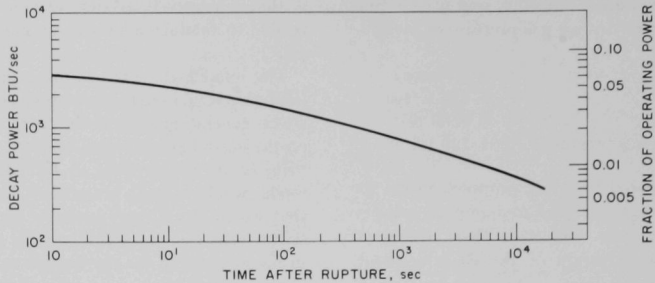
1. The initial reactor temperature following the 10-sec blowdown period is 544°F or 285°C (the operating temperature of the reactor). The assumption ignores the possibility of extra heating from the failure of the reactor to shut down instantaneously or the possibility of extra cooling resulting from the rapid expulsion of water from the core.
2. The initial average decay heating rate is 0.0633 of the operating power level of 256 kw/liter  $UO_2$  and thereafter the decay heating rate follows the time variation given in the LOFT analysis report (see Figure V-36).
3. The decay energy is distributed throughout the core in the same manner as the reactor power during steady-state operation.
4. Heating and possible chemical reaction of support structures in the core are neglected. Only fuel and cladding are considered to be in the reactor core.
5. The temperature distribution across individual fuel rods (fuel and cladding) is flat. Since this assumption ignores the energy stored in the oxide fuel pins, the initial rate of temperature rise is somewhat lower than if pin center temperatures had been considered.
6. There are no heat losses from the reactor core before it collapses.

### a. DISTRIBUTION OF ENERGY IN THE CORE

Since the rate of the zirconium-water reaction is a strong function of temperature, it was necessary to ac-

<sup>29</sup> J. M. Waage et al., Preliminary Safety Analysis Report, LOFT Facility, Report IDO-16981, Phillips Petroleum Co., April 1964.

<sup>30</sup> T. R. Wilson et al., An Engineering Test Program to Investigate a Loss-of-Coolant Accident, Report IDO-17049, Phillips Petroleum Co., October 1964.



108-8491

FIG. V-36. Decay Heat Generation Rate Versus Shut-Down Time for LOFT. (50 Mw operation for 400 hr. Reproduced from LOFT analysis report<sup>29</sup>.)

count for the nonuniform distribution of decay energy throughout the core. The decay energy was assumed to be distributed in the same manner as the operating power (fission energy). A simplified cylindrical model of the core with a central, low-enrichment zone (cylinder) and an outer, high-enrichment zone (in the shape of a hollow cylinder) was used to calculate the power distribution. The LOFT core has 32 central elements of low enrichment (2.82%) and 20 peripheral elements of high enrichment (5.70%).

Two zero power Bessel functions were used to describe the radial power distribution (based on the cross-sectional area). The functions were determined by assuming the power peaks at the center and at the interface of the two zones of enrichment to be equal to 1.6 (the reported peak-to-average radial power ratio of the LOFT design). The ratio of zone enrichments was assumed to fix the power level of the outer edge of the low enrichment zone. The functions were determined to be:

$$\text{low enrichment zone: } P/P_{AR} = 1.6 J_0(1.53 y/r) \quad (39)$$

$$\text{high enrichment zone: } P/P_{AR} \\ = 5.5 J_0(2.504 y/R) \quad (40)$$

where

- $J_0$  = zero order Bessel function,
- $y$  = radial position,
- $r$  = radius of low enriched zone,
- $R$  = radius of the core,
- $P$  = power density, and
- $P_{AR}$  = average radial power density.

A cosine function was used to describe the axial power distribution. Based on the axial peak-to-average ratio of 1.5, the function was

$$P/P_{AX} = 1.5 \cos \frac{\pi x}{2(1.052 X)} \quad (41)$$

where

- $x$  = axial position from center of the core,
- $X$  = one-half height of core,
- $P$  = power density, and
- $P_{AX}$  = average axial power density.

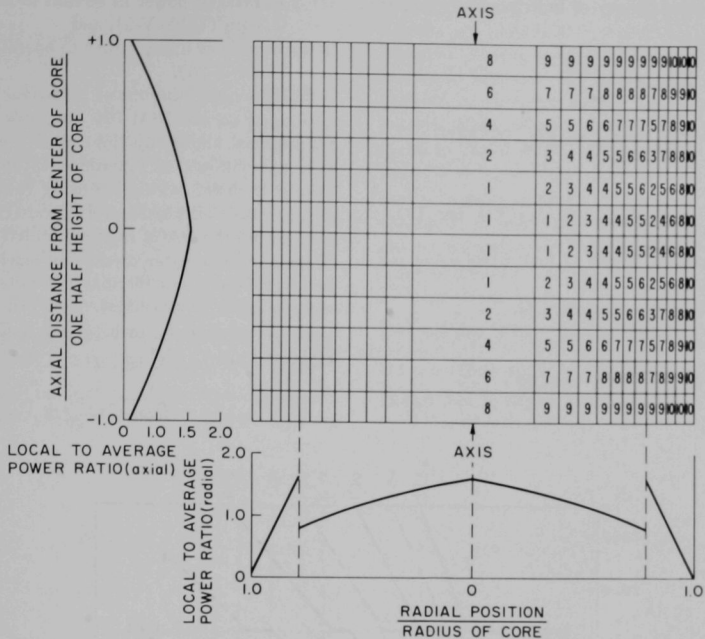
The product of the axial and radial ratios was used to determine the local-to-average volumetric power ratio. The peak-to-average power ratio was 2.4.

In order to facilitate the calculations, the core was segmented and each segment was ascribed a volumetric power ratio. This was accomplished by segmenting the core into thirteen radial zones of equal volume. Eight of these zones were of low enrichment and five were of high enrichment. Each radial zone was further divided into twelve axial segments, also of equal volume. The resulting 156 equal-volume segments (12 cylindrical segments in the center and 144 surrounding doughnut-like segments) were grouped into ten sections based on their average power ratio. The segmentation of the core is illustrated in Figure V-37. The radial and axial power distributions are also shown in this figure.

The power sections were designated by division of the maximum peak-to-average power ratio (2.4) into tenths (i.e., 0-0.24, 0.24-0.48, . . . 2.16-2.4). The percent of the core in each power section is listed in Table V-6.

## b. METHOD OF CALCULATION OF EXTENT OF REACTION AND CHEMICAL AND DECAY ENERGY FOR INDIVIDUAL CORE SECTIONS

The rate of reaction of zirconium with steam when the reaction is not limited by the quantity of steam has been described by the parabolic oxidation law (see ANL-6548, p. 37). When converted into units con-



08 8194

Fig. V-37. Cross Section of Cylindrical Model of LOFT Core Showing Power Distribution. (Numbers refer to power section of core, i.e., 1 = highest and 10 = lowest.)

venient for the present analysis, the rate of reaction may be represented as:

$$-\frac{dr}{dt} = \frac{K}{(r_o - r)} \exp\left(-\frac{\Delta E}{RT}\right) \quad (42)$$

where:

- $r$  = radius of unreacted metal in fuel rod, cm,
- $r_o$  = original radius of fuel rod, 0.991 cm,
- $t$  = time, sec,
- $K$  = rate law constant,  $0.3937 \text{ cm}^2/\text{sec}$ ,
- $\Delta E$  = activation energy, 45.5 kcal/mole,
- $R$  = gas constant,  $1.987 \text{ cal}/(\text{mole})(^\circ\text{C})$ , and
- $T$  = temperature,  $^\circ\text{K}$ .

When the reaction rate is limited by the quantity of steam available for reaction, it becomes necessary to consider factors external to the reactor coolant channels such as the integrity of the reactor pressure vessel, i.e., whether there is an available source of steam and a path for convective steam flow into and out of the core. For purposes of the present analysis, the reaction rate, under steam-limited conditions, was assumed constant:

TABLE V-6. RESULTS OF SEGMENTATION OF LOFT REACTOR CORE INTO TEN SECTIONS

Ratio of Power in Section to Average Power in Core		No. of Core Segments in Power Section	Percent of Core in Power Section
Range	Average		
2.16-2.40	2.28	4	2.56
1.92-2.16	2.04	12	7.69
1.68-1.92	1.80	8	5.13
1.44-1.68	1.56	16	10.26
1.20-1.44	1.32	22	14.10
0.96-1.20	1.08	16	10.26
0.72-0.96	0.84	18	11.54
0.48-0.72	0.60	18	11.54
0.24-0.48	0.36	26	16.67
0-0.24	0.12	16	10.26

$$\frac{dr}{dt} = C \quad (43)$$

where  $C$  = constant depending upon steam flow rate through the reactor core.

The following energy balance was used to calculate

the temperature-time history of individual sections of fuel rod:

$$(C_{p,UO_2} W_{UO_2} + C_{p,Zr} W_{Zr}) \frac{dT}{dt} = Q_C \rho_{Zr} 2\pi r \frac{dr}{dt} + V_{UO_2} Q_D f F(t) \quad (44)$$

where

$C_p$  = specific heat, 0.082 cal/(g)(°C) for  $UO_2$ , 0.088 cal/(g)(°C) for Zr,

$W$  = mass per unit length of fuel, 6.268 g/cm for  $UO_2$ , 1.202 g/cm for Zr,

$Q_C$  = heat of reaction, 1560 cal/g Zr,

$Q_D$  = average reactor power, 61.16 cal/(sec) (cc  $UO_2$ ),

$\rho_{Zr}$  = density of zirconium, 6.5 g/cm<sup>3</sup>,

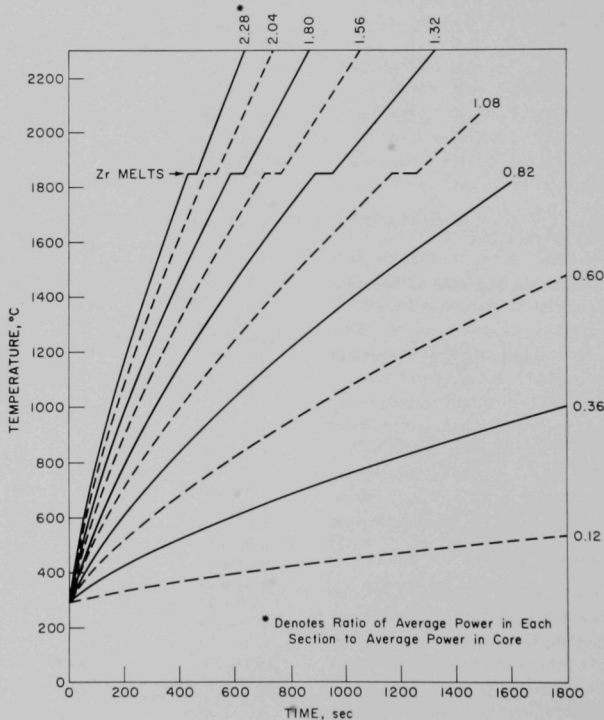
$V_{UO_2}$  = volume of  $UO_2$  per unit length of rod, 0.5858 cm<sup>3</sup>/cm,

$f$  = ratio of power in section to average power in core (Table V-6), and

$F(t)$  = ratio of decay power to operating power (Figure V-36).

Simultaneous solutions of Equations 42 and 44 were performed on the IBM-704 computer for the case of reaction not limited by the quantity of steam. Simultaneous solutions of Equations 43 and 44 were performed by hand calculation using values of the decay energy term which had been integrated on the IBM-704 machine for the case of reaction limited by the quantity of steam. The program used in the machine calculations had a provision for a thermal halt corresponding to the melting point of zirconium (1852°C). When the temperature reached the melting point, Equation 44 was replaced by:

$$(L_{Zr} W_{Zr}) \frac{dF}{dt} = Q_C \rho_{Zr} 2\pi r \frac{dr}{dt} + V_{UO_2} Q_D f F(t) \quad (45)$$



108-8487

FIG. V-38. Calculated Temperature-Time Curves for Each Power Section for the Case of No Metal-Water Reaction in Loss-of-Coolant Accident.

where

$L_{Zr}$  = heat of fusion of Zr, 53.8 cal/g, and  
 $F$  = fraction of metal melted.

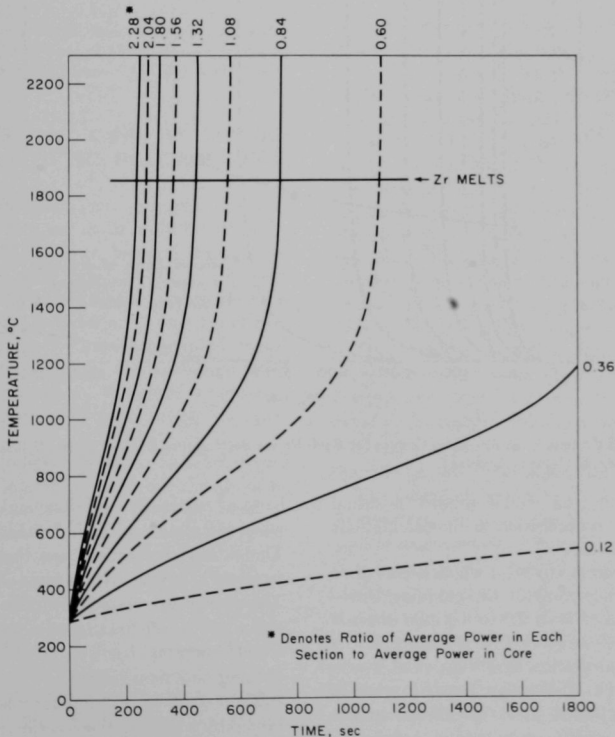
When  $F$  reached a value of 1.0 (fully melted), Equation 44 was again used.

Initial calculations were performed by neglecting the chemical energy (setting  $Q_c = 0$ ) in order to generate reference temperature-time curves. The results are plotted in Figure V-38 where it is apparent that melting of the cladding would begin 430 sec after the blowdown and that one-half of the cladding in the reactor (end of melting in the 6th section) would occur after 1250 sec for the case of no chemical energy generation.

### c. CALCULATIONS FOR CASE OF UNLIMITED STEAM SUPPLY TO THE REACTOR CORE

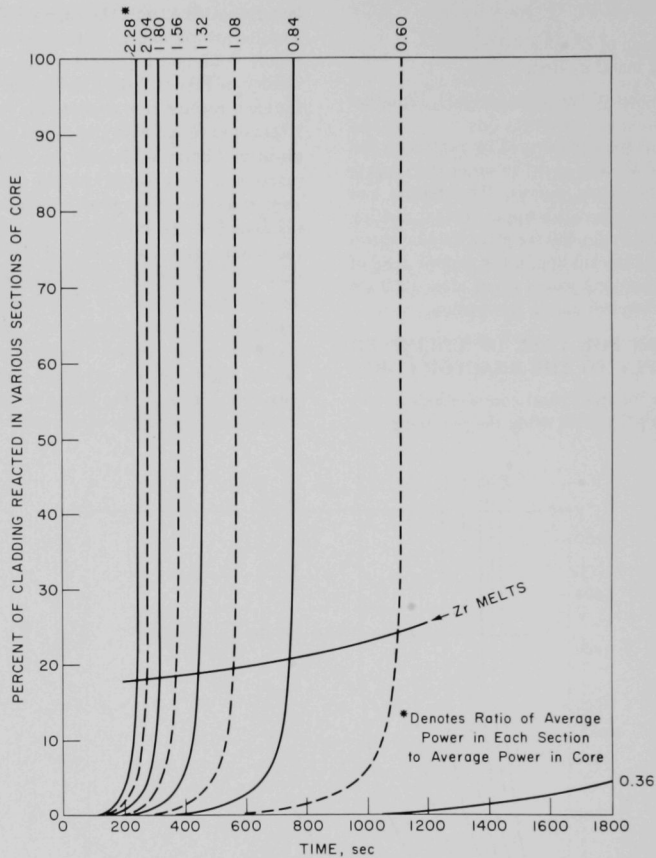
The calculations for individual core sections in unlimited steam were performed using the parabolic rate

law, Equation 42, and the energy balance, Equation 44. Results are plotted as a temperature-time history in Figure V-39 and a percent metal-water reaction-time history in Figure V-40. During the initial time period for each reactor core section, the temperature follows a course identical with the curves for no chemical heat given in Figure V-38, and the extent of metal-water reaction is very small. As the temperature of each section reaches about 800°C, both the temperature and the extent of reaction begin to increase rapidly. Both the temperature rise rate and the reaction rate continue to increase rapidly, indicating ignition. At the melting temperature of the cladding (1852°C), the extent of reaction varies from 18% from the most energetic reactor section (relative power, 2.28) to 24% for the eighth section (relative power, 0.60) as indicated in Figure V-40. The two lowest energy core sections did not ignite within 2000 sec; however, it is



108-8488

FIG. V-39. Calculated Temperature-Time Curves for Each Power Section for the Case of Metal Reacting with an Unlimited Quantity of Steam in the Loss-of-Coolant Accident.



108-8495

FIG. V-40. Calculated Percent Reaction-Time Curves for Each Power Section for the Case of Metal Reacting with an Unlimited Quantity of Steam in Loss-of-Coolant Accident.

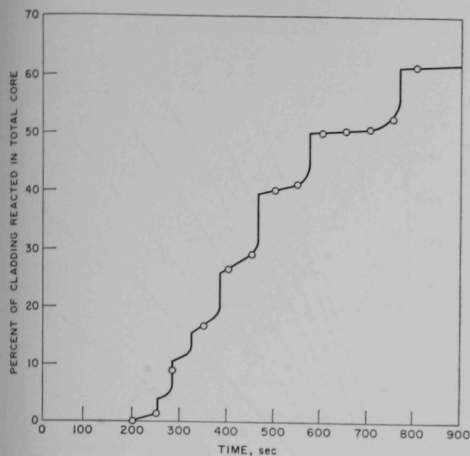
clear that the calculations would predict eventual ignition since there is no provision in the calculations for the effect of heat losses.

The extent of reaction (18 to 24%) which occurs prior to reaching the melting point of the cladding corresponds to the reaction of from 4.5 to 6.0 mils of cladding. These results are in general agreement with the results of a similar calculation by Owens et al.<sup>31</sup> who reported that 5.0 mils of Zircaloy reacted prior to reaching the melting point when calculated on the

<sup>31</sup> J. I. Owens, R. W. Lockhart, D. R. Iltis, and K. Hikido, Metal-Water Reactions VIII, Preliminary Consideration of the Effects of a Zircaloy-Water Reaction During a Loss-of-Coolant Accident in a Nuclear Reactor, GEAP-3279, 1959.

basis of adiabatic conditions and that 5.5 mils reacted when calculated on the basis that heat losses occurred. The extent of reaction and the temperature are interrelated because of the high energy of the reaction. The energy associated with the complete reaction of zirconium is sufficient to raise the temperature of both the cladding and the  $UO_2$  by  $3030^\circ C$ , neglecting phase changes and dissociations.

The extent of reaction for the entire core was obtained by summing the reaction of each section. These data are plotted in Figure V-41. The stepwise character of the plot reflects the ignition of individual core sections.



108-8490

FIG. V-41. Calculated Percent Reaction-Time Curve for Entire Reactor Core for the Case of Metal Reacting with an Unlimited Quantity of Steam in Loss-of-Coolant Accident.

#### d. CALCULATIONS FOR CASE OF LIMITED STEAM SUPPLY TO THE REACTOR CORE

The previous calculation (see subsection c) employed the parabolic rate law as the only factor limiting the reaction rate. It is clear, however, that as the temperature becomes high, the parabolic rate law allows a very rapid reaction. Such a rapid reaction requires that steam is provided at a very rapid rate and, moreover, that the hydrogen generated is removed at an equally rapid rate. A realistic appraisal of a loss-of-coolant accident, therefore, requires a determination of the rate of steam supply to the reactor core.

The rate of steam passing through the reactor core depends to a great extent on the nature of the accident. The LOFT analysis assumes that the pipe break is below the core and that there are no breaks above the core. In this case, there would be a minimum of upward convective flow through the core. If, however, there is also an upper pipe break or a vessel failure resulting from the violence of the blowdown, then there would be a continuous path for convective steam flow. An initial pipe break above the reactor core, which uncovers the core, could also lead to the continuous flow of steam through the core. In this case, any water remaining in the bottom of the reactor vessel after blowdown would have to pass through the core in order to escape the vessel. The steam flow rate

would, of course, depend upon the heat supply to the water pool.

Rather than attempt to specify steam flow rates resulting from various accident conditions at this time, calculations were performed for two reasonable flow rates.

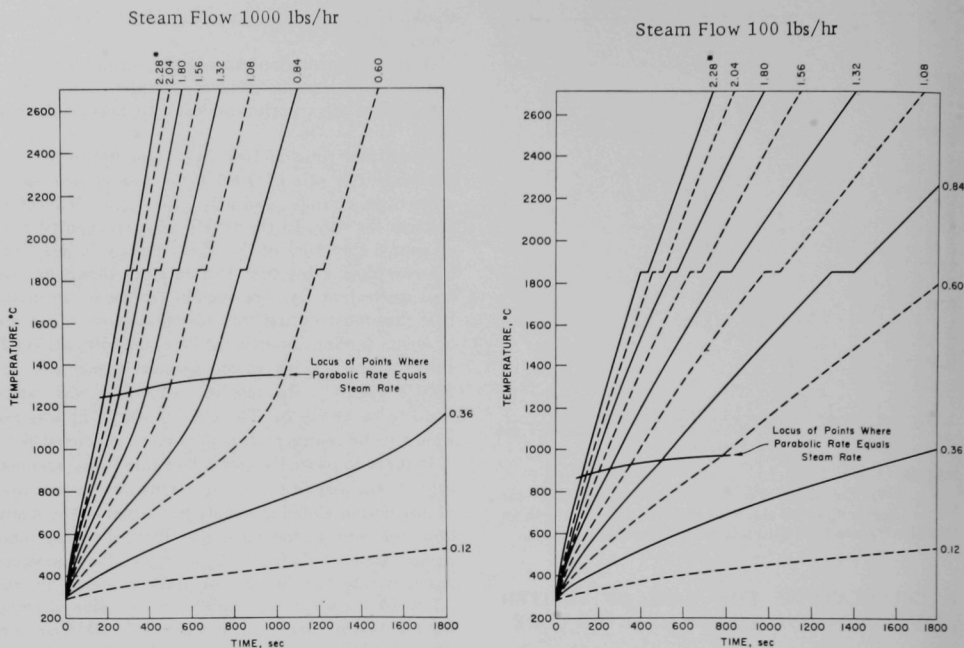
Steam flow rates of 1000 lb/hr and 100 lb/hr were assumed. The rate of 1000 lb/hr was chosen as an order-of-magnitude estimate for free convection through the core. In the LOFT analysis report<sup>29</sup> it is estimated that 10% of the decay energy is lost from the core during the first 15 min after blowdown, by heat convection. By equating ten percent of the decay heat generated during this 15-min period to a mass of steam flowing through the core, entering at 544°F (285°C) and leaving at an assumed temperature of 1800°F (982°C), the rate of steam flow was calculated to be 510 lb/hr. The case of 100 lb/hr was assumed to be representative of a more restricted flow.

In order to relate the steam flow rate to the reaction rate, it was assumed that the maximum reaction rate of any unit of cladding surface was equal to the steam flow rate through the entire core divided by the total surface area of cladding. Accordingly, the maximum reaction rate for the case of 1000 lb steam/hr was  $5.7 \times 10^{-5}$  cm/sec (constant C in Equation 43) and for the case of 100 lb/hr, it was  $5.7 \times 10^{-6}$  cm/sec. The calculations were performed by examining the results for the unlimited-steam case and determining the time at which the reaction rate, limited by the parabolic rate law, reached the steam-limited rates. At this point, calculations were continued for each section of the reactor on the basis that the reaction rate could not increase further.

The results of the calculations for the steam-limited reactions are given in Figures V-42 and V-43. The temperatures and times at which the reaction rates reached the limiting values are indicated in the figures; the temperatures were about 1300°C for a flow rate of 1000 lb/hr and about 900°C for 100 lb/hr.

The extent of reaction for all of the metal cladding in the entire core was obtained by summing the reaction of each section. The results for the two assumed flow rates are plotted in Figure V-44. Comparison of the two shows the marked effect of steam flow rate on the reaction of the core considered as a whole.

The extent of metal-water reaction and hence the steam flow rate has a marked effect on the meltdown history of the cladding. This is shown in Table V-7, where the times corresponding to the beginning of melting of the cladding and the point where one-half of the cladding is melted (end of melting of the 6th section) are tabulated for all of the cases considered.



\*Denotes ratio of average power in section to average power in core.

108-8489

FIG. V-42. Calculated Temperature-Time Curves for Each Power Section for the Case of Metal Reacting with Limited Quantities of Steam in Loss-of-Coolant Accident.

### e. LOSS OF INTEGRITY OF THE REACTOR CORE

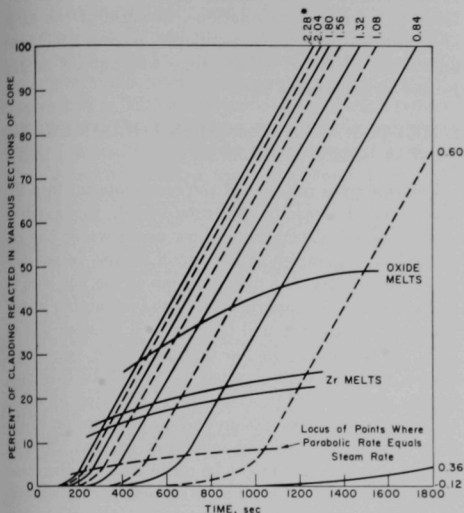
The calculations presented in the previous sections have ignored the loss of integrity of the core due to excessively high temperatures and have assumed that the core structure remains intact. As a result, these calculations eventually predict complete reaction of either the core cladding or the available steam, depending upon which limits the reaction. However, the extreme temperatures reached make it apparent that the core will suffer severe damage and eventually collapse.

It is of major importance to determine the time at which the core melts through the support structures and falls into the bottom of the reactor vessel, since this occurrence will bring to an end the reaction regimes discussed above. As the melted core collapses into the bottom of the reactor vessel, further metal-water reaction may occur during the initial quenching

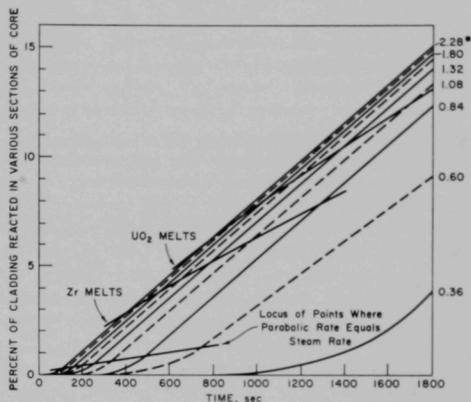
period if water is present, or during a long cooling period of the consolidated mass at the bottom of the reactor vessel or in a catch pan below the reactor vessel if little or no water is present. The metal-water reactions which take place after a total collapse of the core are discussed in the next section (see subsection f).

The temperature at which each section of the core will collapse is not known with certainty. Fuel rods will probably collapse at a temperature somewhere between the melting point of the cladding ( $1852^{\circ}\text{C}$ ) and the melting point of the fuel ( $2800^{\circ}\text{C}$ ). The ability of  $\text{ZrO}_2$  to retain the shape of the original Zircaloy cladding and to retain considerable strength was demonstrated by the furnace experiment in Section VA-1 of this report (see Figure V-4). It is likely, therefore, that the partially oxidized cladding will not collapse at the melting point of zirconium. Interactions between Zircaloy, zirconia, and the fuel could lower the melting

Steam Flow 1000 lbs/hr



Steam Flow 100 lbs/hr



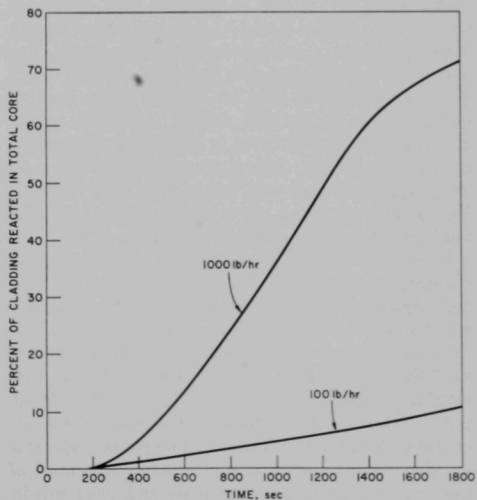
\*Denotes ratio of average power in section to average power in core.

108-8492

FIG. V-43. Calculated Percent Reaction-Time Curves for Each Power Section for the Case of Metal Reacting with a Limited Quantity of Steam in Loss-of-Coolant Accident.

point of the fuel to below 2800°C; however, this has not been established experimentally with any certainty. Rapid collapse of fuel rods and significant downward flow of material in the core will probably require temperatures close to the melting point of ZrO<sub>2</sub> (2600°C) or of UO<sub>2</sub> (2800°C).

Reaction will certainly continue during the period between the beginning of core collapse and the eventual fall of most of the core into the bottom of the reactor vessel. Several complicating factors may affect the reaction during this period. Two of these factors are changes in surface area of the cladding and local blockages of the flow of steam. Since changes in surface area may either be toward greater area (fragmentation) or toward lesser area (coalescence), it is probably a fair assumption to ignore net changes in cladding area. Blockages of convective steam flow probably can also be ignored, at least until a comprehensive model of core behavior during collapse is developed. Since a realistic model of core collapse does not presently exist, some indication of the time when total collapse occurs can be obtained by the method used in the LOFT analysis.<sup>29</sup> In that analysis, it was assumed that the core collapsed at the time when the average of the energy accumulated in the



108-8493

FIG. V-44. Calculated Percent Reaction-Time Curve for Entire Reactor Core for the Case of Metal Reacting with a Limited Quantity of Steam in Loss-of-Coolant Accident.

TABLE V-7. COMPARISON OF THE TIME REQUIRED TO MELT THE CLADDING FOR THE VARIOUS STEAM FLOW RATE CASES

Steam Flow	Time at which Melting of Cladding Begins (sec)	Time to Melt One-Half of Cladding (sec)
Unlimited	240	560
1000 lb/hr	300	680
100 lb/hr	390	1050
No Flow (No Metal-Water Reaction)	430	1250

TABLE V-8. TIME REQUIRED FOR COLLAPSE OF CORE AND EXTENT OF REACTION BASED ON THE AVERAGE NUCLEAR DECAY AND CHEMICAL ENERGY CONTENT

Steam Flow	Case of Average Core Energy Sufficient to Melt Cladding Completely (1852°C)		Case of Average Core Energy Sufficient to Begin To Melt Fuel (2800°C)	
	Collapse Time (sec)	Percent Metal Reacted	Collapse Time (sec)	Percent Metal Reacted
Unlimited	465	40	765	62
1000 lb/hr	740	21	1080	41
100 lb/hr	1200	6.0	2090	13
No Flow (No Metal-Water Reaction)	1400	—	2600	—

core was sufficient to melt the cladding. The times required for the collapse of the core were calculated on the same basis. However, two additional factors were considered: (1) chemical reaction energy was included in addition to decay energy, and (2) times were calculated not only for the zirconium melting point but also for the fuel melting point. The results of this calculation are listed in Table V-8. They demonstrate the major effect of metal-water reaction on the probable time of core failure. Included in Table V-8 is the extent of metal-water reaction for the total core at the time of probable collapse.

In addition to the time required for the core to collapse, time will be required for the slumped core to melt through the  $\frac{3}{8}$ -in. thick stainless steel grid plate which supports the fuel pins in each fuel element. This time was estimated to be 40 sec in the LOFT analysis.<sup>29</sup> Following failure of the grid plate, the hot core material will either funnel through the large holes in the  $1\frac{1}{4}$ -in. thick lower support plate (stainless steel) or will be held for an additional time period while this massive plate is melted. It is most likely that some of the core will fall through the plate and some will be delayed for a considerable period of time. The additional metal-water reaction occurring during these holdup periods can be estimated from the core reaction

rates given in Figures V-41 and V-44 for the three cases calculated if the holdup times can be estimated from heat transfer calculations. Because of the large uncertainties in the core-collapse model itself, the additional effects of holdup time will not be treated further at the present time.

### f. METAL-WATER REACTION FOLLOWING THERMAL CORE COLLAPSE

Following the collapse of the core material into the bottom of the reactor pressure vessel, the reaction conditions will depend upon how much water has remained in the bottom of the vessel. If the vessel bottom is nearly dry, the first portions of the hot core to fall will cause the vaporization of the remaining water. The bulk of the core will then form a random pile of  $UO_2$ ,  $ZrO_2$ , and Zr in the bottom of the vessel and may or may not melt through the vessel. In this case, further reaction will proceed by the diffusion of steam and air into the mass. Steam and air penetration of the mass should be relatively inefficient so that the continuing reaction rate might be quite low. On the other hand, cooling will also be slow so that the debris will remain in a reactive condition for a long time. Detailed analysis of diffusion and heat transfer for this case are lacking.

Should the hot core material fall into a large quantity of water in the bottom of the reactor pressure vessel, then a rapid quenching reaction should occur. If a major portion of the core falls at one time, there would be a chance for a violent steam explosion. Violent steam explosions have occurred on pouring molten aluminum into water.<sup>32</sup> Such an explosion may be a fairly general phenomenon when a quantity of very hot molten material is suddenly discharged into water.<sup>33</sup> It seems unlikely, however, that the entire mass of the reactor core (debris) will drop at one time. The energy generation is greater at the center of the reactor so that it is likely that the supporting structures will fail initially at the center and that failure will then spread radially. In this case, the core debris would enter the water over a period of time, and the chance of a serious explosion would be minimized.

The reaction that occurs during quenching of hot core debris in water has been simulated to some degree by experimental studies. Studies by the condenser discharge method have shown the extent of the zirconium-

<sup>32</sup> G. Long, "Explosions of Molten Aluminum in Water—Cause and Prevention," *Metal Progress* **71**, 107 (May 1957).

<sup>33</sup> L. F. Epstein, "Recent Developments in the Study of Metal-Water Reactions," *Progress in Nuclear Energy Series IV*, Vol. 4, Technology, Engineering and Safety, Pergamon Press, p. 461, 1961.

water reaction that occurs when submerged zirconium wires are heated nearly instantaneously (see ANL-6548). Results indicated that a 2.1-mm sphere of molten zirconium, formed from the electrically heated wires, would react to a maximum of 16% and a 1.05 mm sphere would react to about 40% in heated water. Experiments in TREAT with zirconium-rich, uranium alloys showed that fuel plates reacted to a maximum of 13% as a result of being heated and melted in about 0.5 sec (see ANL-6800, p. 346). The extent of reaction has been found by many investigators to be quite limited so long as there is no mechanism for dispersal of the material into fine particles (smaller than about 2 mm). In both the condenser discharge and the TREAT studies cited above, however, extensive fragmentation and 70 to 100% reaction occurred when the specimens were heated beyond the melting point of  $ZrO_2$  (2600°C) while submerged in water. TREAT experiments with Zircaloy-clad  $UO_2$  fuel specimens gave from 0 to 80% reaction as the energy of the transient and the resulting degree of clad fragmentation were increased (see ANL-6912, p. 90 or ANL-6900, p. 254).

#### g. DISCUSSION

In the analysis of the loss-of-coolant accident presented above, a preliminary attempt was made to predict the general features of such an accident in order to disclose gaps in the knowledge required for a precise analysis. In general, the uncertainty in the analysis increases with increasing time after blowdown. It is believed that the errors in the predictions of the beginning of melting and the initial phases of reaction are not large. A more refined analysis would include the energy stored in the fuel pins due to the temperature gradients which exist during reactor operation. The effects of initial steam cooling of the core and the heat capacity of support structures within the core would also alter the results to a small degree. As core melting and collapse begin, it is clear that uncertainties multiply. It is also clear, however, that an increasing quantity of zirconium is reaching temperatures at which it will react with all of the steam that can enter central regions of the core. The principal uncertainties in the analysis are related to the lack of a meltdown model from which to estimate the failure times of the lower core supporting plates and the temperature of debris falling into the bottom of the reactor vessel. Ultimate analysis of the accident requires calculations of

the steam flow through the core following blowdown and the quantity of water remaining in the lower part of the reactor vessel. In the LOFT analysis, the quantity of water remaining ranged from 0 to about 2000 lb, whereas only 320 lb are required to react with the entire cladding.

One of the uncertainties in the analysis is the relation between the steam flow rate and the limiting reaction rate. Questions concerning the efficiency of reaction of steam flowing upward along individual fuel rods were ignored. In reality, reaction would be greater at lower positions in the core.

One case which was not considered in the analysis presented was that of no net steam flow through the core (i.e., where no rupture in the reactor vessel exists above the core). In this case, there might be some convective circulation of steam, and eventually hydrogen, through the core. Although a detailed calculation of the convective circulation of gases has not been performed, some guide to the extent of metal-water reaction might be gained by noting that the steam present in the entire reactor pressure vessel after the blowdown is sufficient to react with about 8.6% of the cladding.

Two additional uncertainties in the analysis involve chemical phenomena which have not been investigated in sufficient detail to allow assessment of their possible roles in the meltdown accident. These are the reaction of zirconium with hydrogen and the reaction of  $UO_2$  with steam. For a severely steam-limited case, the former reaction could provide a steam-pumping action which would bring steam into the lower portion of the core and form zirconium hydrides in the upper portion of the core.<sup>34</sup> For clean zirconium<sup>34</sup> the hydriding reaction is sufficiently rapid at temperatures of around 1000°C to merit consideration; however, the retarding effect of oxide films on the hydriding reaction at higher temperatures has not been studied extensively. It has been shown that  $UO_2$  will react with water to form  $UO_{2.2}$  and hydrogen in destructive tests in TREAT (see Section V-A4 of this report). The reaction rate has not been evaluated under conditions of high temperature when no violent fragmentation occurs. Although hydrogen is produced in the  $UO_2$ -steam reaction, little or no heat is evolved.

<sup>34</sup> R. B. Bernstein, and D. Cubicciotti, The Permeability of Zirconium to Hydrogen, *J. Phys. Colloid Chem.* **55**, 238 (1951).

## B. FAST REACTOR SAFETY STUDIES

A program of research has been initiated that would bring the experience developed during studies of metal-water reactions to bear on certain potential problems in the area of fast reactor safety. Three problem areas are being studied. These are:

1. the chemical and physical interactions of fuel and cladding materials with molten sodium at high temperature,
2. fuel migration and segregation in mixed uranium-plutonium fuels,
3. transient boiling characteristics of molten sodium to determine the nature of explosive vapor generation.

The survey study of interactions between fast reactor materials and molten sodium has progressed to the apparatus construction stage. Further discussion of the program and a summary of apparatus development is presented in a separate section below.

The study of fuel migration and segregation in mixed uranium-plutonium fuels is in a very preliminary stage. Initial considerations have been given to the development of a furnace to produce a temperature gradient across small samples of mixed fuels such as mixtures of uranium and plutonium oxides, carbides, sulfides, and nitrides. Segregation of the uranium and plutonium compounds within the fuel will be determined by chemical and metallographic analysis. A significant degree of segregation in an operating reactor might seriously decrease the effectiveness of Doppler

broadening as a shutdown mechanism since more time would be required than for an unsegregated fuel before fission heat generated within plutonium-rich regions could be transferred to uranium-rich regions. This additional heat transfer time would delay increased neutron absorption (and decreased reactivity) in a reactor.

Studies of transient heat transfer in liquid sodium are also in a very preliminary stage. Several experimental methods are under consideration in which very hot particles are contacted with liquid sodium. In one of these a swinging arm is employed to drag a heated sphere through a trough of sodium while measuring temperature changes during the event. In another, a falling pellet is heated by a graphite tube furnace prior to contacting the molten sodium. A third method involves the pulling apart of a heated, segmented rod immersed in liquid sodium; this results in contacting fresh surface with the sodium. In the fourth method, a thermite type chemical reaction can be used so that molten material is rapidly generated and sprayed into the sodium. Following orientation studies in the laboratory, it is likely that in-pile meltdowns in TREAT will be required. Determination of the nature of rapid vapor generation in sodium, especially regarding superheating or explosive vapor generation, and the measurement of transient heat transfer coefficients will be valuable in the analysis of fast reactor accidents of either the loss-of-flow or the nuclear excursion type.

### 1. Fuel- and Cladding-Coolant Interaction Studies (D. SWIFT, P. KRAUSE)

A program to study the high temperature interaction between sodium coolant and fast reactor materials has been initiated. The purpose of the investigation is to determine possible sources of chemical energy release and physical effects that would result from a fast reactor meltdown accident. In order to simulate the contact of coolant with reactor material in a meltdown accident, a small sample of reactor material will be heated to a temperature which it would be expected to reach in a meltdown accident and dropped into a pool of liquid sodium. The quenched sample will then be removed from the sodium and examined to determine the extent of chemical or physical interaction.

Initial experiments will be performed with a number of metals and alloys which are either currently being used or are being considered as possible fuel or cladding materials in fast reactors. These include uranium, zirconium, stainless steel (austenitic and ferritic), vanadium, titanium, vanadium-titanium alloys, mo-

lybdenum, tantalum, and niobium. Experiments with iron and chromium are also planned as a part of the investigation of stainless steel. The metals are to be melted in a levitation coil powered by a 15-kw induction generator operating at 250 kc. The coil design and experimental procedure have been described in a previous report (see ANL-6648, p. 196).

The experiments are to be carried out in a standard 2-module glovebox containing an argon atmosphere. The argon is to be circulated through a purification system which will maintain oxygen and water vapor levels below 5 ppm. Oxygen removal will be effected by reaction with hydrogen over a palladium bed, and water vapor will be removed by Linde molecular sieves. Provision is being made to pass a coaxial transmission tube from the step-down transformer of the generator through a glove port to the levitation coil. The coil and coaxial lines are to be oil cooled to preclude the possibility of a sodium-water reaction within the glovebox; thus, a heat transfer loop has been constructed

which includes a pump, flow meter, and oil-water heat exchanger. The sodium is to be contained in a cylindrical well, 2¼ in. in dia. and 7 in. deep, welded to the floor of the glovebox. Thus, the sodium can be heated externally using a mantle heater. By locating the coil near the top of the glovebox, the samples should drop approximately 3 ft before hitting the liquid sodium surface. This should insure that the samples are completely immersed in sodium.

Major emphasis will be given to the detection and evaluation of exothermal alloying reactions which may occur between the metal and sodium at meltdown temperatures (>2000°C). Detection of such reactions can be accomplished by visual observation and/or temperature changes in the sodium in excess of sensible heat addition. Evaluation of the extent of reaction and the reaction products will be accomplished by metallurgical examination of the quenched metallic sample.

These experiments should also indicate physical changes which might occur when molten metal contacts liquid sodium. The possibility of large density

changes (formation of metal froths) is of some importance in evaluating the secondary effects of a molten metal accident. Examination of the quenched metal sample after contact with sodium should indicate what physical changes have occurred. It may also be possible to obtain qualitative information about transient sodium boiling by visual observation of the initial contact between the molten metal and sodium. This information may be of interest because so little is known about the phenomenon of transient sodium boiling.

The second phase of the investigation will be a study of nonmetal-sodium interactions, with particular emphasis given to the interactions with the oxide, carbide, and nitride of uranium. It will be necessary to modify the heating procedure, since these materials cannot be inductively heated in a levitation coil. Consideration is currently being given to a susceptor method of heating using a material such as graphite as the susceptor.

## C. METAL OXIDATION AND IGNITION KINETICS

### 1. Ignition of Irradiated Uranium (J. G. SCHNIZLEIN, D. F. FISCHER)

An important aspect of the ignition of uranium is the effect of irradiation on ignition behavior. Incidents reported in the literature (at Chalk River, Canada<sup>35</sup> and Windscale, England,<sup>36</sup> as well as several ignitions at Hanford<sup>37</sup>) have been interpreted as indicating a greater pyrophoricity of uranium after irradiation. Therefore, studies of the ignition of irradiated uranium were initiated.

It is certain that the release of fission products in the event of ignition of irradiated uranium constitutes a severe hazard. The release of fission products has been studied by Parker *et al.*,<sup>38</sup> Hilliard,<sup>39</sup> Scott,<sup>40</sup> and

Megaw *et al.*<sup>41</sup> at elevated temperatures. Some of these authors indicate a somewhat greater oxidation rate with irradiated uranium than with unirradiated metal, but there were uncertainties as to surface area and extent of irradiation. Increased oxidation rates were noted in air only when uranium was irradiated above  $10^{20}$  nvt ( $10^{-2}$  a/o burnup) at which point fission gas bubbles cause disruption of the oxide and increased surface area.<sup>42</sup>

Zima<sup>37</sup> concludes that "The effect of irradiation on the pyrophoricity or uranium remains obscure. The evidence presented in this review does not indicate a strong irradiation influence. It is submitted that the two main effects of irradiation with respect to fuel element fires are: increase in the potential active surface associated with a given mass of U through the development of cracks, and porosity; self heating from radioactive decay." There have been numerous studies on the effect of irradiation on the mechanical properties of uranium. Directional growth, surface

<sup>35</sup> J. W. Greenwood, Contamination of the NRU Reactor in May 1958, AECL-850 (CRR-836), May 1959.

<sup>36</sup> Accident at Windscale No. 1 Pile on October 10, 1957, Her Majesty's Stationery Office, London, November 1957.

<sup>37</sup> C. E. Zima, Pyrophoricity of Uranium in Reactor Environments, HW-62442, January 1960.

<sup>38</sup> G. W. Parker, G. E. Creek, W. J. Martin, and C. J. Barton, Fuel Element Catastrophe Studies: Hazards of Fission Product Release from Irradiated Uranium, ORNL-CF-60-6-24, June 1960.

<sup>39</sup> R. K. Hilliard, Fission Product Release from Uranium Heated in Air, HW-60689, August 1959.

<sup>40</sup> A. J. Scott, Fission Product Release by High Temperature Uranium-Steam Reaction, HW-62604, November 1959.

<sup>41</sup> W. J. Megaw, R. C. Chadwick, A. C. Wells, and J. E. Bridges, *J. Nuclear Science* **15**, 176 (1961).

<sup>42</sup> R. K. Hilliard, Fission Product Release from Uranium—Effect of Irradiation Level, HW-72321, June 1962.

TABLE V-9. SPECTROGRAPHIC ANALYSIS OF ENRICHED URANIUM USED FOR STUDIES OF THE IGNITION OF IRRADIATED URANIUM

Element	Concentration <sup>a</sup> (ppm)	Element	Concentration <sup>a</sup> (ppm)
Si	300	Mn	5
Fe	300	Mg	20
Ni	20	Cu	50
Al	25	Mo	30
Cr	15		

<sup>a</sup> The concentrations of those constituents not indicated were below the limits of spectrographic detection. Limits of detection (in ppm) are: Ag, 1; As, 20; B, 0.1; Be, 0.5; Bi, 1; Ca, 100; Ce, 5; K, 500; Li, 5; Na, 10; P, 100; Pb, 2; Sb, 5; Sn, 5; Ti, 100; Zn, 50.

roughening, and swelling are commonly observed.<sup>43</sup> These all tend to increase the specific surface area and promote pyrophoricity. Post-irradiation swelling has been noted to occur when highly irradiated uranium is heated to approximately 650°C<sup>44</sup> (see also ANL-6543). This swelling would very likely result in ignition if it occurred in the presence of air. LaPlante (ANL-6569, p. 31) has observed a strongly exothermic reaction with nitrogen at approximately the same temperature.

A brief summary of the proposed ignition program was presented in ANL-6569, p. 185. It was decided at that time to enclose cylindrical uranium samples in constraint jackets in an effort to avoid the complications of surface roughening, directional growth, and swelling during irradiation. Conditions were chosen to maintain a low sample temperature (less than 300°C) during irradiation. A small sample size (0.25 in. long) by 0.20-in. dia. pins) was chosen so that its ignition temperature before irradiation would probably be less than 650°C and thus the complication of post-irradiation swelling would be avoided.

#### a. PREPARATION OF SAMPLES

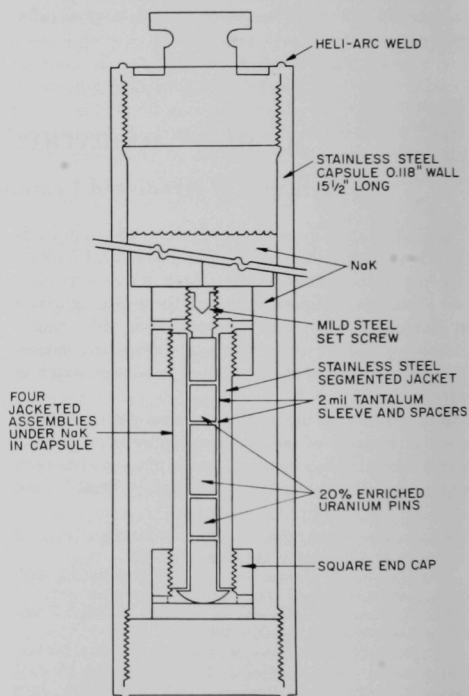
The uranium pins were supplied by the ANL Metallurgy Division. The pins were 20% enriched so that adequate burnup could be obtained in a reasonable time of irradiation. Results of a spectrographic analysis of the uranium are shown in Table V-9.

Three uranium pins (two 0.25-in. long and one 0.5-in. long) were assembled in one segmented stainless steel constraint jacket as shown in Figures V-45 and V-46. (The 0.5-in. long pins were prepared for use in another program not related to ignition in air or oxygen.) Tantalum foil sleeves and spacers en-

veloped the pins to prevent the formation of "fission rivets". Four jacketed assemblies were arranged axially in each irradiation capsule. Free space in the capsules was filled with NaK to serve as a heat transfer medium to conduct fission heat away from the uranium during irradiation. Each capsule was sealed by welding, leak tested, and checked for defects by radiography.

A total of three capsules were prepared. Two of the capsules were submitted for irradiation in MTR; the third was not irradiated. One capsule underwent four irradiation cycles in MTR; the second underwent eight cycles. Subsequent burnup analyses indicated that 0.79% of the <sup>235</sup>U had been fissioned in the one capsule and 1.71% of the <sup>235</sup>U had been fissioned in the second.

During the irradiation sequence, the samples were subjected to thermocycling and were in contact with NaK for an extended period of time. In order to separate any effects of thermocycling and NaK contact

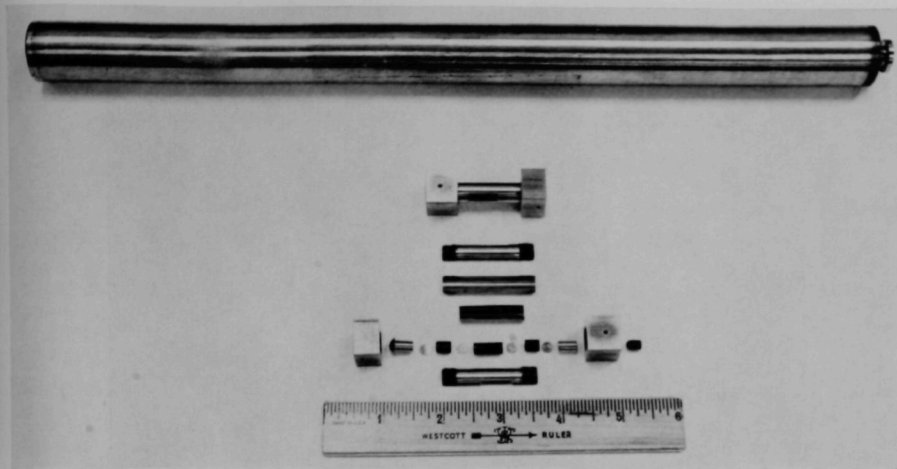


108-8082

FIG. V-45. Capsule and Jacket Assembly for MTR Irradiation of Uranium Ignition Samples (Schematic).

<sup>43</sup> J. H. Kittel and S. H. Paine, Nucl. Sci. Eng. **3**, 250 (1958).

<sup>44</sup> N. R. Chellev and R. K. Steunenberg, Nucl. Sci. Eng. **14**, 1 (1962).



108-7492A

FIG. V-46. Stainless Steel Capsule and Jacket Assembly for MTR Irradiation of Uranium Ignition Samples.

from irradiation effects, the third capsule, while not subjected to radiation was subjected to 17 thermocycles (10 min at 260–270°C, cooled 30 min below 40°C) with NaK in the capsule.

In addition to the irradiated samples and the thermocycled samples, two jacket assemblies were prepared which were neither irradiated, exposed to NaK, nor thermocycled. Samples removed from these assemblies were used as control samples.

#### b. IGNITION APPARATUS

The apparatus was very similar to that developed previously for burning curve ignition experiments with unirradiated uranium (see ANL-5974, p. 11). Because of the high level of radiation from the irradiated samples, new apparatus was constructed which could be operated by electronic manipulators in the Senior Cave Facility. The apparatus, shown in Figure V-47, was constructed and tested outside of the cave and later moved into the cave facility.

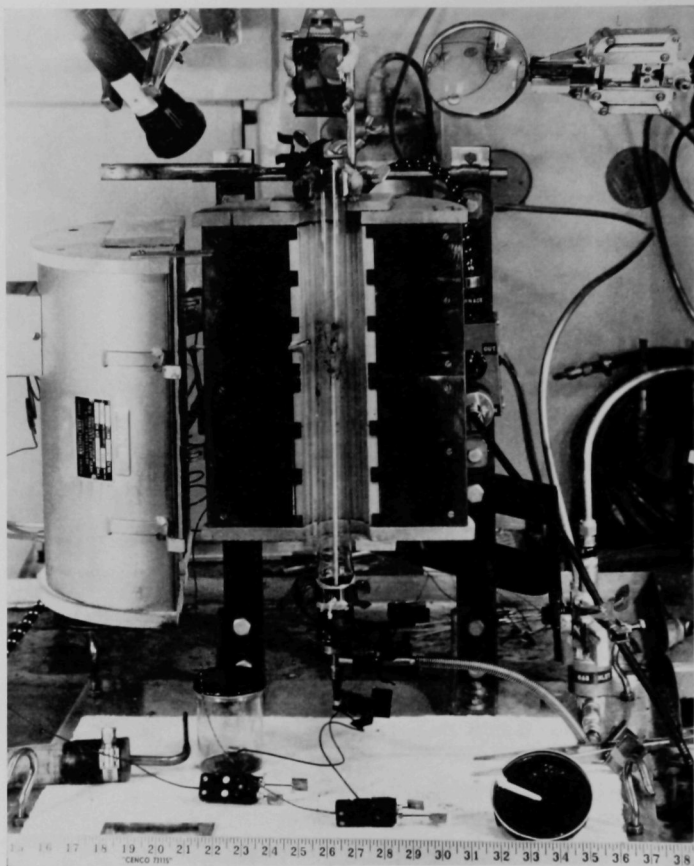
The cylindrical samples were mounted on the top end of a vertical ceramic rod in contact with a thermocouple. The sample and the ceramic rod were enclosed in a quartz tube inside of an electric furnace. Oxygen or air was passed through the tube at a uniform rate of 2000 cc/min, a rate which was sufficient to prevent accumulation of nitrogen around the sample during air oxidations. Furnace temperature, indicated by a thermocouple between the furnace wall and the quartz

tube, was programmed to increase from room temperature at a rate of 10°C per min. Furnace temperature and sample temperature were both recorded as a function of time. The sample temperature-time trace has been referred to as a burning curve (see ANL-5974, p. 12). The sample first self-heats beyond the furnace temperature and then may ignite. Ignition temperature is determined graphically as the intersection point between the pre-ignition heating rate and the post-ignition self-heating rate.

In some of the experiments in air, it was found that the physical contact between the thermocouple and the sample was inadequate for accurate temperature recording. It was concluded that the thermocouple must be imbedded in holes within the sample in order to achieve an accurate temperature-time trace. Accordingly, small holes were drilled in one thermocycled and two irradiated samples. Drilling was difficult but was accomplished with a center drill using short spurts of heavy drilling pressure, while using kerosene as a lubricant.

#### c. RESULTS OF IGNITION TESTS IN PURE OXYGEN

The 20% enriched uranium samples used for the experiments were right cylinders, 0.25 in. long by 0.20 in. dia. and had an apparent specific area between 0.59 and 0.60 cm<sup>2</sup>/g. The appearance of unreacted specimens is shown in Figure V-48. An unirradiated



108-7801A

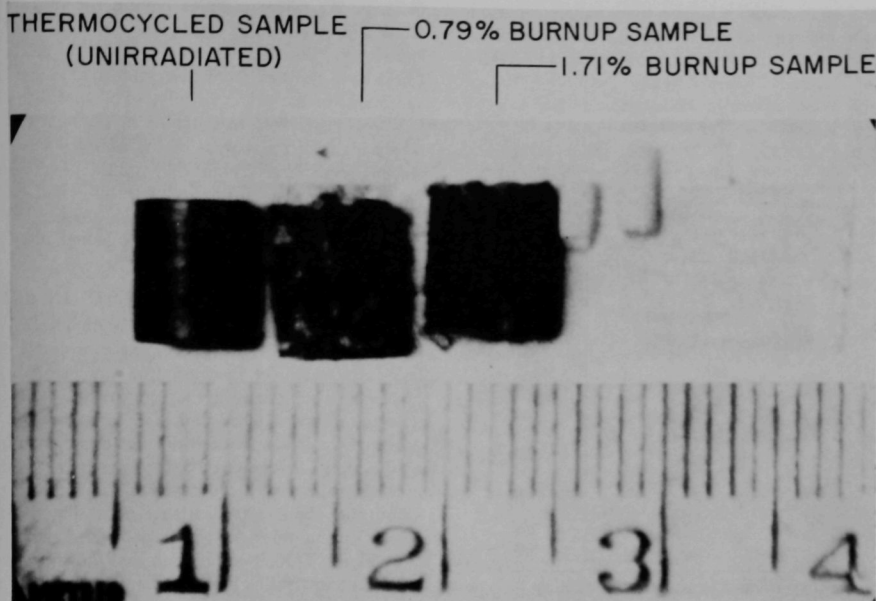
Fig. V-47. Apparatus Used for the Ignition Studies of Irradiated Uranium in the Senior Cave Facility.

thermocycled sample shown at the left of the figure had a relatively smooth surface which was identical with completely untreated control samples. The irradiated samples shown at the right of the figure had some surface roughening in spite of the constraint imposed on the sample during irradiation. The white specks apparent on the 0.79% burnup sample were particles of dessicant used during sample storage.

Typical temperature-time traces (burning curves) obtained in oxygen are plotted in Figure V-49. Ignition temperatures determined from the burning curves are listed in Table V-10, for all of the experiments. There

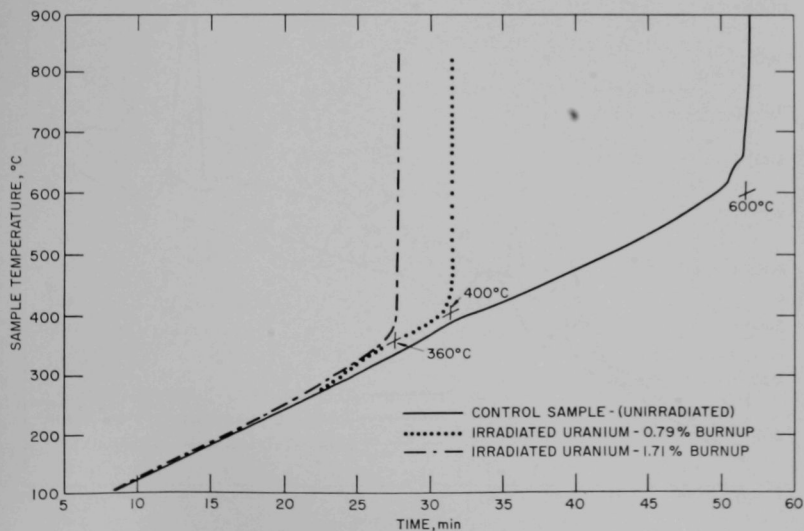
were no significant differences in results for control samples and thermocycled samples, suggesting that the decreased ignition temperature for the irradiated samples resulted from the effects of irradiation and not from incidental thermocycling or NaK contact. There was also no significant difference in burning curve ignition temperature between control samples ignited in the Cave Facility and outside the Cave Facility, indicating no effect of the high background radiation level which existed in the cave.

The ignition temperatures (591–611°C) of the unirradiated cylindrical samples (specific area 0.60 cm<sup>2</sup>/g)



108-8085A

Fig. V-48. Appearance of Specimens Used for the Ignition Studies of Irradiated Uranium.



108-8083

Fig. V-49. Temperature-Time Traces (Burning Curves) of 20% Enriched Uranium Samples Heated in Flowing Oxygen. (Furnace heated at 10°C/min. Ignition temperatures determined by graphical method as indicated.)

in oxygen were slightly higher than values reported previously for pure uranium samples having similar specific areas. This information was reported in ANL-

TABLE V-10. EFFECT OF IRRADIATION ON IGNITION TEMPERATURES OF 20% ENRICHED URANIUM IN OXYGEN

(Burning Curve Ignition Tests with 0.25 in. long by 0.20-in. dia. right cylinders; specific area 0.59-0.60 cm<sup>2</sup>/g)

Run Number	Ignition Temp. (°C)
Control Samples	
12 <sup>a</sup>	600
24	611
Thermocycled, Not Irradiated	
10 <sup>a</sup>	591
11 <sup>a</sup>	597
26	608
27	602
Irradiated in MTR to 0.79% Burnup of <sup>235</sup> U	
20	403
23	403
25	400
Irradiated in MTR to 1.71% Burnup of <sup>235</sup> U	
21	357
22	365

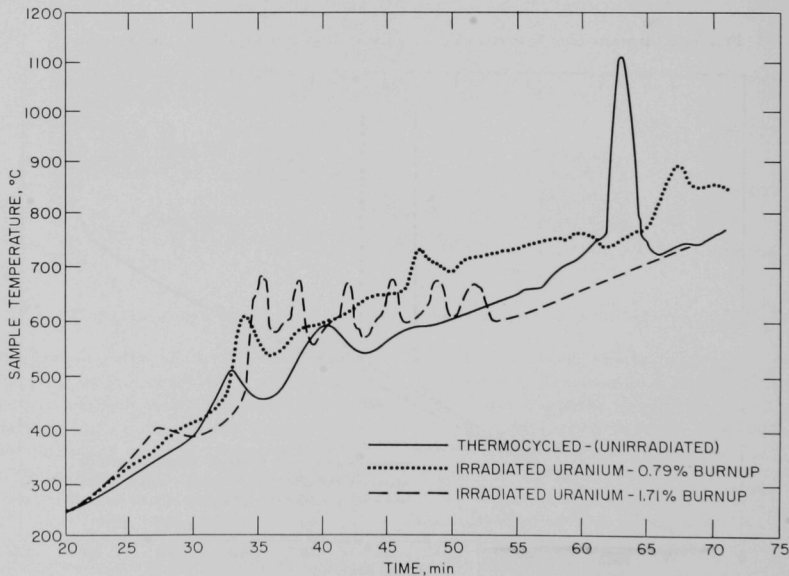
<sup>a</sup> Experiments performed outside of Cave Facility.

5974, p. 27, where samples having specific areas of 0.396 and 0.790 cm<sup>2</sup>/g ignited at 595 and 540°C, respectively. The difference is relatively minor and could have resulted from the cylindrical shape of the specimens in the current study. (The specimens studied previously were rectangular in shape.) The relatively high silicon content of the samples used in the current study (see Table V-9) would have been expected to decrease ignition temperatures if it had any effect at all (see ANL-6596, p. 181). Other impurity contents were probably too small to have had an effect on ignition temperature.

#### d. RESULTS OF IGNITION TESTS IN AIR

Shown in Figure V-50 are results of burning curve experiments in air using samples containing drilled holes into which the thermocouple was inserted. Much of the fine structure in the temperature-time traces was not recorded when undrilled samples were used. Although ignitions as such did not occur with irradiated samples, it is clear that there was a greater degree of self-heating and spontaneous thermocycling, beginning at about 400°C, with the irradiated samples than with the unirradiated, thermocycled samples.

In Figure V-50, it can be seen that the 1.71% burnup sample underwent a sharp temperature rise from about



108-8084

FIG. V-50. Temperature-Time Traces (Burning Curves) of 20% Enriched Uranium Samples Heated in Flowing Air. (Furnace heated at 10°C/min. Thermocouple embedded in drilled specimens.)

400 to about 700°C at 35 min. This sharp rise indicates a tendency toward ignition at the same temperature at which ignition in oxygen occurred (see Figure V-49). Failure to ignite in air was probably due to the formation of a protective oxide at higher temperatures. The formation of protective oxides on uranium in air was demonstrated in previous studies by the finding that a parabolic rate law applied at 600°C and above (see ANL-6725, p. 201). Thus, spontaneous thermocycling

is observed from below 600°C, where a rapid linear oxidation rate law applies, to above 600°C, where a parabolic oxidation law applies.

The ignition at approximately 700°C at 60 min which was observed for the unirradiated specimen in Figure V-50 did not occur with the irradiated samples, probably because the irradiated samples had been completely oxidized before the furnace temperature reached values high enough to initiate this ignition.



## VI. Energy Conversion\* (C. E. Crouthamel, J. C. Hesson, A. D. Tevebaugh)

Emf cells continue to be of interest as devices for the direct conversion of heat to electrical energy. An emf cell would function in one isothermal leg of a Carnot cycle. Regeneration of the cell products could be accomplished ideally by a second cell operating in the high temperature isothermal leg of a Carnot cycle. Practical operation of a high temperature cell would be difficult, however, because of increasing mutual solubility and volatility of the three liquid phases, anode, cathode and electrolyte. The realization of practical high temperature cell operation will probably require the development of solid electrolytes or molten electrolytes in suitable porous ceramic materials. Such electrolytes would be capable of supporting high current densities with low cell polarization, and their use would be expected to reduce the irreversible transfer of the cell reactants at high temperatures to acceptable low levels. Work in this area will be done at a later date. We have concentrated initially on the spontaneous thermal regeneration of the cell products in the systems currently being considered. This type of regeneration requires the physical separation at high temperature of the anode and cathode reactants. Lack of basic data in the pertinent areas—thermodynamic, chemical, physical, kinetic, and solid state—handicaps the application of any regenerative emf cell system. The current program is involved in obtaining selected pieces of fundamental data in all areas except solid state electrolyte phenomena. For the first generation cells the necessity for solid electrolytes has been avoided by careful selection of the cell components. The above considerations have led us to the study of two types of emf cells for possible application in a regenerative cycle. They are the hydride cell and the bimetallic concentration cell.

The hydride cell consists of an anode of liquid lithium metal, an electrolyte of molten lithium halide salts, and a hydrogen gas cathode. In operation, liquid lithium is oxidized to lithium ions, hydrogen gas is reduced to hydride ions, and the two combine to form the cell product, lithium hydride.

The bimetallic concentration cells have two liquid metal electrodes in contact with a molten salt electrolyte. The fused salt electrolyte must be thermodynamically stable with respect to reduction by the anode

metal. The overall cell reaction is the oxidation of the metallic anode to produce metal ions in the electrolyte and the reduction of the metal ions in the electrolyte at the cathode to produce an alloy.

In a previous report, ANL-6900, p. 320, data for the standard emf of the lithium hydride cell as a function of temperature were reported. In this report, results on a series of unsaturated cells to determine lithium hydride activities and activity coefficients in fused salts are given. These data are necessary in defining and optimizing the operating voltage and regeneration characteristics of a lithium hydride cell. Also presented in this report are preliminary results on the kinetics of the electrode reactions of a lithium hydride cell.

The solubilities of  $\text{Na}_3\text{Bi}$  intermetallic and of pure sodium metal in the  $\text{NaI-NaCl-NaF}$  ternary eutectic have been determined. The sodium-bismuth cell has tentatively been selected for some of the first engineering investigations. The ternary salt mixture was selected as the electrolyte system for these cell studies. The solubility data were obtained to aid in understanding the irreversible transfer of both anode and cathode metals in an operating cell. In addition, the studies of solubility are a part of the effort to elucidate the nature and behavior of the intermetallic compounds in fused salts and liquid metals. As another part of this program, the spectral studies of alkali tellurides and alkali bismuthides in fused salts have been continued.

For the regeneration portion of the cycle, knowledge of temperature-pressure-composition relationships in the liquid-vapor equilibria is needed. Nonisothermal isopiestic experiments with the sodium-bismuth system have demonstrated the possible relative extents to which regeneration might proceed for selected condensation temperatures and a fixed regeneration temperature of  $900^\circ\text{C}$ . These experiments also revealed that solid  $\text{Na}_3\text{Bi}$  may deposit in the regenerator if the system pressure and, therefore, the condensation temperature, is too low. The relationships among regeneration and condensation temperatures, anode composition, and compositions of material removed from and returned to the cathode were deduced from a generalized analysis of a fixed isobaric phase diagram.

Engineering studies have been continued. The cycle efficiencies of the Na-Bi, Li-Sn, Na-Sn, and LiH re-

\* A summary of this section is given on pages 15 to 16.

generative cells have been examined and computed, using conservative estimates of operating parameters. A series of static corrosion tests with liquid bismuth and

tin metals were run, and a number of dynamic corrosion tests were made in thermal convection loops containing liquid bismuth.

## A. LITHIUM HYDRIDE CELL STUDIES (C. JOHNSON, R. HEINRICH, C. E. CROUTHAMEL)

The lithium hydride cell may be represented as



for which the cell reaction is  $\text{Li} (\ell) + \frac{1}{2} \text{H}_2 (\text{g}) \rightarrow \text{LiH} (\text{s})$ . The standard emf of the saturated lithium hydride cell was reported in a previous report, ANL-6900, p. 320. Knowing this value, the activity of the cell product, lithium hydride, can be determined in electrolytes of similar cells. This information is important in ascertaining optimum conditions for the regeneration cycle of the cell.

To date, several unsaturated lithium hydride cells have been operated for the purpose of determining the activity of lithium hydride in certain specified electrolytes. The cells utilized an Armco iron "flag" cathode, a lithium anode, and electrolytes of various compositions of lithium hydride in lithium chloride or in lithium chloride-lithium fluoride eutectic mixture. The activity of lithium hydride in each electrolyte can be calculated from the following equation:

$$E = E^\circ - RT/nF \ln \frac{a_{\text{LiH}}}{a_{\text{Li}} a_{\text{H}_2}^{1/2}}$$

For a hydrogen pressure of 760 mm and pure lithium metal, this equation reduces to the form

$$E = E^\circ - RT/nF \ln a_{\text{LiH}}$$

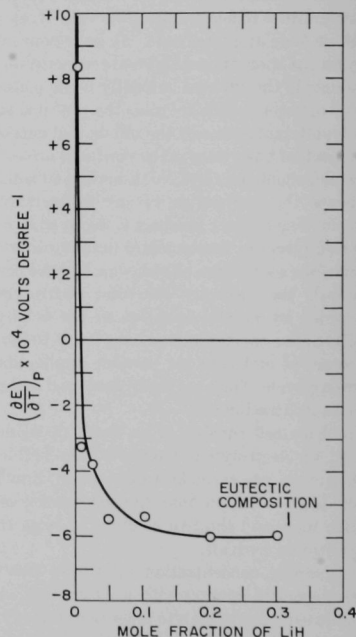
TABLE VI-1. THERMODYNAMIC DATA FOR LiH IN VARIOUS ELECTROLYTES

$T = 873^\circ\text{K} (600^\circ\text{C})$      $E^\circ = 0.244$  volts     $\text{H}_2 = 760$  mm

Cell No.	Electrolyte Composition (m/o)	Cell emf (volts)	$a_{\text{LiH}}$	$\gamma$	$(\partial E/\partial T)_P \times 10^4$ (volts degree <sup>-1</sup> )
1	5.6 LiH-66.1 LiCl-28.3 LiF	0.366	0.20	3.5	-4.7
2	11.0 LiH-62.3 LiCl-26.7 LiF	0.324	0.35	3.1	-4.8
3	1.0 LiH-99.0 LiCl	0.518	0.03	2.5	-3.3
4	5.0 LiH-95.0 LiCl	0.388	0.15	2.9	-5.5
5	10.2 LiH-89.8 LiCl	0.344	0.26	2.6	-5.4
6	20.2 LiH-79.8 LiCl	0.291	0.54	2.7	-6.0
7	~100.0 LiCl (trace amounts of LiH)	0.60	0.009	—	+8.3
8	30.2 LiH-69.8 LiCl	0.263	0.79	2.6	-5.9
9	2.5 LiH-97.5 LiCl	0.438	0.08	3.0	-3.8

The lithium hydride activities for various cell electrolytes have been calculated from the above relationship and the data summarized in Table VI-1. Examination of the data indicates that lithium hydride exhibits strong positive deviations from ideality in lithium chloride as well as lithium chloride-lithium fluoride eutectic.

Also included in Table VI-1 are temperature coefficients of the emf of the cell at a variety of electrolyte compositions. At practical hydride compositions the temperature coefficients are all negative. Since the cell reaction is reversible, the entropy change of the reaction can be determined by  $\Delta S = nF (\partial E/\partial T)_P$ . When the proper substitutions are made,  $\bar{S} = -R \ln a_{\text{LiH}}$ .



108-8714

FIG. VI-1. Temperature Coefficient of EMF of Cells with LiH-LiCl Electrolytes.

As the concentration of the lithium hydride in solution approaches an infinitely dilute solution, the partial molal entropy approaches an infinitely large positive number. This type of relationship is illustrated in Figure VI-1 where the emf-temperature coefficient is plotted against the lithium hydride concentration. Only the data obtained utilizing the lithium hydride-lithium chloride binary electrolyte have been included in this graph.

## B. ELECTRODE KINETICS (J. P. ELDER,\* J. A. PLAMBECK,\*\* C. E. CROUTHAMEL)

A prerequisite for the characterization of the factors controlling the operation of the galvanic lithium hydride cell is an understanding of the mechanism of the individual electrode reactions. Such mechanisms result from an interpretation of the polarization data (electrode potential-current density characteristics) observed for each electrode. Generally, for a specified electrode surface area, at low polarizations (when the departure of the electrode potential from its equilibrium value is small) the transfer of charge across one or the other of the electrode-electrolyte interfaces governs the current output of the cell. The maximum current which may be withdrawn from the cell, however, is governed by the limiting rate, i.e., current density, of one or the other of the electrode processes, which is a mass transfer controlled phenomenon.

To understand the electrode kinetic mechanisms, it was necessary to devise several complementary methods of studying the reactions. Since charge transfer processes at the high temperatures of molten salt media are relatively rapid, the only method of measuring the specific rate constant characterizing the process is by use of perturbation-relaxation techniques. The electrode under study is perturbed from its equilibrium state by application of either a current or a voltage pulse, which induces a transient voltage or current, respectively. From an analysis of the voltage-time or current-time curve, the important kinetic parameters may be evaluated. However, because the complete analysis of the data acquired by employing several of these pulse techniques requires a knowledge of the diffusion coefficient of the soluble ionic component of the appropriate redox couple, it is of importance to measure this parameter independently. This measurement will be carried out by employing the chronopotentiometric technique. Analysis of the data obtained using this technique is greatly simplified if voltammetric data is in turn avail-

able. Voltammetry is a simplified, conventional polarization technique wherein one of the working electrodes is unpolarizable and thus may be employed simultaneously as a reference electrode. This is achieved by employing, as the polarizable working electrode, a thin wire of superficial surface area several orders of magnitude less than the counter electrode. Upon polarizing the microelectrode by means of an external voltage applied across the cell, currents of the order of microamperes flow. The current density at the large counter electrode is so small that it is polarized to a negligible extent.

The necessary apparatus has been acquired whereby the electrochemical characteristics of the lithium hydride cell may be investigated by these several means. Initial experimentation has been directed at developing the voltammetric technique as applied to this reactive system. It is of utmost importance to work with extremely pure materials, since this technique is highly sensitive to the presence of impurities in the electrolyte melt. For this reason, the LiCl-KCl eutectic (59 m/o LiCl), m.p. 352°C, which can be obtained commercially in a high state of purity, has been employed. In order to maximize the sensitivity of the voltammetric method, the area of the working microelectrode should be minimized. Normally, this is achieved by sealing the wire in an insulating material in such a manner that the minimum geometric area is exposed. This technique is not possible in this system owing to the fact that there is a finite solubility of lithium in the electrolyte and, as yet, no suitable insulating material except frozen salt has been found which will completely withstand attack by this metal. Frozen salt, however, is not amenable for fabrication of these electrodes. For this reason, the following arrangement has been employed. A thin tungsten wire (0.035 in. in dia.) is suspended above the electrolyte so that the extremity, sharpened to a needle point, just touches the surface. Since there is lithium in solu-

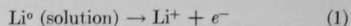
\* Post-doctoral Fellow.

\*\* Graduate Student, University of Illinois.

tion, this microelectrode will respond to the  $\text{Li}/\text{Li}^+$  potential. In the presence of hydrogen above and hydride ion in the electrolyte, the  $\text{H}_2/\text{H}^-$  equilibrium is established at the three phase boundary. Therefore, it is essential to establish first the effect of the presence of dissolved lithium on the polarization of the  $\text{H}_2/\text{H}^-$  electrode.

Preliminary experiments have established the following facts. At all potentials positive with respect to  $\text{Li}/\text{Li}^+$  as reference zero, an anodic process occurs at the microelectrode, regardless of the establishment of the  $\text{H}_2/\text{H}^-$  equilibrium. Presumably, this is the oxida-

tion



When the  $\text{H}_2/\text{H}^-$  equilibrium is established and the microelectrode is polarized, the current-voltage curve can be interpreted as the resultant of the anodic process (1) and the cathodic reduction of hydrogen



For both processes (1) and (2), a limiting current plateau is observed. At the present time, sufficient data for a complete analysis have not been obtained.

## C. INTERMETALLIC SYSTEMS

### I. Sodium-Bismuth Solubility Studies (M. FOSTER, R. EPPLEY, H. SHIMOTAKE, C. E. CROUTHAMEL)

One of the types of regenerative emf cells being considered for engineering studies is the sodium-bismuth bimetallic concentration cell. A bimetallic concentration cell, in general, consists of two liquid metal electrodes in contact with a fused salt electrolyte which is stable in the cell environment, particularly with respect to the anode. Because of the great reducing capability of the alkali metals which are being considered as possible anode materials, only halide salts of the anode metal have been considered as electrolyte constituents.

The overall cell reaction is

Anode Metal  $A$  (liquid)  $\rightarrow$

$A$  dissolved in cathode alloy of  $A$  and  $B$  (liquid).

The interaction of  $A$  and  $B$  in the cathode alloy is usually very strong. (It is this effect that produces useful cell voltages.) As a result of this interaction, as the concentration of  $A$  in  $B$  is increased, solid stoichiometric intermetallic compounds may form in the liquid metal cathode, e.g.,  $\text{Na}_3\text{Bi}$  in the sodium-bismuth cell, and may be solubilized in the molten salt electrolyte.

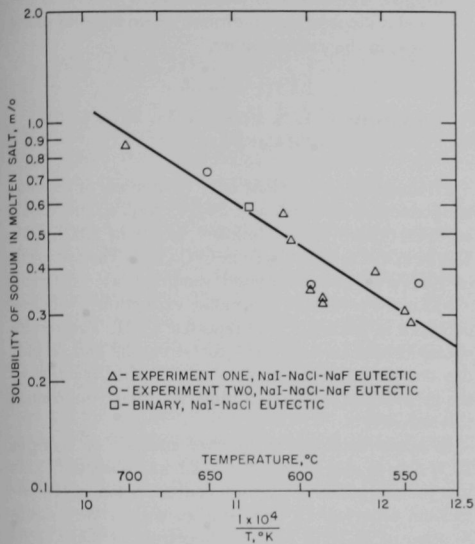
In the operation of a bimetallic concentration cell, the solubilities of both the alkali metal (from the anode) and the intermetallic species (from the cathode) in the fused salt electrolyte give rise to an irreversible transfer of material between electrodes. The irreversible transfer of alkali metal from the anode to the cathode may be overcome by an increased rate of regeneration. However, the irreversible transfer of cathode material to the anode, if appreciable, must be dealt with by other schemes. The rates of these irreversible transfers are expected to be proportional to the solubilities of the species in the electrolyte. Thus, it is of interest

from the standpoint of cell operation to determine the solubilities of alkali metal and intermetallic species in the electrolyte. It is anticipated that by proper selection of cell operating variables and cell components, the effects of these solubilities can be minimized.

The electrolyte selected for use in the sodium-bismuth bimetallic concentration cell was the ternary eutectic 53.2 m/o NaI - 31.6 m/o NaCl - 15.2 m/o NaF. It has a melting point of 530°C, one of the lowest found in any of the sodium halide ternary systems.

In the determination of the solubility of sodium in the ternary mixture two experiments were conducted. In both experiments, the electrolyte, in contact with molten sodium, was held at a given temperature until equilibrium was established. Samples of the electrolyte were taken with tantalum sampling buckets through a tantalum tube immersed in the molten salt. In the first experiment, sodium was observed to deposit on the cooler upper portions of the furnace well containing the melt (melt temperatures, 546 to 697°C). Because of these losses, it was believed that the values obtained for the solubility of sodium might be low. In the second experiment, in order to minimize the volatilization of sodium, a plate with a  $\frac{7}{8}$ -in. dia. hole in the center was used to cover the tantalum crucible containing the melt. The diameter of the hole was further reduced by the insertion of a tantalum tube,  $\frac{3}{4}$  in. in dia. by 28 in. long, through which samples of the melt were taken. Results of these experiments are shown in Figure VI-2. Values for the solubility of sodium in the electrolyte range from 0.3 m/o at 546°C to 0.9 m/o at 697°C. The scatter of the points is somewhat higher than desired; however, since the data show that reasonable reproducibility and

proper temperature dependence for solutions were achieved, the points are believed to indicate true solubility and not dispersions or colloidal solutions. Note that the value given by the one datum point for the

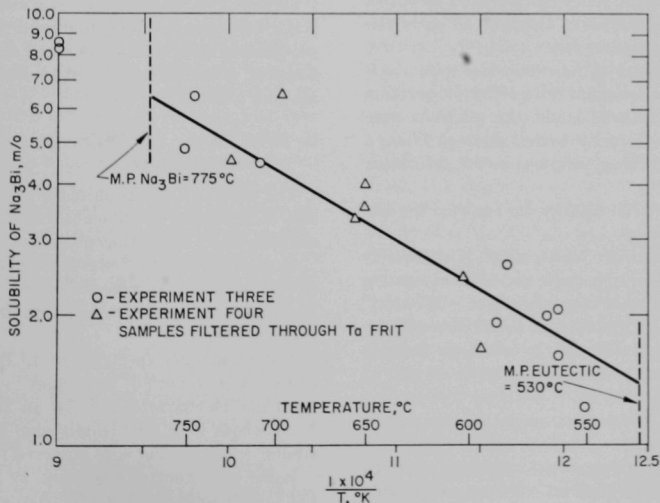


108-8569

Fig. VI-2. Solubility of Sodium in Molten Salt Solvents.

binary eutectic mixture 63.3 m/o NaI - 36.7 m/o NaCl shows essentially the same solubility as for the ternary eutectic mixture at 630°C; this agreement would be expected since NaI and NaCl are the major components of the ternary eutectic.

The solubility of solid  $\text{Na}_3\text{Bi}$  in the ternary eutectic mixture of NaI, NaCl, and NaF has also been studied. Samples of the melt, in equilibrium with  $\text{Na}_3\text{Bi}$ , were taken using  $\frac{1}{2}$ -in. dia. tantalum sampling cups. The samples were dissolved in water, filtered to separate the black bismuth metal precipitate, and the solution titrated with standard acid to determine sodium as the hydroxide. The bismuth was dissolved in nitric acid and titrated complexometrically. In one of the initial experiments, a layer of solid  $\text{Na}_3\text{Bi}$  formed on the surface of the electrolyte after temperature cycling of the melt. The presence of solid  $\text{Na}_3\text{Bi}$  in the electrolyte pointed up the need for a sampling technique which would eliminate any solid particles which might be present as a result of thermal gradients in the system. In subsequent experiments, the samples were taken through a long  $\frac{3}{4}$ -in. dia. tantalum tube which was reduced to a  $\frac{1}{4}$ -in. dia. tube at the bottom. A  $\frac{1}{4}$ -in. tantalum frit (density 9.6) was swaged into the  $\frac{1}{4}$ -in. tube and the melt was forced through the frit by applying a differential helium pressure of approximately 1 to 2 atmospheres by pressurizing the exterior of the tube. The solution in the  $\frac{3}{4}$ -in. tube was sampled by means of a 0.5-in. dia. tantalum cup and analyzed as in the former experiments. The scatter of



108-8556

Fig. VI-3. Solubility of  $\text{Na}_3\text{Bi}$  in the Eutectic Mixture of NaI-NaCl-NaF.

points was reduced markedly by the use of the tantalum filter frits. The results of the latter experiments are shown in Figure VI-3. Values for the solubility of  $\text{Na}_3\text{Bi}$  in the ternary eutectic ranged from 1.2 m/o at  $552^\circ\text{C}$  to 8.5 m/o at  $839^\circ\text{C}$ . The average Na:Bi atom ratios were  $2.98 \pm .03$  and  $2.95 \pm .03$  for experiments 3 and 4, respectively (excluding the two points shown

above the compound melting point at  $839^\circ\text{C}$ , for which the average ratio was  $2.77 \pm .03$ ). In further experiments, the solubility of intermetallic sodium-bismuth alloys which are not of stoichiometric composition will be studied. These will correspond more closely to anticipated cell operating conditions where no solid phase is present in the cathode alloy.

## 2. Intermetallic Compounds in Molten Salt Solutions (M. S. FOSTER, G. McCLOUD, R. L. McBETH,\* D. M. GRUEN,\* C. E. CROUTHAMEL)

Studies designed to elucidate the nature and scope of the phenomena involved in the solubility of intermetallic compounds in molten salt solutions have been continued. These studies are interesting from both theoretical and practical viewpoints. Two types of compounds have been investigated: (a) the alkali metal tellurides,  $\text{M}_2\text{Te}$ , and (b) the alkali metal bismuthides,  $\text{M}_3\text{Bi}$ . The sodium-bismuth bimetallic system has been selected for preliminary engineering studies; however, the relatively high solubility of  $\text{Li}_2\text{Te}$  in fused salts and the high volatility of tellurium suggest that thermal regeneration of the telluride may be possible. Both the alkali metal tellurides and bismuthides have been studied by means of their absorption spectra in molten salt solutions.

### a. SPECTRAL STUDIES OF ALKALI METAL TELLURIDES

The alkali metal tellurides were prepared by direct combination of stoichiometric amounts of each element in an inert atmosphere box.

The absorption spectra of these tellurides were measured in fused silica absorption cells. Before absorption spectra measurements were made, the solutions were filtered through fine-porosity fritted discs of silica, a procedure which gave clear solutions in the absorption cells.

Previous studies (ANL-6900) have reported the absorption spectra of:

1.  $\text{Li}_2\text{Te}$  in  $\text{LiCl-LiF}$  at  $525^\circ\text{C}$ , which is characterized by an absorption peak at  $\sim 469 \text{ m}\mu$  and a charge transfer band commencing at  $\sim 377 \text{ m}\mu$ ;
2.  $\text{Li}_2\text{Te}$  in  $\text{CsCl}$  at  $700^\circ\text{C}$ , with peaks at  $\sim 465 \text{ m}\mu$  and  $\sim 635 \text{ m}\mu$  in addition to a charge transfer band whose longer wavelength edge is located at  $\sim 300 \text{ m}\mu$ ; and
3.  $\text{Cs}_2\text{Te}$  in  $\text{CsCl}$ , whose spectrum is the same as that for  $\text{Li}_2\text{Te}$  in  $\text{CsCl}$ .

Later studies of the absorption spectrum of  $\text{Li}_2\text{Te}$  in  $\text{LiCl}$  revealed a single peak at  $\sim 470 \text{ m}\mu$  comparable to that of  $\text{Li}_2\text{Te}$  in  $\text{LiCl-LiF}$ .

Preliminary calculations have been made of the molar extinction coefficients of  $\text{Li}_2\text{Te}$ ,  $\text{Na}_2\text{Te}$ , and  $\text{Cs}_2\text{Te}$  in  $\text{CsCl}$ . These are as follows:  $\text{Li}_2\text{Te}$  in  $\text{CsCl}$ , 605;  $\text{Na}_2\text{Te}$  in  $\text{CsCl}$ , 602;  $\text{Cs}_2\text{Te}$  in  $\text{CsCl}$ , 838. The spectrum of  $\text{Na}_2\text{Te}$  in  $\text{CsCl}$  exhibited shoulders at  $\sim 570$  and  $\sim 500 \text{ m}\mu$ . Previously, the molar extinction coefficient of  $\text{Li}_2\text{Te}$  in  $\text{LiCl-LiF}$  was reported as 27. The results obtained indicate low oscillator strengths and forbidden transitions, and complete metathetical reaction of the lithium and sodium tellurides with the cesium chloride solvent.

In initial attempts at spectral analysis of  $\text{K}_2\text{Te}$  in  $\text{KCl}$ , only a charge transfer band was observed. This was probably due to the high concentration of the potassium telluride. In later studies with a very dilute solution of  $\text{K}_2\text{Te}$  in  $\text{KCl}$ , the spectrum at  $850^\circ\text{C}$  consisted of a single peak at  $\sim 610 \text{ m}\mu$  in addition to a charge transfer band commencing at  $\sim 345 \text{ m}\mu$ .

Solutions of varying concentrations of  $\text{Na}_2\text{Te}$  in  $\text{NaCl}$  were prepared and submitted for spectral analysis. None of these solutions showed an absorption peak; however, a charge transfer band commencing at  $\sim 490 \text{ m}\mu$  was observed.

### b. SPECTRAL STUDIES OF ALKALI METAL BISMUTHIDES

The alkali metal bismuthides were prepared by direct combination of stoichiometric quantities of each element in an inert atmosphere box.

In contrast with the tellurides, the absorption spectra of the bismuthides were measured in sapphire cells. The solutions were filtered through fine-porosity fritted stainless steel discs.

The absorption spectrum of  $\text{Li}_3\text{Bi}$  in  $\text{LiCl-LiF}$  at  $525^\circ\text{C}$  was reported previously (ANL-6900). The spectrum is characterized by an intense absorption band whose long wavelength edge is at  $\sim 610 \text{ m}\mu$ . A similar spectrum has been observed for  $\text{Li}_3\text{Bi}$  in  $\text{LiCl}$ .

$\text{K}_3\text{Bi}$  was studied spectrally in  $\text{LiCl-KCl}$  and in  $\text{CsCl}$ . The solid intermetallic compound, at  $\sim 280^\circ\text{C}$ , had a pronounced green color. A solution of  $\text{K}_3\text{Bi}$  in  $\text{LiCl-KCl}$  was light purple. At temperatures between

\* ANL Chemistry Division.

500 and 1000°C, the spectrum exhibited an intense charge transfer band and, in addition, an absorption peak at  $\sim 495 \mu$ . Between 600 and 700°C, the spec-

trum of  $K_3Bi$  in CsCl exhibited no distinct peaks; however, the usual charge transfer band edge was observed.

## D. LIQUID-VAPOR RELATIONSHIPS IN THE REGENERATION OF THE Na-Bi CELL (A. K. FISHER, S. JOHNSON, C. E. CROUTHAMEL)

Several experiments were performed under conditions which were intended to approximate those expected to exist in the regeneration cycle of a sodium-bismuth emf cell. These experiments, which can be termed nonisothermal isopiestic experiments, consisted of heating  $Na_3Bi$  in one end of a sealed, evacuated tube while the other end of the tube was maintained at a lower temperature. The hot end was about 900°C, while the cool-end temperature, in different experiments, was 525, 616, 651, and 712°C. A three-day run period was common to all experiments.

After quenching the tubes, the residues at the hot end and the cool end were analyzed for sodium and bismuth. The condensate at the cool end was essentially pure sodium. No bismuth was detected by a method that has a lower limit of detection of less than one part per thousand. The final Na contents of the residues remaining at the hot end of the tubes (900°C) in the four experiments and the corresponding cool-end temperatures were: 15 a/o at 525°C, 48 a/o at 616°C, 54 a/o at 651°C, and 62 a/o at 712°C. These are not equilibrium values, since it must be recognized that equilibrium cannot be achieved in a nonisothermal experiment. The results, therefore, reflect relative possible extents of regeneration under conditions which are similar except for the difference in condensation temperature.

The results of the nonisothermal isopiestic experiments must be considered in conjunction with results from transpiration experiments. The transpiration experiments, in which a carrier gas sweeps away a sample of vapor for condensation and analysis, were designed to yield preliminary information on the composition of the vapor over a Na-Bi alloy at the regeneration temperature. It was found that the vapor over a 50-50 a/o Na-Bi alloy at about 900°C contains about 3 to 3.5 a/o bismuth. This result indicates that:

1. in a regenerative Na-Bi cell fractionation will be needed to obtain high purity sodium for return to the anode, and
2. in the nonisothermal isopiestic experiments such fractionation must have been in operation to account for the high purity of the sodium in the cool end of the tube.

It is of interest to note, then, that the fractionation in the nonisothermal isopiestic experiments was achieved with a tube  $\frac{3}{4}$  in. in dia. and about 18 in. long with no packing inside. The necessary number of theoretical plates would appear to be fairly low.

Of considerable significance is the fact that in the nonisothermal isopiestic experiments, a well-defined band of solid  $Na_3Bi$  deposited on the interior wall at an intermediate site in the temperature gradient. This cannot be taken as evidence that  $Na_3Bi$ , as such, was distilled and deposited, since it is known from mass spectrometric work that  $Na_3Bi$  volatilizes by decomposition. Rather, the re-formation and deposition of solid  $Na_3Bi$  occur as a result of sodium and bismuth vapors coexisting in the proper molar ratio at a suitable temperature and pressure. This can be explained in terms of a temperature-composition phase diagram in which there is a region where vapor and solid phases coexist. Briefly, this kind of a diagram results when the pressure of a system is low enough to cause the liquid-vapor loop to overlap the  $Na_3Bi$ -liquid areas. A region of vapor- $Na_3Bi$  (solid) can be formed. For a cell, the practical consequence of deposition of solid is the eventual plugging of the regenerator. The cure is indicated from an analysis of the phase-diagram relationships: increasing the system pressure will result in a temperature-composition phase diagram in which the vapor-liquid loop no longer overlaps the solid  $Na_3Bi$ -liquid areas and deposition of solid will be impossible. In turn, the system pressure will be maintained at a value determined by: (1) the temperature at the condensation end of the regenerator, and (2) the composition of material being condensed there. These facts indicate that a sufficiently high condensation temperature must be maintained to avoid solid deposition.

By fixing both the temperature and the composition at the condensation site for a two-component system, e.g., sodium-bismuth, a particular isobaric phase diagram is fixed upon, and the entire system behavior must follow this diagram. Some conclusions which came from an analysis of such a fixed diagram in relation to the regenerative cell concept may be summarized as follows:

1. Fixing the composition of the cathode product to

be sent to the regenerator fixes a minimum value for the regeneration temperature which is the bubble point, and also a maximum value which is the dew point. A unique regeneration temperature is not set by fixing the composition of material withdrawn from the cathode.

2. Fixing the composition of material to be returned

to the cathode does fix the regeneration temperature.

3. The cell reaction can generally be carried out at a temperature below the condensation temperature, but not above it unless a pressure gradient exists between the condensation region and the cell proper.

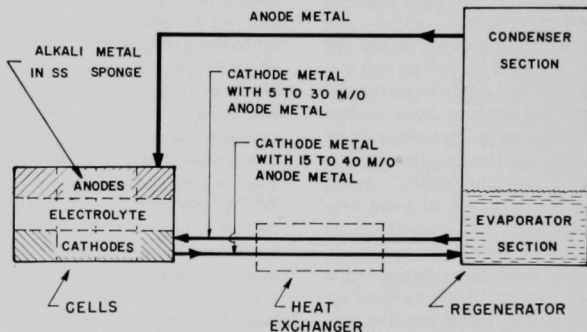
## E. REGENERATIVE Emf CELLS—ENGINEERING STUDIES (J. C. HESSON, H. SHIMOTAKE)

Engineering studies, which were started during the preceding reporting period, have been continued on the feasibility of developing a practical thermally regenerative emf cell, which ultimately would be capable of being coupled to a reactor or other heat source. Both

the bimetallic and lithium hydride cells are being studied; block, flow diagrams for these cell systems are shown in Figures VI-4 and VI-5.

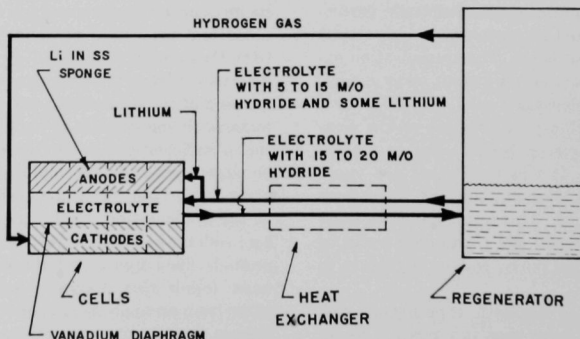
This study involves the following:

1. Anode and cathode metal combinations.



108-8717

FIG. VI-4. Bimetallic Cell System Flow Diagram.



108-8716

FIG. VI-5. Lithium Hydride System Flow Diagram.

2. Cell voltages and cell electrical efficiencies.
3. Electrolyte selection including stability.
4. Electrolyte electrical conductivity.
5. Non-faradaic or mass transfer of anode (and cathode) metals due to their solubility in the electrolyte.
6. Cell configurations and geometry including electrical insulation.
7. Electrolyte and electrode mechanical positioning methods including the possible use of porous or

- sponge metals for the molten metal electrodes and perhaps a ceramic matrix for the electrolyte.
8. Electrode metal transfer between the cell and regenerator including heat exchange.
9. Cell and regenerator operating temperatures.
10. Cell and regenerator efficiencies.
11. Corrosion.
12. Possible cell stacking for higher series voltages and greater compactness.

## 1. Engineering Thermodynamic Studies

Preliminary thermodynamic studies of the regeneration efficiencies for sodium-bismuth, sodium-tin, and lithium-tin bimetallic cell systems and the lithium hydride cell system have been made. In the bimetallic systems, sodium or lithium is the anode metal and bismuth or tin is the cathode metal. In the lithium hydride system, lithium is the anode metal and hydrogen is the cathode material.

### a. BIMETALLIC SYSTEMS

In the bimetallic systems (Figure VI-4) the cell product, which is the cathode metal containing some anode metal, is circulated to and from the regenerator in heat-exchange relationship. In the regenerator the anode metal is separated from the cathode metal by vaporization. The anode metal vapor is condensed and returned to the anode of the cell.

Preliminary studies indicate that for regeneration in the case of the sodium-bismuth system, reflux would be required in the distillation to obtain sodium sufficiently free of bismuth. The requirement of reflux reduces the maximum possible regeneration efficiency below the ideal cycle efficiency. The term "ideal cycle", as used here, does not mean the Carnot cycle, but means the operation of the chosen cycle approaching ideal and adiabatic conditions as nearly as possible, i.e., no heat-exchanger losses, no heat losses through insulation, etc.

In order to limit the recycle rate of the cathode metal to and from the regenerator, it would be desirable that the concentration limits of alkali metal in the cathode alloy range from about 15 to 40 m/o anode metal and that about 10 m/o anode metal be removed in the regenerator.

The temperature at which the heat is rejected (condensing temperature of the anode metal vapor from the regenerator as determined by the regeneration pressure) is dependent both upon the mole fraction of anode metal in the cathode metal being returned from the regenerator to the cell and upon the regeneration temperature (which determines the regeneration pres-

sure). Thus, the condensing temperature increases as the regeneration temperature increases, and the ideal regeneration cycle efficiency is nearly independent of the regeneration temperature. The efficiency is, however, dependent upon the mole fraction of anode metal in the cathode metal. For a given mole fraction of anode metal in the cathode metal, the minimum regeneration temperature, in the case where reflux is not required, is determined by the magnitude of the partial vapor pressure of the anode metal required to obtain reasonable distillation rates. (In the case of liquid metals, a partial vapor pressure of at least 1 mm Hg is usually required for reasonable distillation rates.) In the case where reflux is required, it may be necessary to operate at a temperature above the calculated minimum regeneration temperature in order to avoid solid phase regions. Table VI-2 shows computed values of efficiencies for the bimetallic cell systems. The efficiencies are based on a heat utilization efficiency of 75% of the ideal cycle for the regenerator and a cell electrical efficiency of 60%. The values compare favorably with the expected overall thermal efficiencies of other systems for similar application (for example, mercury vapor cycle, 6 to 10%; thermoelectric cycle, 5%; and thermionic at 1610°K, 8% maximum, and at 2050°K, 16% maximum).

The cell voltage increases as the dissolved mole fraction of anode metal in the cathode metal is decreased. Hence, from a viewpoint of cell voltage low concentrations of anode metal in the cathode metal are desired, but from a viewpoint of regeneration high values are desired.

### b. LITHIUM HYDRIDE SYSTEM

In the lithium hydride system (Figure VI-5) the cell product is lithium hydride, which is soluble in the electrolyte and in the lithium anode metal. The electrolyte (or possibly the lithium anode metal) is circulated to and from the regenerator in heat-exchange relationship, i.e., the electrolyte going to the regener-

TABLE VI-2. COMPUTED EFFICIENCIES FOR BIMETALLIC REGENERATIVE CELL SYSTEMS

Bimetallic System	Mole Fraction AnodeMetal in Cathode Metal			
	0.1	0.2	0.3	0.4
<i>Sodium-Bismuth</i>				
Efficiency, Percent				
Regeneration, Ideal Cycle-No Reflux	41	38	36	34
Regeneration, Ideal Cycle-30% Reflux	29	27	25	23
Regeneration, 75% of Ideal Cycle-30% Reflux	21	20	19	18
System, 60% Cell Electrical Efficiency	13	12	11	10
Estimated Regeneration Temperature, °K, to Avoid Solid Phase Region	1325	1310	1300	1290
<i>Sodium-Tin</i>				
Efficiency, Percent				
Regeneration, Ideal Cycle	30	27	23	20
Regeneration, 75% of Ideal Cycle	22	20	17	15
System, 60% Cell Electrical Efficiency	13	12	10	9
Regeneration Pressure, mm Hg, at 1073°K (800°C)	1.3	5.3	10.0	16.6
Sodium Condensing Temperature, °K, for 1073°K Regeneration Temperature	735	785	830	855
<i>Lithium-Tin</i>				
Efficiency, Percent				
Regeneration, Ideal Cycle	27	24	20	17
Regeneration, 75% of Ideal Cycle	20	18	15	13
System, 60% Cell Electrical Efficiency	12	11	9	8
Regeneration Pressure, mm Hg, at 1323°K (1050°C)	0.33	0.75	1.75	3.3
Lithium Condensing Temperature, °K, for 1323°K Regeneration Temperature	960	1005	1055	1090

TABLE VI-3. COMPUTED PERCENT EFFICIENCIES FOR LITHIUM HYDRIDE CELL SYSTEM

Regeneration Temperature (°K)	Cell Temperature (°K)	Efficiency (%)		
		Ideal Regeneration Cycle	Expected <sup>a</sup> Regeneration	Expected <sup>b</sup> System
1200	773	35	24	12
	873	27	19	9
1300	773	41	29	14
	873	33	23	11
1400	773	45	31	16
	873	38	26	13
1500	773	48	33	17
	873	45	31	15

<sup>a</sup> Based on 70% of Ideal Cycle.

<sup>b</sup> Based on 70% of Ideal Cycle and 50% Cell Electrical Efficiency.

ator is heated by the warmer electrolyte returning to the cell. In the regenerator, the hydride is decomposed into hydrogen and lithium. The hydrogen is returned to the cell cathode, and the lithium is returned to the cell anode.

In order to limit the recycle rate of the electrolyte to and from the regenerator it would be desirable that

the electrolyte contain from about 15 to 25 m/o hydride when going from the cell to the regenerator and that about 10 m/o hydride be decomposed in the regenerator.

In the case of the lithium hydride cell system the temperature at which the heat is rejected (cell operating temperature) is independent of the regeneration temperature. However, the hydrogen regeneration pressure increases with increased regeneration temperature and with increased mole fraction of hydride in the electrolyte. The cell emf increases with increased hydrogen pressure, but decreases as either the cell temperature or the mole fraction of hydride in the electrolyte is increased.

The ideal regeneration cycle efficiency is dependent upon the regenerator and cell operating temperatures but is nearly independent of the mole fraction of hydride in the electrolyte. Table VI-3 shows computed values of efficiencies for the lithium hydride system. Again, they compare favorably with efficiency values of other systems. The efficiencies are based on a heat utilization efficiency of 70% of the ideal cycle for the regenerator and a cell electrical efficiency of 50%. These values of 70 and 50% are less than the corresponding values of 75 and 60% used for the bimetallic systems. Lower values are used for the heat utilization

efficiency because of anticipated lower heat transfer coefficients for the electrolyte; lower values are used for the cell efficiency because of cell voltage losses due to diffusion of hydrogen through the vanadium diaphragm at the cathode.

## 2. Experimental Sodium-Bismuth Cell

### NON-FARADAIC SODIUM TRANSFER

Experimental work on the sodium-bismuth cell was continued. Studies of irreversible or non-faradaic transfer, i.e., without corresponding production of cell current, have been initiated using "open" sodium-bismuth cells. The rate of transfer of sodium from anode to cathode was measured as a function of temperature and also as a function of cell current at constant temperature. The irreversible transfer results from the solubility of sodium in the electrolyte. The electrolyte used in most of the experiments was the sodium chloride-62.5 m/o sodium iodide eutectic. In some experiments, 5 m/o sodium fluoride was added to the electrolyte.

The "open" sodium-bismuth cell consisted of a stainless steel crucible, 1 7/8 in. in dia. by 5 in. high, in which the electrolyte was contained. The 7/8-in. dia. stainless steel cathode cup containing bismuth was immersed in the electrolyte. The anode consisted of a 1-in. dia.

The cell voltage increases as the dissolved mole fraction of hydride in the electrolyte is decreased. Hence, from a viewpoint of cell voltage, low concentrations of hydride in the electrolyte are desired, but from a viewpoint of regeneration, high values are desired.

stainless steel cup with a 7/8-in. dia. hole in its bottom and a layer of stainless steel sponge above the hole. In this manner, sodium was retained in the cup and yet was allowed to contact the electrolyte when the bottom of the cup was dipped slightly into the electrolyte. The distance between the cathode bismuth surface and the anode sodium surface was 2 in.

The non-faradaic transfer is here defined as

$$q = \frac{Q - At}{t}$$

where

$q$  = non-faradaic transfer, g/hr,

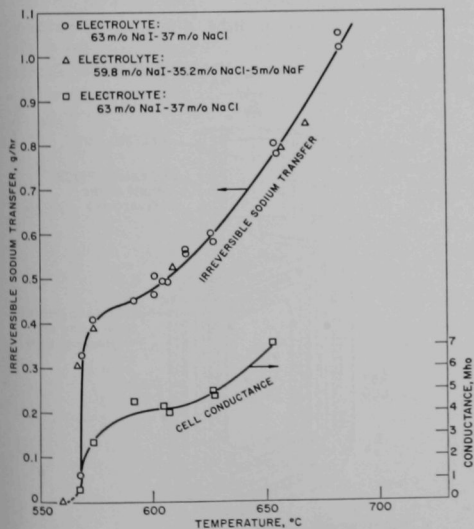
$Q$  = total g of sodium transferred from anode to cathode during run,

$A$  =  $(3600)(23)/96,500 = 0.857$  g/(amp)(hr),

$I$  = average cell current, amp, and

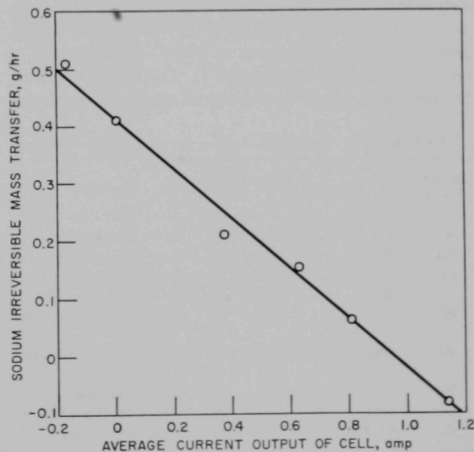
$t$  = time of run, hr.

Figures VI-6 and VI-7 show the results of these tests. From these figures, it is noted that the non-faradaic transfer rate increases as the temperature is increased and decreases as the cell current is increased. The addition of 5 m/o sodium fluoride to the electrolyte did



108-8559

FIG. VI-6. Irreversible Sodium Transfer and Conductance in an Open-Circuit Sodium-Bismuth Cell as a Function of Temperature.



108-8544

FIG. VI-7. Irreversible Sodium Transfer in an Open-Circuit Sodium-Bismuth Cell as a Function of Current.

not noticeably change this transfer rate. The conductance of the cell as a function of temperature is shown in Figure VI-6.

The cell electrical efficiency is a product of the voltage and current efficiencies which in turn are functions of cell conductance, cell current, and the non-faradaic

sodium transfer. While additional experiments will be required to determine optimum parameters, the work to date indicates that cell current efficiencies of about 80% can be obtained during operation at 75% of the open circuit voltage. The resulting overall cell electrical efficiency is about 60%.

### 3. Frozen Electrolyte-Silicone Rubber Insulation-Seal

A closed 3-in. dia. cell has been constructed of stainless steel with a frozen electrolyte-silicone rubber combination electrical insulator-pressure seal. In this cell, the silicone rubber pressure seal is placed about 1½ in. beyond the cell between water cooled flanges which are attached to the cell by ½-in. thick discs to minimize heat transfer. An alumina spacer is placed between the ½-in. discs. The cell body proper is heated by ⅛-in. dia. electric heating elements. In the one test run made

to date, the cell, charged with electrolyte and bismuth, was heated to about 600°C without leaking or developing a short circuit. During this test, an attempt was made to add sodium to the anode through a Teflon stopcock; however, attack of the Teflon by the molten sodium made it necessary to terminate the run at this point. A different heating method of charging sodium will be tried.

### 4. Engineering Material Study

In the proposed regenerative emf cell system, the cathode product, which is a liquid metal alloy of the anode and cathode metals, is transferred to the regenerator in which separation of the anode metal by distillation is effected. The alloy, depleted in anode metal, is returned to the cell cathode after passing through a heat exchanger in which the heat is transferred to the alloy stream coming from the cell cathode and returned to the cell anode. In order to distill the anode metal readily it is necessary to operate the regenerator at a temperature of 800°C or higher and to operate the cell at about 600°C. The exact operating temperatures would be dependent on the properties of

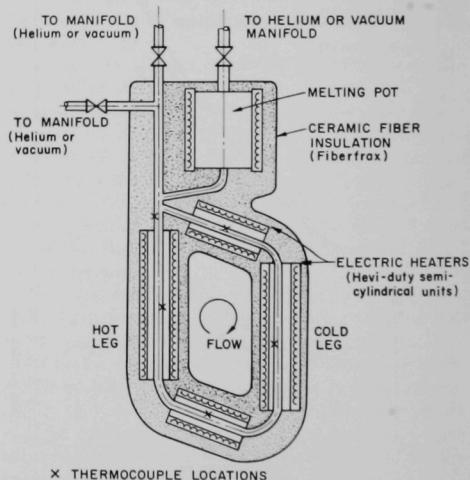
the fused salt electrolytes and electrode metals involved. No container materials have yet been found which are mechanically strong at these temperatures, are readily fabricable, and are also sufficiently resistant to corrosion by the liquid metals at anticipated regeneration temperatures.

During the past six months, a number of corrosion

TABLE VI-4. SUMMARY OF STATIC CORROSION TESTS

Liquid Metal	Test Material	Temp. (°C)	Time (hr)	Remarks
Sn	Ta	900	27	No visible attack
Sn	Ta	1000	96	No visible attack
Sn	Mo	1000	26	No visible attack
Sn	W	1000	96	No visible attack. <sup>a</sup>
Bi	Steel 1020	1000	22	Intergranular penetration
Bi	Steel 1040	1000	100	Intergranular penetration
Bi	Armco Iron	850	24	Shallow attack
Bi	Armco Iron	1000	50	Specimen dissolved
Bi	SS 304	850	97	No visible attack

<sup>a</sup> Electron microprobe examination indicated 10-μ penetration.



108-8721 Rev.

Fig. VI-8. Thermal Convection Loop.

experiments have been carried out to test possible container materials for cells in which bismuth or tin is used as a liquid metal cathode. A series of static tests was run to screen various materials. The material to be tested, along with the particular cathode metal of interest, was contained in a crucible fabricated from Mo-30 w/o W, an alloy which is considered to be nearly inert to attack by bismuth and tin.

The test materials were usually cut from sheet stock in the form of coupons,  $\frac{1}{2}$  by 1 by  $\frac{1}{8}$  in. The loaded crucibles were placed in a stainless steel vessel located in a resistance-heated furnace and were held at the test temperatures for predetermined periods of time. The test results are presented in Table VI-4. No visible attack on the Mo-30 w/o W container was noted.

A series of dynamic corrosion tests was conducted to determine the effect of liquid bismuth on low carbon steel. Four thermal convection loops containing liquid bismuth have been operated under varied temperature conditions. The loops, shown schematically in Fig. VI-8, were constructed of standard  $\frac{1}{4}$ -in. low carbon steel pipe (0.54-in. OD, 0.364-in. ID). The total height of a loop proper is 10 in. and the width is 6 in. The insides of the loops were cleaned with either acid (Loops 1, 2 and 3) or molten sodium hydride-sodium hydroxide (Loop 4) to remove scale, oxides, etc. Loops 3 and 4 were externally sprayed and coated with molten stainless steel for protection against air oxidation in high temperature tests.

Loop 1 was run with a hot leg temperature of 800°C and a cold leg temperature of 700°C for 100 hr. Although the outside of the loop was oxidized severely, no visible mass transfer effect by the liquid metal was found.

Loop 2 was run with a hot leg temperature of 520°C and a cold leg temperature of 420°C for 1,000 hr. The reduction of the pipe wall thickness did not exceed 0.010 in. at the hot leg. Microscopic examinations showed no evidence of intergranular attack.

Loop 3 was run at a hot leg temperature of 800°C and a cold leg temperature of 700°C. After 24 hr of operation, two plugs were formed. Plugging was caused by (1) incomplete descaling of the loop interior before the test, and (2) lodging in the loop of a test coupon which had become loose during the test.

Loop 4 was run at a hot leg temperature of 850°C and a cold leg temperature of 450°C. After 430 hr of operation a leak developed in the hot leg of the loop. Microscopic examination revealed that (1) attack of the steel by bismuth was greatest at the entrance to the hot leg of the loop, and (2) extensive mass transfer had occurred.

The static corrosion tests indicate that tungsten, molybdenum-30 w/o tungsten, molybdenum, and tantalum show sufficient promise for use with tin to be tested dynamically at temperatures up to about 1000°C.

The dynamic corrosion tests indicate that mild steel will not be suitable for the high temperature sections of the apparatus (the regenerator) in which bismuth is circulated with temperature changes from about 800°C to about 600°C, but that mild steel or stainless steel may be suitable for the low temperature sections of the apparatus (the cell).

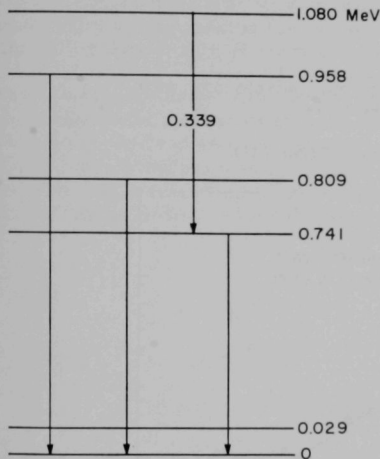
Thermal convection loops are being constructed for dynamic corrosion tests by tin and bismuth on tantalum, molybdenum-30 w/o tungsten, and niobium.



## VII. Nuclear Constants\* (Donald C. Stupegia, A. D. Tevebaugh)

### A. NEUTRON INELASTIC SCATTERING (D. C. STUPEGIA, A. B. SMITH,\*\* J. F. BARRY\*\*\*)

In the preceding report, ANL-6900, a discussion was given of the importance of neutron inelastic scattering in the fast reactor program. Inelastic scattering is the primary reaction by which the neutron energy spec-



108-8541

FIG. VII-1. Energy Levels in Niobium-93.

trum is degraded in a fast reactor. A program for the measurement of the energy and intensity of gamma rays associated with neutron inelastic scattering is being carried out using the 3 MeV pulsed Van de Graaff accelerator of the Reactor Physics Division. In this

\* A summary of this section is given on page 16.

\*\* Reactor Physics Division.

\*\*\* Exchange visitor from Aldermaston, England.

### B. FAST NEUTRON CAPTURE (D. C. STUPEGIA, M. SCHMIDT, A. A. MADSON)

In calculations of the breeding gain of a reactor, capture cross sections of various reactor structural materials, coolants, and control materials are required as a function of neutron energy. In the present program

work the data of interest are:

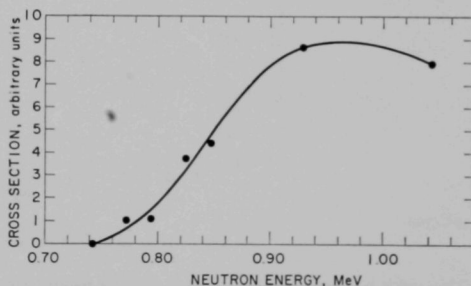
(1) cross sections for the production of gamma rays as a function of neutron energy, and

(2) cross sections for the production of gamma rays at a given neutron energy as a function of angle of gamma ray emission with respect to the neutron beam direction.

Preliminary work has been done on zirconium, holmium, and rhenium. More extensive data have been taken on the production of the 0.741, 0.809, and 0.958 MeV gamma rays resulting from the excitation of levels in niobium-93 (see Figure VII-1).

In Figure VII-2 a plot is given of the relative cross sections for the production of the 0.741 MeV level of <sup>93</sup>Nb as a function of neutron energy.

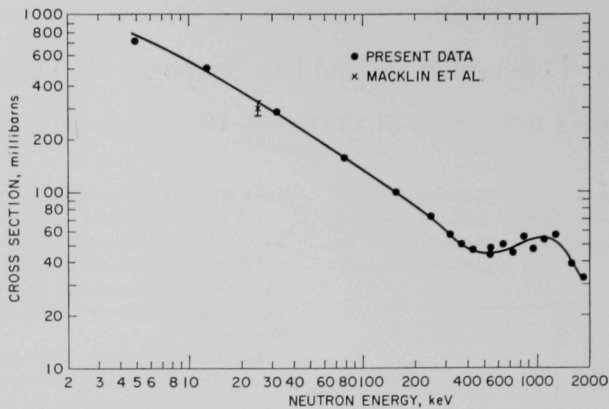
These results will be used to calibrate absolute cross sections when the neutron flux and gamma ray calibrations are completed. Analyses are also being carried out which will yield the cross sections for the production of the 0.809 and 0.958 MeV states.



108-8715

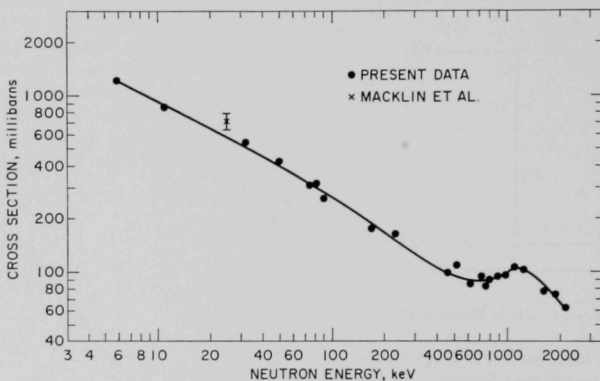
FIG. VII-2. Production of 0.741-MeV Level of Niobium-93 by Inelastic Scattering.

fast neutron capture cross sections have been studied. In the previous report, ANL-6900, nearly complete data were given on the cross sections of <sup>185</sup>Re and <sup>187</sup>Re for neutron energies between 4 keV and 2 MeV.



108-8718

FIG. VII-3. Neutron Capture Cross Section of Erbium-170.



108-8708

FIG. VII-4. Neutron Capture Cross Section of Gadolinium-158.

This work has now been completed and the results are being prepared for publication.

Two other capture cross section curves have been completed. These are erbium-170 and gadolinium-158, which are shown in Figures VII-3 and VII-4. The re-

sults of Macklin, et al.,<sup>1</sup> for 25 keV neutrons, which are also shown in the figures, are in good agreement with the data from the present study.

<sup>1</sup> R. L. Macklin, N. H. Lazar, W. S. Lyon, *Phys. Rev.* **107**, 504 (1957).

### C. CAPTURE-TO-FISSION RATIOS IN EBR-II (D. C. STUPEGIA, A. A. MADSON)

Preparations are being made to measure the ratio of the capture and fission cross sections of uranium and plutonium isotopes as a function of position in the core and blankets of EBR-II. These data will be useful in calculations of the breeding gain of fast reactor systems, as discussed in a previous report, ANL-6900, p. 330.

A total of 71 samples of  $^{233}\text{U}$ ,  $^{235}\text{U}$ ,  $^{238}\text{U}$ ,  $^{239}\text{Pu}$ ,  $^{240}\text{Pu}$ , and  $^{242}\text{Pu}$  have been introduced into stainless steel capsules, 65 of which are now being placed in special EBR-II fuel element tubes. The numbers and types of samples which will be placed in various regions of the core and blankets of EBR-II are summarized in Table VII-1.

Following completion of the experimental work and analysis of the results, the data on capture-to-fission ratios will be compared with their corresponding values as calculated from a multi-neutron group set of cross sections. This cross section set, now being compiled in the Reactor Physics Division, divides the neutron en-

ergy spectrum of EBR-II into 20 energy groups and lists capture and fission cross sections of each isotope for each group. From these values, together with an estimate of the neutron flux in each group, one can calculate the expected capture-to-fission ratio at any position in the reactor. Similar comparisons were made for experimental data obtained in the third loading of EBR-I.

TABLE VII-1. NUMBER OF SAMPLES OF URANIUM AND PLUTONIUM IN CORE AND BLANKETS OF EBR-II

Isotope	Core	Blanket		
		Inner	Outer	Upper
$^{239}\text{Pu}$	8	1	4	3
$^{240}\text{Pu}$	4	1	2	3
$^{242}\text{Pu}$	6	1	4	3
$^{233}\text{U}$	6	0	2	1
$^{235}\text{U}$	6	1	2	2
$^{238}\text{U}$	3	0	2	0



## VIII. Analytical Research and Development\* (R. P. Larsen, R. J. Meyer)

A program for the development of analytical methods for the determination of burnup of fast reactor fuels and for the measurement of fast fission yields is being carried out by the Analytical Group. Although the primary objective of this program is the development of methods for EBR-II fuels, the methods will also be applicable to other fast reactors. Methods for the determination of technetium-99 and lanthanum-139 have been developed, and the uranium-235 fast fission yields for both nuclides have been determined. These data were reported in ANL-6900, p. 336, and in the Idaho Division reports.

The present objective of the program is the determination of other uranium-235 fast fission yields. Of particular interest are those nuclides which are poten-

tially useful fission monitors for other fast reactor fuels and those nuclides which can be used to determine the source of the fissions in fuels which contain two fissile nuclides. EBR-I, Mark-III core material is being used for these determinations. The number of atoms of the fission product is being determined by a combination of spectrophotometric and mass spectrometric analyses; the number of fissions is being determined by a cesium-137 radiochemical analysis. In time this approach will be used with EBR-I, Mark-IV fuel to establish plutonium-239 fast fission yields. More accurate values for the uranium-235 and plutonium-239 fast fission yields, as well as those for uranium-233, will be obtained from materials irradiated in EBR-II for an extended period. However, these irradiations will not be completed before 1969.

\* A summary of this section is given on pages 16 to 17.

### A. URANIUM-235 FAST FISSION YIELDS OF MOLYBDENUM-95, -97, -98, AND -100 (R. J. POPEK)

EBR-I, Mark-III fuel of about 0.3 a/o burnup has been analyzed radiochemically for its cesium-137 content and spectrophotometrically for its molybdenum content. (The molybdenum concentration is about 0.03 w/o.) In the spectrophotometric molybdenum analysis, molybdenum (VI) in sulfuric acid is reduced with tin

(II) to molybdenum (V), the molybdenum (V) is reacted with thiocyanate, the molybdenum-thiocyanate complex is extracted into n-butyl acetate, and the absorbance is measured. Upon completion of mass spectrometric analysis, the fission yields of the molybdenum-95, -97, -98, and -100 isotopes will be calculated.

### B. URANIUM-235 FAST FISSION YIELDS OF RUTHENIUM-101, -102, AND -104 (R. D. OLDHAM)

The yields of the ruthenium isotopes from the fast fission of uranium-235 are also being determined on the Mark-III fuel from EBR-I. Spectrophotometric analysis for the ruthenium content has been completed. Ruthenium was separated from the other fission products and the uranium by distillation of the volatile tetroxide from a dilute sulfuric acid-sodium bismuthate mixture, and the tetroxide was caught in carbon tetrachloride at 0°C. The amount of ruthenium in the distillate was determined spectrophotometrically after

reaction with 1-nitroso-2-naphthol and reduction with ascorbic acid. Because the concentration of ruthenium in the samples was very low, complete recovery of ruthenium in the separation procedure was not achieved. However, a correction for this loss, about 5%, was readily made by analyzing the product and the original solution radiochemically for their ruthenium-106 contents. Upon completion of the mass spectrometric analysis, the fission yields of ruthenium-101, -102, and -104 will be calculated.

**C. IRRADIATIONS IN EBR-II (R. J. MEYER, R. J. POPEK)**

Plans are being made to irradiate 100-mg amounts of the oxides of uranium-233, uranium-235, and plutonium-239 in EBR-II to produce materials that will permit the determination of fast fission yield data of increased accuracy. The samples will be irradiated until 25% of the fissile atoms have been consumed. This will allow the number of fissions from the nuclide of interest to be determined accurately from pre- and post-irradiation mass spectrometric analysis. The number of fission product atoms produced will be determined chemically, radiochemically and/or mass spectrometrically.

Details of this irradiation are now being completed. It appears that an irradiation which is equivalent to more than two years in the reactor at full design power will be necessary to obtain the burnup desired. This will require that the samples irradiated in the core be recycled, since none of the core subassemblies will remain in the reactor for two years. It is estimated that this recycling and the operation of the reactor at somewhat less than full power will increase the time for the irradiation to four or five years.

# IX. Studies and Evaluations\* (W. J. Mecham, W. B. Seefeldt, V. G. Trice, M. Levenson)

## A. GENERAL OBJECTIVES

Studies and evaluations are concerned with the feasibility and costs of projected applications of research and development projects of the Chemical Engineering Division. Such studies may show which step of a process should be further modified in order that the process as a whole may be more economical. Or they may show that some particular step or technique has an economic advantage and that new ways of incorporating this step in other process applications should be sought. The scope and specific objectives of these staff studies and evaluations are expected to vary with the interests of the Laboratory.

\* A summary of this section is given on page 17.

The present studies and evaluation activities by full-time staff members are a continuance of Division activities previously carried on by *ad hoc* committees. The major activities during this year have been concerned with two projects: (1) a Divisional economic study of fuels and reprocessing methods for fast reactors and (2) a contribution to an interdivisional conceptual design study and a feasibility and economic analysis of a large metal-fuel fast breeder power reactor and its integrated fuel cycle system.

Future projects are to be defined for studies and evaluations in the area of fuel cycle operations (especially for fast reactors) and allied process applications.

## B. COST EVALUATION OF METAL-FUELED FAST REACTORS

An interdivisional study group has been organized to evaluate the economy of the generation of electric power by a large metal-fueled fast breeder reactor. A report is being prepared for the use of the U.S. Atomic Energy Commission in which the estimated costs of nuclear power generation by metal-fueled reactors are compared with those reported previously for fast breeder reactors fueled with oxide and carbide fuels.<sup>1-4</sup> The report will encompass all on-site costs for a 1000 Mw(e) plant including the reactor, integral pyrochemical processing, refabrication, interim on-site storage of wastes, and in addition, the ultimate disposal of high activity level wastes at a separate site. Design criteria and specifications have been established for the ANL Reference Metal Fueled Reactor and Integral Fuel Cycle Facility. The ANL Chemical Engineering Division and the Metallurgy Division were assigned the responsibility for the conceptual design and estimation

TABLE IX-1. SPECIFICATIONS OF THE ARGONNE REFERENCE METAL-FUELED FAST BREEDER REACTOR WHICH ESTABLISH THE FUEL PROCESSING REQUIREMENTS

Total Thermal Power, Mw(t)	2513
Net Electrical Power, Mw(e)	1000
Fraction of Total Power Generated in Core	0.87
Total Breeding Ratio	1.55
Internal Breeding Ratio	0.63
Initial Composition of Fuel, w/o:	
Core	
Uranium	79.30
Plutonium	18.75
Titanium	1.95
Blanket	
Depleted Uranium	100
Core Fuel Burnup, percent of actinides	5.5
Blanket Fuel Burnup, percent of actinides	0.32
Composition of Discharged Fuel, w/o:	
Core	
Uranium	75.11
Plutonium	17.55
Titanium	1.95
Fission Products	5.39
Blanket	
Uranium	97.72
Plutonium	1.96
Fission Products	0.32
Reactor Cycle, days	191
Plant Factor, %	80
Quantity of Fuel Discharged per Cycle, kg	
Core	6252
Blanket	15570

<sup>1</sup> Allis-Chalmers, Atomic Power Development Associates, Babcock and Wilcox Company, Large Fast Reactor Design Study, ACNP-64503, January 1964.

<sup>2</sup> Combustion Engineering, Liquid Metal Fast Breeder Reactor Design Study, CEND-200, January 1964.

<sup>3</sup> General Electric Company, Liquid Metal Fast Breeder Reactor Design Study, GEAP-4418, January 1964.

<sup>4</sup> Westinghouse, Liquid Metal Fast Breeder Reactor Design Study, WCAP-3251-1, January 1964.

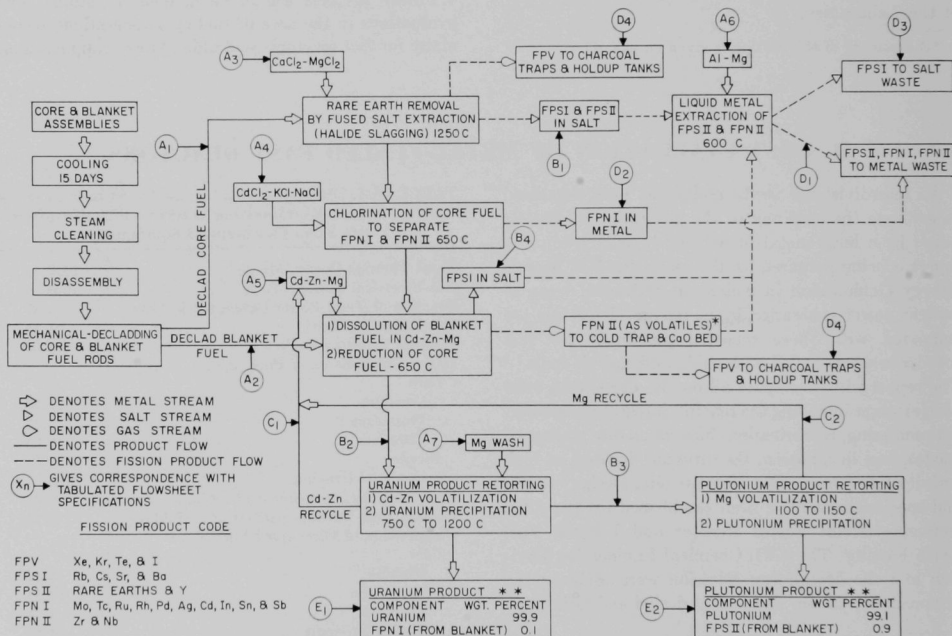
of the cost of the Integral Fuel Cycle Facility. The key specifications of the reference reactor which estab-

lish the fuel reprocessing requirements are presented in Table IX-1.

## 1. Reference Compact Pyrochemical Process for Metal Fast Reactor Fuel

A conceptual process for the decontamination of fuel discharged from a metal-fueled fast breeder reactor and the recovery of plutonium bred in the blanket fuel for use in the refabrication of core fuel elements is described by the flowsheet in Figure IX-1. This flowsheet is for the processing of fuel from a reactor that employs uranium-plutonium alloy in the core and uranium in the blanket. It is also applicable to alloys containing titanium and/or zirconium as a major component of the core fuel. The flowsheet does not represent the only process steps that would satisfy the processing requirements. Alternative process steps are currently

being studied and it is expected that some of these will ultimately lead to more economical processing. However, the reference flowsheet was chosen because it consists of an assemblage of pyrochemical steps for which sufficient supporting evidence is available from laboratory and pilot plant studies to provide a high degree of confidence in the technical feasibility of the steps, and for which enough information is available from component development studies to develop conceptual equipment designs for use in the estimation of processing costs.



108-8532

FIG. IX-1. Principal Steps in the Reference Compact Pyrochemical Process for Metal Fuel (U-Pu Core; U Blanket).

## 2. Preparation of Fuel for Processing

Preliminary operations are employed to prepare the fuel for processing. The core and blanket fuel assemblies are removed from the reactor and transferred to a sodium-cooled tank where they are retained for about 15 days. During the total period of cooling before reprocessing (20 or more days), the heat generation rate from the decay of fission products decreases by a factor of about 10, and affords a substantial reduction

in the heat removal requirements in subsequent process steps. Unlike aqueous processing, the influent streams in pyrochemical processing are not subject to radiation damage, and therefore an extended period of cooling is not required. After cooling, the fuel assemblies are steam cleaned to remove residual sodium and then disassembled and the excess structural metal removed and discarded.

## 3. Removal of Fission Products

*Removal of Fission Products from Core Fuel.* In the flowsheet and in the tabulated data, the principal fission products are grouped as follows:

Fission products, volatile (FPV)	Xe, Kr, Te, I
Fission products, salt-soluble, group I (FPSI)	Rb, Cs, Sr, Ba
Fission products, salt-soluble, group II (FPSII)	Rare earths and Y
Fission products, noble metals, group I (FPNI)	Mo, Tc, Ru, Rh, Pd, Ag, Cd, In, Sn, Sb
Fission products, noble metals, group II (FPNII)	Zr, Nb

The core and blanket fuel are processed separately in the initial process steps. The core fuel is treated to remove all fission products listed above. The reference flowsheet is expected to provide greater than 99% removal of the fission products. Because of the presence of residual amounts of fission products in the fuel processed by this reference process, remote refabrication of core and blanket fuel elements and remote refueling of the reactor is necessary.

Declad core fuel is melted in a beryllia crucible and contacted with a fused salt containing magnesium chloride at 1250°C. Of the separate classes of fission products cited above, the FPV products are volatilized, and the FPSI and FPSII groups are oxidized by the magnesium chloride and extracted into the salt phase. The salt phase is separated and the partially processed metal is further treated to remove the FPNI and FPNII fission products in subsequent processing steps.

The FPNI group of fission products is separated from uranium, plutonium, and the FPNII fission products by treatment of the mixture with cadmium

chloride in a tungsten crucible at 650°C. Uranium, plutonium, and the FPNII group are chlorinated. The FPNI group is not chlorinated and is accumulated in the cadmium metal phase which is formed as a consequence of the reduction of cadmium chloride.

The immiscible metal and salt phases are allowed to separate by the difference in their densities. The metal phase containing the FPNI fission products is transferred to a waste receiver, and the salt phase containing the uranium and plutonium and FPNII fission products is transferred to the vessel used for blanket dissolution. Further process steps for the combined core and blanket fuel are described below.

*Removal of Fission Products from Blanket Fuel and Reduction of Core Fuel.* Declad blanket fuel is dissolved in a liquid metal mixture of cadmium, zinc, and magnesium. Simultaneously, uranium and plutonium in solution in the salt phase from the core fuel chlorination are reduced by the magnesium in the solvent metal. This process step is conducted at 650°C in a 405 stainless steel crucible. Fission products of groups FPV and FPNII (the latter from both the core and blanket) are separated by volatilization. The FPSI fission products are separated by extraction into the salt phase. The salt composition is critical for the volatilization step. From presently available data, the composition 60 m/o  $MgCl_2$  - 25 m/o NaCl - 15 m/o KCl is believed to be satisfactory. The other fission products in the blanket, namely the FPSII and FPNI groups, are not separated and accompany the uranium and plutonium in the solvent metal phase. Titanium, if it is a component in core fuel alloy, is volatilized with the FPNII group.

#### 4. Partitioning of Uranium and Plutonium; Recovery of Uranium and Plutonium as Ingots of Metal

Uranium and plutonium are partitioned in a retorting step. The solvent metal phase from the blanket dissolution step, which contains the uranium and plutonium recovered from the core and blanket fuel, is retorted in a beryllia crucible to volatilize cadmium and zinc. Uranium precipitates because of its negligible solubility in the magnesium solution that remains. The FPNI group of fission products from the blanket fuel accompanies the uranium. Plutonium and the FPSII group remain in solution in the magnesium phase which

is processed in a separate retort furnace for the ultimate recovery of metallic plutonium. The solvent metals volatilized in the retort operations are recycled to the blanket dissolution step.

The precipitated uranium is retorted in a vessel for uranium retorting to an ultimate temperature of 1200°C to remove the residual solvent metal and to consolidate the uranium into an ingot of metal. The plutonium solution is similarly treated in its retort furnace.

#### 5. Composition of Recovered Uranium Ingots and Plutonium Ingots

The products of the reference flowsheet contain the fission products FPSII and FPNI that were generated in the blanket. The blanket burnup specification for the Argonne Reference Reactor is:

Zone	Blanket Burnup (% of U Atoms)	Quantity of Fuel Removed per Cycle (kg)
Axial Blanket	0.27	5730
Inner Radial Blanket	0.27	1420
Outer Radial Blanket	0.37	8420

For the above conditions the composition of the separate products of the processing is estimated to be:

Uranium Product		Plutonium Product	
Uranium (w/o)	FPNI Fission Products (w/o)	Plutonium (w/o)	FPSII Fission Products (w/o)
99.9	0.1	99.1	0.9

On repeated recycle, the FPNI content of the uranium product will build up slowly and may be expected to reach 0.72% after eight radial blanket cycles (34 yr of irradiation). The FPSII concentration in the plutonium product will not build up because the fission products are removed in the processing of core fuel.

#### 6. Estimated Fuel Cycle Costs for the Argonne Reference Metal-Fueled Reactor

Estimates of operating costs, annual charges, and unit fuel cycle costs have been developed for the integral fuel cycle facility associated with the Argonne Reference Reactor. The costs of processing and waste disposal were estimated by the Chemical Engineering Division and those for refabrication by the Metallurgy

TABLE IX-2. COSTS OF THE REFERENCE COMPACT PYRO-CHEMICAL FUEL CYCLE FACILITY FOR THE ARGONNE REFERENCE METAL-FUELED 1000 Mw(e) FAST REACTOR

	Unit Costs	
	mills/kw(e)-hr	\$/kg
Processing and Refabrication	1.02	170
Waste Disposal	0.05	8
Out-of-Reacto Fuel Inventory	0.22	38
One Percent Processing Loss	0.03	5
Plutonium Credit	-0.37	-62
Total	0.95	159

Division. The conceptual design of a plant to process fuel as specified in the reference flowsheet was based on the EBR-II Fuel Cycle Facility. All processing and refabrication operations with highly irradiated fuel are conducted remotely in a large heavily shielded inert atmosphere enclosure. Building and installation cost estimates were largely based on the costs incurred in the construction of the EBR-II Fuel Cycle Facility. Equipment cost estimates were based on the cost of equipment for the EBR-II, the projected cost of plant-scale versions of components currently under development by the Chemical Engineering Division, and manufacturers' quotes.

The estimated unit fuel cycle cost for the Argonne Reference Metal-Fueled Reactor is 0.95 mill/kw(e)-hr. A breakdown of this cost is presented in Table IX-2. The unit cost includes amounts for the return on investment, the replacement of capital and the operating costs. A breakdown of the annual charges is presented in Table IX-3. A 6.75 percent cost of money was used in computing the capital replacement cost. For the re-

turn on investment a rate of 13 percent was used which includes taxes, insurance and the cost of money. These percentage values were based on practices of private utility companies, as reported in the AEC Guide to Nuclear Power Cost Evaluation (TID-7025). The depreciation schedules for the replacement of capital was 30 yr for buildings, 15 yr for out-of-cell and in-cell non-process equipment, and 5 yr for process equipment.

The reference fuel cycle facility is operated at a plant factor of only 37 percent, principally because reactor unloading, cooling, processing, refabrication, and refueling must occur in the 191-day period between reactor cycles. Consequently, the processing campaign

TABLE IX-3. ANNUAL CHARGES FOR THE REFERENCE COMPACT PYROCHEMICAL FUEL CYCLE FACILITY FOR THE ARGONNE REFERENCE METAL-FUELED 1000 Mw(e) FAST REACTOR

Operating Cost	\$4,712,500
Cost of Capital Replacement	654,400
Return on Investment <sup>a</sup>	2,190,900
Inventory Charges	1,577,000
Total Annual Charge	\$9,134,800

<sup>a</sup> The total investment includes plant facilities, contractor's overhead and engineering fees, insurance, site improvement, direct installation costs, start-up costs, and working capital.

### C. DIVISIONAL STUDY OF REPROCESSING OF FAST REACTOR PLUTONIUM FUELS

The purpose of this study is to compare the cost of processing various fast reactor plutonium fuels by alternative processing methods under a consistent set of requirements and restrictions. The set of conditions includes parameters for reactor power, burnup, and other parameters that are expected to correspond to the range of possibilities as to fuel loads, technical specifications, and economic requirements of a projected fast breeder reactor system capable of producing competitively priced electrical power in 1980. The alternative fuels and processes are those whose technical details are being defined and whose practical applications are being demonstrated in current development programs. Three fuel materials are being considered: metal, oxide, and carbide. For each of the reference fuels, three alternative methods are being considered for the recovery of valuable fuel from fission products. The three methods are: (1) an aqueous-solvent extraction, (2) a fluid-bed volatility process, and (3) a com-

TABLE IX-4. UNIT COSTS OF THE REFERENCE COMPACT PYROCHEMICAL FUEL CYCLE FACILITY FOR THREE METAL-FUELED FAST BREEDER REACTORS (2500 Mw(e) TOTAL)

	Unit Costs	
	mills/ kw(e)-hr	\$/kg
Processing and Refabrication	0.83	138
Waste Disposal	0.05	8
Out-of-Reactor Fuel Inventory	0.10	17
One Percent Processing Loss	0.03	5
Plutonium Credit	-0.37	-62
Total	0.63	106

is of 147-day duration per cycle. By increasing the processing plant factor to 80 percent, the output of three reactors totaling 2500 Mw(e) could be handled in the reference fuel cycle facility with only a modest increase in the annual charge, but with a substantial decrease in the unit charge for processing and refabrication. The unit charges for this case appear in Table IX-4. Since the out-of-reactor inventory of the fuel cycle does not increase when a favorable schedule is used with three reactors, the unit inventory charge also is decreased.

pact pyrochemical process. All of the above combinations are being examined for two processing plant sizes, corresponding to different sizes of fast reactor power systems, namely, a single 1000 Mw(e) reactor and ten 1000 Mw(e) reactors. For each of the above reactor systems, the process plant loads also vary in uranium and plutonium throughput according to several reactor design and operation conditions, i.e., various cases of fuel burnup, of plutonium concentration in the discharged core material, and of plutonium concentration in the discharged blanket materials.

Although this study is undergoing revision and the cost evaluations should therefore be considered preliminary, current results are summarized here for the purpose of identifying the variables involved in the comparison of alternative fuels and processes and showing the approximate relative contribution of reprocessing, shipping, and out-of-reactor fuel inventory to the total fuel cycle costs.

## 1. Comparative Cost Analysis

Reference flowsheets for aqueous-solvent extraction, fluid-bed volatility, and pyrochemical processes were selected to serve as a basis for plant cost calculations. Process flow rates, plant size, costs of supplies, services, and chemicals, waste volumes and costs, nuclear safety procedures and other process decisions were based on these flowsheets. The reference reprocessing plants were based on total throughputs of 100 to 1000 kg per day. This range of production covers the total throughput for both the integral processing plant (for one reactor) and the central processing plant (for ten reactors).

The aqueous solvent extraction process is the most highly developed of the three reference processes and could be applied to the specific fuels and processing rates discussed with little change in the flowsheets adopted. However, there are several points in the aqueous process in which this application goes beyond present plant practice:

1. Plutonium enrichment is higher for these fast reactor fuels than for the feed in present aqueous plants, and more difficult criticality problems exist.
2. Solvent degradation under high radiation fields for high burnup fuels is a problem believed to be overcome in the aqueous flowsheet used here by specifying a 120-day fuel cooling period before processing. (Although this cooling time is longer than that specified in this study for the nonaqueous processes, the higher associated cost is at least partially compensated for by other plant savings, for example, less expensive iodine-handling steps for longer-cooled fuel and a lower cost solvent treatment for recycle.)
3. Some complications may be offered to the metal-dissolution step by the presence of alloying agents such as ruthenium, molybdenum, zirconium, and titanium.
4. The presently existing processes for conversion of plutonium oxide to carbide is not yet well developed, although promising developments are underway at Argonne National Laboratory and elsewhere.

The fluid-bed fluoride volatility process is less well developed than the aqueous process, and modifications of the reference flowsheet can be expected in reducing this process to practice. Although the major process steps have been given considerable study at several sites in connection with processing of uranium fuel, plutonium behavior is still less well defined than uranium behavior.

The compact pyrochemical process flowsheets are not as highly developed as the aqueous flowsheet, but all the major steps are under study at Argonne National Laboratory. The metal fuel flowsheet is being reduced to practice at the EBR-II integrated processing facility at the Idaho site. The basic plant concepts for pyrochemical processing, including the associated remote operation and maintenance techniques, are being evaluated at the EBR-II plant.

For each of the three processes, capital and operating costs were calculated for direct processing, shipping, inventory, waste disposal, and process losses. The overall cost associated with reprocessing was taken as the sum of costs in these categories.

The following preliminary conclusions appear from the cost analysis of the cases outlined above. The distinction is made here between direct costs of reprocessing and overall costs of reprocessing and associated handling, which includes losses, inventory charges, shipping costs, and waste disposal, as well as the direct reprocessing costs.

1. Large 10,000 Mw(e) central plants have lower overall and direct unit costs (mills/kw-hr) than do small 1000 Mw(e) integrated plants for all cases calculated. Here it is assumed that shipping by presently acceptable methods will continue to be possible. On this basis, the lower direct processing costs for large plants more than compensate for the cost of shipping.
2. For metal fuels, pyrochemical processes have the lowest direct and overall reprocessing costs, regardless of plant throughput and other variables. This is due to the relative simplicity of the compact pyrochemical process, and the fact that it yields a metal product directly.
3. Waste disposal costs for all cases were lowest for the volatility process, chiefly due to its production of a very low volume solid waste. In some cases, waste disposal for the pyrochemical process was equally low.
4. Fuel inventory and waste disposal for the aqueous solvent extraction process showed substantially the highest costs in all cases. These high costs are due to the relatively long cooling time for the fuel before processing and to the relatively large volumes of process liquid waste, which must be concentrated and solidified.
5. Cost comparisons\* of the aqueous, volatility, and pyrochemical processes are as follows:

\* Only horizontal comparisons are valid.

		High Cost		Low Cost				High Cost		Low Cost	
<i>A. Metal Fuel</i>											
1. <i>Small Integral Plant</i>											
a. Direct Processing:	aqueous	volatility	pyrochem.							volatility	aqueous
b. Overall Processing and Handling:	aqueous	volatility	pyrochem.							pyrochem.	volatility
2. <i>Large Central Plant</i>											
a. Direct Processing:	aqueous		pyrochem.								
	volatility										
b. Overall Processing and Handling:	aqueous	volatility	pyrochem.								
<i>B. Oxide Fuel</i>											
1. <i>Small Integral Plant</i>											
a. Direct Processing:	pyrochem.		volatility								
	aqueous										
b. Overall Processing and Handling:	aqueous	pyrochem.	volatility								
2. <i>Large Plant</i>											
a. Direct Processing:	volatility		pyrochem.								
	aqueous										
b. Overall Processing and Handling:	aqueous		volatility								

## 2. The Cost-Throughput Relation for Reprocessing Plants: The Effect of Burnup

If the form of the relation between mass throughput ( $w$ ) and total annual cost ( $C$ ) is assumed to be of exponential relation  $C = a w^b$ , where  $a$  and  $b$  are constants, then the constant  $b$  is found to be approximately 0.5 for the total annual direct processing costs developed for the reference 100 and 1000 kg/day reprocessing plants.

Since the reprocessing plant throughput is furnished by the rate of discharge of fuel, the core fuel processing rate for a reactor of given power is inversely proportional to burnup. Similarly, the blanket processing rate is inversely proportional to the amount (and therefore the concentration) of plutonium bred in the blanket at the time of discharge.

The unit processing costs, mills/kw(e)-hr, for the reference plants were calculated for various burnups and blanket plutonium concentrations by using the above processing cost-load factor  $b$  and the appropriate processing rates. As long as combined fuel and blanket processing is assumed, such variations of throughput do not change the relative cost advantages (cited above) for the reference processing plants of 100 and 1000 kg/day capacity. However, the fraction of the total unit fuel cycle cost that is due to the direct processing cost in general varies with this change of throughput because of change of burnup.

The general relation of fuel burnup to processing

loads and costs may be described in the following terms. The processing load ( $w$ ) is directly proportional to the rate of power generation ( $P$ ) and inversely proportional to the percent burnup ( $B$ ), other things being equal. Thus, for two reactors,

$$\frac{w_2}{w_1} = \frac{P_2 B_1}{P_1 B_2}$$

From our previous relation between cost ( $C$ ) and throughput ( $w$ ):

$$\frac{C_2}{C_1} = \left( \frac{w_2}{w_1} \right)^{0.5}$$

Thus, for a given total power generation,

$$P_1 = P_2, \text{ and } \frac{C_2}{C_1} = \left( \frac{B_1}{B_2} \right)^{0.5}$$

The significance of this relation is that for a given level of total power generation, the unit costs of reprocessing (in mills/kw(e)-hr) varies not inversely to the first power of burnup, but inversely to the 0.5 power, or whatever power is correct for the cost-throughput relation of the reprocessing plant. Actually, the effect of core fuel burnup on processing costs is even less pronounced because the blanket portion of the processing rate is not changed in general by variations in core fuel burnup.

## 3. Shipping and Inventory Costs

A study of shipping and out-of-reactor fuel inventory costs was made for aqueous, volatility, and pyrochemical processing of fast reactor fuel. The study compared costs for an integrated processing plant for a single 1000 Mw(e) reactor and a central plant large

enough to process the fuel of 10 such reactors. Burnup of core fuel and plutonium concentrations were examined as additional parameters. The assumption was made that presently acceptable rail shipments are feasible for spent reactor fuel.

TABLE IX-5. FUEL SHIPPING CASK FOR SPENT FAST REACTOR FUEL

<b>A. Cask Characteristics</b>	
Weight, loaded, tons	100
Weight of cask shock buffer, tons	25
Capacity	
Full loading, actinides plus fission products, kg	2000
Heat dissipation, kw	50
	% of Cask Cost
<b>B. Interest, Depreciation, and Insurance</b>	
Return on investment	6.75
Sinking fund factor (10 years at 6.75%)	7.33
Income tax	3.40
State and local taxes	2.45
Property insurance on cask	1.00
	20.93
<b>C. Use Charge</b>	
Annual cost of cask and buffer <sup>a</sup>	\$52,000
Annual cost of repairs and supplies	3,000
	\$55,000
Total annual cost	\$55,000
Use Charge (60% use factor)	\$250/day

<sup>a</sup> Total cost of cask and buffer is \$250,000.

Shipping and inventory costs were analyzed together because of the interrelationship between the two costs. The value of the fuel affects both the property insurance cost during shipping and the inventory cost. The shipping costs affect the value of the fuel prior to shipping and, thus, the inventory cost prior to shipping. Finally, for pyrochemical and volatility processing, the combined cost of shipping plus inventory has a minimum value for an optimum cooling period which varies with burnup, plutonium concentration in the discharged fuel, and the cost of plutonium. (However, in this study only a single set of fuel values was used: \$10/g fissile plutonium and \$10/kg other actinides.) Other variables have only a minor effect on this optimum cooling time.

Shipping costs for high-burnup, short-cooled fast reactor fuels cannot be taken directly from cost correlations developed for thermal reactors in terms of cost per kilogram of material shipped because of the higher rate of heat dissipation of fission products in the fast reactor fuel. That is, the cask cooling requirement for the present case of fast reactor fuel is more restrictive as to the cask capacity than is the volume or weight of fuel. The shipping cost, therefore, is more directly a function of the amount of heat which must be dissipated than of the weight of fuel shipped.

In this study of fuel shipping costs for spent fuel of fast reactors the cost estimates were made for rail shipments of casks for delivering spent fuel to the

processing plant and separate shipments for delivering new fuel to the reactor. It was found more economical to ship empty casks on the return trip than to hold casks at the reactors.

The conceptual cask design for fast reactor fuels employed a heavy internal basket for neutronic isolation and heat conduction. Natural air conduction is used internally and forced air convection externally. However, natural air convection externally is satisfactory in an emergency. In general, cask loading was determined by the actual heating value of the fuel. An external crash buffer (25 tons) is employed for additional safety.

A daily use charge was determined for the spent fuel casks on the basis shown in Table IX-5. A similar basis was used to determine a daily charge of \$140 for the cask for shipping refabricated fuel; this latter cask was lighter, 70 tons total, with a 3000 kg capacity.

Liability insurance during shipment was estimated at \$1000 per trip plus \$1 per mile for spent fuel and \$500 per trip plus \$0.50 per mile for refabricated fuel.

Property insurance during shipping was estimated at 0.15% of the basic fuel value for the 500-mile distance and 0.20% of the basic fuel value for the 1000-mile distance. The basic fuel values taken in this study were \$10/g for fissile plutonium and \$10/kg for fertile actinides.

Fuel inventory costs were based on annual fixed charges on fuel value of 13%, following the practice of private utilities for nondepreciating capital cited in the AEC "Guide to Nuclear Power Cost Evaluation" (TID-7025).

Since the basic fuel value was taken to apply to fuel material ready for fabrication, adjustments in value were required for fuel in other stages of the fuel cycle operations. These adjustments depend on costs incurred in reprocessing, shipping, insurance, and refabrication, together with costs due to losses. Only approximate adjustments were made in this study.

The inventory costs for integral (on-site) plants were based on a cooling period of 200 days for aqueous processing with a period after cooling of 160 days. The total time of 360 days corresponds to two reactor unloading cycles in this study. For volatility and pyrochemical processing in integral plants the cooling time was 60 days and the post-cooling period 120 days (one reactor unloading cycle).

The inventory costs for central plants were based on a cooling period of at least 120 days prior to processing for aqueous plants, and it was assumed that longer cooling had no advantage in processing costs. For volatility and pyrochemical processes it was considered that a minimum cooling time of 20 days was required for handling and that longer times had no in-

fluence on the cost of processing. However, cooling times somewhat longer than 20 days were used for the central plant using volatility and pyrochemical processing, since the cooling times were selected as optimized values, giving the lowest total inventory and shipping costs. This calculation involved finding the minima of functions relating cooling time to the heat emission and to the inventory and shipping costs of the fuel.

The costs of inventory and shipping for various fuel recovery processes are summarized in Table IX-6. For aqueous processing there is no incentive for on-site processing (integral plants) because the long out-of-reactor period for the integral plant results in inventory costs higher than the combined inventory and shipping cost for central plant processing. For pyrochemical and volatility processing, the combined inventory and shipping charges for central plants are substantially higher than for integral plants, even of the small 1000 Mw(e) size of this study. However, in determining the overall comparative costs of integral and central plants, the lower unit costs of reprocessing and

TABLE IX-6. COSTS OF INVENTORY AND SHIPPING FOR VARIOUS FUEL RECOVERY PROCESSES

One-thousand Mw(e) reactor, 80% load factor, 20% total plutonium in core fuel, 2% total plutonium in blanket fuel, fissile plutonium valued at \$10/g, fertile actinides valued at \$10/kg.

Burnup (%)	Aqueous Processing (mills/kw-hr)			Pyrochemical and Volatility Processing (mills/kw-hr)		
	On-Site Plant*	Central Plant at Distance Given		On-Site Plant*	Central Plant at Distance Given	
		500 miles	1000 miles		500 miles	1000 miles
3	0.547	0.374	0.417	0.280	0.311	0.378
5	0.339	0.246	0.276	0.176	0.213	0.255
10	0.184	0.144	0.164	0.098	0.126	0.151
20	0.106	0.091	0.104	0.059	0.079	0.093

\* No shipping required.

waste disposal for central plants must be taken into account.

#### 4. Fuel Inventory Costs: Effect of Burnup and Out-of-Reactor Residence Time

The relation of fuel inventory costs to burnup and time required for a complete fuel cycle operation may be illustrated by the following considerations. The power density,  $H$ , of the reactor per kg of actinide fuel,  $L$ , may be expressed as follows:

$$H = \frac{0.95B}{T} = \frac{Pf}{L},$$

where

- $H$  = reactor power density, Mw(t)/kg fuel in reactor
- 0.95 = conversion factor, Mw(t)/kg of fuel fissioned per day
- $B$  = burnup of fuel, weight fraction
- $T$  = irradiation time of fuel in reactor, days
- $P$  = nominal reactor power, Mw(t)
- $f$  = power factor, fraction of total time that reactor is on power
- $L$  = fuel loading in reactor, kg.

The rate of fuel discharged from the reactor in kg/day is  $w$ , and

$$w = \frac{L}{T} = \frac{Pf}{0.95B}.$$

The amount of fuel  $W$  held up outside the reactor in the total fuel cycle operations depends on the total out-of-reactor time  $T_o$ , in days. Thus,

$$W = wT_o = \frac{LT_o}{T} = \frac{Pf}{0.95} \left( \frac{T_o}{B} \right).$$

If two cases are compared wherein  $L$ ,  $P$ , and  $f$  are constant,

$$\frac{W_2}{W_1} = \left( \frac{T_o}{T} \right)_2 / \left( \frac{T_o}{T} \right)_1 = \left( \frac{T_o}{B} \right)_2 / \left( \frac{T_o}{B} \right)_1.$$

For a reactor with a given irradiation time  $T$ , the size of the out-of-reactor fuel inventory is directly proportional to  $T_o$ , the out-of-reactor fuel cycle time. Thus, while lower burnup results in a larger amount of fuel inventory, other things being equal, a shorter out-of-reactor fuel cycle time compensates by lowering the inventory amount. Thus, as an illustration, fuel inventory (and hence the charges) will be the same for the following cases:

	Case 1	Case 2	Case 3
Burnup, %	3	5	10
Time out of reactor, days	72	120	240

Inventory charges are influenced by reactor parameters (especially power density and fuel management schedules) even more than by variants of processing, and the longer cooling time for aqueous than for the nonaqueous processes results in a penalty for aqueous processes that is especially pronounced for the 180-day reactor fueling cycle time on which Table IX-6 was based.

